

*Chukchi Sea Offshore Monitoring in Drilling Area  
(COMIDA): Hanna Shoal Ecosystem Study*  
Final Report

Prepared By:  
Kenneth H. Dunton, Principal Investigator  
University of Texas Marine Science Institute  
750 Channel View Drive, Port Aransas, TX 78373  
(email of corresponding author: [ken.dunton@mail.utexas.edu](mailto:ken.dunton@mail.utexas.edu))

Associate Editor: Susan V. Schonberg

Prepared For:  
Bureau of Ocean Energy Management  
Alaska Outer Continental Shelf Region  
3801 Centerpoint Drive, Suite 500  
Anchorage, AK 99503



Cooperative Agreement No. M11AC00007

Lead Project Scientists:  
Carin Ashjian  
Robert G. Campbell  
Lee W. Cooper  
Jacqueline M. Grebmeier  
H. Rodger Harvey  
Brenda Konar  
David Maidment  
John Trefry  
Tom Weingartner

June 2016



Cooperative Agreement No. M11AC00007

PREFACE

Study, design, oversight, and funding were provided by the U.S. Department of the Interior, Bureau of Ocean Energy Management, Alaska Outer Continental Shelf Region, Anchorage, Alaska, as part of the BOEM Environmental Studies Program, under Number M11AC00007.

DISCLAIMER

This report has been reviewed by the Bureau of Ocean Energy Management (BOEM) and approved for publication. Approval does not signify that the contents necessarily reflect the views and policies of the Bureau, nor does mention of trade names or commercial products constitute endorsement or recommendation for use.

THE CITATION FOR THIS REPORT IS:

Dunton, K.H., C. Ashjian, R.G. Campbell., L.W. Cooper, J.M. Grebmeier, H.R. Harvey, B. Konar, D. M. Maidment, J.H. Trefry, and T.J. Weingartner. 2016. Chukchi Sea Offshore Monitoring in Drilling Area (COMIDA): Hanna Shoal Ecosystem Study. Final Report. OCS Study BOEM 2016-047. Prepared for the Bureau of Ocean Energy Management, Anchorage, AK, by The University of Texas Marine Science Institute, Port Aransas, TX. 352 pp.

THE DATA CITATION IS:

Dunton, K.H., C. Ashjian, R.G. Campbell, L.W. Cooper, J.M. Grebmeier, H.R. Harvey, B. Konar, D.M. Maidment, J.H. Trefry, T.J. Weingartner, and T.L. Whiteaker. 2014. Hanna Shoal Ecosystem Study. OCS Study BOEM 2016-047. Version 1.1. National Oceanographic Data Center, NOAA. doi:10.7289/V5GX48MN

# *Chukchi Sea Offshore Monitoring in Drilling Area (COMIDA): Hanna Shoal Ecosystem Study*

## Final Report

### Lead Project Scientists:



Carin Ashjian  
Woods Hole Oceanographic Institution  
G Redfield 2-46, MS #33  
Woods Hole, MA 02543  
[cashjian@whoi.edu](mailto:cashjian@whoi.edu)



Robert G. Campbell  
University of Rhode Island  
Graduate School of Oceanography  
S. Ferry Rd Narragansett, RI 02882  
[campbell@gso.uri.edu](mailto:campbell@gso.uri.edu)



Lee Cooper  
University of Maryland  
Center for Environmental Science  
P.O. Box 38  
Solomons, MD 20688  
[cooper@umces.edu](mailto:cooper@umces.edu)



Kenneth H. Dunton  
University of Texas  
Marine Science Institute  
750 Channel View Drive  
Port Aransas, TX 78373  
[ken.dunton@utexas.edu](mailto:ken.dunton@utexas.edu)



Jacqueline Grebmeier  
University of Maryland  
Center for Environmental Science  
PO Box 38  
Solomons, MD 20688  
[jgrebmei@umces.edu](mailto:jgrebmei@umces.edu)



H. Rodger Harvey  
Old Dominion University  
Ocean, Earth, and Atmospheric Sciences  
4600 Elkhorn Ave  
Norfolk, VA 23529  
[rh Harvey@odu.edu](mailto:rh Harvey@odu.edu)



Brenda Konar  
University of Alaska Fairbanks  
Institute of Marine Science  
217 O'Neill  
Fairbanks, AK 99775  
[bhkonar@alaska.edu](mailto:bhkonar@alaska.edu)



David Maidment  
University of Texas at Austin  
Center for Research in Water Resources  
1 University Station C1786  
Austin, TX 78712-0273  
[maidment@utexas.edu](mailto:maidment@utexas.edu)



John Trefry  
Florida Institute of Technology  
Dept. of Marine & Environmental Systems  
College of Engineering Edwin A Link, 101  
Melbourne, Florida 32901  
[jtrefry@fit.edu](mailto:jtrefry@fit.edu)



Thomas Weingartner  
University of Alaska Fairbanks  
Institute of Marine Science  
115 O'Neill  
Fairbanks, AK 99775  
[tjweingartner@alaska.edu](mailto:tjweingartner@alaska.edu)

## COMIDA Science Tasks and Participants

<b>Major Tasks</b>	<b>Principal Investigator</b>	<b>Associates/Students</b>
Zooplankton population structure and biology	Dr. Carin Ashjian Dr. Robert G. Campbell	Philip Alatalo Heather McEachen Stephen Elliott Hangzhou Wang Celia Gelfman
Sediment and water column chlorophyll Sediment tracers Infaunal biomass and carbon Sediment grain size and C:N	Dr. Lee Cooper Dr. Jackie Grebmeier	Christopher Paver Michael Gonsior Laura Gemery Christian Johnson Mengjie Zhang Dubrava Kirievskaya Chris Paver Kathleen Marshall Holly Kelly (teacher) Deana Wheeler (teacher)
Infaunal diversity and abundance Food web structure Nutrient fluxes	Dr. Kenneth Dunton	Susan Schonberg Amber Hardison Philip Bucolo Jordann Young Nathan McTigue Christina Bonsell Susan Saupe Andrea Skloss (teacher)
Hydrocarbon extraction Sediment screening	Dr. H. Roger Harvey	Karen Taylor Molly Mikan Ian Salter Rachael Pleuthner Tetiana Muniak Dr. Guoping Zhu
Epifaunal composition and abundance	Dr. Brenda Konar	Alexandra Ravelo Kimberly Powell Tanja Schollmeier Jasmin Groß Thomas Brey
GIS and data management	Dr. David Maidment	Timothy Whiteaker Stephen Jackson Johnny Sullivan
Trace metal analyses in sediments Trace metal analyses in biota	Dr. John Trefry	Robert Trocine Austin Fox Youchao Yan Brena O'Neill
Physical oceanography	Dr. Thomas Weingartner	Dave Leech Ying-Chih Fang Peter Winsor

## Table of Contents

### Introduction

**Hanna Shoal: An Integrative Study of a High Arctic Marine Ecosystem.....1**  
Kenneth H. Dunton

### Tom Weingartner

**Physical Oceanography and Circulation.....9**  
Tom Weingartner, Ying-Chih Fang, and Peter Winsor

### John Trefry

**Trace Metals in Sediments, Water and Biota.....69**  
John Trefry, Robert Trocine, Austin Fox

### Roger Harvey

**Organic Contaminants in Chukchi Sea Sediments and Biota of the Hanna Shoal  
Region.....95**  
H. Rodger Harvey, Karen Taylor

### Carin Ashjian and Robert Campbell

**Mesozooplankton Abundance and Distribution in Association with Hydrography on Hanna  
Shoal, NE Chukchi Sea, During August 2012 and 2013.....114**  
Carin Ashjian, Robert Campbell, Philip Alatalo, Celia Gelfman, Stephen Elliott, Heather  
McEachen

**Physical Control of the Distributions of a Key Arctic Copepod in the Northeast Chukchi  
Sea.....147**  
Stephen Elliott, Carin Ashjian, Zhixuan Feng, Benjamin Jones, Changsheng Chen, Yu Zhang,  
Robert Campbell

### Brenda Konar

**Interannual Variability of Epibenthic Communities in the Chukchi Sea Alaska.....177**  
Kimberly Powell, Brenda Konar, Jaqueline Grebmeier

**Size-frequency Distribution, Growth, and Mortality of Snow Crab (*Chionoecetes opilio*)  
and Arctic lyre crab (*Hyas coarctatus*) in the Chukchi Sea from 2009 to 2013.....199**  
Jasmin Groß, Brenda Konar, Thomas Brey, Jacqueline M. Grebmeier

**Jackie Grebmeier and Lee Cooper**

**Sediment Deposition Patterns on the Chukchi Shelf Using Radionuclide Inventories.....229**

Lee W. Cooper and Jacqueline M. Grebmeier

**Water Column Chemistry, Benthic Macroinfaunal Populations, and Sediment Tracer Measurements.....247**

Jacqueline M. Grebmeier, Lee W. Cooper

**Kenneth Dunton**

**Arctic Shelves as Platforms for Active Biogeochemical Activity: Nitrogen and Carbon Transformations in the Chukchi Sea, AK.....263**

Amber K. Hardison, Nathan D. McTigue, Wayne S. Gardner, Kenneth H. Dunton

**Trophodynamics of the Hanna Shoal Ecosystem (Chukchi Sea, Alaska): Connecting Multiple End-members to a Rich Benthic Food Web.....285**

Nathan D. McTigue, Kenneth H. Dunton

**Distribution, abundance, biomass and diversity of benthic infauna in the northeastern Chukchi Sea, Alaska.....308**

Susan Schonberg, Ken Dunton

**David Maidment**

**Data Management for the Hanna Shoal Ecosystem Study.....321**

Tim Whiteaker, David Maidment

## Figure Captions

### **Introduction to Hanna Shoal: An Integrative Study of a High Arctic Marine Ecosystem:** Kenneth H. Dunton

**Figure 1.** The location of Hanna Shoal and stations occupied in the northeast Chukchi Sea during summers 2009, 2010, 2012, and 2013 for the COMIDA program in relation to oil and gas tracts from Lease Sale 193. Water depths are in meters.

**Figure 2.** A synopsis of major water circulation patterns in the northern Chukchi Sea. Nutrient-rich Bering Sea water flows north through the Central Channel before turning east along the Chukchi Sea shelf break and circumventing Hanna Shoal and exiting through Barrow Canyon to the Beaufort Sea. COMIDA hydrographic and current moorings (in yellow ellipses) deployed on the Hanna Shoal Ecosystem Study are denoted yellow. From Brugler et al., 2014 (with permission).

### **Tom Weingartner**

#### **Physical Oceanography and Circulation:** Tom Weingartner, Ying-Chih Fang, and Peter Winsor

**Figure 1.** The mean, vertically-integrated flow over the Chukchi Sea shelf based on the model study of Spall (2007). Note the clockwise circulation around the northern and eastern sides of Hanna Shoal.

**Figure 2.** A photograph of the assembled COMIDA ADCP and MicroCat TCP mooring. The ADCP electronics are housed in the center well on the syntactic foam float. The MicroCat sits in a separate well with only the sensors exposed.

**Figure 3.** Bathymetric map showing the locations of the COMIDA current meter moorings in 2011 – 12 and 2013 – 14.

**Figure 4.** Timelines of ADCP data recovery from the COMIDA moorings with blue being for 2012-13 and red for 2013-14 deployments.

**Figure 5.** Maps of ADCP mooring locations in the northeastern Chukchi Sea shelf from 2008 – 2015. Yellow dots indicate moorings in which data processing is not yet complete.

**Figure 6.** SSM/I sea ice concentration maps for the Chukchi shelf in 2011: May (left column), June (middle column) and July (right column).

**Figure 7.** Sea ice concentration maps in 2012 for May (left), June (middle), and July (right). The labels on the July 15 map refer to Hanna (HN) and Herald (HE) shoals, the Central Channel (CC), and Herald Valley (HV).

**Figure 8.** Sea ice concentration maps in 2013 for May (left), June (middle), and July (right).

**Figure 9.** Locations of the ice-edge (15% ice concentration contour as determined by the NSIDC) on August 1 and 15 and September 1 and 15 for 2011 (top), 2012 (middle), and 2013 (bottom).

**Figure 10.** Time series of wind vectors over the northeastern Chukchi Sea for the August – November periods of 2011 (top), 2012 (middle), and 2013 (bottom).

**Figure 11.** Ice concentration time series for 2012 – 13 at each mooring location based upward-looking ADCPs.

**Figure 12.** Ice concentration time series for 2013 – 14 at each mooring location based upward-looking ADCPs.

**Figure 13.** The evolution of sea ice concentrations as seen on 30 October (top), 15 November (middle), and 30 November (bottom) for 2012 (left column) and 2013 (right column).

**Figure 14.** Mean vectors and variance ellipses for sea ice (black) and winds (red) for the periods of November 2012 – June 2013 (top) and from November 2013 – June 2014 (bottom).

**Figure 15.** Zonal (U) and Meridional (V) components of velocity as a function of depth and time for moorings HSNW40, HSNW50, NSNE40, HSNE50 for both the 2012 – 13 and 2013 – 14 deployment periods.

**Figure 16.** Zonal (U) and Meridional (V) components of velocity as a function of depth and time for moorings HSNE60 mooring for both the 2012 – 13 and 2013 – 14 deployment periods.

**Figure 17.** Mean vectors and variance ellipses for the uppermost ADCP bin (black) and winds (red) for the 2012 – 2013 deployment (top) and the corresponding period in 2013 – 2014 (bottom).

**Figure 18.** The trajectory of one of nine satellite-tracked drifters released during deployment of the HSNE50 in September 2013, along with time series of the drifter velocity components, SST, and winds along the drifter track. The thick lines on the velocity plots are low-pass filtered currents. The bottommost panel shows the cluster's centroid trajectory and the individual trajectories of the drifters comprising the cluster.

**Figure 19.** The trajectory of one of nine satellite-tracked drifters released during deployment of the HSNE50 in September 2013, along with time series of the drifter velocity components, SST, and winds along the drifter track. The thick lines on the velocity plots are low-pass filtered currents. The bottommost panel shows the cluster's centroid trajectory and the individual trajectories of the drifters comprising the cluster.

**Figure 20.** Mean vectors and variance ellipses for vertically-averaged currents (black) and winds (red) for the periods of November 2012 – June 2013 (top) and the corresponding period in 2013 – 2014.

**Figure 21.** Mean vectors and variance ellipses for currents at 10 mab (black) and winds (red) for the periods of November 2012 – June 2013 (top) and the corresponding period in 2013 – 2014 (bottom).

**Figure 22.** Mean vectors and variance ellipses for currents at 6 mab (black) and winds (red) for the periods of February 2013 (top) and October 2013 (bottom).

**Figure 23.** Time series of vertically averaged current vectors (top), and temperature (middle) and salinity (bottom) at 47 m depth from mooring HSNW50-12. The timing of the temperature maximum ( $T_{\max}$ ) and the descent to the freezing point ( $T_f$ ) are noted.

**Figure 24.** Time series of vertically averaged current vectors (top), and temperature (middle) and salinity (bottom) at 23 m (red) and 47 m (blue) depth from mooring HSNE50-12. The timing of the temperature maximum ( $T_{\max}$ ) and the descent to the freezing point ( $T_f$ ) are noted.



**Figure 25.** Time series of bottom temperature and salinity from the COMIDA 2012 – 13 mooring array.

**Figure 26.** Time series of bottom temperature and salinity from the COMIDA 2012 – 13 mooring array.

**Figure 27.** Mean vertical profiles of velocity for the 2012 – 13 (top) and 2013 – 14 **Figure 28.** Rotary spectra of currents at 45 m depth from HSNE50-12 consisting of clockwise (black) and counterclockwise (blue) spectral components. The symbols  $K_1$ ,  $f$ , and  $M_2$  denote the diurnal tide, inertial, semi-diurnal tide frequencies, respectively.

**Figure 29.** Wavelet analysis results for the clockwise (CW) spectral component at HSNE50-12. The inertial band lies within the 8 – 16 hour period. Periods when the energy levels are significantly greater (at the 95% level) than background are enclosed by black contours.

**Figure 30.** Wavelet analysis from the 2012 – 13 deployments of HSNE40 (upper left) and HSNW40 (upper right) and HSNE50 (lower left) and HSNW50 (lower right). In each panel the time series includes the wind the ice velocity vectors. The lowest panel consists of the time series as a function of depth of clockwise (CW) energy in the near-inertial wave band (8 – 16) hours.

**Figure 31.** COMIDA CTD stations occupied in August 2012. Roman numerals denote the transects used to construct vertical sections shown in separate Figures 34, 36 – 38.

**Figure 32.** CTD stations occupied in August 2013.

**Figure 33.**  $\theta/S$  diagrams from 2012 (top) and 2013 (bottom).

**Figure 34.** Vertical sections of potential temperature (top row) and salinity (bottom row). The sections are from Transects I (left), II (middle), and III (right; see Figure 31 for transect locations). Typical ice concentrations on these transects were 50 – 90%.

**Figure 35.** VM-ADCP vector at 20 m depth in August 2012. Blue numbers indicate the day in August when the data were collected. The bottom panel shows the wind vector.

**Figure 36.** Vertical sections of potential temperature (top) and salinity (bottom) constructed from Transects IV (see Figure 31 for transect locations). Ice concentrations along this transect ranged from 30 – 70% ice cover.

**Figure 37.** Vertical sections of potential temperature (top row) and salinity (bottom row). The sections are from Transects V (left), VI (middle), and VII (right; see Figure 31 for transect locations).

**Figure 38.** Vertical sections of potential temperature (top row) and salinity (bottom row) from along Transect I in 2012 (left) and 2013 (right).

**Figure 39.** Vertical sections of temperature (left) and salinity (right) in August 2013 (top) and July 2014 (bottom) along the sections shown on the maps to the right of each section.

**Figure 40.** The trajectories of two of 13 drifters released near Wainwright Alaska on 11 August 2012. The trajectories are color-coded according to the sea surface temperatures measured by the drifter and given by the scale on the map.

**Figure 41.** Plan views of temperature (left) and salinity (right) in August and September of 2012. The plan views are based on averages of the upper and bottom 10 m of the water column.

**Figure 42.** Plan views of temperature (left) and salinity (right) in August and September of 2011. The plan views are based on averages of the upper and bottom 10 m of the water column. The black line in the bottom right panel shows the location of the vertical sections shown in Figure 43.

**Figure 43.** Vertical sections of temperature (left) and salinity (right) in September 2011 (top row) and 2012 (bottom row).

**Figure 44.** From top to bottom: Vertical sections of (from top to bottom) temperature, salinity, density, chl *a*, particle concentrations, and CDOM (color dissolved organic matter) along the Leg M transect collected by the acrobat towed CTD unit in September 2013. The dotted line shows the approximate position of the MW/BSW front evident at km 30 on the section. The green dot shows the start of the transect, which corresponds to the left side of the section plots.

**Figure 45.** Temperature and salinity distribution along the HSNW mooring line in September 2013 (from Lu et al., 2015).

**Figure 46.** Mean surface current vectors for the week of 5 September 2012, as estimated from HFRs.

**Figure 47.** Color-coded (by SST) trajectory of a satellite-tracked drifter released at the location of the green triangle on 13 August 2012. The drifter's last reported position was on 15 November at the location of the red star.

**Figure 48.** Record-length mean currents and current ellipses for all moorings in the northeast Chukchi Sea, 2011 – 12. Red vectors and ellipses are for winds, grey indicate statistics based on less than one full year of data.

**Figure 49.** Record-length mean currents and current ellipses for all moorings in the northeast Chukchi Sea, 2011 – 12. Red vectors and ellipses are for winds, grey indicate statistics based on less than one full year of data.

### *John Trefry*

**Trace Metals in Sediments, Water and Biota:** John Trefry, Robert Trocine, Austin Fox

**Figure 1.** Sampling stations for 2012 (○) and 2013 (□) field surveys for the Hanna Shoal Ecosystem Study. Inset map shows location of study area off the northwest coast of Alaska. Arrows (→) and asterisks (\*) identify stations where sediment cores and water samples, respectively, were collected. Dashed oval outlines general area of Hanna Shoal.

**Figure 2.** Contour maps for Al in surface sediments from (A) the area of Hanna Shoal and (B) the northeastern Chukchi Sea based on data from 2009, 2010, 2012 and 2013. Inset maps show study area off NW coast of Alaska.

**Figure 3.** Contour map for total organic carbon (TOC) in surface sediments from the area of (A) Hanna Shoal and (B) the northeastern Chukchi Sea. Inset maps show study area off NW Alaska.

**Figure 4.** Concentrations of Al versus (A) V and (B) Ni for surface sediments collected during 2012 and 2013 on and around Hanna Shoal. Solid lines and equations show linear regression fit to data from 2009 and 2010 data (COMIDA Project), dashed lines show 99% prediction intervals, *r* is the correlation coefficient and *p* is the statistical *p* value.

**Figure 5.** Contour maps for total Hg in surface sediments from (A) Hanna Shoal and (B) the northeastern Chukchi Sea based on data from 2009, 2010, 2012 and 2013. Inset maps show study area off NW coast of Alaska.

**Figure 6.** Vertical profiles for (A) Ba, (B) Pb, (C) Be, (D) Tl, (E) As, (F) Fe, (G) Mn and (H) total organic carbon (TOC) in sediment from station H27 north of Hanna Shoal along with and their ratios to Al.

**Figure 7.** Vertical profiles for (A) Ba, (B) Pb, (C) Ni, (D) Hg, (E) As, (F) Fe, (G) Mn and (H) total organic carbon (TOC) for station HS3 on Hanna Shoal along with and their ratios to Al.

**Figure 8.** Vertical profiles for As for sediment cores from stations (A) H107, (B) H112, (C) CBL13 and (D) H32 along with and their ratios to Al.

**Figure 9.** Contour maps for total arsenic (As) in surface sediments from (A) Hanna Shoal and (B) the northeastern Chukchi Sea based on data from 2009, 2010, 2012 and 2013. Inset maps show study area off NW coast of Alaska.

**Figure 10.** Vertical profiles for dissolved oxygen (DO), redox potential (Eh) and pH for sediment cores from stations (A) HS3 near Hanna Shoal and (B) H27 to the north of Hanna Shoal in deeper water. Note difference in sediment depth scale for DO (millimeters) relative to Eh and pH (centimeters).

**Figure 11.** Vertical profiles for (A) temperature and salinity, and dissolved (B) As, (C) Sb, (D) Cd, (E) phosphate and (F) Ba for station H21 located west of Hanna Shoal.

**Figure 12.** Vertical profiles for (A) temperature and salinity and dissolved (B) Cd and (C) phosphate for station H2 located west of Hanna Shoal.

**Figure 13.** Concentrations of dissolved Cd versus dissolved phosphate for water samples collected during (A) 2012 and (B) 2013 from the northeastern Chukchi Sea with a focus on the area around Hanna Shoal.

**Figure 14.** Log transformed concentrations of THg in ng/g (d.wt.) versus fish length in cm. 95% prediction interval is from 2010 data.

**Figure 15.** Concentrations of inorganic and monomethyl Hg in biota collected from the northeastern Chukchi Sea during 2012 and 2013.

### **Roger Harvey**

#### **Organic Contaminants in Chukchi Sea Sediments and Biota of the Hanna Shoal Region: H. Rodger Harvey, Karen A. Taylor**

**Figure 1.** Summed concentrations of parent and alkylated polycyclic aromatic hydrocarbons present in surface sediments of the Hanna Shoal study. Circles are scaled to concentrations present in surface (0-1cm) sediments. Detailed information on the distribution of the 31+ individual PAH's seen and their concentrations are available through the Hanna Shoal database.

**Figure 2.** Summed concentrations of normal and odd chain alkane hydrocarbons present in surface sediments of the Hanna Shoal Ecosystem study. Circles are scaled to concentrations present in surface (0-1cm) sediments. Details on the distribution of individual hydrocarbons and concentrations are available through the Hanna Shoal database.

**Figure 3.** The distribution of parent and alkyl substituted polycyclic aromatic hydrocarbons (PAH) seen in the foot muscle of the Northern Neptune whelks and their eggs. For comparison sediment burdens at sites nearest the collection site of each animal are also included (note scale on right for sediments). Tissue normalized concentrations were higher in larger individuals while sediments showed no significant trends among the 4 sites. This suggest that *Neptunea* does appear to bio accumulate organic contaminants in muscle tissue. In contrast, only a small fraction of PAHs are transferred from female whelks to their eggs, with a strong bias towards the accumulation of alkylated structures.

**Carin Ashjian and Robert Campbell**

**Mesozooplankton Abundance and Distribution in Association with Hydrography on Hanna Shoal, NE Chukchi Sea, During August 2012 and 2013:** Carin J. Ashjian, Robert G. Campbell, Philip Alatalo, Celia Gelfman, Stephen Elliott, Heather McEachen

**Figure 1.** Station locations of the Bongo tows for the two years. Station number noted for each. See also Appendix I for station locations.

**Figure 2.** Integrated water column zooplankton biomass as carbon (estimated from displacement volume) for the two years.

**Figure 3.** Integrated water column abundance and composition of genera of calanoid copepods from the 150  $\mu\text{m}$  mesh net zooplankton tows for the two years. (Abbreviations: Pseudocal.= *Pseudocalanus* spp.; C. hyper=*Calanus hyperboreus*; Neocal.=*Neocalanus* spp., Acartia=*Acartia longiremus*; Metridia=*Metridia* spp.; Microcal.=*Microcalanus pygmaeus*)

**Figure 4.** Integrated water column abundance and composition of the three copepod species *Calanus glacialis* (*C. glacialis*), *C. hyperboreus* (*C. hyp.*), and *Neocalanus* spp. (*Neocal.*) from the 150  $\mu\text{m}$  mesh net zooplankton tows for the two years.

**Figure 5.** Integrated water column abundance and composition of the life stages of the copepod *Calanus glacialis* from the 150  $\mu\text{m}$  mesh net zooplankton tows for the two years. AF=adult female, CV=copepodid stage V, CIV=copepodid stage IV, CIII=copepodid stages CI-CIII. Note log scale for abundance.

**Figure 6.** Integrated water column abundance and composition of the life stages of the copepod *Calanus glacialis* from the 150  $\mu\text{m}$  mesh net zooplankton tows for the two years for the Barrow Canyon region only. AF=adult female, CV=copepodid stage V, CIV=copepodid stage IV, CIII=copepodid stages CI-CIII. Note log scale for abundance.

**Figure 7.** Integrated water column abundance and composition of genera of non-calanoid copepods and of non-copepod holoplankton from the 150  $\mu\text{m}$  mesh net zooplankton tows for the two years.

**Figure 8.** Water column integrated abundances of euphausiids. Open circles indicate locations where no euphausiids were captured. On station (57) from 2012 had extremely high abundances of euphausiids and is plotted separately as the black triangle.

**Figure 9.** Integrated water column abundance and composition of meroplankton taxa from the 150  $\mu\text{m}$  mesh net zooplankton tows for the two years. (Abbreviations: Barn Naup = Barnacle nauplii; Barn Cyp= Barnacle cyprids; Poly Larv=Polychaete larvae; Poly trochophores =

Polychaete trochophores; Echinoderm = Echinoderm larvae; Gastropod = Gastropod larvae; Bivalve=Bivalve larvae; Crust Larv = Crustacean Larvae

**Figure 10.** Plots of PC1 vs. PC2 and PC3 for each year, grouped according to similarity using position on the graph. Groups are differentiated by color. Station numbers indicated for some groups. Note, station 53 from 2012 was not included in the analysis because of dramatically different plankton composition.

**Figure 11.** Stations grouped using PCA of integrated abundances of zooplankton taxa. For each year, different colors indicate stations that were grouped together on the basis of their taxonomic composition. Analyses were conducted independently for each year so there is no correspondence in station types between the two years. Upper water column (25.5, 23 m for 2012 and 2013, respectively) velocities measured using the hull-mounted acoustic Doppler current profiler also are shown (gray vectors).

**Figure 12.** Temperature-salinity plots for the different stations grouped using PCA for 2012. Dot colors correspond to the different stations types from Figures 10 and 11. TS properties for station 55 (lower right, cyan) were more consistent with those of station 53 (dark blue, temperatures 8°C and greater).

**Figure 13.** Temperature-salinity plots for the different stations grouped using PCA for 2013. Dot colors correspond to the different stations types from Figures 10 and 11.

**Figure 14.** Proportions of different haplotypes of the mtCOI gene from *C. glacialis* collected at 6 stations in each year. For each location, station number is indicated.

**Figure 15.** Temperature-salinity diagrams for stations where mtCOI genetic analysis was conducted. Numbers refer to stations identified in Figure 13.

### **Physical Control of the Distributions of a Key Arctic Copepod in the Northeast Chukchi**

**Sea:** Stephen M. Elliott, Carin J. Ashjian, Zhixuan Feng, Benjamin Jones, Changsheng Chen, Yu Zhang, Robert G. Campbell

**Figure 1.** Chukchi Sea geographic features and dominant advective pathways (adapted from Brugler et al., 2014).

**Figure 2.** Central nodes of AO-FVCOM in the area of interest. The green box represents Hanna Shoal.

**Figure 3.** Locations over Hanna Shoal sampled using net tows in August of 2012 and 2013.

**Figure 4.** Spatially interpolated depth averaged mean modeled currents for selected months in 2012 and 2013.

**Figure 5.** Integrated water column abundances of *C. glacialis* over Hanna Shoal in 2012 and 2013. Abundances (# individuals m<sup>-2</sup>) are differentiated into seven life stages (Copepodid 1-6, adult males (AM), adult females (AF)).

**Figure 6.** Filtered Probability Distribution of Adult *C. glacialis* on a) 15 December 2012 and b) 15 December 2014 and Hotspots from the Filtered Probability Distribution of Adult *C. glacialis* on c) 15 December 2012 and d) 15 December 2012.

**Figure 7.** Filtered probability distributions of adult *C. glacialis* on 03 March 2012 and 03 March 2013 (left) and of *C. glacialis* egg release locations in 2012 and 2013 (right).

**Figure 8.** Difference between the 2012 and 2013 probability distributions for diapausing copepods from the sink experiments. The probability distributions for 2013 were subtracted from those from 2012 at each location. All values greater than  $5 \times 10^{-5}$  were retained. Positive values indicate sink locations for 2012 but not 2013 while negative values indicate sink locations for 2013 but not for 2012.

**Figure 9.** Difference between the probability distributions on 3 March from the 2012 and 2013 primary source experiments for a) adult females and b) egg release. The result for 2013 was subtracted from the 2012 result and all values greater than  $5 \times 10^{-5}$  were retained.

**Figure 10.** Effect of depth of release – sink experiment. a) The distribution of the 130,000 deepest copepods on 15 December 2012 subtracted from the distribution of the 130,000 shallowest copepods on 15 December 2012. b) The distribution of the 130,000 deepest copepods on 15 December 2013 subtracted from the distribution of the 130,000 shallowest copepods on 15 December 2013.

**Figure 11.** Effect of depth of release –source experiment. The distribution of the 130,000 deepest copepods on 3 March 2012 subtracted from the distribution of the 130,000 shallowest copepods on 3 March 2012 for adult copepods and egg release locations (top). The distribution of the 130,000 deepest copepods on 3 March 2013 subtracted from the distribution of the 130,000 shallowest copepods on 3 March 2013 for adult copepods and egg release locations (bottom).

### **Brenda Konar**

**Interannual Variability of Epibenthic Communities in the Chukchi Sea Alaska:** Kimberly Powell, Brenda Konar, Jaqueline M. Grebmeier

**Figure 1.** Epibenthic stations sampled in 2009, 2010, 2012, and 2013 in the Chukchi Sea, Alaska. The color of the circles represent the number of years that a station was sampled. Square symbols denote stations only sampled in one year, and circles are stations sampled in multiple years. Circled stations are a subset of stations with the maximum spatial overlap for all years based on ArcGIS spatial analysis.

**Size-frequency Distribution, Growth, and Mortality of snow crab (*Chionoecetes opilio*) and Arctic lyre crab (*Hyas Coarctatus*) in the Chukchi Sea from 2009 to 2013:** Jasmin Groß, Brenda Konar, Thomas Brey, Jacqueline M. Grebmeier

**Figure 1.** Map displaying the stations that were used for the analyses of the size frequency distribution of *Chionoecetes opilio* (left) and *Hyas coarctatus* (right) in the years 2009, 2010, 2012 and 2013. Stations allocated to a specific region are encircled with a black line, and the attached symbol indicates the region number.

**Figure 2.** The combined size frequency distribution of *Chionoecetes opilio* females (top) and males (bottom) from 2009 (A), 2010 (B) and 2013 (C). Arrows indicate the mean with the standard deviation in brackets. n = sample size, S = Skewness, K = Kurtosis.

**Figure 3.** The combined size frequency distribution of *Hyas coarctatus* females (top) and males (bottom) from 2009 (A), 2010 (B) and 2012 (C). Arrows indicate the mean with the standard deviation in brackets. n = sample size, S = Skewness, K = Kurtosis.

**Figure 4.** The mean (A, C) and mode (B, D) of the combined SFD data of all stations across years of *Chionoecetes opilio* (A, B) and *Hyas coarctatus* (C, D) males and females separated in regions.




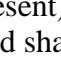
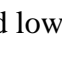
**Figure 5.** Linear growth model shown as a size-at-age graph for males (right) and females (left) of *Chionoecetes opilio* (A, B) and *Hyas coarctatus* (C, D), including the corresponding equation to the fitted linear trendline.

**Figure 6.** The natural logarithm of the frequency of crabs caught in an age group plotted against age for males and females of *Chionoecetes opilio* (top) for the years 2009 (left), 2010 (middle) and 2013 (right) and *Hyas coarctatus* (bottom) for the years 2009 (left), 2010 (middle) and 2012 (right), including the corresponding equation to the fitted linear trendline and the mortality factor (Z).

**Jacqueline Grebmeier and Lee Cooper**

**Sediment Deposition Patterns on the Chukchi Shelf Using Radionuclide Inventories:** Lee W. Cooper and Jacqueline M. Grebmeier

**Figure 1.** Location of the cores studied in the Chukchi and adjacent East Siberian Sea. Red circles were stations sampled in 2009 and black circles were sampled in 2013. Station names are adjacent to the symbols. A few stations (with two station names next to circles) were sampled in

both 2009 and 2012. Sediment profile categories based upon <sup>137</sup>Cs distributions:  Cores collected in productive areas with high benthic bioturbation and high sedimentation;  Cores with sedimentation exceeding bioturbation (<sup>137</sup>Cs maximum present);  Cores where bioturbation influence exceeded sedimentation (no clear <sup>137</sup>Cs maximum present);  cores collected in Hanna Shoal area showed generally low sediment deposition and shallow if any <sup>137</sup>Cs maxima;  high current area cores with shallow if any <sup>137</sup>Cs maxima and lower overall <sup>137</sup>Cs inventories.

**Figure 2.** Maximum depth (in cm) of radiocesium maximum observed in cores collected in 2009 and 2012.

**Figure 3.** Radiocesium activity at the depth where maximum activity was observed. Data are corrected to core collection data in 2009 or 2013.

**Figure 4.** Radiocesium distributions in sediment cores categorized as having more influence from bioturbation than sedimentation and located in areas of high biological activity north of Bering Strait. In general these are cores with no identifiable <sup>137</sup>Cs maxima and even distribution of radiocesium throughout the sediment core.

**Figure 5.** Radiocesium distributions in two cores collected from a biologically active location on the southeast side of Hanna Shoal. As with cores shown in Figure 4, these are cores with no identifiable <sup>137</sup>Cs maxima and even distribution of radiocesium throughout the sediment core.

**Figure 6.** Radiocesium distributions in sediment cores categorized as having more influence from bioturbation than sedimentation. In general these are cores with no identifiable  $^{137}\text{Cs}$  maxima and even distribution of radiocesium throughout the sediment core.

**Figure 7.** Radiocesium distributions in sediment cores categorized as having more influence from sedimentation than bioturbation. In general these are cores with identifiable  $^{137}\text{Cs}$  maxima.

**Figure 8.** Radiocesium distributions in sediment cores collected from Hanna Shoal that show relatively low deposition and shallow maxima.

**Figure 9.** Radiocesium distributions in sediment cores collected from high current regions within Herald Canyon, showing relatively low deposition and shallow maxima.

**Figure 10.** Radiocesium distributions in sediment cores collected north of Wrangel Island and in Long Strait, generally showing relatively low current flow and lower bioturbation than from Herald Canyon (Figure 8).

**Figure 11.** Radiocesium distributions in two sediment cores with low overall deposition south of Wrangel Island and in the northeast Chukchi Sea.

**Figure 12.** Radiocesium distribution in a sediment core collected on the Bering continental slope (400 m water depth) in June 2007 from the USCGC Healy. Station location is  $60.0469^\circ\text{N}$ ,  $179.6632^\circ\text{W}$ .

**Figure 13.** Log of  $^{210}\text{Pb}$  excess regressions relative to sediment depth for 14 cores (of 40) where there was a steady decline in excess  $^{210}\text{Pb}$  (above background or supported), moving down the sediment core. Background or supported  $^{210}\text{Pb}$  provided for each core is based upon activities at the base of the core (number of activities averaged is given as  $n=$ ). Sedimentation estimates from  $^{210}\text{Pb}$  were calculated from the activity co-efficient for  $^{210}\text{Pb}$  ( $-0.1352 \text{ year}^{-1}$ ) divided by slope of the line relating log excess  $^{210}\text{Pb}$  to sediment depth (cm). The yellow checked circles indicate cores where there was good agreement between sedimentation rate estimates provided by both  $^{210}\text{Pb}$  and  $^{137}\text{Cs}$ .

### **Water Column Chemistry, Benthic Macroinfaunal Populations, and Sediment Tracer Measurements:** Jacqueline Grebmeier, Lee Cooper

**Figure 1.** Stations sampled during Healy 1201 (August 2012) and Healy1301 (July-August 2013).

**Figure 2.** Bottom water nutrients (nitrate/nitrite, silica and ammonium for (left) HLY1201 and (right) HLY1301.

**Figure 3. Figure 3.**  $\delta^{18}\text{O}$  for a. surface seawater and b. bottom seawater during HLY1301 in 2013. c. Sea ice fraction present in surface waters during HLY 1201 in 2012. See text for brief description of three end member mixing model that was used.

**Figure 4.** Water column chlorophyll *a*, integrated from sea surface to bottom, during HLY1201, August 2012 (a.) and HLY1301, late July-August 2013 (b). Sediment chlorophyll *a* on surface sediments (0-1 cm) during HLY1201, August 2012 (c.) and HLY1301, late July-August 2013 (d.).



**Figure 5.** Stable carbon isotope ratios observed in the organic fraction of surface sediments during a. HLY1201 and b. HLY1301 (b.) and surface sediment C/N ratios for c. HLY1201 and d. HLY1301.

**Figure 6.** Grain size distributions ( $\geq 5 \phi$ ) in surface sediments for a. HLY1201 and b. HLY1301 and total organic carbon content (%) for c. HLY1201 and d. HLY1301.

**Figure 7.** a. Depth of  $^{137}\text{Cs}$  maximum and b. radioactivity at that depth.

**Figure 8.** a. Distribution of macroinfaunal station biomass (grams wet weight per  $\text{m}^2$  (gww/ $\text{m}^2$ ) in the main study area in the northern Chukchi Sea for HLY1201 and HLY1301 and b. the dominant macrofauna by biomass in relation to total station biomass.

**Figure 9.** Distribution of sediment community oxygen uptake (SCOC;  $\text{mmol O}_2/\text{m}^2/\text{d}$ ) during HLY1201 and HLY1301.

**Figure 10.** Distribution of  $\delta^{13}\text{C}$  in various amino acids for different trophic level components of the NE Chukchi Sea food web (phytoplankton, crustacean, bivalves and polychaetes) at station CBL11.

### Kenneth Dunton

**Arctic shelves as platforms for active biogeochemical activity: nitrogen and carbon transformations in the Chukchi Sea, AK.:** Amber K. Hardison, Nathan D. McTigue, Wayne S. Gardner, Kenneth H. Dunton

**Figure 1.** Sample stations along the Hanna Shoal in the Northeast Chukchi Sea, Alaska. Depth contour lines are 20 m increments.

**Figure 2.** Gas ( $\text{O}_2$ ,  $\text{N}_2$ ) and nutrient ( $\text{NH}_4^+$ ,  $\text{PO}_4^{3-}$ ,  $\text{NO}_3^-$ ,  $\text{NO}_2^-$ ) fluxes at the sediment-water interface measured in control cores. Values are mean (SE) for duplicate cores. In panel A, grey bars correspond to total  $\text{O}_2$  utilization (TOU) from core incubations while circles correspond to diffusive  $\text{O}_2$  utilization (DOU) from microelectrode profiles. Error bars for DOU represent SE for duplicate cores. Letters in italics designate groups from a post-hoc Tukey's test. Means with the same letter are not significantly different. In panel A, letters correspond to TOU values.

**Figure 3.**  $\text{NH}_4^+$  cycling rates at the sediment-water interface measured in  $^{15}\text{NH}_4^+$  treated cores. Values are mean (SE) for replicate sampling days. Letters in italics designate groups from a post-hoc Tukey's test. Means with the same letter are not significantly different. REG = regeneration;  $U_{\text{pot}}$  = potential uptake;  $U_{\text{act}}$  = actual uptake; SAD = sediment  $\text{NH}_4^+$  demand.

**Figure 4.** Relationship between measured  $\text{N}_2$  fluxes and estimated  $\text{N}_2$  fluxes based on station depth and equation developed in Chang and Devol (2009). Rates are  $\text{mmol N m}^{-2} \text{d}^{-1}$ .

**Trophodynamics of the Hanna Shoal Ecosystem (Chukchi Sea, Alaska): connecting multiple end-members to a rich benthic food web:** Nathan D. McTigue, Kenneth H. Dunton

**Figure 1.** Jitterplot projecting the distribution of  $\delta^{13}\text{C}$  and  $\delta^{15}\text{N}$  values for six trophic guilds.

**Figure 2.**  $\delta^{13}\text{C}:\delta^{15}\text{N}$  biplot for all organisms analyzed for stable isotopes. Color and shape denotes trophic guild membership. Solid lines correspond to the standard ellipse for each trophic guild and are color-coded respectively.

**Figure 3.**  $\delta^{13}\text{C}:\delta^{15}\text{N}$  biplot for species in the suspension feeder guild (a), deposit feeder guild (b), and predator/scavenger guild (c). Solid lines correspond to the standard ellipse for each trophic guild and are color-coded, respectively, per plot. Axes represent the same range in each plot.

**Figure 4.1.** Boxplots of the distribution of possible dietary contributions for consumers in the suspension feeder guild (a-c), and deposit feeder guild (d-f.).

**Figure 4.2.** Boxplots of the distribution of possible dietary contributions for consumers in the suspension feeder guild (a-c), deposit feeder guild (d-f), and predator/scavenger guild (g-i). Outliers were omitted for clarity. Contributions are represented as proportions (0-1). The whiskers extend to the 95% credible interval. The three end-members used in the mixing model were ice algae (a, d, g), MPB (b, e, h), and phytoplankton/SOM (c, f, i).

### **Distribution, abundance, biomass and diversity of benthic infauna in the northeastern Chukchi Sea, Alaska:** Susan Schonberg, Ken Dunton

**Figure 1.** Map of COMIDA Hanna Shoal 2012 and 2013 infaunal sampling station locations.

**Figure 2.** Percent abundance (top graph) and percent biomass of major phyla of infauna samples collected in the COMIDA Hanna Shoal project (2012 and 2013 combined).

**Figure 3.** COMIDA CAB (2009, 2010) and COMIDA Hanna Shoal (2012, 2013) infaunal station abundance (top) and biomass (bottom) means ( $\text{m}^{-2}$ ).

**Figure 4.** Percentage of station infaunal abundance that is composed of amphipods (top), polychaetes (middle), and bivalves (bottom).

**Figure 5.** Percentage of station infaunal biomass that is composed of amphipods (top), polychaetes (middle), and bivalves (bottom).

**Figure 6.** COMIDA Hanna Shoal 2012 and 2013 infaunal abundance data. Station means (top), Simpson Diversity Index values (middle) and Pielou's Evenness Index (bottom).

**Figure 7.** COMIDA Hanna Shoal 2012 and 2013 infaunal biomass data. Station means (top), Simpson Diversity Index values (middle) and Pielou's Evenness Index (bottom).

**Figure 8.** A Principal Components Analysis (PCA) plot of environmental data collected at 24 stations located in the Hanna Shoal study area.

### **Data Management for the Hanna Shoal Ecosystem Study:** Tim Whiteaker, David Maidment

**Figure 1.** Distribution of data values by sample medium.

**Figure 2.** Distribution of data values by broad category.

**Figure 3.** Distribution of variables by broad category.

**Figure 4.** BioODM enhancements to the CUAHSI Observations Data Model.

**Figure 5.** Simplified Entity Relationship Diagram for Downloadable Data

**Figure 6.** Example folder structure of project sampling results dataset

## Table Legends

### Tom Weingartner

**Physical Oceanography and Circulation:** Tom Weingartner, Ying-Chih Fang, and Peter Winsor

**Table 1.** 2012-13 Mooring specifics. 2012 deployments were conducted in ice; recoveries were undertaken in open water.

**Table 2.** 2013-14 Mooring specifics. All mooring operations in 2013 and 2014 were conducted in ice-free waters.

### John Trefry

**Trace Metals in Sediments, Water and Biota:** John Trefry, Robert Trocine, Austin Fox

**Table 1.** Summary of sediment and water samples collected for metals.

**Table 2.** Summary of biota samples analyzed for metals.

**Table 3.** Concentrations of metals and total organic carbon (TOC) in surface sediments from COMIDA: Hanna Shoal Project for 2012.

**Table 4.** Concentrations of metals and total organic carbon (TOC) in surface sediments from COMIDA: Hanna Shoal Project for 2013.

**Table 5.** Concentrations of dissolved metals in seawater from the COMIDA: Hanna Shoal Project for 2012 from stations BSR5, H1, H2, H4, H6, H16, H21, H24, H30, H32 and BC5.

**Table 6.** Concentrations of dissolved metals in seawater from the COMIDA: Hanna Shoal Project for 2013 from stations BRS5, HS3, H7, H9, H28, H29, H102, H107, H111, H114, BarC4 and CBL11.

**Table 7.** Concentrations of dissolved trace metals in the Chukchi Sea from this study and for the North Pacific Ocean from Donat and Bruland (1995).

**Table 8.** Concentrations of metals (on a dry weight basis) in zooplankton (150  $\mu\text{m}$  mesh, n = 16) collected during 2012 and 2013 from the northeastern Chukchi Sea.

**Table 9.** Concentrations (on a dry weight basis) of metals in whole clams (*Astarte borealis*, n = 11) collected during 2012 and 2013 from the northeastern Chukchi Sea.

**Table 10.** Concentrations (on a dry weight basis) of whelk muscle (*Neptunea borealis*, n = 12) collected during 2012 and 2013 from the northeastern Chukchi Sea.

**Table 11.** Concentrations (on a dry weight basis) of metals in snow crab muscle (*Chionocetes opilio*, n = 12) collected during 2012 and 2013 from the northeastern Chukchi Sea.

**Table 12.** Concentrations (on a dry weight basis) of metals in arctic cod muscle (*Boreogadus saida*, n = 12) collected during 2012 and 2013 from the northeastern Chukchi Sea.

**Roger Harvey**

**Organic Contaminants in Chukchi Sea Sediments and Biota of the Hanna Shoal Region:** H. Rodger Harvey, Karen A. Taylor

**Table 1.** Target polycyclic aromatic hydrocarbons (PAHs) measured in Hanna Shoal samples, including number of rings and method detection limit values (MDL). PAH's observed in sediments or invertebrates in this project are denoted by (#). For comparison, (\*) is included to denote those PAH's that were detected previously in Chukchi Sea sediments from the COMIDA09/10 campaign.

**Table 2.** Target n-alkanes measured in Hanna Shoal Ecosystem Study samples, including method detection limit values (MDL). Alkanes observed seen in this study are shown by (#). For comparison, (\*) denotes n-alkanes detected in Chukchi sediments seen in the previous COMIDA-CAB 09/10 study.

**Table 3.** A comparison of total PAH and alkane hydrocarbon concentrations observed across multiple years from the COMIDA and Hanna Shoal Research Program cruises.

**Carin Ashjian and Robert Campbell**

**Mesozooplankton Abundance and Distribution in Association with Hydrography on Hanna Shoal, NE Chukchi Sea, During August 2012 and 2013:** Carin J. Ashjian, Robert G. Campbell, Philip Alatalo, Celia Gelfman, Stephen Elliott, Heather McEachen

**Table 1.** Average abundances and ranges ( $\# \text{ m}^{-3}$ ) of selected taxa from studies in the northeastern Chukchi Sea collected during August of each year using 150  $\mu\text{m}$  mesh nets. Data from 1950 and 1951 were collected by Johnson (1956), data from 2002 were collected by Lane et al. (2008), and data from 2012 and 2013 were collected as part of this study. Details of the 1959, 1951, and 2002 data are described in Lane et al. (2008). For 2012 and 2013, only those stations that lay in regions also sampled by the Lane et al. (2008) study were included; these regions were along the northern edge of the Shoal (depth  $> \sim 50 \text{ m}$ ) into the shelf-break and slope and in Barrow Canyon.

**Physical Control of the Distributions of a Key Arctic Copepod in the Northeast Chukchi Sea:** Stephen M. Elliott, Carin J. Ashjian, Zhixuan Feng, Benjamin Jones, Changsheng Chen, Yu Zhang, Robert G. Campbell

**Table 1.** Model experiments conducted. The number of runs of each configuration also is noted.

**Table 2.** Statistics Comparing Sensitivity to Perturbation to Interannual Differences. CoM = Center of Mass.

**Brenda Konar**

**Interannual Variability of Epibenthic Communities in the Chukchi Sea Alaska:** Kimberly Powell, Brenda Konar, Jaqueline M. Grebmeier

**Table 1.** R-values, or the scaled degree of separation between years, based on the analysis of similarity (ANOSIM) test for epibenthic abundance and biomass.

**Table 2.** Top: One-way analysis of variance (ANOVA) of major taxa based on relative abundance and biomass within spatially overlapping stations by year. Asterisks represent statistically significant changes in taxon abundances over time. Bottom: Tukey test p-values for spatially overlapping stations of taxa with statistically significant differences in years: *C. opilio*, *Pagurus* spp., and Caridea

**Table 3.** Mean values for relative abundance and biomass for taxa that varied significantly between 2009, 2010, 2012, and 2013.

**Table 4.** Mean values for the important environmental variables for 2009, 2010, 2012, and 2013.

**Table 5.** One-way analysis of variance (ANOVA) of important environmental variables for abundance and biomass within spatially overlapping stations by year. Asterisks represent statistically significant differences environmental variables over time. Bottom: Tukey test p-values for spatially overlapping stations of Environmental variables with statistically significant differences.

**Size-frequency Distribution, Growth, and Mortality of snow crab (*Chionoecetes opilio*) and Arctic lyre crab (*Hyas Coarctatus*) in the Chukchi Sea from 2009 to 2013:** Jasmin Groß, Brenda Konar, Thomas Brey, Jacqueline M. Grebmeier

**Table 1.** Table displaying the average maximum size (Max) of the highest percentile (10% largest individuals), sample number (n) and standard deviation (SD) for males and females of both sexes.

**Table 2.** Tukey's HSD results comparing the average maximum size of the highest percentile for both species, *Chionoecetes opilio* and *Hyas coarctatus*, among all possible pairs of the factor year, showing the p-values with a significance level of  $\alpha=0.05$  (\* denotes significant results). The dash (-) indicates that values were not calculated.

**Table 3.** PERMANOVA results for both species, *Chionoecetes opilio* and *Hyas coarctatus*, showing the Pseudo-F statistic with corresponding degrees of freedom (df) and p-values with a significance level of  $\alpha=0.05$  (\* denotes significant results).

**Table 4.** Pairwise comparison of the factors that showed a significant result in the PERMANOVA for both species *Chionoecetes opilio* and *Hyas coarctatus*. Displayed are the t-statistic with the corresponding degrees of freedom (df) and the p-values with a significance level of  $\alpha=0.05$  (\* denotes significant results). The dash (-) indicates that values were not calculated.

**Table 5.** DistLM results for *Chionoecetes opilio* showing the variable, the relative contribution to the explained variation (Contrib.), the cumulative contribution of the explained variation (Cum.) and p-values with a significance level of  $\alpha=0.05$  (\* denotes significant results).

**Table 6.** DistLM results for *Hyas coarctatus* showing the variable, the relative contribution to the explained variation (Contrib.), the cumulative contribution of the explained variation (Cum.) and p-values with a significance level of  $\alpha=0.05$  (\* denotes significant results).

**Table 7.** ANCOVA results for the growth model of *Chionoecetes opilio* and *Hyas coarctatus*, with sex as the categorical factor, age as the covariate and size as the dependent variable. Displayed are the test statistic (F-value), the degrees of freedom (df) and the significance value (p-value) at a 0.05 significance level (\* denotes significant results).

**Table 8.** ANCOVA results for the mortality model of both sexes of *Chionoecetes opilio* and *Hyas coarctatus*, with year as the categorical factor, age as the covariate and natural logarithm (ln) of the frequency as the dependent variable. Displayed are the test statistic (F-value), the degrees of freedom (df) and the significance value (p-value) at a 0.05 significance level (\* denotes significant results). The dash (-) indicates that models without the interaction term were more appropriate than the ones with the interaction term.

### Jacqueline Grebmeier and Lee Cooper

#### **Water Column Chemistry, Benthic Macroinfaunal Populations, and Sediment Tracer Measurements:** Jacqueline Grebmeier, Lee Cooper

**Table 1.** Summary of HLY1201 stations (stn) by number (#), name, macroinfaunal abundance (#/m<sup>2</sup>) and wet weight biomass (grams wet weight, gww/ m<sup>2</sup>), number of taxa, and percent of top 3 dominant family types in each station (abundance and biomass).

### Kenneth Dunton

#### **Arctic shelves as platforms for active biogeochemical activity: nitrogen and carbon transformations in the Chukchi Sea, AK.:** Amber K. Hardison, Nathan D. McTigue, Wayne S. Gardner, Kenneth H. Dunton

**Table 1.** Characterization of bottom water and surface sediment. Sediment TOC, TN, and benthic chlorophyll *a* were measured in top 2 cm. CTD and sediment organic content from McTigue et al. 2016; Benthic chl *a* from Dunton (unpublished).

**Table 2.** Gas and nutrient benthic fluxes in control cores. Values are mean (SE). “DNF eff.” = denitrification efficiency

**Table 3.** NH<sub>4</sub><sup>+</sup> recycling rates from <sup>15</sup>NH<sub>4</sub><sup>+</sup> cores. All units are μmol N m<sup>-2</sup> h<sup>-1</sup>. Values are mean (SE).

**Table 4.** Literature comparison of N<sub>2</sub>, O<sub>2</sub>, and nutrient fluxes in the Chukchi Sea.

**Table 5.** Pearson Correlation coefficients (R) between benthic fluxes and environmental parameters. Values in bold are significant at the p<0.05 level.

**Table 6.** Organic carbon remineralization estimates. Carbon mineralization estimate from DOU uses 106C:138O Redfield ratio. Carbon oxidation via denitrification uses 1N:1.25C ratio (Hardison et al., 2015). Percent of export production is based on summer export production = 13.2 +/- 13 mmol C m<sup>-2</sup> d<sup>-1</sup>, Moran et al., 2005.

#### **Trophodynamics of the Hanna Shoal Ecosystem (Chukchi Sea, Alaska): connecting multiple end-members to a rich benthic food web:** Nathan D. McTigue, Kenneth H. Dunton

**Table 1.** Statistics describing the SEAs for the Hanna Shoal food web. Units are %.

**Table 2.** Overlapped area of trophic guild SEAs. Overlap refers to area (%<sup>2</sup>) that g1 overlaps with g2. Area 1 and Area 2 respectively correspond with g1 and g2.

**Table 3.** SEAs for species analyzed by SIBER. SEAc is corrected for sample size. Units are %.

**Table 4.** End-member discrimination correlations reported by the mixing model as its effectiveness to discern differences in end-member contribution for consumers. High negative correlations indicate poor discrimination. For the column labeled Trophic, susp = suspension feeder, depo = deposit feeder, and pred = predator/scavenger. Group indicates position on x-axis in Figure 4.

**Table 5.** Probabilities that Group 1 has a larger SEA than Group 2 from the Bayesian fitting of multiple SEAs (see Methods).

### **Distribution, abundance, biomass and diversity of benthic infauna in the northeastern Chukchi Sea, Alaska:** Susan Schonberg, Ken Dunton

**Table 1.** Environmental data collected during the 2012 and 2013 COMIDA Hanna Shoal project and used for the Principal Component and Biota and Environment Analyses. Bottom water temperature are from the ship's CTD and all other data were processed from samples at The University of Texas. Grain size data are available from J. Grebmeier.

### **Data Management for the Hanna Shoal Ecosystem Study:** Tim Whiteaker, David Maidment

**Table 1.** Examples of the types of data collected in various sample media.

**Table 2.** DataValues - numerical values representing sampling results.

**Table 3.** LabMethods - descriptions of the laboratory methods used to analyze physical samples for specific constituents.

**Table 4.** Methods - the methods used to collect samples and any additional information about the method.

**Table 5.** ShipCourse - the ship course for cruises undertaken during the Hanna Shoal Ecosystem Study. The table is intended to be visualized as a point feature class in a geographic information system, i.e., a set of point locations in a map.

**Table 6.** Sites - the spatial location at which data values have been collected. The table is intended to be visualized as a point feature class in a geographic information system, i.e., a set of point locations in a map.

**Table 7.** Sources - the source organization and contact which originated the data values.

**Table 8.** Taxonomy - the taxonomy information to describe organisms in the study.

**Table 9.** Variables - descriptive information about what variables have been measured.

**Table 10.** Relationships - these relationships define ancillary information about data values.

**Table 11.** Number of updates to CUAHSI controlled vocabularies.

## **Introduction**

### **Hanna Shoal: An Integrative Study of a High Arctic Marine Ecosystem**

**Kenneth H. Dunton**

The University of Texas at Austin Marine Science Institute  
750 Channel View Dr.  
Port Aransas, Texas 78373

[ken.dunton@utexas.edu](mailto:ken.dunton@utexas.edu)

## **1. Background**

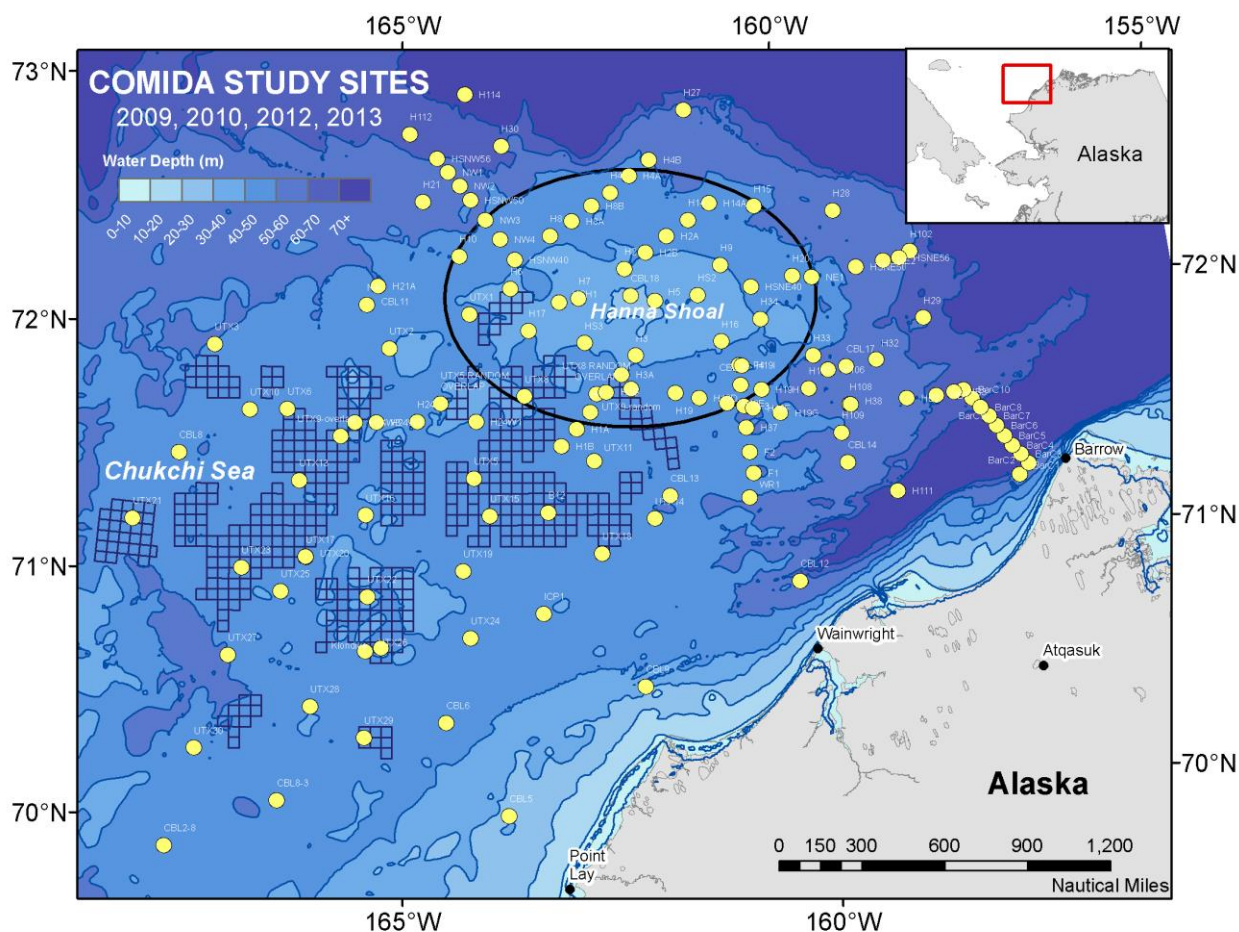
Hanna Shoal is a shallow topographic feature of the northeastern Chukchi Sea that lies about 160 km northwest of Barrow, Alaska at latitude 72° N (Figure 1). Water depths on various parts of the Shoal are as shallow as 20 m, compared to 55 to 60 m on the surrounding seabed. In contrast to the soft muddy sediments characteristic of the Chukchi Shelf, the shallow areas of Hanna Shoal are heavily ice gouged and scoured, resulting in a seabed characterized by unsorted coarse materials, including sand, gravel, small pebbles, and even an occasional boulder. These areas contain a relatively depauperate fauna, in part due to the heavy scouring by ice that effectively removes most long-lived biota. In contrast, the deeper flanks of the Shoal are biologically rich, as reflected in the historically high concentration of walrus there in the summer that actively feed on the abundance of molluscs, crustaceans, polychaete worms, and other benthic fauna. Walrus forage and rest from ice floes trapped on the Shoal that endure long into late summer. But even following ice retreat by late-summer, walrus are known to make the 300-mi round-trip from haul-outs on the northwestern Arctic coast to feed around Hanna Shoal (Jay et al., 2012).

Oceanographers attribute the high productivity of Hanna Shoal, and the northeastern Chukchi Sea shelf in general, to the unique physics that steer highly productive water masses into the region, the relatively shallow average depth (42 m on the northeastern Chukchi Shelf), and weak grazing pressure from low zooplankton abundance during spring. These factors facilitate the deposition of a large proportion of pelagic primary production to the seabed, thus providing a major carbon subsidy to the benthic food web. The result is high diversity and biomass of benthic fauna that coincides with high water column chlorophyll *a* in localized “hotspots” of the Chukchi Sea, first noted nearly three decades ago by Grebmeier et al. (1988). The strong consumptive link between carbon produced in the water column and consumed on the seabed (or pelagic-benthic coupling) has continued to receive strong attention and is now well documented, especially in shallow western arctic shelf ecosystems (Dunton et al., 2005).

### **1.1 Baseline Studies of the Northeastern Chukchi Sea Region**

For decades, arctic oceanographers have been aware of the Hanna Shoal’s unique biological significance and its importance as a feeding ground for marine mammals (Fay, 1982; Jay et al., 2012). In 2008, intensive field studies of the northern Chukchi Sea, including areas bordering Hanna Shoal, were launched following the Chukchi Sea OCS Oil and Gas Lease Sale 193, which produced a record \$2.67 billion in revenue for the federal government. In response to the sale, industry-sponsored biological studies on tracts leased by Shell, ConocoPhillips, and Statoil





**Figure 1.** The location of Hanna Shoal stations occupied in the northeast Chukchi Sea during summers 2009, 2010, 2012 and 2013 for the COMIDA program in relation to oil and gas tracts from Lease Sale 193. Graphic credit: Tim Whiteaker and Susan Schonberg.

began in 2008 under the Chukchi Sea Environmental Studies Program (CSESP; see Hopcroft and Day, 2013).

About the same time, our group conducted spatially extensive biological and chemical benthic surveys on some 107,000 km<sup>2</sup> of seabed on a separate project, the Chukchi Sea Offshore Monitoring in Drilling Area-Chemical and Benthos (COMIDA CAB) study (Dunton et al., 2012; COMIDA CAB web site, 2014 [<http://arcticstudies.org/comidacab/index.html>]; Dunton et al. 2014). This study was followed by a more interdisciplinary and focused field program on Hanna Shoal in 2012 and 2013 (COMIDA Hanna Shoal web site, 2016 [<http://arcticstudies.org/hannashoal/index.html>]). Both the COMIDA CAB and Hanna Shoal studies are initiatives funded by the Bureau of Ocean Energy Management (BOEM), although Shell Exploration and Production complemented these interdisciplinary studies with partial support for ship operations. Our recent work, along with the studies conducted by our CSESP colleagues, has greatly enriched our knowledge of this very productive area in the northern Chukchi Sea that we regard as the Pacific Gateway to the Arctic Ocean.

The COMIDA study provided baseline information on the biological, chemical, and physical characteristics of the northern Chukchi Sea, including a description of its trophic structure and identification of key benthic processes during a period of sea-ice loss and climate change. We found that the sediments of the northern Chukchi Sea are essentially pristine with extremely low concentrations of aliphatic hydrocarbons and polycyclic aromatic hydrocarbons (PAHs); 17 trace metals were present in sediments at natural background levels (Trefry et al., 2014; Harvey et al., 2014). The only exception was confined to two previous (1989) exploratory drill sites, but there was no evidence that bioaccumulation of these substances occurred above natural concentrations. Nutrients were found at low concentrations during late summer, but our ship-board experiments revealed that nutrients are recycled extremely rapidly (~1 day), presumably taken up by phytoplankton that are responsible for the region's high primary productivity.

## **1.2 Links to Earlier Research and Marine Megafauna**

Our biological studies of the northern Chukchi under the COMIDA study confirmed earlier observations that the high primary productivity of the region (as noted by Grebmeier et al., 2006), combined with its relatively shallow depths and favorable circulation regimes, sustains a rich epibenthic and infaunal benthos dominated by polychaete worms, molluscs, crustaceans, and echinoderms (Konar et al., 2014; Schonberg et al., 2014). Benthic food webs are complex, as defined by their trophic redundancy and diversity of both the infauna and epifauna. The high biodiversity and complex trophic relationships are signs of robust benthic communities that likely possess some degree of resiliency to disturbance.

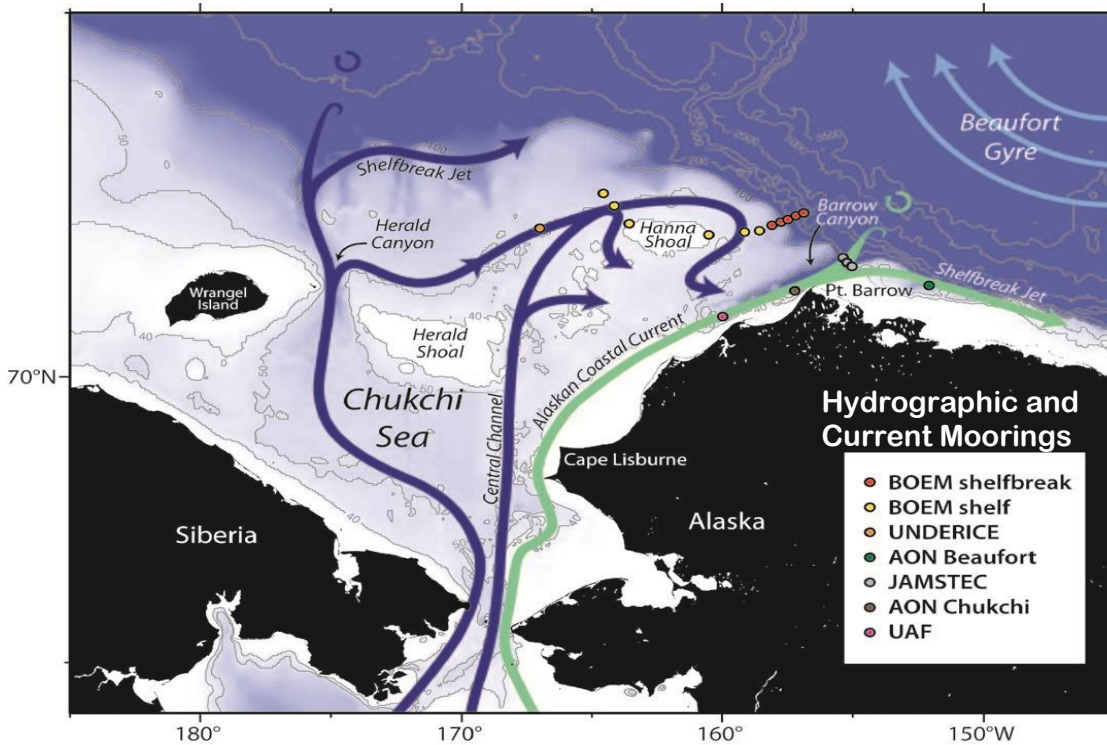
Analysis of benthic infaunal biomass through the COMIDA study area revealed areas of potentially very high biomass on the south and southeastern flanks of Hanna Shoal and provide good agreement with earlier (1970s and 1980s) quantitative benthic studies. Taken together, these observations suggest that the high productivity of the region is a persistent feature of the northern Chukchi Shelf that is in part responsible for its importance as a feeding area for marine mammals.

For example, Schonberg et al. (2014) found that gray whales, which feed on benthic-dwelling amphipods, were almost exclusively concentrated over an area between Wainwright and Point Barrow, a region shown to have great concentrations of amphipods that were first noted in the 1970s. In addition, although the area south of Hanna Shoal is dominated by the favored prey of walrus, including infaunal bivalves and polychaetes, walrus distribution was observed to be closely associated with remnant sea-ice distributions. Walrus concentrated offshore on ice near Hanna Shoal as long as sea-ice was available but moved nearer to shore and to coastal haul-out locations when the ice retreated off the shelf. As noted above, the observed concentration of marine mammals in these areas over decades suggests a temporal stability of available benthic prey items. However, recent decreases in ice extent and persistence during the summer months is likely resulting in a reduction of available time for walrus to forage the rich benthos near Hanna Shoal (Jay et al., 2012).

## **1.3 Water Circulation around Hanna Shoal and Implications for Zooplankton**

The circulation pattern around Hanna Shoal and its corresponding water mass properties have been studied extensively by a number of oceanographers during this project and others over the past couple of years. Thanks to their cooperative and coordinated efforts, a much clearer picture of the complex interplay of bathymetry, water mass contributions, and formation of dense winter

water is emerging as outlined recently by Weingartner et al. (2013). Circulation patterns (see Figure 2 and Brugler, 2014) show a general clockwise flow around the north and east sides of the Shoal as well as on the west flank based on moorings deployed from both the USCGC *Healy* in 2012 (retrieved in September 2014) and other mooring deployments and CTD (conductivity, temperature, depth) data. However, the generation of both very cold and salty waters during winter sea ice formation, as well as and fresher ice meltwaters in summer complicate this overall pattern. In addition, eddies form with the infiltration of northward-flowing, nutrient-rich Bering Sea water.



**Figure 2.** A synopsis of major water circulation patterns in the northern Chukchi Sea. Nutrient-rich Bering Sea water flows north through the Central Channel before turning east along the Chukchi Sea shelf break and circumventing Hanna Shoal and exiting through Barrow Canyon to the Beaufort Sea. The location of hydrographic and current moorings deployed around Hanna Shoal Ecosystem are denoted by yellow circles. Graphic credit: Robert Pickart. Adapted from Brugler et al., 2014 (with permission).

The currents and water mass movements around Hanna Shoal have profound impacts on water column chlorophyll *a* biomass and zooplankton distribution, abundance, and composition in shelf waters (see Ashjian et al., 2005 and Grebmeier et al., 2006). High chlorophyll *a* levels were noted on the western, northern, and eastern sections of Hanna Shoal over the period of our study, which is consistent with more nutrient-rich Bering Sea water flowing clockwise around the flanks of Hanna Shoal. Integrated water column chlorophyll *a* levels approached  $200 \text{ mg m}^{-2}$ , among the higher values recorded in the northeastern Chukchi (Grebmeier et al., 2006).

In both field years of our study, Bongo net tows produced the greatest biomass of zooplankton along the edges of the Shoal, particularly on the northwest quadrant, which is dominated by Bering Sea Water, compared to on the eastern side, which is dominated by less-productive

Alaskan Coastal Water (see Figure 2). We found the copepod *Calanus glacialis/marshallae* ubiquitous across Hanna Shoal, which is a key species for the planktivorous bowhead whale. Analysis of data is continuing, with particular emphasis on the large bodied copepod *Calanus hyperboreus* and euphausiids (krill).

#### **1.4 Sediment Chemistry**

Sediment samples were collected using a variety of equipment (grabs, box corers, gravity cores, etc.) from the *Healy*. Analyses revealed that total organic carbon was highest in fine-grained sediments from stations on the flanks of the Shoal and that, interestingly, up to 35% of the organic matter is from terrigenous sources, likely from coastal erosion and inputs from arctic rivers (e.g., the Yukon). No Hanna Shoal stations exhibited trace metal contamination, and evidence from gravity cores, which record decades to centuries of deposition, indicate there has been no detectable anthropogenic contributions. Similarly, concentrations of a suite of 52 targeted PAHs were very low and were present at background levels in surface sediments surrounding Hanna Shoal with few exceptions. As part of a separate study, chemical analysis of muscle tissues in the whelk *Neptunea* revealed that this omnivorous species is a valuable indicator of anthropogenic inputs because, as a long-lived resident of the benthic community, ingestion of sediments leads to long-term accumulation of trace metals (e.g., mercury) and PAHs. Sedimentation studies using natural and bomb fallout radionuclides indicate little deposition on Hanna Shoal, with higher sedimentation rates on the periphery of the Shoal, where there is considerable bioturbation by benthic animals.

#### **1.5 Benthic Biology**

As mentioned above, a shallow shelf and weak grazing pressure allows a large proportion of pelagic production to reach the shallow benthos, providing a major carbon subsidy to the benthic food web of the Chukchi. Consequently, it has been hypothesized that Arctic shelf sediments can act as repositories for the various pelagic microalgae that sink to the bottom, essentially creating “food banks” (Pirtle-Levy et al., 2009) for benthic grazers. These areas of seabed can be identified by the high chlorophyll *a* concentrations in the sediments that have been deposited since ice retreat that include contributions from both phytoplankton and ice algae (Cooper et al., 2009).

To assess the importance of such chlorophyll *a*-rich sediment “food banks,” our team performed hundreds of extractions on benthic grab samples. Using both fluorescence and high-performance liquid chromatography (HPLC), we found chlorophyll *a* concentrations among the highest ever reported in marine sediments (up to 665 mg m<sup>-2</sup>). Levels varied depending on the overlying water mass type (rich offshore Bering Sea-Anadyr water compared to Alaskan coastal water), again revealing the link between productivity and the physical dynamics of the system.

Our HPLC measurements revealed an abundance of fucoxanthin, which confirmed that most of the chlorophyll *a* was derived from diatoms, which are highly prevalent in melting sea ice. Yet even more interesting were the concentrations of chlorophyll *a* degradation products (pheopigments) in the sediments. McTigue et al. (2015) found an abundance of various pheopigments that indicate active consumption of chlorophyll *a* by benthic fauna. In addition, despite the active assimilation of sediment chlorophyll *a* by scavenging fauna and natural degradation, the ratio of chlorophyll *a* to total pheopigments was generally >1, suggesting that viable cells in the sediments may be continuing to produce under low light levels. These

observations further corroborate stable isotopic measurements that “food banks” of chlorophyll *a* and other deposited organic matter provide a critical source of carbon to a rich and diverse benthic food web that includes representatives from virtually every major invertebrate taxonomic group, including those actively consumed by fish, diving birds, and marine mammals.

### The Epibenthic and Infaunal Community

Congruent with the benthos functioning as a “food bank” for the benthic consumers, estimates of epibenthic and infaunal organisms around Hanna Shoal, collected using plumb staff beam trawls and van Veen grabs, are enormous. Epibenthic assemblages range to 500 g m<sup>-2</sup> (and thousands of individuals m<sup>-2</sup>); infaunal biomass and abundances approach 820 g m<sup>-2</sup> and 5,500 individuals m<sup>-2</sup>, respectively. In both sampling years, the greatest biomass was not on the Shoal itself, but on its northwest and southeast flanks (or both), which receive Bering Sea water that originates in the North Pacific (see Figure 2). Brittle stars and shrimp dominated the epibenthos of the study area, although many other invertebrates are often very common at particular locations (e.g., the gastropod *Neptunea*, hermit crabs, snow crabs, and sea cucumbers). Extensive statistical analysis of the observed patterns in species biomass, abundance, and distribution are ongoing, but depth, temperature, and sediment grain size appear to be among the most important environmental drivers of benthic community structure.

Bivalves, sipunculids, and polychaete worms generally dominate the infaunal assemblages. Some of our more recent analyses reveal that for bivalves, areas of highest abundance, biomass, and caloric value are centered on the southeast side of Hanna Shoal, which corresponds to feeding areas for Pacific walrus, based on satellite telemetry (Jay et al, 2012). In addition, taxonomic specialists have found a plethora of undescribed polychaete species in our samples. Some of these worm species are simply mis-identified, but many others are new species to science.

## 2. Summary

The location of Hanna Shoal on the northern shelf edge of the Chukchi Sea is associated with physical oceanographic conditions that have led to the development of rich biological assemblages on the flanks of the Shoal. The bifurcation of nutrient-rich Bering Sea waters around Hanna Shoal, the formation of ice melt waters and cold salty winter waters, and the entrapment of summer ice on the ice on the Shoal all contribute to a highly dynamic and changing hydrography. In particular, the relatively slow retreat of sea ice from Hanna Shoal in summer makes it a productive feeding ground for the large numbers of walrus that use the ice as a platform to access the abundant populations of bivalves, crustaceans, and polychaete worms on the seabed. The Hanna Shoal region will continue to draw attention as long as the area holds promise for significant oil and gas reserves and polar amplification of a warming climate continues to produce biological changes in response to decreases in ice extent and duration.

## 3. Acknowledgements

The Hanna Shoal Ecosystem Study was funded by the U.S. Department of Interior, Bureau of Ocean Energy and Management (BOEM), Alaska Outer Continental Shelf Region, Anchorage, Alaska under BOEM Cooperative Agreement No. M11AC00007. I am deeply appreciative to Heather Crowley of BOEM for her participation on the research cruises, unqualified support of our research, and active role in project planning. Funds for partial support of ship operations

were provided by Shell Exploration and Production through the dedicated efforts of Michael Macrander to enhance our scientific knowledge of this productive system.

I thank the crew and commanding officers of the USCGC Healy for their support of our oceanographic operations and Jackie Grebmeier and Lee Cooper for serving as chief scientists on both Hanna Shoal cruises. I am very grateful to an extremely talented group of students, technicians, and research scientists who were instrumental in the success and productivity of this program. To my life-long sea mates, who composed the Hanna Shoal Ecosystem PI team, my sincere thanks for contributing immensely to our understanding of the northern Chukchi Sea. They include Carin Ashjian (Woods Hole Oceanographic Institution); Bob Campbell (University of Rhode Island); Lee Cooper and Jackie Grebmeier (University of Maryland Center for Environmental Science); Rodger Harvey (Old Dominion); Brenda Konar (University of Alaska Fairbanks), Susan Schonberg (University of Texas at Austin), John Trefry (Florida Institute of Technology), and Tom Weingartner (University of Alaska Fairbanks). I am also very appreciative to co-PIs David Maidment and Tim Whiteaker (University of Texas at Austin) for data management, creation and maintenance of a dedicated web site and providing all of us with desperately needed assistance with graphics in ArcGIS. Finally, a heartfelt thanks goes to The University of Texas at Austin Project Manager Susan V. Schonberg who handled the task of extracting final reports from 10 very busy PI's (p.iii), and formatting 13 reports into a cohesive final report, while also contributing her own section on the infaunal assemblages.

#### 4. References

- Ashjian C.J., Gallager, S.M., Plourde, S., 2005. Transport of plankton and particles between the Chukchi and Beaufort Seas during summer 2002, described using a Video Plankton Recorder. *Deep-Sea Res. II* 52, 3259-3280.
- Brugler, E.T., Pickart, R.S., Moore, G.W.K., Roberts, Weingartner, T.J., Statscewich, H., 2014. Seasonal to interannual variability of the Pacific Water boundary current in the Beaufort Sea. *Progr. Oceanogr.* 127, 1-20, [dx.doi.org/10.1016/j.pocean.2014.05.002](https://doi.org/10.1016/j.pocean.2014.05.002).
- COMIDA CAB web site, 2014. <http://arcticstudies.org/comidacab/index.html>
- COMIDA Hanna Shoal web site, 2016. <http://arcticstudies.org/hannashoal/index.html>
- Cooper L.W., Lalande, C., Pirtle-Levy, R., Larsen, I.L., Grebmeier, J.M., 2009. Seasonal and decadal shifts in particulate organic matter processing and sedimentation in the Bering Strait Shelf region. *Deep-Sea Res. II* 56, 1316-1325.
- Dunton, K.H., Cooper, L.W., Grebmeier, J.M., Harvey, H.R., Konar, B., Maidment, D., Schonberg, S.V., Trefry, J., 2012. Chukchi Sea Offshore Monitoring in Drilling Area (COMIDA): Chemical and Benthos (CAB). Final Report prepared for Bureau of Ocean Energy Management, Anchorage, AK, by University of Texas Marine Science Institute, Port Aransas, TX. 26 pp.+appendices.
- Dunton, K.H., Goodall, J.L., Schonberg, S.V., Grebmeier, J.M., Maidment, D.R., 2005. Multi-decadal synthesis of benthic-pelagic coupling in the western Arctic: Role of cross-shelf advective processes. *Deep-Sea Res. II* 52, 3462-3477.

- Dunton, K.H., Grebmeier, J.M., Trefry J.H., 2014. The benthic ecosystem of the northeastern Chukchi Sea: An overview of its unique biogeochemical and biological characteristics. *Deep-Sea Res. II* 102, 1-8.
- Fay, F.H. 1982. Ecology and biology of the Pacific walrus, *Odobenus rosmarus divergens*. *N. American Fauna* 74, 1-279.
- Grebmeier, J.M., McRoy, C.P., Feder H.M., 1988. Pelagic-benthic coupling on the shelf of the Northern Bering and Chukchi Seas .I. Food-supply source and benthic biomass. *Mar. Ecol. Progr. Ser.* 48, 57-67.
- Grebmeier, J.M., Cooper, L.W., Feder, H.M., Sirenko, B.I., 2006. Ecosystem dynamics of the Pacific-influenced northern Bering and Chukchi Seas in the Amerasian Arctic. *Progr.Oceanogr.* 71, 331-361.
- Harvey, H.R., Taylor, K.A., Pie, H.V., Mitchelmore, C.L., 2014. Polycyclic aromatic and aliphatic hydrocarbons in Chukchi Sea biota and sediments and their toxicological response in the Arctic cod, *Boreogadus saida*. *Deep-Sea Res. II* 102:32-55.
- Jay, C.V., Fischbach, A.S., Kochnev A.A., 2012. Walrus areas of use in the Chukchi Sea during sparse sea ice cover. *Mar. Ecol. Progr. Ser.* 468, 1-13.
- Konar B., Ravelo, A., Cooper, L., Grebmeier, J., Trefry, J., 2014. Size frequency distributions of key epibenthic organisms in the eastern Chukchi Sea and their correlations with environmental parameters. *Deep-Sea Res. II* 102, 107-118.
- McTigue, N.D., Bucolo, P, Liu, Z., Dunton K.H., 2015. Pelagic-benthic coupling, food webs, and organic matter degradation in the Chukchi Sea: Insights from sedimentary pigments and stable carbon isotopes. *Limnol. Oceanogr.* 60, 429-445.
- Pirtle-Levy, R., Grebmeier, J.M., Cooper, L.W., Larsen, I.L., 2009. Chlorophyll a in Arctic sediments implies long persistence of algal pigments. *Deep-Sea Research Part II-Topical Studies in Oceanography* 56, 1326-1338.
- Schonberg, S.V., Clarke J.T., Dunton, K.H., 2014. Distribution, abundance, biomass and diversity of benthic infauna in the northeast Chukchi Sea, Alaska: relation to environmental variables and marine mammals. *Deep-Sea Res. II* 102, 144-163.
- Trefry, J.H., Trocine, R.P., Cooper, L.W., Dunton, K.H., 2014. Trace metals and organic carbon in sediments of the northeastern Chukchi Sea. *Deep-Sea Res. II* 102, 18-31.

# Physical Oceanography and Circulation

**Tom Weingartner, Ying-Chih Fang, Peter Winsor**

University of Alaska Fairbanks  
Institute of Marine Science 115 O'Neill  
Fairbanks, AK 99775  
[tjweingartner@alaska.edu](mailto:tjweingartner@alaska.edu)

## Abstract

We examined the time-varying circulation and water mass properties of the Chukchi Sea shelf surrounding Hanna Shoal using shipboard surveys and oceanographic moorings funded through the BOEM COMIDA program. The COMIDA data were complimented by other data sets whose collection was supported by Shell, ConocoPhillips, Statoil, the North Slope Borough, and other BOEM-supported projects in the region. We found that the sea ice and associated surface meltwaters are transported westward on average in response to the prevailing northeasterly winds. The vertically-averaged flow was eastward and parallel to the isobaths northwest of Hanna Shoal, in agreement with many circulation models but this flow component was negligible or slightly westward northeast of Hanna Shoal, in contrast to these same models. These observations imply that there should be, on average, zonal convergence in the flow north of Hanna Shoal. Presumably this convergence is associated with an off-shelf deflection of the eastward-flowing water observed to the northwest of Hanna Shoal. The near-bottom circulation flows clockwise around the northwest and northeast sides of Hanna Shoal on average, and this finding agrees with the numerical models. The circulation differences between the model and observations on the northeast side of Hanna Shoal are due to baroclinic pressure gradients. These oppose the barotropic forcing and tend to drive a counterclockwise flow, around the Shoal. This inference is consistent with the mean vertical velocity shear from the moorings and the fall hydrographic data. We also found that the water column on the shelf to the east of Hanna Shoal remains strongly stratified year-round with this stratification maintained by cold, dilute meltwater in the upper 15 – 20 m and near-freezing, salty winter water on the bottom. This winter water is advected into the region by the bottom flow. Its source is elsewhere on the Bering or Chukchi Sea shelves. It is transported into the area east of Hanna Shoal after being carried northward through the Central Channel and then around Hanna Shoal and or northward through Herald Valley and then eastward across the outer shelf. Some winter water may form locally over Hanna Shoal, especially in years when grounded ice atop the Shoal results in the formation of latent heat polynyas. Our results also imply that waters on the shelf east of Hanna Shoal are renewed much more slowly than elsewhere in the Chukchi Sea.

In summer and fall meltwater and winter water were the major water masses in the COMIDA study area. Bering Sea summer waters (Alaskan Coastal Water and Bering Sea Water) were often found south of  $\sim 71.5^\circ\text{N}$ . The boundary separating the water masses to the north from those to the south consists, in most years, of a strong, surface front between the meltwater and the Bering waters and, perennially, by a sub-surface front between the winter and Bering water masses. The subsurface front is not necessarily contiguous with the surface front. The subsurface front appears to extend zonally from the southwest side of Hanna Shoal eastward to the head of Barrow Canyon. Very likely this front extends northward and parallel to the eastern side of the Central Channel along the west side of Hanna Shoal. The latter inference is consistent with



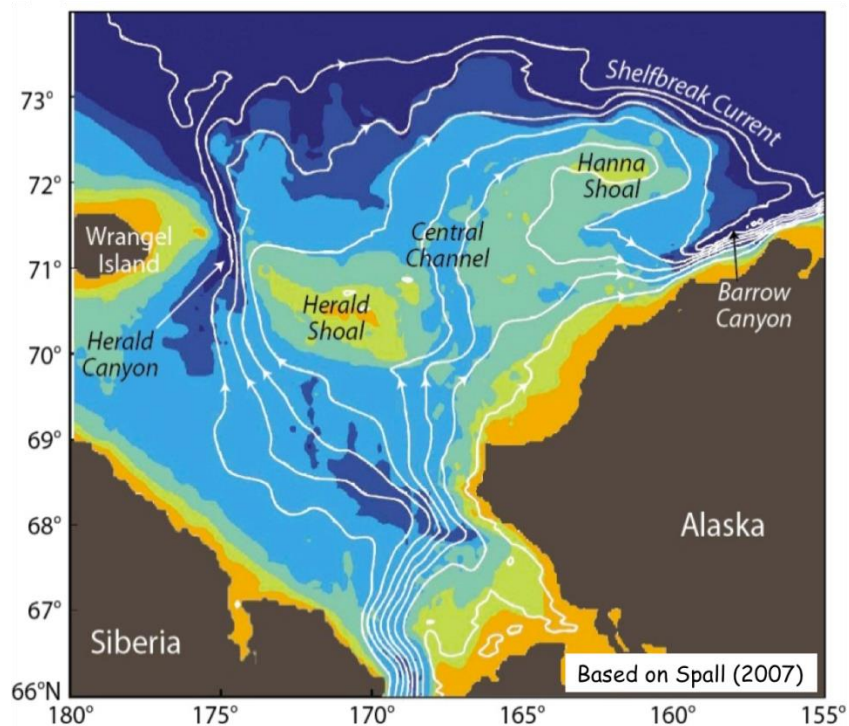
summer sea ice concentration maps, which effectively delineate the northward path of the Bering Sea Water in the Channel, COMIDA CTD sections collected along the northwest side of Hanna Shoal in August 2012 and 2013, which captured waters clearly influenced by BSW, and the September 2013 acrobat section that detected intrapycnocline eddies along the HSNW mooring line. The meltwater/Bering summer water fronts are baroclinically unstable, a process which leads to the formation of intrapycnocline, anticyclonic eddies that propagate across the front carrying Bering summer waters. The existence of these fronts (and the associated frontal processes) and the strength and depth of the pycnocline in the COMIDA sampling area depends upon the vertical and horizontal distributions of meltwater, winter water, and Bering Sea summer waters. In contrast to 2012 and 2013, there was no evidence of surface fronts in 2011 and the shelf stratification in that year was much weaker. These differences were attributed to the dearth of meltwater on the northeastern Chukchi shelf in 2011 compared to the other years.

The sub-surface front is likely a perennial feature of the shelf and it appears to be an effective barrier that prevents waters from south of Hanna Shoal from moving onto the shelf to the east of the Shoal. Consequently, north of the front, the shelf has an arctic-flavor insofar as it is heavily stratified due to surface meltwater and very dense winter waters over the bottom. The circulation also changes on either side of the front. South of the front the summer waters are carried northward over the shelf from Bering Strait and then into Barrow Canyon. Here the shelf circulation is engaged in the meridional transfer of Pacific Ocean waters into the Arctic Ocean. North of the front the exchange appears to be primarily zonal. Meltwater and sea ice are advected westward and dense bottom waters are transported eastward.

## **1. Introduction**

There were two main goals of the COMIDA physical oceanography component. The first was to understand the time-varying circulation and water mass properties of the Chukchi shelf around Hanna Shoal. The second, and closely linked, goal was to provide the physical oceanographic context for the biological and chemical components of COMIDA. Numerical models (e.g., Winsor and Chapman, 2004; Spall, 2007) indicate that the mean circulation around Hanna Shoal includes a clockwise flow around the north and east sides of the Shoal (Figure 1). Until this study, however, there were no systematic observations available upon which to evaluate these model results. Thus an essential aspect of this study was to compare these model predictions with the observations. This report summarizes some of the results from the 2012 - 14 field programs.

The Hanna Shoal portion of the Chukchi Sea shelf is, as suggested by the models (Figure 1), intimately connected to the broader Chukchi Sea circulation field, including Bering Strait. From Figure 1, these connections include flow moving eastward across the outer shelf and shelfbreak which derives from Herald Canyon (or Valley). According to the model, the northward flow through the Central Channel rounds the western side of Hanna Shoal and joins the flow moving eastward from the Herald Valley. Some of this merged flow feeds the eastward-flowing shelfbreak current that continues into the Beaufort Sea (e.g. Pickart, 2004; Nikolopoulos et al., 2005) and some continues southward and back onto the northeastern Chukchi shelf east of Hanna Shoal. Eventually this component of the flow exits the shelf via Barrow Canyon. According to the model the mean flow on the shelf east of Hanna Shoal is very sluggish because the streamlines are far apart here) in comparison to the much swifter flow on the northwest side of Hanna Shoal (and Barrow Canyon and the Central Channel for that matter).



**Figure 1.** The mean, vertically-integrated flow over the Chukchi Sea shelf based on the model study of Spall (2007). Note the clockwise circulation around the northern and eastern sides of Hanna Shoal.

In addition one of the streamlines wraps nearly around the south side of Hanna Shoal before reflecting eastward. This implies that fluid is being carried from the north side of Hanna Shoal to the south side. In contrast, the streamlines farther south indicate a mean eastward flow that transports water across the central shelf from the Central Channel and the southern Chukchi Sea toward Barrow Canyon. The Hanna Shoal circulation affects regional ecosystem processes; including distribution of biogeochemical properties and benthic and planktonic organisms. Indeed, as will be evident, the circulation greatly affects the hydrographic properties around Hanna Shoal in the summer months, at the very least, when COMIDA sampling took place.

The physical oceanographic measurements supported by COMIDA included oceanographic moorings, shipboard CTDs and Vessel-Mounted ADCPs (VM-ADCP). There were, however, many additional data sets derived from other projects, including those supported by BOEM, the oil industry (primarily through the Chukchi Sea Environmental Studies Program; CSESP), the North Slope Borough-Shell Baseline Studies Program, and the Alaska Ocean Observing system. These data sets include additional oceanographic moorings and high-frequency radar (HFR) deployed along the Chukchi Sea coast (Weingartner et al., 2013a), satellite-tracked drifters (Weingartner et al., 2015), and shipboard CTD data sets (Weingartner et al., 2012, 2013b, 2014). Many of these data sets are still being analyzed and some have only recently become available. The expanded data sets allow us to extend the COMIDA results in time and space. The COMIDA data sets complement these other programs insofar as many of the COMIDA measurements were made in previously un- or undersampled regions of the Chukchi Sea shelf. In aggregate, these various data sets will allow a comprehensive synthesis of the physical

oceanography of the northeastern Chukchi Sea shelf. Although we include elements of these data sets herein, this synthesis will be part of the BOEM-supported NE Chukchi Circulation Study.

## 2. Methods

### 2.1 COMIDA Moorings

The COMIDA mooring component included 6 current meter moorings. These were initially deployed in August 2012 from the *USCG Healy*. They were then recovered and re-deployed in September 2013 from the *Norseman II* under the direction of Chief Scientist, Peter Winsor (UAF). The same vessel and Chief Scientist conducted the recoveries in September 2014. The moorings were targeted for deployment on the 40, 50, and 60 m isobaths to the northwest and northeast of Hanna Shoal. By choosing the same isobaths on either side of Hanna Shoal we could test for continuity of mass transport under the assumption that the mean flow is primarily geostrophic, as predicted by the models. In practice we deployed the deepest moorings on the 56 m isobath in 2012 and 2013 because heavy ice impeded *Healy* from reaching the deeper depths on the northwest side of Hanna Shoal in a timely manner. The mooring nomenclature is a combination of Hanna Shoal (HS) and the direction from the Shoal (northwest or northeast), the isobath depth, and the deployment year. For example, HSNW60-12 is the mooring deployed on the 56 m isobath northwest of Hanna Shoal in 2012.

The mooring positions and deployment times are listed in Tables I and II for the respective years. In both years each mooring had an ADCP and a MicroCat temperature/conductivity/pressure (T/C/P) recorder mounted about 3 m above bottom (Figure 2). Moorings HSNE50-12 and HSNE60-12 included an ISCAT at ~25 and 30 m depth, respectively. The ISCAT is a T/C/P sensor that records data internally and onto a data logger mounted to the mooring float 3 m above bottom. The ISCAT includes a weak link mechanism that allows it to detach from the mooring should a deep ice keel snare the ISCAT and begin dragging the mooring. The ISCAT and MicroCat pairs on these moorings were designed to measure changes in water column stratification.

Similarly configured moorings were deployed in 2013 using fresh equipment. Unfortunately the two ISCATs scheduled for re-deployment in 2013 were not functioning correctly and consequently were not deployed. Overall the data quality was very good, however, the ADCP on mooring HSNW60-12 failed about 1 month after deployment. Furthermore, this mooring could not be recovered in 2014 following its second deployment. The acoustic release did not respond to shipboard interrogations and a tight ship schedule and poor weather precluded undertaking extensive search and dragging operations for this mooring. It is quite possible that HSNW60-12 is still in position and that it can be recovered by a future dragging operation. Figure 3 shows a high-resolution map of the 2012-14 COMIDA mooring locations and Figure 4 shows the time lines of available data from each COMIDA mooring.

Figure 5 shows the locations of the COMIDA moorings in 2012 and 2013 along with the other moorings for which we have acquired data over the years from 2008-2009 through 2014-2015. Most of these moorings were sponsored by the oil industry. UAF recently obtained these data sets and will combine them with the Hanna Shoal moorings. There were also a comprehensive



**Figure 2.** A photograph of the assembled COMIDA ADCP and MicroCat TCP mooring. The ADCP electronics are housed in the center well on the syntactic foam float. The MicroCat sits in a separate well with only the sensors exposed.

set of moorings in Barrow Canyon (indicated by the prefix BC), which were jointly funded by industry and BOEM (2010-2012), then by BOEM (2012-2014), and finally by UAF (2014-2015). Under separate BOEM funding, Dr. Robert Pickart deployed an array of 6 moorings (CS1 – CS5; FM1) that extended across the shelfbreak and slope from the end of the COMIDA HSNE line. These moorings were deployed from the USCG *Healy* in October 2013 and recovered in fall 2014.

Of particular relevance to the COMIDA array is the 2011-2012 industry array, which included a set of three moorings to the NW of Hanna Shoal (HS01 – HS03). Data from these moorings will be valuable in comparing with the COMIDA array because, as we will show, the ice and water properties in late summer and fall of 2011 were quite different than in 2012-14. In addition the three industry moorings (HS04 – 06) on the southeast side of Hanna Shoal will be used to assess flow in here. Finally we note that the moorings in Central Channel (Crackerjack), Site 1 (or CPAI01) in Klondike, and Burger and Statoil all provide records that will be useful in addressing circulation around Hanna Shoal and interannual variations in the circulation over this shelf.

**Table 1.** 2012-2013 Mooring specifics. 2012 deployments were conducted in ice; recoveries were undertaken in open water.

Mooring	Deployment date 2012	Latitude (° ' N)	Longitude (° ' W)	Depth* (m)	Instruments
<sup>2</sup> HSNW56-12	August 16	72 41.745	164 31.935	56.2	ADCP/uCat
<sup>1,2</sup> HSNW50-12	August 16	72 31.517	164 5.944	50.3	ADCP/uCat
<sup>2</sup> HSNW40-12	August 16	72 16.85	163 32.034	40.7	ADCP/uCat
<sup>3</sup> HSNE40-12	August 21	72 07.267	160 29.735	40.4	ADCP/uCat
<sup>4</sup> HSNE50-12	August 21	72 09.749	159 07.346	49.7	ADCP/uCat/IC <sup>6</sup>
<sup>4</sup> HSNE56-12	August 21	72 10.88	158 33.092	56.2	ADCP/uCat/IC <sup>6</sup>

<sup>1</sup>Mooring was to include ISCAT (IC), but this was snagged on ice and broke from mooring during deployment. ISCAT was recovered and was used on NE moorings.

<sup>2</sup>Moorings were deployed in rotting broken ice, with local concentrations of ~40 – 60%.

<sup>3</sup>Mooring was deployed in rotting broken ice, with regional concentrations of ~70%.

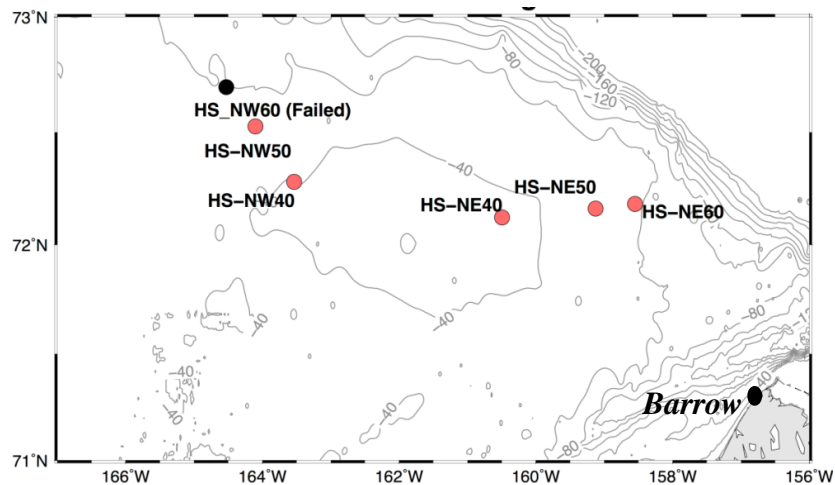
<sup>4</sup>Moorings were deployed in rotting broken ice, with regional concentrations of ~50%.

<sup>6</sup>HSNE50 ISCAT was at 24.9 m below surface, or 24.8 meters above bottom (mab)

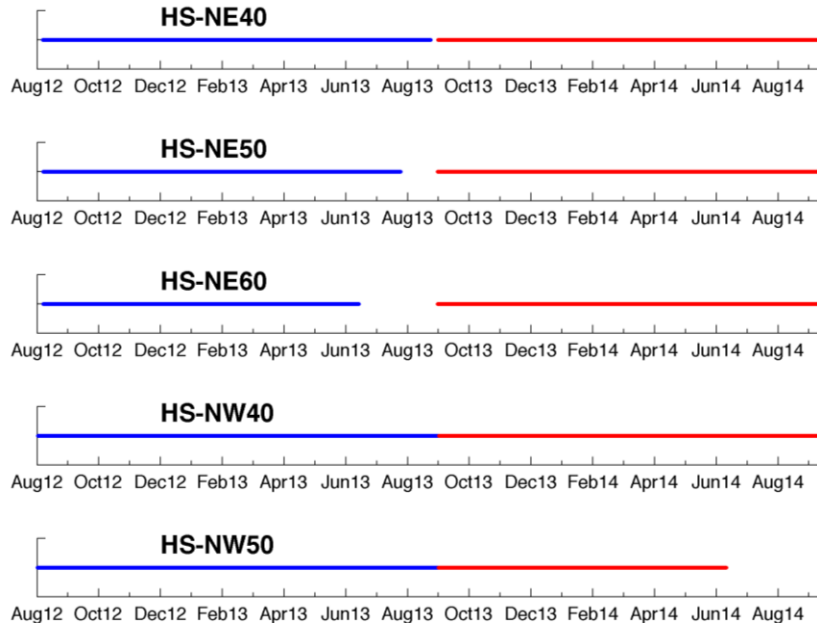
<sup>6</sup>HSNE56 ISCAT was at 29.5 m below surface, or 26.7 meters above bottom (mab)

**Table 2.** 2013-2014 Mooring specifics. All mooring operations in 2013 and 2014 were conducted in ice-free waters.

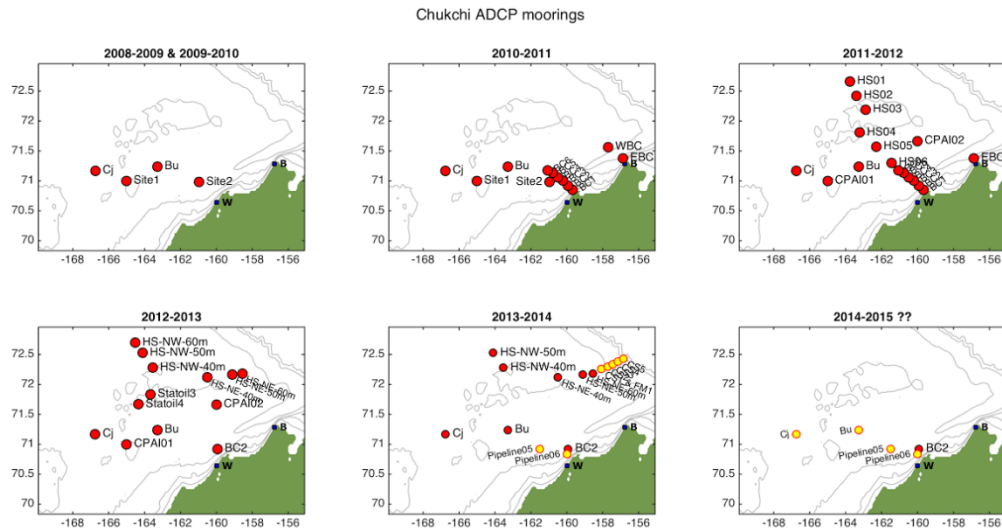
Mooring Name	Deployment Date 2013	Latitude (° ' N)	Longitude (° ' W)	Depth (m)	Instruments
HSNE-40-13	September 8	72°07.257'	160°29.540'	41	ADCP/uCat
HSNE-50-13	September 8	72°09.768'	159°07.297'	50	ADCP/uCat
HSNE60-13	September 8	72°10.892'	158°33.069'	57	ADCP/uCat
HSNW-40-13	September 9	72°16.852'	163°32.073'	41	ADCP/uCat
HSNW-50-13	September 9	72°31.514'	164°05.949'	51	ADCP/uCat
HSNW60-13	September 9	72°41.753'	164°31.943'	57	ADCP/uCat



**Figure 3.** Bathymetric map showing the locations of the COMIDA current meter moorings in 2011 – 12 and 2013 – 14.



**Figure 4.** Timelines of ADCP data recovery from the COMIDA moorings with blue being for 2012-2013 and red for 2013-2014 deployments.



**Figure 5.** Maps of ADCP mooring locations in the northeastern Chukchi Sea shelf from 2008 – 2015. Yellow dots indicate moorings in which data processing is not yet complete.

## 2.2 CTD and VM-ADCP Data

The *Healy* COMIDA cruises enabled the collection of CTD and VM-ADCP data using a 150 kHz unit. Winsor’s cruises, which serviced the COMIDA moorings, also occupied several CTD sections around Hanna Shoal and over the HSNW and HSNE and Chukchi slope array of Pickart. Data along these sections were collected with a towed-vehicle (Acrobat) that provides high resolution (~250 m in the horizontal and 1 m in the vertical) CTD data along the transect. Weather and schedule constraints did not permit sampling extensively over the slope array. The *Norseman II* also carries a 300-kHz vessel-mounted ADCP (VM-ADCP), which enabled us to

collect velocity data in both 2013 and 2014. Pickart also conducted CTD and VM-ADCP sections on either side of Hanna Shoal in summer 2014 from the USCG *Healy* as part of his NSF-funded program in the Chukchi Sea. All of these data sets are presently being processed.

We used the 3-hourly winds produced by NOAA's North American Regional Reanalysis (NARR) models (Mesinger et al., 2006) derived for gridpoints north ( $72.5^{\circ}\text{N}$ ,  $161.5^{\circ}\text{W}$ ) and south ( $71.3^{\circ}\text{N}$ ,  $161.5^{\circ}\text{W}$ ) of Hanna Shoal as a representation of the wind field over the northeastern Chukchi Sea. Ice-concentration maps for May, June, July, October, and November of 2011 - 2013, were prepared based on data obtained by the Special Sensor Microwave Imager (SSM/I) satellite sensor and processed according to Spreen et al. (2008). More detailed maps of the ice edge for the August – September periods of each year were prepared based on analyses performed by the National Snow and Ice Data Center (NSIDC).

### **3. Results**

#### **3.1 Sea Ice**

The annual formation and decay of sea ice exerts a tremendous influence on the circulation and water properties of the Chukchi Sea shelf. In general, ice begins forming in late October and effectively covers the entire shelf, including Bering Strait, by late December. Ice retreat commences in late April or early May with northward retreat in Bering Strait. By mid-July the ice edge is typically north of  $70^{\circ}\text{N}$ , with prominent embayments forming in Herald Valley, the Central Channel, and Barrow Canyon (Paquette and Bourke, 1981; Martin and Drucker, 1997). Ice continues to retreat through September, although it may remain over Hanna Shoal throughout the summer. In fact, the interannual variability in summer/early fall ice cover over Hanna Shoal is probably very large. To illustrate this we show maps of the seasonal evolution of ice retreat for May, June, and July 2011 - 2013 (Figures 6 – 8). Figure 9 has more detailed maps of the ice edge (defined by 15% ice concentration limit per NSIDC) in the northeastern Chukchi Sea for the August – September period of the same years.

The sequence of SSM/I ice concentration maps provides a broader perspective of the seasonal evolution in sea ice retreat over the Chukchi shelf prior to the 2012 and 2013 surveys and also contrasts these years with 2011. In each year, substantial ice retreat began in Bering Strait by the third week of May. In 2011 (Figure 6), ice began retreating simultaneously from the northwest coast of Alaska in May, with a substantial fraction of the northeastern Chukchi Sea (south of  $70^{\circ}\text{N}$ ) ice-free by the 3<sup>rd</sup> week of June. Ice continued to retreat northward through July, with the shelf effectively ice-free by the end of July. In contrast, ice retreated more slowly in 2012 and 2013. In 2012 (Figure 7), ice retreated in Bering Strait and along the northwest coast of Alaska through mid-June, but then the retreat stalled, or even reversed, into mid-July. At this time the ice-edge embayments in Herald Valley, the Central Channel and Barrow Canyon were evident, but substantial concentrations of ice remained over Hanna Shoal. In 2013 (Figure 8), the ice-edge embayments were evident by 1 July and the southernmost limit of sea ice in the northeastern Chukchi at  $\sim 70^{\circ}\text{N}$  by mid-June. By late July much of the western Chukchi Sea was ice-free, but heavy concentrations of ice remained over the northeastern shelf, particularly east of, and over Hanna Shoal.

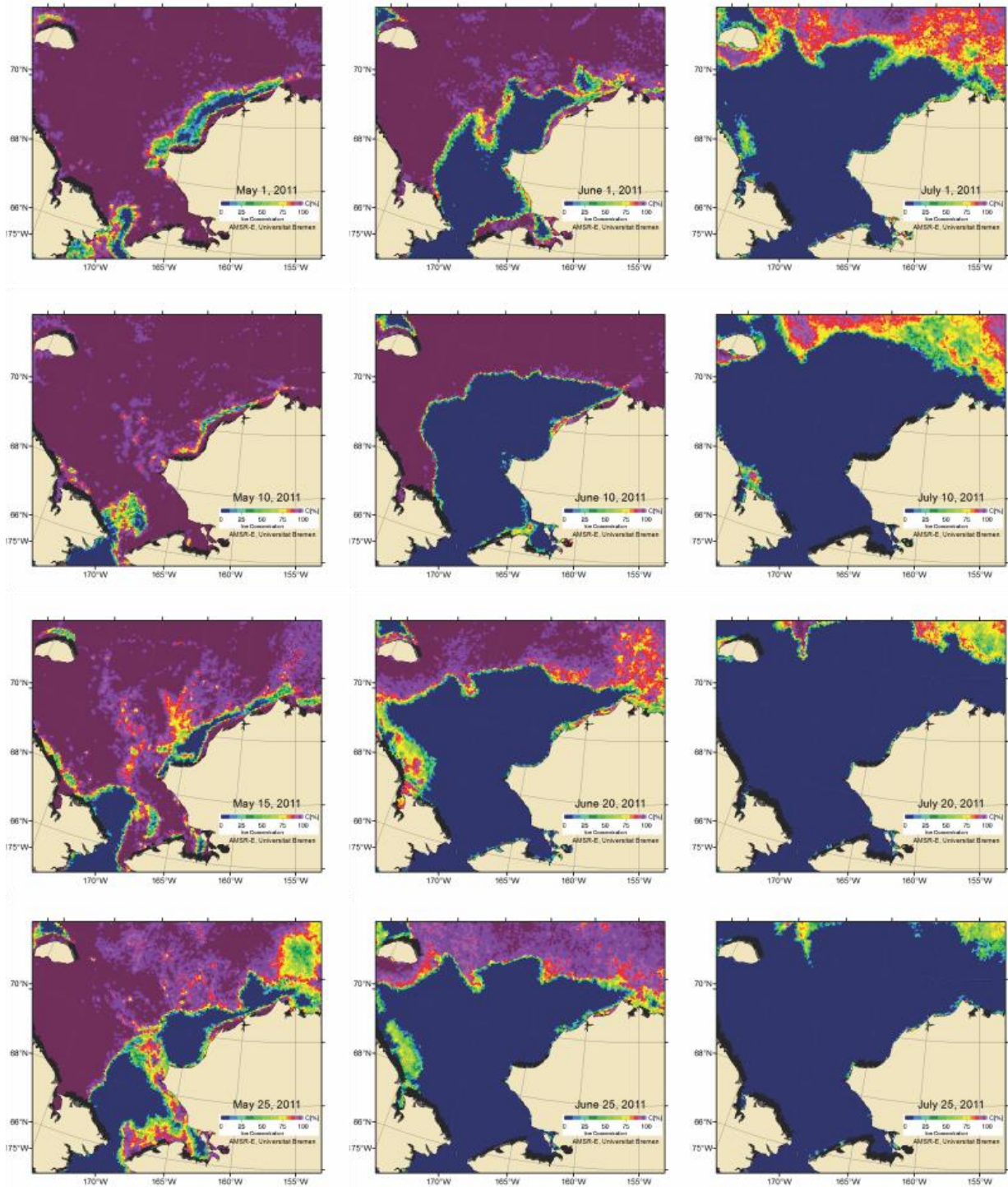
The northeastern Chukchi Sea was, for all practical purposes ice-free in August and September 2011 (Figure 9, top). In 2012 ice remained over Hanna Shoal and portions of the shelf south of Hanna Shoal into mid-September (Figure 9, middle). This same basic pattern held in 2013 (Figure 9, bottom), except that the ice-edge retreated rapidly from south of Hanna Shoal on 1 September to north of the shelfbreak by mid-September. In both of the August COMIDA cruises visual observations from the bridge of the *Healy* indicated that thick ice was grounded atop Hanna Shoal. According to A. Mahoney [University of Alaska, Fairbanks, AK, pers. comm. January 2015], this thick ice grounded on Hanna Shoal in late winter of both 2012 and 2013. Eicken and Mahoney (2015) argue that the source of this ice is, in general, not pack ice that drifts southwestward from the polar basin, but heavily deformed ice displaced westward after detaching from the stamukhi zone of the Alaskan Beaufort Sea. . (Other potential sources for this thick ice would be from Ellesmere and Banks Island regions of the Arctic Ocean, where the thickest multi-year ice of the Arctic Ocean is traditionally found.)

The reasons for these year-to-year differences in ice retreat are not readily apparent, but they do not appear to be related to August and September winds (Figure 10). In both 2011 (light ice year) and 2013 (heavy ice year) the winds were persistently from the northeast (and moderately strong). In contrast, the winds in August 2012 (heavy ice year) were from the south and southwest. By fall in all years the winds strengthened and were generally northeasterly.

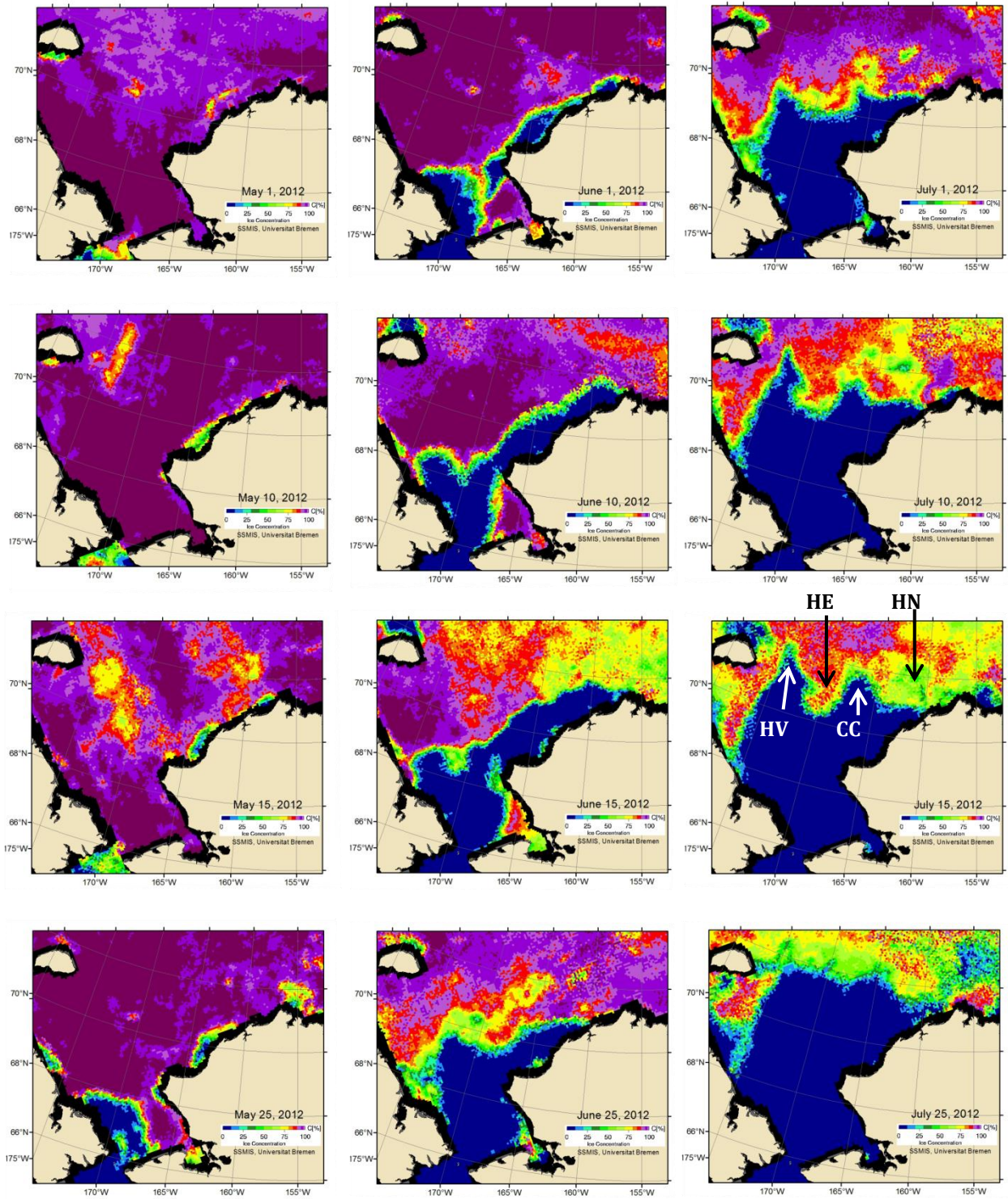
On an even more local level Figures 11 and 12 show the evolution of sea ice as detected by the upward-looking ADCPs at each mooring location for the 2012 – 2013 and the 2013 – 2014 deployments, respectively. In 2012 ice concentrations increased very rapidly in late October at all locations simultaneously. This appears to have been largely due to advection of the pack ice from the basin onto the shelf due to northerly winds. Later we show that the stratification over this portion of the shelf is shallow, very strong and persistent. As such, the stratification may enhance the onset of ice formation by confining ocean heat loss to the atmosphere to a very shallow surface layer. Figure 13 shows the SSMI ice concentrations, which indicate open water was present over all mooring sites in late October 2012, but that 100% coverage had developed by mid-November. Ice concentrations of ~100% persisted through June 2013, although it appears that the springtime decrease in ice concentrations began earlier at the HSNW moorings than at the HSNE moorings. This is consistent with the late June and early July 2013 ice concentrations maps (Figure 8), which indicates lower ice concentrations on the western and northwestern sides of Hanna Shoal compared to the eastern side.

Sea ice concentrations also increased more or less simultaneously at all locations in late October 2013 as well. The ice cover developed much more erratically than in 2012, however, as ice concentrations varied between 0 and 100% between late October and mid-November before uniform concentrations of 100% set in by late November. The ice concentration time series in Figure 12 indicates that the ice actually set up later at the HSNW moorings than at the HSNE moorings. This asymmetry in the timing of ice setup is also evident in the SSMI fall ice concentration maps for 2013 (Figure 13). The mooring time series ended too early in summer 2014 to tell if there was an asymmetric retreat of the ice on either side of Hanna Shoal. SSMI imagery from summer 2014 (not shown) indicates that ice concentrations decreased more rapidly on the western side of the Shoal compared to the east, at least through mid-July. Thereafter, the ice retreat appeared to progress more uniformly on either side of the Shoal.

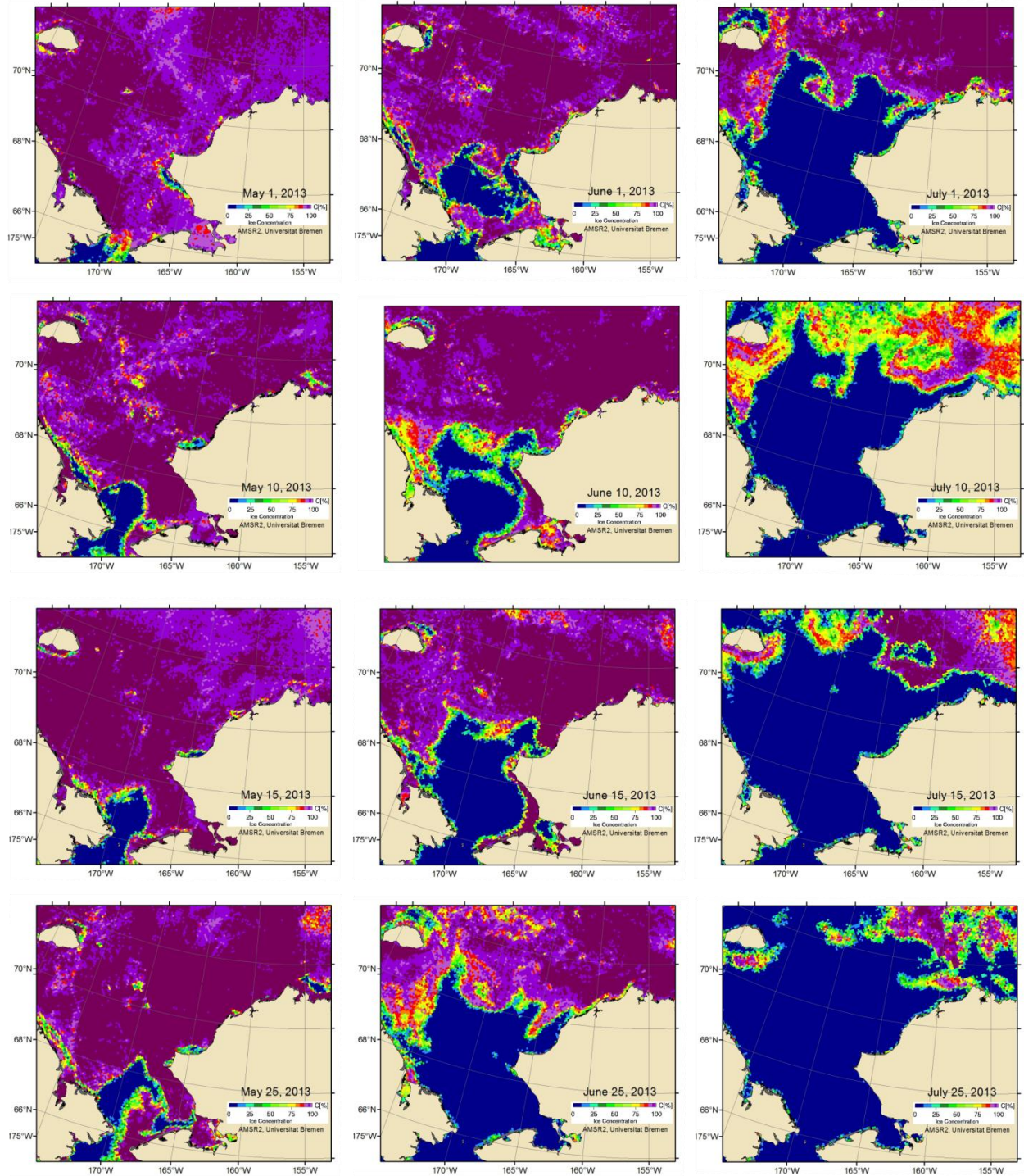




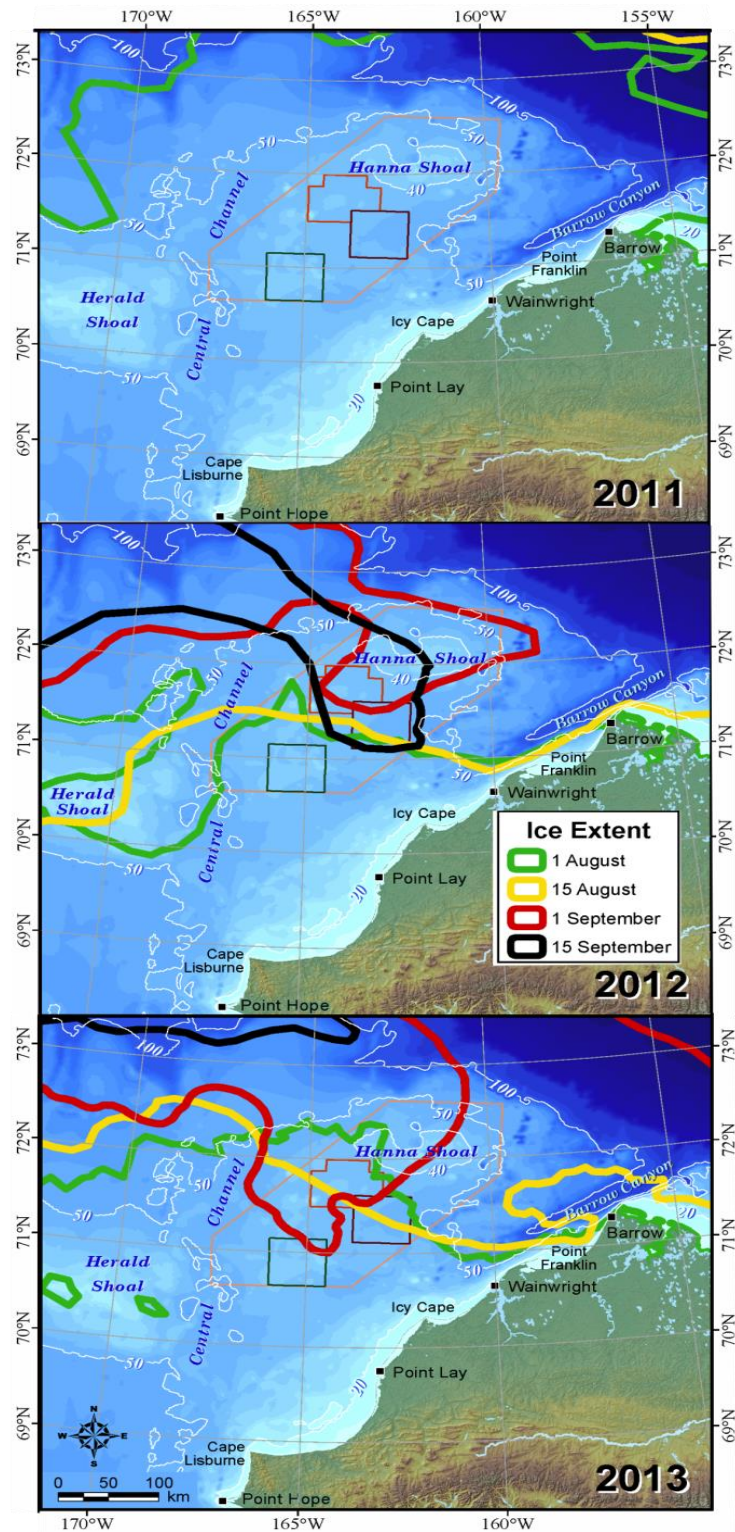
**Figure 6.** SSM/I sea ice concentration maps for the Chukchi shelf in 2011: May (left column), June (middle column) and July (right column).



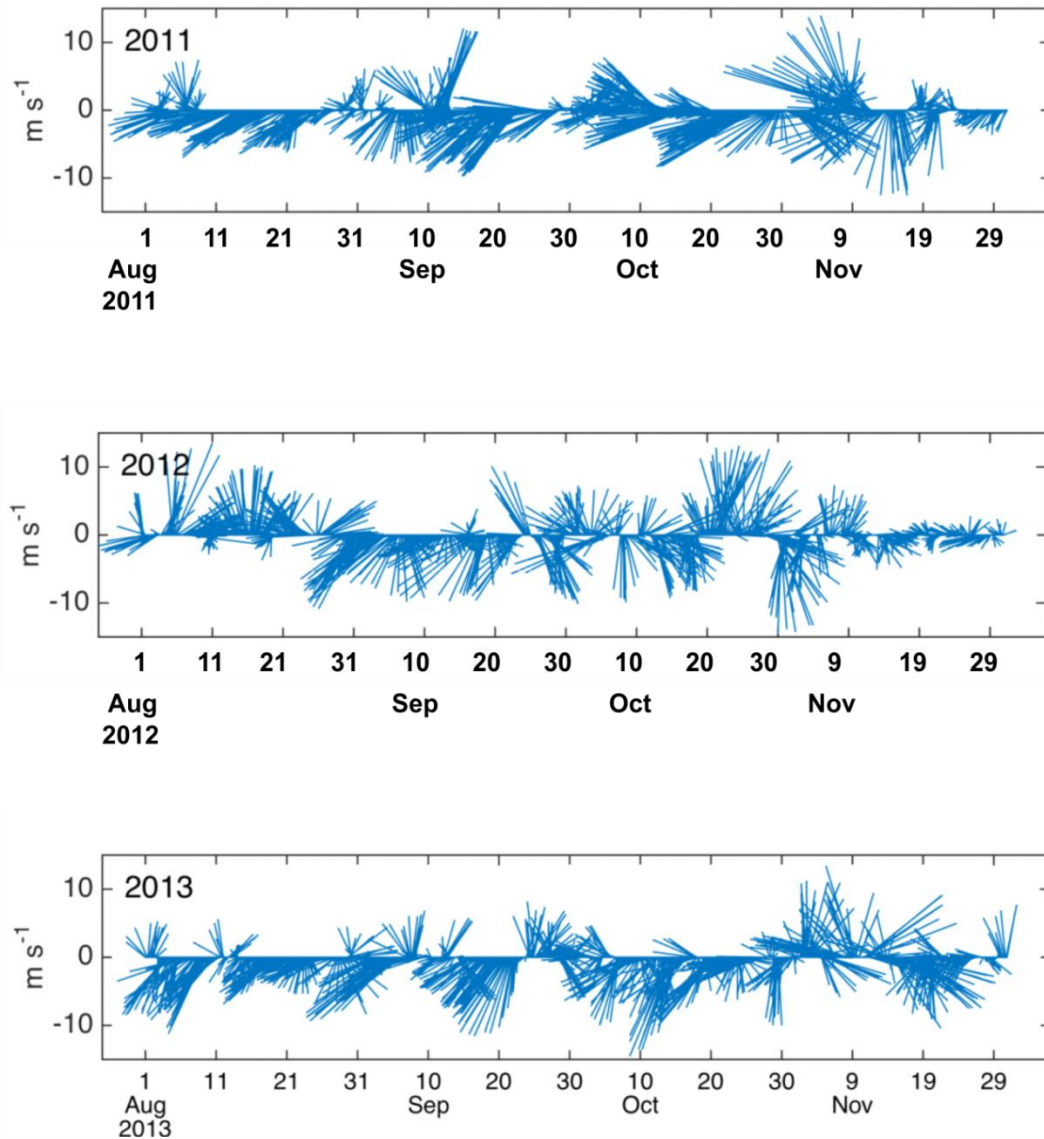
**Figure 7.** Sea ice concentration maps in 2012 for May (left), June (middle), and July (right). The labels on the July 15 map refer to Hanna (HN) and Herald (HE) shoals, the Central Channel (CC), and Herald Valley (HV).



**Figure 8.** Sea ice concentration maps in 2013 for May (left), June (middle), and July (right).



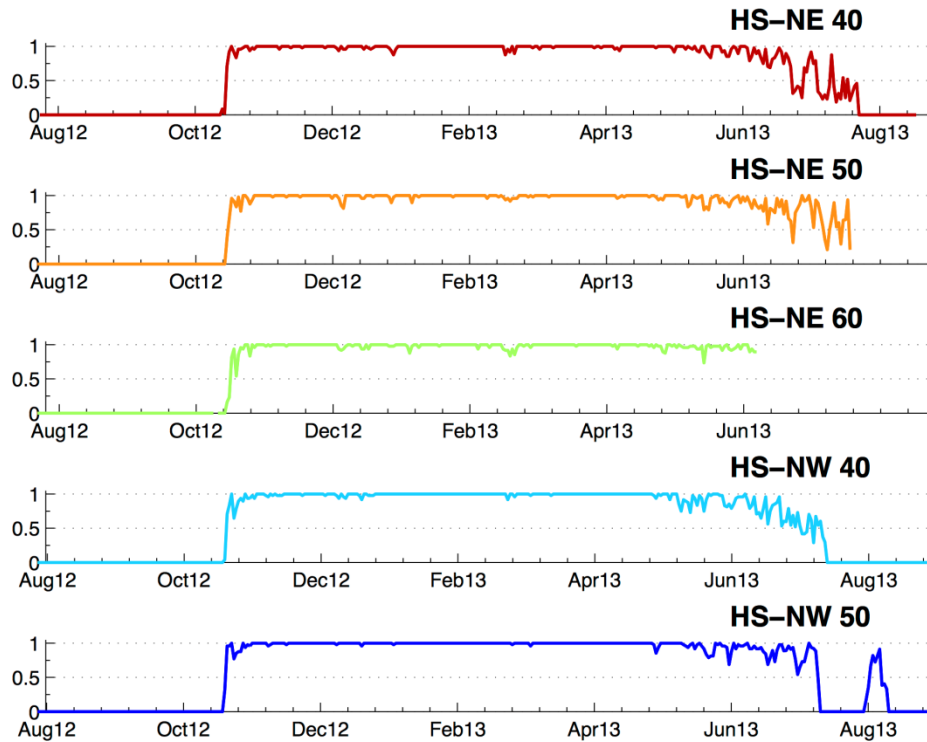
**Figure 9.** Locations of the ice-edge (15% ice concentration contour as determined by the NSIDC) on August 1 and 15 and September 1 and 15 for 2011 (top), 2012 (middle), and 2013 (bottom).



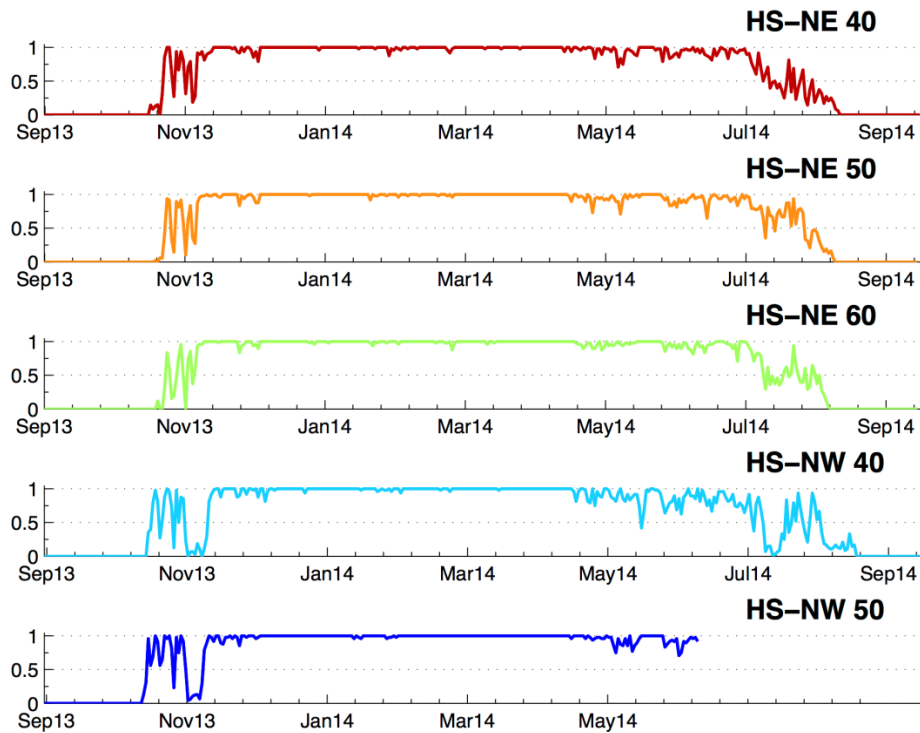
**Figure 10.** Time series of wind vectors over the northeastern Chukchi Sea for the August – November periods of 2011 (top), 2012 (middle), and 2013 (bottom).

The interannual and spatial differences in the timing of autumn ice set-up will result in different patterns of air-sea heat flux because sea-ice is an effective insulator of the ocean. Spatial differences in these heat fluxes may well leave spatial signatures in the fall distribution of ocean surface temperatures and salinities.

The bottom-tracking capability of the ADCP instruments enabled measuring sea ice velocities and the ice drift is summarized in Figure 14. In both years, the mean ice drift was westward at 2 - 5  $\text{cm s}^{-1}$ . The variance ellipses indicate that the standard deviations are 2 – 4 times the magnitude of the mean. The ellipse orientations are approximately zonal, implying that the variability in ice drift is primarily in the east-west direction, although for the most part these ellipses are not strongly polarized. Interestingly the ellipse orientations with the largest polarizations are at HSNE50-13 and at HSNE60-13; the former was zonally polarized while the latter was meridionally-polarized. The drift was spatially coherent and, at all sites, directed approximately

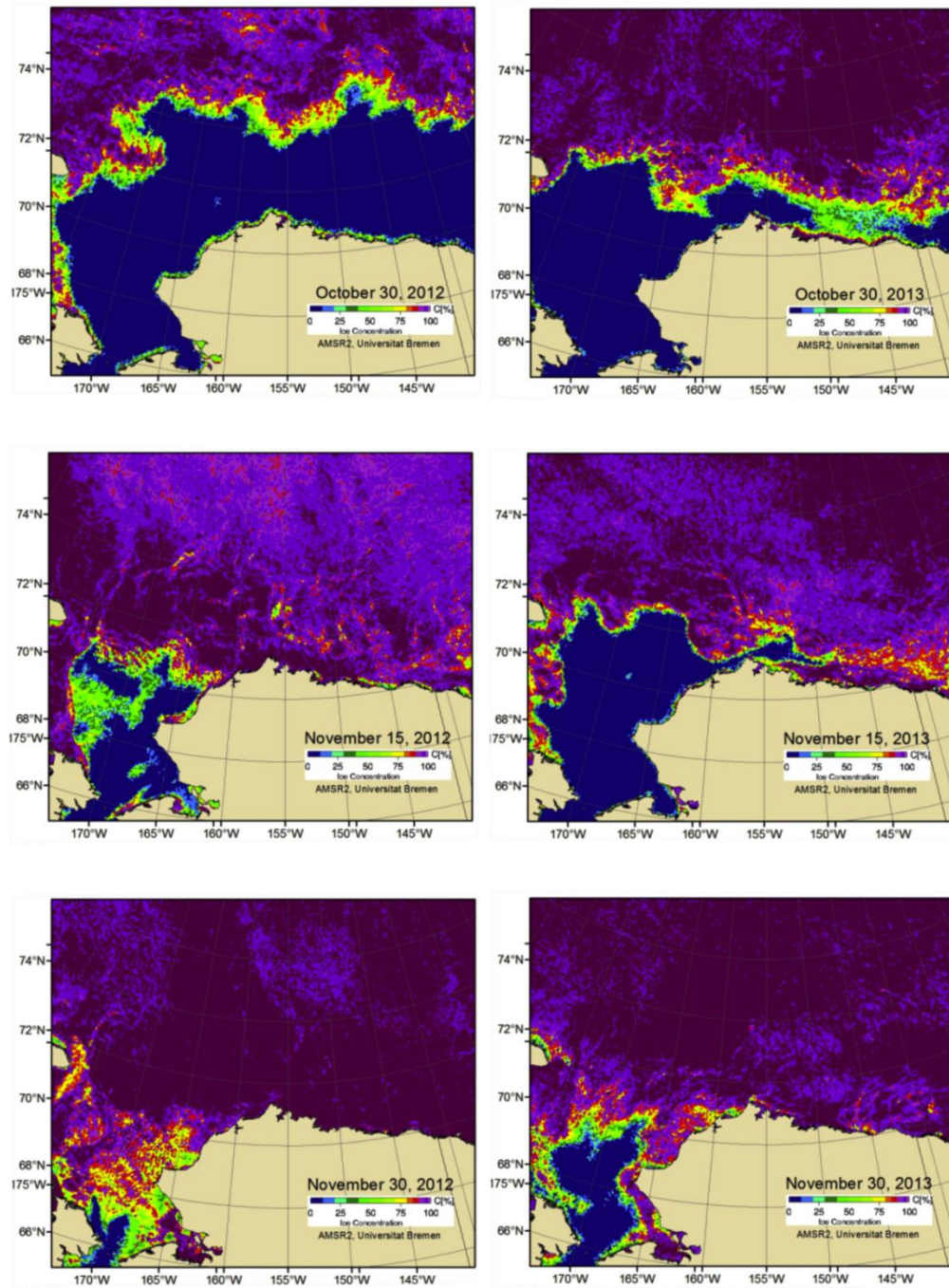


**Figure 11.** Ice concentration time series for 2012 – 13 at each mooring location based upward-looking ADCPs.



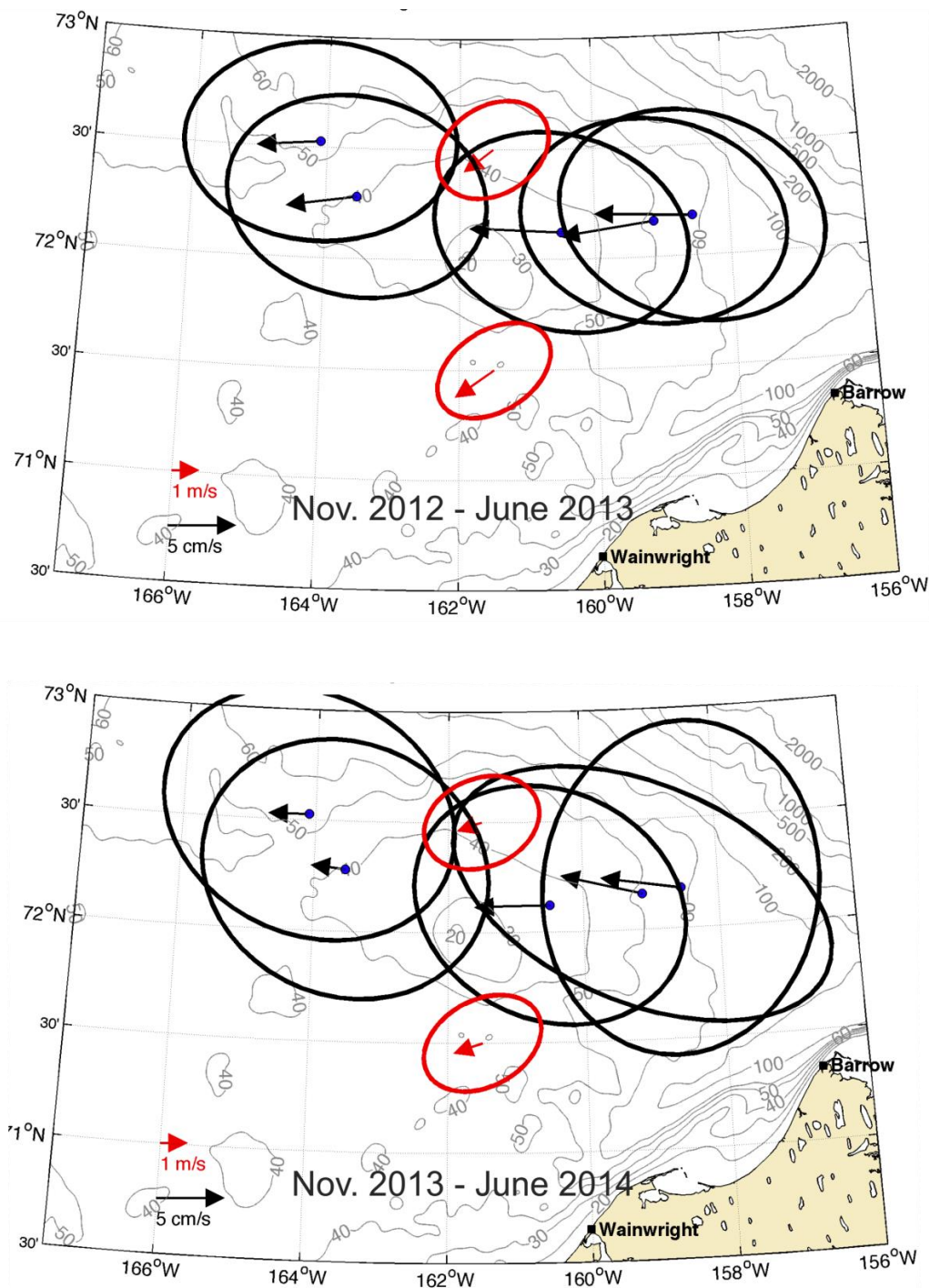
**Figure 12.** Ice concentration time series for 2013 – 14 at each mooring location based upward-looking ADCPs.

45° to the right of the wind. Note that the winds in both years were from the northeast with the mean speed in 2012 – 13 being about 3 m s<sup>-1</sup> and in 2013 – 14 the mean speed was ~1.5 m s<sup>-1</sup>.



**Figure 13.** The evolution of sea ice concentrations as seen on 30 October (top), 15 November (middle), and 30 November (bottom) for 2012 (left column) and 2013 (right column).

Finally, the mean 2013 – 14 ice velocities at the HSNW moorings were about half those at the HSNE moorings. Although the scales over which we view these differences are large, the means suggests that the ice drift may have been convergent over Hanna Shoal in 2013 – 14. Such convergence could lead to deformation of the ice pack and grounding. Based on the mean ice velocities, there was no evidence of convergence over the 2012 – 13 deployment.



**Figure 14.** Mean vectors and variance ellipses for sea ice (black) and winds (red) for the periods of November 2012 – June 2013 (top) and from November 2013 – June 2014 (bottom).



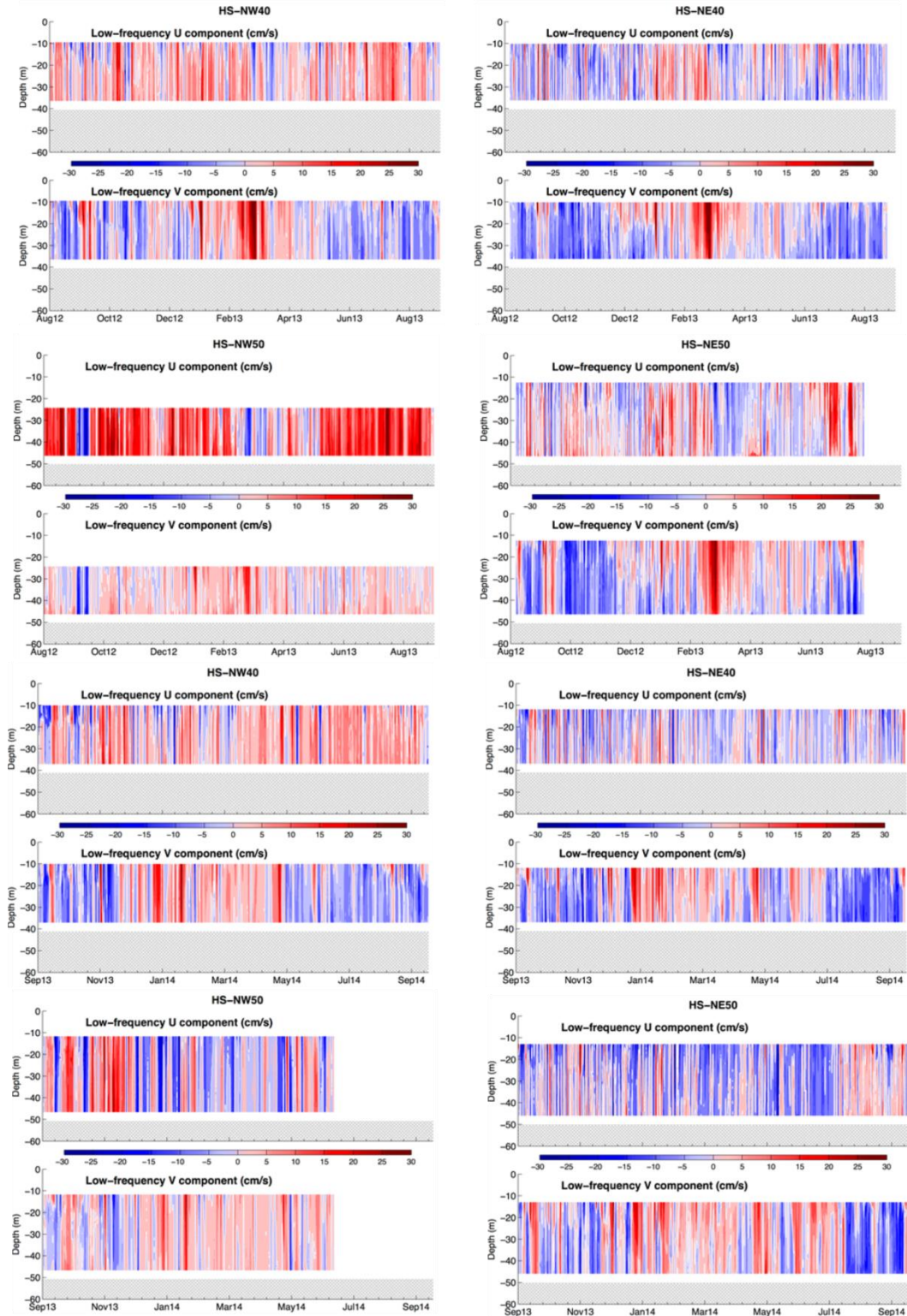
### 3.2 Sub-inertial Currents

In this section we examine the current variability at both long and short periods; long periods are the sub-inertial motions of 3 days or longer. The shorter period current variations of interest are inertial ( $\sim 12$  hour) and the subject of Section 3.3. The sub-inertial currents were formed by low-pass filtering the original time series with a 40-hr cutoff period. Figure 15 shows the low-pass filtered current components at each site in both years for the 40 and 50 m moorings. Figure 16 shows the same data sets for both years from HSNE60. Several general observations emerge from these figures. First, in both years the currents at the NE moorings had greater vertical shear than those at the NW moorings. Second, in 2012 – 13 the flow at both HSNW50 and HSNW40 was mainly eastward, whereas in 2013 – 14 there were more westward flow events, with these occurring primarily in winter. Third, there were also more westerly flow events in the NE moorings in 2013 – 14 compared to the 2012 – 13. Fourth, the velocity data at the NW mooring do not appear to be strongly correlated with the velocities at the NE moorings. This last impression was confirmed by computing the rotary coherences among mooring pairs. Although not shown, we have done this for the currents at the near-surface, the mid-depth (22 m), and bottom (10 m above bottom). Over the low-frequency portion of the current spectrum (e.g., periods  $> 3$  days), the rotary coherence squared values vary from 0.4 to 0.6 for moorings within  $\sim 60$  km of one another, but decrease to  $\sim 0.3$  or less at distances  $> 60$  km.

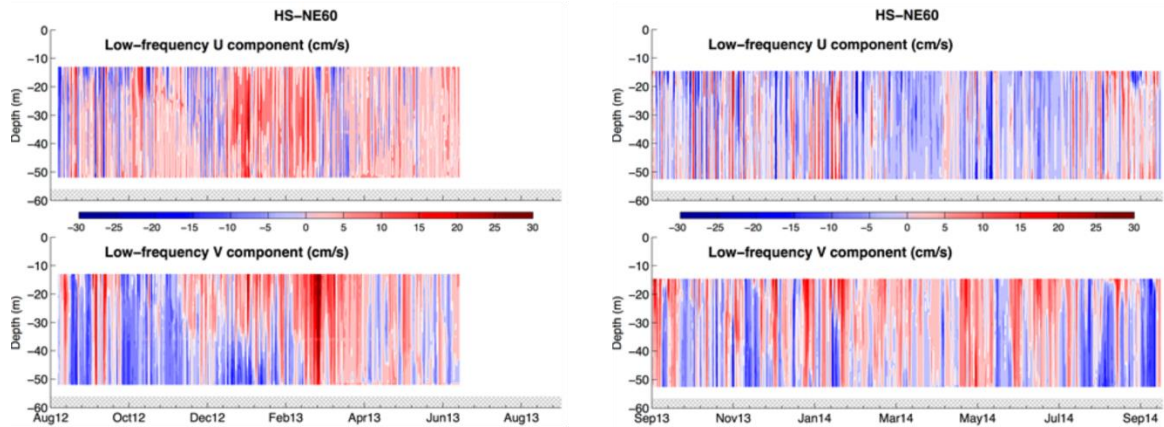
Using the same plotting convention as applied to the ice drift, Figure 17 summarizes the record length means and variances for the near-surface currents for both deployment periods. The means and ellipses for these currents were very similar to the ice drift. In both years the near-surface drift was nearly westward with current speeds averaging  $\sim 3$  cm  $s^{-1}$  at the HSNE moorings in 2012 – 13 and about half that at the HSNW moorings for the same deployment period. For the 2013 – 14 deployment, the record-length means were approximately twice as large as those from the corresponding sites in the previous year. Upper ocean current ellipses were large and isotropic.

The near-surface record-length average currents were consistent with the trajectories of satellite-tracked drifters released at the time of deploying the HSNE50-13 and HSNW50-13 moorings (Figures 18 and 19, respectively). The cluster-averaged speeds were  $\sim 5$  cm  $s^{-1}$  although maximum sustained speeds were  $\sim 40$  cm  $s^{-1}$ . In both cases the clusters drifted  $\sim 200$  km westward in less than 2 months under the prevailing northeasterly winds. Although the winds are the presumable causative agent for this drift, we note that the winds only explain about 30% (20%) of the current variability for the HSNE (HSNW) cluster.

Figure 20 shows the record-length means and ellipses for the vertically-averaged currents. In both years the vertically-averaged flow was eastward on the northwest side of Hanna Shoal at speeds of from 3 to 7 cm  $s^{-1}$ . On the east side of the Shoal the mean flow was negligible for the 2012 – 13 deployment but westward at  $\sim 2$  cm  $s^{-1}$  for the 2013 – 14 average. The current ellipses tend to be oriented parallel to the isobaths and their semi-major and –minor axes indicate that the standard deviations are many times the magnitude of the mean. These results have major implications on the along-isobath continuity of the flow field around the north side of Hanna Shoal for they imply that the flow is convergent between the northwest and northeast sides of Hanna Shoal. How that convergence arises is unclear, but it implies a cross-isobath transport,



**Figure 15.** Zonal (U) and Meridional (V) components of velocity as a function of depth and time for moorings HSNW40, HSNW50, NSNE40, HSNE50 for both the 2012 – 13 and 2013 – 14 deployment periods.



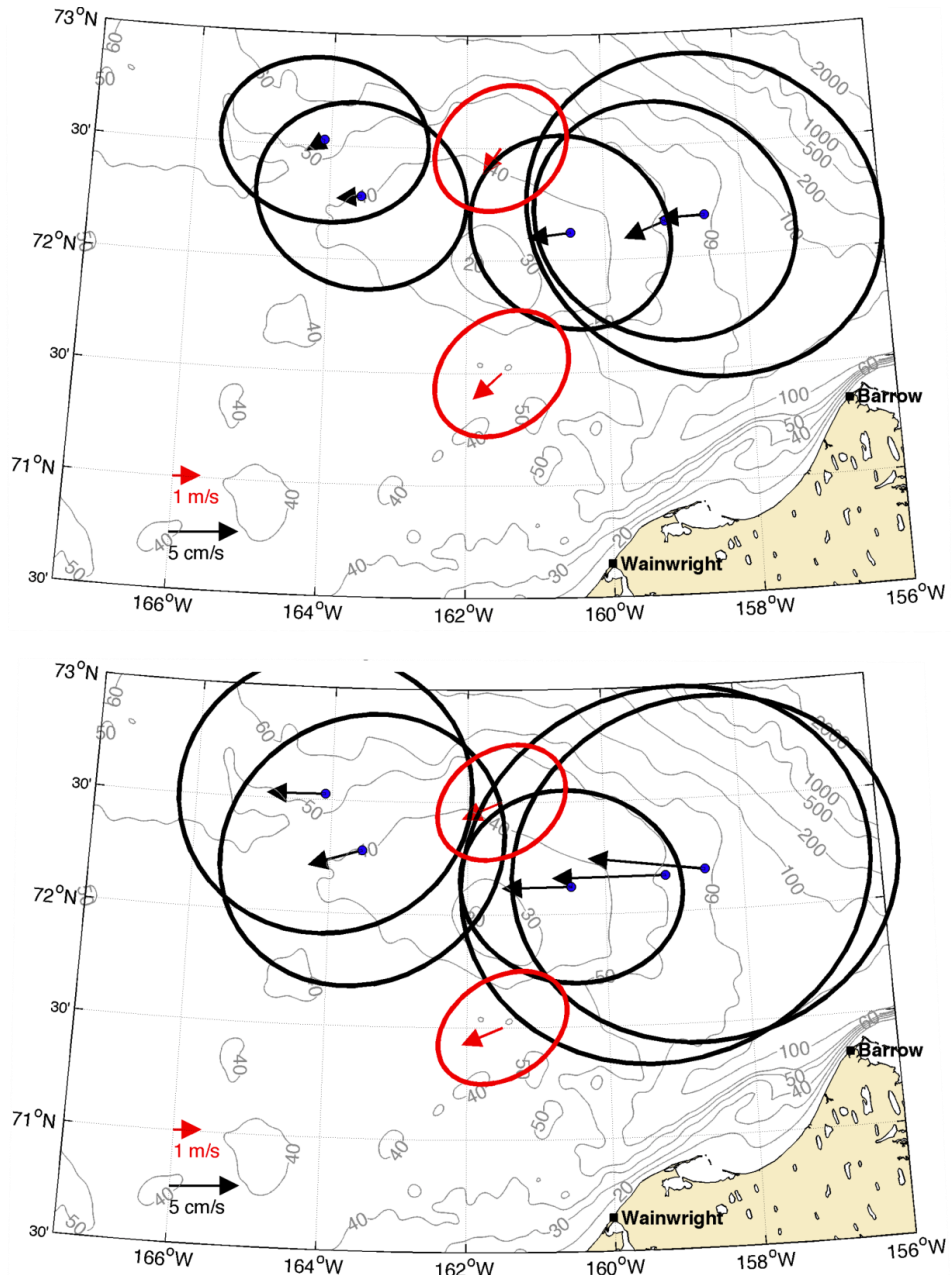
**Figure 16.** Zonal (U) and Meridional (V) components of velocity as a function of depth and time for moorings HSNE60 mooring for both the 2012 – 13 and 2013 – 14 deployment periods.

which presumably would be directed toward the shelfbreak and deeper water rather than southward and onto Hanna Shoal.

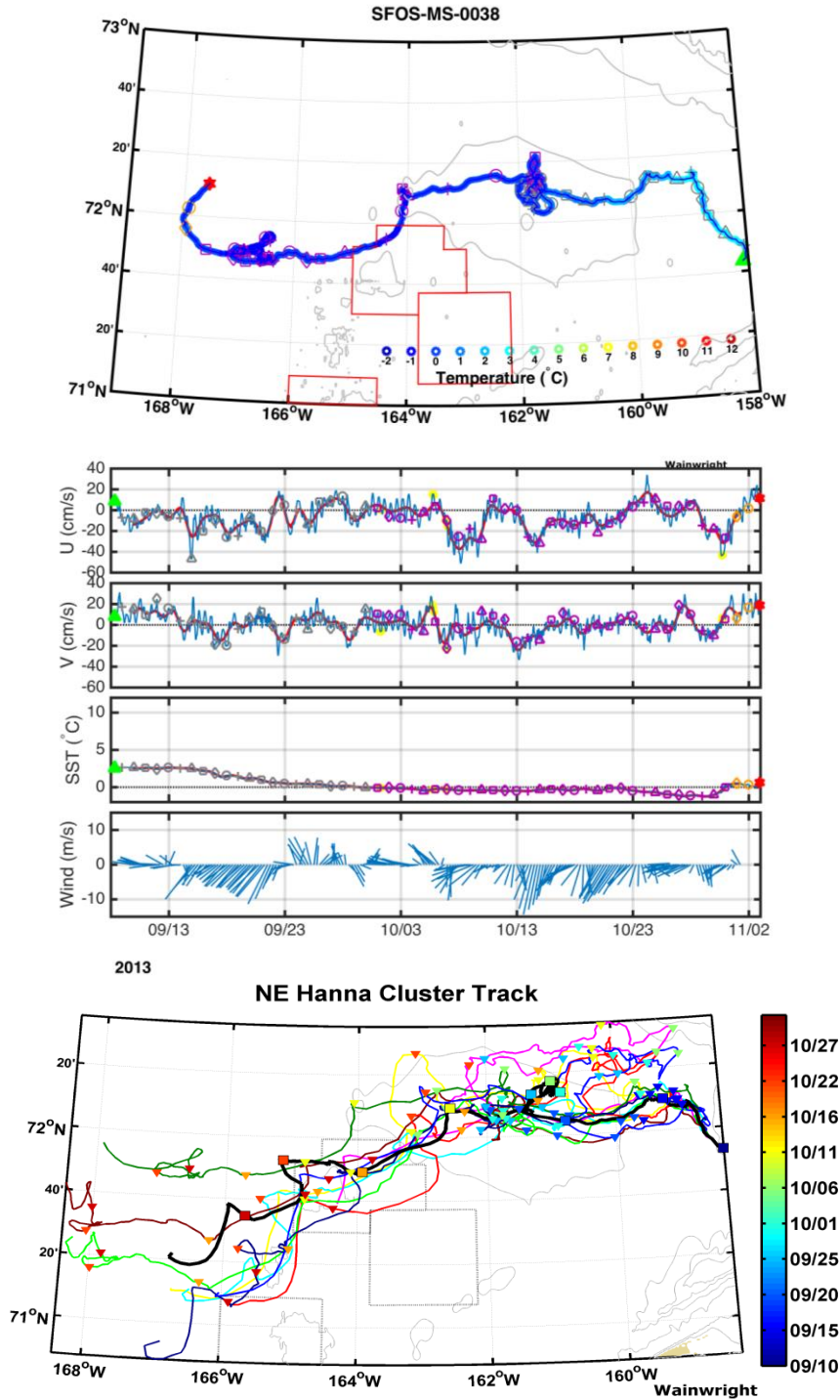
We next examine the near-bottom currents (e.g., 10 meters above bottom; mab) in Figure 21. Northwest of Hanna Shoal the currents were eastward and in the same direction as the vertically-averaged flow and opposite in the direction of the near-surface flow. Turning to the east side of Hanna Shoal the bottom currents were southward in 2012 – 13 and, although not shown, were somewhat stronger in summer and fall than in winter. In 2013 – 14, the bottom currents were considerably weaker east of Hanna Shoal, but nevertheless showed a southward tendency at least at HSNE40 and HSNE60.

In summary, the record-length means from both mooring deployments indicate a westward drift of sea ice and surface waters on either side of Hanna Shoal. The vertically-averaged flow was convergent on the north side of the Shoal, with an eastward flow on the northwest side of Hanna Shoal and weak or westward flow on the eastern side of the Shoal. The bottom water followed a clockwise circulation pattern with swifter flow on the northwest side of the Shoal and weaker and southward flow on the eastern side of the Shoal.

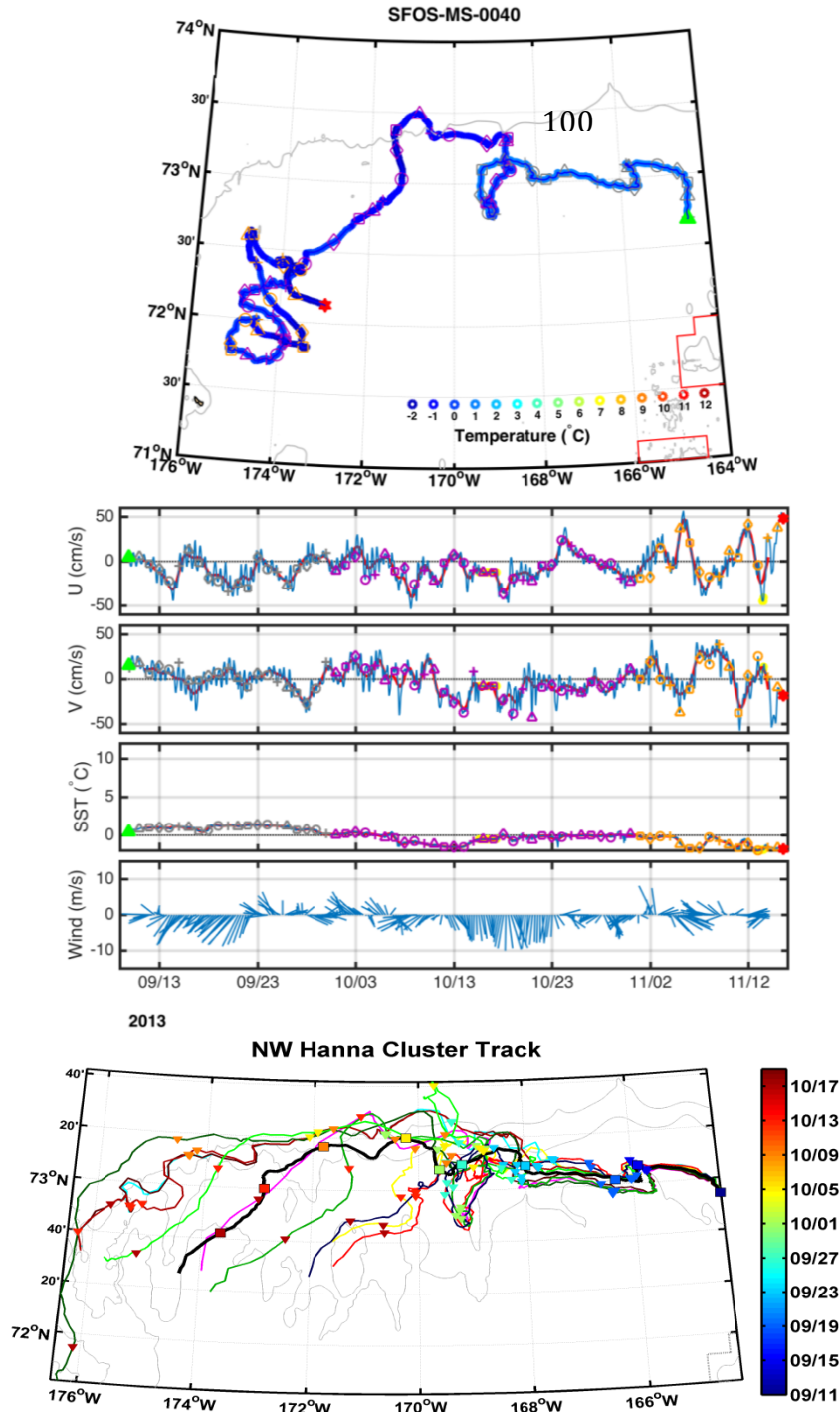
As noted previously in our description of the drifters, the local winds did not account for a large fraction of the current variations. A particularly good example of the loose connection between the winds and currents is evident upon comparing the mean February and October 2013 current vectors and ellipses (Figure 22). The mean winds in both of these months were quite similar;  $\sim 5 \text{ m s}^{-1}$  from the northeast. In February 2013 the bottom water flowed northward on average at  $\sim 5 \text{ cm s}^{-1}$  at all locations. By contrast in October 2013 the mean bottom water flow was southward at all locations except HSNW50, where the flow was eastward. These differential responses to similar “local” winds suggest that the circulation around Hanna Shoal is, at least, in part remotely forced. The exact nature of this forcing is uncertain at this time, but a more inclusive analysis, which includes a large amount of additional mooring data, may resolve this issue.



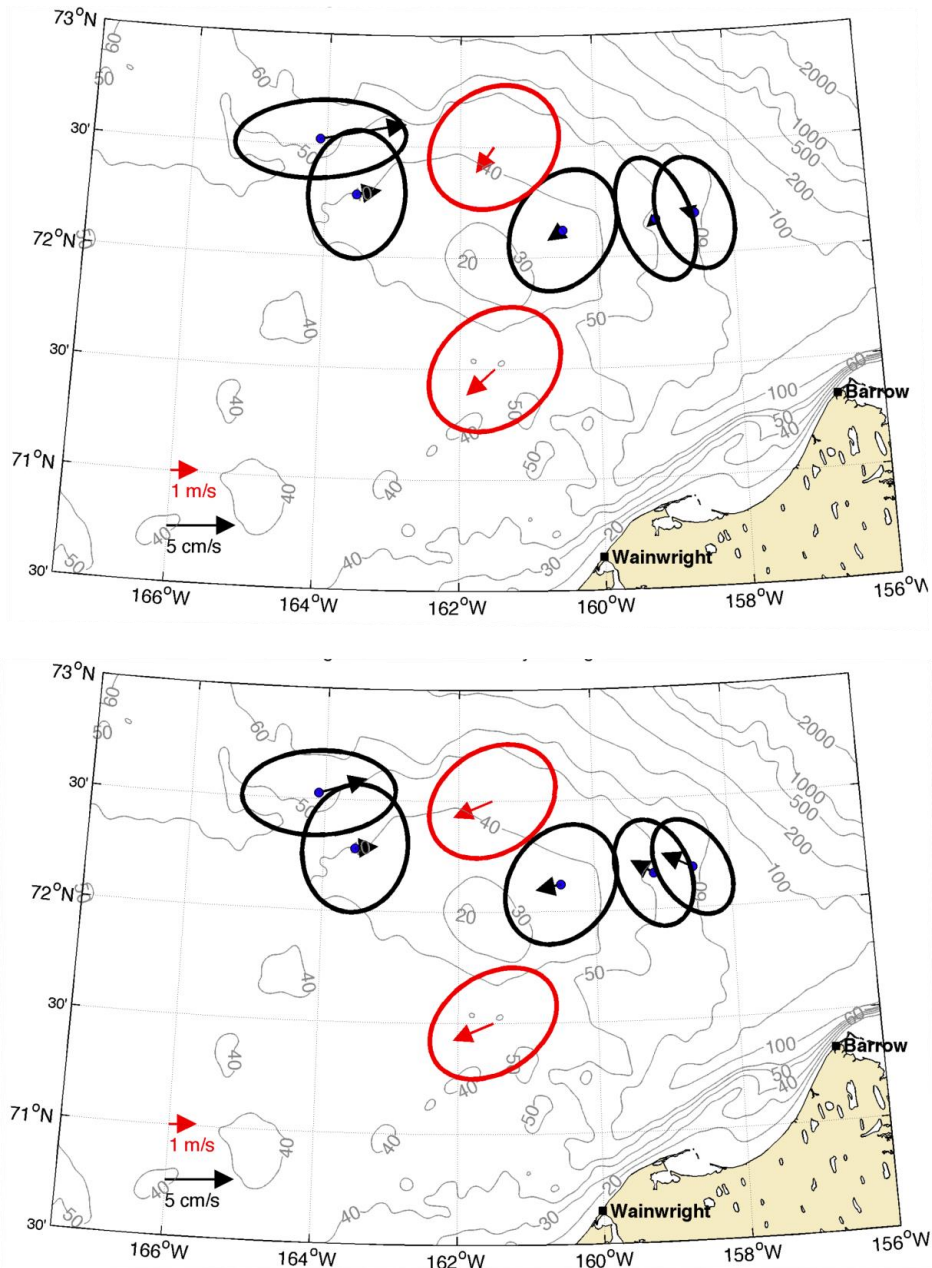
**Figure 17.** Mean vectors and variance ellipses for the uppermost ADCP bin (black) and winds (red) for the 2012 – 2013 deployment (top) and the corresponding period in 2013 – 2014 (bottom).



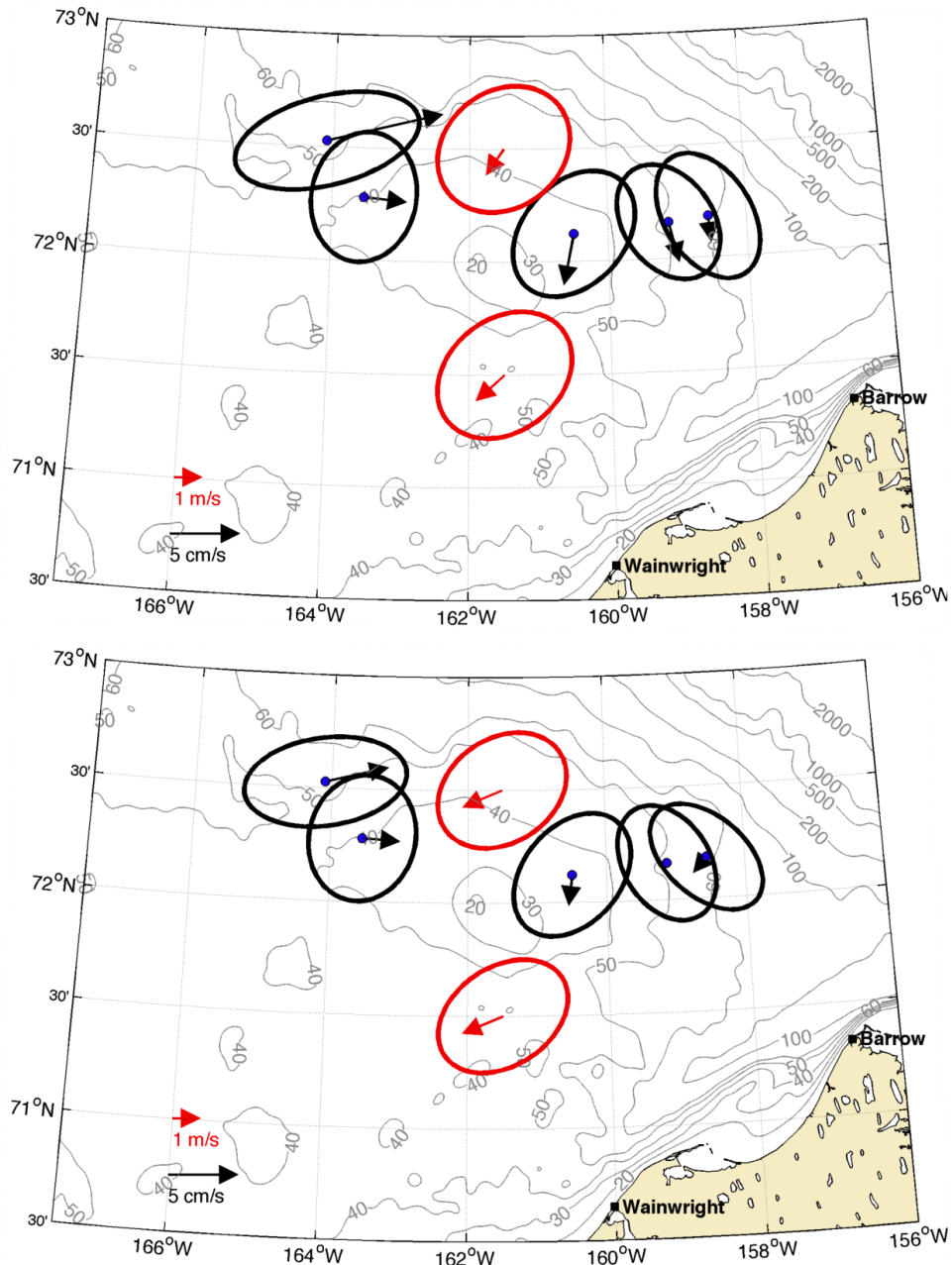
**Figure 18.** The trajectory of one of nine satellite-tracked drifters released during deployment of the HSNE50 in September 2013, along with time series of the drifter velocity components, SST, and winds along the drifter track. The thick lines on the velocity plots are low-pass filtered currents. The bottommost panel shows the cluster's centroid trajectory and the individual trajectories of the drifters comprising the cluster.



**Figure 19.** The trajectory of one of nine satellite-tracked drifters released during deployment of the HSNE50 in September 2013, along with time series of the drifter velocity components, SST, and winds along the drifter track. The thick lines on the velocity plots are low-pass filtered currents. The bottommost panel shows the cluster's centroid trajectory and the individual trajectories of the drifters comprising the cluster.

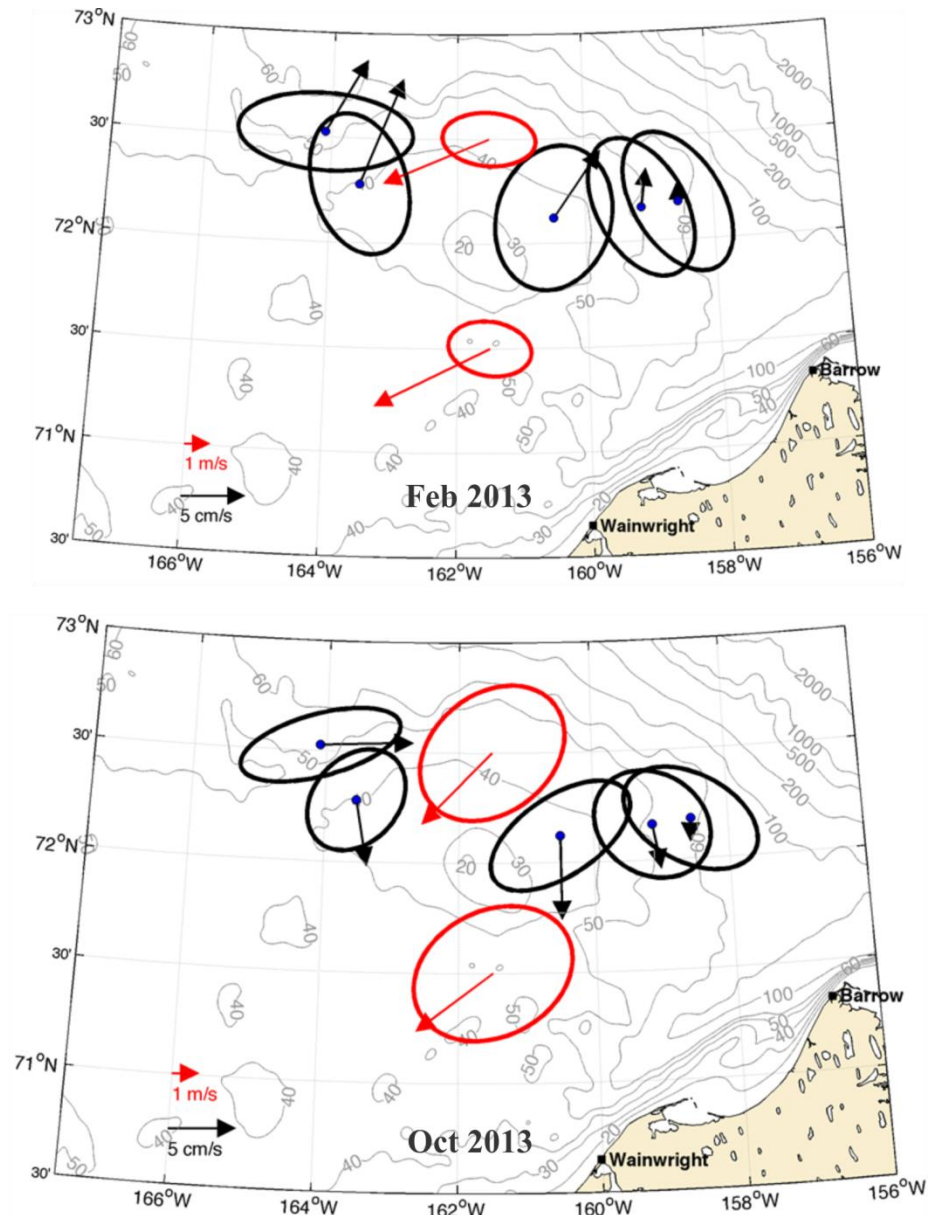


**Figure 20.** Mean vectors and variance ellipses for vertically-averaged currents (black) and winds (red) for the periods of November 2012 – June 2013 (top) and the corresponding period in 2013 – 2014.



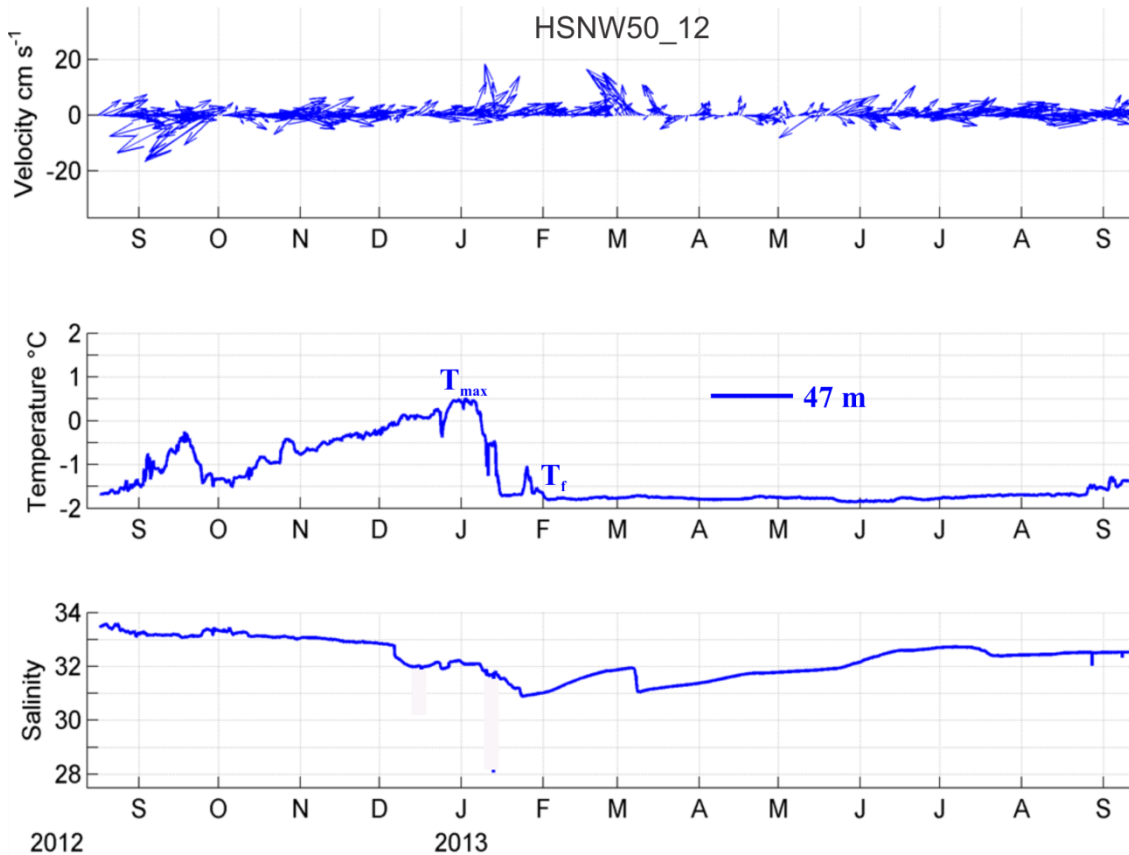
**Figure 21.** Mean vectors and variance ellipses for currents at 10 mab (black) and winds (red) for the periods of November 2012 – June 2013 (top) and the corresponding period in 2013 – 2014 (bottom).





**Figure 22.** Mean vectors and variance ellipses for currents at 6 mab (black) and winds (red) for the periods of February 2013 (top) and October 2013 (bottom).

We conclude this section by comparing the seasonal changes in vertically-averaged currents and temperature and salinity at HSNW50-12 (Figure 23) with the corresponding time series at HSNE50-12 (Figure 24). The latter figure includes the time series of temperature and salinity from both the ISCAT moored at 23 below the surface and the MicroCat at 43 m depth. At HSNW50-12, the vertically-averaged flow was eastward generally; there was a reversal to the southwest in September 2012 and a burst of northward flow in March 2013. The record-length average flow was  $\sim 7 \text{ cm s}^{-1}$  westward. At the beginning of the record in August bottom temperatures were close to the freezing point ( $\sim -1.8^\circ\text{C}$ ), but they then increased to  $\sim -0.5^\circ\text{C}$  in late September. This increase was followed by a brief cooling event in early October and then a



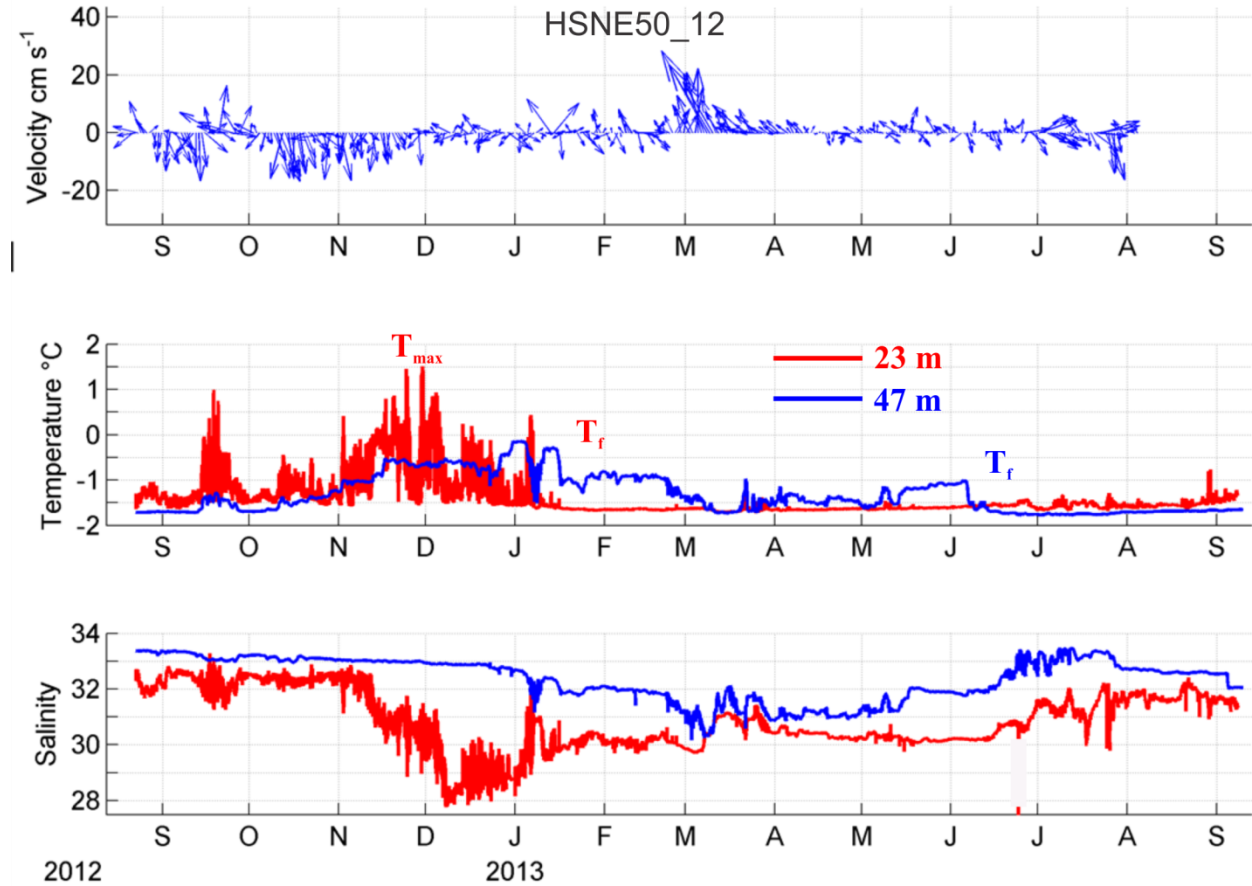
**Figure 23.** Time series of vertically averaged current vectors (top), and temperature (middle) and salinity (bottom) at 47 m depth from mooring HSNW50-12. The timing of the temperature maximum ( $T_{max}$ ) and the descent to the freezing point ( $T_f$ ) are noted.

monotonic increase to a maximum of  $0.5^{\circ}\text{C}$  by late December. In January, the temperature decreased rapidly until it reached the freezing point by 1 February. Salinities were initially  $\sim 33.5$  in September but gradually decreased to a minimum of  $\sim 31$  in mid-January. Over the remainder of the record the salinity increased very slowly and attained  $\sim 32.5$  by September 2013. The December-January transition in bottom waters consisted of a change from being cool and saline to warm and fresh is of particular interest. For reasons outlined later, we believe that this transition was primarily associated with vertical mixing.

At HSNW50-12 the vertically-averaged velocity was quite variable through time, and over the record averaged to  $0 \text{ cm s}^{-1}$ . In fall the flow was primarily south-southeastward but with the exception of the strong northward flow event in March, the flow was weak and variable from December to August. Consider next the salinity records at 23 and 47 m, which provide an index of the bulk vertical stratification because of the density dependence upon salinity. In fall the vertical salinity difference between was  $\sim 1$ , but this increased to  $\sim 5$  by mid-December. This change came about primarily because of freshening at 23 m even though the bottom salinity had also decreased slightly through fall! The shallow salinity decrease was associated with increasing temperatures, which were a maximum of  $\sim 1.5^{\circ}\text{C}$  in mid-December. Salinities then increased at 23 m through February, but continued to decrease at the bottom. In March, the salinity difference was a minimum of  $<1$ . This change in stratification was associated with northward flow and an

increase in salinity at both depths, which suggests that the change reflects the advection of a less stratified water column from the south rather than local mixing.

After March, the stratification increased again, due primarily to a slight salinity increase (decrease) at the bottom (mid-depth). Bottom and mid-depth salinities both increased in July and remained nearly constant into August. The salinity record indicates that the vertical stratification over this portion of the Chukchi Sea shelf remains intact throughout the year, which is a remarkable and unexpected finding!



**Figure 24.** Time series of vertically averaged current vectors (top), and temperature (middle) and salinity (bottom) at 23 m (red) and 47 m (blue) depth from mooring HSNE50-12. The timing of the temperature maximum ( $T_{max}$ ) and the descent to the freezing point ( $T_f$ ) are noted.

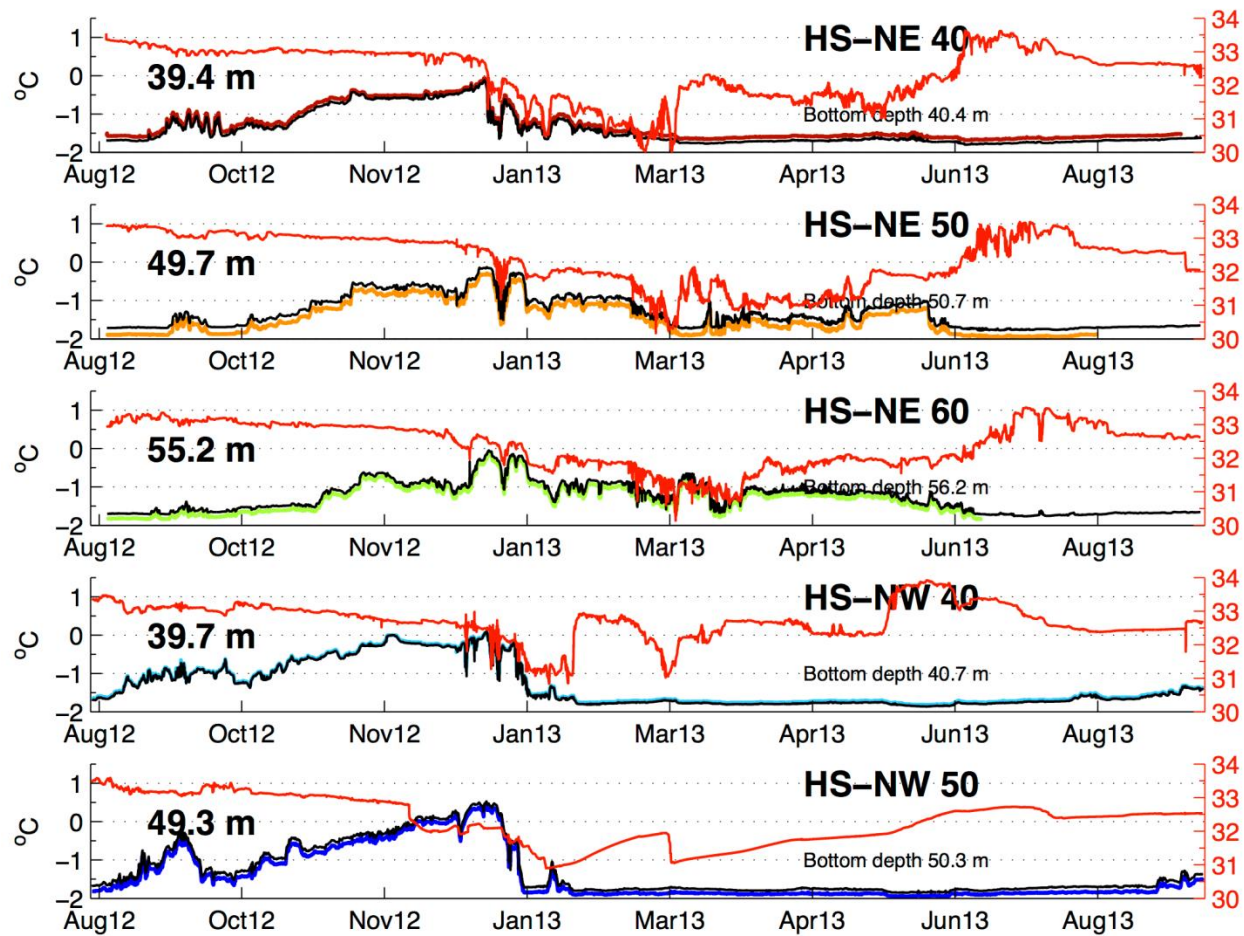
Bottom temperatures at HSNE50-12 increased slowly through fall and reached their maximum ( $\sim 0^\circ\text{C}$ ) in January. They remained fairly constant through the first week of June, with the exception being the decrease to the freezing point ( $T_f$ ) during the northward flow event in March. The decrease to  $T_f$  coincided with a bottom salinity increase, further suggestive that these winter-formed waters were advected into the area. Bottom temperatures decreased again to the freezing point (and salinity increased in conjunction with the temperature decrease) in the second week of June.

This change occurred well after the onset of spring ice melt and bottom conditions remained that way through the end of the record. Again, advection has to account for the presence of these winter waters at this time of the year. The mean flow from August through September at both HSNE50 and HSNE60 was to the southeast at this time indicating that the source of this winter water was from the northern side of Hanna Shoal.

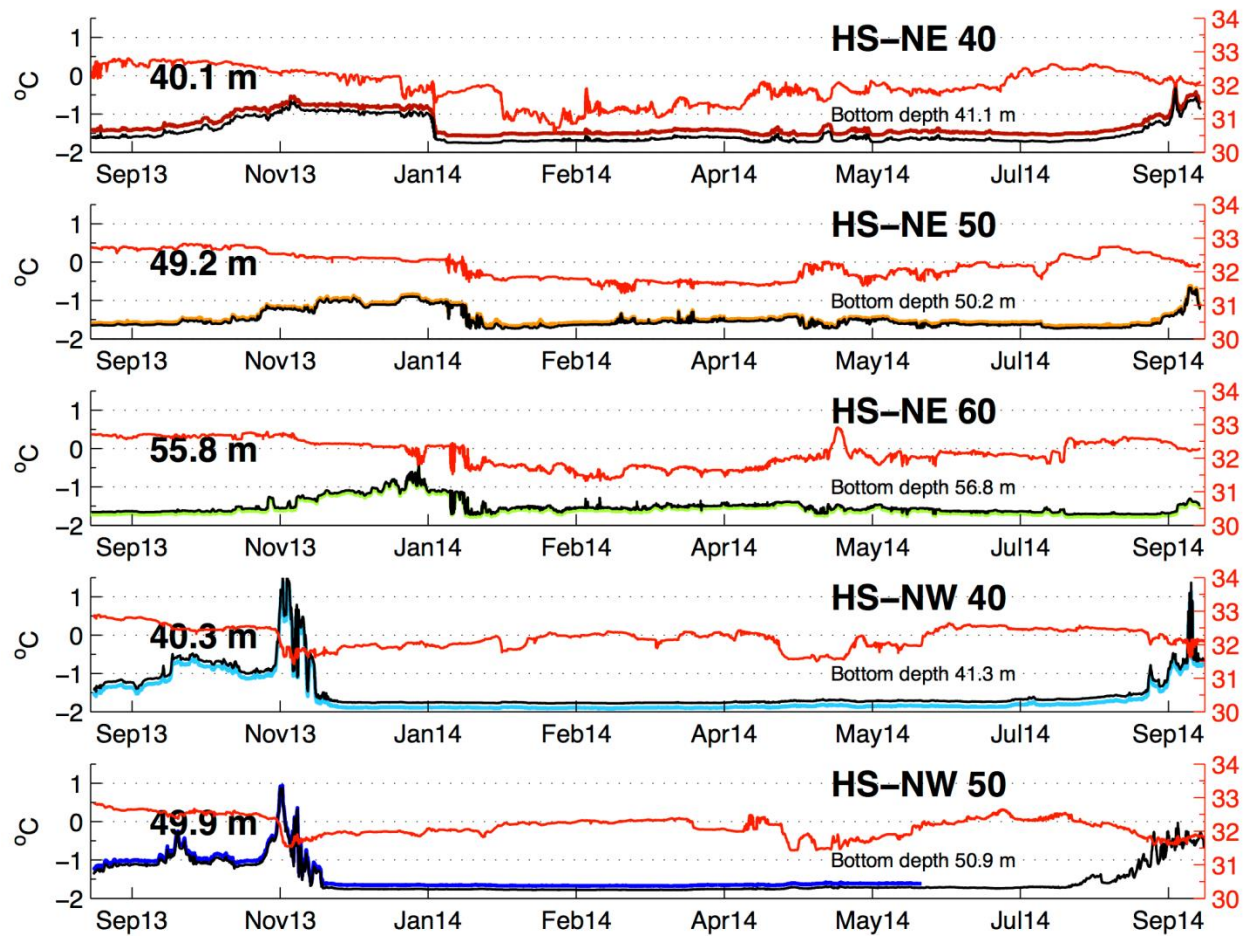
The mid-depth temperature record reached its maximum in December and then decreased to the freezing point in early January. That decrease was most likely due to local freezing at the surface and convective mixing. Nevertheless, the mixing was insufficient to penetrate entirely to the bottom. Mid-depth temperatures remained at the freezing point through early June but began to increase at about the same time that the bottom temperatures collapsed to the freezing point. We speculate that the mid-depth temperature increase may be associated with penetrating solar radiation as sea ice begins breaking up and meltponds allow solar radiation to penetrate through the ice and into the water column (Light et al., 2008).

An important feature of the mid-depth temperature and salinity records is the signature of very high-frequency oscillations. These were present throughout fall, and especially from November through early January. We contend that the MicroCat at 23 m depth was very likely in the midst of a strong pycnocline and that these high frequency fluctuations are internal wave signals.

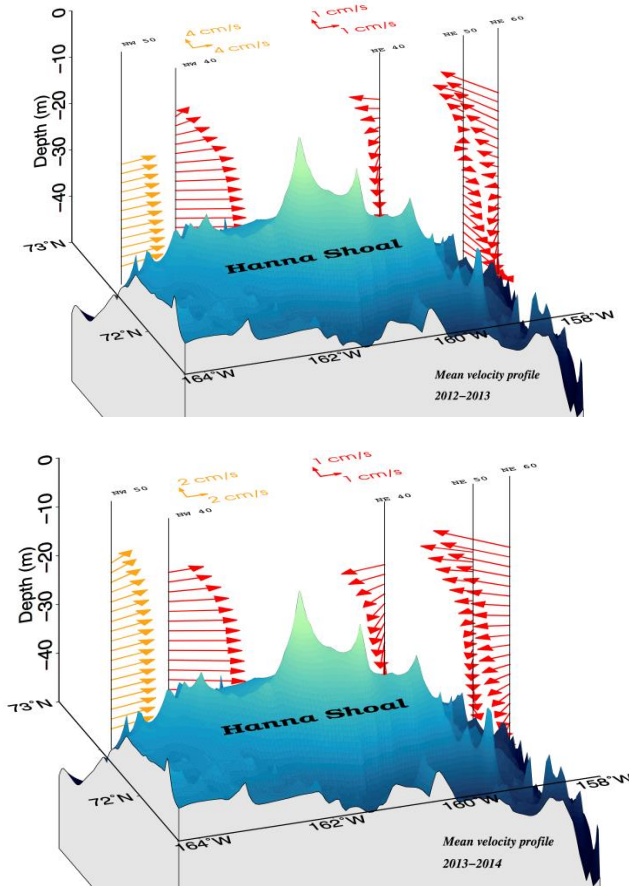
The bottom temperature and salinity records from the 2013 – 14 HSNE deployments (Figure 26) show the same basic seasonal evolution in temperature and salinity as was observed in 2012 – 13. However, the seasonal evolution was quite different at the HSNW moorings (Figure 26). The annual maximum in temperature occurred in mid-November 2013, nearly two months earlier than in the previous year. Temperatures then dropped to the freezing point in early December and remained at the freezing point into July. These differences may be related to the differences in ice concentration between fall 2012 and fall 2013 as discussed in relation to Figures 11 – 13. In 2012, we surmised that the northerly winds rapidly advected ice over the both northeastern Chukchi Sea with coverage being spatially uniform at ~100% by mid-November. In 2013 by contrast, the development of 100% ice cover was slower and included episodic advance and retreats before finally setting up. Moreover, 100% ice cover developed sooner on the east side of the Shoal than in the Central Channel and northwest side of the Shoal. These differences in ice cover (in conjunction with the assumed differences in stratification) on either side of the Shoal would lead to earlier cooling at the HSNW moorings compared to the HSNE moorings.



**Figure 25.** Time series of bottom temperature and salinity from the COMIDA 2012 – 13 mooring array.



**Figure 26.** Time series of bottom temperature and salinity from the COMIDA 2012 – 13 mooring array.

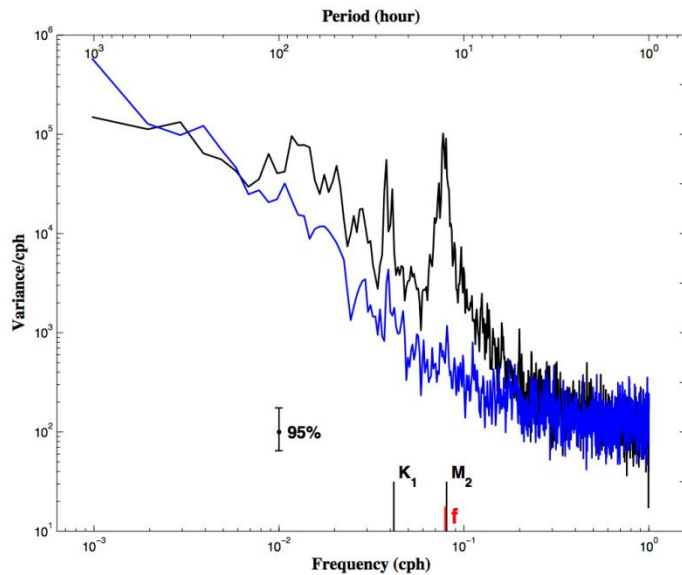


**Figure 27.** Mean vertical profiles of velocity for the 2012 – 13 (top) and 2013 – 14 (bottom) deployments.

We conclude this section with two summary figures that show the mean velocity profiles at all HS mooring sites for 2012 – 13 and 2013 – 14 (Figure 27). These show that the velocity shear was greater on the eastern of Hanna Shoal than on the western side in both years. On the eastern side of the Shoal, the surface flow was generally westward and the velocity vectors veered counterclockwise with depth. This veering amounted to  $\sim 180^\circ$  at HSNE50-12 but closer to  $90^\circ$  at the other HSNE moorings. On the western side of the Shoal the flow tended to be more unidirectional with current magnitudes increasing with depth. Note that the large shear on the northeastern side of the Shoal explains the weak vertically-averaged flow. There may be several reasons for the difference in mean shear on either side of the Shoal. First, some of the shear differences may be associated with differences in surface stress, especially if the ice at the NWS moorings was less mobile than the ice on the eastern side of the Shoal. Horizontal density gradients, associated with either fronts and or sloping isopycnals, will produce a geostrophic shear via the thermal wind (with the degree of veering proportional to the strength of the horizontal density gradients.) The counterclockwise veering at HSNE50 implies that water densities increased moving westward toward the Shoal. This implies the existence of baroclinic pressure gradients that, on their own, would drive a vertically-sheared counterclockwise, flow around the eastern side of Hanna Shoal. If this baroclinic pressure field exists, then it works in opposition to the barotropic (and geostrophic) motion associated with the clockwise flow around Hanna Shoal.

### 3.3. High-frequency current variations

Thus far we have emphasized the low-frequency current variations and differences in the circulation on either side of Hanna Shoal. There are also important spatial and seasonal differences in the higher-frequency currents, especially those associated with near-inertial motions. Figure 28 shows the rotary spectra at 45 m depth from HSNE50-12, which is typical of the rotary spectra at other locations. At low-frequencies the variance is equally distributed between clockwise (CW) and counterclockwise (CCW) current components. At periods  $<1$  day, CW energy dominates the spectrum, especially at the inertial ( $f$ ) and semi-diurnal ( $M_2$ ) tidal frequencies. Our sampling rate was insufficient to resolve the inertial and semi-diurnal tides. Consequently harmonic analysis for the purposes of isolating the  $M_2$  tide will be biased by contamination from inertial motions. Inertial energy is intermittent, however, whereas the semi-diurnal barotropic tide is periodic and deterministic. Wavelet analysis allows determining how energy in a particular frequency band changes through time. We applied rotary wavelet analyses to our data to distinguish periods of enhanced inertial energy from periods when inertial motions were absent or subdued. We focused on the CW component (because inertial and  $M_2$  currents rotate clockwise) and identified periods when inertial motion was statistically different from background energy levels.



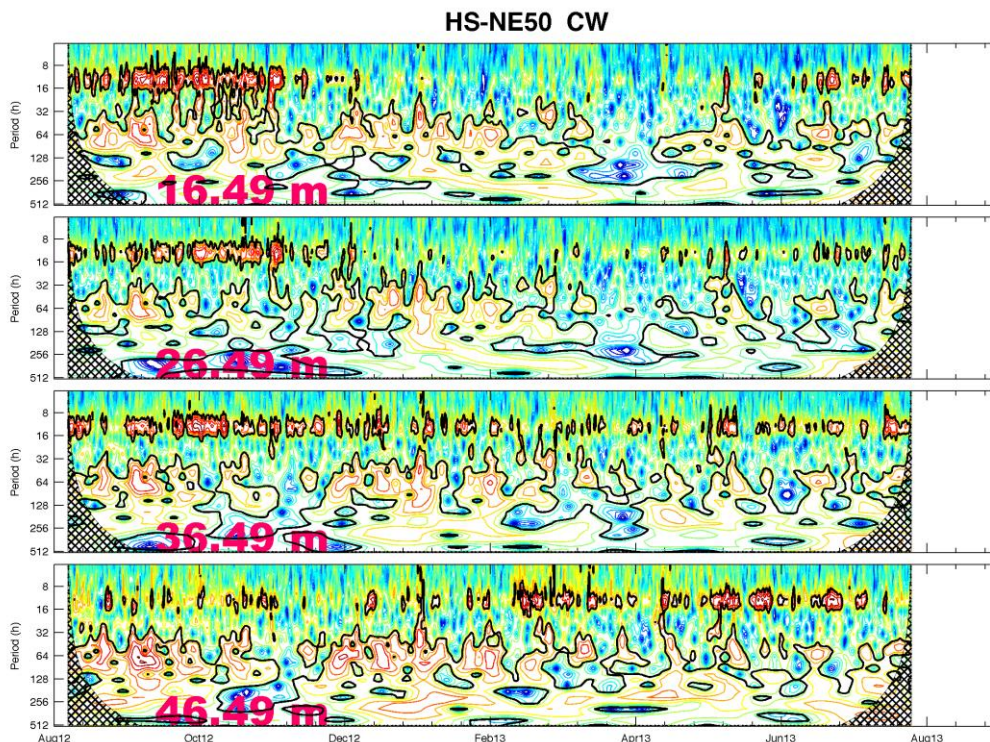
**Figure 28.** Rotary spectra of currents at 45 m depth from HSNE50-12 consisting of clockwise (black) and counterclockwise (blue) spectral components. The symbols  $K_1$ ,  $f$ , and  $M_2$  denote the diurnal tide, inertial, semi-diurnal tide frequencies, respectively. The width of the 95% confidence interval (95%) for the spectral estimates is included.

Figure 29 shows an example of the wavelet analyses for several depths for HSNE50-12. Inertial energy, contained within the 8 – 16 hour period band, was observed at all depths, and while highly intermittent varied seasonally and was a maximum in fall.

Figure 30 shows examples of the wavelet analyses from HSNE40 and HSNW40 for the 2012 – 13 deployment and from HSNE 50 and HSNW50 for the 2013 – 14 period. Two key results of these analyses are that a) the near-inertial energy tends to decrease when sea ice is present on both sides of Hanna Shoal and b) there is more inertial energy on the northeast side of Hanna Shoal than on the northwest side of the Shoal. These results are common to both years. The general reduction in inertial wave energy in the presence of ice may be due to the ice containing most of this energy and perhaps dissipating it through ice-ice interactions. It is not clear why



there are differences in inertial wave energy on either side of Hanna Shoal, although we noted earlier that the mean ice velocities were smaller at the HSNW moorings than at the HSNE moorings. If the ice on the NW side of Hanna Shoal was less mobile than the ice on the east side of the Shoal, then the reduction in ice mobility could impede inertial wave generation.

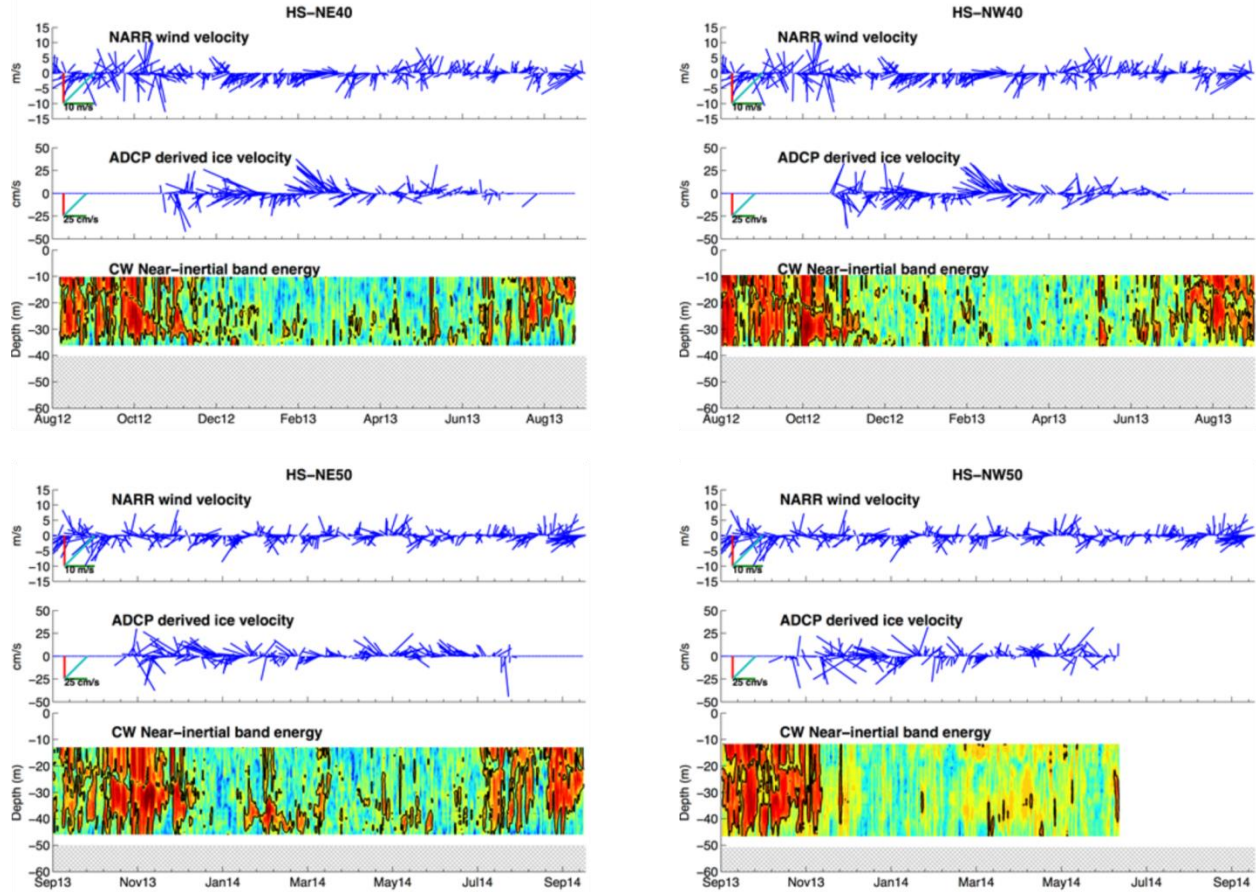


**Figure 29.** Wavelet analysis results for the clockwise (CW) spectral component at HSNE50-12. The inertial band lies within the 8 – 16 hour period. Periods when the energy levels are significantly greater (at the 95% level) than background are enclosed by black contours.

### 3.4 Hydrography

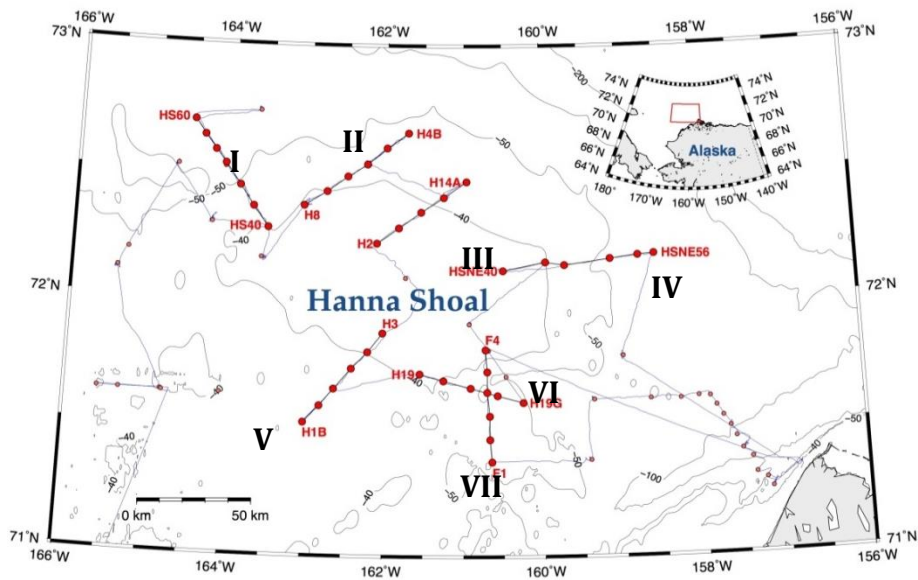
The presentation of shipboard hydrographic data relies on two different sources: the data sets collected under the auspices of the COMIDA program from the USCG *Healy* and data sets collected by other programs including those supported by BOEM and the oil industry. We supplement the *Healy* data with that from other programs, because the *Healy* sampling approach did not permit acquiring data to form quasi-synoptic hydrographic sections, which are most helpful in understanding the circulation and water mass distribution.

The *Healy* CTD stations occupied in August 2012 and 2013 are shown in Figures 31 and 32. Note that in 2013 the sampling extended across the shelf and shelfbreak to the northeast of Hanna Shoal. We constructed potential temperature-salinity ( $\theta/S$ ) diagrams for each cruise (Figures 33 and 34) as an aid in identifying the various water masses that were present based on the Coachman et al., (1975) nomenclature. There were four water masses present in both years: Alaskan Coastal Water (ACW), Bering Sea Water (BSW), meltwater (MW) and winter water (WW). In addition Atlantic Water (AW) was observed in 2013 only.

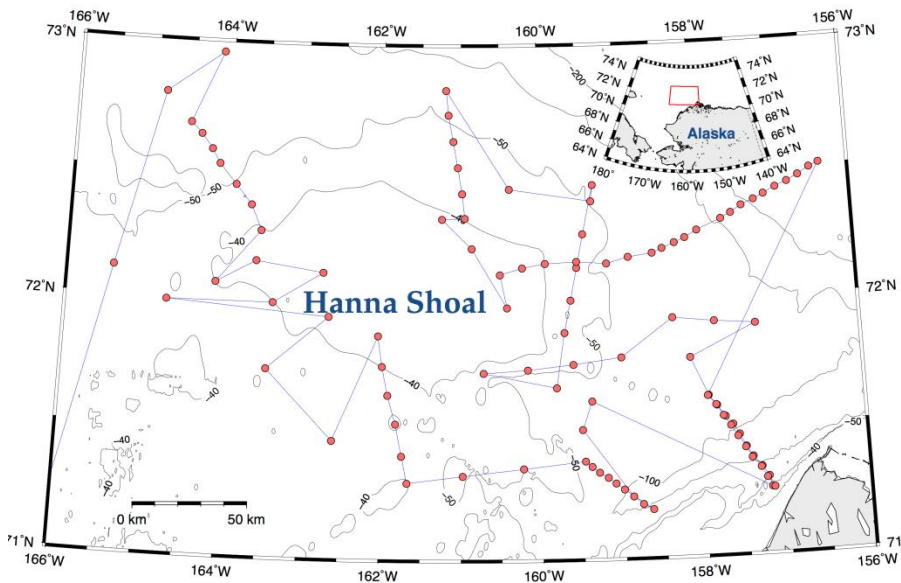


**Figure 30.** Wavelet analysis from the 2012 – 13 deployments of HSNE40 (upper left) and HSNW40 (upper right) and HSNE50 (lower left) and HSNW50 (lower right). In each panel the time series includes the wind the ice velocity vectors. The lowest panel consists of the time series as a function of depth of clockwise (CW) energy in the near-inertial wave band (8 – 16) hours.

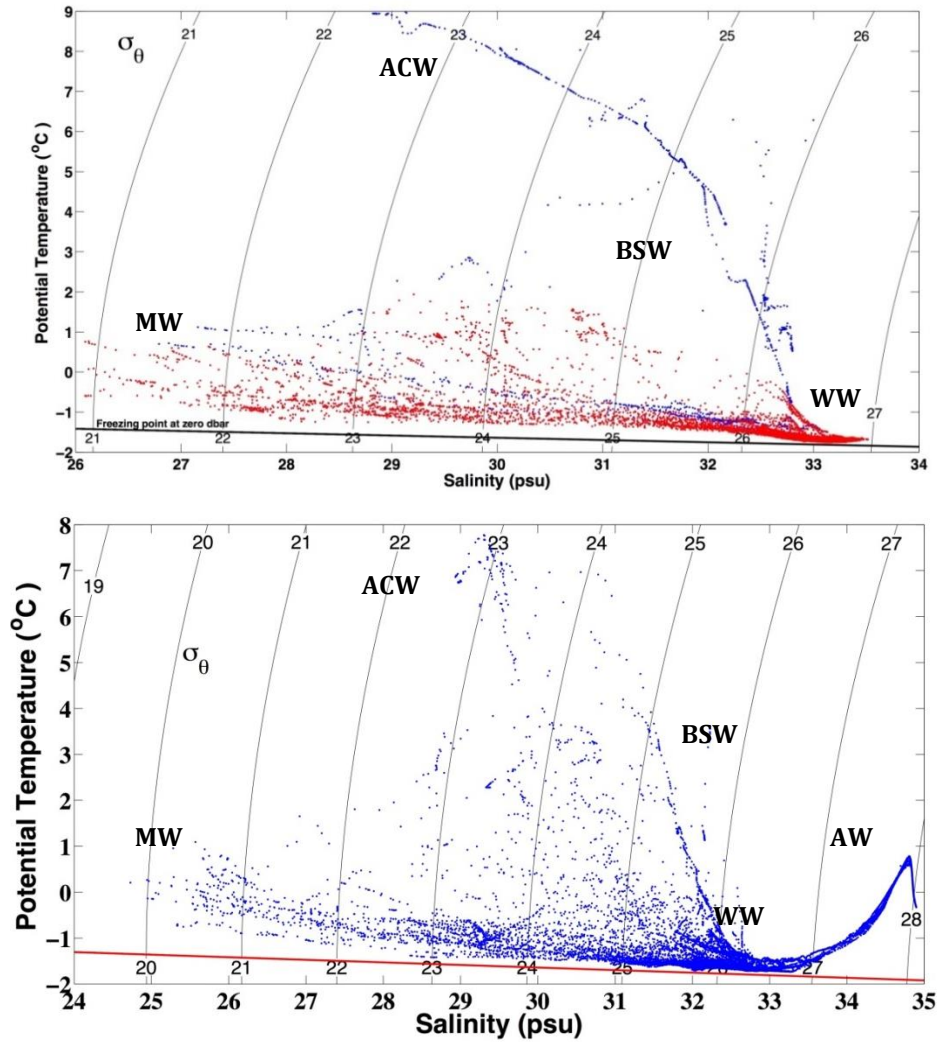
ACW is fresh ( $<31.5$ ) and the warmest ( $\geq 5^{\circ}\text{C}$ ) water mass. In general it occurred closest to the coast and within Barrow Canyon. BSW is saltier ( $31.5 - 32.5$ ) and cooler ( $\leq 5^{\circ}\text{C}$ ) than ACW and was generally found in the Central Channel and south of Hanna Shoal. Both ACW and BSW are water masses that have flowed northward from Bering Strait during the summer. MW is cool ( $<1^{\circ}\text{C}$ ) and is the freshest ( $<30$ ) water mass. It is a result of ice melt and was found at the surface of nearly all stations. The freshest and coldest MW fractions were at stations with melting ice. WW is very salty ( $\geq 32.5$ ) and the coldest water mass with temperatures at or very close to the freezing point. WW is formed in winter due to salt rejection from growing ice. Finally, AW is the saltiest water mass having salinities  $>33.2$  and temperatures  $>-1.5^{\circ}\text{C}$ . AW spans a range of temperatures from  $-1.5^{\circ}\text{C}$  to  $\sim 1^{\circ}\text{C}$ . As is evident from the figure, each of these water masses tend to blend with one another to form intermediate products. Mixing occurs either vertically through the action of the winds or through horizontal exchange processes (e.g., Lu et al., 2015). The exceptions are the ACW in 2013 and the AW in 2014. The former was observed only in the surface waters in Barrow Canyon where it resided at depths shallower than the BSW and WW. The AW was located seaward of the shelfbreak and beneath the Arctic Ocean's halocline, which contains shelf-derived WW.



**Figure 31.** COMIDA CTD stations occupied in August 2012. Roman numerals denote the transects used to construct vertical sections shown in separate Figures 34, 36 – 38.

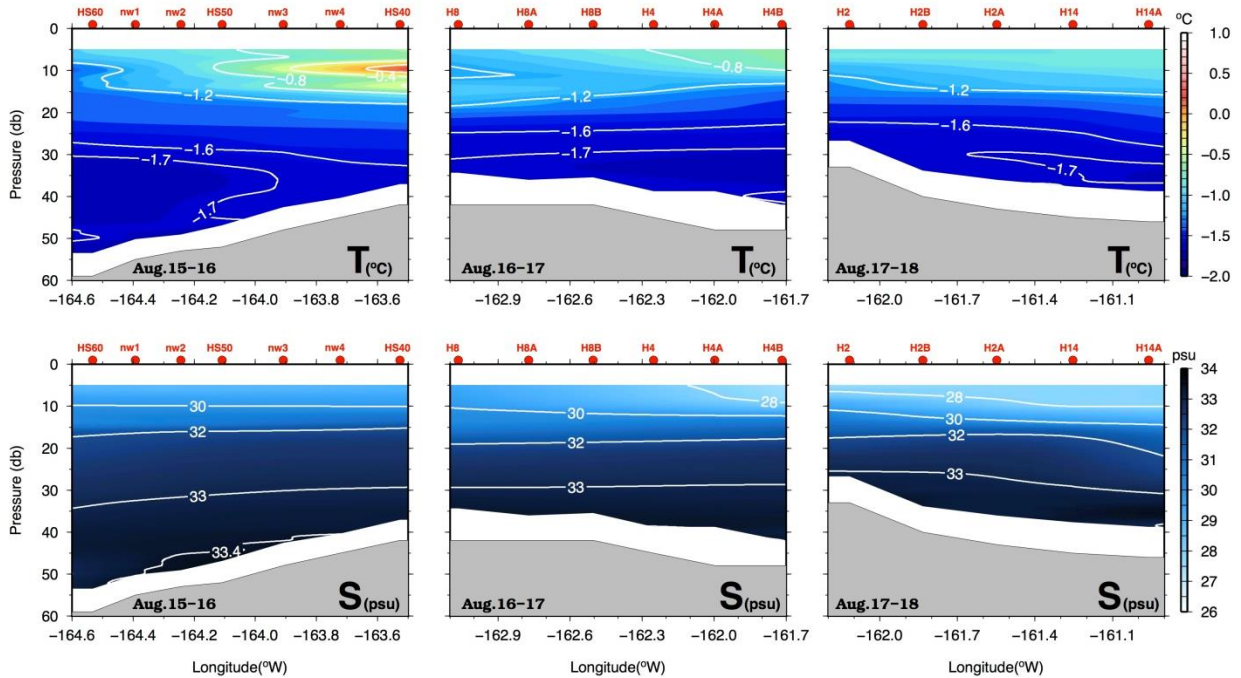


**Figure 32.** CTD stations occupied in August 2013.



**Figure 33.**  $\theta/S$  diagrams from 2012 (top) and 2013 (bottom).

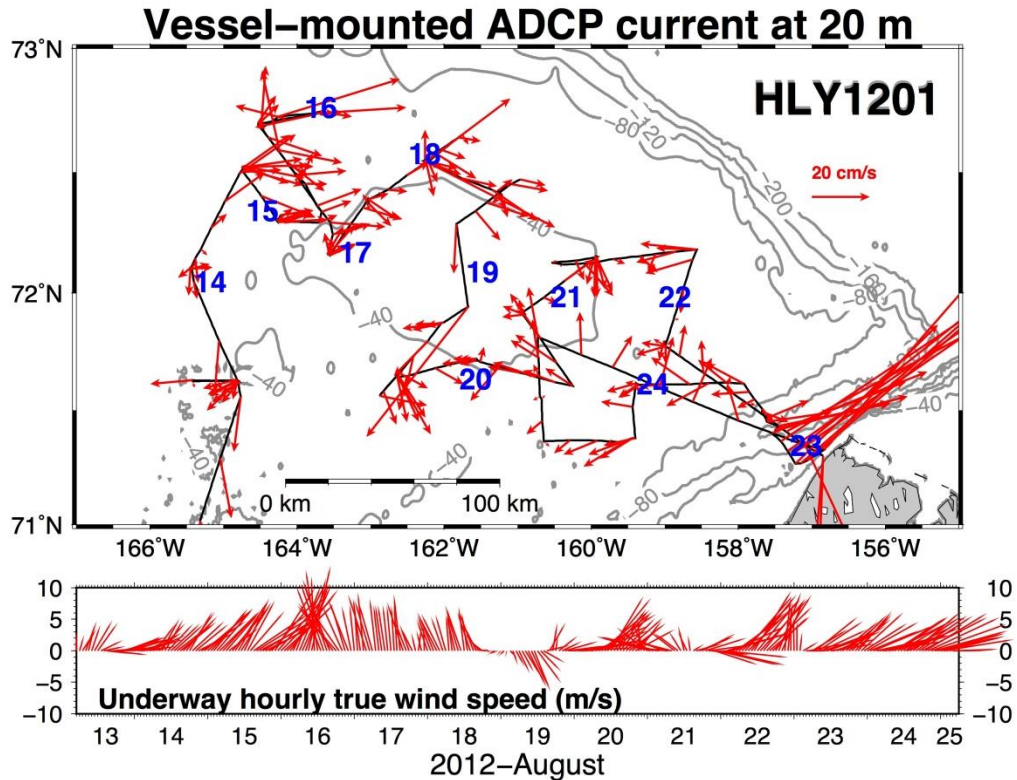
From the 2012 CTD survey we constructed seven hydrographic vertical sections along transects that surrounded the Shoal (Figure 31). Three of the sections (I, II, and III) were from transects occupied on the northwestern and northern sides of the Shoal (Figure 34), a fourth section (IV) was from the eastern side (Figure 36) and the remaining three sections (V, VI, and VII) were from transects distributed along the southern flanks of the Shoal (Figure 37). Several features are common to all sections. First below ~20 m depth the water column consists entirely of WW with salinities >32.5 and temperatures <-1.6°C. The most saline waters (>33.3) were found along transects VII and IV, south of and east of Hanna Shoal, respectively. Second the surface waters were all <30 and quite cold ( $\leq 0^\circ\text{C}$ ) indicating that these waters were from melting sea ice.



**Figure 34.** Vertical sections of potential temperature (top row) and salinity (bottom row). The sections are from Transects I (left), II (middle), and III (right; see Figure 31 for transect locations). Typical ice concentrations on these transects were 50 – 90%.

Third, the water column was strongly stratified due to the large vertical differences in salinity. The halocline was thin, amounting to a salinity change of  $\sim 4$  over 10 m depth, which corresponds to a density difference of  $0.4 \text{ kg m}^{-4}$  across the pycnocline. Fourth the isohalines (and isopycnals) tend to slope downward and away from the Shoal. Fifth, surface fronts, manifested as large horizontal salinity changes, were evident only along Transects II, V and VII, although these fronts were not well-resolved because of the coarse station spacing. Subsurface fronts were also present particularly on the east (Figure 36) and south sides (Figure 37) of Hanna Shoal along Transects IV and VII, respectively. In both cases these subsurface fronts were associated with the most saline winter waters observed during the cruise.

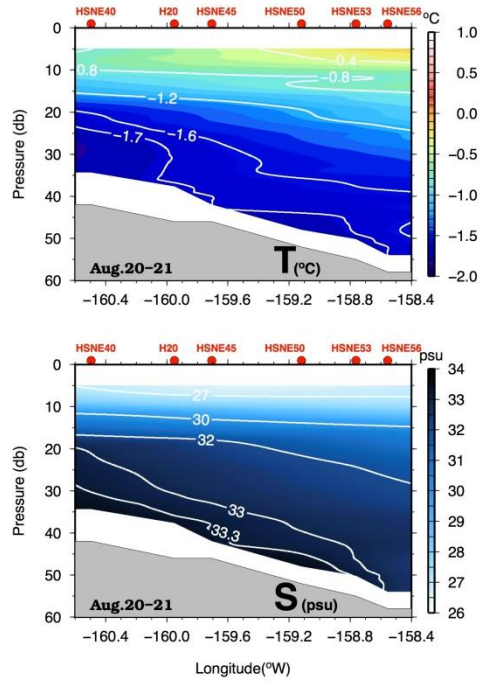
Surface waters showed considerably more variability in their temperature and salinity properties than deeper waters. Along Transects I – III (Figure 34) temperatures decreased moving northward and away from the Shoal. For example the maximum temperature ( $\sim 0^\circ\text{C}$ ) was observed closest to the Shoal and below the surface along Transect I. On the other two transects the temperature maxima were observed at the northernmost stations at the surface and were smaller. For example, the temperature maximum along Transect III was  $\sim -1^\circ\text{C}$ . Coincident with the decrease in the temperature maximum was a decrease in salinity, suggesting that these changes coincided with an increase in ice melt along the path of the temperature maximum. If this is the case, then the horizontal pathway of this warm water is eastward along the north side of Hanna Shoal and consistent with the mean eastward flow observed at moorings HSNW50 and HSNW40. It is also consistent with the VM-ADCP data at 20 m depth (Figure 35), which shows



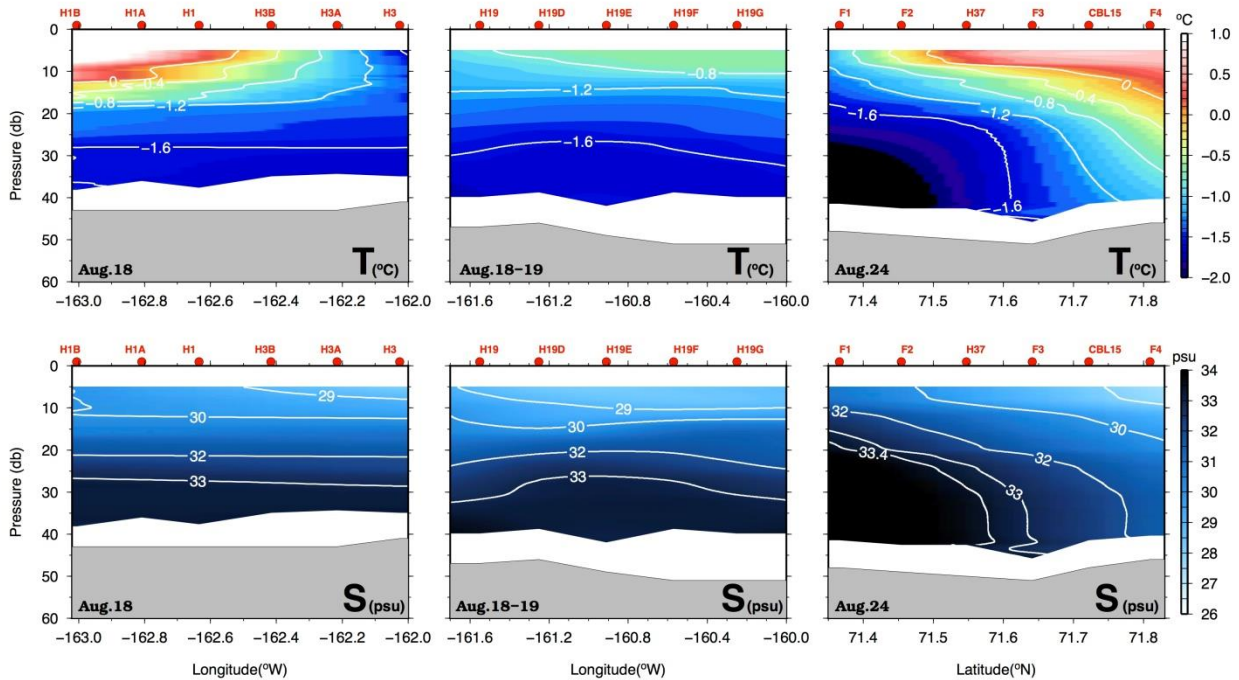
**Figure 35.** VM-ADCP vector at 20 m depth in August 2012. Blue numbers indicate the day in August when the data were collected. The bottom panel shows the wind vector.

a clockwise circulation of  $\sim 0.15 \text{ cm s}^{-1}$  around the northwest side of Hanna Shoal. A rough approximation of the heat flux divergence over the upper 20 between Transects I and III is  $50 \text{ W m}^{-2}$ , based on the temperature changes between the sections and the VM-ADCP data. This assumed ocean-to-ice heat flux is roughly half the clear sky net solar radiation flux of  $120 \text{ W m}^{-2}$ . Much of the region in which we operated, however, was subjected to dense fog, so that the ocean heat flux to the bottom of the ice may have been equivalent to the radiative flux at the ice surface.

The warm surface waters observed along the other transects were warmer than those along Transects II and III. These stations were occupied later in the cruise, however, and their elevated surface temperatures most likely reflect the effects of increased solar radiation.

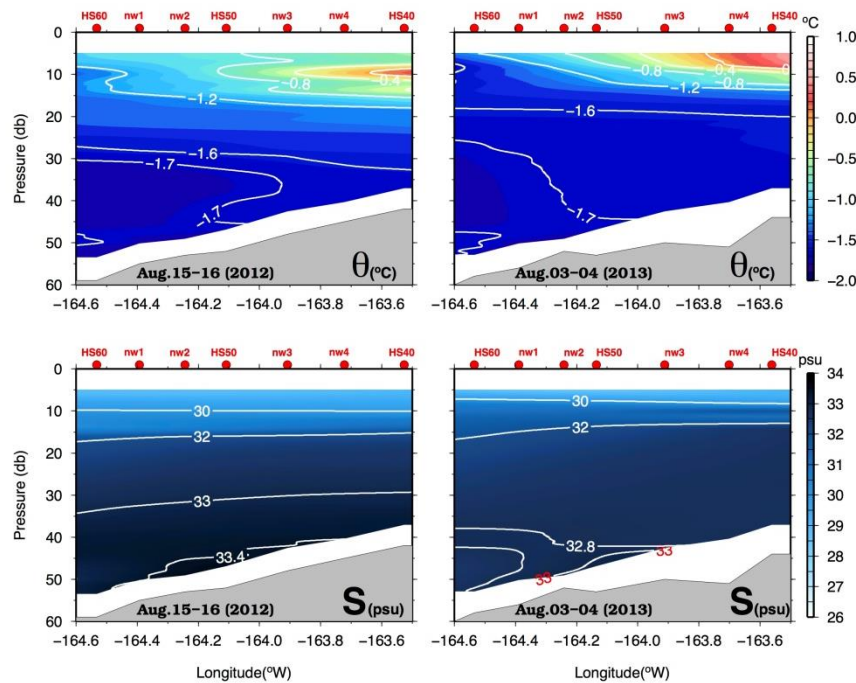


**Figure 36.** Vertical sections of potential temperature (top) and salinity (bottom) constructed from Transect IV (see Figure 31 for transect locations). Ice concentrations along this transect ranged from 30 – 70% ice cover.



**Figure 37.** Vertical sections of potential temperature (top row) and salinity (bottom row). The sections are from Transects V (left), VI (middle), and VII (right; see Figure 31 for transect locations).

In 2013, schedule constraints limited us to two transects for synoptic sampling. The first of these was similar in location to Transect I from the 2012 survey. Two important features emerge upon comparing the vertical sections from both of these occupations (Figure 38). The first is that the wedge of warm, surface waters occurred at identical locations, e.g. close to the northwest side of the Shoal. These waters, with a salinity of 30 – 31, are probably a mixture between warm, moderately salty Bering Sea Water (BSW) and meltwater (MW). The origin of the BSW is the northward flow in the Central Channel. This notion is consistent with the northward and preferential erosion of sea ice in the Central Channel (cf. Figures 7 – 9) compared to the shelf regions immediately to the west and east of the Channel. The second point of interest is that the bottom waters in 2012 were considerably saltier (by ~0.5) than those in 2013. The reason for this is not completely clear, although when grounded ice occurs atop Hanna Shoal in winter, latent heat polynyas may form in the lee of the grounding (typically over the south side of the Shoal). The very heavy and broad distribution of grounded ice over Hanna Shoal in the winter of 2012 likely led to extensive polynya development in that year. In that case, vigorous ice growth would have led to salinization of the waters over and around the Shoal. If this was the cause for the salinity differences between these years then the summer observations imply that dense winter water tends to be trapped to the Shoal.

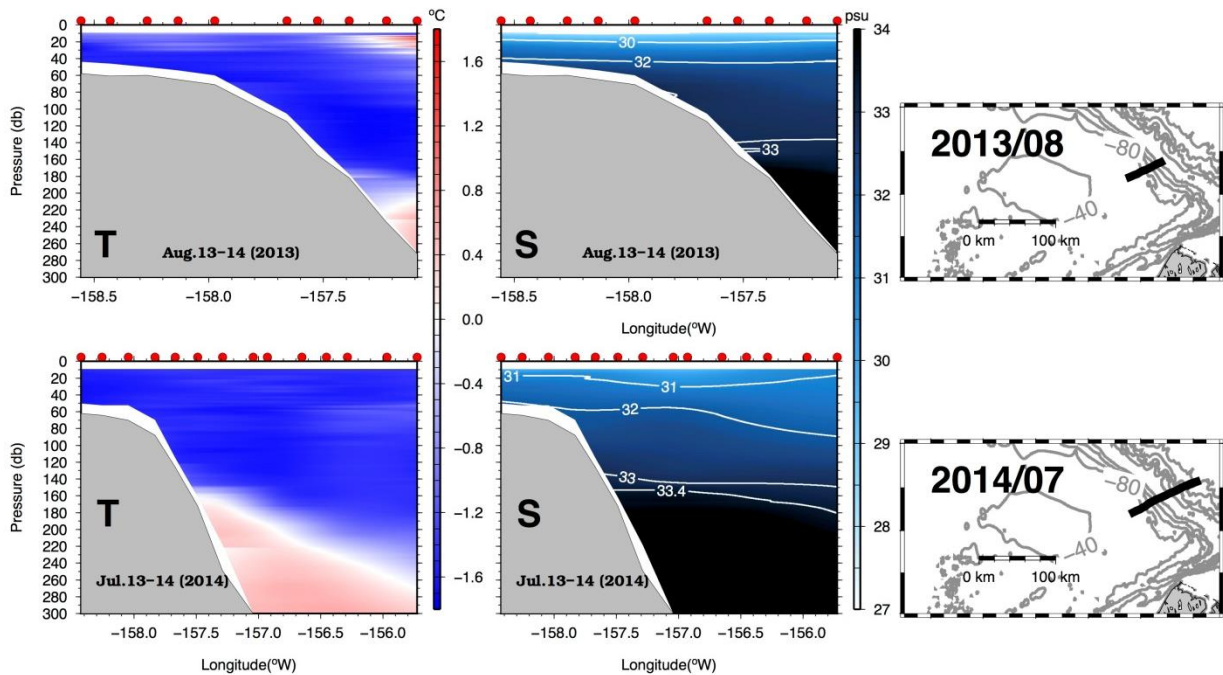


**Figure 38.** Vertical sections of potential temperature (top row) and salinity (bottom row) from along Transect I in 2012 (left) and 2013 (right).

During the August 2013 COMIDA cruise, we occupied a CTD transect that crossed the shelfbreak along the northeast side of Hanna Shoal. The shelf and slope were partially ice-free at this time (Figure 9). In July 2014, Dr. Robert Pickart completed a CTD survey in roughly the same area. The temperature and salinity sections from each of these surveys are compared in Figure 39. In August 2013, the near-surface waters were strongly stratified (more so than in July 2014) due to low salinity (<30) waters. Upper ocean temperatures were > -1.0°C except offshore where surface temperatures were >0.0°C but <1.0°C. (We will address the possible sources of

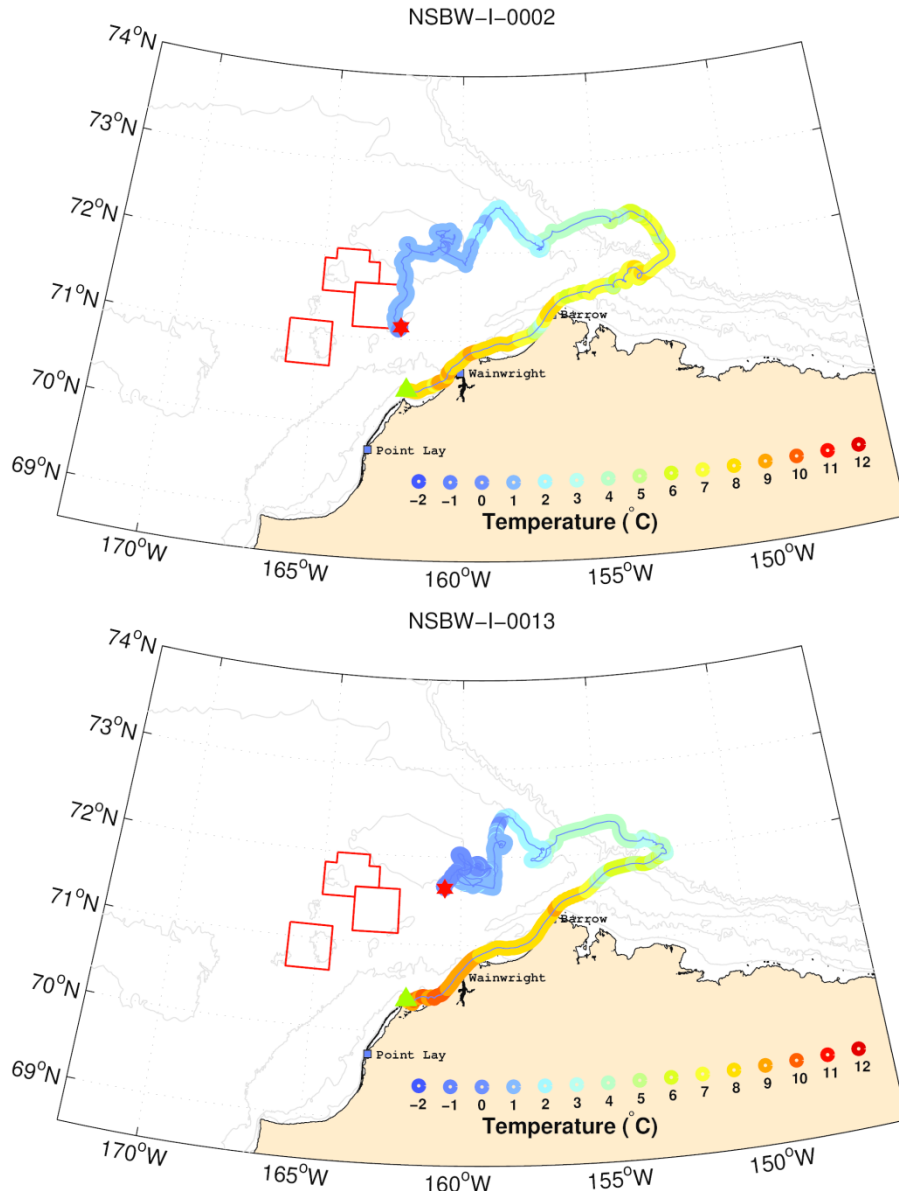


this warm water below.) Shelf salinities beneath the pycnocline were  $\sim 32$  in both years and temperatures were  $< -1.5^\circ\text{C}$ . The hydrographic structure also differed between these sections seaward of the shelfbreak ( $\sim 80$  m isobath) and at depths greater than 100m. In 2013, warm ( $> 0.0^\circ\text{C}$ ) salty ( $> 33$ ) water was confined to depths greater than 180m and the deep, warm isotherms were relatively flat or sloped downward toward the bottom. In July 2014, the isotherms and isopycnals had a pronounced upward tilt over the slope with warm ( $\sim 0.5^\circ\text{C}$ ), salty ( $> 33.1$ ) Atlantic Water observed at  $\sim 140$  m depth. The sloping of the isotherms and isohalines at this time are suggestive of active shelfbreak upwelling. Upwelling favorable winds occurred in June 2014, but winds were weak and variable in July. Hence the upwelling-structure observed in 2014 might not have been a local response to the winds, but rather the signature of an upwelling-coastal trapped wave that was propagating eastward along the slope. The July 2014 section also indicates that the 32 isohaline bows upward and the 33 isohaline bows downward suggesting an anticyclonic eddy centered at  $\sim 157^\circ\text{W}$  and within the Arctic Ocean's halocline. Such eddies are not unusual features along the continental slopes of the Chukchi and Beaufort seas (Weingartner et al. 1998; Spall et al. 2008; von Appen et al. 2012).



**Figure 39.** Vertical sections of temperature (left) and salinity (right) in August 2013 (top) and July 2014 (bottom) along the sections shown on the maps to the right of each section.

The source of the warm surface waters observed seaward of the shelfbreak in August 2013 is of some interest. We doubt that it was formed locally as a consequence of solar radiation. If that was the case, then we would have expected surface temperatures along the entire section to be nearly as warm. Instead we believe that this water is ACW advected westward from the mouth of Barrow Canyon. We base our speculation on the behavior of a cluster of 13 drifters released near Icy Cape, Alaska, at the head of Barrow Canyon on 11 August 2012. Two of the trajectories



**Figure 40.** The trajectories of two of 13 drifters released near Wainwright Alaska on 11 August 2012. The trajectories are color-coded according to the sea surface temperatures measured by the drifter and given by the scale on the map.

are shown in Figure 40 (and the other trajectories can be found at University of Alaska, School of Fisheries and Ocean Sciences web site ([http://dm.sfos.uaf.edu/chukchi-beaufort/data/floaters/float\\_map\\_2012.php](http://dm.sfos.uaf.edu/chukchi-beaufort/data/floaters/float_map_2012.php))). During the first week the drifters moved ~400 km northeastward to the mouth of the canyon.

During this time the temperatures decreased from ~10 to 5°C. During the next week they drifted westward along the Chukchi continental slope and temperatures decreased to ~3°C. Over the next month, several of the drifters moved back onto the shelf to the east of Hanna Shoal where they slowly meandered over this portion of the shelf before dying. It is clear from both the trajectories and the drifters' SST records that ACW water is at least occasionally advected

westward from Barrow Canyon along the Chukchi shelfbreak and onto the shelf east of Hanna Shoal. Aside from the heat brought onto this portion of the Chukchi Sea shelf, the ACW also carries relatively fresh water so this flux may also impact the local salt budget.

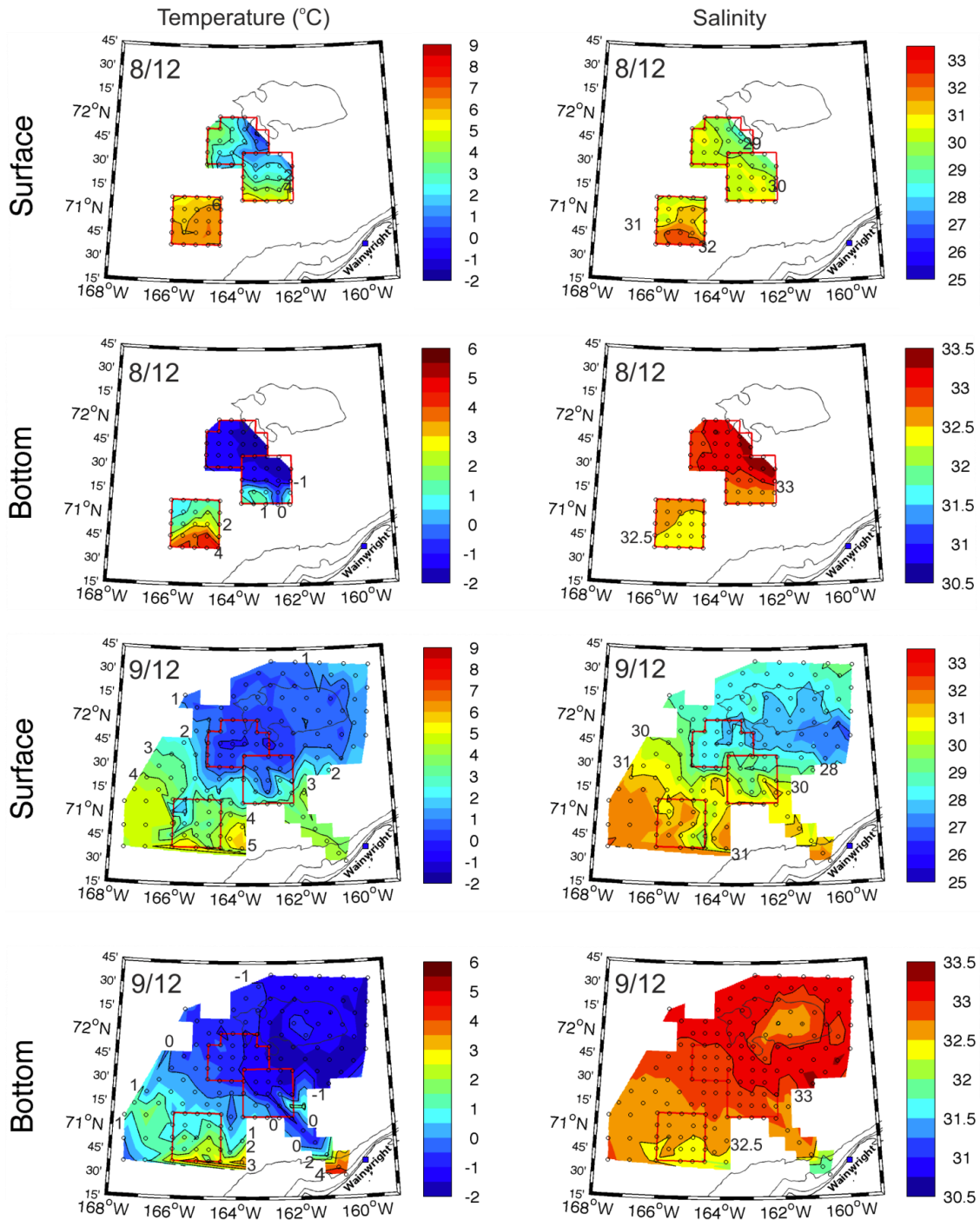
Time constraints prevented us from conducting extensive CTD surveys south of Hanna Shoal in both years. In order to place the COMIDA CTD data in a broader spatial and temporal context, we use hydrographic data from other BOEM-supported studies and the industry-supported CSESP program to show that the region south of the Shoal is different in several noteworthy respects from the shelf to the north of the Shoal. We will also use these data sets to outline some of the large interannual variability in hydrography that can occur around Hanna Shoal (and presumably the Chukchi Sea shelf).

We begin by examining plan views of the vertical average of the upper and bottom 10 m of the water column in both August and September 2012 (Figure 41). In August the surface waters between 70° - 71°N, and 164° - 165°W were warm (6°C) and moderately salty (31 – 32). Bottom waters were slightly colder and saltier, but both water masses are consistent with this being BSW. North of this location and over the south flank of Hanna Shoal, the surface waters were cooler and fresher, suggesting mixing between MW and BSW. In contrast the bottom waters were WW as these were very cold and salty. The more complete coverage from September 2012 underscores the broad spatial extent occupied by the MW at the surface. The BSW distribution was also quite broad as it extended northward in the Central Channel along 166°W as well as eastward toward the coast at Wainwright. Overall these data suggest a zonally-elongated front that ran eastward along about 71.5°N from the southwest edge of Hanna Shoal to the head of Barrow Canyon. The hydrography collected by the 2013 CSESP surveys was broadly similar to that of 2012 in terms of the distributions of water masses and locations of the MW/BSW frontal system (Weingartner et al., 2014).

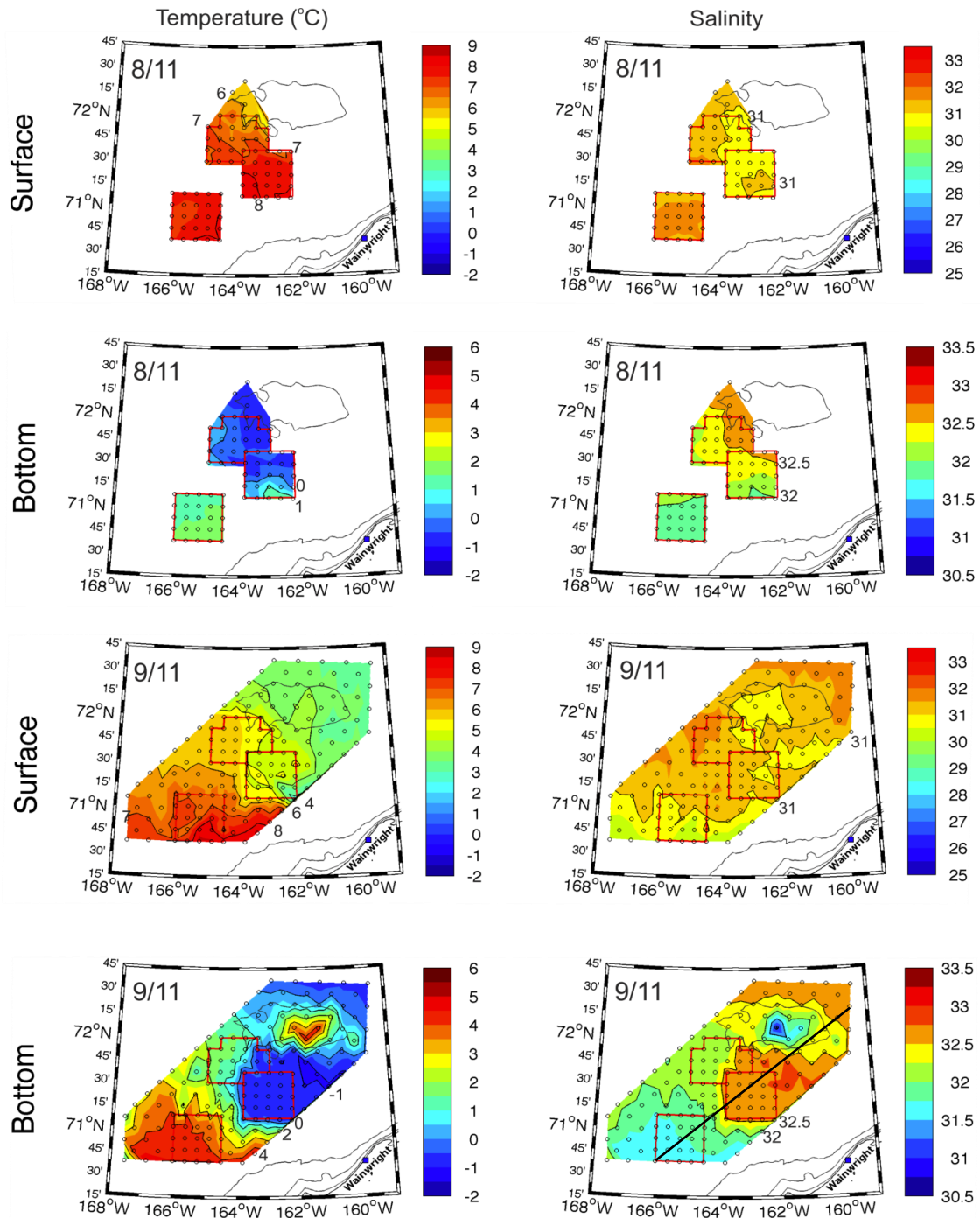
In contrast, the situation in 2011 was quite different in several significant ways (Figure 42). In contrast to 2012, the surface waters in both August and September were horizontally homogeneous and consisted of BSW. The absence of MW is consistent with the very early retreat of sea ice over in 2011 (Figures 6 and 9) and also resulted in the absence of surface fronts. In August the bottom waters between 70° - 71°N and 164° - 165°W were BSW, while bottom waters north of that location and along the southern side of Hanna Shoal consisted of WW. In September, BSW protruded prominently northward in the Central Channel, occupied the shelf south of ~71°N, and occurred over the bottom atop the shallowest portions of Hanna Shoal. WW occurred elsewhere including within a prominent lobe that extended westward toward the Central Channel and along the south side of Hanna Shoal. A prominent frontal system delineates this lobe of WW from the BSW.

An alternative perspective on these data is provided in Figure 43 which shows two, 300-km long vertical sections occupied in September 2011 and 2012. The sections ran from the southwest (beginning at ~70.5°N, 166°W) to the northeast (ending at ~72.5°N, 160°W) along the northeast side of Hanna Shoal (their location is shown in the lower right panel of Figure 42). In 2011 warm, moderately salty BSW occupied the uppermost 20 m over the entire area, while WW was confined to either side of Hanna Shoal. Fronts (primarily associated with temperature gradients) separated the BSW along the bottom over the southern portion of the section (south of km 100) from the WW to the north. In contrast, the 2012 section consisted of a strong, frontal system

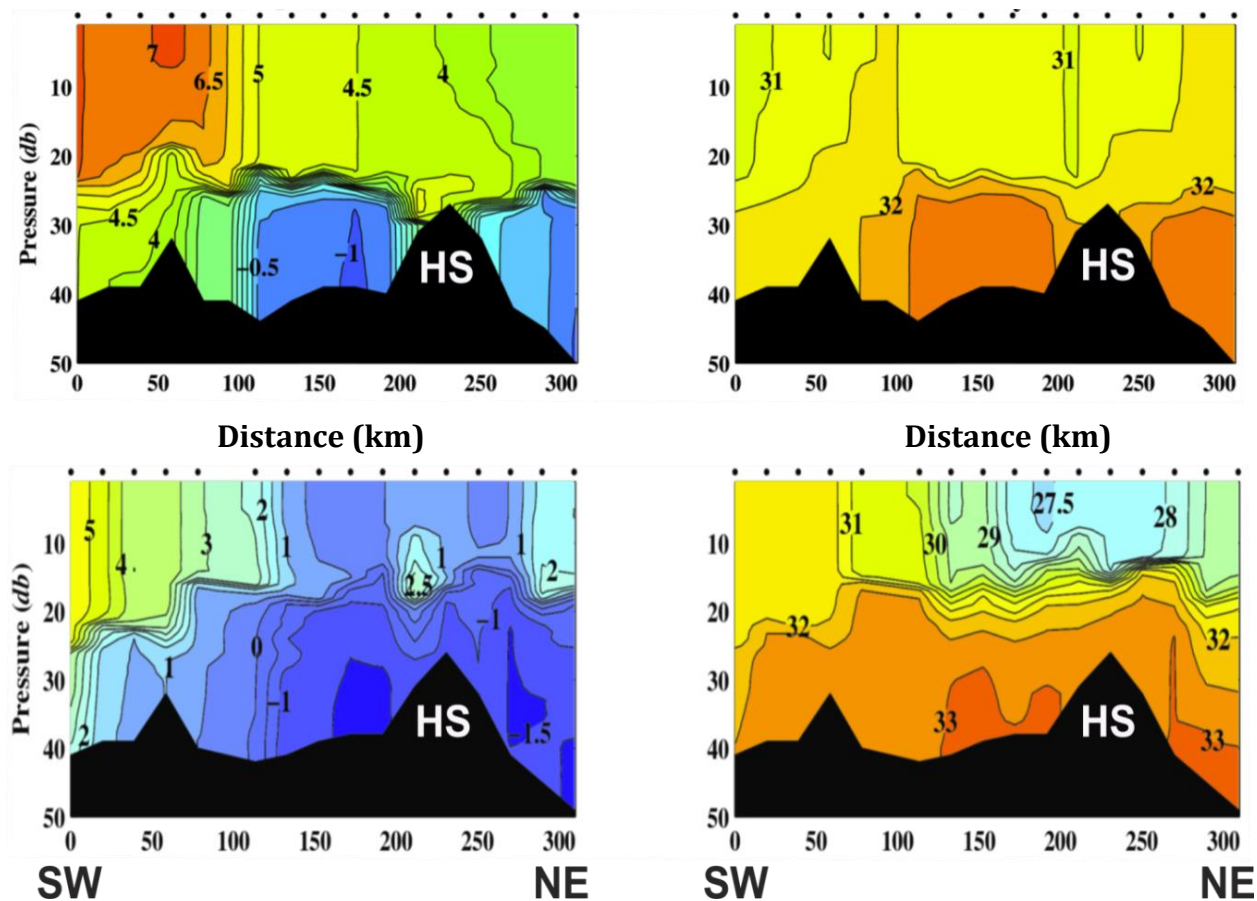
associated with the MW and BSW at km 140 in addition to weaker MW frontal systems at km 175 and km 200. Similar to 2011, the WW was primarily observed around Hanna Shoal. The sections also differ with respect to vertical stratification. In both years the stratification was dominated by salinity, however, in 2012 the stratification was twice as strong as in 2011. These interannual



**Figure 41.** Plan views of temperature (left) and salinity (right) in August and September of 2012. The plan views are based on averages of the upper and bottom 10 m of the water column.



**Figure 42.** Plan views of temperature (left) and salinity (right) in August and September of 2011. The plan views are based on averages of the upper and bottom 10 m of the water column. The black line in the bottom right panel shows the location of the vertical sections shown in Figure 43.

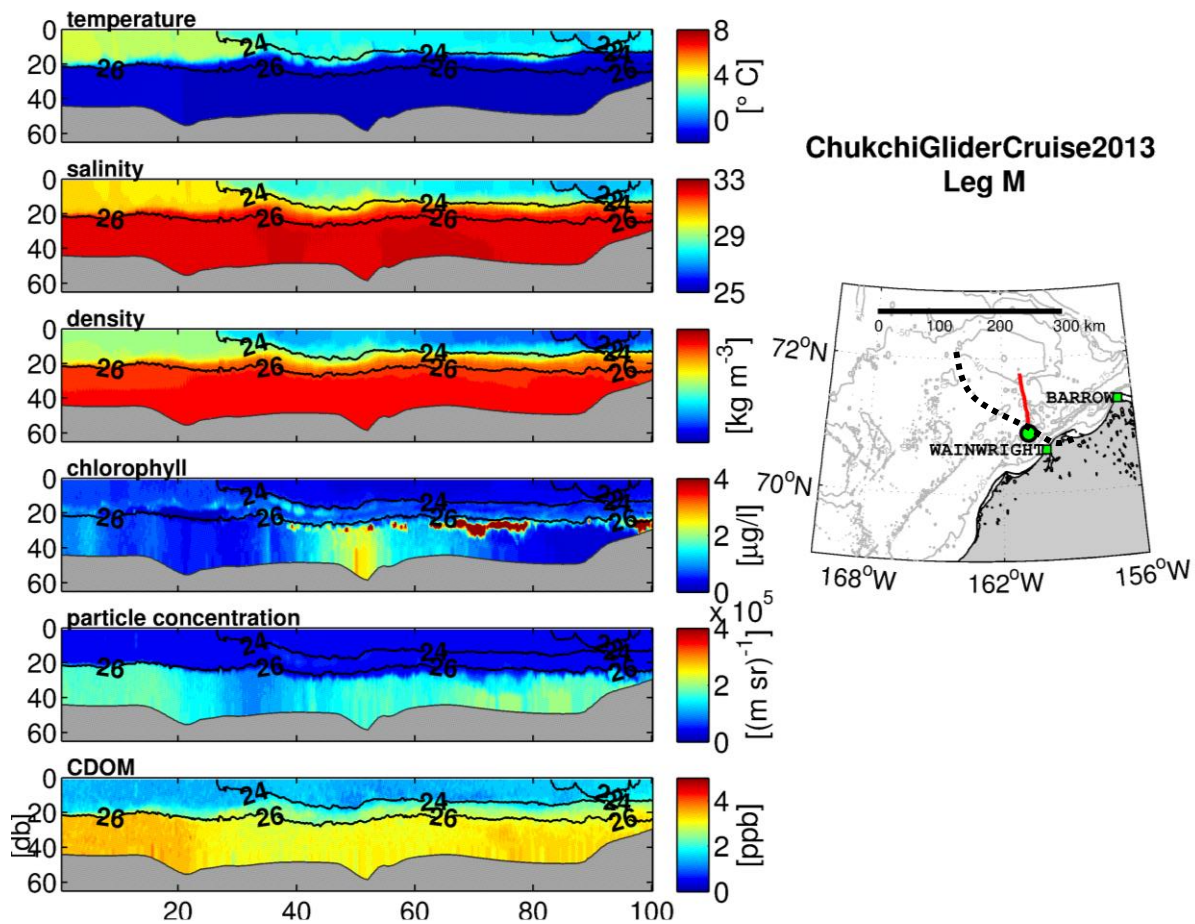


**Figure 43.** Vertical sections of temperature (left) and salinity (right) in September 2011 (top row) and 2012 (bottom row).

differences in stratification were due to the absence of MW in 2011 and its presence in 2012 (and in 2013).

Another important feature observed in the 2012 section was the presence, at km 225, of a “blob” of warm ( $\sim 2^{\circ}\text{C}$ ) water, which was enclosed by the upward-bowing of the 29 isohaline above the blob and the downward-bowing of the 32 isohaline below it. This feature is probably an anticyclonic, intrapycnocline eddy that formed via a baroclinic instability of the MW/BSW front (Lu et al., 2015). The eddies appear to be common features of these frontal systems and are an important agent for lateral mixing and as a potential heat source for the underside of ice (Lu et al., 2015). The coarse resolution of the CESP CTD sampling did not permit adequate horizontal resolution of these fronts. A more highly-resolved view of this front is shown in Figure 44, which was constructed from data obtained from the Acrobat towed-CTD data collected in September 2013 during the Norseman II recovery of the COMIDA moorings. The horizontal resolution of the hydrographic data on this section is  $\sim 250$  m and more than adequate to resolve the  $\sim 10$  km-wide MW BSW front centered at about km 30. Also included on the map to the right of the sections is a dotted line denoting the approximate location of the MW/BSW front as ascertained from CESP data and other Acrobat sections. We infer that the front is zonally-oriented and aligned along about the  $71.5^{\circ}\text{N}$  parallel. At its offshore end, the front very likely bends northward and parallels the Central Channel west of Hanna Shoal. It also bends northward along the western half of Barrow Canyon.

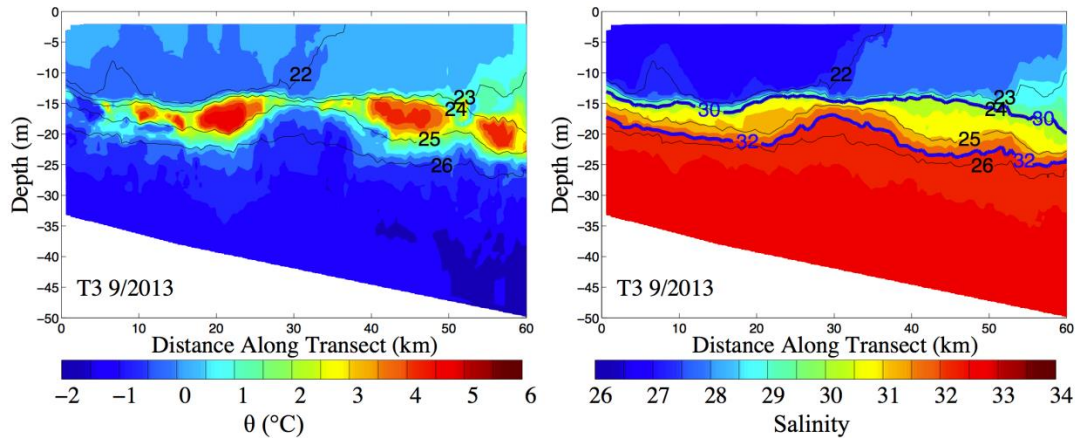
The figure also shows that there was a striking contrast in the chl *a* distribution to the south and north of the front. South of the front, the chl *a* concentrations were low and diffuse, but north of the front high chl *a* concentrations were compressed into thin sheets slightly below the pycnocline (the bottom of which coincides with the 26  $\sigma_t$  isopycnal). These sheets were not horizontally continuous, but instead quite patchy. The lack of chlorophyll south of the front (associated with the BSW) is because these waters are nutrient-poor on the northeast shelf in August; phytoplankton having consumed the nutrients in these waters during their transport northward from Bering Strait. MW is devoid of nutrients whereas the WW is nutrient-rich (Codispoti et al., 2005). By residing at the base of the pycnocline phytoplankton growth was presumably aided by the availability of nutrient-rich water while residing within the euphotic zone. These thin patches embedded in the pycnocline may be very productive from summer through late fall, with much of this fixed carbon sinking to the bottom given the generally weak currents in this area.



**Figure 44.** Vertical sections of (from top to bottom) temperature, salinity, density, chl *a*, particle concentrations, and CDOM (color dissolved organic matter) along the Leg M transect collected by the acrobat towed CTD unit in September 2013. The dotted line shows the approximate position of the MW/BSW front evident at km 30 on the section. The green dot shows the start of the transect, which corresponds to the left side of the section plots.

Figure 45 consists of vertical sections collected along the HSNW mooring line in September 2013 and provides another example of these eddy-like features. In this case several anticyclones were evident in the form of warm, intrapycnocline features encapsulated between the vertically-distended 30 and 32 isohalines. The temperature and salinity properties of these features clearly indicates a BSW source, because the waters above and below the pycnocline were MW and WW, respectively. Very likely these features arose due to frontal instability within the Central Channel.

We conclude with two other examples of these MW/BSW fronts. The first, shown in Figure 46, is a map of the weekly mean surface velocity vectors collected over the northeastern Chukchi Sea shelf during the week of 5 September 2012 from shore-based high frequency radars (HFR) in Barrow Wainwright, and Pt. Lay. The vector distribution suggests a convergence zone extending from west to east along about 71.5°N. North of this zone the surface flow is southward (and downwind based on the mean wind vector at Barrow during this time). South of the zone, the flow is northeastward. The convergence is roughly aligned with the position of the fronts discussed previously and appears to extend eastward to Barrow Canyon.

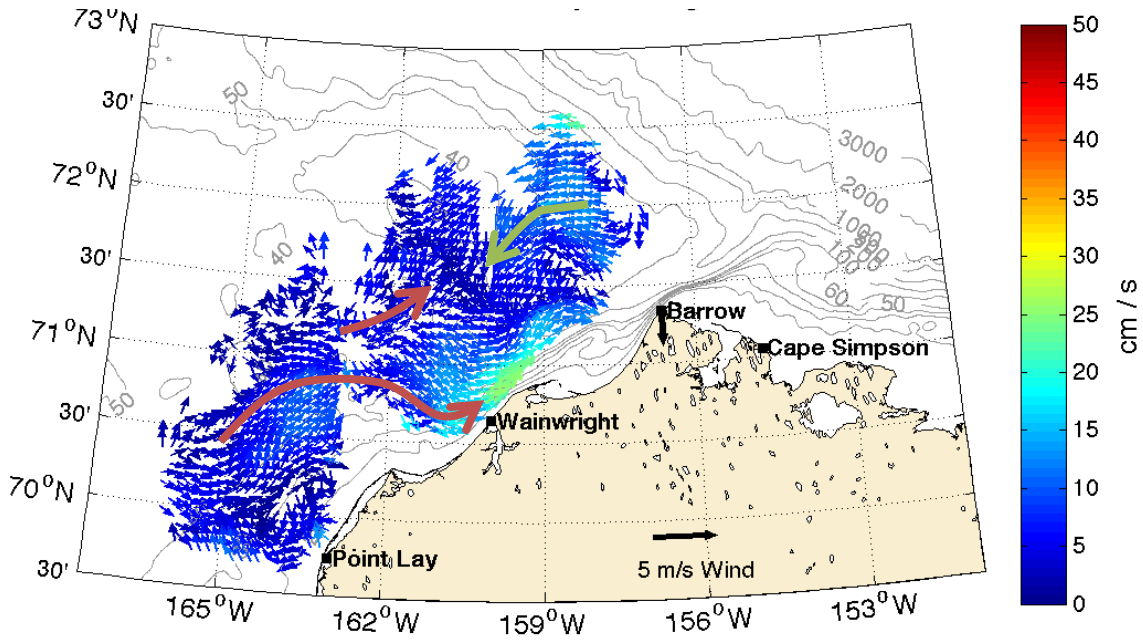


**Figure 45.** Temperature and salinity distribution along the HSNW mooring line in September 2013 (from Lu et al., 2015).

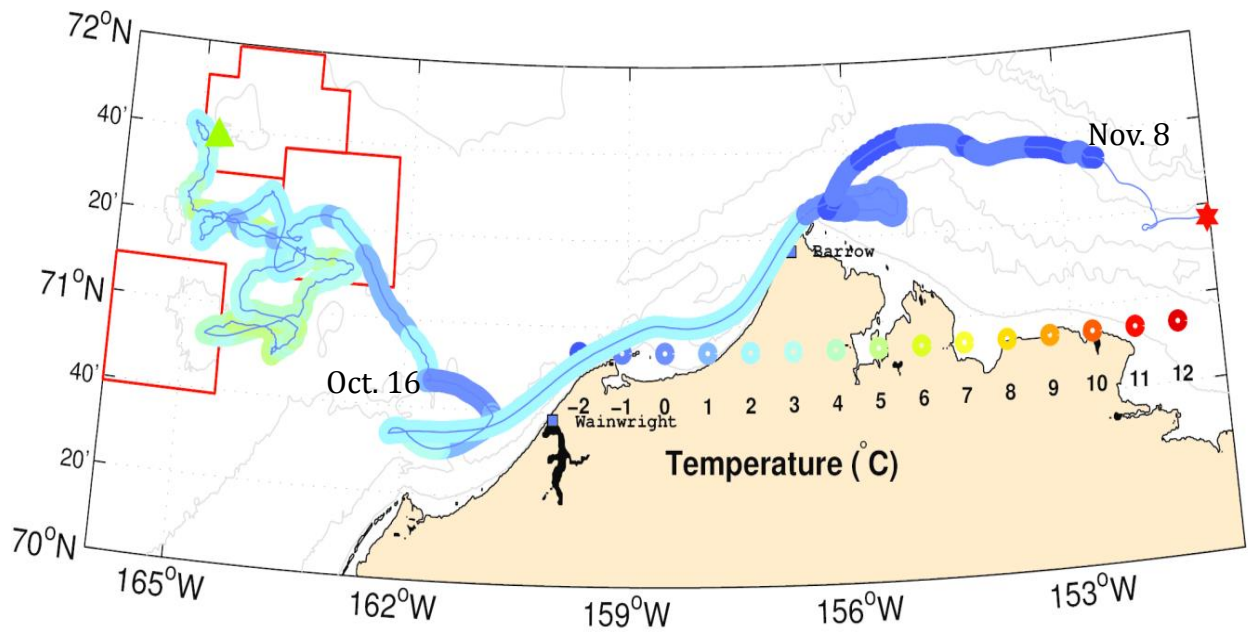
Surface current vector maps obtained in August and September 2011 showed no such features, which is consistent with the hydrography from that year. As might be expected the presence of mesoscale motions should yield differences in surface current variability. In 2011, the variance in both the zonal and meridional velocity components across the radar mask was half that for the same components in 2012. These differences cannot be attributed to differences in the wind regime between these two years for the variances in both wind vector components were identical in both years.

Figure 47 shows the trajectory of a 10-m drogued, satellite-tracked drifter that was released from the USCG *Healy* on 13 August 2012. Over its first 45 days the drifter's trajectory included a number of meanders and large excursions in SST, neither of which were associated with changes in winds. These variations in SST and trajectory path are suggestive (but not conclusive) that the drifter was entrained into mesoscale motions associated with frontal instability.





**Figure 46.** Mean surface current vectors for the week of 5 September 2012, as estimated from HFRs.



**Figure 47.** Color-coded (by SST) trajectory of a satellite-tracked drifter released at the location of the green triangle on 13 August 2012. The drifter's last reported position was on 15 November at the location of the red star.

## 4. Discussion and Conclusions

The goals of the physical oceanography component of the COMIDA program were to understand the time-varying circulation and water mass properties of the Chukchi shelf surrounding Hanna Shoal and to provide the physical context for the biological and chemical components of the program. In part our measurements were meant to address the results from numerical ocean circulation models (e.g., Winsor and Chapman, 2004; Spall, 2007) that suggested that mean circulation is clockwise around Hanna Shoal. We found that the ice and surface meltwaters are transported westward on average in response to the prevailing northeasterly winds. The vertically-averaged flow was eastward and parallel to the isobaths northwest of Hanna Shoal, in agreement with the models. Over the shelf to the northeast of Hanna Shoal the vertically-averaged flow was negligible or westward, in contrast to the models. These observations imply that there should be, on average, zonal convergence in the flow field north of Hanna Shoal. Presumably this convergence is associated with an off-shelf deflection of the eastward flowing water observed to the northwest of Hanna Shoal. Finally, in agreement, with the numerical models, the near-bottom circulation appears to be clockwise around the northwest and northeast flanks of Hanna Shoal. Other differences in the circulation characteristics between the northwestern and northeastern sides of Hanna Shoal included the enhancement in inertial energy and the greater vertical velocity shear of the sub-inertial flow in the east compared to the west.

There are several possible reasons for the differences in the circulation characteristics between the east and west sides of the Shoal. First the strong geostrophic, barotropic flow along the northwest side of the Shoal must weaken (although the transports should not change) proceeding clockwise around the Shoal because the isobaths diverge on the eastern side of the Shoal. Note that this weakening in the circulation implies a longer residence time for the waters east of the Shoal. This difference may be reflected in the chemical and biological composition of the water column and sediments. Second, the weaker geostrophic flow will be more susceptible to wind-driven reversals. In particular, these reversals will be confined primarily to the strongly, stratified surface layer. Recall that we inferred that the stratification eroded in early winter on the northwest side of Hanna Shoal, but remained strong and intact year-round over the shelf east of the Shoal. Third, the fall CTD data sets suggested that there may be horizontal density gradients, with less dense water moving eastward from the eastern side of Hanna Shoal. These density gradients will impel a counterclockwise baroclinic, geostrophic flow, via the thermal wind relationship, over the shelf east of the Shoal. If these density gradients prevail year-round they will compete against the clockwise barotropic flow.

The strong stratification, the deep clockwise barotropic motion, and persistent baroclinic pressure gradients should lead to greater velocity shear on the east side of the Shoal compared to the west side. Indeed, we found that the mean velocity profile on the shelf east of the Shoal had substantial shear, whereas the profile to the northwest of the Shoal had little shear.

These findings have significant implications on the disposition of various shelf water masses. The bottom waters to the northwest and northeast of Hanna Shoal vary seasonally in their composition. In late fall and early winter their temperatures were a maximum of from  $-1^{\circ}\text{C}$  to  $1^{\circ}\text{C}$  and their salinities were a minimum of 31 – 32.5. Shelf waters south of Hanna Shoal typically reach the freezing point temperature in October or November (Weingartner et al., 2005). The fact that the bottom temperatures north of Hanna Shoal were well-above the freezing

point indicates that these bottom waters had 1) originated earlier in the summer from south of Bering Strait and 2) had minimal exposure to the surface waters during their northward transit in fall. There are two possible pathways by which these waters reached the northwest side of Hanna Shoal: via the Central Channel or Herald Valley. The latter is the more circuitous route (see Figure 1) as it involves westward flow across the Hope Sea Valley, northward flow in Herald Valley, and then eastward flow across the outer shelf north of Herald Valley. We tentatively suggest that Herald Valley is the source of this warm water at depth (Woodgate et al., 2005; Pickart et al., 2010) in late fall and winter, because previous (albeit limited) measurements indicate that temperatures are at or near the freezing point in the Central Channel by mid-fall (Weingartner et al. 2005).

During our summer and fall CTD surveys the bottom waters around Hanna Shoal consisted of dense winter-formed waters. The mooring time series shows that these winter waters appeared northwest of Hanna Shoal in late January when the observed ice cover of 100% effectively insulated the ocean. Winter waters occurred northeast of Hanna Shoal only in the following summer, well after melting had commenced. This implies that at both locations dense water was advected into the region from elsewhere; either from ice formation regions well to the south of Hanna Shoal or from around the immediate periphery of Hanna Shoal when latent-heat polynyas form in the lee of grounded ice on the Shoal. Our summer CTD observations indicated that very salty (>33) and near-freezing waters were trapped around the Shoal in both summer surveys. According to A. Mahoney (University of Alaska, August 2015), satellite images indicate that grounded ice was atop the Shoal during the winters of both 2012 – 13 and 2013 – 14 and that there were (at least) occasional polynyas formed in the lee of the grounded ice. This dense winter water and the meltwater released from ice the following summer are key ingredients in the formation of the strong regional stratification. We argued that this stratification eroded in late January northwest of Hanna Shoal, some 2 – 3 months later than the breakdown of stratification on the shelf south of the Shoal (Weingartner et al., 2005). A surprising finding was that heavy stratification remained intact year-round on the shelf to the east of the Shoal.

Our understanding of the hydrographic conditions around Hanna Shoal was aided by the inclusion of hydrographic data obtained by surveys undertaken by other programs around Hanna Shoal, including those well to the south of Hanna Shoal and much later in the fall to the northwest and northeast of Hanna Shoal. These data sets showed that Bering Sea summer waters (Alaskan Coastal Water and Bering Sea Water) were often found south of  $\sim 71.5^{\circ}\text{N}$  in 2012 and 2013, with this approximate boundary defined by a strong, surface front (and a sub-surface front, not necessarily contiguous with the surface front) that separates the Bering summer waters from the meltwater. Although a complete characterization of this front was not achieved, it appears to extend zonally from the southwest side of Hanna Shoal eastward to the head of Barrow Canyon. We further surmise that the front extends northward and parallel to the eastern side of the Central Channel along the west side of Hanna Shoal. This supposition is based on three lines of evidence: the summer sea ice concentration maps, which effectively delineate the northward path of the Bering Sea Water in the Channel, both COMIDA CTD sections collected along the northwest side of Hanna Shoal in August, which captured waters clearly influenced by BSW, and the September 2013 acrobat section that detected intrapycnocline eddies along the HSNW mooring line.

These MW/BSW fronts appear to be baroclinically unstable, a process which leads to the formation of intrapycnocline, anticyclonic eddies that propagate across the front and that contain Bering summer waters. The existence of these fronts (and the associated frontal processes) and the strength and depth of the pycnocline in the COMIDA sampling area depends upon the meltwater distribution and its juxtaposition with winter water and Bering summer waters. In contrast to 2012 and 2013, there was no evidence of surface fronts in 2011 and the shelf stratification in that year was much weaker. These differences were attributed to the dearth of meltwater on the northeastern Chukchi shelf in 2011.

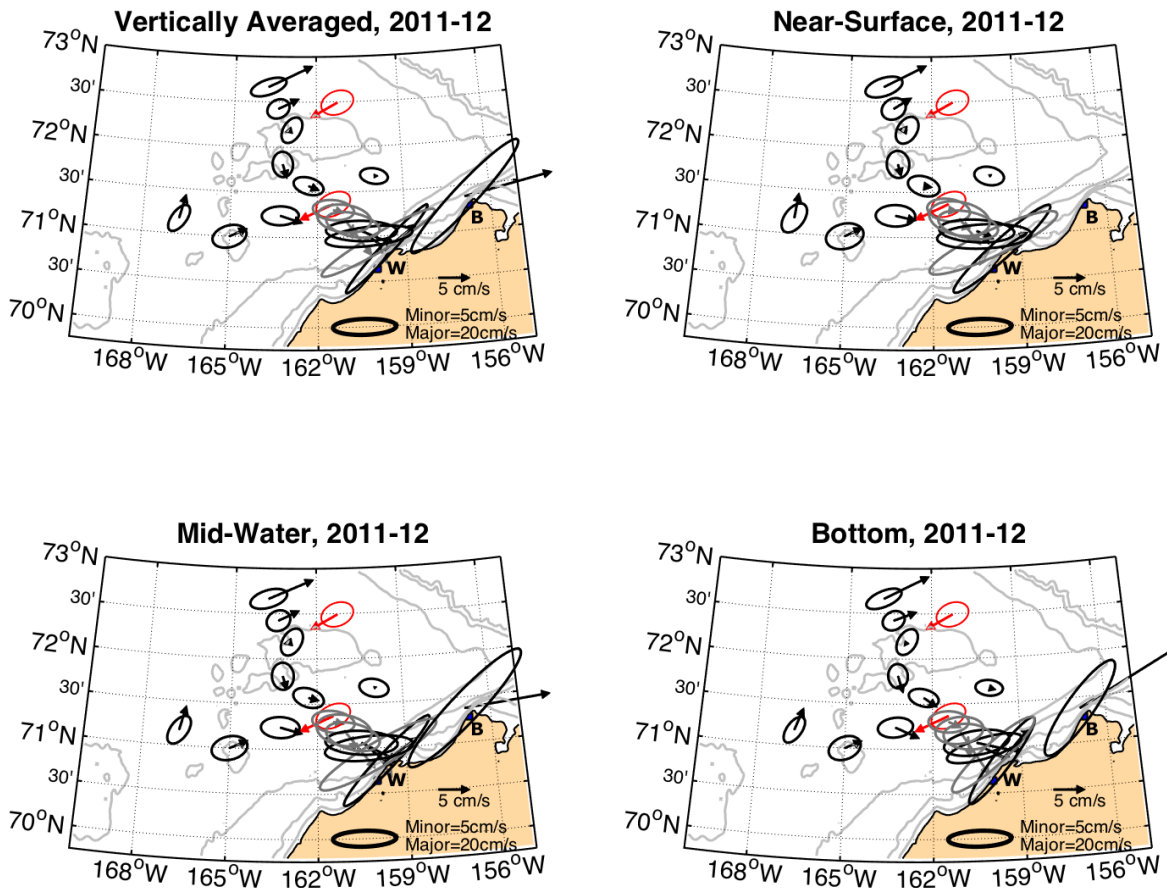
In addition to the meltwaters north of this front, cold, salty, winter-formed waters persist over the shelf bottom around Hanna Shoal throughout most of the year. This sub-surface front was present in all years and is likely a perennial feature of the shelf. Both the surface and sub-surface fronts are somewhat pliable boundaries that effectively divide the southern and northern portions of the northeastern shelf. South of the front, shelf water properties vary seasonally due to the annual influx of Bering Sea summer waters. The front constrains the northward movement of these summer waters (except through frontal instabilities). North of the front, the shelf has more of an arctic-flavor insofar as it is heavily stratified due to surface meltwater and very dense winter waters over the bottom. The circulation also changes on either side of the front. South of the front the summer waters are carried northward over the shelf from Bering Strait and then into Barrow Canyon. Here the shelf circulation is engaged in the meridional transfer of Pacific Ocean waters into the Arctic Ocean. North of the front the exchange appears to be primarily zonal. Meltwater and sea ice are advected westward and dense bottom waters are transported eastward.

We have begun processing the recently acquired industry data sets and while we are not in a position to discuss these in detail, two summary figures further substantiate some of the conclusions thus far stated and others reveal additional information on the circulation around Hanna Shoal. Figure 48 shows record length mean currents and variance ellipses for all moorings over the 2011 – 2012 deployment period in the northeastern Chukchi Sea. Maps were prepared for the vertically-averaged currents as well as those near the surface, mid-depth, and near bottom.

During the 2011 – 2012 deployment, the currents northwest of Hanna Shoal were eastward at all depths. With the exception of the surface currents, this result is identical to that obtained from the COMIDA moorings. The single mooring to the east of Hanna Shoal revealed negligible flow at all depths except at the bottom where the mean currents were eastward at  $\sim 1 \text{ cm s}^{-1}$ . Along the southern flank of Hanna Shoal the flow was southeastward on average at  $\sim 3 \text{ cm s}^{-1}$ . This flow would have transported waters from the southwest side of Hanna Shoal and the northern end of the Central Channel toward Barrow Canyon. These current vectors, as well as those closer to the canyon, also indicate that there is no net exchange between the shelf to the east and south of Hanna Shoal. (This contrasts with Spall's [2007] model prediction that on average some of the water east of Hanna Shoal flows over the shelf south of Hanna Shoal.) This supports our contention that the shelf east of Hanna Shoal is isolated from the shelf to the immediate south of the Shoal. Perhaps not surprisingly, these vectors are aligned roughly parallel to the sub-surface front that forms in summer between BSW to the south and WW to the north.

Consider next the currents measured by the three moorings south of  $71.5^\circ\text{N}$ . Within the Central Channel ( $\sim 71.2^\circ\text{N}$ ,  $167.5^\circ\text{W}$ ) the flow was northward at all depths at  $\sim 5 \text{ cm s}^{-1}$ . The two

moorings to the east of the Channel registered a mean eastward current of  $2 - 3 \text{ cm s}^{-1}$  implying that this flow would carry water from the Central Channel toward Barrow Canyon. Northeastward flow occurs only in Barrow Canyon.

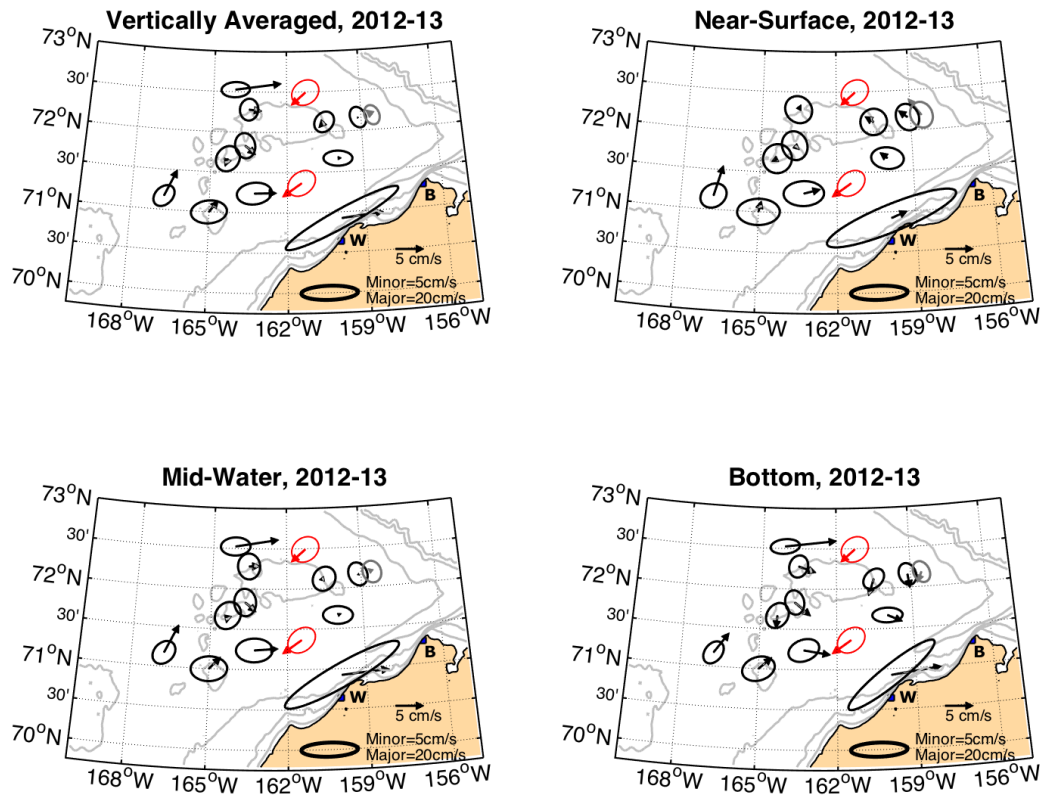


**Figure 48.** Record-length mean currents and current ellipses for all moorings in the northeast Chukchi Sea, 2011 – 2012. Red vectors and ellipses are for winds, grey indicate statistics based on less than one full year of data.

Figure 49 consists of similar maps for the 2012 – 2013 deployment. Although the mooring locations differ somewhat between the two years, there is remarkable similarity between the two deployments insofar as there is northward flow in the Central Channel and eastward flow south of Hanna Shoal toward Barrow Canyon. The mooring east of Hanna Shoal and south of the HSNE array shows results similar to the preceding year, i.e., very weak vertically-averaged flow, but a bottom flow that was eastward at  $\sim 2 \text{ cm s}^{-1}$ .

These and additional mooring data from the northeastern Chukchi Sea are presently being analyzed to assess flow variations on shorter time and space scales and to examine potential forcing mechanisms. We will also be exploring the circulation coherence over this portion of the Chukchi shelf. Our measurements underscore the critical role that meltwater plays in this region.

In summer, the amount of meltwater present on the shelf depends upon the rate of sea ice retreat from Hanna Shoal and the adjacent northeastern shelf. We found no compelling evidence



**Figure 49.** Record-length mean currents and current ellipses for all moorings in the northeast Chukchi Sea, 2011 – 2012. Red vectors and ellipses are for winds, grey indicate statistics based on less than one full year of data.

that the local winds controlled the August sea ice distribution over the COMIDA sampling domain. Nor have we found strong evidence that the winds from May through June affect the amount of summer ice cover in the Hanna Shoal region. We suggest that local and remote (in both time and space) processes are involved in determining the summer ice distribution. Recall that the COMIDA summer sampling occurred following winters when extensive grounded ice covered Hanna Shoal. Eicken and Mahoney (2015) contend that the thick ice that grounds on Hanna Shoal derives primarily from the highly deformed seaward edge of the landfast ice of the Alaskan Beaufort Sea. There are two requirements for this to happen. The first is that sufficiently thick (e.g., deformed) ice be produced by detachment from the seaward edge of the landfast ice zone. The second ingredient is that the detached ice drifts westward. Our ice drift measurements from the moored ADCPs show a mean westward ice drift and surface flow under northeasterly winds, which is the vehicle for transporting ice from the Alaskan Beaufort Sea to Hanna Shoal. We speculate that once grounded on Hanna Shoal, the ice may serve as a barrier to pack ice drifting over the Shoal that promotes additional deformation, grounding, and ice accumulation. We further hypothesize that if there is sufficient accumulation (and grounding) then the ice

remains intact well into summer. Hence, both a local process (e.g., grounding due to the local bathymetry) and remote processes (ice deformation, breakout, and the trajectory of thick ice floes during the winter) may be important in regulating the summer ice distribution over the Hanna Shoal region.

As an additional comment, we note that the interannual variability in ice concentrations over Hanna Shoal do not appear to be closely tied to variability in ice concentrations over the Arctic basin. For example, the heavy sea ice concentrations in the northeastern Chukchi Sea in summer of 2012 occurred when the arctic-wide sea ice extent was the third lowest in record (the other summers being 2007 and 2011) since the onset of satellite-based sea-ice record in 1979 (National Snow and Ice Data Center).

Interannual variations in the northward flux of heat through Bering Strait may also affect year-to-year differences in ice concentrations on the northeastern shelf. This heat flux increased nearly twofold between 2008 and 2011, primarily due to an increase in the mass transport through the Strait (Woodgate et al. 2012). The heat flux subsequently decreased to 2008 levels in 2012 before slightly increasing again in 2013 (Woodgate et al., 2015). A key difference amongst these years was that the sea-surface height difference between the Aleutian Basin in the Bering Sea and the Chukchi Sea shelf was much greater in 2011 than in the later years (Danielson et al., 2014) so that the large-scale pressure gradient that forces flow northward through the Strait and over the Chukchi shelf was stronger in 2011 than in 2012 and 2013. Interannual changes in this pressure gradient also will affect the magnitude of the wind-forced response of the shelf flow field. The interannual differences in heat flux from 2011 through 2013 roughly correspond to similar variations in the ice cover. The processes by which this oceanic heat flux may influence ice melt may depend upon more local processes, however, and include the wind-driven circulation, the degree of stratification of the summer waters moving northward from the Strait, and mesoscale processes associated with the marginal ice zone (Lu et al., 2015).

Summer sea ice concentration maps (including those presented here) consistently show an ice-edge embayment extending northward in the Central Channel and along the west side of Hanna Shoal. That indentation has been ascribed to the northward flow in the Central Channel (Weingartner et al., 2005 and see Figures 48 and 49) as well as the Taylor-column effect ascribed to Hanna and Herald shoals (Martin and Drucker, 1997). Our CTD measurements showed warm water moving clockwise around the northwest side of Hanna Shoal, consistent with inferences from satellite-imagery that the Central Channel is this heat source. We estimated that the ocean heat flux convergence (approximate at best and assumption dependent) was  $\sim 50 \text{ W m}^{-2}$ , which must represent a substantial contribution to ice melt especially when dense fog (as was common on the August COMIDA cruises) scatters and absorbs the incoming solar radiation. Figures 48 and 49 indicate the mean northward flow in Central Channel. Our preliminary inspection of the Central Channel mooring time series (from 2008 – 2015) suggests that this northward flow varies but little from year-to-year and rarely reverses. As noted earlier, we do not believe that all of the water flowing along the northwest side of Hanna Shoal derives from the Central Channel. Rather we posited that some fraction of this transport derives from Herald Valley.

The COMIDA mooring data indicates that there must be flow convergence on the north side of Hanna Shoal. How this convergence arises is unclear, but one candidate mechanism is associated with the counterclockwise pressure gradient due to the inferred baroclinic pressure gradient on

the east side (at least) of Hanna Shoal. Regardless of the mechanism the observations imply that there is a cross-isobath transport, which would direct the flow northward toward the shelfbreak and deeper water rather than southward toward Hanna Shoal. If our contention is correct then it means that Chukchi shelf waters are being transported into the basin north of Hanna Shoal.

#### **4.1 Recommendations**

The results from the physical oceanography component of the COMIDA program have yielded an abundance of new information and insights on the Hanna Shoal portion of the northeastern Chukchi Sea. There are, however, a number of key issues that have emerged from our analyses that deserve future study. These are:

There is a strong eastward flow along the northwest side of Hanna Shoal, which extends to at least as far to the northwest as the 60 m isobath, but very likely even farther. This flow likely consists of water emanating from both the Central Channel and the mouth of Herald Valley farther to the west. Information is needed on how much water is flowing eastward from Herald Valley. This can be determined by deploying an array of moorings from south to north slightly east of the Russian-US Convention Line. We recommend that a meridional array of moorings be deployed between the 50 and 100 m isobaths to assess this transport.

Closely coupled to this issue is the need to quantify better the transport in the Central Channel. We believe that this could be done by deploying 2 – 3 moorings at the southern end of the Channel and 2 – 3 at the northern end to the west of Hanna Shoal. The moorings in recommendation 1 and 2 should include T/C/P recorders at multiple depths in order to assess the stratification.

We hypothesized that flow convergence occurs over the shelf to the north of Hanna Shoal. This possibility should be explored by conducting a zonal sequence of meridionally-oriented synoptic transects to examine water properties and the circulation here. This survey would benefit from concurrent VM-ADCP data and consideration should be given to deploying deep-drogued (i.e., 35 m) satellite tracked drifters to assess the deep circulation on the north side of the Shoal.

Two surprising and related observations were the year-round presence of heavy stratification and the inferred year-round counterclockwise baroclinic pressure tendency on the shelf east of Hanna Shoal. We surmised that the baroclinic pressure field opposed the barotropic pressure field in the upper half of the water column. These competing pressure fields are critical to establishing the weak circulation, the inferred convergence north of the Shoal and the water properties east of the Shoal. Verification of this baroclinicity could be done easily with carefully deployed array of moorings using ISCATS (which were deployed successfully in COMIDA) and/or a string of T/C/Ps. This deployment could be done in conjunction with the Chukchi Environmental Observatory (Danielson, pers comm.)

The persistence of sea ice (or lack thereof) in summer on Hanna Shoal has a profound influence on the regional circulation and hydrography. In addition, it also affects the regional biology through control of stratification and as habitat for walrus and other marine mammals. It may also play a key role in governing sources and sinks of carbon and the structure of the benthos. A prudent area of investigation would be to determine the sources of ice on Hanna Shoal, the mechanisms controlling these sources and those that affect its persistence or its ablation.



## 5. Acknowledgements

This study was funded by the US department of the Interior, Bureau of Ocean Energy Management (BOEM), Alaska Outer Continental Shelf Region, Anchorage, Alaska under BOEM Cooperative Agreement No. M11AC00007 as part of the Chukchi Sea Offshore Monitoring in Drilling Area (COMIDA).

## 6. References

- Coachman, L., Aagaard, K., Tripp, R.B., 1975. Bering Strait: The Regional Physical Oceanography, Univ. of Washington Press, Seattle, 172 pp.
- Codispoti, L., Flagg, C., Kully V., Swift J.H., 2005. Hydrographic conditions during the 2002 SBI process experiments. *Deep-Sea Res. II*, 52 (24-26): 3199 – 3226.
- Eicken, H., Mahoney, A.R., 2015. Sea ice: hazards, risks, and implications for disasters. In: Ellis, J.T., Sherman, D.J. (Eds.), *Sea and Ocean Hazards, Risks, and Disasters*. Elsevier, Oxford, United Kingdom, pp. 381–401. doi:10.1016/B978-0-12-396483-0.00013-3.
- Light, B., Grenfell, T.C., Perovich, D.K., 2008. Transmission and absorption of solar radiation by Arctic sea ice during the melt season, *J. Geophys. Res.*, 113, C03023, doi:10.1029/2006JC003977.
- Lu, K., Weingartner, T., Danielson, S., Winsor, P., Dobbins, E., Martini, K., Statscewich, H., 2015. Lateral mixing across ice meltwater fronts of the Chukchi Sea shelf. *Geophys. Res. Lett.*, 42, 6754–6761, doi:10.1002/2015GL064967.
- Martin, S., Drucker, R., 1997. The effect of possible Taylor columns on the summer sea ice in the Chukchi Sea. *J. Geophys. Res.*, 102 (5), 10473 – 10482.
- Mesinger, F., 19 Coauthors, 2006. North American regional re-analysis, *Bull. Amer. Meteor. Soc.*, 87, 343–360.
- Nikolopoulos, A., Pickart, R.S., Fratantoni, P.S., Shimada, K., Torres D.J., Jones E.P., 2009. The western Arctic boundary current at 152°W: Structure, variability, and transport. *Deep-Sea Res. II*, 56, 1164-1181.
- Paquette, R.G., Bourke, R.H., 1981. Ocean circulation and fronts as related to ice melt-back in the Chukchi Sea. *J. Geophys. Res.*, 86, 4215-4230.
- Pickart, R.S., 2004. Shelfbreak circulation in the Alaskan Beaufort Sea: Mean structure and variability. *J. Geophys. Res.*, 109(C4), C04024 10.1029/2003JC001912.
- Pickart, R.S., Pratt, L.J., Torres, D.J., Whitledge, T.E., Proshutinsky, A.Y., Aagaard, K., Agnew T.A., Moore G.W.K., Dail H.J., 2010. Evolution and dynamics of the flow through Herald Canyon in the Western Chukchi Sea. *Deep-Sea Res. II*, **57**, 5-26.
- Spall, M.A., 2007. Circulation and water mass transformation in a model of the Chukchi Sea. *J. Geophys. Res.* 112, C05025, doi:10.1029/2005JC002264.
- Spall, M., Pickart, R.S., Fratantoni, P., Plueddemann, A., 2008. Western Arctic Shelfbreak Eddies: Formation and transport. *J. Phys. Oceanogr.*, 38, 1644-1668.

- Spreen, G., Kaleschke, L., Heygster, G., 2008. Sea ice remote sensing using AMSR-E 89 GHz channels. *J. Geophys. Res.* 113, C02S03, [doi:10.1029/2005JC003384](https://doi.org/10.1029/2005JC003384).
- University of Alaska School of Fisheries and Ocean Sciences. [http://dm.sfos.uaf.edu/chukchi-beaufort/data/drifters/drifter\\_map\\_2013.php](http://dm.sfos.uaf.edu/chukchi-beaufort/data/drifters/drifter_map_2013.php)
- von Appen, W.-J., Pickart, R.S., 2012: Two Configurations of the Western Arctic Shelfbreak Current in Summer. *J. Phys. Oceanogr.*, 42, 329–351.
- Weingartner, T., Irvine, C., Dobbins, L., Danielson, S., DeSousa, L., Adams, B., Suydam, R., Neatok, W., 2015. Satellite-tracked drifter measurements in the Chukchi and Beaufort seas. Final Report, OCS Study 2015-022, Bureau of Ocean Energy Management. 171 p. <http://www.boem.gov/Alaska-Reports-2015/>
- Weingartner, T., Danielson, S., Dobbins, L., Potter, R., 2014. Physical oceanographic measurements in the Northeastern Chukchi Sea: 2013. Technical report prepared for ConocoPhillips, Inc., Shell Exploration & Production Company and Statoil USA E&P, Inc. 52 p.
- Weingartner, T., Winsor, P., Potter, R., Statscewich, H., Dobbins, E., 2013a. Application of High Frequency Radar to Potential Hydrocarbon Development Areas in the Northeast Chukchi Sea. Final Report to the U.S. Department of the Interior Bureau of Ocean Energy Management, Alaska Outer Continental Shelf Region, ConocoPhillips, Inc., and Shell Exploration & Production Company (Cooperative Agreement No: M09AC15207 as part of the BOEM Alaska Environmental Studies Program). 162 p.
- Weingartner, T., Danielson, S., Dobbins, L., Potter, R., 2013b. Physical oceanographic measurements in the Northeastern Chukchi Sea: 2012. Technical report prepared for ConocoPhillips, Inc., Shell Exploration & Production Company and Statoil USA E&P, Inc., 64 p.
- Weingartner, T., Dobbins, E., Danielson, S., Winsor, P., Potter, R., Statscewich, H., 2013c. Hydrographic variability over the northeastern Chukchi Sea shelf in summer-fall 2008–2010. *Cont. Shelf Res.* <http://dx.doi.org/10.1016/j.csr.2013.03.012>
- Weingartner, T., Danielson, S., Dobbins, L., R. Potter, R., 2012. Physical oceanographic measurements in the Northeastern Chukchi Sea: 2011. Technical report prepared for ConocoPhillips, Inc., Shell Exploration & Production Company and Statoil USA E&P, Inc., 38 p.
- Weingartner, T., Aagaard, K., Woodgate, R., Danielson, S., Sasaki, Y., Cavalieri, D., 2005. Circulation on the North Central Chukchi Sea Shelf. *Deep-Sea Res. II* 52: 3150-3174, [doi:10.1016/j.dsr2.2005.10.015](https://doi.org/10.1016/j.dsr2.2005.10.015).
- Weingartner, T.J., Cavalieri, D.J., Aagaard, K., Sasaki, Y., 1998. Circulation, dense water formation, and outflow on the northeast Chukchi shelf. *J. Geophys. Res.*, 103: 7647 – 7661.
- Winsor, P., Chapman, D.C., 2004. Pathways of Pacific Water across the Chukchi Sea: A numerical model study. *J. Geophys. Res.* 109, C03002, [doi: 1029/2003JC001962](https://doi.org/10.1029/2003JC001962).
- Woodgate, R.A., Aagaard, K., Weingartner, T.J., 2005b. A year in the physical oceanography of the Chukchi Sea: Moored measurements from autumn 1990-1991, *Deep-Sea Res. II*, 52(24-26), 3116-3149.

Woodgate, R.A., Weingartner, T.J., Lindsay, R., 2012. Observed increases in Bering Strait oceanic fluxes from the Pacific to the Arctic from 2001 to 2011 and their impacts on the Arctic Ocean water column. *Geophysical Research Letters* 39, L24603. doi:10.1029/2012GL054092.

Woodgate, R.A., Stafford K.M., Pahl, F.G., 2015. A Synthesis of Year-round Interdisciplinary Mooring Measurements in the Bering Strait (1990-2014) and the RUSALCA years (2004-2011). *Oceanography* 28(3):46-67, [doi:10.5670/oceanog.2015.57](https://doi.org/10.5670/oceanog.2015.57).

## Trace Metals in Sediments, Water and Biota

John Trefry, Robert Trocine, Austin Fox

Department of Marine & Environmental Systems, Florida Institute of Technology,  
150 West University Boulevard, Melbourne, FL 32901

[jtrefry@fit.edu](mailto:jtrefry@fit.edu)

### Abstract

As part of the Hanna Shoal Ecosystem Study, concentrations of trace metals in sediments, seawater and marine biota were determined to establish a baseline for future reference and to explain observed spatial and temporal trends for selected essential or potentially toxic metals. This study was carried out during a period marked climatic change and increased human activity in the Arctic. Concentrations of 17 trace metals (Ag, As, Ba, Be, Cd, Cr, Cu, Hg, Mn, Ni, Pb, Sb, Se, Sn, Tl, V and Zn) in 44 surface sediments and 278 sediment core samples from the Hanna Shoal area of the northeastern Chukchi Sea (NECS) were essentially all at natural, background values. Ratios of metals/Al were used to determine background metal concentrations. All concentrations of the potentially toxic metals Ag, Cd, Hg, Pb and Zn were below published sediment quality criteria. No elevated Ba concentrations were found in contrast to previous studies in the NECS when sampling included historic drilling sites for oil and gas. Concentrations of As and Mn were high in some surface sediments and could be linked to subsurface, diagenetic remobilization of these metals with subsequent reprecipitation in surface sediments. Concentrations of dissolved trace metals in seawater were low and in close agreement with values for North Pacific surface water (As, Ba, Cr, Pb, Sb, Se and Tl) or North Pacific deep water for nutrient-type metals (Cd, Cu, Ni, and Zn). Concentrations of As, Sb and Tl varied by <10% in the NECS and followed salinity. Values for Cd, Ni and Zn were higher in bottom water; Cd correlated especially well with dissolved phosphate with a slope of 0.37 (Cd/P, mole basis) in close agreement with values of 0.34-0.40 for the northwest Pacific Ocean. Concentrations of Ag, As, Ba, Cd, Cr, Cu, Fe, Total Hg, MMHg, Mn, Ni, Sb, Se, Sn, V and Zn were determined for the following organisms and tissue types during 2012 and 2013: mixed zooplankton, whole clams (*Astarte borealis*), whelk muscle (*Neptunea borealis*), snow crab muscle (*Chionocetes opilio*) and arctic cod muscle (*Boreogadus saida*). The primary focus of this effort was on total Hg and monomethyl Hg (MMHg) in biota because of the keen interest and concern for Hg contamination in the Arctic. Concentrations of MMHg biomagnified from 4 ng/g (d. wt.) in zooplankton to 13 ng/g (d. wt.) in clams to 165 ng/g (d. wt.) in whelk. Despite this distinct biomagnification of MMHg, concentrations of inorganic Hg were relatively uniform at  $20 \pm 5$  ng/g (d. wt.) across the food web with no discernible biomagnification. Results for other metals are also presented and discussed here to provide a baseline for future assessments.

## 1. Introduction

The broad shelf of the northeastern Chukchi Sea (NECS) is presently at a crossroad with respect to sea-ice retreat, northward migration of species, coastal erosion and offshore energy development (Holland et al., 2006; Grebmeier et al., 2010; Ping et al., 2011). These ongoing events follow a long geological history of extensive sea level changes that have greatly influenced both the sedimentary environment and human activity in the Chukchi Sea (Hopkins, 1967). Six major sea level regressions exposed the seabed in the Chukchi Sea during the Pleistocene and Holocene epochs with the most recent exposure occurring just 13,000–17,000 years BP (Creager and McManus, 1965). Despite such a dynamic history, only 2–10 m of sediment were deposited throughout most of the Chukchi Sea during the past 1.8 million years (Grantz et al., 1982). Present-day events are likely to have a significant impact on the Chukchi Sea, one that is just beginning to be recorded in the sediments.

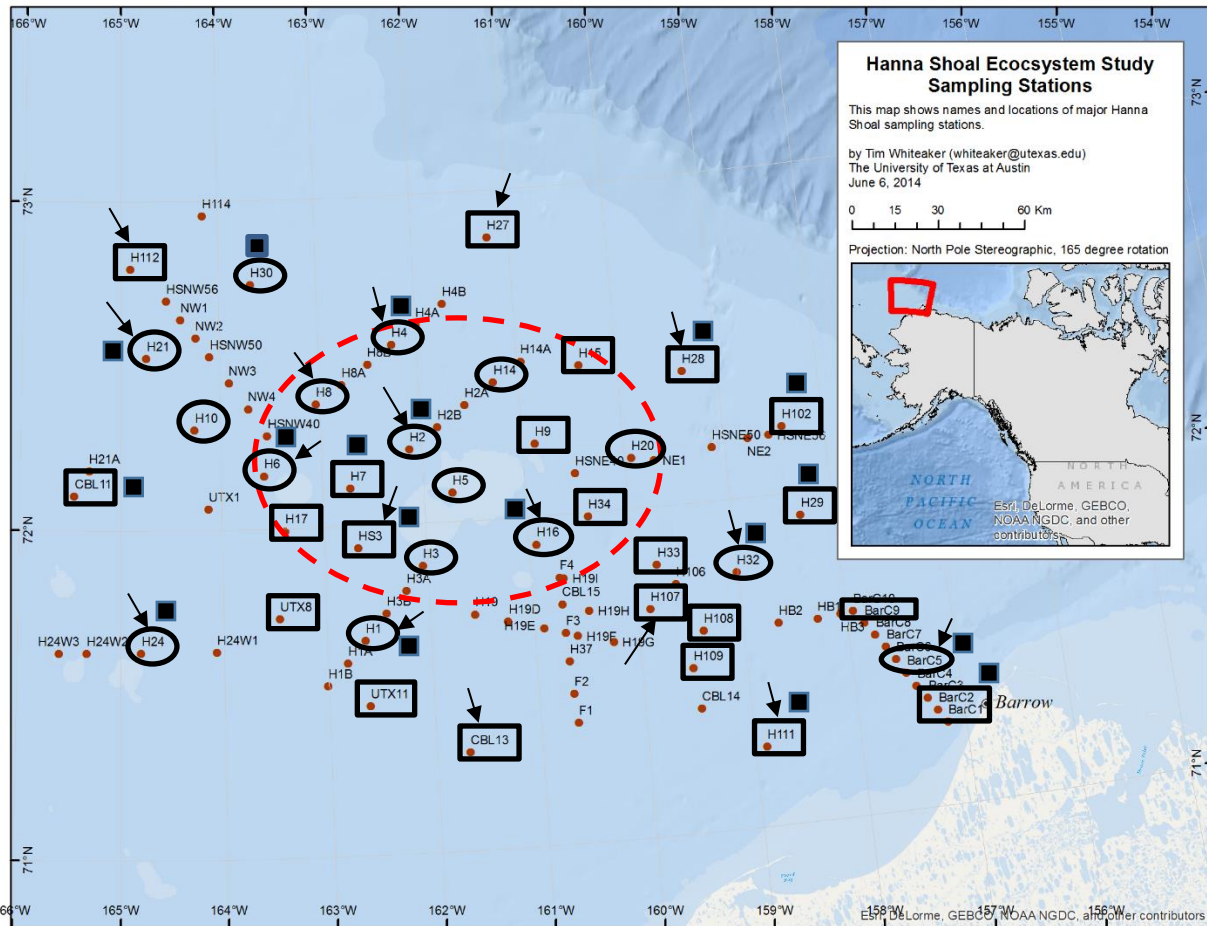
Sediments in the Chukchi Sea support a vibrant infaunal assemblage characterized by polychaete worms, small mollusks and crustaceans (Feder et al., 1994). Biota from higher trophic levels include arctic cod, walrus, seals, polar bears, sea birds and migrating bowhead whales. Bioaccumulation of Hg in plankton yields cellular Hg concentrations that are thousands of times greater than in surrounding seawater. Continued bioaccumulation in pelagic and benthic predators yields an exponential increase in Hg concentrations (biomagnification) with increasing trophic level (TL). In the Arctic, Hg biomagnifies by >50 fold in higher TLs (sea birds and marine mammals) relative to primary consumers (zooplankton and bivalves). For example, Wagemann et al. (1998) found an increase in total Hg (THg) from ~20 ng/g dry weight for arctic zooplankton to >1,500 ng/g dry weight in ringed seal muscle.

With a specific focus on the Hanna Shoal area in the NECS, the objectives of this part of the Hanna Shoal Ecosystem Study are to determine: (1) background concentrations of trace metals in sediments and identify any anthropogenic inputs of metals to the sediments, (2) the geographical distribution of trace metals in surface and subsurface sediments, (3) baseline concentrations and vertical and horizontal trends for dissolved trace metals in the water column and (4) baseline concentrations of trace metals in marine biota and trace the biomagnification of mercury in marine organisms of the NECS.

## 2. Methods

### 2.1. Study Area

The study area for this project is the NECS (Figure 1). This region is north of the previous 2009–2010 surveys during the COMIDA: Chemical and Benthos Project (Dunton et al., 2012) and does not include any historic (1989–1992) exploratory drilling sites for oil and gas. The sediments are silty sand and mud with <10% silt plus clay nearshore and >90% silt plus clay in offshore areas (Naidu et al., 1997, Trefry et al., 2014). The provenance of these sediments is considered to be the Yukon and other rivers, with transport from the Bering Sea to the Chukchi Sea by the Alaska Coastal Current (McManus et al., 1969).



**Figure 1.** Sampling stations for 2012 (○) and 2013 (◻) field surveys for the Hanna Shoal Ecosystem Study. Inset map shows location of study area off the northwest coast of Alaska. Arrows (→) and solid squares (■) identify stations where sediment cores and water samples, respectively, were collected. Dashed oval outlines general area of Hanna Shoal.

## 2.2. Sample Collection

Sampling for this study was carried out during August 2012 and 2013 using the USCGC *Healy*. Stations were selected using a probability-based, hexagonal grid approach of White et al. (1992) to ensure random selection with an even distribution of sites. Sediment sampling was conducted at 18 stations in the 2012 and 23 stations in 2013 (Figure 1 and Table 1). Sediment cores were collected at 10 and 7 of the sediment stations in 2012 and 2013, respectively (Table 1 and Figure 1). Surface sediments were collected using a pre-cleaned, double van Veen grab that obtained two side-by-side samples, each with a surface area of 0.1 m<sup>2</sup> and a depth of ~15 cm. Samples (top 1 cm and subsurface layers) were carefully collected from one of the two grabs and placed in separate containers for metals, organic C and grain size. The companion grab was used for sampling benthic biota. A HAPS corer (Kannevorff and Nicolaisen, 1973) with a 30-cm acrylic liner was deployed at numerous sites and a Benthos gravity core with a 1-m long barrel, 7.5-cm diameter plastic liner was deployed into stiff sediments at several sites. Core samples were split

**Table 1.** Summary of sediment and water samples collected for metals.

<b>2012</b>	<b>Surface Sediments</b>	<b>Sediment Cores with (# samples)</b>	<b>Water Samples</b>
# of samples	18 (0-1 cm and 0-2 mm)	10 (159)	77
Stations sampled	H1, H2, H3, H4, H5, H6, H8, H10, H14, H16, H19, H20, H21, H23, H24, H30, H32, H38, BC5	H1, H2, H4, H6, H8, H16, H21, H24, H38, BC5	BSR5, H1, H2, H4, H6, H16, H21, H24, H30, H32, BC5
<b>2013</b>	<b>Surface Sediments</b>	<b>Sediment Cores with (# samples)</b>	<b>Water Samples</b>
# of samples	23 (0-1 cm)	7 (119)	72
Stations sampled	HS3, H7, H9, H15, H17, H27, H28, H29, H33, H34, H102, H107, H108, H109, H111, H112, BarC1, BarC2, BarC9, CBL11, CBL13, UTX8, UTX11	HS3, H27, H28, H107, H111, H112, CBL13	BRS5, HS3, H7, H9, H28, H29, H102, H107, H111, H114, BarC4, CBL11

into 1- to 2-cm thick layers aboard ship under clean conditions. All sediments samples, except those for grain size analysis, were frozen shipboard.

Water column samples were collected at 11 stations (77 samples) in 2012 and 12 stations (72 samples) in 2013 with repeat sampling at the Bering Strait (Table 1). These samples were collected using HCl-washed, Teflon-lined, 10-L GoFlo bottles that were mounted on an epoxy-coated rosette and opened at ~10 m by hydrostatic pressure. Samples were vacuum filtered through polycarbonate filters (Poretics, 47-mm diameter, 0.4- $\mu$ m pore size) in a laminar flow hood aboard ship immediately after collection. Filters were pre-washed in 5N HNO<sub>3</sub> and rinsed three times using 18 M $\Omega$ -cm deionized water (DIW) and then weighed three times to the nearest  $\mu$ g under cleanroom conditions. Precision for replicate filtrations averaged <4% (i.e., <0.04 mg/L). Filtered samples were collected in Teflon bottles (Hg) and low density polyethylene bottles (other metals) and preserved with Fisher Optima HNO<sub>3</sub>. Particle-bearing filters were sealed in acid-washed petri dishes, labeled and then double-bagged in plastic and stored until dried and re-weighed at Florida Institute of Technology (FIT). Samples for particulate organic carbon (POC) were filtered through pre-combusted Gelman Type A/E glass fiber filters mounted on acid-washed filtration glassware within a Class-100 laminar-flow hood.

Twenty-seven species or groups of organisms (e.g., phytoplankton and zooplankton) were collected based on availability and their potential as bioindicators of Hg contamination, a pre-defined focus of the COMIDA: Hanna Shoal Project (Table 2). Samples of mixed zooplankton (n = 16), clams (*Astarte borealis*, n = 11), whelk (*Neptunea borealis*, n = 12), snow crab (*Chionocetes opilio*, n = 18) and arctic cod (*Boreogadus saida*, n = 12) also were collected to determine concentrations of Ag, As, Ba, Cd, Cr, Cu, Fe, Mn, Ni, Sb, Se, Sn, V and Zn.

**Table 2.** Summary of biota samples analyzed for metals.

<b>2012</b>	<b>Biota samples analyzed for various trace metals</b>	<b>Biota samples analyzed for total Hg and monomethylmercury</b>
# of samples	40	47
Stations sampled	BarC10, CBL11, CBL14, H1, H10, H14, H16, H19, H2, H20, H24, H3, H30, H32, H38, H4, H6, H8	BarC10, CBL11, CBL14, H1, H10, H14, H16, H19, H20, H21, H23, H24, H3, H30, H32, H38, H6, H8
Organisms analyzed	zooplankton (8), clams (8), crabs (8), whelk (8), arctic cod (8)	zooplankton, clams, crabs, whelk , arctic cod
<b>2013</b>	<b>Biota samples analyzed for various trace metals</b>	<b>Biota samples analyzed for total Hg and monomethylmercury</b>
# of samples	51	527
Stations sampled	BarC 3, BarC 5, BarC 6, CBL 11, CBL 13, CBL 15, H102, H107, H109, H15, H17, H20, H27, H29, H32, H34, H6, HS3, UTX 1, UTX 11, UTX 8, UTX8	BarC 10, BarC 3, BarC 5, BarC 6, BarC 6, BarC 7, BarC 9, BRS 5, CBL 11, CBL 13, CBL 14, CBL 15, H102, H107, H108, H109, H111, H112, H114, H15, H17, H19, H20, H27, H28, H29, H32, H33, H34, H6, H7, H9, HS3, UTX 1, UTX 11, UTX8
Organisms analyzed	phytoplankton (1), zooplankton (9), clams (4), crabs (19), whelk (7), arctic cod (4)	Food web spectrum including phytoplankton, zooplankton, amphipods, clams, crabs, whelk , arctic cod

Zooplankton were obtained by vertical tows using a bongo net with 150- $\mu$ m mesh. Benthic biota were collected from one side of a 0.1 m<sup>2</sup> double van Veen grab; samples were sieved through a 1-mm mesh to remove sediments and then organisms were sorted to the species level and counted (Schonberg et al., 2014). The second 0.1-m<sup>2</sup> section of the grab was used to collect surface sediments for chemical analysis. Biota also were collected using an epibenthic, 3.05-m plum-staff beam trawl, with a 7-mm mesh and a 4-mm cod end liner. Trawl samples were sorted by species, counted and sizes of selected species were measured to the nearest mm (Konar et al., 2014; Ravelo et al., 2014). Muscle tissue from biota samples was dissected using stainless steel blades aboard ship in a laminar flow hood and stored frozen until laboratory analysis. Samples of whole organisms were frozen immediately aboard ship and kept frozen until laboratory analysis.



### 2.3. Laboratory Methods

Total concentrations of Ag, Al, As, Ba, Be, Cd, Cr, Cu, Fe, Hg, Mn, Ni, Pb, Re, Sb, Se, Sn, Tl, V, Zn and organic carbon were determined for 41 surface sediments and 278 samples from 17 sediment cores (Table 1 and Figure 1). Sediment samples for metal analysis were homogenized and a wet portion was set aside for Hg analysis. The remaining sediment was freeze-dried to obtain percent water content and dry sediment for acid digestion for other metals. A separate, wet sediment sample from each location was set aside for grain size analysis.

Sediment samples for metal analysis, except Hg, were homogenized, completely digested in Fisher Trace Metal Grade HF, HNO<sub>3</sub> and HClO<sub>4</sub> and analyzed for Al, Cr, Cu, Fe, Mn, V and Zn using a Perkin-Elmer Model 4000 atomic absorption spectrometer and for Ag, As, Ba, Be, Cd, Ni, Pb, Sb, Se, Sn and Tl using a Varian Model 820-MS inductively coupled plasma mass spectrometer according to established laboratory methods (Trefry et al., 2003). Standard reference material (SRM) #2709 (soil with certified Ba value) from National Institute of Standards and Technology (NIST) was processed with each batch of samples; all values were within the 95% confidence intervals for certified values. Analytical precision ranged from 1% (Al, Cu, Fe, and Pb) to 4% (Hg). Method detection limits were 25 (Cu) to >5,000 (Ba, Pb) times lower than the lowest value obtained for field samples.

Sediment digestion for Hg was carried out using high-purity HNO<sub>3</sub> and H<sub>2</sub>SO<sub>4</sub>. The sediment Certified Reference Material (CRM) MESS-3 from the National Research Council of Canada (NRC) was digested and analyzed with each group of sediment samples. Concentrations of the remaining metals were determined using dry sediment that was totally dissolved using high-purity HF, HNO<sub>3</sub> and HClO<sub>4</sub>. The sediment digestions included MESS-3 and the Standard Reference Material (SRM) #2709 from the NIST. Analysis was by cold-vapor atomic absorption spectrometry (Trefry et al., 2007).

Sediment total organic carbon (TOC) concentrations were determined by treating freeze-dried sediment with 10% HCl to remove inorganic carbon, followed by high-temperature combustion and infra-red CO<sub>2</sub> quantification. Grain size analyses of surface sediment samples were carried out using the classic method of Folk (1974) that includes a combination of wet sieving and pipette techniques.

The POC content was determined using acid-treated samples of filtered particles that were combusted in ceramic boats at 900°C in a Shimadzu TOC-5050A carbon system with a SSM-5000A solid sampling module. A four-point calibration curve was used with pure sucrose as the standard. Precision was 1.6% and results for the certified reference material (CRM) MESS-2, marine sediment issued by the National Research Council of Canada (NRC) were within the 95% confidence limits for the certified value.

Seawater concentrations of dissolved As, Cd, Cr, Cu, Ni, Pb, Sb, Se, Tl and Zn were determined on extracts obtained using a reductive precipitation procedure derived from Nakashima et al. (1988). In this procedure, ultra-high purity Pd, Fe and NaBH<sub>4</sub> were used to precipitate the metals that were then collected by filtration and redissolved in ultra-high purity HNO<sub>3</sub> and HCl. This procedure was carried out using 400 mL of seawater and a seawater CRM (CASS-3 issued

by the NRC) with final extract volumes of ~4 mL (by weighing and determining density), resulting in a ~100-fold increase in concentration of the seawater metals prior to analysis. The extracts were transferred to acid-washed 7.5-mL LDPE bottles, sealed, labeled and then stored in a plastic bag until analysis by ICP-MS using a Varian Model 820 instrument.

Concentrations of dissolved silica, phosphate and nitrate were determined using standard methods (Grasshoff, 1976). Reagent blanks, laboratory replicates and certified standards were analyzed for quality control. Analysis was by UV-visible spectrometry.

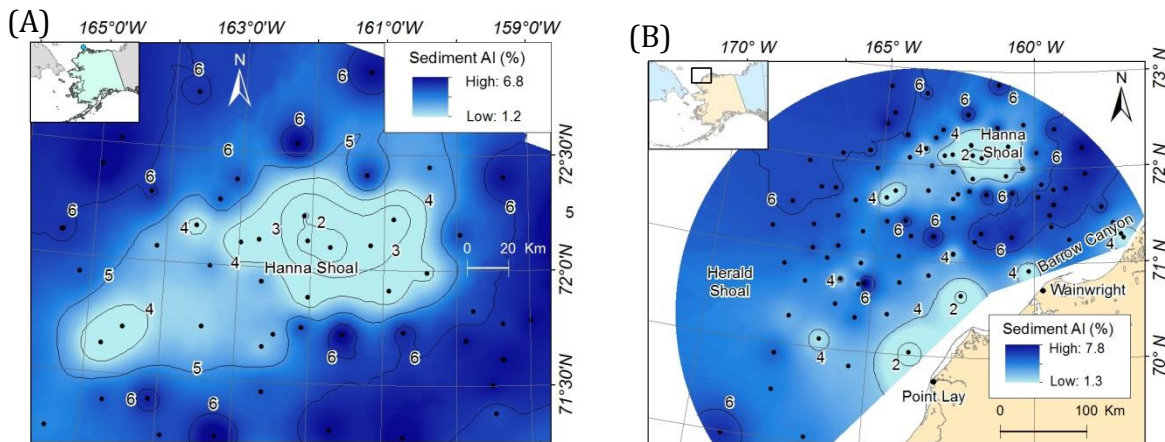
Freeze-dried tissue samples were homogenized and completely digested in Fisher Trace Metal Grade HNO<sub>3</sub> and H<sub>2</sub>O<sub>2</sub> and analyzed for Cu, Fe, Mn and Zn using a Perkin-Elmer Model 4000 atomic absorption spectrometer, for THg using a Laboratory Data Control cold vapor atomic absorption spectrometer and for other metals by ICP-MS according to established laboratory methods (Trefry et al., 2007, 2013). SRM #1566b (oyster tissue) from the NIST was processed with each batch of samples; all values were within the 95% confidence intervals for the certified values. Analytical precision was better than 6% for all analytes.

Samples for MMHg analysis were digested using an acid bromide/methylene chloride extraction. The aqueous phase was analyzed using ethylation, isothermal gas chromatography separation and detection by CVAFS based on methods from Bloom and Crecelius (1983) and Bloom (1989). The CRM DORM-3 from the NRC was processed with each batch of samples and all values were within the 95% confidence interval for the certified value. Analytical precision was better than 7% for lab replicates. Concentrations of inorganic Hg (Hg<sub>inorg</sub>) were determined by subtracting concentrations of MMHg from THg (Hg<sub>inorg</sub> = THg - MMHg). Concentration data for metals in biota are reported on a dry weight (d. wt.) basis to account for variability in water content among species. All values are reported as mean ± standard error (SE) as a measure of uncertainty between the sample mean and an estimate of the population mean.

### **3. Results and Discussion**

#### **3.1. Metal Distributions in Sediments**

Data from 41 locations on and around Hanna Shoal show that sediments on the shoal and to the southwest are predominantly quartz sand with low clay content. Concentrations of sediment Al, a proxy for clay minerals, were as low as 1.2% on Hanna Shoal relative to values >6.0% in the adjacent NECS (Figure 2A, B, Tables 3 and 4). Fine-grained sediments have been winnowed from Hanna Shoal over time to leave a residual coarse fraction dominated by sand (Tomil and Grantz, 1976). Aluminum-poor, coarse-grained sediments also have been found nearshore (Figure 2B). Sediments richest in Al (6–6.8%) and silt + clay (>75%) were found away from the shoals in deeper water and offshore areas (Figure 2B). Concentrations of TOC also were low (<0.6%) on Hanna Shoal and highest (~1.5%) in fine-grained sediments (Figure 3). Data for the δ<sup>13</sup>C of sediment organic carbon show that nearshore sediments contain >50% terrigenous organic matter whereas all other stations contain <35% terrigenous organic matter (i.e., >65% marine organic matter, Trefry et al., 2014).



**Figure 2.** Contour maps for Al in surface sediments from (A) the area of Hanna Shoal and (B) the northeastern Chukchi Sea based on data from 2009, 2010, 2012 and 2013. Inset maps show study area off NW coast of Alaska.

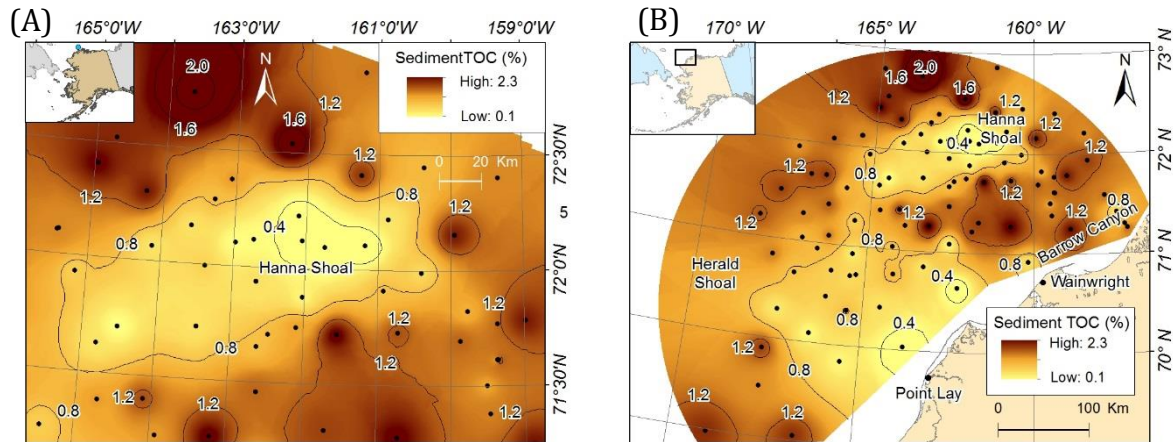
Data from the present study (Tables 3 and 4) agree very well with and complement previous results for Al, Fe, Mn, Cu, Cr, V, Ni and Zn by Naidu et al. (1997) and Trefry et al. (2014). Large ranges in values for each metal were found throughout the study area with maximum/minimum concentrations that varied from ~2 (Ag and Ba) to 18 (Hg, Tables 3 and 4). Metal concentrations directly correlated with sediment grain size ( $r = 0.9$ ) and variations in sediment metal concentrations directly related to silt + clay content. Concentrations of Al and other trace metals generally correlate well with concentrations of silt + clay because concentrations of both Al and most metals are very low in coarse-grained quartz sand or carbonate shell material and much higher in fine-grained aluminosilicates. Aluminum is rarely introduced by anthropogenic activities and is present at percent levels in most sediment relative to part per million (ppm or  $\mu\text{g/g}$ ) levels for trace metals. Thus, concentrations of trace metals were normalized to Al (i.e., use of metal/Al ratios) as a proxy for the metal controlling variables of grain size, organic carbon content and mineralogy. Concentrations of sediment Al have been previously shown to correlate strongly ( $r = 0.7\text{--}0.9$ ) or very strongly ( $r > 0.9$ ) with clay content and concentrations of selected trace metals (Trefry et al., 2003, 2013, 2014). Therefore, concentrations of other metals, such as V and Ni, in sediments follow trends observed for Al very strongly (Figure 4). Concentrations of total Hg were as low 5 ng/g (ppb) on Hanna Shoal (Figure 5A) relative to a maximum value of 57 ng/g in fine-grained sediment (Figure 5B, Tables 3 and 4). Most metals studied (Ag, Ba, Be, Cd, Cr, Cu, Fe, Ni, Pb, Sb, Se, Sn, Tl, V, Zn) showed a spatial distribution that paralleled general trends for Al and Hg. No metal contamination has been identified in any sediment collected to date from Hanna Shoal. Exceptions to this trend, are described in more detail below, have been observed for As and Mn due to diagenetic remobilization of these metals followed by enrichment in the surface layer due to oxidative precipitation (Trefry et al., 2014). All concentrations of the potentially toxic metals (Ag, Cd, Hg, Pb and Zn) were below published sediment quality criteria (Long et al., 1995). No elevated Ba concentrations were found during 2012 and 2013 in contrast to previous studies in the NECS when sampling included historic drilling sites for oil and gas (Trefry et al., 2013, 2014).

**Table 3.** Concentrations of metals and total organic carbon (TOC) in surface sediments from COMIDA: Hanna Shoal Project for 2012.

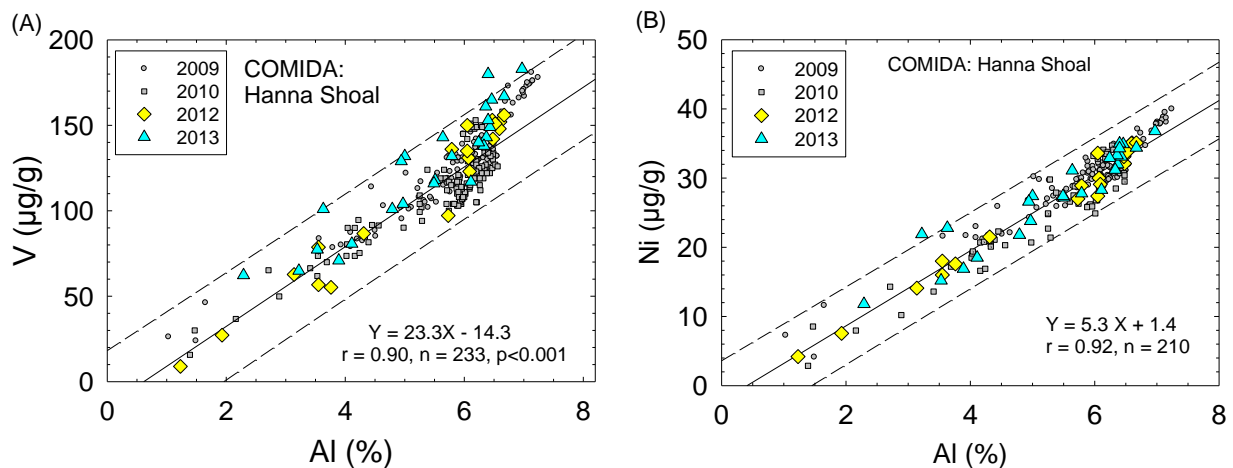
Surface Sediment	Statistic	Ag (µg/g)	Al (%)	As (µg/g)	Ba (µg/g)	Be (µg/g)	Cd (µg/g)	Cr (µg/g)	Cu (µg/g)	Fe (%)	Hg (ng/g)
Cumulative (0-1 cm)	Mean	0.13	5.00	11.1	613	1.17	0.18	68.7	13.5	2.82	28
	Std. Dev.	0.02	1.73	4.9	72	0.36	0.05	22.2	5.4	1.12	12
	n	18	18	18	18	18	18	18	18	18	18
	Maximum	0.15	6.67	20.9	767	1.51	0.28	90.2	20.3	4.20	48
	Minimum	0.08	1.23	3.2	412	0.36	0.07	11.1	3.4	0.49	5
	Median	0.14	5.92	11.3	625	1.33	0.17	79.7	14.8	3.25	31
Surface Sediment	Statistic	Mn (µg/g)	Ni (µg/g)	Pb (µg/g)	Sb (µg/g)	Se (µg/g)	Sn (µg/g)	Tl (µg/g)	V (µg/g)	Zn (µg/g)	TOC (%)
Cumulative (0-1 cm)	Mean	293	24.7	11.4	0.58	0.75	1.41	0.40	106	73.0	1.11
	Std. Dev.	102	9.7	2.7	0.14	0.26	0.45	0.07	47	30.5	0.56
	n	18	18	18	18	18	18	18	18	18	18
	Maximum	507	35.1	14.7	0.73	1.07	1.89	0.49	156	106	2.27
	Minimum	85	4.2	5.9	0.26	0.18	0.30	0.22	8.9	10.2	0.22
	Median	320	28.2	11.9	0.62	0.83	1.59	0.42	127	86.6	1.21

**Table 4.** Concentrations of metals and total organic carbon (TOC) in surface sediments from COMIDA: Hanna Shoal Project for 2013.

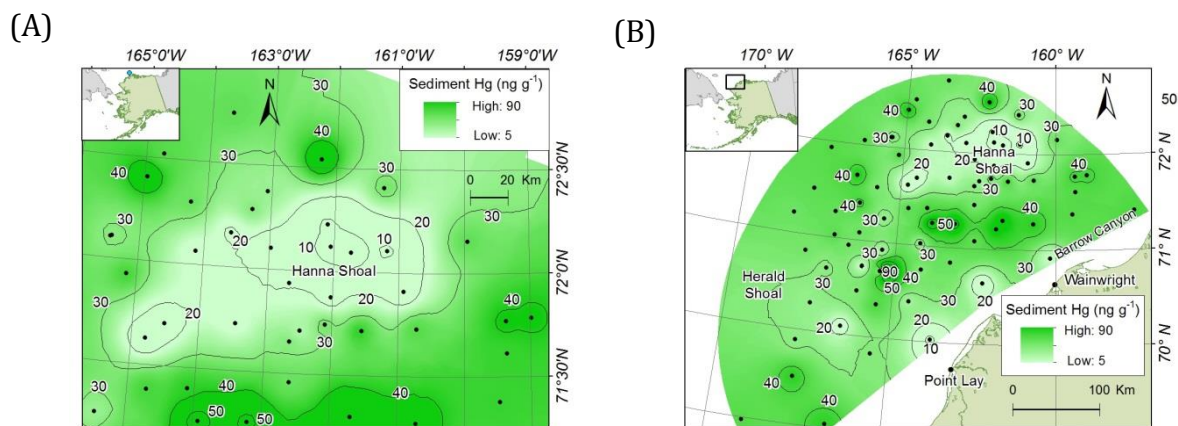
Surface Sediment	Statistic	Ag (µg/g)	Al (%)	As (µg/g)	Ba (µg/g)	Be (µg/g)	Cd (µg/g)	Cr (µg/g)	Cu (µg/g)	Fe (%)	Hg (ng/g)
Cumulative (0-1 cm)	Mean	0.11	5.35	17.7	613	1.23	0.20	75.5	15.2	3.29	32
	Std. Dev.	0.01	1.32	7.6	75	0.22	0.04	16.4	4.6	0.99	15
	n	23	23	23	23	23	23	23	23	23	23
	Maximum	0.14	6.97	38.8	823	1.53	0.31	94.0	22.2	5.21	57
	Minimum	0.09	2.29	8.18	443	0.70	0.14	34.9	7.7	1.41	10
	Median	0.11	5.79	15.5	628	1.30	0.19	80.6	16.1	3.48	26
Surface Sediment	Statistic	Mn (µg/g)	Ni (µg/g)	Pb (µg/g)	Sb (µg/g)	Se (µg/g)	Sn (µg/g)	Tl (µg/g)	V (µg/g)	Zn (µg/g)	TOC (%)
Cumulative (0-1 cm)	Mean	310	27.5	11.9	0.64	1.08	1.65	0.42	125	80.6	0.93
	Std. Dev.	80	7.1	2.3	0.13	0.22	0.40	0.06	37	23.7	0.27
	n	23	23	23	23	23	23	23	23	23	23
	Maximum	404	36.8	16.6	0.85	1.35	2.19	0.53	183	116	1.49
	Minimum	118	11.8	8.14	0.38	0.62	0.87	0.30	62.3	31.4	0.44
	Median	319	28.3	11.8	0.65	1.13	1.71	0.44	132	84.0	0.91



**Figure 3.** Contour map for total organic carbon (TOC) in surface sediments from the area of (A) Hanna Shoal and (B) the northeastern Chukchi Sea. Inset maps show study area off NW Alaska.



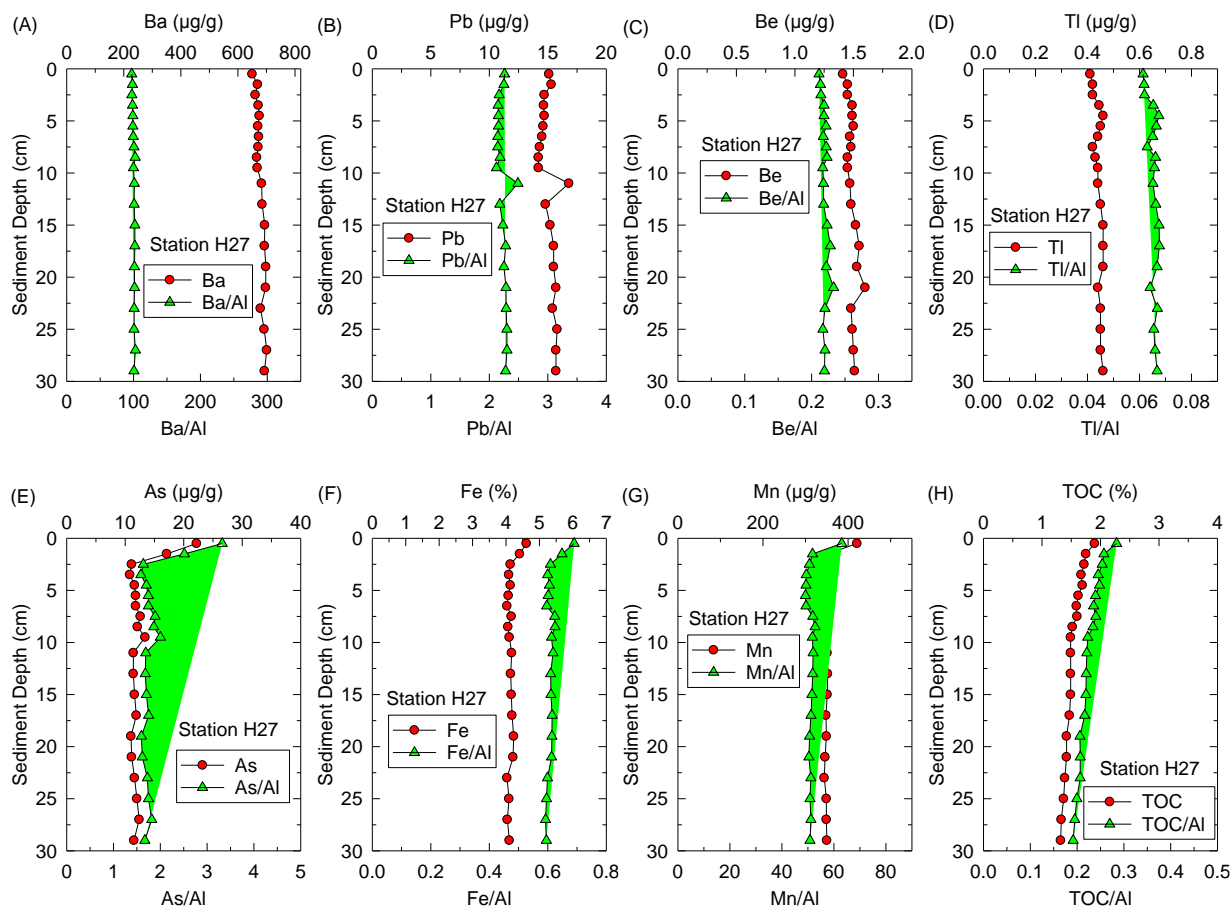
**Figure 4.** Concentrations of Al versus (A) V and (B) Ni for surface sediments collected during 2012 and 2013 on and around Hanna Shoal. Solid lines and equations show linear regression fit to data from 2009 and 2010 data (COMIDA Project), dashed lines show 99% prediction intervals,  $r$  is the correlation coefficient and  $p$  is the statistical  $p$  value.



**Figure 5.** Contour maps for total Hg in surface sediments from (A) Hanna Shoal and (B) the northeastern Chukchi Sea based on data from 2009, 2010, 2012 and 2013. Inset maps show study area off NW coast of Alaska.

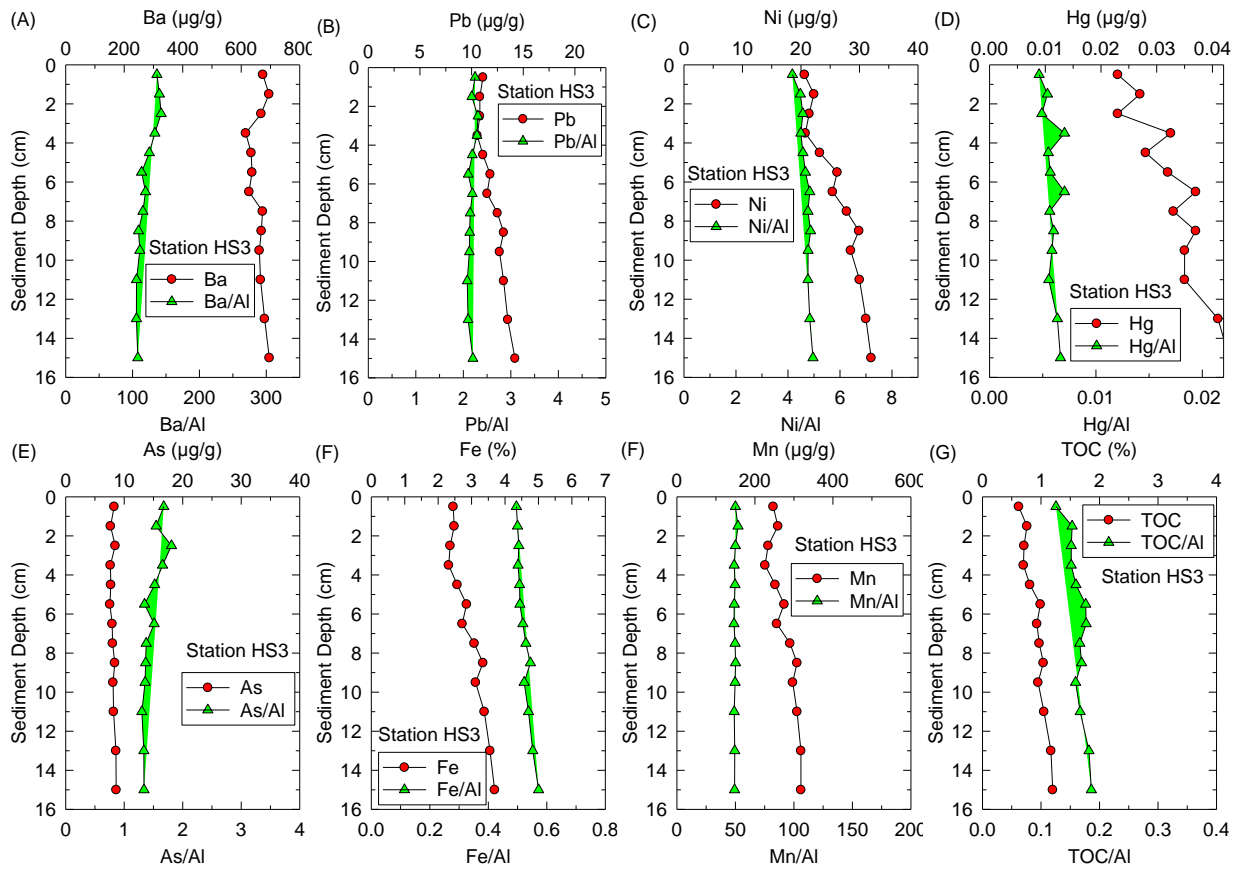
Vertical profiles for metals in sediment cores in the Hanna Shoal area showed two trends. The most common trend was essentially straight vertical profiles for the metal/Al ratio with very little variation (Figures 6A-D and 7A-D). Uniform metal/Al ratios throughout the cores were found for most metals, including Ba (Figures 6A and 7A), Pb (Figure 6B and 7B), and Hg (Figure 7D). This same observation was described by Trefry et al. (2014) for locations south of Hanna Shoal. These sediment cores likely record decades to centuries of uniform metal/Al ratios with no detectable anthropogenic or diagenetic modification. Although mixing can mute anthropogenic or diagenetic anomalies, such alteration, if any, must be small to support the uniform metal/Al ratios observed.

The second trend was elevated As values in the surface layers (0-5 cm) of sediment from some cores (Figure 6E), but not others (Figure 7E). Higher As concentrations (and the As/Al ratio) in the surface layers of sediment (Figure 6E) are caused by diagenetic remobilization of As in subsurface, reducing sediments. Subsequent upward diffusion moves dissolved As toward the oxic, sediment-water interface where it can precipitate with Fe oxides (Figure 6F) or diffuse into the overlying seawater (Farmer and Lovell, 1986; Linge and Oldham, 2002). Diagenetic enrichment of As in surface sediments (based on As/Al was observed to occur at just 8 of 58 stations during the previous COMIDA CAB study, 6 of which were located in the northeast quadrant of the study area, east of Hanna Shoal (Trefry et al., 2014). Arsenic enrichment was found in surface sediments at 6 of 18 stations sampled during the 2012 Hanna Shoal cruise (H4, H6, H14, H16, H30, H32) and 6 of 7 cores analyzed from the 2013 cruise (H27, H28, H107, H111, H112 and CBL13; but not HS3) (Figures 6E, 7E and 8A-D). Coring during 2013 focused on areas that were thought to be prone to diagenetic remobilization of As. Manganese remobilization and surface enrichment also was observed in many of the cores where As values were elevated in surface sediments (e.g., Figure 6G). The process is similar to that described above for As and previously observed in many studies (e.g., Lynn and Bonatti, 1965; Trefry and Presley, 1982).

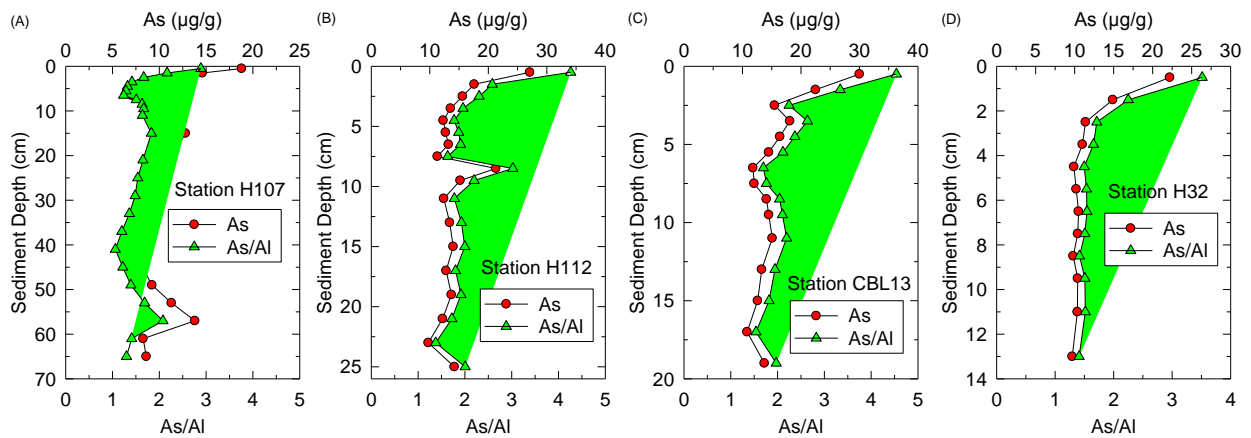


**Figure 6.** Vertical profiles for (A) Ba, (B) Pb, (C) Be, (D) Tl, (E) As, (F) Fe, (G) Mn and (H) total organic carbon (TOC) in sediment from station H27 north of Hanna Shoal along with and their ratios to Al.

During the 2013 cruise, we determined concentrations of dissolved oxygen (DO) and values for redox potential (Eh) and pH in sediment cores using an oxygen microelectrode and standard Eh and pH electrodes. This effort was added to help explain observed diagenetic remobilization of As and Mn at some sites relative to others (Figure 9). At station HS3 (no As enrichment) on the southern side of Hanna Shoal, for example, DO approached zero at about 5 mm and the total integrated amount of sediment oxygen was 27 nmol/cm<sup>2</sup> (Figure 10A). In contrast, the DO at station H27 (As enrichment) approached zero at 15 mm and the total integrated oxygen was ~3.4 times higher at 91 nmol/cm<sup>2</sup> (Figure 10B).

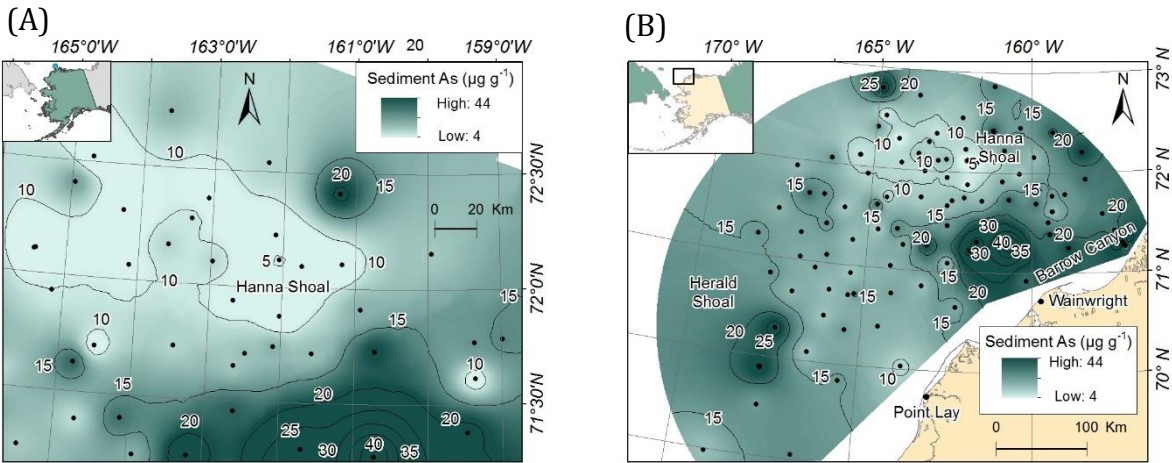


**Figure 7.** Vertical profiles for (A) Ba, (B) Pb, (C) Ni, (D) Hg, (E) As, (F) Fe, (G) Mn and (H) total organic carbon (TOC) for station HS3 on Hanna Shoal along with and their ratios to Al.

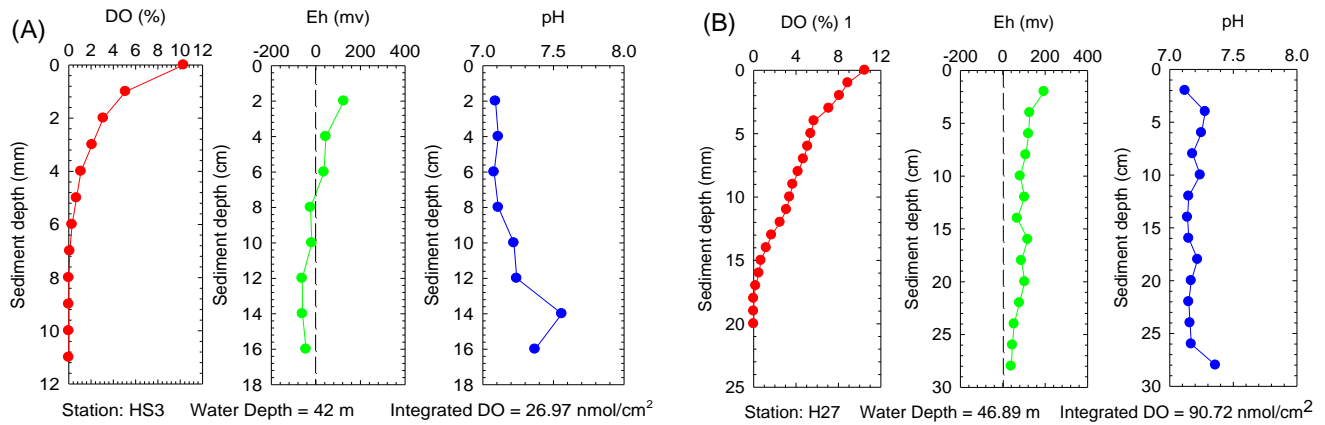


**Figure 8.** Vertical profiles for As for sediment cores from stations (A) H107, (B) H112, (C) CBL13 and (D) H32 along with and their ratios to Al.





**Figure 9.** Contour maps for total arsenic (As) in surface sediments from (A) Hanna Shoal and (B) the northeastern Chukchi Sea based on data from 2009, 2010, 2012 and 2013. Inset maps show study area off NW coast of Alaska.



**Figure 10.** Vertical profiles for dissolved oxygen (DO), redox potential (Eh) and pH for sediment cores from stations (A) HS3 near Hanna Shoal and (B) H27 to the north of Hanna Shoal in deeper water. Note difference in sediment depth scale for DO (millimeters) relative to Eh and pH (centimeters).

### 3.2. Dissolved Trace Metals and Nutrients

Concentrations of dissolved As, Sb and Tl were very relatively uniform throughout the Hanna Shoal area during both 2012 and 2013 with relative standard deviations [ $RSD = (\text{mean}/\text{standard deviation}) \times 100$ ] that averaged  $<10\%$  for all 135 data points (Tables 5 and 6). Such uniformity also was observed for salinity in the same 152 samples ( $S = 30.9 \pm 1.6$ ,  $RSD \sim 5\%$ ). Dissolved As values averaged  $\sim 18\%$  were lower than reported for surface water in the North Pacific Ocean (Table 7); some of this difference was due to 12% lower salinities in our Chukchi Sea samples ( $S = 30.9$ ) versus the North Pacific Ocean ( $S = 35$ ). Vertical profiles for dissolved As in the Hanna

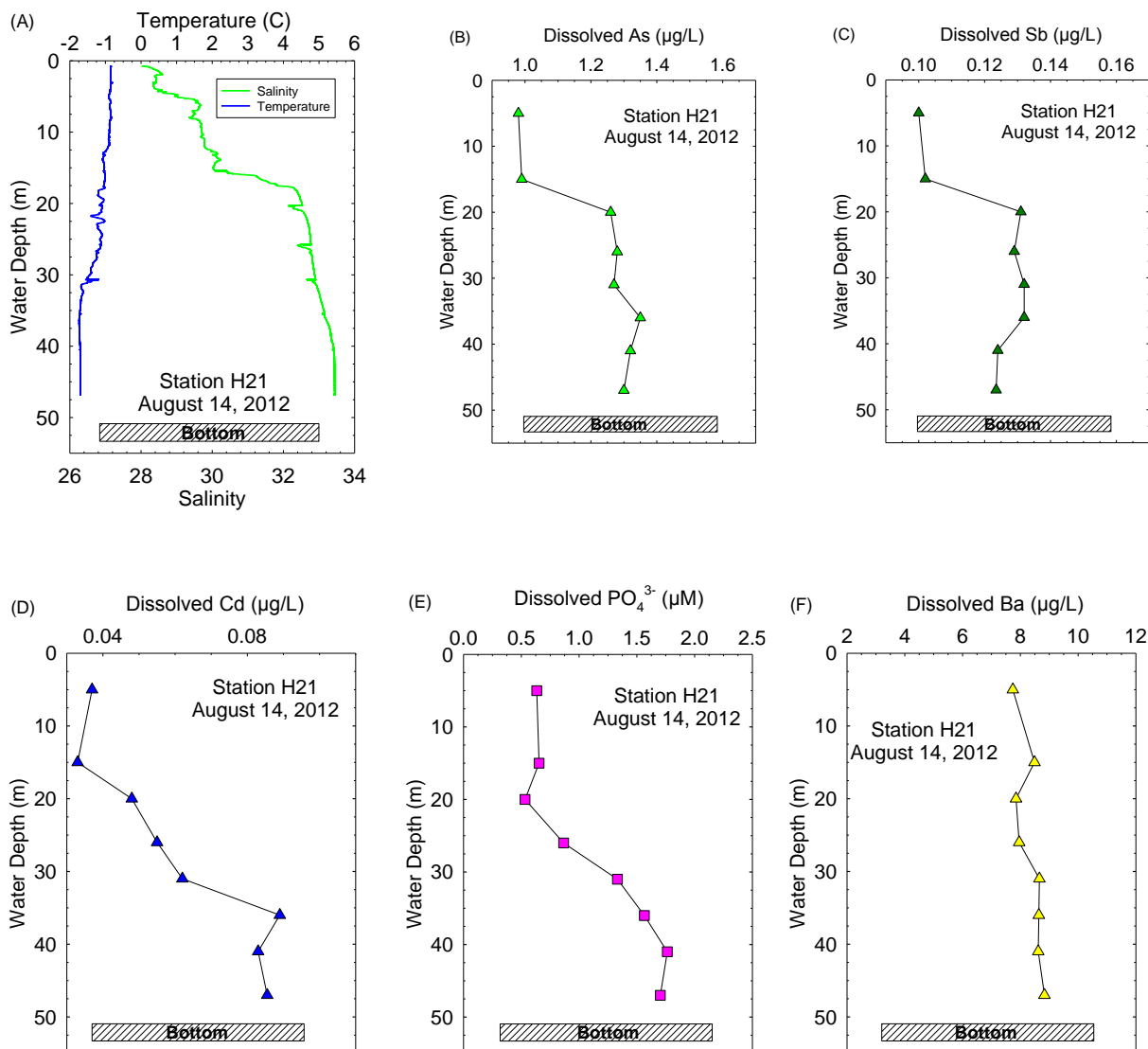
Shoal area followed a trend similar to that observed for salinity as shown for station H21 (Figure 11B). Overall, concentrations of dissolved As varied directly as a function of salinity. Trends for Sb were somewhat similar as shown by the vertical profile for dissolved Sb at station H21 (Figure 11C); however, the relationship between dissolved Sb and salinity was weak ( $r < 0.3$ ), most likely due to the small RSD for dissolved Sb (~9%), combined with an analytical precision of about ~4%. Concentrations of both As and Sb show relatively little variation in the northeastern Chukchi Sea. Both metals have relatively long residence times in the ocean (As at 40, 000 years and Sb at 6,000 yrs; Broecker and Peng, 1981) and have somewhat limited reactivity.

**Table 5.** Concentrations of dissolved metals in seawater from the COMIDA: Hanna Shoal Project for 2012 from stations BSR5, H1, H2, H4, H6, H16, H21, H24, H30, H32 and BC5.

Statistic	Salinity (g/L)	As ( $\mu\text{g/L}$ )	Ba ( $\mu\text{g/L}$ )	Cd ( $\mu\text{g/L}$ )	Cr ( $\mu\text{g/L}$ )	Cu ( $\mu\text{g/L}$ )	Ni ( $\mu\text{g/L}$ )	Pb ( $\mu\text{g/L}$ )	Sb ( $\mu\text{g/L}$ )	Se ( $\mu\text{g/L}$ )	Tl ( $\mu\text{g/L}$ )	Zn ( $\mu\text{g/L}$ )
Mean	31.2	1.23	8.79	0.071	0.095	0.291	0.347	0.021	0.126	0.043	0.012	0.313
Std. Dev.	1.6	0.16	0.90	0.027	0.026	0.075	0.057	0.021	0.018	0.010	0.001	0.165
n	77	77	77	77	77	77	77	77	77	77	77	77
Maximum	33.0	1.61	10.9	0.144	0.197	0.635	0.494	0.137	0.166	0.065	0.015	0.840
Minimum	27.0	0.94	5.71	0.029	0.042	0.131	0.206	0.003	0.097	0.017	0.008	0.062
	32.0	1.24	8.79	0.075	0.097	0.283	0.342	0.012	0.125	0.042	0.012	0.278

**Table 6.** Concentrations of dissolved metals in seawater from the COMIDA: Hanna Shoal Project for 2013 from stations BRS5, HS3, H7, H9, H28, H29, H102, H107, H111, H114, BarC4 and CBL11.

Statistic	Salinity (g/L)	As ( $\mu\text{g/L}$ )	Ba ( $\mu\text{g/L}$ )	Cd ( $\mu\text{g/L}$ )	Cr ( $\mu\text{g/L}$ )	Cu ( $\mu\text{g/L}$ )	Ni ( $\mu\text{g/L}$ )	Pb ( $\mu\text{g/L}$ )	Sb ( $\mu\text{g/L}$ )	Se ( $\mu\text{g/L}$ )	Tl ( $\mu\text{g/L}$ )	Zn ( $\mu\text{g/L}$ )
Mean	30.8	1.22	8.36	0.052	0.080	0.295	0.345	0.007	0.113	0.035	0.011	0.270
Std. Dev.	1.5	0.12	0.91	0.022	0.026	0.050	0.056	0.003	0.010	0.008	0.001	0.110
n	75	75	75	75	75	75	75	75	75	75	75	75
Maximum	33.0	1.45	10.2	0.112	0.157	0.419	0.468	0.016	0.133	0.056	0.013	0.682
Minimum	26.0	0.97	5.13	0.027	0.031	0.192	0.214	0.002	0.091	0.019	0.009	0.126
Median	31.5	1.24	8.37	0.042	0.078	0.294	0.343	0.007	0.112	0.035	0.011	0.253



**Figure 11.** Vertical profiles for (A) temperature and salinity, and dissolved (B) As, (C) Sb, (D) Cd, (E) phosphate and (F) Ba for station H21 located west of Hanna Shoal.

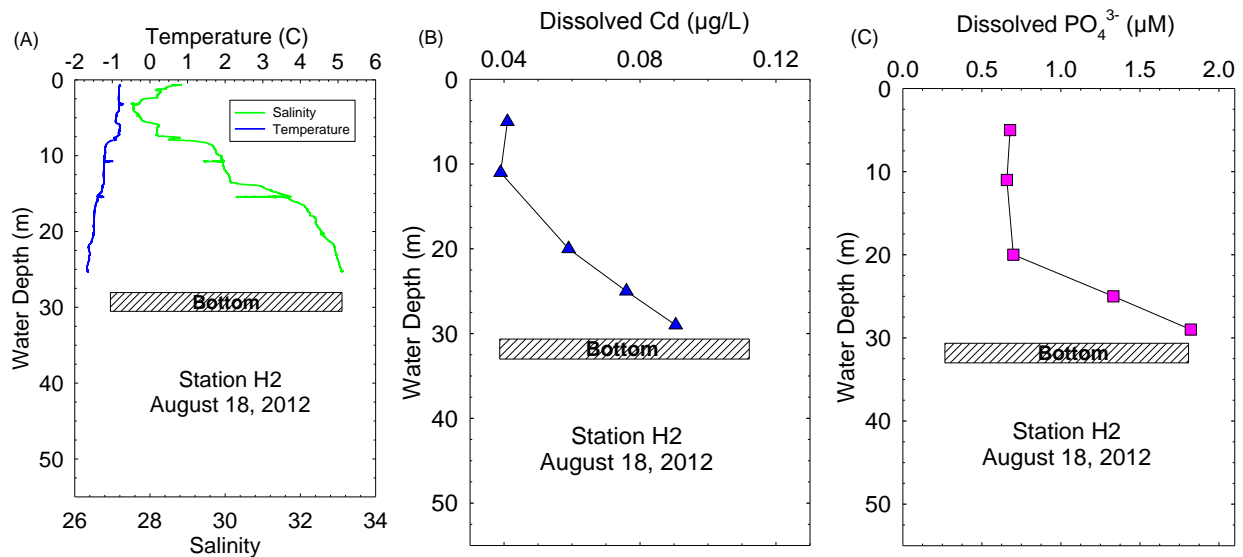
Concentrations of Cd, Cu and Ni were more variable than observed for As and Sb with values for the RSD that ranged from 16 to ~50% (Tables 5 and 6). Vertical profiles for Cd (Figures 11D and 12B) and Ni looked similar to those for As and Sb in that they followed salinity. However, the ratios of concentrations for bottom water to surface water for Ba, Cd and Ni were 1.7, 2.8 and 1.8, respectively, relative to values of <1.2 for both As and Sb. In contrast with As, concentrations of dissolved Cd did not correlate with salinity and the maximum/minimum for Cd was >5 at a salinity of 32 (chosen as reference) relative to a maximum/minimum ratio (at S = 32) of 1.3 for dissolved As.

**Table 7.** Concentrations of dissolved trace metals in the Chukchi Sea from this study and for the North Pacific Ocean from Donat and Bruland (1995).

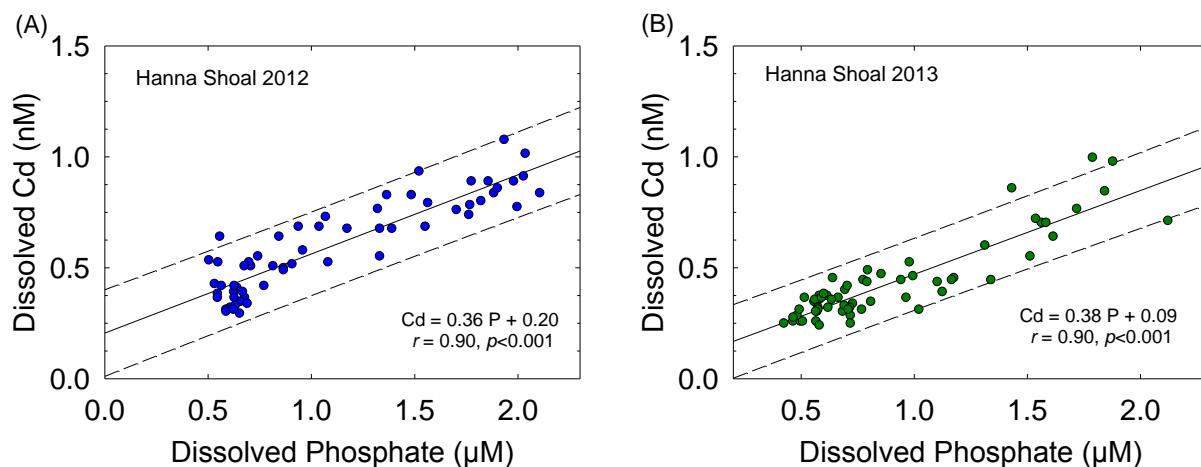
Metal	Mean This Study ( $\mu\text{g/L}$ )	Mean This Study (nM)	North Pacific Surface <sup>1</sup> (nM)	North Pacific Deep <sup>1</sup> (nM)
As	1.2	16	20	24
Cd	0.060	0.5	$\leq 0.01$	1
Cr	0.085	1.3	3	5
Cu	0.30	4.5	0.5-1.3	4.5
Ni	0.35	5.9	2	11-12
Pb	0.010	48 pM	14-50 pM	3-6 pM
Sb	0.11	0.9	0.7-1.1	-
Se	0.04	0.5	0.5	2.3
Tl	0.012	60 pM	60-80 pM	80 pM
Zn	0.3	5	0.1-0.2	2-10

<sup>1</sup>Donat and Bruland (1995).

Concentrations of Cd, Cu, Ni and Zn in the shallow (~50 m) bottom water of the NECS were more closely matched with those for the deep North Pacific Ocean (Table 7) and show a nutrient-type behavior. Thus, the vertical distributions of these metals follow those for the deep sea, even though the NECS is shallow. The strong Cd versus phosphate relationship for the Chukchi Sea (average slope Cd/P = 0.37 for our data, Figure 13) is within the range of 0.34–0.40 found for the northwest Pacific Ocean and the Sea of Okhotsk (Abe, 2002) and other global trends. Therefore, the vertical distribution of the nutrient-type metals in the NECS corresponds to observed trends in the deep sea. Concentrations of Cr, Pb and Se correspond with values for surface water in the North Pacific Ocean (Table 7). These metals do not show nutrient-type profiles.



**Figure 12.** Vertical profiles for (A) temperature and salinity and dissolved (B) Cd and (C) phosphate for station H2 located west of Hanna Shoal.



**Figure 13.** Concentrations of dissolved Cd versus dissolved phosphate for water samples collected during (A) 2012 and (B) 2013 from the northeastern Chukchi Sea with a focus on the area around Hanna Shoal.

### 3.3. Metals in Biota

Concentrations of Ag, As, Ba, Cd, Cr, Cu, Fe, Total Hg, MMHg, Mn, Ni, Sb, Se, Sn, V and Zn were determined for the following organisms and tissue types from the Hanna Shoal area during 2012 and 2013: mixed zooplankton, whole clams (*Astarte borealis*), whelk muscle (*Neptunea borealis*), snow crab muscle (*Chionocetes opilio*) and arctic cod muscle (*Boreogadus saida*) (Tables 8-12). The primary focus of this effort was on THg and MMHg in biota because of the keen interest and concern for Hg contamination in the Arctic (e.g., [Campbell et al., 2005](#)). Results for other metals are also presented and discussed here to provide a baseline for future assessments.

Average concentrations of THg in mixed zooplankton (150-µm mesh) from the NECS were  $13 \pm 1$  ng/g (d. wt., Table 8). Zooplankton from the NECS have THg concentrations at the low end of a range of values reported for zooplankton in the Arctic. For example, [Campbell et al. \(2005\)](#) found an average THg of  $25 \pm 15$  ng/g (d. wt.) for *Calanus hyperboreus* from the Northwater Polynya. [Pucko et al. \(2014\)](#) reported THg concentrations of  $14 \pm 6$  ng/g (d. wt.) for *Calanus hyperboreus* collected in the Amundsen Gulf and the Canadian Beaufort Sea whereas [Stern and Macdonald \(2005\)](#) reported an average of  $85 \pm 9$  ng/g (d. wt.) for the Canadian basin. The large range of THg values reported for *Calanus hyperboreus* are most likely due to seasonal shifts in physiology and regional differences in food availability with the lowest concentrations identified during late summer when lipid and caloric energy content are highest ([Percy and Fife, 1981](#); [Pucko et al., 2014](#)).

Concentrations of THg in zooplankton from the NECS were 2-10 times lower than values reported for non-arctic regions. [Knauer and Martin \(1972\)](#) reported a mean THg of  $119 \pm 46$  ng/g for mixed zooplankton along a transect from Monterey Bay to Hawaii. [Bargagli et al. \(1998\)](#) found an average of  $65 \pm 16$  ng/g for mixed zooplankton from Terra Nova Bay in the Antarctic.

**Table 8.** Concentrations of metals (on a dry weight basis) in zooplankton (150 µm mesh, n = 16) collected during 2012 and 2013 from the northeastern Chukchi Sea.

Statistic	Ag (µg/g)	As (µg/g)	Ba (µg/g)	Cd (µg/g)	Cr (µg/g)	Cu (µg/g)	Fe (µg/g)	Total Hg (ng/g)	MMHg (ng/g)	Mn (µg/g)	Ni (µg/g)	Se (µg/g)	Sn (µg/g)	V (µg/g)	Zn (µg/g)
Mean	0.32	5.7	14.0	2.6	1.4	22.0	426	13.4	4.3	5.7	0.10	2.3	0.57	1.5	125
SD	0.41	3.5	7.0	2.0	1.2	25.7	337	4.9	2.6	7.9	0.04	0.8	0.30	1.0	98
Median	0.15	4.6	13.5	2.1	1.1	9.6	295	11.8	4.0	2.2	0.11	2.4	0.55	1.2	88
Max	1.65	16.3	26.2	9.1	3.8	86.3	1415	22.5	8.7	30.4	0.18	3.6	0.99	3.7	428
Min	0.05	2.7	5.2	0.5	0.2	3.3	104	6.8	<1.5	0.4	0.02	0.6	0.01	0.3	15

Lower concentrations of THg in arctic zooplankton from this and other studies likely result from (1) lower deposition rates for atmospheric Hg in the Arctic, (2) lower concentrations of THg in arctic phytoplankton and (3) greater use of POM, sediment OM and benthic algae as food sources. Zooplankton from the NECS contained MMHg in the range of <1.5–8.7 ng/g (d. wt.) with an average of  $37 \pm 7\%$  of the THg as MMHg in the 10 zooplankton samples for values above the MDL (Table 8).

Among the other metals in zooplankton, average concentrations of Ag, Cr, Ni, Sn and V were <2 µg/g with RSDs >50% (Table 8). When the RSD is high, it is difficult to observe statistically significant changes in metal concentrations over time and space. Average concentrations of As, Ba, Cd, Mn and Se were 2-14 µg/g (d. wt.) and also had high RSDs at 35 to >100%. In contrast, essential elements such as Cu, Zn and Fe were present at higher yet variable values of 22, 125 and 426 µg/g, respectively.

Average concentrations of THg in whole bivalves (*Astarte borealis*) from this study were  $48 \pm 13$  ng/g (d. wt., Table 9) with average MMHg content at  $20 \pm 7\%$  of the THg (MMHg =  $13 \pm 9$  ng/g). The % MMHg in bivalves decreased with increasing THg due to the increased relative abundance of Hg<sub>inorg</sub>. Pan and Wang (2011) reported that the relative concentrations of THg in bivalves were directly correlated with the efflux rates for inorganic Hg (Hg<sub>inorg</sub>) which is consistent with data from this study. Bivalves from the NECS had THg concentrations in whole organisms that were at the lower end of the range of values previously reported for other bivalves from lower latitudes. Kimbrough et al. (2008) reported lower Hg concentrations for bivalves from Alaska (60-120 ng/g, d. wt.) than bivalves from the contiguous U.S. (up to 1,280 ng/g, d. wt.) during the NOAA National Status and Trends (NST), Mussel Watch Program. Apeti et al.

**Table 9.** Concentrations (on a dry weight basis) of metals in whole clams (*Astarte borealis*, n = 11) collected during 2012 and 2013 from the northeastern Chukchi Sea.

Statistic	Ag (µg/g)	As (µg/g)	Ba (µg/g)	Cd (µg/g)	Cr (µg/g)	Cu (µg/g)	Fe (µg/g)	Total Hg (ng/g)	MMHg (ng/g)	Mn (µg/g)	Ni (µg/g)	Se (µg/g)	Sn (µg/g)	V (µg/g)	Zn (µg/g)
Mean	0.23	11.0	14.8	22.8	1.3	9.2	869	48	13	14.1	3.8	8.2	0.29	2.0	89.9
SD	0.31	2.4	8.2	4.6	0.3	4.4	180	17	9	5.9	3.4	1.5	0.52	0.4	38.0
Median	0.12	10.4	13.3	22.0	1.2	8.9	820	42	10	12.5	3.2	8.0	0.07	2.0	79.2
Max	1.14	16.6	35.8	29.5	1.7	19.9	1215	120	36	23.9	13.4	11.2	1.64	2.6	189.1
Min	0.10	8.4	5.2	15.9	0.9	3.7	664	26	8	7.6	1.1	5.9	0.01	1.5	62.4

(2012) also as part of the NST, reported average THg and MMHg concentrations of 119 and 44 ng/g (d. wt.), respectively, for whole oyster tissue collected from the Gulf of Mexico, 45% and 300% greater, respectively, than average values identified for bivalves in this study (Table 9). Lower Hg concentrations in arctic bivalves likely result from (1) lower rates of atmospheric deposition, (2) reduced concentrations of Hg in arctic phytoplankton (Hammerschmidt and Fitzgerald, 2006) and (3) an essentially pristine sedimentary environment with respect to Hg (Fox et al., 2014).

Average concentrations of Ag, Cr, Sn and V also were <2 µg/g in clams with RSDs that were lower for Cr and V than in zooplankton at 20-30% (Table 9). Average concentrations of As, Cd, Mn and Se were 8-23 µg/g (d. wt.) with RSDs at ~20%. Such values make the clams a more useful organism for long-term monitoring.

The whelk *Neptunea borealis* had average THg in muscle that ranged from 19-402 ng/g (d. wt.) (Table 10) and MMHg accounted for 91 ± 4% of the THg (Table 10). The highest concentrations of THg for *N. borealis* were found for larger whelk, with significantly greater concentrations for whelk ≥5 cm in shell length relative to whelk <5 cm ( $p = 0.04$  and  $0.01$  respectively, t-test one-tailed, assuming equal variance). This muscle tissue had very low (<1 µg/g) concentrations of Ag, Ba, Cd, Cr, Mn, Ni, Se and V (Table 10). Average concentrations of the essential elements Fe and Zn were considerably higher at 76 and 73 µg/g, respectively.

**Table 10.** Concentrations (on a dry weight basis) of whelk muscle (*Neptunea borealis*, n = 12) collected during 2012 and 2013 from the northeastern Chukchi Sea.

Statistic	Ag (µg/g)	As (µg/g)	Ba (µg/g)	Cd (µg/g)	Cr (µg/g)	Cu (µg/g)	Fe (µg/g)	Total Hg (ng/g)	MMHg (ng/g)	Mn (µg/g)	Ni (µg/g)	Se (µg/g)	Sn (µg/g)	V (µg/g)	Zn (µg/g)
Mean	0.19	54.5	0.34	0.22	0.12	14.6	76	158	173	0.085	0.032	1.9	0.12	0.17	73
SD	0.07	26.0	0.18	0.09	0.04	5.5	32	114	117	0.044	0.017	0.3	0.21	0.06	11
Median	0.19	62.7	0.43	0.21	0.13	14.3	68	133	145	0.082	0.032	1.9	0.05	0.19	70
Max	0.31	101.9	0.53	0.40	0.16	21.5	121	402	525	0.149	0.073	2.5	0.68	0.26	96
Min	0.07	15.1	0.02	0.05	0.03	5.2	31	19	25	0.003	0.005	1.6	0.03	0.04	64

Concentrations of THg in muscle tissue from the snow crab (*Chionocetes opilio*) averaged 112 ± 50 ng/g, d. wt., (Table 11). No comparison between genders was possible because all large snow crabs (>3 cm) collected in this study were males, and all small snow crabs (<3 cm) were pooled with mixed gender prior to analysis. No significant ( $p = 0.637$ ) relationship was identified between carapace width (size) and concentrations of THg; this is consistent with previous results for snow crabs from the NECS (Fox et al., 2014). Concentrations of MMHg averaged 89 ± 41 ng/g (d. wt.) and the % MMHg averaged 76 ± 6%. Concentrations of Ag, Ba, Cd, Cr, Ni, Sn and V were <1 µg/g (d. wt., Table 11). Concentrations of the essential metals Cu, Fe and Zn were much higher at 16, 28 and 123 µg/g (d. wt., Table 11).

**Table 11.** Concentrations (on a dry weight basis) of metals in snow crab muscle (*Chionocetes opilio*, n = 12) collected during 2012 and 2013 from the northeastern Chukchi Sea.

Statistic	Ag (µg/g)	As (µg/g)	Ba (µg/g)	Cd (µg/g)	Cr (µg/g)	Cu (µg/g)	Fe (µg/g)	Total Hg (ng/g)	MMHg (ng/g)	Mn (µg/g)	Ni (µg/g)	Se (µg/g)	Sn (µg/g)	V (µg/g)	Zn (µg/g)
Mean	0.69	35.7	0.63	0.14	0.26	15.5	28	112	89	4.3	0.11	4.1	0.19	0.21	123
SD	0.27	15.1	0.34	0.07	0.20	4.8	14	50	41	4.6	0.07	1.6	0.19	0.04	12
Median	0.65	31.5	0.67	0.11	0.21	16.3	22	100	77	2.2	0.08	3.5	0.12	0.20	122
Max	1.32	74.8	1.13	0.33	0.77	21.5	65	217	168	13.9	0.27	8.4	0.66	0.27	149
Min	0.35	18.0	0.13	0.09	0.09	4.8	14	46	34	1.0	0.03	2.9	0.01	0.15	107

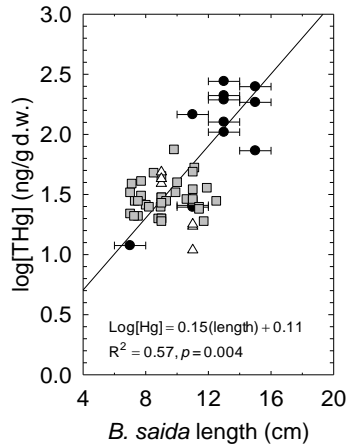
Concentrations of THg in muscle from arctic cod (*Boreogadus saida*) collected in 2012 and 2013 ranged from 11–49 ng/g (d. wt.) with an overall average of  $30 \pm 13$  ng/g (Table 12). Log<sub>10</sub>-transformed concentrations of Hg versus fish length showed a strong correlation ( $r = 0.75$ ) for all data (2010, 2012, 2013, Figure 14). When only fish from the 2012 and 2013 surveys were considered, the mean THg value of ~30 ng/g in muscle was ~4 times lower than found in 2010 and clearly related to smaller cod in 2012 and 2013 (Figure 14). Size-frequency distributions for arctic cod from all three years followed a normal distribution (normal probability plot,  $R^2 = 0.90$ ,  $p < 0.001$ ). No significant correlations were identified between Hg concentrations and any site specific or environmental variables measured during this study including spatial distribution (i.e., latitude or longitude).

Relative to previous studies, average THg concentrations for arctic cod muscle from this study were 2–4 times lower than concentrations reported for the Canadian Arctic of: (1)  $190 \pm 30$  ng/g (d. wt.) (Atwell et al., 1998), (2)  $270 \pm 40$  ng/g (d. wt.) (Stern and Macdonald, 2005), (3)  $158 \pm 13$  ng/g (d. wt.) (van der Veldeen et al., 2013) and (4)  $363 \pm 42$  ng/g (d. wt.) (Clayden et al., 2015). Lower concentrations of Hg in this study versus the Canadian Arctic were not explained by differences in fish size and are consistent with ~4 times lower concentrations of THg ( $85 \pm 5$  ng/g, d. wt.) reported by Stern and Macdonald (2005) for arctic cod collected from the Chukchi Sea.

**Table 12.** Concentrations (on a dry weight basis) of metals in arctic cod muscle (*Boreogadus saida*, n = 12) collected during 2012 and 2013 from the northeastern Chukchi Sea.

Statistic	Ag (µg/g)	As (µg/g)	Ba (µg/g)	Cd (µg/g)	Cr (µg/g)	Cu (µg/g)	Fe (µg/g)	Total Hg (µg/g)	MMHg (ng/g)	Mn (µg/g)	Ni (µg/g)	Se (µg/g)	Sn (µg/g)	V (µg/g)	Zn (µg/g)
Mean	0.34	9.0	0.7	0.22	0.15	4.9	40	30	27	2.1	0.11	2.6	1.8	0.3	51.8
SD	0.20	5.5	0.4	0.18	0.08	1.2	20	13	6	1.0	0.05	0.5	3.5	0.1	11.3
Median	0.31	8.5	0.6	0.21	0.13	4.9	41	28	29	1.9	0.13	2.5	0.4	0.2	49.8
Max	0.68	21.8	1.6	0.58	0.30	7.1	72	49	35	4.6	0.21	3.5	8.9	0.4	73.4
Min	0.12	3.0	0.1	0.02	0.04	3.4	18	11	12	1.0	0.04	1.9	0.3	0.2	37.4

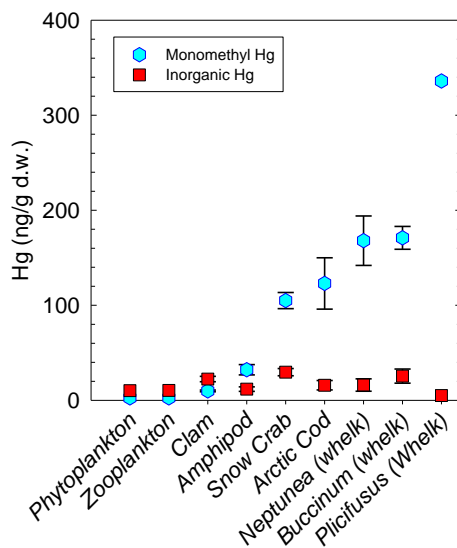




**Figure 14.** Log transformed concentrations of THg in ng/g (d.wt.) versus fish length in cm. 95% prediction interval is from 2010 data.

Concentrations of MMHg in muscle accounted for an average of  $97 \pm 6\%$  of the THg concentrations in *B. saida* (Table 12) consistent with values of  $>90\%$  MMHg from previous studies (Lavoie et al., 2010; Douglas et al., 2012). Again, average concentrations of Ag, Ba, Cd, Cr, Ni, and V were  $<1 \mu\text{g/g}$  with only minor amounts of these metals incorporated in muscle. The RSDs for these metals ranged from 22 to  $>100\%$  and averaged 54%.

Overall, concentrations of MMHg increased from 4 ng/g (d. wt.) in zooplankton to 13 ng/g (d. wt.) in clams to 165 ng/g (d. wt.) in whelk (Figure 15). Despite the distinct biomagnification of MMHg, concentrations of  $\text{Hg}_{\text{inorg}}$  stay relatively uniform at  $20 \pm 5 \text{ ng/g}$  (d. wt.) across the food web (Figure 15).



**Figure 15.** Concentrations of inorganic and monomethyl Hg in biota collected from the northeastern Chukchi Sea during 2012 and 2013.

## 4. Acknowledgements

We thank Heather Crowley of the Bureau of Ocean Energy Management (BOEM), U.S. Department of Interior, for her interest and enthusiasm for studies of metals in biota. We also thank the crew, officers and commanding officer onboard the USCGC *Healy* for logistical and sampling support. We thank Ken Dunton for his leadership as Chief Scientist for the Hanna Shoal Ecosystem Study and Jackie Grebmeier and Lee Cooper for serving as Chief Scientists on the two cruises. This field and laboratory study was funded by the U.S. Department of the Interior, Bureau of Ocean Energy Management (BOEM), Alaska Outer Continental Shelf Region, Anchorage, Alaska under Cooperative Agreement No. M11AC00007 as part of the Hanna Shoal Ecosystem Project and the BOEM Alaska Environmental Studies Program.

## 5. References

- Abe, K., 2002. Preformed Cd and PO<sub>4</sub> and the relationship between the two elements in the northwestern Pacific and the Okhotsk Sea. *Mar. Chem.* 79, 27-36.
- Apeti, D.A., Lauenstein, G.G., Evans, D.W., 2012. Recent status of total mercury and methyl mercury in the coastal waters of the northern Gulf of Mexico using oysters and sediments from NOAA's mussel watch program. *Mar. Pollut. Bull.* 64, 2399-2408.
- Atwell, L., Hobson, K.A., Welch, H.E., 1998. Biomagnification and bioaccumulation of mercury in an arctic marine food web: insights from stable nitrogen isotope analysis. *Can. J. Fish. Aquat. Sci.* 55, 1114-1121.
- Bargagli, R., Monaci, F., Sanchez-Hernandez, J.C., Cateni, D., 1998. Biomagnification of mercury in an Antarctic marine coastal food web. *Mar. Ecol. Prog. Ser.* 169, 65-76.
- Bloom, N.S., Crecelius, E.A., 1983. Determination of mercury in seawater at sub-nanogram per liter levels. *Mar. Chem.* 14, 49-59.
- Bloom, N., 1989. Determination of picogram levels of methylmercury by aqueous phase ethylation, followed by cryogenic gas-chromatography with cold vapor atomic fluorescence detection. *Can. J. Fish. Aquat. Sci.* 46, 1131-1140.
- Broecker, W.S., Peng, T.-H., 1982. *Tracers in the Sea*. Lamont-Doherty Geological Observatory, Palisades, NY, 690 pp.
- Campbell, L.M., Norstrom, R.J., Hobson, K.A., Muir, D.C.G., Backus, S., Fisk, A.T., 2005. Mercury and other trace elements in a pelagic Arctic marine food web (Northwater Polynya, Baffin Bay). *Sci. Total Environ.* 351-352, 247-263.
- Clayden, M.G., Arsenault, L.M., Kidd, K.A., O'Driscoll, N.J., Mallory, M.L., 2015. Mercury bioaccumulation and biomagnification in a small Arctic polynya ecosystem. *Sci. Total Environ.* 509-510, 206-215.
- Creager, J.S., McManus, D.A., 1965. Pleistocene drainage patterns on the floor of the Chukchi Sea. *Mar. Geol.* 3, 279-290.
- Donat J.R., Bruland, K.W., 1995. Trace elements in the oceans. pp. 247–281 in: Salbu B, Steinnes E, ed. *Trace elements in natural waters*. CRC Press, Boca Raton.

- Douglas, T.A., Loseto, L.L., Macdonald, R.W., Outridge, P., Dommergue, A., Poulain, A., Amyot, M., Barkay, T., Berg, T., Chetelat J., Constant, P., Evans, M., Ferrari, C., Ganter, N., Johnson, M.S., Kirk, J., Kroer, N., Larose, C., Lean, D., Gissel, N., Poissant, L., Rognerud, S., Skov, H., Sorensen, S., Wang, F., Wilson, S., Zdanowicz, C.M., 2012. The fate of mercury in arctic terrestrial and aquatic ecosystems, a review. *Environ. Chem.* 9, 321-355.
- Dunton, K.W. et al., 2012. Chukchi Sea Offshore Monitoring in Drilling Area (COMIDA): Chemical and Benthos (CAB). OCS Study BOEM 2012-012. Final Report to Bureau of Ocean Energy Management, Alaska Outer Continental Shelf Region, Anchorage, Alaska,
- Farmer, J.G., Lovell, M.A., 1986. Natural enrichment of arsenic in Lock Lomond sediments. *Geochim. Cosmochim. Acta* 50, 2059–2067.
- Feder, H.M., Naidu, A.S., Jewett, S.C., Hameedi, J.M., Johnson, W.R., Whitley, R.E., 1994. The northeastern Chukchi Sea: benthos-environment interactions. *Mar. Ecol. Prog. Ser.* 111, 171–190.
- Folk, R.L., 1974. *Petrology of Sedimentary Rocks*. Hemphill Publishing Co., Austin.
- Fox, A.L., Hughes, E.A., Trocine, R.P., Trefry, J.H., Schonberg, S.V., McTigue, N.D., Lasorsa, B.K., Konar, B., Cooper, L.W., 2014. Mercury in the northeastern Chukchi Sea: Distribution patterns in seawater and sediments and biomagnification in the benthic food web. *Deep-Sea Res. II*, 102, 56-67.
- Grantz, A., Dinter, D.A., Hill, E.R., Hunter, R.E., May, S.D., McMullen, R.H., Philips, R.L., 1982. Geologic framework, hydrocarbon potential and environmental conditions for exploration and development of proposed oil and gas lease sale 85 in the central and northern Chukchi Sea - A Summary Report. U.S. Geological Survey Open-File Report, p. 1053.
- Grasshoff, K., 1976. *Methods of Seawater Analysis*. Verlag Chemie, New York, 317 pp.
- Grebmeier, J.M., Moore, S.E., Overland, J.E., Frey, K.E., Gradinger, R., 2010. Biological response to recent Pacific Arctic sea ice retreats. *Eos, Trans. Am. Geophys. Union* 91, 161-168.
- Hammerschmidt, C.R., Fitzgerald, W.F., 2006. Methylmercury in freshwater fish linked to atmospheric mercury deposition. *Environ. Sci. Technol.* 40, 7764-7770.
- Holland, M.M., Bitz, C.M., Tremblay, B., 2006. Future abrupt reductions in the summer Arctic sea ice. *Geophys. Res. Lett.* 33, L23503.
- Hopkins, D.M., 1967. *The Bering Land Bridge*. Stanford University Press, Stanford, Calif.,
- Kanneworff, E., Nicolaisen, W., 1973. The "HAPS:" A frame supported bottom corer. *Ophelia* Suppl. 10, 119-129.
- Kimbrough, K.L., Johnson, W.E., Lauenstein, G.G., Christensen, J.D., Apeti, D.A., 2008. An assessment of two decades of contaminant monitoring in the nation's coastal zone. Silver Spring, MD. NOAA Technical Memorandum NOS NCCOS 74.
- Knauer, G.A., Martin, J.H., 1972. Mercury in a pelagic food chain. *Limnol. Oceanogr.* 17, 868-876.

- Konar, B., Ravelo, A., Grebmeier, J., Trefry, J.H., 2014. Size frequency distributions of key epibenthic organisms in the eastern Chukchi Sea and their correlations with environmental parameters. *Deep-Sea Res. II* 102, 107-118.
- Lavoie, R.A., Hebert, C.E., Rail, J., Braune, B.M., Yumvihoze, E., Hill, L.G., Lean, D.R.S., 2010. Trophic structure and mercury distribution in a Gulf of St. Lawrence (Canada) food web using stable isotope analysis. *Sci. Total Environ.* 408, 5529-5539.
- Linge, K.L., Oldham, C.E., 2002. Arsenic remobilization in a shallow lake: The role of sediment resuspension. *J. Environ. Qual.* 31, 822-828.
- Long, E.R., Macdonald, D.D., Smith, S.L., Calder, F.D., 1995. Incidence of adverse biological effects with ranges of chemical concentrations in marine and estuarine sediments. *Environ. Manage.* 19:81-97.
- Lynn, D.C., Bonatti, E., 1965. Mobility of manganese in diagenesis of deep sea sediments. *Mar. Geol.* 3, 457-474.
- McManus, D.A., Kelley, J.C., Creager, J.S., 1969. Continental Shelf Sedimentation in an Arctic Environment. *Geol. Soc. Am. Bull.* 80, 1961.
- Nakashima, S., Sturgeon, R.E., Willie, S.N., Berman, S.S., 1988. Determination of trace elements in sea water by graphite-furnace atomic absorption spectrometry after preconcentration by tetrahydroborate reductive precipitation. *Anal. Chim. Acta* 207, 291-299.
- Naidu, A.S., Blanchard, A., Kelley, J.J., Goering, J.J., Hameed, M.J., Baskaran, M., 1997. Heavy metals in Chukchi Sea sediments as compared to selected circum-arctic shelves. *Mar. Pollut. Bull.* 35, 260-269.
- Pan, K., Wang, W.-X., 2011. Mercury accumulation in marine bivalves: Influences in biodynamics and feeding niche. *Environ. Pollut.* 159, 2500-2506.
- Percy, J. A., Fife, F. J., 1981. The biochemical composition and energy content of Arctic marine macrozooplankton. *Arctic* 34, 307-313.
- Ping, C.-L., Michaelson, G.J., Guo, L., Jorgenson, M.T., Kanevskiy, M., Shur, Y., Dou, F., Liang, J., 2011. Soil carbon and material fluxes across the eroding Alaska Beaufort Sea coastline. *J. Geophys. Res.* 116, G02004.
- Pucko, M., Burt, A., Walkusz, W., Wang, F., Macdonald, R.W., Rysgaard, S., Barber, D.G., Tremblay, J.-E., Stern, G.A., 2014. Transformation of Mercury at the Bottom of the Arctic Food Web: An Overlooked Puzzle in the Mercury Exposure Narrative. *Environ. Sci. Technol.* 48, 7280-7288.
- Ravelo, A.M., Konar, B., Trefry, J.H., Grebmeier, J.M., 2014. Epibenthic community variability in the northeastern Chukchi Sea continental shelf. *Deep-Sea Res. II* 102, 119-131.
- Schonberg, S.V., Clarke, J.T., Dunton, K.W., 2014. Distribution, abundance, biomass and diversity of benthic infauna in the Northeast Chukchi Sea, Alaska: Relation to environmental variables and marine mammals. *Deep-Sea Res. II* 102, 144-163.
- Stern, G.A., Macdonald, R.W., 2005. Biogeographic provinces of total and methyl mercury in zooplankton and fish from the Beaufort and Chukchi Seas: results from the SHEBA drift. *Environ. Sci. Technol.* 39, 4707-4713.

- Tomil, L.J., Grantz, A., 1976. Origin of a Bergfield at Hanna Shoal, northeastern Chukchi Sea, and its influence on the sedimentary environment. AIDJEX (Arctic Ice Dynamics Joint Experiment) Bull. 34, 1-42.
- Trefry, J.H., Presley, B.J. (1982) Manganese fluxes from Mississippi delta sediments. *Geochim. Cosmochim. Acta.* 46, 1715–1726.
- Trefry, J.H., Rember, R.D., Trocine, R.P., Brown, J.S., 2003. Trace metals in sediments near offshore oil exploration and production sites in the Alaskan Arctic. *Environ. Geol.* 45, 149-160.
- Trefry, J.H., Trocine, R.P., McElvaine, M.L., Rember, R.D., Hawkins, L.T., 2007. Total mercury and methylmercury in sediments near offshore drilling sites in the Gulf of Mexico. *Environ. Geol.* 53, 375-385.
- Trefry, J.H., Dunton, K.H., Trocine, R.P., Schonberg, S.V., McTigue, N.D., Hersh, E.S., McDonald, T.J., 2013. Chemical and biological assessment of two offshore drilling sites in the Alaskan Arctic. *Mar. Environ. Res.* 86, 35-45.
- Trefry, J.H., Trocine, R.P., Cooper, L.W., Dunton, K.H., 2014. Trace metals and organic carbon in sediments of the northeastern Chukchi Sea. *Deep-Sea Res. II*, 102, 18-31.
- van de Velden, S., Dempson, J.B., Evans, M.S., Muir, D.C.G., Power, M., 2013. Basal mercury concentrations and biomagnification rates in freshwater and marine food webs: Effects on Arctic char (*Salvelinus alpinus*) from eastern Canada. *Sci. Total Environ.* 444, 531-542.
- Wagemann, R., Trebacz, E., Boila, G., Lockhardt, W.L., 1998. Methylmercury and total mercury in tissues of arctic marine mammals. *Sci. Total Environ.* 218, 19-31.
- White, D., Kimerling, J. A., Overton, W. S., 1992. Cartographic and geometric components of a global sampling design for environmental monitoring. *Cartogr. Geogr. Inform.* 19, 5–22.

# Organic Contaminants in Chukchi Sea Sediments and Biota of the Hanna Shoal Region

H. Rodger Harvey, Karen A. Taylor

Department of Ocean, Earth, and Atmospheric Sciences  
Old Dominion University, Norfolk, VA 23529

[rharvey@odu.edu](mailto:rharvey@odu.edu)

## Abstract

The Hanna shoal Ecosystem Study expanded the initial Chukchi Sea Offshore Drilling Area (COMIDA) project northward to include important areas of sediment transport and deposition. This program determined the concentrations of organic contaminants (aliphatic hydrocarbon and polycyclic aromatic hydrocarbons, PAHs) in surface sediments (0-1 cm) from 36 sites in the Hanna Shoal region of the Chukchi Sea. Up to 31 total PAHs, including parent and alkyl homologues, were detected with total concentrations ranging over 6-fold in surface sediments from a low of 168 ng g<sup>-1</sup> at station H34 to 1147 ng g<sup>-1</sup> at station BarC5 (Figure 1). Alkyl PAHs were slightly more abundant than parent structures and accounted for 53-64% of the total. These values across the Hanna Shoal region are considered at background levels (< 1600 ng g<sup>-1</sup>). Alkanes were higher, as expected, and ranged from 4.3 µg g<sup>-1</sup> at HS3 to 31 µg g<sup>-1</sup> at H14. In contrast to COMIDA sediments stations were often dominated by short chain (C<sub>15</sub>-C<sub>22</sub>) alkanes. In biota, a diversity of PAHs were detected in the northern whelk *Neptunea heros* foot muscle with total concentrations ranging from 0.14-1.5 µg/g dry tissue wt. Larger (and presumably older) animals showed higher levels of PAH per unit muscle tissue, suggest that animal bioaccumulate PAH's over time, but do not appear to transfer these hydrocarbons to internal and external eggs present in females.

## 1. Introduction

The interest in resources and ecosystem processes in the Arctic Ocean has led to a crucial need to carry out baseline assessments of the distribution and concentration of key organic compounds. Located between northern Alaska and the Siberian coast, the Chukchi Sea is part of the largest continental shelf in the world and its northern location puts it at the crossroads of recent observed changes in global climate. Recent decadal scale observations of warming temperatures makes it highly susceptible to the effects of sea-ice retreat, ecosystem shifts and offshore energy development (Grebmeier et al., 2010). This study builds upon the initial BOEM supported COMIDA program which documented both biotic and chemical inventories in the southern region of the Chukchi Sea (see Dunton et al., 2012; Dunton et al, 2014 and references therein). This study expanded that work northward with measures of aliphatic n-alkane and polycyclic aromatic hydrocarbons (PAHs) were targeted which expanded previous work in the region (Harvey et al, 2014). These two hydrocarbon classes were emphasized based on their ability to trace specific sources of anthropogenic contamination (i.e. fossil fuel combustion) and natural inputs (i.e. oil seeps, terrestrial debris) and to establish baseline values of the suite of hydrocarbons across the Hanna Shoal region.

Hydrocarbon biomarkers found in the Arctic represent a mixture of natural background and petroleum hydrocarbon sources with concentrations of aliphatic n-alkanes significantly greater than those of PAHs. Major contributors to the elevated n-alkane signal (C<sub>27</sub> and C<sub>29</sub>) in Arctic Ocean sediments are varied but largely derive from persistent inputs of terrigenous material from rivers and coastal erosion (Belicka et al., 2002; Belicka and Harvey, 2009; Yamamoto et al., 2008; Yunker et al., 2005). Although PAHs represent only a small (0.2-7%) fraction of the total composition of crude oil, their aromatic structures represent one of the major contributors to its toxicity (Neff, 2002; NRC, 2003). This component of the Hanna Shoal study was to document organic contaminant levels in sediments as seen as PAH and aliphatic hydrocarbons and to document tissue specific concentrations in tissues of important invertebrates (e.g. *Neptunea heros*). Previous work had already established only minor toxicological responses by the low levels of PAH and hydrocarbons observed to the native fish *B. saida* (Harvey et al., 2014).

## **2. Methods**

### **2.1 Field collections**

Sampling in the Chukchi Sea in both 2012 and 2013 was accomplished aboard the USCGC *HEALY* by scientists H. Rodger Harvey and Karen Taylor from Old Dominion University. Collections included a suite of sediments, particles and associated biota. Surface sediment (0-1 cm) samples were collected using several types of samplers, predominantly a 0.25 m<sup>2</sup> stainless steel box core (KC – Denmark), which was subsequently sectioned as described below. On occasion a stainless double Van-Veen sampler was used where undisturbed sediment samples were available. All samplers were protected from stack smoke, grease drips from winches and wire, and other potential airborne contamination during sampling.

### **2.2 Sediments**

On shipboard all cores were sectioned into 1 cm intervals in the upper 10 cm of sediment, and 2 cm intervals below for chemical analysis. During the collection and handling of sediment samples, extreme care was taken to avoid contact with potential hydrocarbon sources. Contamination blanks for deck and laboratory processing of all samples are described in the QA/QC section. Only clean glassware and other materials of high purity that may come in contact with the samples were used. All sediments for PAH and hydrocarbon analysis were stored in pre-cleaned plastic I-Chem jars with Teflon-lined screw cap lids and immediately frozen.

### **2.3 Invertebrates**

Our previous work documented concentrations of both PAH and alkanes hydrocarbons from the foot muscle in 35 individuals of the *Neptunea* whelk which had been pooled into three size classes based on shell length (0-5, 5-8, >8 cm - see Harvey et al., 2014). That analysis showed a diversity of PAHs in muscle tissues with alkyl-substituted compounds dominating over parent species among all size classes. What was surprising, however, was that the total concentration of PAHs decreased in larger organisms while aliphatic n-alkanes in *Neptunea* muscle showed the opposite trend. To assess organic contaminants in higher trophic level benthic invertebrates,

additional female Northern Neptune whelk (*Neptunea heros*) with eggs cases were collected when observed in benthic trawls to further investigate body burdens in muscle tissue and the possible transfer to attached eggs. Four female *Neptunea* whelks ranging in size from 4.8-11.4 cm were collected from stations CBL-11, H6, and H17 during the 2013 Hanna Shoal Ecosystem Study cruise. In addition, several individual *Neptunea* carried both internal (with albumen) and external eggs (removed from their casings) among those collected through bottom trawls. Sterile tools were used for the dissection and removal of foot muscles on the ship, which were stored in pre-combusted foil and immediately frozen until analysis. Sterile tools were used for the dissection and removal of foot muscles on the ship, which were stored in pre-combusted foil and immediately frozen.

During the Healy 1201 expedition, several individuals of the mussel *M. discors* were present in box core collections obtained from the BarC5 site (Barrow Canyon). Following a similar protocol as for *N. heros* PAH and alkane hydrocarbons were determined in dissected muscle tissues from these benthic inhabitants and compared to surface sediments adjacent to their burrows.

## **2.4 Laboratory analysis of hydrocarbons in surface sediments and invertebrates**

### **2.4.1 Extraction of hydrocarbons**

Surface sediments (0-1 cm) from 36 sites, several tissue types from *Neptunea* and muscle tissue of *M. discors* were analyzed for both aromatic and aliphatic hydrocarbons. Each sediment sample was lyophilized to a fine powder and thoroughly homogenized prior to chemical analysis. *Neptunea* foot muscle and eggs (both internal and external cases) were extracted wet. Lyophilized sediment or tissue were transferred to Green Chem glass vessels with Teflon screw-cap lids. Six perdeuterated PAHs (Acenaphthene-d<sub>10</sub>, Phenanthrene-d<sub>10</sub>, Benz(a)anthracene-d<sub>12</sub>, Benzo(a)pyrene-d<sub>12</sub> and Benzo(g,h,i)perylene-d<sub>12</sub>, and n-Octadecane-d<sub>38</sub>) were added prior to extraction and served as internal standards for calculation of recoveries and hydrocarbon concentrations (refinement of EPA Method 8270). Sediments and tissues were extracted with hexane: acetone (1:1, 35ml) at 80°C for 30 min and stirred on high using a MARS microwave assisted extraction system (CEM Corp., Matthews, NC) operating at 1200 W (refinement of EPA Method 3546). After extraction, vessels were allowed to cool to room temperature before being opened. The supernatant was first filtered through pre-cleaned and combusted glass wool and then combined with 2-4 ml hexane: acetone (1:1) rinses of the extraction vessel containing the sample. Sediment and muscle tissue extracts were concentrated to 3 ml using rotary evaporation and then split for the analysis of PAHs and aliphatic hydrocarbons.

Labware (glass or Teflon) used in the extraction process was washed in Alconox, soaked in RBS-35 detergent, and then 15% HCl each for 24 hr. and then rinsed three times with RO or UV Nanopure water after each washing step. Glassware was dried and then combusted at 450°C for 4 hr. to remove any possibility of remaining organics. All labware was pre-rinsed with solvent three times before sample addition. A procedural blank was prepared and analyzed in parallel with each round of samples extracted.



**Table 1.** Target polycyclic aromatic hydrocarbons (PAHs) measured in Hanna Shoal samples, including number of rings and method detection limit values (MDL). PAH's observed in sediments or invertebrates in this project are denoted by (#). For comparison, (\*) is included to denote those PAH's that were detected previously in Chukchi Sea sediments from the COMIDA09/10 campaign.

PAH Targets	# of rings	MDL (ng/g dry wt.)	PAH targets (continued)	# of rings	MDL (ng/g dry wt.)
Naphthalene #*	2	1.12	Fluoranthene#*	4	0.22
2-Methylnaphthalene#*	2	0.57	Pyrene#*	4	0.20
1-Methylnaphthalene#*	2	0.28	Benzo(a)fluorene	4	0.03
Biphenyl#*	2	0.18	Retene#*	4	0.15
1-ethylnaphthalene#	2	0.10	Methylfluoroanthracene #	4	0.12
2,7-Dimethylnaphthalene #*	2	0.07	Benzo(b)fluorine*	4	0.02
1,3-Dimethylnaphthalene #*	2	0.08	Cyclopenta(c,d)pyrene	4	0.02
1,6-Dimethylnaphthalene #*	2	0.09	Benz(a)anthracene#*	4	0.03
1,4-Dimethylnaphthalene #*	2	0.04	Chrysene+Triphenylene#	4	0.03
1,5-Dimethylnaphthalene #*	2	0.03	Naphthacene*	4	0.08
Acenaphylene	2	0.02	4-Methylchrysene#*	4	0.02
1,2-Dimethylnaphthalene	2	0.02	Benzo(b)fluoranthene	4	0.04
1,8-Dimethylnaphthalene	2	0.39	Benzo(k)fluoranthene	4	0.02
Acenaphthene	2	0.11	Dimethylbenz(a)anthracene	4	0.03
2,3,5-Trimethylnaphthalene*	2	0.03	Benzo(e)pyrene#	5	0.04
Fluorene#	2	0.11	Benzo(a)pyrene*	5	0.08
1-Methylfluorene#*	2	0.05	Perylene#*	5	0.06
Dibenzothiophene#*	3	0.04	3-Methylchloanthrene	5	0.08
Phenanthrene#*	3	0.62	Indeno(1,2,3-c,d)pyrene	5	0.01
Anthracene	3	0.03	Dibenz(a,h+ac)anthracene	5	0.02
2-Methyldibenzothiophene#*	3	0.09	Benzo(g,h,i)perylene*	6	0.02
1-Methyldibenzothiophene#	3	0.04	Anthanthrene	6	0.01
2-Methylphenanthrene#*	3	0.15	Corenene	7	0.00
2-Methylanthracene#*	3	0.03			
4,5-Methylenephenanthrene	3	0.04	<b>Internal standards:</b>		
1-Methylanthracene#*	3	0.04	Acenaphthene-d <sub>10</sub>	3	
1-Methylphenanthrene#*	3	0.13	Phenanthrene-d <sub>10</sub>	3	
9-Methylanthracene	3	0.03	Benzo(a)anthracene-d <sub>12</sub>	4	
3,6-dimethylphenanthrene#*	3	0.10	Benzo(a)pyrene-d <sub>12</sub>	5	
9,10-Dimethylanthracene#*	3	0.16	Benzo(g,h,i)perylene-d <sub>12</sub>	6	

#### **2.4.2 Gas Chromatography-Mass Spectrometry analysis of PAHs**

PAHs were analyzed by capillary gas chromatography (GC) with an Agilent 6890 system coupled to an Agilent 5973 Network Mass Selective Detector (MS) operated in electron ionization mode. The GC-MS system was equipped with a J&W Scientific DB-5MS fused silica column (30 m, 0.25 mm id, 0.25 film thickness) and operated in selected ion monitoring (SIM) mode. Samples were injected in splitless mode at an initial oven temperature of 50°C and an injector temperature of 250°C with helium as the carrier gas. The oven temperature was ramped at 15°C/min to 120°C and then 3.5°C/min to 300°C before holding at 300°C for 10 min. The base peak area response of selected ions was adjusted relative to that of the appropriate perdeuterated-PAH internal standard, which is based on the number of carbons (refinement of EPA Method 8270D). Target PAHs and method detection limits are listed in Table 1 below together with those detected in Hanna Shoal samples.

#### **2.4.3 Purification and structural analysis of aliphatic hydrocarbons**

Due to the complex matrix and varied organic matter content of sediments and invertebrate tissues, it was necessary to further purify total extracts for hydrocarbon analysis via hydrolysis and fractionation by normal phase-high performance liquid chromatography (HPLC). This process was identical to that used in the previous COMIDA CAB project sample analysis. In brief, a fraction of each sediment extract was subjected to alkaline hydrolysis with a solution of 0.5 N KOH in methanol. The resulting neutral fractions were concentrated to 250 µl and separated with an Agilent HPLC system equipped with a Luna silica analytical column (5 µm; 250 mm x 4.6 mm id) and guard column cartridge of similar material (Phenomenex Torrance, CA). Separation of fractions was achieved at ambient temperature with an injection volume of 50 µl and flow rate of 0.5 ml min<sup>-1</sup> with the following solvent gradient (modified slightly from Tolosa and de Mora, 2004): 100% A (0-10 min); 80% A and 20% B (at 15 min); 100% B (at 20 min) and then isocratic hold to 30 min, followed by 50% B and 50% C (at 35 min) and then isocratic hold to 60 min (where A = hexane, B = methylene chloride and C = MeOH; all HPLC grade). Once fractions were collected, the flow rate was increased to 1 ml min<sup>-1</sup> and the column re-equilibrated before the start of the next run with 100% B (to 65 min); 100% A (to 70 min) and then isocratic hold to 80 min. The elution of n-alkanes occurs in the first fraction (0-10 min). Once collected, solvent was concentrated to 80 µl with a stream of N<sub>2</sub> gas before capillary gas chromatography (GC) and GC-mass spectrometric analysis.

Aliphatic n-alkanes were quantified by capillary GC using Agilent 6890N Network GC System and flame ionization detection (FID) with hydrogen as the carrier gas. The base peak area response of n-alkanes were determined relative to that of the perdeuterated internal standard (n-Octadecane-d<sub>38</sub>). Identification of n-alkanes was carried out by GC-MS operated in full scan mode. The column and temperature programs are similar to that described above. Target n-alkanes included a broad range of alkanes including those targeted in our previous COMIDA study are shown in Table 2 below.

**Table 2.** Target n-alkanes measured in Hanna Shoal Ecosystem Study samples, including method detection limit values (MDL). Alkanes observed seen in this study are shown by (#). For comparison, (\*) denotes n-alkanes detected in Chukchi sediments seen in the previous COMIDA-CAB 09/10 study.

n-Alkane Targets	n-Alkane Targets (continued)
n-C <sub>10</sub>	n-C <sub>27</sub> #*
n-C <sub>11</sub>	n-C <sub>28</sub> #*
n-C <sub>12</sub>	n-C <sub>29</sub> #*
n-C <sub>13</sub>	n-C <sub>30</sub> #*
n-C <sub>14</sub>	n-C <sub>31</sub> #*
n-C <sub>15</sub> #*	n-C <sub>32</sub> #*
n-C <sub>16</sub> #*	n-C <sub>33</sub> #*
n-C <sub>17</sub> #*	n-C <sub>34</sub>
n-C <sub>18</sub> #*	n-C <sub>35</sub>
n-C <sub>19</sub> #*	n-C <sub>36</sub>
n-C <sub>20</sub> #*	n-C <sub>37</sub>
n-C <sub>21</sub> #*	n-C <sub>38</sub>
n-C <sub>22</sub> #*	n-C <sub>39</sub>
n-C <sub>23</sub> #*	n-C <sub>40</sub>
n-C <sub>24</sub> #*	
n-C <sub>25</sub> #*	Internal Standard:
n-C <sub>26</sub> #*	n-C <sub>18-d</sub> <sub>38</sub>

#### 2.4.4 Quality Assurance and Quality Control

A quality assurance (QA) plan that includes quality control (QC) procedures and analyses applied during the COMIDA-CAB program was continued for the Hanna Shoal Ecosystem Study program. Important QC components include analytical balance calibration, instrument tuning and calibration (MARS, GC-MS), standard recoveries, procedural and field blank analysis, and duplicate sample analysis. Calibration and tuning of the mass spectrometer was carried out after each set of 10 samples using perfluorotributylamine (PFTBA) as the calibrant to automatically adjust the MS parameters to meet the predefined criteria for operation in EI mode. Internal standard recoveries of perdeuterated PAH (83-102%) and n-alkane (9%) standard reference compounds were determined based on measurements obtained both before and after microwave assisted extraction and processing (MARS system). For each round of 12 samples, one procedural blank was prepared to monitor potential contamination resulting from glassware, solvents, and processing procedures. These blanks were processed along with field samples and followed the same handling and analytical scheme. A second set of field blanks were used on board to account for shipboard air and particles. Procedural blanks corrected for individual compounds in each PAH and n-alkane concentrations observed in samples, respectively. Field blanks collected during all cruises were processed in parallel to field samples and followed the same handling and analytical scheme. Field blanks including ship laboratory air and DI

water blanks were obtained on glass-fiber filters at the start and end of each cruise. Target hydrocarbon concentrations detected in field blanks were subtracted from those in field samples observed in samples, respectively. Individual and summary information for all blanks are contained in the Hanna Shoal database (<http://arcticstudies.org/hannashoal/data.html>). Duplicate sample analysis was prepared for 17% of the total samples and provided a measure of processing and analytical precision. This report provides measurements of the abundance and distribution of 52 targeted polycyclic aromatic hydrocarbons (PAH) and 15 normal-alkanes in surface sediments (0-1 cm) and their potential to bioaccumulate in the muscle tissue and eggs of upper trophic level organisms.

### **3. Results**

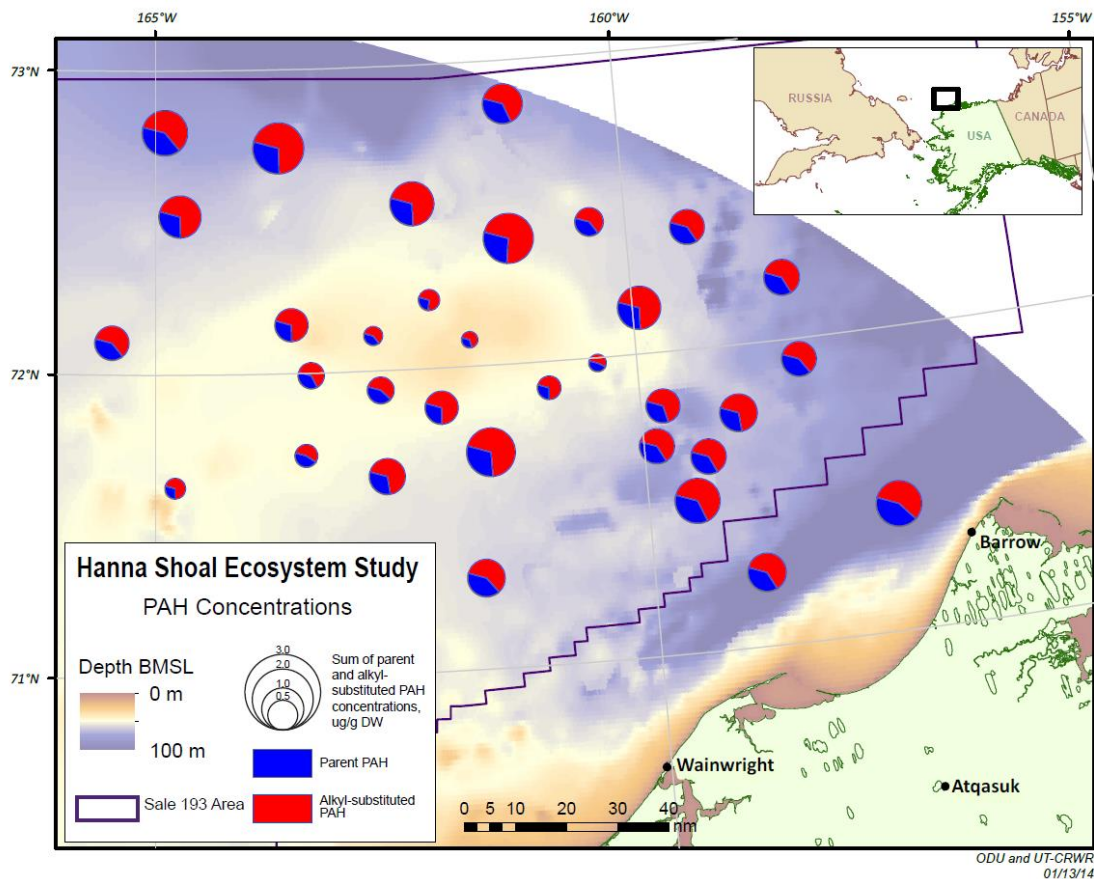
#### **3.1 Analysis of polycyclic aromatic hydrocarbons (PAHs) in Hanna Shoal surface sediments**

The PAH abundance and distribution was measured in surface sediments (0-1 cm) from 17 individual sites collected during the 2012 Hanna Shoal Ecosystem Study cruise and 19 individual sites occupied during the 2013 cruise. All sediments were analyzed following strict protocols for quantitative measurement with multiple standards to track recovery and allow quantitative measures of concentration and multiple procedural and process blanks were incorporated in the protocol to assure accurate values. PAHs were identified and quantified by gas chromatography-mass spectrometry (GC-MS) operated in single ion monitoring (SIM) mode following standard and widely approved protocols. Up to 53 individual PAHs representing both parent and alkyl-substituted aromatic compounds were targeted and detected in surface sediments across the region (see figure 1) Total PAH concentrations observed in HLY 1301 sediment samples (0.17-1.2 µg/g dry wt.; Avg. 0.66 µg/g) were similar to those we documented in sediments collected during the 2012 Hanna Shoal cruise expedition (0.15-1.5 µg/g dry wt.; Avg. 0.80 µg/g) with similar distributions generally also seen. Overall, PAH concentrations could be viewed as very low and with few exceptions were present at background levels in surface sediments spanning the Hanna Shoal region.

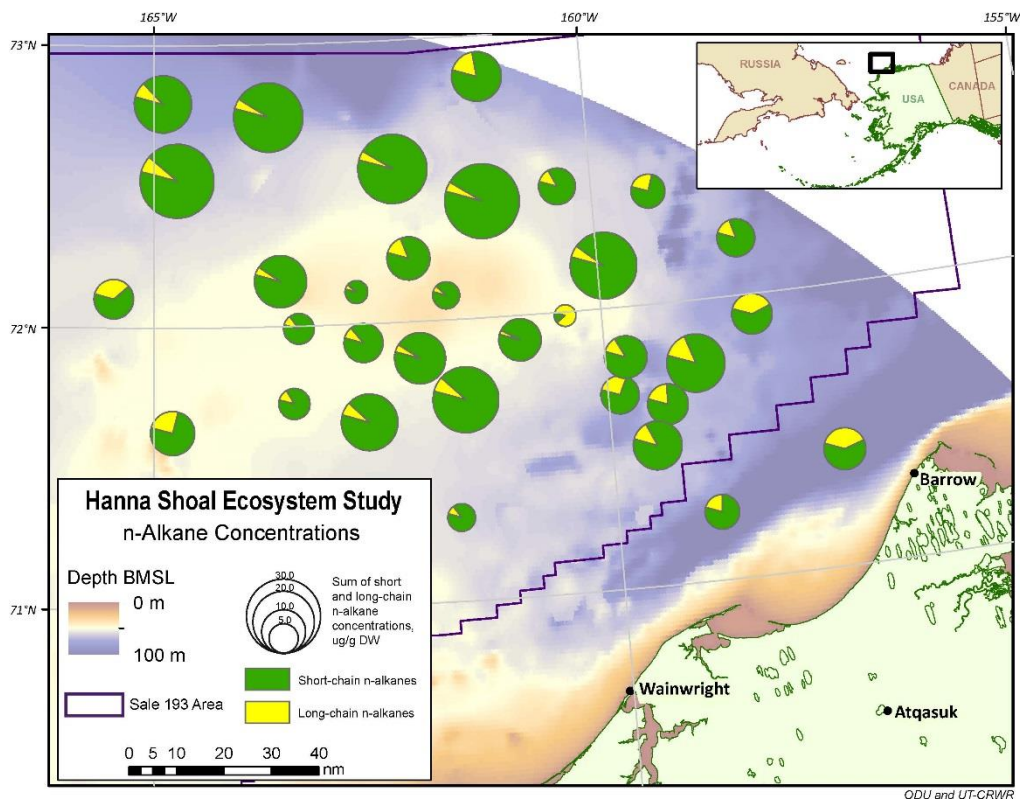
#### **3.2 Alkane hydrocarbons in Hanna Shoal Sediments**

The analysis of straight-chain n-alkanes was completed for all sediments collected in 2012 and 2013 and summarized in Figure 2. To obtain useful quantitative and qualitative information, n-alkanes were further isolated and purified from extracts of sediments (described above) through hydrolysis and subsequent normal phase-high performance liquid chromatography (NP-HPLC) methods. Alkanes were identified by GC-MS and quantified by GC with flame ionization detection (FID) as described previously (Harvey et al., 2014). Up to 16 individual n-alkanes ranging from C<sub>15</sub>-C<sub>31</sub> were measured in sediments collected. Total concentrations ranged from 2.6-18.2 µg/g dry wt. (avg. 8.3 µg/g) at sites where sediments were collected in 2013 and were slightly lower than seen in the 2012 analysis set (4.1-31.0 µg/g dry wt.; avg. 19.2 µg/g). Although concentrations did vary among years, hydrocarbon distributions in all Hanna Shoal sediments were dominated by shorter chain alkanes (C<sub>15</sub>-C<sub>22</sub>) which accounted for the majority

(avg. of 84%) among all alkanes observed. These alkanes are common to biogenic sources suggest a mixture of terrestrial natural products with small amounts of petrogenic materials.



**Figure 1.** Summed concentrations of parent and alkylated polycyclic aromatic hydrocarbons present in surface sediments of the Hanna Shoal study. Circles are scaled to concentrations present in surface (0-1cm) sediments. Detailed information on the distribution of the 31+ individual PAH's seen and their concentrations are available through the Hanna Shoal database.



**Figure 2.** Summed concentrations of normal and odd chain alkane hydrocarbons present in surface sediments of the Hanna Shoal Ecosystem study. Circles are scaled to concentrations present in surface (0-1cm) sediments. Details on the distribution of individual hydrocarbons and concentrations are available through the Hanna Shoal database.

### 3.3 Sediment organic contaminant comparisons over time

While the Hanna Shoal study was unique in many locations, several sites visited during the field program were designed to overlap with the COMIDA-CAB study sites conducted in 2009-2010 which allowed several of those sites to be revisited. This provided an opportunity to compare previous results with more recent sediment collections for hydrocarbons. While a number of factors might lead to differences among sediments collected several years apart and site locations are defined broadly (5km cross section), the initial hypothesis was that sediments should show similar total values overall and little change in concentration. The results of those comparisons for sites analyzed during the COMIDA program and revisited during the Hanna Shoal Ecosystem Study in 2012 and 2013 are shown below for PAH and alkane hydrocarbons (Table 3). An examination of total PAH and alkane concentrations across the three cruises in general show very similar concentrations. For HLY1201 and HLY 1301 in particular, revisits found sediment PAH concentrations differed no more than 15%, and much less at the other two sites. Alkanes values were low but variable at all sites, with BarC5 also showing the greatest difference at repeat visits. The higher variability seen at BarC5 is interesting as it is also the site of intense biological activity and is an area of enhanced carbon deposition (Grebmeier and McRoy, 1989;

Trefry et al., 2014). While overall concentrations remained low, PAH and alkane values determined in the Hanna Shoal program did show some differences when compared to the earlier COMIDA results for overlapping sites, but no consistent trend was apparent (Table 3).

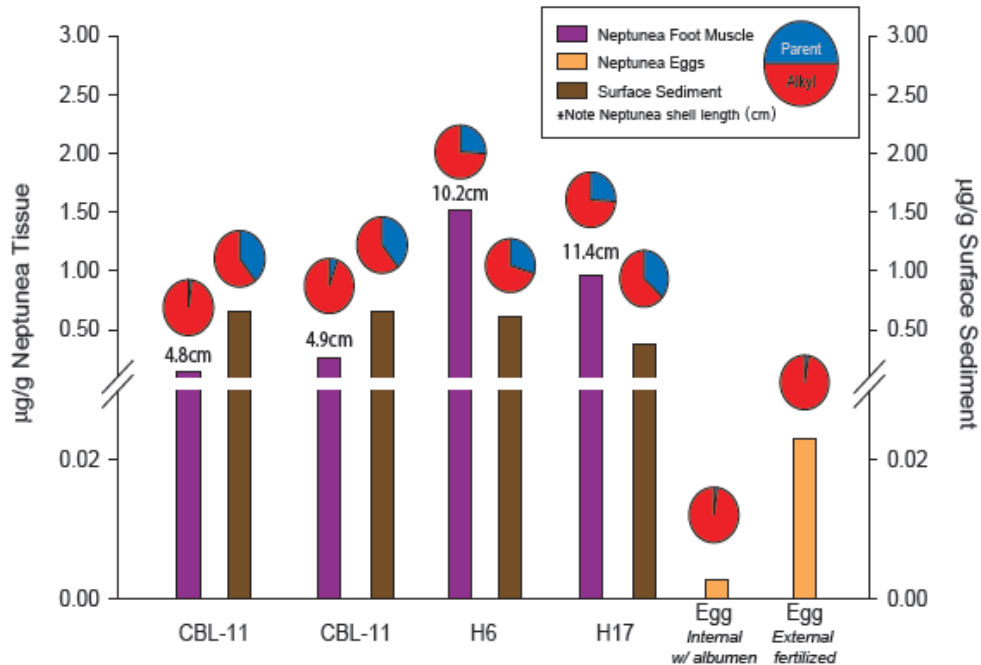
**Table 3.** A comparison of total PAH and alkane hydrocarbon concentrations observed across multiple years from the COMIDA and Hanna Shoal Research Program cruises.

<b>Total PAH (ng / g dry sediment)</b>			
<b>Station</b>	<b>COMIDA 09,10</b>	<b>HLY1201</b>	<b>HLY1301</b>
H38/H108		677.03	688.91
BARC5		1354.58	1147.01
CBL11		638.29	649.51
CBL13	461.60		779.10
UTX8	410.80		296.07

<b>Total Alkanes (µg / g dry sediment)</b>			
<b>Station</b>	<b>COMIDA 09,10</b>	<b>HLY1201</b>	<b>HLY1301</b>
H38/H108		17.01	9.23
BARC5		26.01	8.66
CBL11		18.10	8.52
CBL13	12.32		9.82
UTX8	6.95		5.40

### **3.4 Organic contaminants in tissues of the northern Neptune whelks (*Neptunea heros*) and muscle tissue of the mussel *M. discors*.**

The present study expanded upon previous COMIDA information which described the bioaccumulation of organic contaminants in muscle tissue of the Neptune whelk. In addition to muscle tissue previously examined, *Neptunea* foot muscle in four females plus eggs in several stages of development were extracted and analyzed for PAH and alkane hydrocarbon concentrations to examine the potential for trophic transfer of these compound to offspring. A comparison of body burdens for those animals and their eggs are shown in Figure 3 below together with sediment values at the station nearest to the benthic trawl collections. While the small sample size limits insight, an important observation were significant concentrations of PAH's were present in muscle tissues, suggesting that ingestion of sediments can lead to long term accumulation. In eggs, concentrations were low with strong preference of alkylate PAH's.



**Figure 3.** The distribution of parent and alkyl substituted polycyclic aromatic hydrocarbons (PAH) seen in the foot muscle of the Northern Neptune whelks and their eggs. For comparison sediment burdens at sites nearest the collection site of each animal are also included (note scale on right for sediments). Tissue normalized concentrations were higher in larger individuals while sediments showed no significant trends among the 4 sites. This suggest that *Neptunea* does appear to bio accumulate organic contaminants in muscle tissue. In contrast, only a small fraction of PAHs are transferred from female whelks to their eggs, with a strong bias towards the accumulation of alkylated structures.

### 3.5 Organic contaminants of the mussel, *M. discors*

For comparative purposes with the whelk *Neptunea*, muscle tissues of the mussel *M. discors* collected during the HLY 1201 cruise were also analyzed for PAH and alkane hydrocarbons. While these represent a single station in the Barrow Canyon area (Bar5), they provide useful contrast with information on a sessile benthic resident. Up to 26 individual PAHs and 8 alkane hydrocarbons ranging from C<sub>22</sub>-C<sub>29</sub> were detected in the tissues (excluding gut) of *M. discors*. In mussels, PAH concentrations were not elevated compared to values seen in surface sediments (1146.9 ng/gm) with total PAH values of 32.9 ng/gm wet tissue seen in pooled samples. The distribution between parent and alkylated species were similar to sediments with 43.9% present as parent compounds in tissues and phenanthrene as the dominant structure. The remaining 56% comprised alkylated species. Alkanes (C<sub>22</sub> - C<sub>29</sub>) were similarly low with total concentrations of 4.14 µg/gm tissue observed compared to sediments (total of 26.01 µg/gm dry sediment). Based on the values observed for this single collection, PAH concentrations were much lower than surrounding surface sediments, suggestion no active bioaccumulation of either PAH or alkanes for this population.



## 4. Discussion

### 4.1 PAHs in Surface Sediments

Surface and subsurface sediments collected from the Chukchi shelf during the Hanna Shoal field seasons establish a baseline data set to identify future impacts from oil and gas exploration in this region. PAH concentrations in surface sediments (0-1cm) spanning the study area were spatially variable and ranged from 168-1147 ng g<sup>-1</sup> (Figure 1; detailed concentration information is contained in the Hanna Shoal database). The mean ( $\pm$  std. dev.) concentrations observed here at 657  $\pm$ 294 ng g<sup>-1</sup> is remarkably similar to that seen in the COMIDA study (683  $\pm$ 483) and can be considered at background levels for this pristine environment. They are comparable to the total PAH values of 500 ng g<sup>-1</sup> (Yunker et al., 2011) and 614  $\pm$ 611 ng g<sup>-1</sup> (Naidu et al., 2001) reported in other Arctic sediments. These results and the broader values seen in COMIDA study are, however lower relative to total PAH measurements in Camden Bay (961+334 ng g<sup>-1</sup>; Brown et al., 2010), Elson Lagoon (1299 +1698 ng g<sup>-1</sup>) and Canadian Beaufort shelf sediments (1900 +470 ng g<sup>-1</sup>) Yunker et al., 1993).

The PAH concentrations in Chukchi shelf surface sediments comprised both parent and alkyl-substituted PAHs, which represent a mixture of pyrogenic, petrogenic and biogenic sources that are typical of this region. Alkyl-PAHs account for the majority of the total (68-72%) and were dominated by various methyl and dimethyl-naphthalenes, phenanthrenes and pyrene, which are likely derived from petroleum or combustion inputs throughout the study area. This dominance of alkyl-PAHs appears widespread and has also been also reported in sediments from the Chukchi (Harvey et al., 2014) and Beaufort Sea (Yunker et al., 1993; Yunker et al., 1996) shelves. While it is possible that these petrogenic markers originate in oil from seeps on the Chukchi shelf (Gautier et al., 2009), organic-rich peat, shales and bitumens that occur in Alaska's North Slope tundra also provide likely sources and stable matrices for the transport of alkyl-PAHs over long distances via turbidity currents or ice rafting of sediments (Jones and Yu, 2010; Mull, 1995). Additional sources of parent PAHs to the Arctic region include sea-ice (Kawamura et al., 1994; Masclet and Hoyau, 1994) and snow (Welch et al., 1991), which arrive in the Arctic through long-range atmospheric transport of emissions from fossil fuel and biomass burning in temperate regions and sequestered (Becker et al., 2006; Patton et al., 1991). This is supported by significant amounts of pyrogenic PAHs seen in airborne particles from long-term Canadian air monitoring (Becker et al., 2006; Halsall et al., 1997). While parent PAHs (excluding perylene) in these Hanna Shoal surface sediments contribute a mean of 25%  $\pm$  2% to the total PAH signal, several studies (Yunker et al., 2002; Yunker and MacDonald, 1995) suggest that atmospheric transport of PAHs have a minor influence on sedimentary PAH distributions in the Arctic Ocean due to their volatility and substantial losses during snow/ice-melt and passage through the water column. This leaves the resulting sediment composition with a much lower proportion of pyrogenic PAHs than the original combustion sources.

Among the suite of PAHs measured in Chukchi shelf surface sediments, Hanna Shoal sediments were similar to work on the COMIDA study with perylene is one of the most abundant structures observed (avg. 76 ng g<sup>-1</sup>). This compound is found naturally in many sedimentary environments and generally thought to originate from organic matter diagenesis (Meyers and Ishiwatari, 1993). Values observed in Chukchi sediments for this biogenic PAH is comparable to the estimate of 60

ng g<sup>-1</sup> reported by Yunker et al. (2011) in a surface sediment from the same region. Overall, however, total PAH concentrations in surface sediments of all sites examined in this study are present at levels considered to be background values for pristine areas (< 1600 ng g<sup>-1</sup>) with the highest levels seen at the Barrow Canyon site (BarC5 -1147 ng g<sup>-1</sup>). This is lower than the single highest station from the previous study where station 26 sediments contained total PAHs of 2956 ng g<sup>-1</sup>.

Compared to overall PAH values, alkane hydrocarbons in surface sediments (0-1cm) spanning the 19 sites of the study area varied spatially and showed higher concentrations (3 and 18 μg g<sup>-1</sup>). Average total n-alkane concentrations (8.3 ± 3.8 μg g<sup>-1</sup>) were comparable to that reported in surface sediments from the COMIDA sites (Harvey et al., 2014), Beaufort Sea inner shelf (7.2 ± 5.1 μg g<sup>-1</sup>; Naidu et al., 2001), but lower relative to Mackenzie shelf sediments (9.8 ± 1.7 μg g<sup>-1</sup>; Yunker and MacDonald, 1995), which include more direct inputs of terrigenous organic matter. Among subsets of the alkanes, the mean value for the longer-chain C<sub>23-31n</sub>-alkanes (1.6 ± 1.01 μg g<sup>-1</sup>) was very similar to that measured by Yunker et al. (2011) for select sites on the Chukchi shelf (4.8 μg g<sup>-1</sup>).

## 4.2 Aliphatic n-alkanes in surface sediments

Though concentrations varied spatially, surface sediments throughout the study area showed the greatest average abundance of lower chain alkanes n-alkanes (C<sub>15</sub>-C<sub>22</sub>) except for station H34 where they accounted for only 16% of total alkane hydrocarbons at 0.41 μg g<sup>-1</sup>. The distribution of lower molecular weight n-alkanes (C<sub>15-22</sub>) seen in Chukchi shelf surface sediments likely represent a mixture of both algae/bacteria and petroleum sources (Figure 2). The contributions of C<sub>17</sub> and C<sub>19</sub> n-alkanes are often suggested as algal and photosynthetic bacterial markers (Giger et al., 1980; Wakeham, 1990; Xiao et al., 2008), while even carbon short-chain n-alkanes (C<sub>16-22</sub>) are more typical of petroleum sources (Boehm et al., 1990; Boehm et al., 1987; Brown et al., 2004; Steinhauer and Boehm, 1992). Station H34 was also the station where a distinct odd-over-even carbon predominance of higher molecular weight alkanes (C<sub>23</sub>-C<sub>31</sub>) was observed and accounted for the majority (64%) of total alkanes. Higher molecular weight n-alkanes have also been documented in the Beaufort Sea nearshore sediments with a dominance of C<sub>27</sub> or C<sub>29</sub> and a well-defined odd-over-even predominance (Wainwright and Humphrey, 1984; Yunker et al., 1993); as an indication of terrestrial source material (Bianchi et al., 1989; Kalkreuth et al., 1998; Tuo et al., 2003).

A number of studies (e.g. Belicka et al., 2002; Belicka et al., 2004; Boucsein and Stein, 2000; Goñi et al., 2000; Schubert and Calvert, 2001; Stein et al., 1994; Taylor and Harvey, 2011) have used various suites of organic carbon signatures (i.e. long-chain n-alkanes, fatty acids and alcohols, triterpenoids) to quantify the input and movement of terrestrial carbon to the western Arctic. The Arctic Ocean receives significant inputs of terrigenous material from rivers and coastal erosion and the n-alkane distribution seen in Chukchi shelf surface sediments represent a mixture of terrestrial and petroleum hydrocarbons sources (Figure 2). The sources for such alkanes include major inputs eastward of our study area in the Beaufort Sea where annual sediment loads from the Mackenzie River alone have been estimated at 127 Mt (Macdonald et al., 1998). These inputs are supplemented with terrestrial contributions by rapid erosion (0.5 to 6 m yr<sup>-1</sup>) of the peat-enriched Alaskan coastline (Are et al., 2008; Macdonald et al., 1998;

Solomon, 2005). Sea-ice transport provides one mechanism to link plant alkanes seen in sediments with their terrestrial origin. Sediment resuspension and coastal erosion near the Alaskan shoreline allow sea-ice to entrain significant quantities of terrigenous material during freezing (Eicken et al., 2005). This material is subsequently redistributed to the Chukchi Sea upon thawing, with predicted trajectories of sea-ice movement showing a westward direction (Eicken et al., 2005). Of particular importance to the Chukchi Sea is the Yukon River which empties directly into the eastern Chukchi shelf and provides a direct source of terrigenous organic matter and n-alkanes to sediments. The Yukon River Basin drains 853,300 km<sup>2</sup> and discharges annual sediment loads of approximately 60 Mt into Bering Sea (Walvoord and Striegl, 2007) with waters turning northward as the Alaskan Coastal Current. Early work by Naidu et al. (1982) traced the movement and subsequent deposition of clay minerals originating from the Yukon River northward through Bering Strait and into the Chukchi Sea, supporting another potential mechanism of the delivery of terrestrial organic carbon to Chukchi shelf sediments. Guo and Macdonald (2006) used several lines of evidence to support organic material transport as well. The rather low values seen for alkane hydrocarbons in the Hanna Shoal study sites and dominance of lower chain alkanes together with the previous COMIDA values suggest that apart from areas of direct river influence, terrestrial carbon is a relatively small fraction of organic material distributed across the Chukchi region. Similar to PAH distributions, n-alkanes in Chukchi shelf sediments are detected at background levels and represent a combination of natural background biogenic and petrogenic hydrocarbons.

### 4.3 Hydrocarbons in *Neptunea heros*

Hydrocarbons can be accumulated by benthic invertebrates through desorption from sediments in which they reside and ingestion of food. Compared to the previous COMIDA study, only a small set of animals (4) were available for analysis among Hanna Shoal trawl collections and the results thus present limited information on organic contaminants and their biotic distribution (See Figure 3.) Two of the larger female whelks, however, did contain internal and external eggs which allows some evaluation on the potential for trophic transfer of hydrocarbons to offspring. For adults a diversity of PAHs were detected in *Neptunea* foot muscle with total concentrations ranging from 0.14-1.5 µg/g dry tissue weight. The fact that larger (and presumably older) *Neptunea* have higher levels of PAH per unit muscle tissue than smaller whelks suggest that organisms bioaccumulate PAH's over time, particularly given that sediments where the organisms were observed did not show large differences in concentration. Larger adults also increased their proportion of parent PAH structures, which might imply altered feeding tactics as they mature. Based on the analysis of both internal and external eggs, it does appear that female *Neptunea* transfer a small fraction of PAHs (<2% relative to muscle) to their eggs with alkylated structures as the dominant form seen. In general, *Neptunea* appears to bioaccumulate the organic contaminants observed in muscle tissue, with a small fraction of PAHs transferred from female whelks to their eggs.

In contrast to PAHs, short chain alkanes (C<sub>15</sub>-C<sub>22</sub>) accounted for 77-99% of the total alkanes present in the muscle tissues with tissue concentrations ranging from 10.7 to 54.5 µg/ gm tissue and with concentrations, much higher in the two larger animals. For those females with eggs, alkanes were not detected in either internal or external egg masses. This is contrary to typical studies that have observed depuration of hydrocarbons by invertebrates with lower molecular

weight hydrocarbons selectively lost (Malins, 1977). In this case, however, a comparison to sediments where animals were collected showed similar distributions, albeit with very low concentrations (all less than 15  $\mu\text{g}/\text{gm}$ ) and with lower chain alkanes comprising at least 90% of the alkanes seen in sediments. These low concentrations may have resulted in no selective loss with alkane distributions in tissues reflecting sediments where organisms were collected.

## 5. Summary

This study represents the second phase of an important examination of spatially explicit concentrations of hydrocarbons across the Chukchi shelf and its retention by an important benthic invertebrate. The low levels seen in both PAH values and alkanes across the broad region of shelf sites surveyed indicate that this ecosystem is relatively pristine with limited accumulation of petrogenic carbon in surface sediments. Although a broad suite of 31 individual PAHs were detected in Hanna Shoal surface sediments, total PAH concentrations are low with alky substituted forms as the dominate form present in the observed distribution little anthropogenic input. While alkane hydrocarbons are often 10-fold higher in sediments than observed PAH's, they represent mainly natural sources with concentrations substantially below that often observed in coastal shelves.

## 6. Acknowledgements

This study was funded by the US department of the interior, Bureau of Ocean Energy Management (BOEM), Alaska Outer continental Shelf Region, Anchorage, Alaska under BOEM Cooperative Agreement No. M11AC00007 as part of the Chukchi Sea offshore Monitoring in Drilling Area (COMIDA). John Trefry and crew are thanked for organic carbon values and many helpful discussions and Rachel Pleuthner capably assisted in logistics. Tim Whiteaker is thanked for preparation of GIS graphics and management of database issues.

## 7. References

- Are, F., Reimnitz, E., Grigoriev, M.N., Hubberten, H.-W., Rachold, V., 2008. The influence of cryogenic processes on the erosional Arctic shoreface. *J. Coastal Res.* 24, 110–121.
- Becker, S., Halsall, C.J., Tych, W., Hung, H., Attewell, S., Blanchard, P., Li, H., Fellin, P., Stern, G., Billeck, B., Friesen, S., 2006. Resolving the long-term trends of polycyclic aromatic hydrocarbons in the Canadian Arctic atmosphere. *Environ. Sci. Technol.* 40, 3217–3222.
- Belicka, L.L., Macdonald, R.W., Harvey, H.R., 2002. Sources and transport of organic carbon to shelf, slope, and basin surface sediments of the Arctic Ocean. *Deep-Sea Res.* I 49, 1463–1483.
- Belicka, L.L., Macdonald, R.W., Yunker, M.B., Harvey, H.R., 2004. The role and depositional regime on carbon transport and preservation in Arctic Ocean sediments. *Mar. Chem.* 86, 65–88.
- Belicka, L.L., Harvey, H.R., 2009. The sequestration of terrestrial organic carbon in Arctic Ocean sediments: A comparison of methods and implications for regional carbon budgets. *Geochim. Cosmochim. Acta* 73, 6231–6248.

- Bianchi, G., Avato, P., Scarpa, O., Murelli, C., Audisio, G., Rossini, A., 1989. Composition and structure of maize epicuticular wax esters. *Phytochemistry* 28, 165–171.
- Boehm, P., Steinhauer, M., Crecelius, E., Neff, J.M., Tuckfield, 1987. Analysis of trace metals and hydrocarbons from outer continental shelf (OCS) activities, final report. OCS Study MMS 87-0072, Anchorage, Alaska: USDO, Minerals Management Service.
- Boehm, P., LeBlanc, L., Trefry, J., Marajh-Whittemore, P., Brown, J., Sohtzberg, A., Kick, A., 1990. Monitoring hydrocarbons and trace metals in Beaufort Sea sediments and organisms, final report. OCS Study MMS 90-500, Anchorage, Alaska: USDO, Minerals Management Service.
- Boucein, B., Stein, R., 2000. Particulate organic matter in surface sediments of the Laptev Sea (Arctic Ocean): application of maceral analysis as organic-carbon source indicator. *Mar. Geol.* 162, 573–586.
- Brown, J.S., Trefry, J.H., Cook, L.L., Boehm, P.D., 2004. ANIMIDA Task 2: Hydrocarbon and metal characterization of sediments, bivalves and amphipods in the ANIMIDA study area, final report. OCS Study MMS 2004-024, Anchorage, Alaska: USDO, Minerals Management Service.
- Brown, J.S., Trefry, J.H., Cook, L.L., Boehm, P.D., 2010. Continuation of the Arctic nearshore impact monitoring in the development area (CANIMIDA): synthesis, 1999-2007, final report. OCS Study BOEMRE 2010-032, Anchorage, Alaska: USDO, Bureau of Ocean Energy Management, Regulation, and Enforcement.
- Dunton, K.H., Cooper, L.W., Grebmeier, J.M., Harvey, H.R., Konar, B., Maidment, D., Schonberg, S.V., Trefry, J., 2012. Chukchi Sea offshore monitoring in drilling area (COMIDA: chemical and benthos (CAB)). Final Report Prepared for the Bureau of Ocean Energy Management, Anchorage, AK. by the University of Texas Marine Science Institute, Port Aransas, TX, 26 pp. + appendices.
- Dunton K.H., Grebmeier, J.M., Trefry, J.H. 2014. The benthic ecosystem of the northeastern Chukchi Sea: An overview of its unique biogeochemical and biological characteristics, *Deep-Sea Res. II: Topical Studies in Oceanography.* 102, 1-8, doi.org/10.1016/j.dsr2.2014.01.001.
- Eicken, H., Gradinger, R., Gaylord, A., Mahoney, A., Rigor, I.G., Melling, H., 2005. Sediment transport by sea ice in the Chukchi and Beaufort seas: Increasing importance due to changing ice conditions? *Deep-Sea Res. II* 52, 3281–3302.
- Goñi, M.A., Yunker, M.B., Macdonald, R.W., Eglinton, T.I., 2000. Distribution and sources of organic biomarkers in arctic sediments from the Mackenzie River and Beaufort Shelf. *Mar. Chem.* 71, 23–51.
- Grebmeier, J.M., McRoy, C.P., 1989. Pelagic-benthic coupling on the shelf of the northern Bering and Chukchi Seas. III. Benthic food supply and carbon cycling. *Mar. Ecol. Prog. Ser.* 53, 79-91.
- Grebmeier, J.M., Moore, S.E., Overland, J.E., Frey, K.E., Gradinger, R., 2010. Biological response to recent pacific Arctic sea ice retreats. *EOS* 91, 161-163.
- Guo, L., and Macdonald R. W. 2006. Source and transport of terrigenous organic matter in the upper Yukon River: Evidence from isotope ( $\delta^{13}\text{C}$ ,  $\Delta^{14}\text{C}$ , and  $\delta^{15}\text{N}$ ) composition of

- dissolved, colloidal, and particulate phases, *Global Biogeochem. Cycles*, 20, GB2011, doi: 10.1029/2005GB002593.
- Halsall, C.J., Barrie, L.A., Fellin, P., Muir, D.C.G., Billeck, B.N., Lockhart, L., Rovinski, F.Y., Kononov, E.Y., Pastukhov, B.V., 1997. Spatial and temporal variation of polycyclic aromatic hydrocarbons in the Arctic atmosphere. *Environ. Sci. Technol.* 31, 3593-3599.
- Harvey, H.R., K.A. Taylor, H.V. Pie, and C. L. Mitchelmore. 2014. Polycyclic aromatic and aliphatic hydrocarbons in Chukchi Sea biota and sediments and their toxicological response in the Arctic cod, *Boreogadus saida*. *Deep-Sea Res. II.* 102, 32-55
- Jones, M.C., Yu, Z., 2010. Rapid deglacial and early Holocene expansion of peatlands in Alaska. *Proc. Nat. Acad. Sci.* 107, 7347-7352.
- Kalkreuth, W.D., Keuser, C., Fowler, M.G., Li, M., McIntyre, D.J., Püttmann, W., Richardson, R.J., 1998. The petrology, organic geochemistry and palynology of Tertiary age Eureka Sound Group coals, Arctic Canada. *Org. Geochem.* 29, 799–809.
- Kawamura, K., Suzuki, I., Fujii, Y., Watanabe, O., 1994. Ice core record of polycyclic aromatic hydrocarbons over the past 400 years. *Naturwissenschaften.* 81, 502-505.
- Macdonald, R.W., Solomon, S.M., Cranston, R.E., Welch, H.E., Yunker, M.B., Gobeil, C., 1998. A sediment and organic carbon budget for the Canadian Beaufort Shelf. *Mar. Geol.* 144, 255-273.
- Malins, D.C., 1977. Biotransformation of petroleum hydrocarbons in marine organisms indigenous to the Arctic and Sub-Arctic, in: Wollie, D.A. (Ed.), *Fate and Effects of Petroleum Hydrocarbons in Marine Organisms and Ecosystems*. Pergamon, New York, pp. 47-59.
- Masclet, P., Hoyau, V., 1994. Evidence for the presence of polycyclic aromatic hydrocarbons in the polar atmosphere and in polar ice. *Analysis Magazine.* 22, M31-M33.
- Meyers, P.A., Ishiwatari, R., 1993. Lacustrine organic geochemistry: An overview of indicators of organic matter sources and diagenesis in lake sediments. *Org. Geochem.* 20, 867–900.
- Mull, C.G., 1995. Preliminary evaluation of the hydrocarbon source rock potential of the Tingmerkpuk sandstone (Neocomian) and related rocks, northwestern De Long Mountains, Brooks Range, Alaska. Public Data File 95-30. State of Alaska, Dept. of Natural Resources, Div. of Geological and Geophysical Surveys, Fairbanks, AK.
- Naidu, A.S., Goering, J.J., Kelley, J.J., Venkatesan, M.I., 2001. Historical changes in trace metals and hydrocarbons in the inner shelf sediments, Beaufort Sea: Prior and subsequent to petroleum-related industrial developments, final report. OCS Study MMS 2001-061. University of Alaska Coastal Marine Institute, University of Alaska Fairbanks and USDOI, MMS, Alaska OCS Region.
- Naidu, A.S., Cooper, L.W., Grebmeier, J.M., Whitley, T.E., Hameedi, M.J., 2003. The continental margin of the North Bering-Chukchi Sea: concentrations, sources, fluxes, accumulation and burial rates of organic carbon, in: Stein, R., Macdonald, R.W. (Eds.), *The Organic Carbon Cycle in the Arctic Ocean*. Springer-Verlag, Berlin, pp. 193–203.
- National Research Council (NRC). 2003. *Oil in the Sea: Inputs, Fates, and Effects*. National Academies Press, Washington, DC.

- Neff, J.M., 2002. Polycyclic aromatic hydrocarbons in the ocean, in: *Bioaccumulation in Marine Organisms: Effect of Contaminants from Oil Well Produced Water*. Elsevier, Oxford, pp. 241-313.
- Patton, G.W., Walla, M.D., Bidleman, T.F., Barrie, L.A., 1991. Polycyclic aromatic and organochlorine compounds in the atmosphere of Northern Ellesmere Island. *Can. J. Geophys. Res.* 96, 10867-10877.
- Schubert, C.J., Calvert, S.E., 2001. Nitrogen and carbon isotopic composition of marine and terrestrial organic matter in Arctic Ocean sediments: Implications for nutrient utilization and organic matter composition. *Deep-Sea Res. II* 48, 789-810.
- Solomon, S.M., 2005. Spatial and temporal variability of shoreline change in the Beaufort-Mackenzie region, Northwest Territories, Canada. *Geo-Mar. Lett.* 25, 127-137.
- Stein, R., Nam, S., Schubert, C., Vogt, C., Fütterer, D., Heinemeier, J., 1994. The last deglaciation event in the eastern central Arctic Ocean. *Science* 264, 692-696.
- Steinhauer, S.S., Boehm, P.D., 1992. The composition and distribution of saturated and aromatic hydrocarbons in nearshore sediments, river sediments and coastal peat of the Alaskan Beaufort Sea: Implications for detecting anthropogenic hydrocarbon inputs. *Mar. Environ. Res.* 33, 223-253.
- Taylor, K.A., Harvey, H.R., 2011. Bacterial hopanoids as tracers of organic carbon sources and processing across the western Arctic continental shelf. *Org. Geochem.* 42, 487-497.
- Thain, J.E., Vethaak, A.D., Hylland, K., 2008. Contaminants in marine ecosystems: developing an integrated indicator framework using biological-effect techniques. *ICES J. Mar. Sci.* 65, 1508-1514.
- Tolosa, I., de Mora, S., 2004. Isolation of neutral and acidic lipid biomarker classes for compound-specific-carbon isotope analysis by means of solvent extraction and normal-phase high-performance liquid chromatography. *J. Chromatog. A* 1045, 71-84.
- Tuo, J., Wang, X., Chen, J., Simoneit, B.R., 2003. Aliphatic and diterpenoid hydrocarbons and their individual carbon isotope compositions in coals from the Liaohe Basin, China. *Org. Geochem.* 34, 1615-1625.
- Trefry, J. H., Trocine, R.P., Cooper, L.W., Dunton, K.H., 2014. Trace metals and organic carbon in sediments of the northeastern Chukchi Sea. *Deep Sea Research II* 102, 18-31.
- Wainwright, P.F., Humphrey, B., 1984. Analysis of sediment data from the Beaufort Shorebase Monitoring Program, 1982-1984.
- Walvoord, M. A., and Striegl, R.G. 2007. Increased groundwater to stream discharge from permafrost thawing in the Yukon River basin: Potential impacts on lateral export of carbon and nitrogen, *Geophys. Res. Lett.*, 34, L12402, doi: 10.1029/2007GL030216.
- Wakeham, G., 1990. Algal and bacterial hydrocarbons in particulate matter and interglacial sediment of the Cariaco Trench. *Geochim. Cosmochim. Acta* 54, 1325-1336.
- Welch, H.E., Muir, D.C.G., Billeck, B.N., Lockhart, W.L., Brunskill, G.J., Kling, H.J., Olson, M.P., Lemoine, R.M., 1991. Brown snow: A long-range transport event in the Canadian Arctic. *Environ. Sci. Technol.* 25, 280-286.

- Xiao, L., Zhu, L.P., Wang, Y., Wang, J., Xie, M.P., Ju, J.T., Mausbacher, R., Schwalb, A., 2008. Environmental changes reflected by n-alkanes of a lake core in Nam Co on the Tibetan Plateau since 8.4 ka. *P. Chin. Sci. Bull.* 53, 3051–3057.
- Yamamoto, M., Okino, T., Sugisaki, S., Sakamoto, T., 2008. Late Pleistocene changes in terrestrial biomarkers in sediments from the central Arctic Ocean. *Org. Geochem.* 39, 754–763.
- Yunker, M.B., Macdonald, R.W., Cretney, W.J., Fowler, B.R., McLaughlin, F.A., 1993. Alkane, terpene and polycyclic aromatic hydrocarbon geochemistry of the Mackenzie River and Mackenzie shelf: Riverine contributions to Beaufort Sea coastal sediment. *Geochim. Cosmochim. Acta* 57, 3041–3061.
- Yunker, M.B., Macdonald, R.W., 1995. Composition and origins of polycyclic aromatic hydrocarbons in the Mackenzie River and on the Beaufort Sea shelf. *Arctic* 48, 118–129.
- Yunker, M.B., Snowdon, L.R., Macdonald, R.W., Smith, J.N., Fowler, M.G., Skibo, D.N., McLaughlin, F.A., Danyushevskaya, A.I., Petrova, V.I., Ivanov, G.I., 1996. Polycyclic aromatic hydrocarbon composition and potential sources for sediment samples from the Beaufort and Barents Seas. *Environ. Sci. Technol.* 30, 1310–1320.
- Yunker, M.B., Backus, S.M., Graf Pannatier, E., Jeffries, D.S., Macdonald, R.W., 2002. Sources and significance of alkane and PAH hydrocarbons in Canadian arctic rivers. *Estuar. Coast. Shelf Sci.* 55, 1–31.
- Yunker, M.B., Belicka, L.L., Harvey, H.R., Macdonald, R.W., 2005. Tracing the inputs and fate of marine and terrigenous organic matter in Arctic Ocean sediments: a multivariate analysis of lipid biomarkers. *Deep-Sea. Res. II* 52, 3478–3508.
- Yunker, M.B., Macdonald, R.W., Snowdon, L.R., Fowler, B.R., 2011. Alkane and PAH biomarkers as tracers of terrigenous organic carbon in Arctic Ocean sediments. *Org. Geochem.*, doi: 10.1016/j.orggeochem.2001.06.007.



# Mesozooplankton Abundance and Distribution in Association with Hydrography on Hanna Shoal, NE Chukchi Sea, During August 2012 and 2013

Carin J. Ashjian<sup>1</sup>, Robert G. Campbell<sup>2</sup>, Philip Alatalo<sup>1</sup>, Celia Gelfman<sup>2</sup>, Stephen Elliott<sup>1</sup>, Heather McEachen<sup>3</sup>

<sup>1</sup>Woods Hole Oceanographic Institution  
266 Woods Hole Road,  
Woods Hole, MA 02543-1050

<sup>2</sup>Graduate School of Oceanography, University of Rhode Island  
S. Ferry Road  
Narragansett, RI 02882

<sup>3</sup>School of Fisheries and Ocean Sciences, University of Alaska  
905 N. Koyukuk Drive, 245 O'Neill Building  
Fairbanks, AK 99775

[cashjian@whoi.edu](mailto:cashjian@whoi.edu); [rgcampbell@uri.edu](mailto:rgcampbell@uri.edu); [palatalo@whoi.edu](mailto:palatalo@whoi.edu); [cgelfman@uri.edu](mailto:cgelfman@uri.edu); [stephenmelliott@gmail.com](mailto:stephenmelliott@gmail.com); [h.mceachen@alaska.edu](mailto:h.mceachen@alaska.edu)

## Abstract

Hanna Shoal, in the northeastern Chukchi Sea, is potentially vulnerable to ecosystem disruption under ongoing climate change, however aspects of its ecology, particularly of its zooplankton, were poorly understood. Mesozooplankton distribution, taxonomic composition, and abundance were described from across Hanna Shoal in August 2012 and 2013 as part of the multidisciplinary COMIDA Hanna Shoal Program. Zooplankton were collected using vertical tows of paired Bongo nets equipped with 150  $\mu\text{m}$  and 500  $\mu\text{m}$  mesh nets; samples from the 150  $\mu\text{m}$  mesh nets were enumerated to identify taxa, copepod species, and copepod life stages and to calculate abundances. Zooplankton distributions and abundances were considered together with hydrographic (temperature, salinity) characteristics and current pathways. Haplotypes of the mt COI gene were used to differentiate Bering and Arctic haplotype groups of the copepod *Calanus glacialis* and to differentiate *C. glacialis* and its close congener *C. marshallae*. The meroplankton were an important component of the zooplankton and meroplankton taxonomic composition differed between the eastern and western portions of the Shoal and between years, with bivalve larvae, and in 2012 echinoderm larvae, being important on the eastern portion but much less important on the western portion. Different regions identified on the basis of taxonomic composition were associated with different water masses and current pathways. The northeast corner of the Shoal in particular was differentiated from the crest of the shoal and from Barrow Canyon. Bering Sea Summer water, and intrinsic plankton, was observed in the southwest portion of the Shoal. Comparison of plankton composition and abundances with historic and recent studies done near Hanna Shoal demonstrated that similar plankton compositions were present across a broad region of the Chukchi Sea and that abundances of the

copepod *C. glacialis* appear to be increasing on the time scale of decades, potentially through increased input from the northern Bering Sea. Because the Chukchi Sea is highly advective, it is likely that zooplankton populations over Hanna Shoal are lost to the Canada Basin to the north and must be re-established annually through input from the northern Bering Sea. Under this scenario, enhancement of a resident Hanna Shoal zooplankton community that would retain a significant proportion of the primary production in the water column is unlikely.

## 1. Introduction

Hanna Shoal, in the northeastern Chukchi Sea, lies near the juxtaposition of the Chukchi and Beaufort Seas. It is at the northern front of the northward advection of water, and plankton, of northern Bering Sea origin through the Chukchi Sea to the Canada Basin and central Arctic to the north. The Shoal is important to a range of upper trophic level animals including seabirds and marine mammals that are subsistence for local indigenous Alaskan coastal human communities. The region is benthically rich, as is typical of the Chukchi Sea, with at least one benthic “hot-spot” in the southeastern corner of the shoal that supports high abundances of benthically-feeding walrus (Grebmeier et al., 2015). Hanna Shoal also lies on the path of bowhead whales during their fall migration from the Canadian Arctic to the northern Bering Sea (Quakenbush et al., 2010; Citta et al., 2014); it is unknown if bowhead whales feed on Hanna Shoal during their passage. The Western Arctic, including Hanna Shoal, is the Arctic region most dramatically impacted by diminished sea ice in response to ongoing Arctic warming. Despite the importance and the vulnerability of the region, there have been few studies of the physical oceanography and ecology of Hanna Shoal. Most studies in the northern Chukchi Sea have focused on the shelf-break region (e.g., Shelf Basin Interactions Program, Grebmeier and Harvey, 2005), the oil and gas lease area to the south of the Shoal (e.g., Chukchi Sea Environmental Studies Program, Day et al., 2013), and Barrow Canyon and the Beaufort Sea to the east (e.g., Ashjian et al., 2010). Work on Hanna Shoal proper as part of the COMIDA program began in 2009 but did not include a zooplankton component (e.g., Dunton et al., 2014). This studies focuses on the zooplankton of Hanna Shoal during late summer (August) of 2012 and 2013 as an extension of the ongoing COMIDA Hanna Shoal effort.

Hanna Shoal is seasonally sea-ice covered and sea ice lingers over the region late into the summer, retained both by the prevailing circulation and also by grounding of large ice floes. The circulation of Hanna Shoal is complex. Generally, the Shoal lies between two northward pathways of water that enter the Chukchi Sea through the Bering Strait. The western pathway runs through the central Chukchi Sea (Central Valley) and in summer contains Bering Sea Summer water while the eastern pathway runs along the coast of Alaska and through Barrow Canyon and contains Alaskan Coastal Water (e.g., Weingartner et al., 2005, 2013; Brugler et al., 2014). Circulation on the Shoal itself is frequently clockwise, encircling the shallowest regions. Complex pathways mix water from the Shoal with the northward flowing currents to the east. Along the northern edge of the Shoal, over the shelf break and slope, the shelf break jet usually flows from west to east but can reverse and flow to the west under strong upwelling favorable easterly winds (e.g., Nikolopoulos et al., 2009).

The zooplankton of the northern Chukchi Sea, including Hanna Shoal, is a mixture of endemic animals, animals advected into the region from the Bering Sea, and animals that are moved onto

the shelf by upwelling or southward flow in Barrow Canyon from the adjacent Arctic Basin (e.g., Lane et al., 2008; Hopcroft et al., 2010; Questel et al., 2013). It is believed that much of the plankton in the Chukchi Sea originates in the Bering Sea (e.g., Hopcroft et al., 2010; Matsuno et al., 2011; Questel et al., 2013; Ershova et al., 2015). There are few studies of zooplankton on Hanna Shoal proper, with most work being conducted on the adjacent Chukchi and Beaufort Seas shelf breaks/slopes or in Barrow Canyon (e.g., Lane et al., 2008; Campbell et al., 2009; Llinás et al., 2009; Questel et al., 2013). From the few reports available, zooplankton biomass and abundance on Hanna Shoal is lower than that observed on the adjacent shelf break and slope regions. Hanna Shoal experiences elevated nutrient and phytoplankton concentrations and clearly much of that production is falling unconsumed to seafloor, and supporting an abundant benthos, rather than being consumed by an abundant pelagic zooplankton community (Campbell et al., 2009).

Taxonomic and species diversities on Hanna Shoal are lower than that observed in the adjacent basin (Lane et al., 2008; Lane and Smith unpub.). The copepod community numerically is dominated by small copepods such as *Oithona similis* and *Pseudocalanus* spp. and in terms of biomass by the larger *Calanus glacialis* (a shelf/slope species) and, to a lesser extent, *C. hyperboreus* (a basin species). Species of Pacific/Bering Sea origin might also be present on Hanna Shoal, adjacent to it in Barrow Canyon, or off the shelf to the north, such as the large copepods *Neocalanus* spp. (Cooper et al., 2007) and *C. marshallae*. Genetic sequencing can differentiate species of Pacific and Arctic *Calanus* spp. and describe the interconnectedness of *Calanus* spp. populations from the adjacent seas (Campbell et al., in prep., Nelson et al., 2009). Euphausiids, or krill, have been collected in high abundances on the neighboring Beaufort Shelf where they are consumed by planktivorous bowhead whales (e.g., Ashjian et al., 2010; Moore et al., 2010). However there are few reports of euphausiids collected elsewhere in the Chukchi Sea. Modeling has demonstrated that the euphausiids found near Barrow could be easily advected there from the Bering Sea in 4-6 months (Bérline et al., 2008).

*Calanus* spp. and *Neocalanus* spp. are of particular interest since they are large bodied, lipid rich copepods that provide energy rich food for upper trophic level predators including Arctic cod, planktivorous seabirds, and bowhead whales and because they are indicators of different water mass types. Three species of *Neocalanus* are characteristic of the Bering Sea, *C. hyperboreus* is characteristic of the Arctic Ocean, and *C. glacialis* has both Arctic and Bering populations. A third species of *Calanus*, *C. marshallae*, is characteristic of the Gulf of Alaska and southern Bering Sea, is observed only in very low abundances in the Chukchi Sea, and is very difficult to differentiate taxonomically from *C. glacialis*.

The low abundance and biomass of the zooplankton in the region is surprising, since bowhead whales are known annually cross and utilize the northern portion of Hanna Shoal during their fall migration (Quakenbush et al., 2010). Bowhead whales require dense patches of their plankton prey to feed efficiently. Analyses of bowhead whale stomach contents collected during the Iñupiat subsistence hunt in neighboring Barrow demonstrate that bowhead whales in this region are feeding primarily on large copepods (*Calanus* spp.) and euphausiids (Carroll et al., 1987; Lowry et al., 2004; Moore et al., 2010). The tendency of the bowhead whales to congregate on northern Hanna Shoal, then, appears enigmatic given that our limited understanding of the zooplankton community there does not indicate that the region contains elevated abundances of

bowhead prey. One possibility is that euphausiids and large copepods are episodically transported from the adjacent Chukchi shelf/slope or Barrow Canyon onto Hanna Shoal in upwelling events such as is observed on the Beaufort Shelf (Okkonen et al., 2009; Ashjian et al., 2010), however the source (Barrow Canyon, shelf-break current) of these euphausiids remains elusive. Further description of the zooplankton on and adjacent to Hanna Shoal is critical to an understanding of utilization of this region by the bowhead whales.

The overall goal of this work was to describe the abundance and community composition of the zooplankton on Hanna Shoal and the association of those distributions with physical oceanographic features such as water mass and circulation. The secondary objective was to differentiate the congeneric copepod species *Calanus glacialis* and *C. marshallae* using molecular techniques (*C. marshallae* and *C. glacialis* cannot be differentiated reliably using morphometrics). The abundances of the large bodied *Calanus* spp. and euphausiids (krill) were of particular interest as they are key prey species for the planktivorous bowhead whale.

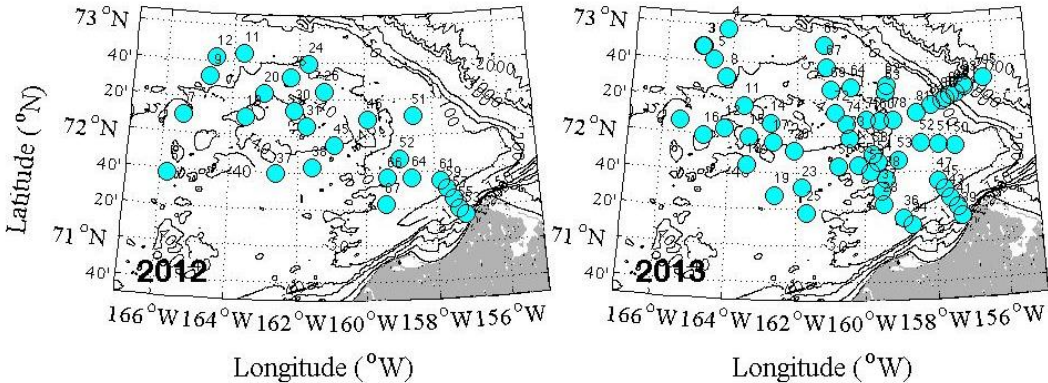
## 2. Methods

Cruises were conducted on Hanna Shoal during August of 2012 and 2013 from the *USCGC Healy*. The zooplankton sampling was part of a multidisciplinary effort that included hydrographic sampling with conductivity-temperature-depth sensors and determination of water column velocities from a hull-mounted acoustic Doppler current profiler (ADCP; RD Instruments (150 kHz). Tides were not removed from the ADCP data but are quite small in this region and should not have a large effect on the direction and magnitude of the currents. Sea ice remained anchored on Hanna Shoal with extensive ice cover in 2012 but was less extensive during 2013. Sampling spanned a longer period in 2013 (August 1-14) than in 2012 (August 11-23), permitting more extensive coverage of Hanna Shoal in 2013 including to locations off the shoal to the NW, N, and NE. A transect across Barrow Canyon that is part of the Distributed Biological Observatory also was sampled in both years.

### 2.1 Zooplankton net sampling

Zooplankton samples were collected with vertical tows of a paired Bongo net frame equipped with 150 and 500  $\mu\text{m}$  black mesh nets, flow meters, and a time-depth recorder. Casts were conducted from surface to ~2 m off of the seafloor. The net also was equipped with a strobe to increase the potential to capture euphausiids; strobes on nets have been shown to yield greater abundances of euphausiids (e.g., Wiebe et al., 2004, 2013). Samples were preserved in 4% formalin seawater immediately following collection. Upon return to the laboratory at the University of Rhode Island, total biomass for each sample was estimated using the non-destructive displacement volume method (Ahlstrom and Thraillkill, 1963) and converted to equivalent wet and carbon weights using the functional regressions of Wiebe (1988). Samples were enumerated to species and life stage in successive splits until at least 300 of the dominant copepod taxa were identified. Four species of *Pseudocalanus* spp. are found in the Chukchi Sea (Hopcroft and Kosobokova, 2009) and are very difficult to accurately differentiate; for this analysis, *Pseudocalanus* was not differentiated to species. Similarly, *C. glacialis* and *C. marshallae* were not differentiated and abundances of *C. glacialis* reported here should be considered as *C. glacialis/marshallae*. For larger fauna such as amphipods and larval fish,

abundances were determined from the entire sample. Abundances and biomass for each station were calculated based on the volume filtered by each net as measured by the flow meters. Integrated abundances were calculated using the concentration of plankton ( $\# \text{ m}^{-3}$ ) multiplied by total water column depths (m) for each sample that were measured using the time-depth recorder. Bongo net tows were conducted at 38 and 50 locations in 2012 and 2013, respectively (Appendix I; Figure 1). Samples were enumerated for the whole zooplankton community from 26 and 34 locations in 2012 and 2013, respectively. Five additional samples were enumerated for only euphausiids in 2012.



**Figure 1.** Station locations of the Bongo tows for the two years. Station number noted for each. Hanna Shoal falls within the 40 m isobaths between 72 and 73 deg. N and 158 and 164 deg. W. See also Appendix I for station locations.

At most locations, 1-2 additional ring net tows were conducted using a 1-m<sup>2</sup> ring net equipped with black 250  $\mu\text{m}$  mesh, a time-depth recorder, and a large non-filtering cod end. *Calanus glacialis/marshallae* from some of these tows were selected using microscopy for genetic analysis. Plankton from these net tows were used also by the Dunton and Trefry groups.

## 2.2 Genetic sequencing

Late copepodid stage or adult female *Calanus glacialis/marshallae* were collected in the field and preserved in 95% ethanol. The mt CO1 gene was sequenced for a total of 180 individuals from 12 stations (2012: Sts 6,11,19,37,45,51; 2013: Sts. 2,4,25,43,72,95). Specimens were sorted from the sample and their prosome length measured prior to genetic analysis. The DNA was extracted from individual specimens, purified, and then amplified by PCR using published protocols (e.g. Bucklin et al., 1995, Hill et al., 2001, Nelson et al. 2009), with slight modifications developed in the laboratory at the University of Rhode Island (URI). The 1384 5'- GGT CAT GTA ATC ATA AAG ATA TTG G -3' (Machida et al, 2004), and 2198 5'- TAA ACT TCA GGG TGA CCA AAA AAT CA -3' (Folmer et al 1994) primers were used for COI gene amplification. Sequences were determined at the URI Genomics and Sequencing Center using a fluorescence-based genetic analysis system (ABI 3130xI Genetic Analyzer). Sequences for mt COI (720 bp), mt16S rRNA (500 bp) and nuclear 18S rDNA (1710 bp) and 28S rRNA (630 bp) genes have been successfully determined for *Calanus* species at the URI laboratory. The mt CO1 gene was chosen for use because its greater variability allows better discrimination

of different populations as well as close examination of the phylogeny of *C. marshallae*, *C. glacialis* and their subpopulations.

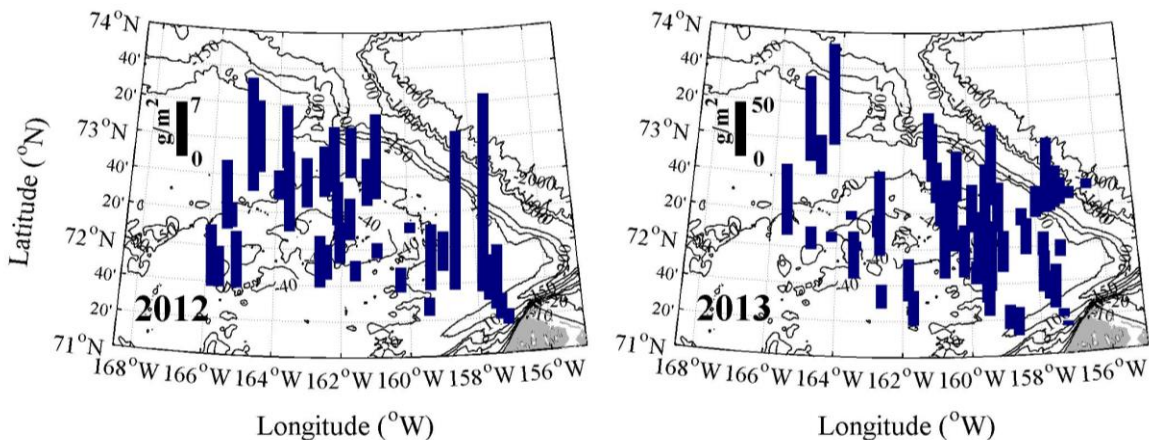
## 2.3 Data Analyses

Life stages of dominant copepod species were summed. Composition and abundance was plotted as pie charts, with the size of each pie indicating abundance for three different sets of the dominant taxa: calanoid copepods, non-calanoid copepods and non-copepod holoplankton, and meroplankton. Principal component analysis was used to group stations separately for each of the two years on the basis of their taxonomic composition. For these analyses, the total abundance of the copepod *C. glacialis* was broken out into the life stage categories of copepodid CI-CIII, copepodid CIV, copepodid CV, and adult females AF. Different groups of stations were identified by visual inspection of 3-D plots of the first three principal components for each station. For 2012, one station (53) was not included because the taxonomic composition was radically different and inclusion of the data so dominated a single principal component that consideration of other variability became difficult. Water column temperature and salinity described using the CTD (see Weingartner report) and water column velocity described using the 150 kHz hull-mounted acoustic Doppler current profiler were related to taxonomic distributions and stations grouped on the basis of taxonomic composition. All data analyses were conducted using Matlab (Mathworks, Inc.).

## 3. Results

### 3.1 Zooplankton Biomass

Zooplankton biomass, estimated from displacement volume, was significantly greater (analysis of variance,  $p < 0.01$ ) in 2013 ( $36.9 \pm 21.8 \text{ g/m}^2$ ) than in 2012 ( $7.5 \pm 5.3 \text{ g/m}^2$ ) (Figure 2). This may have resulted from increased concentrations of phytoplankton being retained in the nets during 2013 than during 2012 that would artificially increase the biomass estimate because of the



**Figure 2.** Integrated water column zooplankton biomass as carbon (estimated from displacement volume) for the two years.

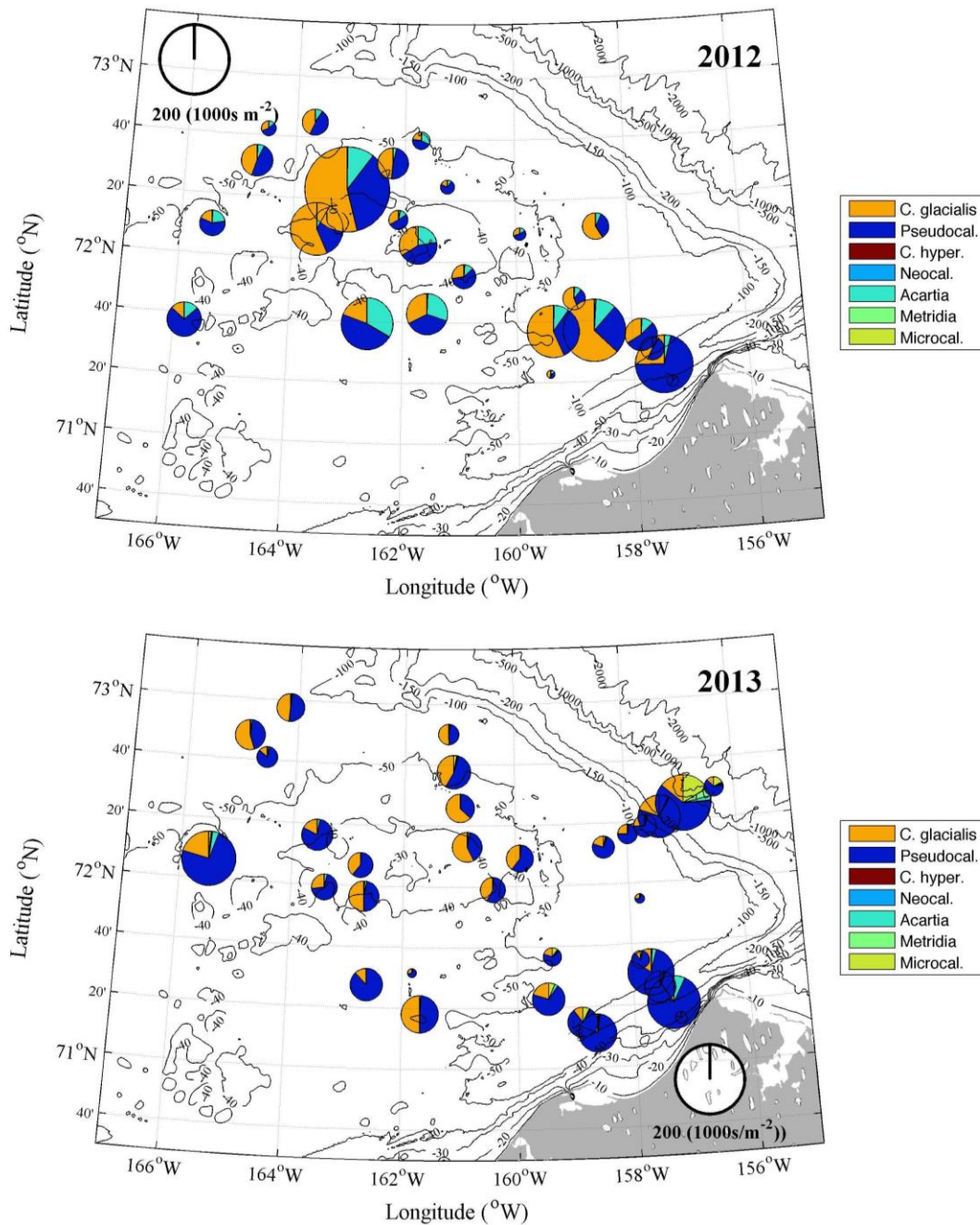
greater displacement volume of the sample. Although the locations with lowest biomass were observed in shallower portions of the Shoal, the shallow portion of the Shoal overall did not have consistently low biomass. For both years, biomass was reduced on the eastern side of Barrow Canyon, consistent with the regular location of the Alaskan Coastal Current.

### 3.2 Zooplankton Abundance

Abundances of zooplankton varied by location and showed different abundance patterns between the two years, although some patterns were consistent between years and between most locations. For calanoid copepods, *Calanus glacialis/marshallae* and *Pseudocalanus* spp. were the dominant types at most locations (Figure 3). In 2012, *Acartia longiremus* was also important but was not a significant proportion of the calanoid copepods in 2013. *Microcalanus pygmaeus*, usually found in the deeper Arctic basin, was important at a few locations in 2013, particularly at deeper locations on the upper Chukchi Sea slope. Highest abundances of calanoid copepods were seen on the NW corner of the Shoal in 2012 and on the eastern side of the Shoal in 2013. In 2013, the *Pseudocalanus* spp. complex was dominant on the eastern Shoal and in Barrow Canyon.

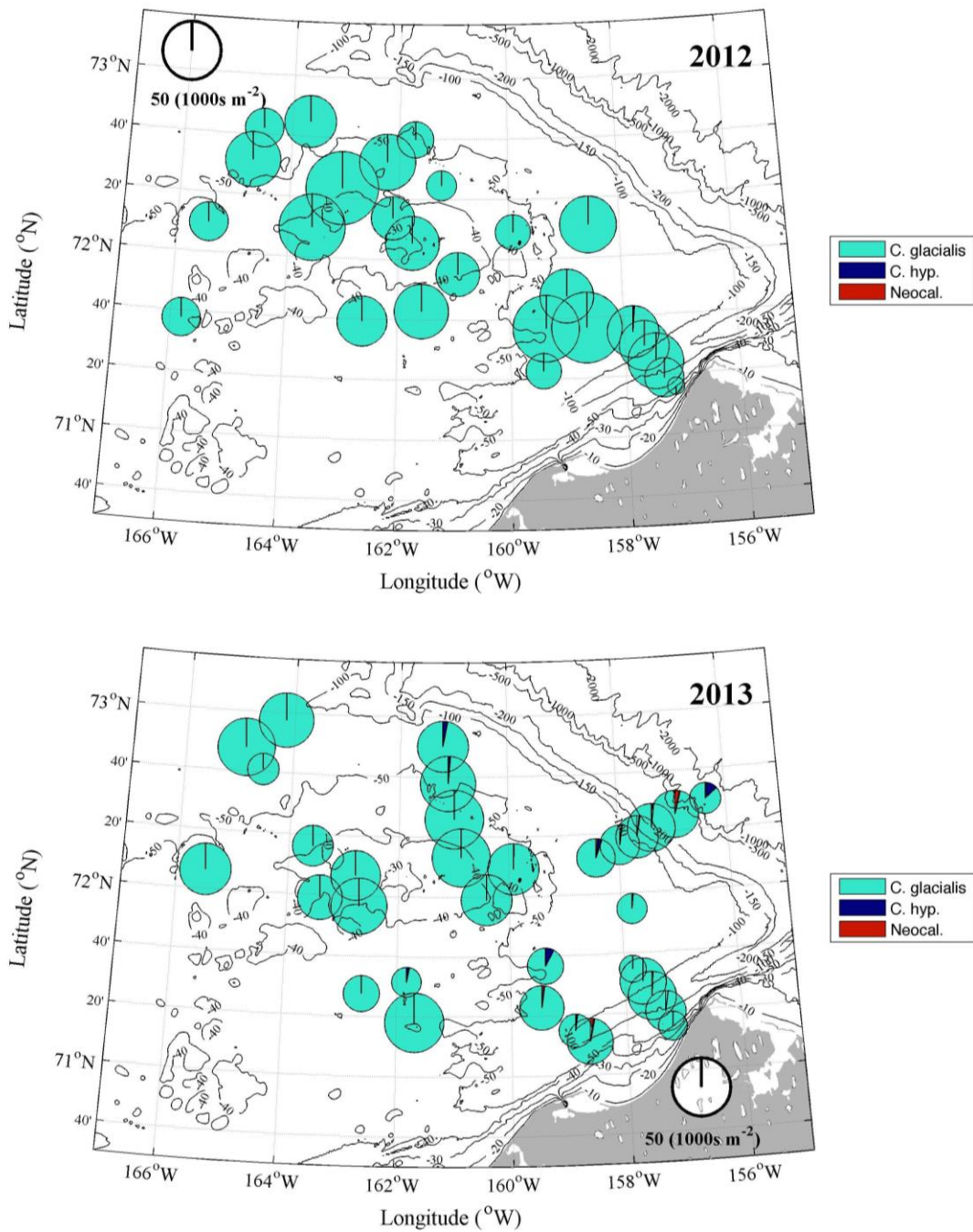
*Calanus glacialis* was the dominant lipid-rich large calanoid copepod (Figure 4). Very low proportions of *C. hyperboreus* and *Neocalanus* spp. were observed along the northern edge of Hanna Shoal in 2013 and in Barrow Canyon and at 1-2 locations on the eastern side of the Shoal in both years.

At most locations *C. glacialis* was dominated by copepodid stages CI-CIII, with proportions of older copepodid stages and adult females being much lower (Figure 5). Notable exceptions included stations to the SW and in Barrow Canyon (Figure 6) in both years where greater proportions of older copepodid stages CIV and CV were present.

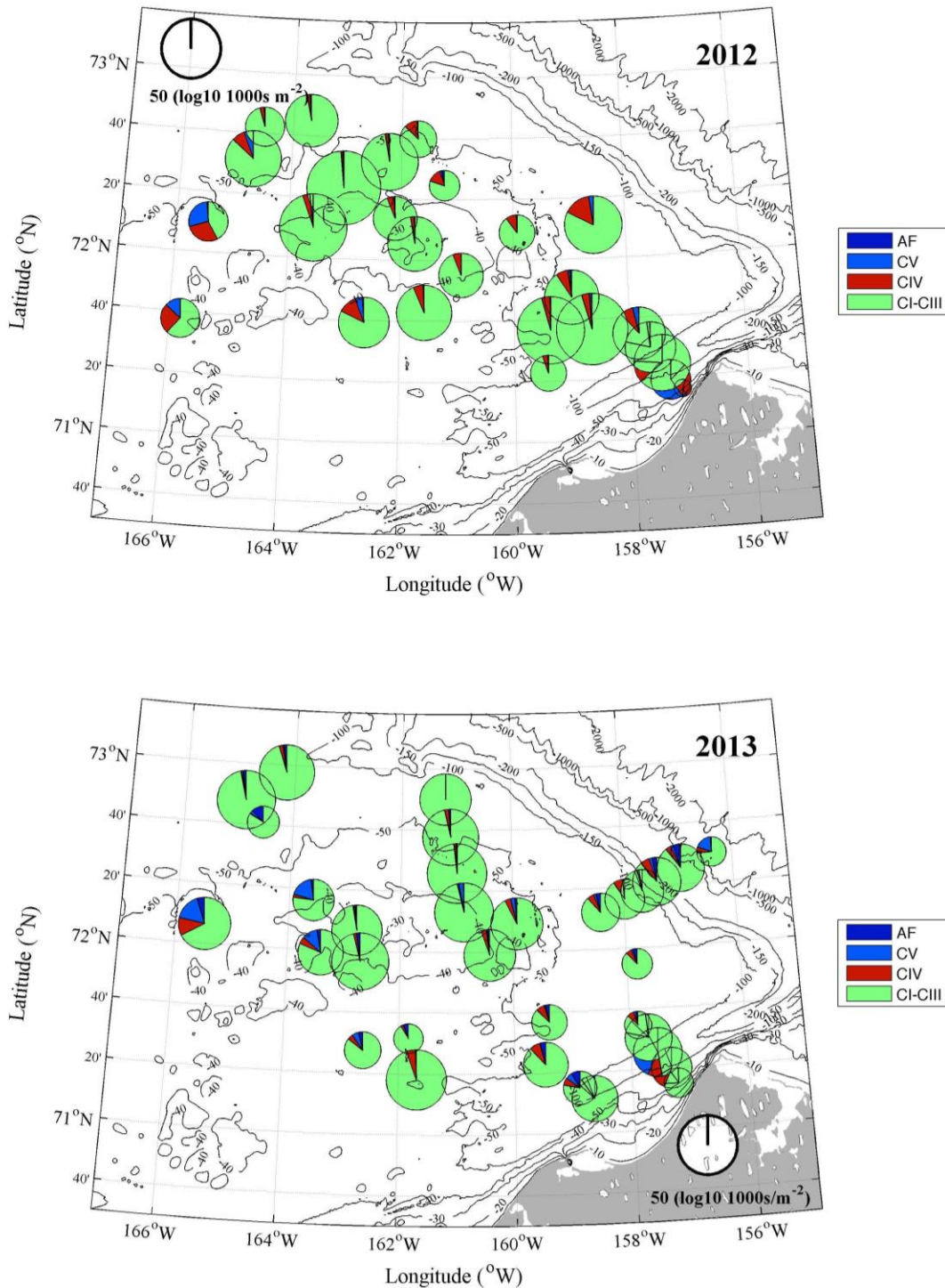


**Figure 3.** Integrated water column abundance and composition of genera of calanoid copepods from the 150  $\mu\text{m}$  mesh net zooplankton tows for the two years. (Abbreviations: Pseudocal.= *Pseudocalanus* spp.; C. hyper=*Calanus hyperboreus*; Neocal.=*Neocalanus* spp., Acartia=*Acartia longiremus*; Metridia=*Metridia* spp.; Microcal.=*Microcalanus pygmaeus*)

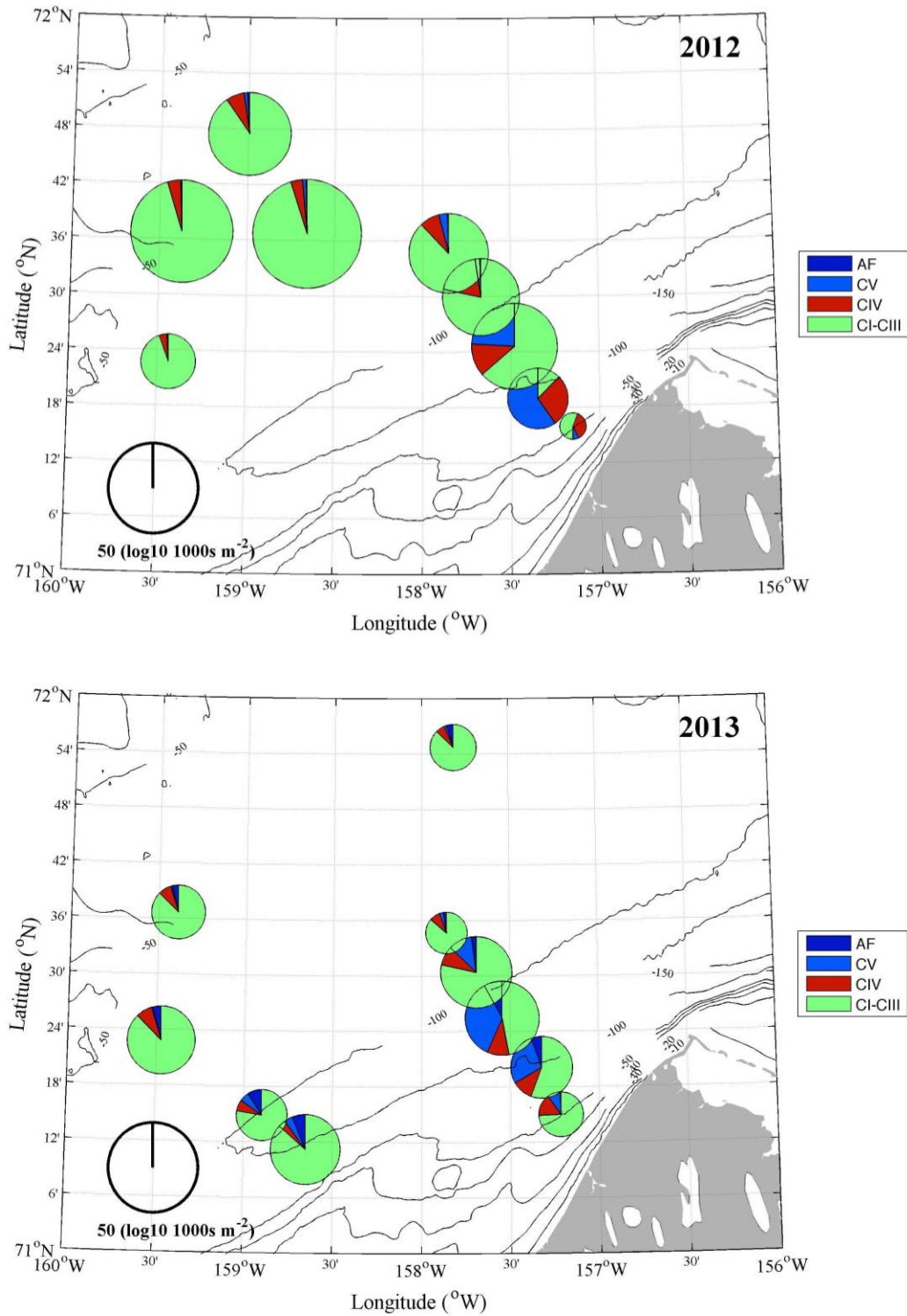




**Figure 4.** Integrated water column abundance and composition of the three copepod species *Calanus glacialis* (*C. glacialis*), *C. hyperboreus* (*C. hyp.*), and *Neocalanus* spp. (*Neocal.*) from the 150  $\mu$ m mesh net zooplankton tows for the two years.



**Figure 5.** Integrated water column abundance and composition of the life stages of the copepod *Calanus glacialis* from the 150  $\mu$ m mesh net zooplankton tows for the two years. AF=adult female, CV=copepodid stage V, CIV=copepodid stage IV, CIII=copepodid stages CI-CIII. Note log scale for abundance.

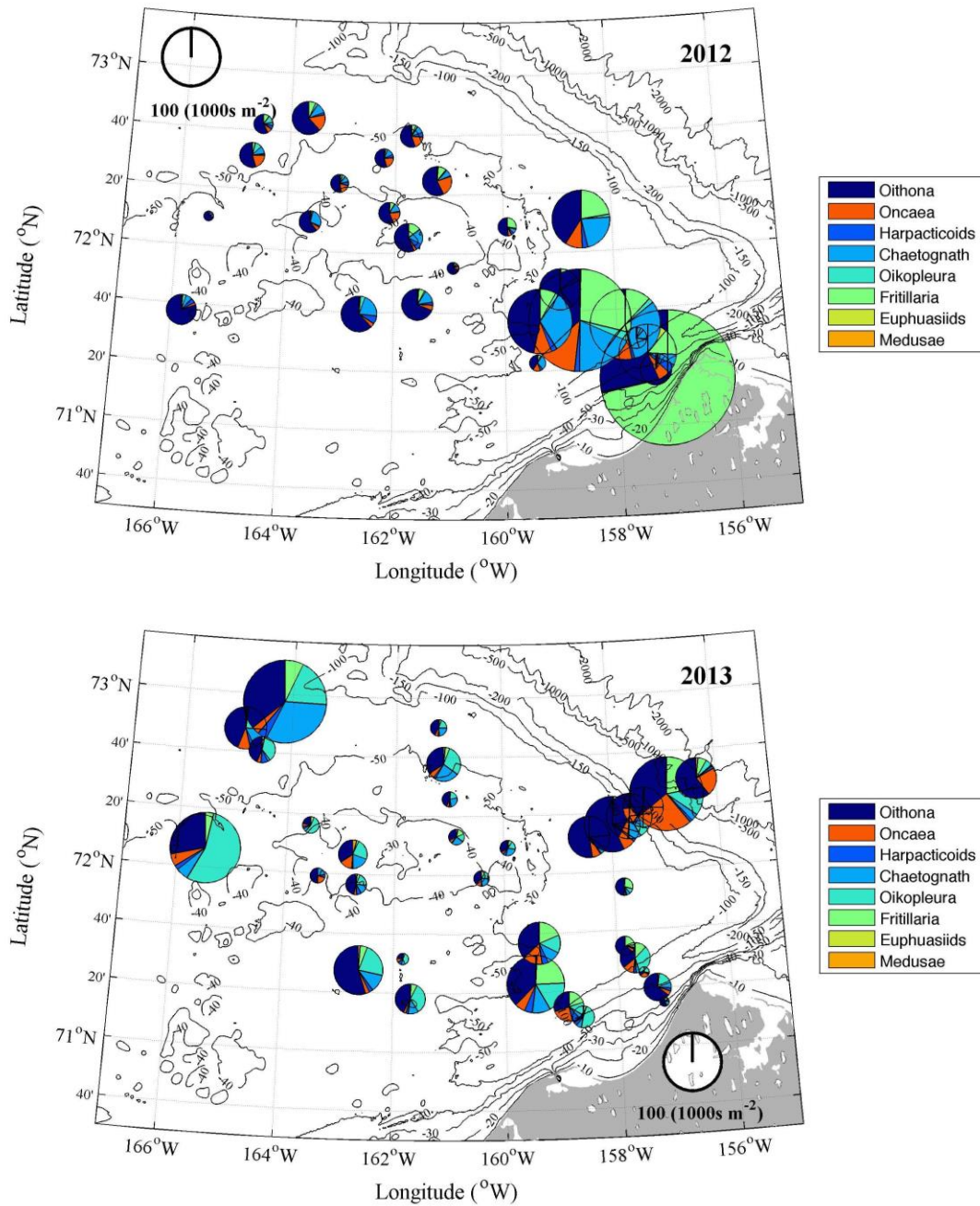


**Figure 6.** Integrated water column abundance and composition of the life stages of the copepod *Calanus glacialis* from the 150  $\mu$ m mesh net zooplankton tows for the two years for the Barrow Canyon region only. AF=adult female, CV=copepodid stage V, CIV=copepodid stage IV, CIII=copepodid stages CI-CIII. Note log scale for abundance.

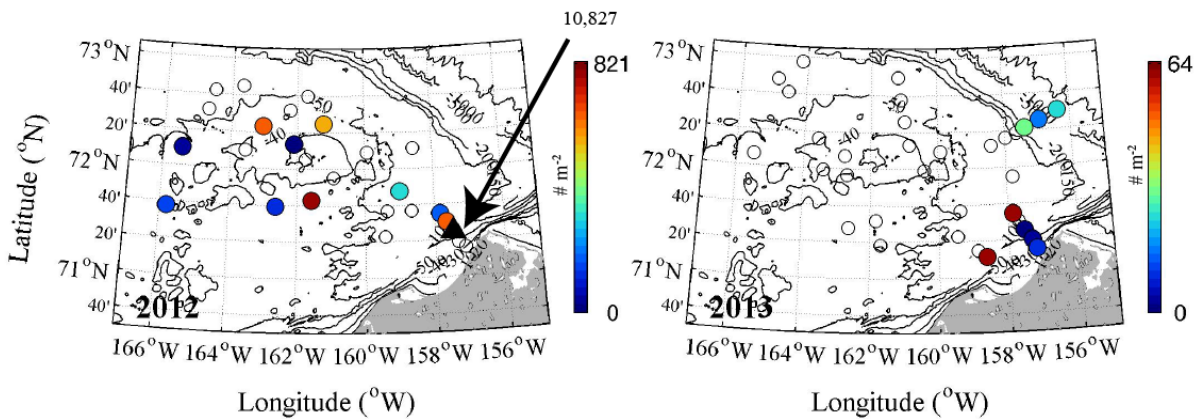
Abundances of the non-calanoid copepods and non-copepod holoplankton showed marked variation with location on the Shoal and between years (Figure 7). For both years, abundances were lowest on the Central Shoal. Abundances in 2012 usually were dominated by the very small cyclopoid copepods *Oithona similis* and *Oncaea* sp. However, high abundances in Barrow Canyon and on the NE corner of the Shoal were dominated by the appendicularian *Fritillaria* spp. Chaetognaths were also common, particularly in the central-eastern Shoal. In 2013, *O. similis* and *Oncaea* were again dominant at most locations and most particularly over the eastern portion of the study region. Chaetognaths again were a consistent member of the community. In addition to *Fritillaria* spp., the appendicularians *Oikopleura* spp. also were important at a few locations.

Euphausiids were rare in the region for both years, although far fewer were observed in 2013 than in 2012 (Figure 8). In 2012, euphausiids were seen at a four locations over the crest of the Shoal, with greatest water column abundances of 821/m<sup>2</sup>. Euphausiids also were present across Barrow Canyon and were extremely abundant (10,827/m<sup>2</sup>) in the middle of the Canyon (Station 57). In 2013, euphausiids were observed only at locations on the edges of the study area, off of the Shoal to the north over the shelf break and slope and in Barrow Canyon, and abundances were an order of magnitude lower than seen at most locations in 2012 (and three orders of magnitude lower than those seen in 2012 in Barrow Canyon).

Meroplankton (the planktonic larval stage of benthic organisms) also showed spatial and inter-annual differences (Figure 9). In 2012, eastern Hanna Shoal and Barrow Canyon had markedly elevated meroplankton abundances that were dominated by echinoderm and bivalve larvae. Lower meroplankton abundances on the central and western Shoal frequently were dominated by other taxa such as barnacle nauplii and polychaete larvae and trochophores and abundances of echinoderm and bivalve larvae were markedly reduced. In 2013, abundances of meroplankton were more evenly distributed across the study region. Abundances of echinoderm larvae were much reduced. Bivalve larvae still were important at many locations on the eastern Shoal and in Barrow Canyon. Locations in the southwestern portion of the study area had high proportions of barnacle nauplii and cyprids and of polychaete larvae and trochophores. Meroplankton were an important component of the zooplankton community, representing 33% of the total numerical abundance for both years (range for 2012: 8-79%; range for 2013: 10-79%).



**Figure 7.** Integrated water column abundance and composition of genera of non-calanooid copepods and of non-copepod holoplankton from the 150  $\mu$ m mesh net zooplankton tows for the two years.

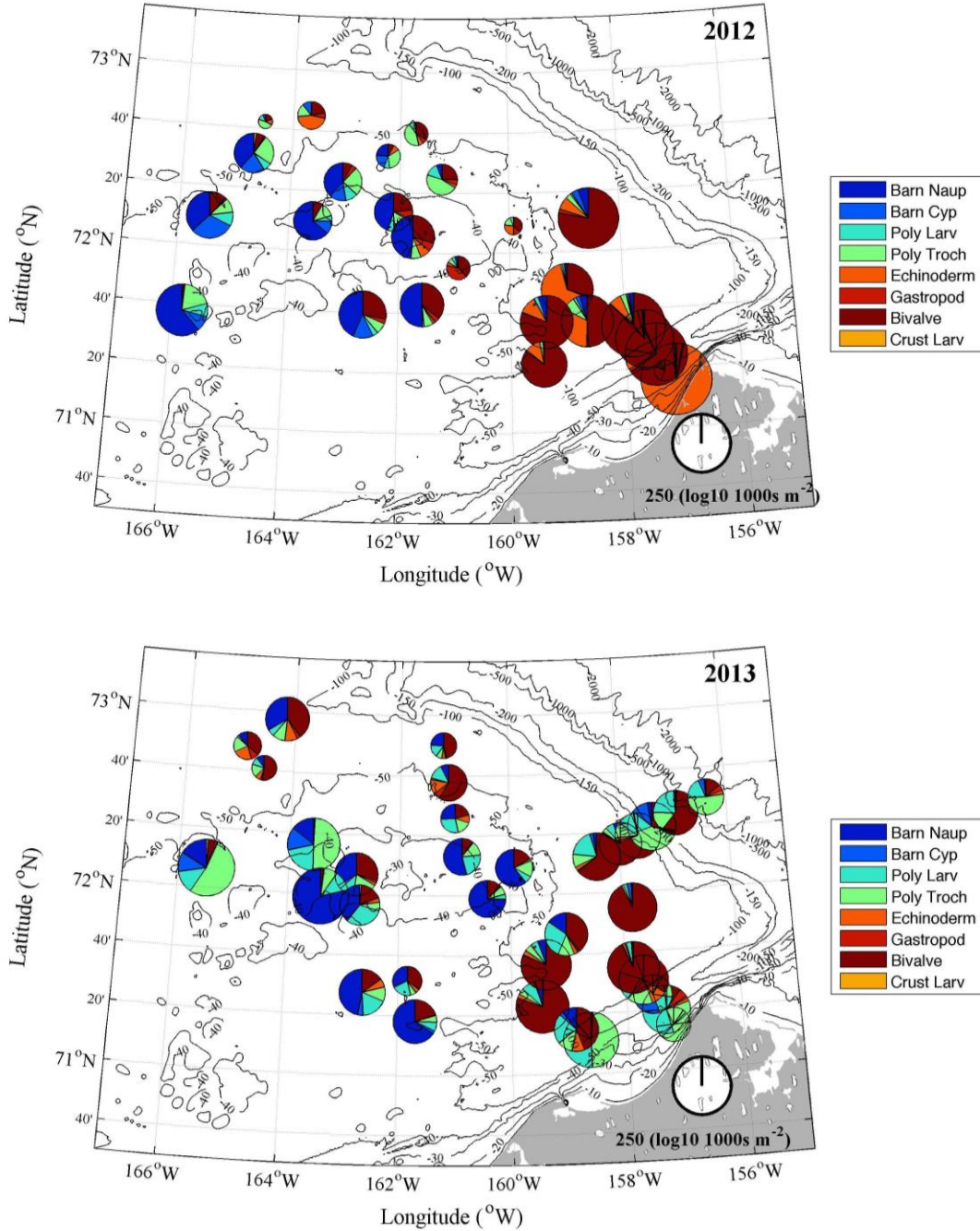


**Figure 8.** Water column integrated abundances of euphausiids. Open circles indicate locations where no euphausiids were captured. On station (57) from 2012 had extremely high abundances of euphausiids and is plotted separately as the black triangle.

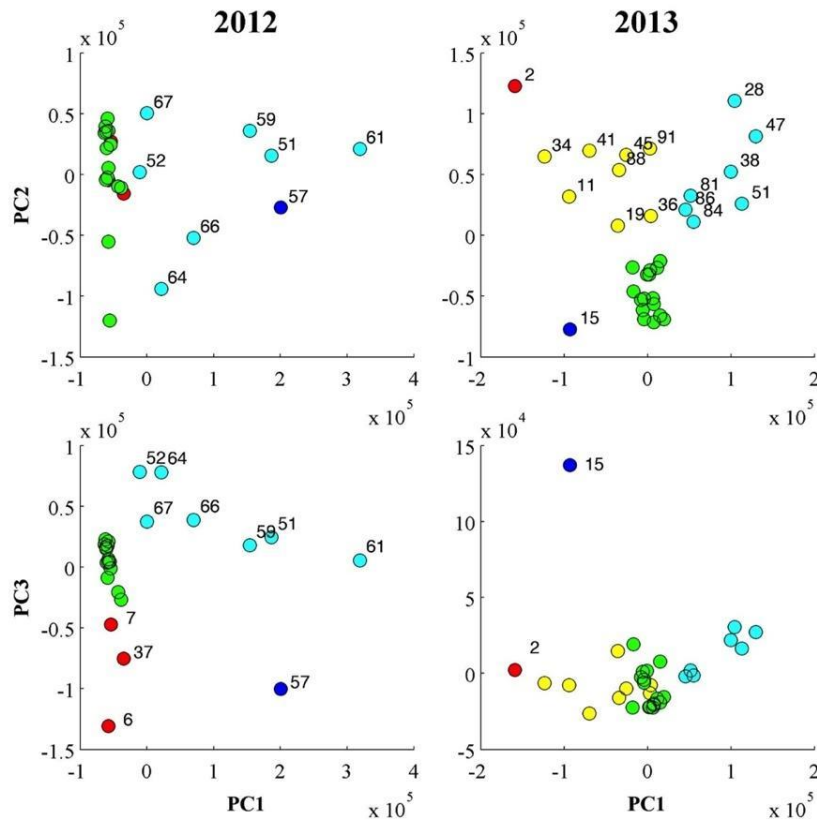
### 3.3 Principal Component Analyses

Principal component analysis (PCA) of the plankton abundances yielded four groups of stations for 2012 and five groups of stations for 2013 (Figures 10 and 11). For 2012, the first three principal components embodied 93.3% of the total variance (Appendix II). Principal component (PC) 1 was dominated positively by bivalve larvae, PC2 negatively by *C. glacialis* CI-CIII and to a lesser extent positively by *Pseudocalanus* spp., and PC3 negatively by both *Pseudocalanus* spp. and barnacle nauplii abundances with lesser positive contributions by *C. glacialis* CI-CIII. The situation was more confusing for 2013 and the first three principal components embodied only 79.6% of the total variance. Both PC1 and PC2 had greatest contributions (positive) by bivalve larvae. *Pseudocalanus* spp. and polychaete trochophores were significant additional negative contributions to PC1 and significant additional positive contributions to PC2. The third PC was positively dominated by barnacle nauplii. For both analyses, meroplankton abundances were very important, perhaps because the meroplankton demonstrated greater spatial variability in abundance and composition than other taxa. Four station groups were identified for 2012 and five for 2013 (Figure 10).

In 2012, the different types of stations classified according to the PC groupings were spatially distributed in a coherent pattern across the Shoal. One set of stations was observed in the SW corner and southern edge of the crest (Figure 11; red stations) and were differentiated by high values of PC3 (Figure 10). A second set of stations was clustered on the central Shoal (Figure 11; green stations). The third type of stations were found on the eastern Shoal and on the western edge of Barrow Canyon (cyan stations); these stations were dominated by bivalve larvae (Figure 9) and were differentiated in PC space by positive values of PC1 that was driven by abundances of bivalve larvae. Finally, two stations in Barrow Canyon comprised the fourth group (dark blue stations); this group was only loosely defined by the PC analysis since one of the stations was so radically different in its taxonomic composition that it was not included in the analysis (st. 53) and the other was not associated with any of the groups (st. 57) and had very high abundances of euphausiids (Figure 8).



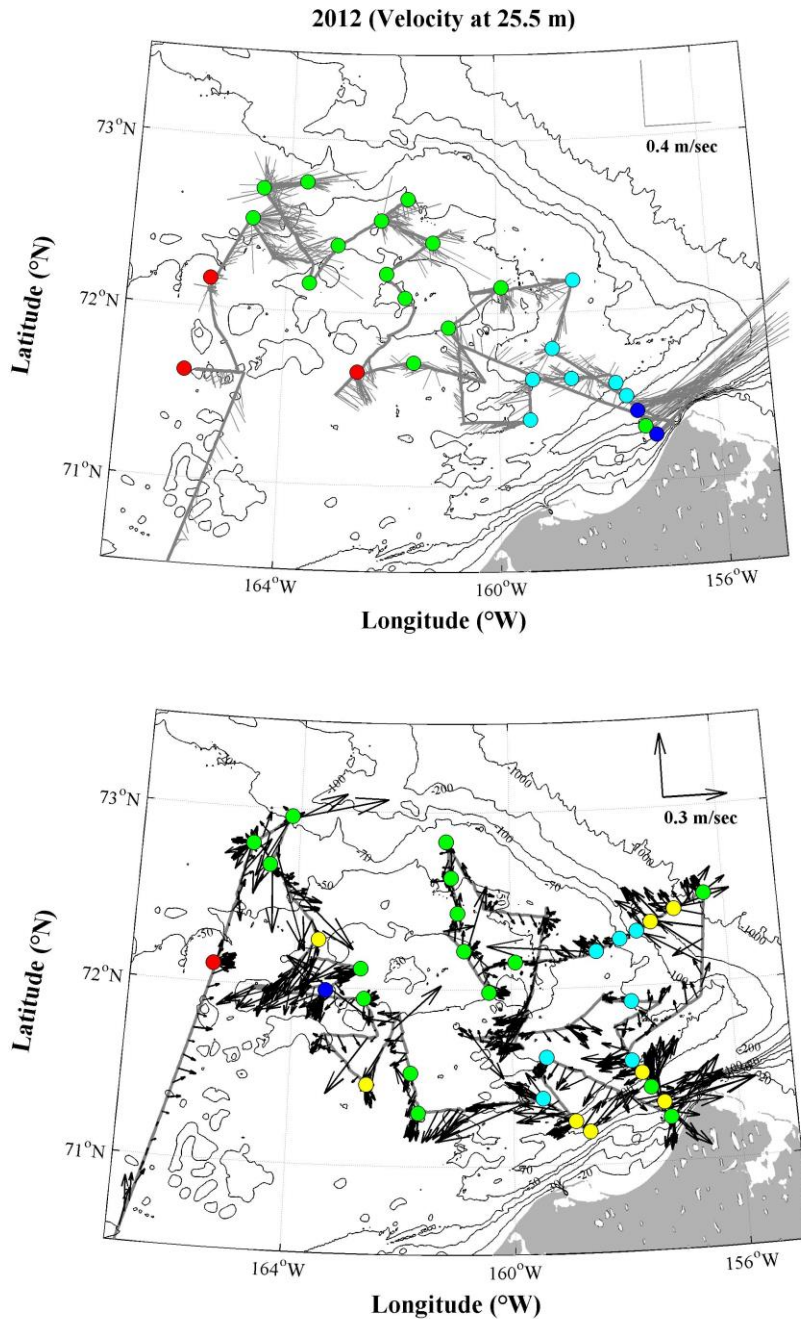
**Figure 9.** Integrated water column abundance and composition of meroplankton taxa from the 150  $\mu$ m mesh net zooplankton tows for the two years. (Abbreviations: Barn Naup = Barnacle nauplii; Barn Cyp= Barnacle cyprids; Poly Larv=Polychaete larvae; Poly trochophores = Polychaete trochophores; Echinoderm = Echinoderm larvae; Gastropod = Gastropod larvae; Bivalve=Bivalve larvae; Crust Larv = Crustacean Larvae)



**Figure 10.** Plots of PC1 vs. PC2 and PC3 for each year, grouped according to similarity using position on the graph. Groups are differentiated by color. Station numbers indicated for some groups. Note, station 53 from 2012 was not included in the analysis because of dramatically different plankton composition.

For 2013, stations were less coherently grouped. One station in the SW corner of the study region stood apart from the others (Figure 11; red station). Stations in the NE corner of the shoal grouped together (Figure 11; cyan stations); these were locations where bivalve larvae were abundant (Figure 9) and as a result PC2 was high (Figure 10). One station (15; dark blue station) was significantly different from all others (Figure 10), likely because of the very high proportion of barnacle nauplii found there (Figure 3). The remaining stations (green, yellow stations; Figure 11) were only loosely differentiated in PC space (Figure 10) and were distributed across the Shoal, onto the shelf and slope to the north, and in Barrow Canyon.



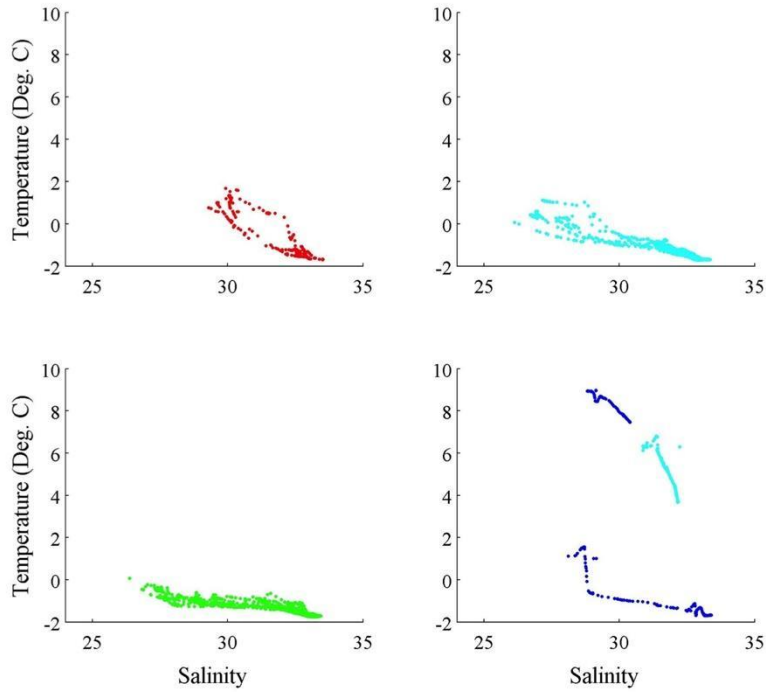


**Figure 11.** Stations grouped using PCA of integrated abundances of zooplankton taxa. For each year, different colors indicate stations that were grouped together on the basis of their taxonomic composition. Analyses were conducted independently for each year so there is no correspondence in station types between the two years. Upper water column (25.5, 23 m for 2012 and 2013, respectively) velocities measured using the hull-mounted acoustic Doppler current profiler also are shown (gray vectors).

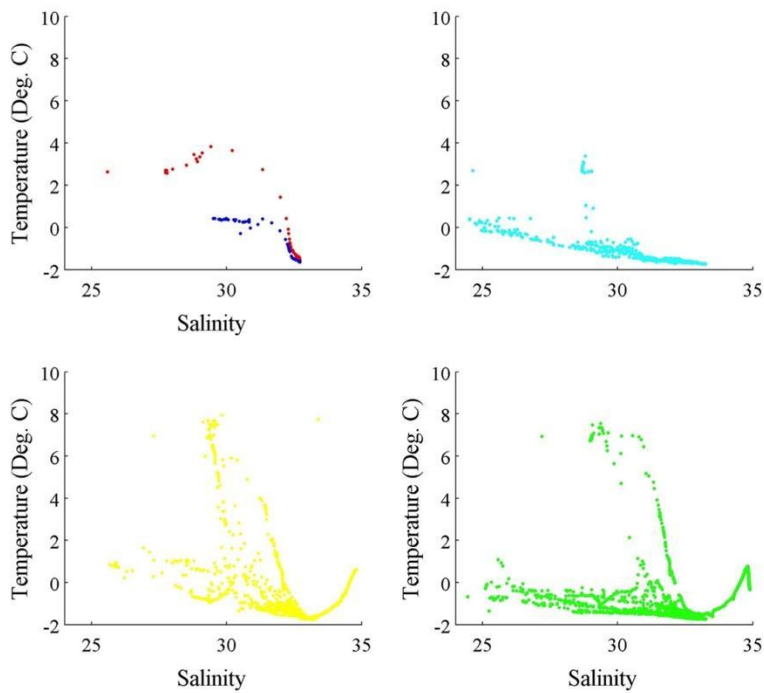
### 3.4 Associations of Station Groups with Hydrographic Conditions and Circulation

Temperature-salinity diagrams were used as a means to identify different water masses that may be associated with the different groups of stations (see Weingartner et al. chapter in this report for more discussion of water masses). This was not entirely successful, as the different types of stations were not consistently associated with different water masses, particularly in 2013. In 2012, very warm water characteristic of Bering Sea summer water or the Alaskan Coastal Current only was observed at stations located in Barrow Canyon (blue stations, Figure 12). There was evidence of warmer water at stations in the SW corner of the study area (red), suggesting an influence of water from the Bering Sea at that location. These stations also did not show the fresh water characteristic of sea ice melt, again supporting a Bering Sea influence likely resulting from northern advection of water from there. Stations on the Shoal (green stations) had low temperatures throughout the water column with a range of salinities including fresh water originating from sea ice melt. Stations on the Shoal were most consistently covered with sea ice during the cruise. Stations on the eastern end of the Shoal and on the western side of Barrow Canyon (cyan stations), characterized by high abundances of bivalve larvae, showed some evidence of warming of fresher water in the upper water column, perhaps originating from solar heating of sea ice melt water. Two stations in Barrow Canyon (lower right plot, stations 53 and 55) had much higher water temperatures than at other locations, likely because of the presence of warm, Alaskan coastal water, however these two stations were placed in different station groups on the basis of plankton composition. A third station in Barrow Canyon (lower right plot) had much lower temperatures and some mixing with warm Alaskan Coastal Water near the surface (2°C) but also with very different plankton composition from other stations (Station 57, Figure 10).

The situation is much more confusing for 2013. Again, the stations in the SW corner of the Shoal (blue, red) were distinct from other locations in having little evidence of the fresher water resulting from ice melt, suggesting that this was water that had been advected in from the south, and had different plankton compositions from other stations and from each other. All stations located in Barrow Canyon (34-45, Figure 1) had Alaskan Coastal Water in the upper water column (T°C 4-8, Salinity 28-32; cyan, yellow, green; Figure 13). Nonetheless, stations with Alaskan Coastal Water were placed into three different station groups based on plankton composition. All other locations showed evidence of warming of fresh sea ice melt water in the upper water column, with greatest warming for located around the edges of the shoal (yellow, Figures 11 and 13) and lesser warming for those on the crest (green) and on the NE corner (cyan) of the Bank



**Figure 12.** Temperature-salinity plots for the different stations grouped using PCA for 2012. Dot colors correspond to the different stations types from Figures 10 and 11. TS properties for station 55 (lower right, cyan) were more consistent with those of station 53 (dark blue, temperatures 8°C and greater).



**Figure 13.** Temperature-salinity plots for the different stations grouped using PCA for 2013. Dot colors correspond to the different stations types from Figures 10 and 11.

Circulation, demonstrated by upper-water column velocity measured using the 150 kHz ADCP, during 2012 showed some features characteristic of the region that also were associated with the different types of stations defined by zooplankton composition (Figure 11; see also Weingartner et al. chapter from this report). Clockwise circulation was observed on the shallow portion of the Shoal. Currents flowed to the east or SE along the southern edge of the shoal. A strong Alaskan Coastal Current (ACC) ran along the eastern edge of Barrow Canyon, with weak flow to the south and west along the western side of the Canyon as well as on the northeast corner of the shoal.

Station types in 2012 were associated with the regions of different circulation or flow region. One type of station (green) was associated with the clockwise circulation on the crest and along the inner edges of the crest. A second taxonomic composition was seen along the southern edges of the Shoal associated with flow to the southeast (red stations). Two types of stations (blue, green) were associated with the ACC in Barrow Canyon, one type with plankton characteristic of the ACC and the second with plankton similar to those found on the crest of the Shoal. Finally, the northeast portion of the Shoal and western side of Barrow Canyon, with southwest flow, had a fourth type of plankton community (cyan stations). The characteristic Arctic basin copepod *C. hyperboreus* was observed only at one of these stations (61; Figure 1), presumably advected to that location from the neighboring basin.

In 2013, the circulation was much less cohesive and showed much less evidence of a clockwise circulation on the Shoal than in 2012 (Figure 11). Flow over much of the southern portion of the Shoal was to the south or southwest while flow on the northern portion of the central Shoal was weaker and much more variable in direction. In Barrow Canyon, the ACC was broader and weaker than in 2012, with flow to the SW only seen at the western side of the Canyon. Significant southwestern flow extended south to the west of the ACC in the Canyon. Along the shelf break/slope, the usually eastward flowing shelf-break jet had reversed and flow was to the west-northwest. The northeast corner of the shoal also showed flow to the west-northwest, although of lower velocity.

Plankton communities in 2013 also were associated with different flow regions, although much more spatially mixed. The community found on the crest of the Shoal (green stations) extended much further to the south than in 2012, resulting from advection in the southwesterly currents, and also was seen in the ACC and at the northern end of the northern transect, likely due to complex advective pathways near the head of and through Barrow Canyon. Stations seen primarily on the periphery of the Shoal (yellow stations) were interspersed with crest stations (green) both along the southern edge and in the ACC. The eastern-northeastern corner of the Shoal contained a characteristic community composition (cyan) that likely was distributed to the NW and to the SW in the variable flow in that region.

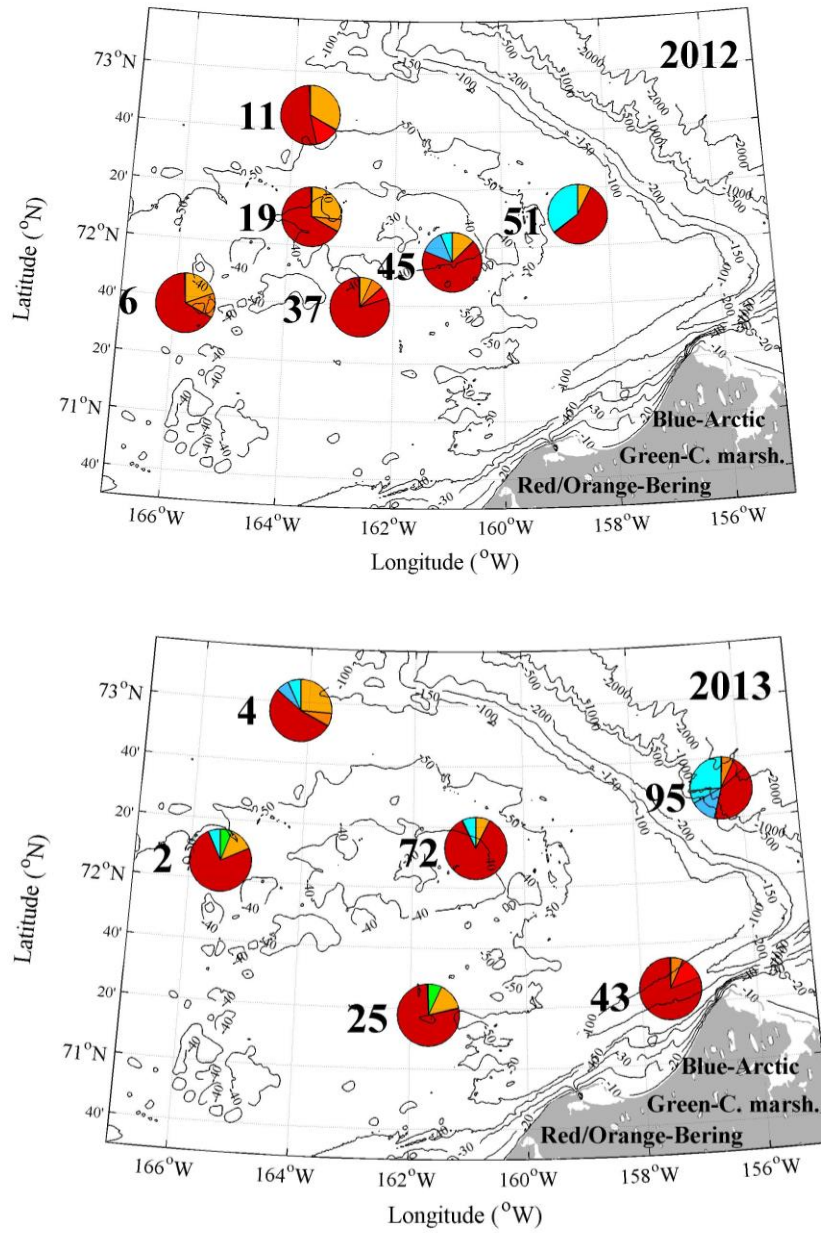
The reduced coherence in flow patterns and marked difference in flow direction in 2013 relative to 2012 likely resulted because the upper water column (23 m) velocities considered here are susceptible to wind direction. The magnitude of the wind was similar for both cruises ( $9.5 \pm 3.7$  and  $10.7 \pm 3.5$  (knots, mean  $\pm$  std.dev), 2012 and 2013 respectively). However, mean wind direction was from the SE and much less variable during 2012 ( $162^\circ \pm 44^\circ$ ) than during 2013 when mean winds were from the E and highly variable ( $105^\circ \pm 109^\circ$ ). If the last two days of

sampling (August 13 & 14) are excluded from the 2013 mean, winds were much less variable and from the NE for the much of the cruise ( $71^{\circ}\pm 51^{\circ}$ ). This persistent NE wind likely drove the widespread S-SW currents observed over much of the Shoal as well as the westerly flowing along shelf current along the northern edge of the Shoal. Although the currents here are termed “upper water column”, they do represent a substantial portion of the total water column at many locations since the water depths on the Shoal were only 30-50 m. Sea ice cover also was somewhat reduced during 2013 relative to 2012 (although both are considered to be “heavy ice” years; Weingartner et al., this report) and the greater extent of open water in that year may have resulted in a greater importance of the local winds to circulation.

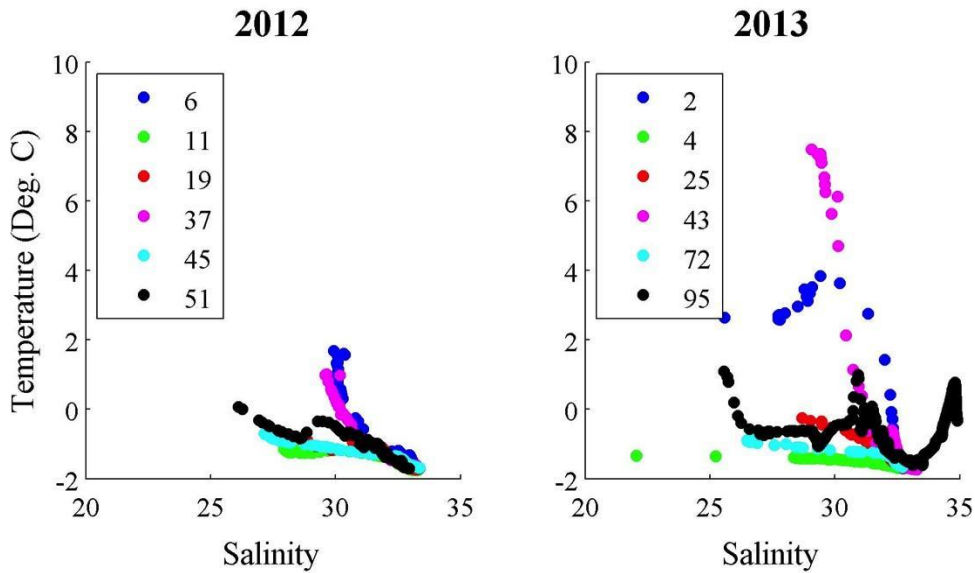
### 3.5 Genetic Analyses

Four haplotypes characteristic of the Bering Sea and three haplotype groups characteristic of the Arctic Ocean were detected in the sequencing of the mtCOI gene from *C. glacialis* at six different locations in each sampling year. Individuals of the congeneric species *C. marshallae*, characteristic of the southern Bering Sea and Gulf of Alaska, also were detected (Figure 14). The region was more genetically diverse in 2013 than in 2012, with both Arctic and Bering Sea haplotypes detected at four of the six locations in 2013 but at only two of the six locations in 2012. The greatest proportion of Arctic haplotypes were found on the NE corner of the Shoal (2012) or off of the Shoal in the Canada Basin to the north (2013), although individuals with Arctic haplotypes were also found along the western side of the Shoal and on the crest in 2013. *Calanus marshallae* was detected at two locations, one in the SW corner of the shoal and one at the southern side of the Shoal near Barrow Canyon, in 2013 but was not detected in 2012. The distribution of haplotypes and species thus was consistent with the known pathways of advection and water masses, including some exchange of water between the Canada Basin and the region of the Shoal particularly in 2013.

Temperature-salinity characteristics for each station were analyzed as independent evidence of the source locations of the water and haplotypes present (Figure 15). In 2012, water at four of the six locations was generally cold with some slight warming of the fresher sea ice melt water in the upper water column. However, the two locations on the southern side of Hanna Shoal did not contain sea ice melt water, consistent with a Bering Sea source, and also only showed Bering Sea haplotypes. In 2013, water mass characteristics were much more variable and several stations likely had a mixture of different water types as well as *C. glacialis* haplotypes and the presence of *C. marshallae*. Station 2 had Bering Sea water ( $4^{\circ}\text{C}$ ), both Bering Sea and Arctic haplotypes, and *C. marshallae*. Station 43, located in Barrow Canyon, showed Alaskan Coastal Water and only Bering Sea haplotypes of *C. glacialis*. Station 95, located off of the Shoal over the Chukchi Slope to the north showed evidence of Alaskan Coastal Water, Bering Sea Water, and Atlantic Water (warmer, high salinity at depth) and had the greatest proportion of Arctic haplotypes.



**Figure 14.** Proportions of different haplotypes of the mtCOI gene from *C. glacialis* collected at 6 stations in each year. For each location, station number is indicated.



**Figure 15.** Temperature-salinity diagrams for stations where mtCOI genetic analysis was conducted. Numbers refer to stations identified in Figure 13.

#### 4. Discussion

The distributions and abundances of mesozooplankton across Hanna Shoal showed variation associated with the different topographic regions and observed hydrographic characteristics and circulation, embodied in the identification of different station types on the basis of plankton composition. Overall, abundances of most taxa did not vary greatly between regions and between years, although abundances and diversity usually were reduced on the crest of the Shoal. There were some notable exceptions, however. Abundances of non-calanoid copepods and non-copepod holoplankton were greater in Barrow Canyon and on the northeastern corner than elsewhere on the Shoal in 2012, particularly because of high abundances of the larvacean *Fritillaria* spp. For both 2012 and 2013, abundances of these taxa were greater on the peripheries of the Shoal than on the Crest. Meroplankton were present in different proportions and abundances across the different regions, with bivalves and echinoderms being important and abundant particularly at eastern locations and barnacles (larvae and cyprids) and polychaetes being more important in western portions. In particular, very high abundances of bivalve and echinoderm larvae were observed on the northeast corner in 2012. Associations with hydrographic conditions and currents were better in 2012 than in 2013, potentially because of local wind forcing differed between the two years with prevailing winds from the south-southeast in 2012 driving clockwise circulation on the Shoal and an easterly shelf-break jet while prevailing winds from the northeast in 2013 driving the shelf-break jet towards the west and generating much less cohesive and more meandering current pathways on the Shoal and in Barrow Canyon. It is also important to note that the plankton were collected over the entire water column so that vertical differences in abundance that might be associated with specific water types could not be identified. This might account also for some of the less tight associations between water types and station groups defined on the basis of taxonomic composition, since the TS characteristics are shown for the entire water column while the

taxonomic composition could be driven by zooplankton present only in the upper or lower portion of the water column (for example).

The focus copepod species *Calanus glacialis* was the dominant species of the large Calanidae on the Shoal, with very few *C. hyperboreus*, *Neocalanus* spp., or *C. marshallae* observed. *Calanus glacialis* usually dominated the calanoid copepod taxonomic composition over the Shoal. It is possible that different populations of *C. glacialis* were present in the different regions, based both on the relative proportion of older life stages (more CIV-Adults) and on the proportions of the different haplotype groups. Populations of *C. glacialis* in the Canada Basin from the north have been observed to have different life stage compositions than those on the Chukchi Shelf (Ashjian and Campbell, unpub.). Here, different life stage compositions over the northern edges of the Shoal relative to those on the southern side coupled to the presence of Arctic haplotypes suggest that mixing of *C. glacialis* populations coming in from the Bering Sea and populations coming onto the Shoal from the north was occurring.

Few euphausiids were observed on Hanna Shoal proper and, in 2013, even on the periphery of the Shoal to the north or in Barrow Canyon. Only at one location in Barrow Canyon in 2012 was a substantial abundance of euphausiids observed. Historically, euphausiids have been rare in zooplankton collections in the Chukchi Sea yet bowhead whales at Barrow feed on euphausiids as seen in whale stomach contents from whales harvested during the annual fall Inūpiat hunt (e.g., Moore et al., 2010). Bowhead whales require dense patches of their prey to feed; such patches are generated on the shelf to the northeast of Barrow by local wind forcing, shelf break upwelling, and current path modifications (e.g., Ashjian et al., 2010; Okkonen et al., 2011; Citta et al., 2015). It is generally believed that euphausiids are not endemic to the Chukchi Sea and are brought to Barrow from the Bering Sea in the prevailing currents where they provide a reliable prey supply for the bowhead whales in fall (e.g., Bérline et al., 2008). It was somewhat surprising not to find more euphausiids, given that the sampling intersected some of those dominant advective pathways. Euphausiids are notoriously difficult to catch because they are highly motile and have good vision so the vertical hauls of the Bongo nets used in this study might have been easy for the animals to elude, despite the use of the strobe on the nets. This cannot entirely explain the dearth of euphausiids seen in 2013, however, since a portion of the net tows was conducted at night when euphausiid vision, and thus net avoidance, is more limited. Euphausiids also are extremely patchy and this might have limited catch success and collections, if the station locations and times happened to not coincide with the presence of a euphausiid patches. Regardless, it is clear that euphausiids are not present in great abundance and a significant component of the zooplankton across Hanna Shoal. Thus, although the fall migration route of bowhead whales frequently crosses Hanna Shoal, bowhead whales are not likely to be feeding during this portion of their migration. This might suggest that the Barrow feeding region for bowhead whales is of greater importance for the whales since dense patches of their prey are not available over Hanna Shoal and prey may not be available until the whales reach the Anadyr Current and Chukotka coast in the western Chukchi Sea.

Only a few previous studies focused on the zooplankton near Hanna Shoal with which comparisons can be made. Lane et al. (2008) concentrated on the shelf-break region in August 2002. Some of the stations sampled for that study were located near those sampled along the northern edge of Hanna Shoal in 2013 for the present study, although there was little overlap for



2012, and both studies occurred during August. Zooplankton composition in 2002 was similar to those in 2012 and 2013, with large bodied copepods, small bodied copepods, other holoplankton, and meroplankton present. Zooplankton from Lane et al. (2008) also were associated with different hydrographic conditions. *Calanus glacialis* was numerous, particularly the younger copepodid stages, but the smaller copepod species including *Pseudocalanus* spp. and *Oithona similis* dominated numerically. Meroplankton also were present, especially barnacle nauplii and echinoderm larvae. Lane et al. (2008) compared abundances of selected taxa with those from samples collected in the early 1950s by Johnson (Johnson, 1956) and concluded that there was a trend towards greater abundances in 2002 for all of the taxa except barnacle nauplii. Comparison of abundances for those same taxa from 2012 and 2013 from stations along the northern edge of Hanna Shoal and in Barrow Canyon, in the same general regions as those sampled by Lane et al. (2008), did not show increased abundances since 2002 for most of the taxa (Table 1).

Abundances of *C. hyperboreus*, the basin type copepod, were approximately equivalent for all of the years. Abundances of *O. similis*, the microcalanids (*Pseudocalanus* spp. and *Microcalanus pygmaeus*), barnacle nauplii, and appendicularians were approximately equivalent to those from 2002 and greater than those observed in the early 1950s. However, abundances of *C. glacialis* from both 2012 and 2013 appeared to be substantially increased relative to both of the earlier periods and showed a consistent trend of increasing abundance over the 63 years. This also was consistent with a recent synthesis of Chukchi Sea zooplankton data over a much greater spatial region and longer period that showed increasing abundances of *C. glacialis*, and other calanoid copepod species that are advected into the Chukchi Sea from the northern Bering Sea, (Ershova et al. 2015).

**Table 1.** Average abundances and ranges (# m<sup>-3</sup>) of selected taxa from studies in the northeastern Chukchi Sea collected during August of each year using 150 µm mesh nets. Data from 1950 and 1951 were collected by Johnson (1956), data from 2002 were collected by Lane et al. (2008), and data from 2012 and 2013 were collected as part of this study. Details of the 1959, 1951, and 2002 data are described in Lane et al. (2008). For 2012 and 2013, only those stations that lay in regions also sampled by the Lane et al. (2008) study were included; these regions were along the northern edge of the Shoal (depth > ~ 50 m) into the shelf-break and slope and in Barrow Canyon.

	Year of Sampling				
	1950	1951	2002	2012	2013
<i>C. hyperboreus</i>	5 (0-7)	3 (0-5)	6 (0-19)	1 (0-5)	3 (0-19)
<i>C. glacialis</i>	18 (3-54)	40 (2-69)	87 (1-241)	379 (10-867)	238 (23-845)
Microcalanids	293 (67-516)	354 (119-662)	900 (24-2547)	509 (20-937)	745 (151-1395)
<i>O. similis</i>	74 (14-157)	180 (34-461)	526 (40-1625)	738 (245-3078)	296 (61-870)
Barnacle nauplii	50 (0-202)	55 (0-202)	8 (0-63)	99 (0-345)	49 (0-239)
Appendicularians	24 (0-76)	55 (0-108)	437 (17-1821)	716 (21-5194)	211 (28-443)

A three-year study of the mesozooplankton of the lease sale areas located to the south of Hanna Shoal during multiple cruises in July-October 2008-2010 (Day et al., 2013; Questel et al., 2013) showed similar overall patterns of abundance and taxonomic composition although there is

little/no overlap in sampling locations and regions between that work and the Hanna Shoal study. Total holozooplankton (3977, 3213 m<sup>-3</sup>, 2012 and 2013 respectively) and meroplankton (2603, 1437 m<sup>-3</sup>, 2012 and 2013) abundances (150 µm mesh nets) on Hanna Shoal were similar to those just to the south (holoplankton ~2400-7400 m<sup>-3</sup>; meroplankton ~625-9315 m<sup>-3</sup>; Questel et al., 2013), with meroplankton comprising 28, 8, and 56% of the total numerical abundance for 2008-2010, respectively, compared to the 33% total numerical abundance on Hanna Shoal in both 2012 and 2013. Holoplankton and meroplankton abundances also were similar to those reported by Hopcroft et al. (2010) from the southern Chukchi Sea in August 2004, suggesting consistency in total zooplankton abundance over this period across the Chukchi Sea. Taxonomic composition to the south in 2008-2010 (Questel et al., 2013) was similar to that observed on Hanna Shoal in 2012 and 2013, with the copepods *C. glacialis*, *Pseudocalanus* spp., and *O. similis*, larvaceans, and meroplankton dominating numerically. Note however that the Questel et al. (2013) study was conducted over a broader range of seasons (July-October) and these abundances and proportions were derived across the range of seasons; this likely accounts for the higher variability observed between years for the Questel et al. (2013) study relative to the Hanna Shoal work. In both the Hopcroft et al. (2010) and Questel et al. (2013) studies zooplankton composition and abundance also were associated with different hydrographic conditions and advective characteristics. Euphausiids were similarly scarce in all of these studies of the Chukchi Sea, suggesting that patchiness and difficulty in capturing the animals as well as their potential limited distribution within particular currents and water masses precludes their regular collection.

The similarity in mesozooplankton abundances on Hanna Shoal to those across these multiple regions of the Chukchi Sea suggests that the role of mesozooplankton in the carbon cycle on the Shoal is similar to that role in other regions of the Chukchi Sea. The Chukchi Sea is known for its high production and benthic biomass; much of the primary production is transferred to the benthos and is not consumed in the water column by the zooplankton. Micro- and mesozooplankton from the Chukchi shelf-break and slope region have been shown to together consume only up to 40% of the total primary production (Campbell et al., 2009). Other studies have estimated that the mesozooplankton can only consume a fraction of the primary production and available chlorophyll in the Chukchi Sea (e.g., Lane et al., 2008; Hopcroft et al., 2010; Questel et al., 2013). Given that the abundances of mesozooplankton on Hanna Shoal are similar to those in other regions of the Chukchi Sea, it is likely that a similar low utilization of primary production is ongoing on the Shoal that contributes to a high input of carbon to the benthos and sustains the rich benthic biomass found there.

At least two different types of populations of the copepod *C. glacialis*, as demonstrated by the haplotypes of the mtCOI gene, were present on the Shoal. The southern portions contained almost exclusively haplotypes characteristic of the Bering Sea while those on the northern edge of the Shoal contained a mixture of Bering Sea and Arctic Ocean haplotypes. These results are consistent with those observed by Nelson et al. (2009), using the 16s ribosomal gene, and also with ongoing work by Campbell et al. (in. prep.) across the Chukchi, Bering, and Beaufort Seas. The increased proportion of Arctic haplotypes along the shelf-break and on the slope also is consistent with suggestions of different populations in the Chukchi and Beaufort Seas based on population age structures (proportion of life stages) observed over several cruises including the

two Hanna Shoal cruises (Ashjian and Campbell, in prep.). All of these observations support a Bering Sea origin for most of the *C. glacialis* present in the Chukchi Sea.

At present, Hanna Shoal and the Chukchi Sea are benthically-dominated and sustain an abundant benthos that is critical feeding habitat for a number of important and endangered upper trophic level animals (e.g., Grebmeier et al., 2015). Under ongoing climate change, ecosystem structure and function in seas such as the Chukchi and on Hanna Shoal may change. It has been suggested that the Chukchi Sea might become increasingly pelagic, with a greater role of the water column consumers in consumption and cycling of primary production carbon. The observed increasing abundances of the copepod *C. glacialis* might support such a transition. However, the Chukchi Sea is also incredibly advective, with much of the zooplankton present being brought in each year through Bering Strait and likely swept off of the northern Shelf within a year. Therefore, it is difficult to envision the establishment or persistence of resident Chukchi Sea populations. Increases in abundance of zooplankton in the Chukchi can realistically only be accomplished through increases in their input through Bering Strait resulting from increased volume transport through the Strait, from increased abundance in the water entering through the Strait, or a combination of both increased volume transport and increased concentration of plankton in that water. Given the likelihood of populations being swept out of the Chukchi Sea in less than a year (e.g., Bérline et al., 2008), it is likely that the Chukchi Sea zooplankton must be reset or re-established each year. Under these conditions, it is likely that Hanna Shoal will continue to support a rich and abundant benthos and serve as a critical feeding location for upper trophic level benthic animals.

## 5. Acknowledgements

The Captain, officers, and crew of the USCGC Healy provided invaluable assistance and support during the two cruises. Special thanks also to our colleagues in the COMIDA Hanna Shoal study for their collaboration and camaraderie, particularly T. Weingartner and Y.-C. Fang for assistance with the physical oceanography data, J. Grebmeier and L. Cooper for their leadership as chief scientists for the cruises, and K. Dunton for his leadership of the program. Many thanks to H. Crowley for her support of this work. This study was funded by the U.S. Department of the Interior, Bureau of Ocean Energy Management (BOEM), Alaska Outer Continental Shelf Region, Anchorage, Alaska under BOEM Cooperative Agreement No. M11AC00007 as part of the Chukchi Sea Offshore Monitoring in Drilling Area (COMIDA).

## 6. References

- Ahlstrom, E.H., Thraillkill, T.R. 1963. Plankton volume loss with time of preservation. CalCOFI Report 9, 57-73.
- Ashjian, C.J. Braund, S.R., Campbell, R.G., George, J.C., Kruse, J. Maslowski, W., Moore, S.E., Nicolson, C.R., Okkonen, S.R., Sherr, B.F., Sherr, E.B., Spitz, Y. 2010. Climate variability, oceanography, bowhead whale distribution, and Iñupiat subsistence whaling near Barrow, AK. Arctic 63, 179-194
- Bérline, L., Spitz, Y.H., Ashjian, C.J., Campbell, R.G., Maslowski, W., Moore, S.E. 2008. Euphausiid transport in the Western Arctic Ocean. Mar. Ecol. Progr. Ser. 360, 163-178.

- Brugler, E.T., Pickart, R.S., Moore, G.W.K., Roberts, S., Weingartner, T.J., Statscewich, H. 2014. Seasonal to interannual variability of the Pacific Water boundary current in the Beaufort Sea. *Prog. Oceanogr.* 127, 1–20. <http://dx.doi.org/10.1016/j.pocean.2014.05.002>.
- Bucklin, A., Frost, B.W., Kocher, T.D., 1995. Molecular systematics of six *Calanus* and three *Metridia* species (Calanoida: Copepoda). *Mar. Biol.* 121 (4), 655-664.
- Campbell, R.G., Sherr, E.B., Ashjian, C.J., Plourde, S., Sherr, B.F., Hill, V., Stockwell, D.A., 2009. Mesozooplankton prey preference and grazing impact in the western Arctic Ocean. *Deep-Sea Res. II* 56, 1274–1289. doi:10.1016/j.dsr2.2008.10.027
- Carroll, G.M, George, J.C, Lowry, L.F, Coyle, K.O. 1987. Bowhead whale (*Balaena mysticetus*) feeding near Point Barrow, Alaska, during the 1985 spring migration. *Arctic* 40: 105-110.
- Citta, J. Quakenbush, L.T., Okkonen, S.R., Druckenmiller, M.L., Maslowski, W., Clement-Kinney, J., Ashjian, C.J., George, J.C., Brower, H., Small, R.J., Harwood, L.A., Heide-Jorgensen, M.P. 2014. Ecological characteristics of core areas used by western Arctic bowhead whales, 2006-2012. *Prog. Oceanogr.* 136, 201-222.doi: 10.1016/j.pocean.2014.08.012.
- Cooper, L.W., Ashjian, C.J., Smith, S.L., Codispoti, L.A., Grebmeier, J., Campbell, R.G., Sherr, E.B. 2006. Rapid seasonal sea-ice retreat in the Arctic could be impacting Pacific walrus (*Odobenus rosmarus divergens*) recruitment. *Aquatic Mammals* 32: 98-102.
- Day, R.H., Weingartner, T.J., Hopcroft, R.R., Aeirts, L.A. M., Blanchard, A.L., Gall, A.E., Gallaway, B.J., Hannay, D.E., Holladay, B.A., Mathis, J.T., Norcross, B.L., Questel, J.M., Wisdom, S.S. 2013. The offshore northeastern Chukchi Sea, Alaska: A complex high-latitude ecosystem. *Cont. Shelf. Res.* 67, 147-165.
- Dunton, K.H., Grebmeier, J.M., Trefry, J. 2014. The benthic ecosystem of the northeastern Chukchi Sea: An overview of its unique biogeochemical and biological characteristics. *Deep Sea Res. II* 102, 1-8
- Ershova, E.A., Hopcroft, R.R., Kosbokova, K.M., Matsuno, K., Nelson, R.J., Yamaguchi, A., Eisner, L.B. 2015. Long-term changes in summer zooplankton communities of the western Chukchi Sea, 1945-2012. *Oceanography* 28, 100-115.
- Folmer, O., Black, M., Hoeh, W., Lutz, R., & Vrijenkoek, R. 1994. Molecular Marine Biology and Biotechnology. DNA primers for amplification of mitochondrial cytochrome c oxidase subunit I from diverse metazoan invertebrates, 3, 294-299.
- Grebmeier, J.M., Harvey, H.R. 2005. The Western Arctic Shelf–Basin Interactions (SBI) Project: an overview. *Deep Sea Res. II* 52,109–3115.
- Grebmeier, J.M., Bluhm, B.A., Cooper, L.W., Danielson, S.L., Arrigo, K.R., Blanchard, A.L., Clarke, J.T., Day, R.H., Frey, K.E., Gradinger, R.R., Kedra, M., Konar, B., Kuletz, K.J, Lee, S.H., Lovvorn, J.R., Norcross, B.L., Okkonen, S.R. 2015. Ecosystem characteristics and processes facilitating persistent macrobenthic biomass hotspots and associated benthivory in the Pacific Arctic. *Prog. Oceanogr.* 136, 92-114. <http://dx.doi.org/10.1016/j.pocean.2015.05.006>.
- Hill, R.S., Allen, L.D., Bucklin, A. 2001. Multiplexed species-specific PCR protocol to discriminate four N. Atlantic *Calanus* species, with an mtCOI gene tree for ten *Calanus*

- species. *Mar. Biol.* 139, 279-287.
- Hopcroft, R.R., Kosobokova, K.N. 2009. Distribution and egg production of *Pseudocalanus* species in the Chukchi Sea. *Deep-Sea Res. II* 57, 49-56.
- Hopcroft, R.R., Kosobokova, K.N., Pinchuk A.I. 2010 Zooplankton community patterns in the Chukchi Sea during summer 2004. *Deep-Sea Res II* 57, 27–39.
- Johnson, M.W. 1956. The plankton of the Beaufort and Chukchi Sea areas of the Arctic and its relation to the hydrography. Arctic Institute of North America, Technical Paper, vol. 1. 32 pp.
- Lane, P.V., Llinás, L., Smith, S.L., Pilz, D. 2008. Zooplankton distribution in the western Arctic during summer 2002: hydrographic habitats and implications for food chain dynamics. *J. Mar. Sys.* 70, 97-133.
- Llinás, L., Pickart, R.S., Mathis, J.T., Smith, S.L. 2009. Zooplankton inside an Arctic Ocean cold-core eddy: Probably origin and fate. *Deep-Sea Res. II* 56: 1290-1304.
- Lowry, L.F., Sheffield, G., George, J.C. 2004. Bowhead whale feeding in the Alaskan Beaufort Sea, based on stomach contents analyses. *Journal of Cetacean Research & Management* 6: 215-223.
- Machida, R. J., Miya, M. U., Yamauchi, M. M., Nishida, M., Nishida, S. 2004. Organization of the mitochondrial genome of Antarctic krill *Euphausia superba* (Crustacea: Malacostraca). *Marine Biotechnology* 6(3), 238-250.
- Matsuno K., Yamaguchi, A., Hirawake, T., Imai, I. 2011. Year-to-year changes of the mesozooplankton community in the Chukchi Sea during summers of 1991, 1992 and 2007, 2008. *Polar Biol* 34, 1349–1360. doi:10.1007/s00300-011-0988-z.
- Moore, S.E., George, J.C., Sheffield, G., Bacon, J., Ashjian, C.J. 2010. Bowhead whale distribution and feeding in the western Alaskan Beaufort Sea during late summer, 2005-2006. *Arctic* 63: 195-205.
- Nelson, R.J., Carmack, E.C., McLaughlin, F.A., Cooper, G.A. 2009. Penetration of Pacific zooplankton into the eastern Arctic Ocean tracked with molecular population genetics. *Mar. Ecol. Prog. Ser.* 381, 129-138.
- Nikolopoulos, A., Pickart, R.S., Fratantoni, P.S., Shimada, K., Torres, D.J., Jones, E.P. 2009. The western Arctic boundary current at 152 W: Structure, variability, and transport. *Deep-Sea Res. II* 56, 1164-1181.
- Okkonen, S.R., Ashjian, C.J., Campbell, R.G., Maslowski, W., Clement-Kinney, J.L., Potter, R., 2009. Intrusion of warm Bering/Chukchi waters onto the shelf in the western Beaufort Sea. *J. Geophys. Res.* 114: C00A11.
- Okkonen, S.R., Ashjian, C.J., Campbell, R.G., Clarke, J., Moore, S.E., Taylor, K.D. 2011. Satellite observations of circulation features associated with the Barrow area bowhead whale feeding hotspot. *Remote Sensing of Environment* 115, 2168-2174.
- Quakenbush, L.T., Citta, J.J., George, J.C., Small, R.J., 2010. Fall and winter movements of bowhead whales (*Balaena mysticetus*) in the Chukchi Sea and within a potential petroleum development area. *Arctic*. <http://doi.org/10.1098/rsbl.2011.0731>.

- Questel, J.M., Clarke, C., Hopcroft, R.R. 2013. Seasonal and interannual variation in the planktonic communities of the northeastern Chukchi Sea during the summer and early fall. *Cont. Shelf Res.* 67, 23–41.
- Wiebe, P., 1988. Functional regression equations for zooplankton displacement volume, wet weight, dry weight, and carbon: a correction. *Fishery Bulletin* 86, 833-835.
- Wiebe, P.H., Ashjian, C., Gallagher, S., Davis, C., Lawson, G., Copley, N. 2004. Using a high powered strobe light to increase the catch of Antarctic krill. *Mar. Bio.* 144 (3), 493 - 502.
- Wiebe, P.H., Lawson, G.L., Lavery, A.C., Copley, N.J., Horgan, E., Bradley, A. 2013. Improved agreement of net and acoustical methods for surveying euphausiids by mitigating avoidance using a net-based LED strobe light system. *ICES J. Mar. Sci.* 70(3), 650-664  
doi:10.1093/icesjms/fst005.
- Weingartner, T., Aagaard, K., Woodgate, R., Danielson, S., Sasaki, Y., Cavalieri, D. 2005. Circulation on the north central Chukchi Sea shelf. *Deep-Sea Res. II* 52, 3150–3174.
- Weingartner, T., Dobbins, E., Danielson, S., Potter, R., Statscewich, H., Winsor, P., 2013. Hydrographic variability of the northeastern Chukchi Sea shelf in summer-fall 2008–2010. *Continental Shelf Research* 67, 5–22.

## Appendix I.

Locations, station numbers, dates, bottom depths, and tow depths for net tows conducted during the two cruises.

Year	Station Number	Station Name	Date (local)	Time (local)		Latitude (Deg. N)	Longitude (Deg. W)	Bottom Depth (m)	Tow Depth (m)
				Hour	Minute				
2012	1	BRS5	8/11/12	20	22	65.737	168.8425	53	53
	3	H24W1	8/13/12	2	18	71.629	165.0750	44	39
	5	H24W3	8/13/12	4	14	71.627	165.6010	41	35
	6	H24	8/13/12	6	46	71.627	165.8039	40	36
	7	CBL11/H23	8/13/12	18	1	72.165	165.4385	47	37
	8	H21A	8/14/12	1	53	72.183	165.3084	48	na
	9	H21	8/14/12	7	7	72.524	164.7066	51	na
	10	H10	8/14/12	19	16	72.321	164.2300	46	na
	11	H30	8/15/12	10	34	72.749	163.6744	65	55
	12	NSNW40-12	8/15/12	19	19	72.703	164.5275	59	49
	16	NW3	8/16/12	3	55	72.452	163.8934	50	25
	19	H6	8/16/12	10	5	72.165	163.5658	41	30
	20	H8	8/16/12	18	54	72.388	163.0428	42	32
	22	H8B	8/17/12	2	53	72.488	162.4998	42	38
	24	H4B	8/17/12	6	57	72.663	161.7087	48	43
	25	H4	8/17/12	10	26	72.537	162.2209	45	41
	26	H14	8/17/12	21	29	72.410	161.2237	45	42
	27	H14A	8/18/12	2	43	72.471	160.9532	46	42
	30	H2	8/18/12	9	12	72.228	162.1050	34	28
	31	H5	8/18/12	15	23	72.090	161.7449	29	21
	32	H3	8/18/12	22	25	71.873	162.0369	42	39
	34	H3B	8/19/12	3	58	71.726	162.4333	43	n/a
	37	H1	8/19/12	9	1	71.655	162.6175	44	30
	38	H19	8/19/12	17	35	71.714	161.5725	46	35
	42	H19G	8/20/12	4	28	71.604	160.2524	52	44
	45	H16	8/20/12	9	54	71.920	160.9278	41	37
	46	H20	8/20/12	20	45	72.150	159.9297	46	38
	51	HSNE56	8/21/12	13	12	72.182	158.5649	58	52
	52	H32	8/21/12	18	49	71.790	158.9925	53	37
	53	BARC1	8/22/12	11	34	71.266	157.1542	49	32
	55	BARC3	8/22/12	15	6	71.316	157.3494	85	65
	57	BARC5	8/22/12	19	8	71.410	157.4782	131	126
	59	BARC7	8/23/12	1	56	71.499	157.6665	89	82
	59	BARC7	8/23/12	2	12	71.502	157.6631	89	65
61	BARC9	8/23/12	5	3	71.578	157.8492	66	61	
64	HB2	8/23/12	10	4	71.612	158.6567	57	46	

	66	H38	8/23/12	13	28	71.613	159.3722	53	41
	67	CBL-14	8/23/12	21	15	71.379	159.4333	53	45
<b>2013</b>	1	BRS5	8/1/13	0	43	65.725	168.8558	52	38
	2	CBL11	8/2/13	8	32	72.107	165.4887	47	33
	3	H112	8/2/13	21	20	72.798	164.8883	64	63
	3	H112	8/2/13	22	34	72.794	164.9307	64	50
	4	H114	8/3/13	9	6	72.959	164.1648	76	74
	5	HSNW60	8/3/13	13	15	72.681	164.5515	57	55
	8	HSW50	8/3/13	17	55	72.528	164.1531	53	49
	11	HSW40	8/3/13	22	0	72.270	163.5694	43	41
	12	UTX1	8/4/13	0	53	72.060	164.1570	42	24
	14	H7	8/4/13	9	35	72.113	162.7745	40	35
	15	H17	8/4/13	16	44	71.986	163.4052	41	37
	16	CC1	8/5/13	0	54	71.984	164.7504	42	33
	17	HS3	8/5/13	7	14	71.943	162.6993	42	34
	18	UTX8	8/5/13	15	2	71.728	163.4575	38	36
	19	UTX11	8/5/13	21	0	71.459	162.6154	43	41
	20	H3	8/6/13	4	8	71.870	162.0572	42	43
	23	TW3	8/6/13	8	24	71.527	161.8297	47	38
	25	CBL13	8/6/13	11	44	71.302	161.6874	50	48
	28	CBL14	8/7/13	0	8	71.380	159.4715	55	50
	34	TW14	8/7/13	5	45	71.187	158.6512	97	90
	36	H111	8/7/13	8	23	71.248	158.8971	113	106
	37	H109	8/7/13	14	6	71.501	159.5127	53	48
	38	H108	8/7/13	20	14	71.611	159.3889	54	50
	39	BARC1	8/8/13	6	47	71.250	157.2169	52	40
	41	BARC3	8/8/13	10	37	71.335	157.3230	96	91
	43	BARC5	8/8/13	14	27	71.424	157.5438	128	112
	45	BARC7	8/8/13	21	45	71.507	157.6886	85	83
	47	BARC9	8/8/13	22	43	71.578	157.8584	67	58
	50	CA2	8/9/13	5	50	71.895	157.3120	79	67
	51	CA3	8/9/13	7	38	71.912	157.8169	70	61
	52	H29	8/9/13	10	56	71.930	158.3318	66	59
	53	H32	8/9/13	19	33	71.778	159.0177	54	54
	54	H106	8/9/13	23	54	71.758	159.6005	53	47
	55	CA4	8/10/13	2	50	71.739	160.1804	51	46
	56	CBL15	8/10/13	5	8	71.731	160.7488	48	34
	57	H107	8/10/13	9	35	71.676	159.8290	54	50
	58	H33	8/10/13	16	48	71.837	159.7370	50	44
	60	YF2	8/11/13	1	8	72.137	159.5267	47	43
	62	YF4	8/11/13	5	9	72.459	159.3080	52	48
	63	H28	8/11/13	6	59	72.398	159.3371	53	50
	64	H15	8/11/13	13	3	72.446	160.3758	52	46
	65	H27	8/11/13	19	58	72.835	161.2053	53	47
	67	CP2	8/12/13	1	18	72.629	161.1082	51	48



69	CP4	8/12/13	3	35	72.431	160.9920	47	46
72	H9	8/12/13	8	31	72.218	160.8667	38	35
73	H34	8/12/13	14	17	71.983	160.4128	40	36
74	HSNE40	8/12/13	18	56	72.112	160.5057	42	39
75	H20	8/12/13	21	33	72.153	159.9237	47	38
78	HSNE50	8/13/13	1	0	72.149	159.1439	54	51
81	H102	8/13/13	6	35	72.202	158.4207	62	56
84	RP3	8/13/13	13	23	72.268	157.9775	69	63
86	RP5	8/13/13	15	27	72.308	157.6557	113	107
87	RP6	8/13/13	16	31	72.323	157.5216	147	144
88	RP7	8/13/13	17	48	72.355	157.3869	192	178
89	RP8	8/13/13	19	0	72.376	157.2279	228	223
91	RP10	8/13/13	21	8	72.422	156.9379	331	300
93	RP12	8/13/13	23	50	72.451	156.9592	604	300
95	H103	8/14/13	3	17	72.498	156.3617	1529	300

## Appendix II.

Coefficients for the first three principal components and cumulative proportion of the variance explained by each for the principal component analyses for each year. Coefficients normalized to maximum value; sign of coefficient retained with normalization. Coefficients with greatest weigh indicated with yellow highlighting.

		Mode 1	Mode 2	Mode 3
<b>2012</b>	<i>C. glacialis</i> AF	0.000	0.000	0.002
	<i>C. glacialis</i> C5	0.006	-0.001	-0.065
	<i>C. glacialis</i> C4	0.010	-0.007	-0.020
	<i>C. glacialis</i> CI-CIII	0.019	-1.000	0.612
	<i>Pseudocalanus</i>	0.059	-0.509	-1.000
	<i>C. hyperboreus</i>	0.000	0.000	0.000
	<i>Acartia</i> spp.	-0.016	-0.158	-0.248
	<i>Metridia</i> spp.	0.000	-0.004	0.007
	<i>Oithona similis</i>	0.072	-0.174	-0.075
	<i>Oncaea borealis</i>	0.024	-0.041	0.146
	Harpacticoid	0.004	-0.016	-0.026
	Barnacle nauplii	-0.010	-0.143	-0.959
	Barnacle cyprids	0.001	-0.017	-0.194
	Chaetognaths	0.068	-0.126	0.233
	Polychaete larvae	0.002	-0.018	-0.091
	Polychaete trochophores	0.050	-0.085	-0.456
	<i>Oikopleura</i>	0.002	-0.013	0.021
	<i>Fritillaria</i>	0.045	-0.135	0.246
	Echinoderms	0.095	-0.127	0.479

	Euphausiids	0.009	-0.011	-0.060
	Gastropod larvae	0.010	0.002	-0.022
	Bivalve larvae	1.000	0.089	-0.012
	Cumulative Variance	77.900	87.600	93.300
<b>2013</b>	<i>C. glacialis</i> AF	-0.007	0.008	-0.002
	<i>C. glacialis</i> C5	-0.035	0.017	-0.005
	<i>C. glacialis</i> C4	-0.011	0.014	0.002
	<i>C. glacialis</i> CI-CIII	-0.071	-0.303	-0.045
	<i>Pseudocalanus</i>	-0.612	0.903	-0.079
	<i>C. hyperboreus</i>	0.003	0.000	-0.002
	<i>Neocalanus</i> spp.	0.000	0.004	-0.001
	<i>Acartia</i> spp.	-0.032	0.046	-0.004
	<i>Metridia</i> spp.	-0.005	0.014	-0.005
	<i>Microcalanus pygmaeus</i>	0.019	0.087	-0.023
	<i>Oithona similis</i>	0.097	0.278	0.017
	<i>Oncaea borealis</i>	0.011	0.090	-0.015
	Harpacticoid	0.000	0.012	0.005
	Barnacle nauplii	-0.481	-0.322	1.000
	Barnacle cyprids	-0.180	0.185	-0.066
	Chaetognaths	0.015	-0.045	0.032
	Polychaete larvae	-0.312	0.311	0.066
	Polychaete trochophores	-0.743	0.656	-0.031
	<i>Oikopleura</i>	-0.214	0.276	-0.044
	<i>Fritillaria</i>	0.129	0.205	0.019
	Echinoderms	0.011	0.033	-0.009
	Euphausiids	0.000	0.000	0.000
	Hydromedusae	0.002	-0.004	-0.001
	Gastropod larvae	-0.010	0.013	-0.005
	Bivalve larvae	1.000	1.000	0.401
	Cumulative Variance	36.9	63.8	79.6

# Physical Control of the Distributions of a Key Arctic Copepod in the Northeast Chukchi Sea

Stephen M. Elliott<sup>1</sup>, Carin J. Ashjian<sup>1</sup>, Zhixuan Feng<sup>1</sup>, Benjamin Jones<sup>1</sup>, Changsheng Chen<sup>2</sup>, Yu Zhang<sup>2</sup>, Robert G. Campbell<sup>3</sup>

## <sup>1</sup>Woods Hole Oceanographic Institution

266 Woods Hole Road,  
Woods Hole, MA 02543-1050

## <sup>2</sup>University of Massachusetts Dartmouth

706 S. Rodney French Blvd  
New Bedford, MA 02744-1221

## <sup>3</sup>Graduate School of Oceanography, University of Rhode Island

S. Ferry Road  
Narragansette, RI 02882

[stephenmelliott@gmail.com](mailto:stephenmelliott@gmail.com); [cashjian@whoi.edu](mailto:cashjian@whoi.edu); [zfeng@whoi.edu](mailto:zfeng@whoi.edu); [btjones@mit.edu](mailto:btjones@mit.edu);  
[c1chen@umassd.edu](mailto:c1chen@umassd.edu); [y Zhang@umassd.edu](mailto:y Zhang@umassd.edu)

## Abstract

The Chukchi Sea is a highly advective regime dominated by a barotropically driven northward flow modulated by wind driven currents that reach the bottom boundary layer of this shallow environment. A general northward gradient of decreasing temperature and food concentration leads to geographically divergent copepod growth and development rates between north and south. The physics of this system establish the biological connection potential between specific regions. The copepod *Calanus glacialis* is a key grazer, predator, and food source in Arctic shelf seas. Its summer distribution and abundance have direct effects on much of the food web, from phytoplankton to migrating bowhead whales. In August 2012 and 2013, *C. glacialis* distributions were observed over Hanna Shoal in the northeast Chukchi Sea. Here the Finite Volume Community Ocean Model i-State Configuration Model is used to advect and develop these distributions forward and backward in time to determine the source and sink regions of the transient Hanna Shoal *C. glacialis* population. Hanna Shoal supplies diapause competent *C. glacialis* to both the Beaufort Slope and the Chukchi Cap, mainly receives juveniles from the broad slope between Hanna Shoal and Herald Canyon and receives second year adults from as far as the Anadyr Gulf and as close as the broad slope between Hanna Shoal and Herald Canyon. The 2013 sink region was shifted west relative to the 2012 region and the 2013 adult source region was shifted north relative to the 2012 region. These connection potentials were not sensitive to precise times and locations of release, but were quite sensitive to depth of release.

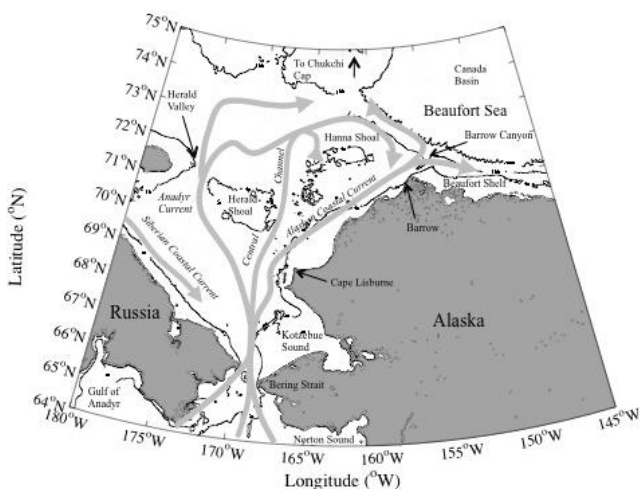
## 1. Introduction

The Chukchi Sea is a dynamic, shallow, marginal sea where water masses from the Pacific, Atlantic and Arctic Oceans meet, resulting in a complex and highly productive ecosystem. Hanna Shoal in the northeastern Chukchi Sea, like much of that shallow arctic shelf sea, exhibits tight pelagic-benthic coupling and supports a rich population of pinnipeds (Hunt et al., 2013; Grebmeier et al., 2014) that provide subsistence food for Alaskan coastal communities. In recent years, climate change has dramatically modified the sea ice and ocean conditions over Hanna Shoal with changes to the ecosystem of the Shoal expected in response. Yet many aspects of the ecology of Hanna Shoal remain poorly understood, making prediction and detection of potential climate change driven ecosystem shifts difficult at best. These interests, in addition to an oil and gas interests south of the shoal, motivated a two-year field study of the ecology of Hanna Shoal in summer, including of one of the dominant copepod species *Calanus glacialis* (BOEM 2015).

The Chukchi Sea has been described as a flow-through shelf, with plankton populations in the significantly influenced by the predominant advective pathways of the region (e.g., Carmack and Wassmann, 2006). The mean circulation of the Chukchi Sea is generally northward, primarily along one of three pathways: Eastern Chukchi and Barrow Canyon, the Central Channel, and Herald Canyon (e.g., Weingartner et al., 2005, 2013) (Figure 1). Annual mean transport through the Chukchi is estimated to be of order 0.8 Sv, although recent measurements have indicated that this transport is increasing (Woodgate et al., 2005; 2012). Mean northwards flow in this shallow shelf sea is modulated by wind-driven circulation that can cause local flow reversals and variability in circulation pathways (Weingartner et al., 2005; Weingartner et al., this report). Residence time in the Chukchi Sea was estimated to be between one and six months with the lowest values expected in late summer and the highest values expected in the late winter, when conditions are the least variable and surface winds have the least effect on circulation (Woodgate et al., 2005). These circulation pathways carry plankton from the northern Bering Sea through the Chukchi to the Arctic Ocean (e.g., Hopcroft et al., 2010). Hanna Shoal, in the northeastern Chukchi Sea, lies at the convergence of the three northward advection pathways and thus should be significantly influenced by input of populations of Bering Sea plankton as well as those endemic to the Chukchi Sea and those that are moved onto the shelf, perhaps by upwelling, from the adjacent Arctic Basin. The exact route followed by the Bering Sea Water arriving in the Chukchi is variable from year to year which seems to drive much of the interannual variation in zooplankton populations (Day et al. 2013).

There are few studies of zooplankton on Hanna Shoal proper, with most work being conducted on the adjacent Chukchi and Beaufort Seas shelf breaks/slopes or in Barrow Canyon (e.g., Lane et al., 2008; Campbell et al., 2009; Llinás et al., 2009; Day et al., 2013; Questel et al., 2013). At present, the zooplankton community, including *C. glacialis*, only grazes a small proportion of the total primary production, leaving the remainder to sink to the seafloor where it supports a rich and abundant benthos (e.g., Campbell et al., 2009; Grebmeier et al., 2014). The copepod community numerically is dominated by small copepods such as *Oithona similis* and *Pseudocalanus* spp. and in terms of biomass by the larger *Calanus glacialis* (a shelf/slope species). *Calanus glacialis* is a key species in the Arctic zooplankton community in terms of biomass, and its role as an energy concentrator is essential for ecosystem function (Falk-Petersen et al., 2009). This relatively long-lived planktonic crustacean is present over Hanna Shoal in August in all of its life stages and may serve as an important food source for migrating bowhead

whales in the fall (Quakenbush et al., 2010). In the highly advective regime western Arctic, *C. glacialis* populations in the adjacent Arctic basin are impacted by the success of populations in the Chukchi Sea, while populations in the Chukchi Sea are dependent on the success of populations in the Anadyr Gulf and the rest of the Northern Bering Sea. Yet the physical processes that mediate these connections remain poorly understood. To predict the strength of the *C. glacialis* population over Hanna Shoal and the effects of this population on those in the western Arctic, it is necessary to identify the strongest upstream sources and strongest downstream sinks of the *C. glacialis* population over Hanna Shoal.



**Figure 1.** Chukchi Sea geographic features and dominant pathways (adapted from Brugler et al., 2014).

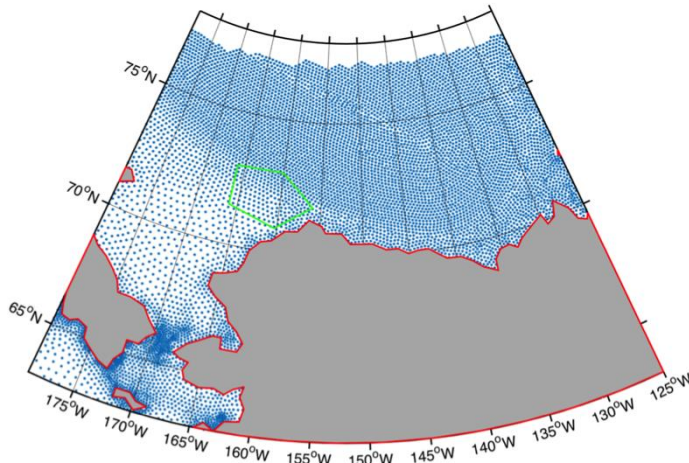
*glacialis* populations were advected forward and backward in time to determine the geographic regions that have tight links to Hanna Shoal and the sources and sinks of the populations observed on Hanna Shoal during each August. The interannual stability of these linkages, as well as their sensitivity to sampling location, time and depth provided insight into whether interannual differences in the observed populations were due to differences in advective pathways or to differences in biological and physical conditions in source regions. Persistent physical oceanographic features critical to controlling the distribution of *C. glacialis* in the northeast Chukchi Sea also were identified.

## 2. Materials and Methods

### 2.1 Physical Ocean Model

The physical ocean model is the Arctic Ocean Finite Volume Community Ocean Model (AO-FVCOM) (Chen et al., 2009). The model domain encompasses 61°N to 77°N and is pan Arctic. For this study, 8,032 control volumes are output in the area of interest defined as 63°N to 78°N and 179°W to 121°W (Figure 1), with average horizontal resolution of 21.7 km and an average area of approximately 218 km<sup>2</sup> for each control volume. As this is an unstructured grid, the horizontal resolution varied between 5.1 km in the Bering Strait and 61.1 km in the central Chukchi. Approximately 200 control volumes represent Hanna Shoal (Figure 2). The model

The remote and harsh nature of the northeast Chukchi Sea makes long-term spatially widespread data difficult and expensive to obtain, thus using direct observation to find source and sink regions is currently impractical. Coupling field observations with oceanographic models is an effective way to extrapolate on the limited data that can be collected in order to make broader conclusions. Here a physical ocean model is coupled to an individual based copepod development model to explore the sources and sinks of the *C. glacialis* populations on Hanna Shoal. Observed life stage specific distributions of *C. glacialis* in August of 2012 and 2013 were used as initialization for the simulations. The observed *C.*



**Figure 2.** Central nodes of AO-FVCOM in the area of interest. The green box represents Hanna Shoal.

surface winds, and atmospheric pressure gradients. Daily mean values were generated for the period of August 2011-December 2013 of velocity and temperature.

## 2.2 Individual Based Modeling of Temperature Dependent *C. glacialis* Development

The individual based development model was the FVCOM i-State Configuration Model (FISCM). The model consists of two parts: a Lagrangian tracking module and temperature dependent development module. The first was used to advect each copepod forward or backward in time using the velocity output from AO-FVCOM. This was done using a 10-minute time step. The second was used to modify the development stage of each copepod forward or backward in time using the temperature output from AO-FVCOM. This was done using a four-hour time step. The development rate of copepods of the species *Calanus finmarchicus*, a congener of *C. glacialis*, at any specific developmental stage has been experimentally found by Campbell et al. (2001) to follow

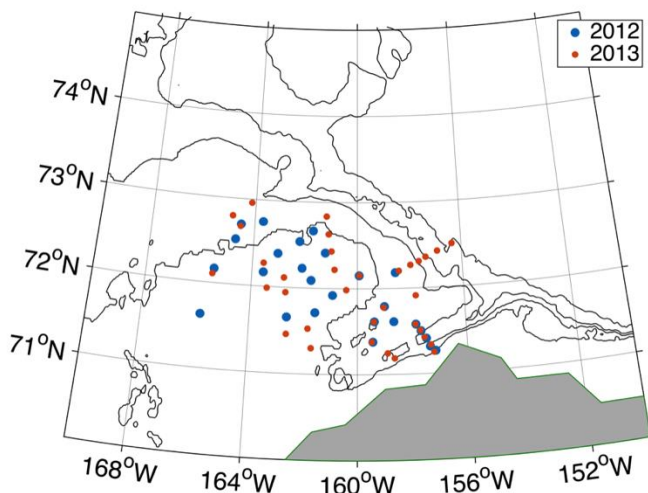
$$D = a(T + \alpha)^\beta \quad (\text{Equation 1})$$

Where T is temperature in degrees Celsius and a,  $\alpha$  and  $\beta$  are parameters fitted to experimental data.  $\beta$  is considered similar for all copepods. Corkett et al. (1986) found the mean  $\beta$  of 11 copepod species to be 2.05, so that is what we will use in this set of experiments. The coefficient “ $\alpha$ ” is considered species specific; 13.04 was used for *C. glacialis*, as determined by Corkett et al. (1986) in laboratory studies. The coefficient “a” is both species and stage specific. The stage specific “a” values for *C. glacialis* used in this experiment were: Egg-839 N1-548 N2-819 N3-1958 N4-1070 N5-1011 N6-1186 C1-1363 C2-1905 C3-2014 C4-3057 C5-5761 (Campbell et al., 2001; Ji et al., 2012).

The approach was to seed the Hanna Shoal region of the modeled fields with *C. glacialis*, using locations, life stage, and abundance (# m<sup>-2</sup>) distributions from field data rather than the more classic IBM approach of using a uniform distribution across the spatial domain of interest. In August 2012 and 2013, two cruises were conducted on *USCGC Healy* in the Northeast Chukchi Sea in support of the Hanna Shoal Ecosystem Study, an extension of the Chukchi Sea Offshore

uses a hybrid terrain following coordinate with 45 sigma layers. Within the area of interest, vertical resolution varies between 11 cm and 118 m. Most of the Chukchi Sea is represented with a vertical resolution of less than 2 meters. The AO-FVCOM is operated as a nested model within the global FVCOM. The merged global-AO FVCOM was initialized by running it for 50 years under climatologic meteorological forcing and river discharge and forced by observed data to capture the impact of tides, river discharge, surface heating, net surface precipitation,

Monitoring in Drilling Area (COMIDA) study. Between 13 and 23 August in 2012 and 1 and 14 August in 2013, paired Bongo nets equipped with 150  $\mu\text{m}$  and 500  $\mu\text{m}$  mesh nets, flow meters, and time-depth recorders were towed vertically from 5 m off the bottom to the surface at different sites across the geographic extent with particular attention given to areas around the periphery (Figure 3). Samples were preserved in 5% formalin seawater and enumerated to species and life stage at the University of Rhode Island.



**Figure 3.** Locations over Hanna Shoal sampled using net tows in August of 2012 and 2013.

At each site, *C. glacialis* water column abundances ( $\# \text{m}^{-2}$ ) from the 150  $\mu\text{m}$  mesh net were used to seed the model simulations on the day of the field observation; *C. glacialis* nauplii and eggs are too small to be sampled quantitatively using a 150  $\mu\text{m}$  net and so were not used for model seeding. Once seeded, the copepods were advected and developed forward or backward in time, depending on the experiment being conducted. Fewer copepods were observed in 2013; a total of 950,574 individual *C. glacialis* stages copepodid I-VI were observed in 2012 and 803,532 in 2013. In order to make model results from the two years entirely comparable, the

observed distribution in 2013 was scaled up by 1.183 to result in the almost the same total number of particles ( $950574 \approx 950578$ ). This had no effect to the relative contribution from different stages or different sampling locations. Since the numbers were acquired through vertical net tows, it is not possible to know the vertical distribution pattern. For this reason, the model copepods were spread evenly between the 45 depth layers represented by FVCOM. All sampling sites had depths less than 225 m, so the model layers were always evenly spaced.

## 2.3 Experiments

A total of 46 experiments were conducted including four primary experiments based on observed distributions of *C. glacialis* and a series of 42 perturbations of the time and location of release (Table 1) to quantify potential spatial and temporal variability in the simulations originating from the specificity of the release conditions. During all experiments, copepods were locked in their depth of release and did not conduct diurnal vertical migration. Boundaries were nonabsorbent. Parameters remained constant throughout all 46 experiments, with the exception of the direction the model was run. All other differences between experiments were constrained to seeding and forcing.

The sink experiments were designed to identify the regions in the Western Arctic that were supplied with copepods originating on Hanna Shoal. These experiments were run for the time period of August 1<sup>st</sup> through December 15<sup>th</sup> for both 2012 and 2013 (Table 2.1) using FVCOM forcing for the last five months of the year in question. The 15<sup>th</sup> of December was chosen as a

representative date by which all surviving *C. glacialis* individuals should have entered diapause if they have developed to the diapausing stage copepodid four (C4) (e.g., Falk-Petersen et al., 2009). Throughout these experiments the juvenile copepods developed according to (Equation 1) based on the daily encountered temperature. Mortality was not considered. The distributions of diapause capable (C4 and above) copepods from Hanna Shoal on the final day were compared interannually and the sensitivities of these solutions were tested through the perturbation analyses.

**Table 1.** Model experiments conducted. The number of runs of each configuration also is noted.

Number	Seeding Distribution	Class	Direction
1	2012	Primary	Forward/Sink
2	2013	Primary	Forward/Sink
3	2012	Primary	Backward/Source
4	2013	Primary	Backward/Source
5-16	2012	Spatial Perturbation	Forward/Sink
17-28	2012	Temporal Perturbation	Forward/Sink
29-31	2013	Spatial Perturbation	Forward/Sink
32-34	2013	Temporal Perturbation	Forward/Sink
35-37	2012	Spatial Perturbation	Backward/Source
38-40	2012	Temporal Perturbation	Backward/Source
41-43	2013	Spatial Perturbation	Backward/Source
44-46	2013	Temporal Perturbation	Backward/Source

The source experiments were designed to identify the regions that were supplying copepods to Hanna Shoal. These experiments were run for the period of August 31<sup>st</sup> backwards to March 3<sup>rd</sup> for both 2012 and 2013 using FVCOM forcing for September backwards through March of the year in question. The 3<sup>rd</sup> of March was chosen as a representative early date when *C. glacialis* adults in the Bering Sea and southern Chukchi might begin to be reproductively active (e.g., Durbin and Casas, 2013) and by which the modeled copepods should have developed backwards to the egg stage. Throughout these experiments juvenile copepods observed over Hanna Shoal undergo neoteny, or juvenilization as they iterate backward through developmental stages according to (Equation 1) based on the temperature they experience. When a copepod reaches the beginning of the egg stage, backwards advection and development are halted as this is the putative location where the egg was released from its parent to avoid juvenilizing a copepod whose stage is less than one and to remove them from the active pool of particles, significantly speeding up the remaining calculations. Since the ages of the adult copepods collected on Hanna Shoal were not known, we choose to have adults remain adult for the duration of the experiment. This assumes that the adults we observed over Hanna Shoal matured to at least C4 during the previous growth season.

Simulation of predation or mortality was not attempted. Therefore, the forward/sink simulation shows areas that have the potential to hold mature copepods later in the year. If the distribution



experiences uneven mortality and predation the shape of the resulting distribution could be dramatically different. The backward/source simulation shows the locations that supplied copepods to Hanna Shoal but does not attempt to re-create the population of copepods earlier in the year, as those population were reduces by mortality and predation during advection to Hanna Shoal. For each successful arrival, there were likely many more that left the source region. The modeling does show the maximum possible spatial extent of the sink region and the minimum possible extent of the source region.

## 2.4 Perturbation Analysis

Clearly the *C. glacialis* distribution over Hanna Shoal is much more continuous than 26 observations made across two weeks and the currents over the shoal are highly variable, particularly in Barrow Canyon. Tracking the source or sink of these specific copepods alone could result in the importance of source and sink regions being overly inflated and conclusions being strongly biased by the very arbitrary exact times and locations of the sampling effort. Perturbation analysis provides a mean to describe some the central tendency of the different distributions and to accommodate variation in the identified source and sink regions that results from variability in the starting locations of the simulations.

Accordingly, each observed starting distribution was perturbed both in time and space. For the 2012 forward/sink experiment, 12 of each perturbation were completed. For the other three primary experiments, only three of each perturbation were completed (Table 1). Perturbations were achieved using the “rand” function in MATLAB, which outputs a number between zero and one from a uniform distribution of pseudorandom numbers. In temporal perturbations each of the observation times were modified by up to 40 hours in either direction using a call to “rand” for the sign of the change and a call to “rand” for magnitude of the change. In spatial perturbations each of the observation positions was modified by up to 14.14 km using four calls to “rand”. Both the horizontal and vertical coordinates were modified by up to  $\pm 10$  km. The scale of the spatial perturbation was chosen to correspond roughly to the horizontal resolution of the model, meaning it could move the release point to one of the three neighboring control volumes. The scale of the temporal perturbation was chosen to correspond roughly to the possibility of moving the release time up to 1.5 days earlier or 1.5 days later.

## 2.5 Statistical Methods

The version of FISCAM used did not incorporate diffusive properties or any random processes; it was entirely deterministic. Since our starting distribution was very concentrated the initial result was also very concentrated. The results were filtered to better account for both subgridscale processes and the uncertainty inherent in the solution. The ending positions and developmental stage of the copepods released for each experiment were converted to a probability distribution by creating a two dimensional histogram with a 5 km grid spacing and then dividing by the total number of copepods in the experiment and passing a Gaussian filter over the probability distribution first in the horizontal and then in the vertical direction. The filter was the length or width of the domain as appropriate, with a standard deviation of 12.5 km.

The perturbation mean distribution was created by adding together the results of the relevant experiments, then dividing by the number of experiments involved. In this way the sum of the

perturbation mean distribution remains one. For the 2012 forward/sink experiment, means were compared using 3, 6 and 12 perturbations. In the other three primary experiments, a mean was calculated using the 3 perturbations conducted. Three different methods were used to compare the different distributions.

The simplest approach calculated a variation between two probability distributions according to Equation 2, where  $P_1$  and  $P_2$  are the probabilities for two different experiments in each model grid cell and the statistic is calculated by summing this difference across all grid cells. This approach makes no distinction between several small differences and a single large difference. It also does not discriminate between large and small offsets.

$$V = \sum |P_1 - P_2| / 2 \quad (\text{Equation 2})$$

Hotspot analysis was used to discriminate between small and large offsets and to deflate small differences. Probability distributions were first thresholded by eliminating all values lower than a critical value (here  $10^{-4}$ ) so that what remains represents a hotspot. In the sink experiments an east and west hotspot for each distribution was created using the exit from Barrow Canyon at  $155^\circ\text{W}$  as the dividing point. In the source experiments three hotspots were created, one for the egg release points and two for the adult distributions. Each adult distribution at Bering Strait ( $65.8^\circ\text{N}$ ) was split to create a north and south hotspot.

The hotspots for different distributions were compared using both a center of mass comparison and a modification of Rose et al.'s (2009) Slip and Slide method for comparing spatial model output. The center of mass for each hotspot was calculated by taking the result of the two dimensional histogram with a 5 km grid spacing and finding the gray-level-weighted center of mass in units of pixels. This position was then projected into the projected coordinates for either the source or sink experiment as appropriate. Comparisons were then made by taking the straight-line distance in projected coordinates between two centers of mass.

For the slip and slide method the parameters in equations 3 and 4 that minimize the differences between the hotspots generated by two different model runs were optimized using the MATLAB function “fminsearch”:

$$x_{\text{new}} = (y \times \sin(\theta_r) + x \times \cos(\theta_r)) \times M_x + A_x \quad (\text{Equation 3})$$

$$y_{\text{new}} = (y \times \cos(\theta_r) - x \times \sin(\theta_r)) \times M_y + A_y \quad (\text{Equation 4})$$

where  $x$  and  $y$  are the coordinates of all copepod location probabilities in a two dimensional matrix,  $\theta_r$  is the rotation applied to the hotspot being manipulated,  $M_x$  and  $M_y$  is the degree to which the hotspot being manipulated is stretched or squeezed in each direction,  $A_x$  and  $A_y$  is the degree to which the hotspot being manipulated is slid in each direction, and  $x_{\text{new}}$  and  $y_{\text{new}}$  are the new coordinates of the manipulated hotspot.

The “fminsearch” function uses multidimensional unconstrained nonlinear minimization, specifically the Nelder-Mead simplex direct search method, to find the parameters in equations 3 and 4 that minimize a residual function, in this case defined as the percent variation (Equation 5) between the two model hotspots:

$$PV = \frac{\sum |P_1 - P_2|}{\sum (P_1 + P_2)} \quad (\text{Equation 5})$$

where  $PV$  is percent variation,  $P_1$  is the two dimensional matrix of copepod location probabilities in the hotspot that will be manipulated and  $P_2$  is the two dimensional matrix of copepod location probabilities in the hotspot that will be used as reference, typically a perturbation mean or a different year in the case of interannual comparison.

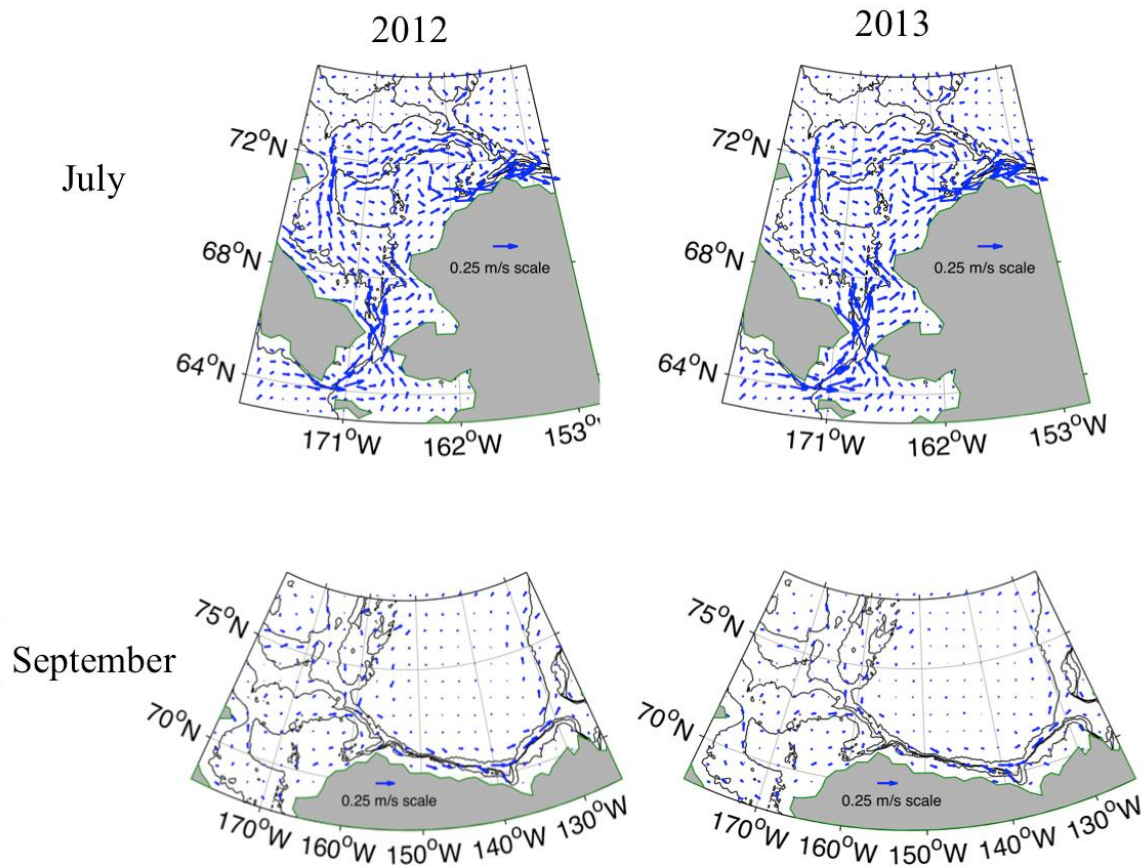
The hotspots start off on the exact same grid, but after manipulation one grid is no longer uniform. A gridded linear interpolant is defined to permit the residual function to query the manipulated hotspot at all the points for which it has values in the reference hotspot. The application of this method not only allows us to quantification the difference between two model outputs, it also allows better characterization of the differences themselves.

### **3. Results**

#### **3.1 Circulation Patterns**

Modeled circulation patterns in July and September of both years were remarkably similar and demonstrated the key features of the Chukchi Sea circulation (Figure 4) that transport copepods to and from Hanna Shoal. Northward flow in three dominant pathways was seen, with flow intensified through Barrow and Herald Canyons and Bering Strait. Clockwise circulation centered on Hanna Shoal is seen in the Northern Chukchi Sea, with flow turning south before being entrained into the Barrow Canyon outflow. In 2013, the Anadyr Current and flow through the Bering Strait are more energetic while the Siberian Coastal current is weaker than in 2012.

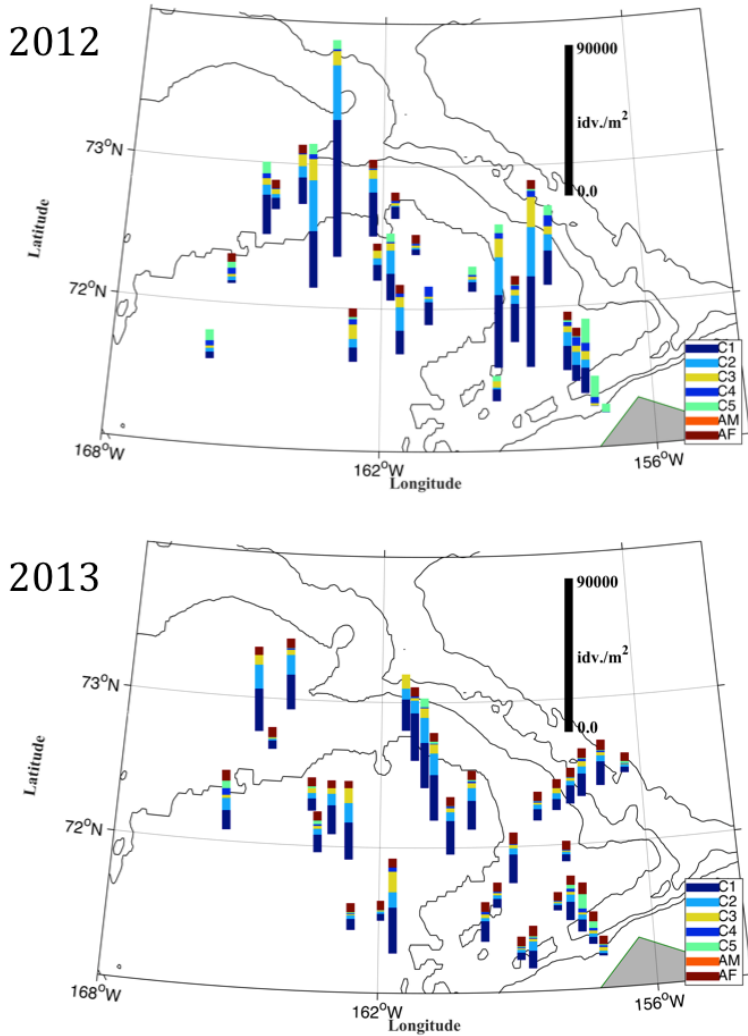
In September of both years, the strength of the Barrow Canyon outflow is masked by the scale of the spatial interpolation. On a monthly averaged basis this flow is strongly northward and consistent. The eastward shelf break jet to the south of the Beaufort Gyre is clearly a dominant feature. The Chukchi slope current traveling westwards from Barrow Canyon to the base of the Chukchi Cap along the southwestern corner of the Canada Basin is barely visible because it is so narrow (Figure 4). Only two interannual differences are worthy of mention. The shelf break current is slightly less energetic in 2013. Also, the Chukchi slope current has a larger northward component than in 2012.



**Figure 4.** Spatially interpolated depth averaged mean modeled currents for selected months in 2012 and 2013.

### 3.2 *C. glacialis* Observed Distributions

Fewer *C. glacialis* were observed on Hanna Shoal in 2013 than had been seen in 2012 (Figure 5). Abundances also were more uniform in 2013 than in 2012. For both years, abundances in Barrow Canyon were among the lowest seen. Both years show greater proportions of earlier life stages as expected based on the timing of the sampling relative to the *C. glacialis* growth season. This was particularly true in 2012 when adults were seen at only 50% of the stations and no adult males were observed. Later stages, particularly adult females in 2013, are found in higher proportions in Barrow Canyon and on the eastern extremis of the shoal, while earlier stages were more common over the center and western extremis of the shoal.

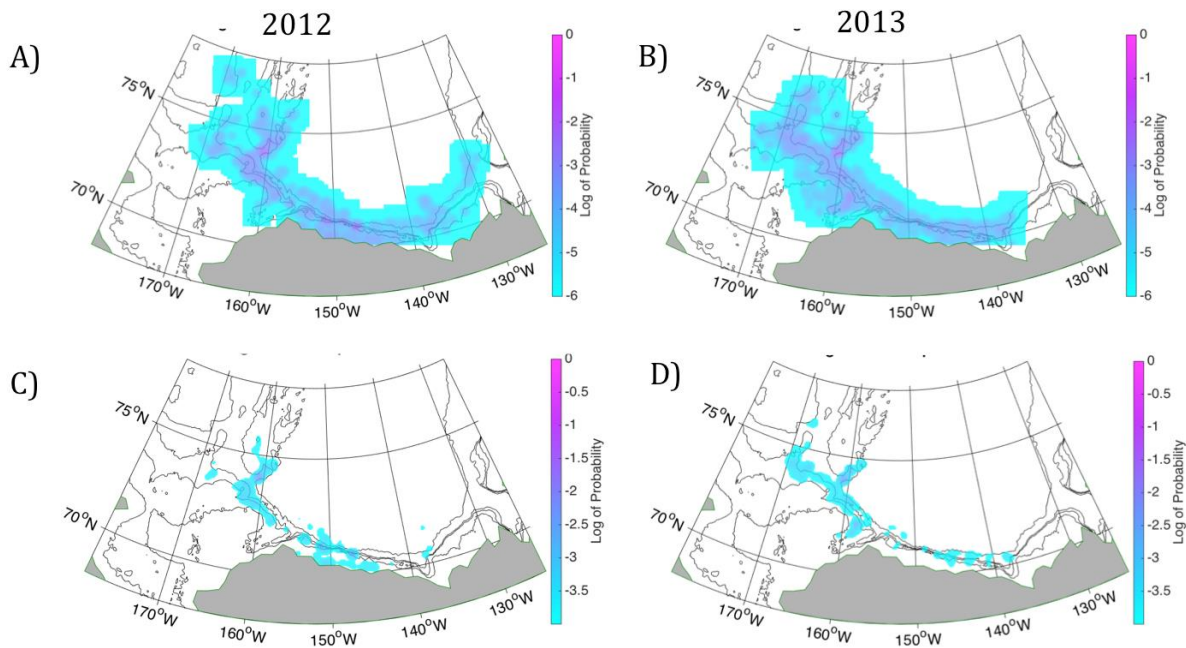


**Figure 5.** Integrated water column abundances of *C. glacialis* over Hanna Shoal in 2012 and 2013. Abundances (# individuals  $m^{-2}$ ) are differentiated into seven life stages (Copepodid 1-6, adult males (AM), adult females (AF)).

### 3.2.1 Sink Experiments

The sink experiments identified locations to which *C. glacialis* observed on Hanna Shoal in August of both 2012 and 2013 could have been advected by December of those years. Despite differences in the circulation regimes between the two years (Figure 2), both simulations suggested that the vast majority of the copepods observed over Hanna Shoal in August enter diapause over the shelf break at the southern extent of the Canada Basin and along the southeastern buttress of the Chukchi Cap (Figures 6 a, b), with significant concentrations also along the coast to the east of Barrow. In 2013, the entire distribution in the Chukchi is shifted west with many more copepods advected over the Chukchi Cap instead of just along its periphery. Low abundances also remain over Hanna Shoal, although much less than elsewhere. The distributions of only the hotspots (Figures 6c, d) shows that the two key sink regions are a western area at the southeastern buttress of the Chukchi Cap and an eastern area split between

the coast and the shelf break halfway from Barrow to the Canadian border. In 2013, the eastern sink region is much less concentrated than in 2012 and is constrained to the shelf break and the western sink region is more important and extends around the northern tip of Hanna Shoal.

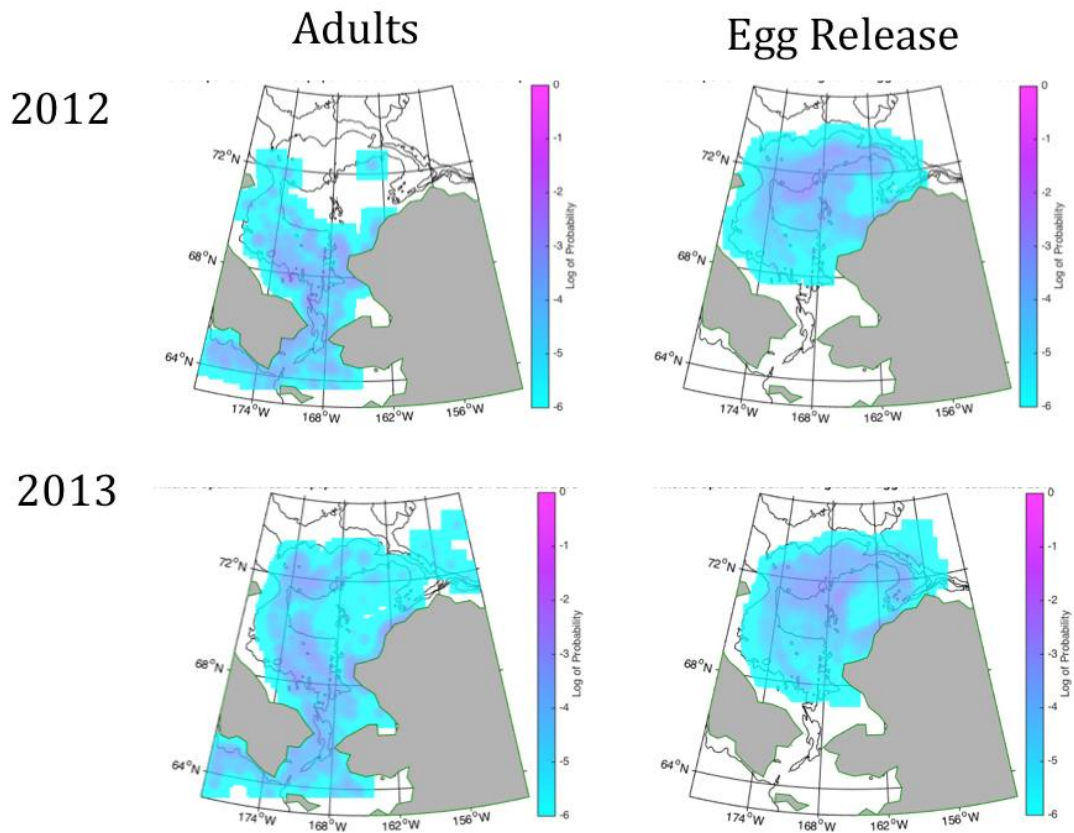


**Figure 6.** Filtered Probability Distribution Of Adult *C. glacialis* on a) 15 December 2012 and b) 15 December 2014 and Hotspots from the Filtered Probability Distribution Of Adult *C. glacialis* on c) 15 December 2012 and d) 15 December 2012.

The development rate model assumes food saturation and only temperature constrains development. Development in both years is very rapid: 50% of the copepods are competent to diapause by September 21, 2012 or September 11, 2013 and 90% are competent to diapause by September 30, 2012 and Sept. 21, 2013, with the differences between years being due to warmer water temperatures in 2013. Thus, critical development is complete before the end of the production season and food conditions would become limiting and the vast majority of the copepods had the potential to reach diapause unless consumed by predators.

### 3.2.2 Source Experiments

These simulations identified locations where *C. glacialis* females observed on Hanna Shoal in August would have been on March 2 of each year. For younger stages of *C. glacialis* observed on Hanna Shoal, the simulation develops the copepods of each of the life stages backwards until the day of egg release is reached to identify the locations where those copepods were produced. Most adult copepods observed over Hanna Shoal both years originated south and west of the shoal, in the southern Chukchi Sea and northern Bering Sea, with only a very small proportion starting over the shoal itself (Figure 7). The distribution almost covers the entire Chukchi, but is skewed to the west, particularly at the northern and southern extent. In 2013, adults also originated in the northern Chukchi Sea and in the Beaufort Sea, although these locations were not hotspots of abundance. The branches of northward advection are evident as elevated probabilities, including the Herald canyon, Central Channel, and Alaska Coastal Current.

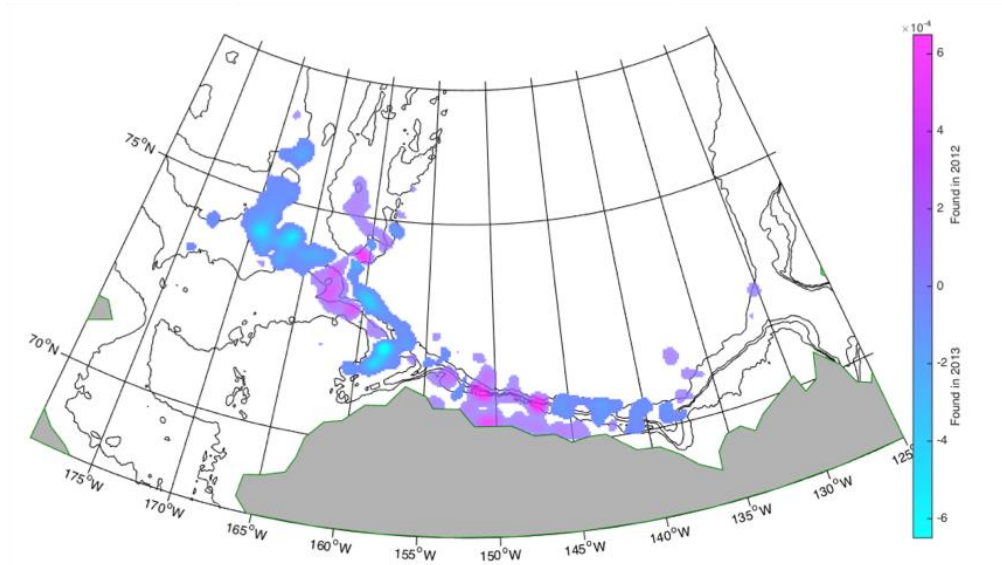


**Figure 7.** Filtered probability distributions of adult *C. glacialis* on 03 March 2012 and 03 March 2013 (left) and of *C. glacialis* egg release locations in 2012 and 2013 (right).

For younger stages observed on Hanna Shoal in August, all had aged back to their putative release by May 1 in both years and most release locations were north of 68°N (Figure 7). Egg release locations were concentrated primarily in Herald Valley and the Central Channel but some were also released along the northern edge of Hanna Shoal and in the Alaska Coastal Current. Again, pathways of advection were clear in the distributions of the egg release locations. Because egg release was reached by May 1 of both years, the backwards advection was shorter than the adult females (ending March 2) and the distributions of egg release sites are much less dispersed than the adult starting position distributions.

### 3.3 Interannual differences in sink and source locations

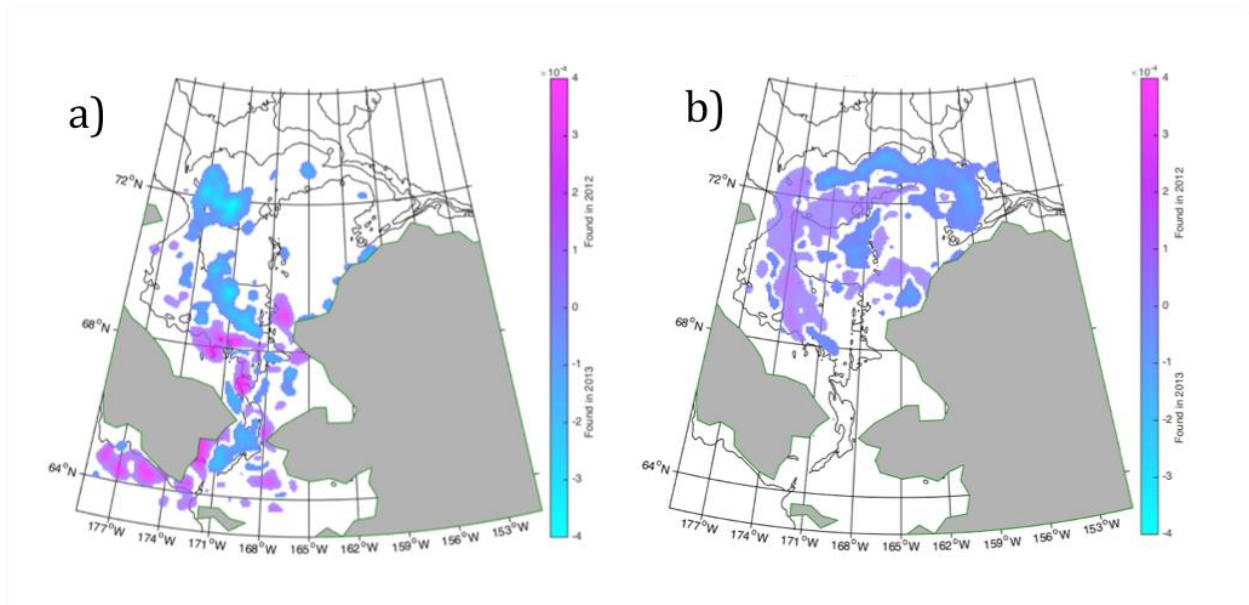
Different regions were greater sinks for diapausing copepods for each of the two years (Figure 8). The westward shift of the distribution in 2013 is striking, particularly the large concentration over the Chukchi Cap and the high concentration just to the west of Barrow Canyon. Although copepods in the 2012 experiment reached the Eastern edge of the Canada Basin their numbers were small. However, many more were seen on the Beaufort Shelf in 2012 than in 2013.



**Figure 8.** Difference between the 2012 and 2013 probability distributions for diapausing copepods from the sink experiments. The probability distributions for 2013 were subtracted from those from 2012 at each location. All values greater than  $5 \times 10^{-5}$  were retained. Positive values indicate sink locations for 2012 but not 2013 while negative values indicate sink locations for 2013 but not for 2012.

The differences between the 2012 and 2013 egg release distributions were highly cohesive (Figure 9). Egg release distributions shift further to the north and east in 2013, with Herald Canyon and the shallower portion of the broad slope east of the exit from Herald Canyon being more important in 2012 and the deeper portion of the Chukchi shelf and slope and Hanna Shoal more important in 2013 (Figure 9b). For the adult females, the differences in the source locations are much less cohesive (Figure 9a). These distributions included far fewer copepods than the others, and thus a more patchwork distribution could be expected. More females originated in the southern portion of the study area in 2012 than in 2013, consistent with the shift in the distributions of the egg release locations between the two years.

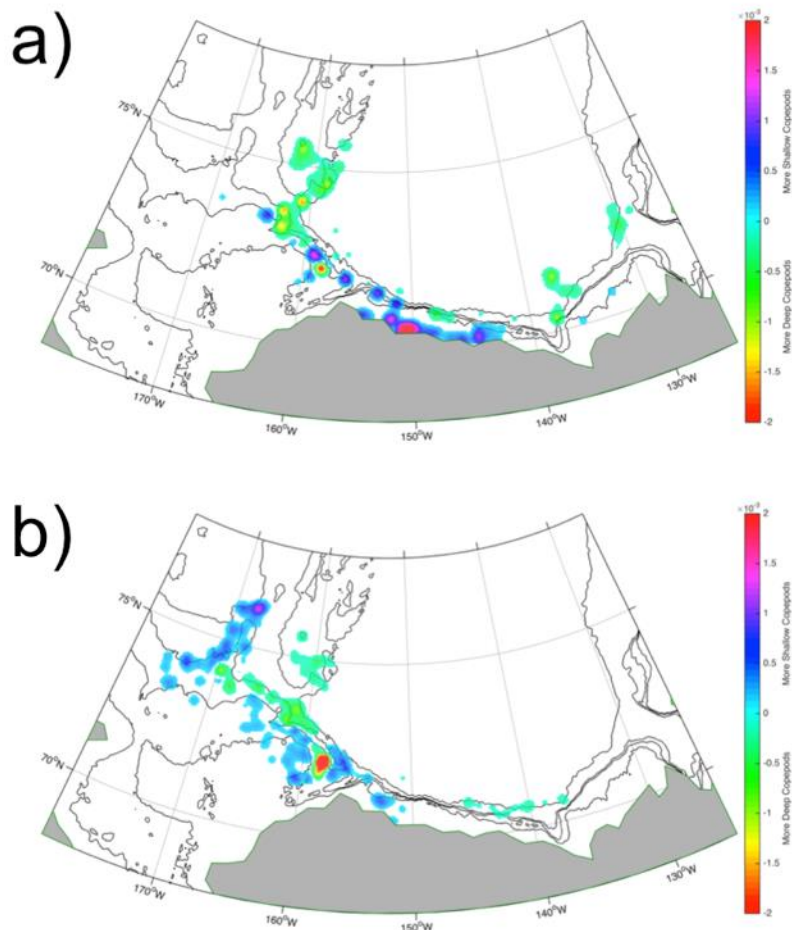




**Figure 9.** Difference between the probability distributions on 3 March from the 2012 and 2013 primary source experiments for a) adult females and b) egg release. The result for 2013 was subtracted from the 2012 result and all values greater than  $5 \times 10^5$  were retained.

### 3.4 Sink Experiments Sensitivity to Depth of Release

The distributions of copepods at the end of the sink experiments were highly sensitive to the depths at which they were released. In general deep particles travel further than shallow particles, but there were differences between years. In 2012, deep model copepods composed the majority of the distributions at the east and west extremes of the total distribution (Figure 10a). Although the particles close to the Alaskan coast were exclusively shallow, the concentration on the shelf break appeared to be a mixture of both deep and shallow copepods. The strong dipole just to the west of Barrow Canyon is notable for its uniqueness. In 2013, the copepods that traveled furthest east (Figure 10b) had more deep constituents than shallow ones. It appears that the shallow copepods that ended up on the Alaskan coast in 2012 ended up on top of the Chukchi Cap in 2013, traveling further west than any of the deep copepods. Deep copepods are still prominent along the western edge of the Canada Basin and on the western edge of Barrow Canyon. Instead of a dipole, a larger peak of deep copepods surrounded by regions dominated by shallower copepods is seen.

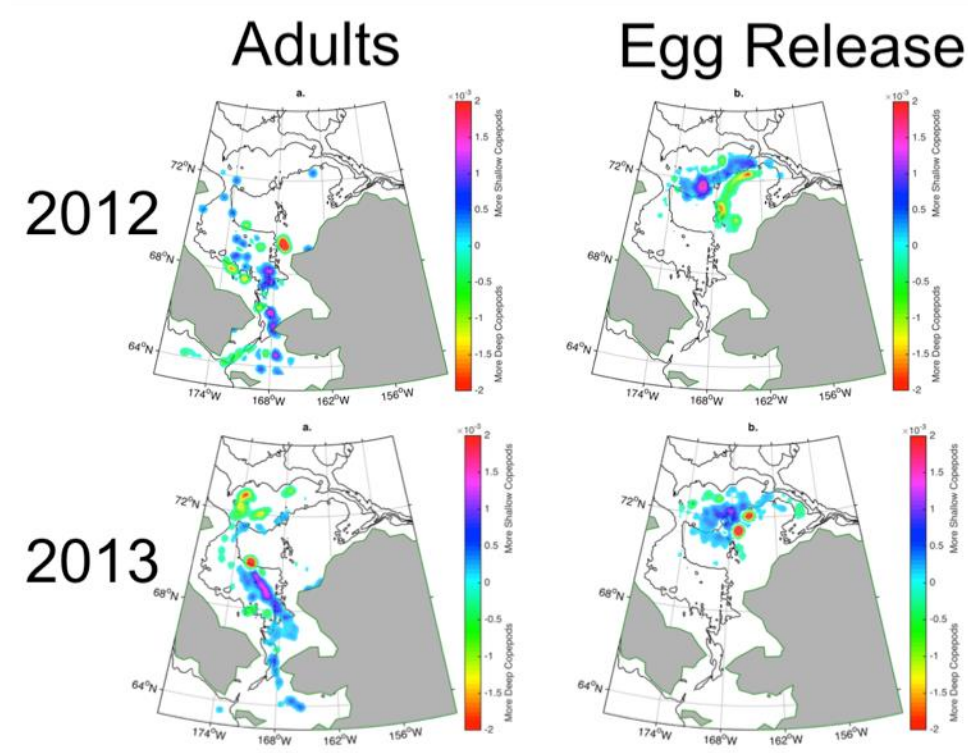


**Figure 10.** Effect of depth of release – sink experiment. a) The distribution of the 130,000 deepest copepods on 15 December 2012 subtracted from the distribution of the 130,000 shallowest copepods on 15 December 2012. b) The distribution of the 130,000 deepest copepods on 15 December 2013 subtracted from the distribution of the 130,000 shallowest copepods on 15 December 2013.

### 3.5 Source Experiments Sensitivity to Depth of Release

In 2012 deep adult copepods tended to start their growing season to the west of shallow copepods with the very notable exception of a large number of adult copepods that started at the base of the central channel just off Cape Lisburne (Figure 11a). Shallow copepods were concentrated in three regions: the northern entrance to Norton Sound, the southern entrance to Kotzebue Sound and the northern entrance to Kotzebue Sound. The less divergent 2012 distribution of egg release sites is divided into two coherent regions when depth of release is considered. Deep copepods are released in a region connecting eastern Hanna Shoal with the Central Channel while the shallow copepods are released over the broad slope connecting Herald Canyon with Hanna Shoal. In 2013 the differences between the adult distributions of deep and shallow copepods are much more coherent (Figure 11b). The shallow copepods started further south from a region that links the Bering Strait with the entrance to Herald Canyon. The deep

copepods started in Herald Canyon and on the broad slope that connects the canyon with Hanna Shoal. The differences between the egg release site distributions are very similar to 2012 except that the deep copepods are concentrated in two locations instead of the broader swath seen in 2012 and conversely the shallow copepods are in a broader swath than they were in 2012.



**Figure 11.** Effect of depth of release –source experiment. The distribution of the 130,000 deepest copepods on 3 March 2012 subtracted from the distribution of the 130,000 shallowest copepods on 3 March 2012 for adult copepods and egg release locations (top). The distribution of the 130,000 deepest copepods on 3 March 2013 subtracted from the distribution of the 130,000 shallowest copepods on 3 March 2013 for adult copepods and egg release locations (bottom).

### 3.6 Sensitivity to Time and Location of Release

Comparison of the results of individual perturbation experiments and the corresponding primary experiment (not shown) demonstrated the sensitivity of the “solution” to small-scale (in terms of the model resolution) temporal and spatial changes in the physical forcing and identified regions that were not found to be important in the primary experiment but to have the physical potential to be important. For the 2012 sink experiment, both the spatial and temporal perturbation means were greater than the primary experiment along the southeastern buttress of the Chukchi Cap and in the region between Barrow and the Canadian Border. These are the same regions where the 2012 distribution was found to be stronger than the 2013 distribution (Figure 8). The differences between the 2013 sink experiment and its corresponding spatial and temporal perturbation means were much less coherent and smaller in magnitude than the differences observed in 2012.

The differences observed between the results of 2012 and 2013 primary experiments could be the result of interannual differences in the biological conditions, differences in the physical forcing, or the semi-arbitrary times and locations of sampling. The differences between the 2012 and 2013 perturbation means were by and large the result of interannual differences in physical forcing.

### **3.7 Statistical Treatment of Sensitivity and Interannual Differences**

The calculated interannual variations for the both the sink and source experiments were more than twice the variations calculated between the primary experiment for either year and any of their corresponding perturbation means (Table 2). When the variation between a mean of three perturbations and a mean of six perturbation was compared to the variation between a mean of six perturbations and a mean of twelve perturbations, the variation fell by roughly half in both the temporal and spatial perturbation cases.

In 2013, the center of mass of the eastern hotspot of the sink distribution moved more than twice the distance between eastern centers of mass in the sink experiment for either year and either of their corresponding perturbation means (Table 2). In 2013 the center of mass of the western hotspot of the sink distribution moved roughly the same distance as its corresponding perturbation means (Table 2).

In 2013 the center of mass of the hotspot of the egg release distribution moved almost twice the distance between egg release centers of mass in the source experiment for either year and either of their corresponding perturbation means (Table 2). In 2013, the center of mass of the northern hotspot of the adult distribution moved more than six times the distance between northern centers of mass in the source experiment for either year and either of their corresponding perturbation means (Table 2). In 2013, the center of mass of the southern hotspot of the adult distribution moved more than ten times the distance between southern centers of mass in the source experiment for either year and either of their corresponding perturbation means (Table 2).

The slip and slid method never reduced the variation between solutions by more than 14% and typical reductions were less than 10% (Table 2). After slip and slide transformation, the interannual variation remained twice the largest value in a corresponding perturbation mean.

**Table 2.** Statistics Comparing Sensitivity to Perturbation to Interannual Differences. CoM = Center of Mass.

Year	2012-2013	2012-2013	2012-2013	2012	2013	2012	2013	2012	2013	2012	2013	2012	2013	2012	2013
Perturbation	Interannual	Interannual	Interannual	Spatial	Spatial	Spatial	Spatial	Spatial	Spatial	Temporal	Temporal	Temporal	Temporal	Temporal	Temporal
Experiment	Sink	Source	Egg	Sink	Sink	Source	Source	Source	Source	Sink	Sink	Source	Source	Source	Source
Class	All	Adult	Egg	All	All	Egg	Egg	Adult	Adult	All	All	Egg	Egg	Adult	Adult
<b>Variation</b>	<b>0.4929</b>	<b>0.5458</b>	<b>0.2172</b>	0.1983	0.1388	0.0654	0.0849	0.2437	0.2435	0.1709	0.1174	0.0594	0.0784	0.2105	0.202
<b>CoM Dist. North (km)</b>	-	<b>139.5</b>	-	-	-	-	-	7.239	14.71	-	-	-	-	20.813	9.1312
<b>CoM Dist. South (km)</b>	-	<b>179.6</b>	-	-	-	-	-	3.042	17.844	-	-	-	-	17.125	14.07
<b>CoM Dist. East (km)</b>	<b>161.7</b>	-	-	75.617	24.987	-	-	-	-	80.113	50.373	-	-	-	-
<b>CoM Dist. West (km)</b>	<b>36.7</b>	-	-	20.765	8.722	-	-	-	-	3.808	35.224	-	-	-	-
<b>CoM Dist. (km)</b>	-	-	<b>13.5</b>	-	-	1.076	7.014	-	-	-	-	2.077	1.549	-	-
<b>East Initial Variation</b>	<b>0.867</b>	-	-	0.3454	0.4351	-	-	-	-	0.3019	0.4588	-	-	-	-
<b>Slip/Slide Variation</b>	<b>0.7535</b>	-	-	0.3289	0.4095	-	-	-	-	0.2967	0.4249	-	-	-	-
<b>West Initial Variation</b>	<b>0.471</b>	-	-	0.1829	0.1329	-	-	-	-	0.1387	0.1114	-	-	-	-
<b>Slip/Slide Variation</b>	<b>0.4662</b>	-	-	0.1734	0.1278	-	-	-	-	0.1327	0.1088	-	-	-	-
<b>Eggs Initial Variation</b>	-	<b>0.4323</b>	-	-	-	0.1123	0.1434	-	-	-	-	0.0786	0.0972	-	-
<b>Slip/Slide Variation</b>	-	<b>0.3584</b>	-	-	-	0.1074	0.1409	-	-	-	-	0.0753	0.0951	-	-
<b>Adults North Initial Variation</b>	-	-	<b>0.6772</b>	-	-	-	-	0.2889	0.3165	-	-	-	-	0.2867	0.2818
<b>Slip/Slide Variation</b>	-	-	<b>0.6741</b>	-	-	-	-	0.2812	0.3117	-	-	-	-	0.2783	0.2658
<b>Adults South Initial Variation</b>	-	-	<b>0.6985</b>	-	-	-	-	0.2991	0.335	-	-	-	-	0.2947	0.2859
<b>Slip/Slide Variation</b>	-	-	<b>0.614</b>	-	-	-	-	0.2941	0.3295	-	-	-	-	0.2876	0.272

## 4. Discussion

This study linked temperature dependent development rates, modeled circulation and ocean temperature, and observed life stage specific distributions of *C. glacialis* on Hanna Shoal in August to explore the source regions for that population and the potential sink regions where they might potentially overwinter. The coupled biophysical modeling efforts demonstrated that most of the *C. glacialis* present on Hanna Shoal in August were born further to the south in the Chukchi Sea or northern Bering Sea and were advected out of the Chukchi Sea into the Beaufort Sea and Chukchi Slope prior to diapause and overwintering. These results also demonstrated that *C. glacialis* are effectively swept through the Chukchi Sea from south to north from March - December, resulting in a residence time in the Chukchi Sea of under one year.

### 4.1 *C. glacialis* Source and Sink Regions for Hanna Shoal

*Calanus glacialis* that have achieved copepodid stage 1 over Hanna Shoal by August will have the potential to mature to a diapause competent stage before the productive season ends in fall. Most of the copepods present over the Shoal in August do not remain there, but instead are advected off the Shoal, generally through Barrow Canyon. After entering the Beaufort Sea, some travel east in the shelf break jet while others travel west in the countercurrent. Hanna Shoal has the potential to be connected both with the *C. glacialis* population entering diapause over the Beaufort Shelf and Slope and the population entering diapause on southeastern corner of the Chukchi Cap. The relative strength of this connection changes on an interannual basis.

*Calanus glacialis* copepodids observed over Hanna Shoal in August are likely to be less than two months in age and were released by adult females within 450 km of it. Given the relatively short amount of time they have had to be advected, it is unsurprising that the distribution of their starting positions is a single cohesive region. This source region is centered at the northern end of the Central Channel and appears to include eggs released by adults moving northeast after exiting Herald Canyon as well as adults traveling through Central Channel itself. Although the shape and the center of mass of this distribution does change interannually, the differences are slight and do not appear to be very meaningful.

Adults over Hanna Shoal have a much less cohesive distribution of their starting locations in early March; it is stretched over 1500 km from the southwest corner of the Beaufort Sea to the Gulf of Anadyr. One quarter to one third of the adults originated south of the Bering Strait at that time. This southern source region strongly favors the Gulf of Anadyr over Norton Sound. This is likely due to the greater strength of the Anadyr Current relative to the Alaskan Coastal Current. Bérline et al. (2008), using particle tracking in a physical model, found that euphausiids in the vicinity of Barrow could have origins either in the Anadyr Gulf or in the Shpanberg Strait at the mouth of Norton Sound, however the authors did not try to evaluate the relative importance of these source regions. In the present study, the northern source region is fragmented between individuals in three different pathways: Herald Canyon to the west, the Alaskan coast to the east and Central Channel in the middle. The latitudinal compression or extension of this northern source region appears to vary significantly from year to year. The Beaufort Sea to the north also can supply copepods to Hanna Shoal but this varies interannually: in 2013 a very small proportion of adult *C. glacialis* on Hanna Shoal in August originated in the Beaufort Sea while in 2012 not a single adult came from there.

The lack of substantial overlaps between the source and sink regions in the Chukchi emphasizes that populations of this species over the northern Chukchi do not appear to have the potential to be self-sustaining but rather are dependent on transients, mainly from southern populations. *Calanus glacialis* individuals have been observed reproducing in the Beaufort Sea (Plourde et al., 2005; Daase et al., 2013) and populations are seen in the Slope and the Beaufort Gyre provides a retentive region that would allow self-sustainment assuming individuals can survive periods in the central Arctic. Observations of healthy *C. glacialis* at 80°N (Ashjian et al., 2003; Nelson et al., 2009) suggest this may be the case.

Genetic work conducted by Nelson et al. (2009) on *C. glacialis* sampled in July 2002 from the Chukchi Sea and Arctic Ocean identified two dominant haplotypes of 16s ribosomal RNA : a North Pacific/Bering type and an Arctic type. This indicates that *C. glacialis* at the northern extent of its range is able to sustain itself without contributions from the south. The Chukchi Sea was dominated by the southern haplotype, consistent with the results of the source experiment. The southern haplotype also was present over the southern Chukchi Cap, consistent with the sink experiment, but interestingly two sites over the Beaufort Shelf contained only the northern haplotype. This could mean that southern expatriates advected to this sink region do not survive, however Nelson et al.'s low sampling resolution leaves open the possibility that they just missed the southern expatriates. Furthermore, wind and resulting current patterns in 2002 could have been markedly different from those in the years modeled here, resulting in little advection of Bering Sea *C. glacialis* populations to the Beaufort Sea. Genetic work conducted by R. Campbell (pers. comm.) with the mitochondrial COI gene also demonstrated that the southern haplotype dominates in the Chukchi Sea and that the northern (Arctic) haplotype is present only in the Beaufort Sea and Canada Basin to the north, along the Chukchi Sea shelf break and on the northern edge of Hanna Shoal, or where significant southward advective events in Barrow Canyon have brought Arctic haplotypes south.

Advection and development to the diapausing stage are not the only factors determining whether an individual or population of individuals can successfully overwinter in the different regions achieved by December (as simulated in this study). As previously suggested, predation may significantly reduce population abundances and predation by upper trophic levels such as ice-associated Arctic cod, jellyfish, or even bowhead whales may differentially reduce population abundances in the regions. Copepods of the genus *Calanus* are believed to require ontogenetic migration to depths greater than seen on the Chukchi and Beaufort Shelves (e.g., Falk-Petersen et al., 2009) and *C. glacialis* in the Central Arctic overwinters in the warm Atlantic water at ~200 m depth (e.g., Ashjian et al., 2003). If there is a critical depth that must be achieved for successful overwintering, it is likely that it is greater than the mean depth of the Chukchi Sea (~50 m) and Beaufort Shelf (~20 m). Therefore, although *C. glacialis* from Hanna Shoal are capable of achieving the diapause state, according to temperature-dependent development, the locations to which they are advected may not be hospitable to successful overwintering. This also highlights how interannual variability in physical forcing (winds, currents) could result in differential overwintering success between the years. For example, in 2012 prevailing upwelling winds and shelf-break upwelling along the Beaufort Shelf break appears to have concentrated *C. glacialis* on the Beaufort Shelf, a location potentially too shallow for successful overwintering. By contrast, in 2013, *C. glacialis* in the Beaufort Sea was concentrated along the shelf-break and slope where overwintering depths could more easily be achieved and overwintering success could be enhanced. It is evident from genetic data that Bering Sea populations of *C. glacialis* are

present in only low proportions in the Arctic Basins, indicating low recruitment of those populations in the Arctic environment that could have resulted in part by low survival during overwintering.

#### **4.2 Physical Control of *C. glacialis* Distribution**

Although the daily mean currents provided by the physical model were highly variable over the course of the month, copepods in these experiments moved more or less in line with the monthly mean conditions. The generally consistent northward currents with very little recirculation place severe limits on long-lived plankton such as *C. glacialis* by restricting the regions between which each population is connected. The physical conditions set the maximum limits of the source and sink regions, while predation, mortality and food conditions will result in source and sink regions that are a subset of these regions.

In this set of experiments, several specific physical oceanographic features were found to have oversized impacts on determining the upstream and downstream connections of Hanna Shoal with other regions. In the sink experiment, the Barrow Canyon outflow was of utmost importance. In the source experiment the Bering Strait inflow and outflow played a defining role. Very few copepods left Hanna Shoal without passing through Barrow Canyon; they followed the clockwise circulation around the shoal until they were entrained in the energetic outflow. The junction between the outflow and the shelf break current proved to be a particularly deterministic point in their journey. The physical model represented this point as a particularly strong vorticity dipole with strong positive vorticity on the west side and negative vorticity on the east side. Pickart et al. (2005) explain that this feature results from the incomplete adjustment of water exiting the canyon as it sinks, stretches and decelerates. The exact position of a copepod relative to this feature would determine whether it would be advected to population concentrations in the east or in the west. A difference of five kilometers between the positions of two copepods in this region could result in over 800 km of difference between the same two copepods on December 15<sup>th</sup>. This feature is clearly not an artifact of the model as similar behavior has been observed in drifters released over the Chukchi Sea (Weingartner, pers. comm.).

Adult copepods arrived over Hanna Shoal following one of three routes: Herald Canyon, Central Channel and the Alaskan Coastal Current. The tendency of the Bering Strait outflow to favor the western route led the Herald Canyon to be the most important of the three. The strength of the Anadyr Current as it enters Bering Strait limits the flow into the Strait from Norton Sound and the region east of St. Lawrence Island. If copepods were released at the same latitude in Norton Sound and the Anadyr Gulf, those released in the Anadyr Gulf would be hundreds of kilometers further north by the beginning of August.

While the exact time and location of release had fairly minimal effect on the locations of the source and sink regions, relatively small differences in depth of release had strong effects on both starting positions at the end of the source experiment and ending positions at the end of the sink experiment. This is due to the importance of topographic steering that results from the shallow nature of the Chukchi. Bérline et al. (2008) found that euphausiids released near the bottom in the Anadyr Gulf and Shpanberg Strait were more concentrated in Barrow canyon than those released near the surface. Here, although the trajectories were different, the deep copepods



were no more concentrated than the shallow copepods (Figure 10). In the source experiment, the furthest travelling shallow copepods were more likely to come from the vicinity of Shpanberg Strait while the furthest travelling deep copepods were more likely to come from Anadyr Gulf (Figure 11).

### 4.3 Sensitivity to Perturbation

The decrease in the variation between different numbers of perturbation means with the increase in the number of perturbation means included indicated that the solution was converging and allows comparisons without fear that the low number of perturbations could be concealing important differences. Since interannual variation is so much larger than the variation between experiments and their corresponding perturbation means, the observed interannual differences in both the source and the sink distributions are indeed important. The hotspot analysis exposes that significant interannual differences in the sink distribution were isolated to the Alaskan coast and that all portions (North, South and Egg Release) of the source distribution exhibit significant interannual differences. The slip and slide analysis confirmed that the observed variation is not simply a translation, rotation or distortion of the same distribution.

The hotspots in the source and sink distributions were not more sensitive to temporal than to spatial perturbations. In 2012 the temporal distances were longer in three out of the five cases. In 2013 the exact opposite pattern is seen with the spatial distances being longer in the same three out of five cases (Table 2). Since the scales of the perturbations were specifically chosen to be similar, this was not surprising.

### 4.4 Assumptions and Limitations

The number of assumptions inherent in the work limits the impact of our conclusions. Similar to the work of Ji et al. (2012), it was assumed that AO-FVCOM output represents the actual current field. The modeled current regime provided by AO-FVCOM appears to be a reasonable approximation of the actual currents in the domain (Chen et al., 2009) and thus this assumption is reasonable. Also similar to Ji et al. (2012), the effects of food limitation on development rate, of mortality on copepod numbers, and of depth varying behavior by the copepods were neglected in the copepod IBM. The diel vertical migration behavior of Arctic species is highly influenced by daylight cycles in the Arctic and is not fully understood and difficult to replicate in a model. Locking the copepods into their release depth during simulations results in the loss of detail, since depth should have a measureable effect on source and sink distributions. The assumptions relative to food and mortality may have different impacts in the sink and source experiments.

The sink experiment shows the maximum extent of the early winter distribution of the *C. glacialis* that were observed over Hanna Shoal in August. The lack of mortality in the modeling means that the true distribution of *C. glacialis* from Hanna Shoal likely is actually smaller than simulated. Therefore it is very likely that regions outside the reported distribution are not supplied by *C. glacialis* from Hanna Shoal. For example, observational studies have not found *C. glacialis* close to shore on the Beaufort Shelf while the 2012 distributions here show a large concentration of *C. glacialis* originating from Hanna Shoal very close to that shore.

The distributions generated by the source experiment have a different set of limitations. While

the distributions track copepods that are known to have survived, the number of copepods that were present in the source regions at the start of the advection is unknown. Consequently, a strong concentration in the source distribution could have resulted from a peak in the *C. glacialis* distribution in that region in early March or from *C. glacialis* from that region experiencing lower mortality than other regions as they were advected to Hanna Shoal. If a putative source region were to suffer a decline in *C. glacialis* abundance, populations on Hanna Shoal would be reduced, but if a putative source region had an increase in *C. glacialis* abundances on Hanna Shoal may not be enhanced since density dependent mortality might prevent the additional copepods from reaching Hanna Shoal.

The treatment of diffusion also represents a series of assumptions. By simply passing a filter over the probability distributions, it is assumed that each release point serves as the center of a 2-D normal distribution with fixed dimensions that is advected and developed only by the conditions found in the center. In a more realistic simulation, the distribution would slowly diffuse over time. The edges of this more realistic distribution would be affected differently than the center due to spatial variability of currents and water temperatures and the final solution at the end of the simulation would look different. The limitations imposed by the assumptions were mitigated using perturbation analysis. If the differences in forcing between the center and the edges of our distributions fundamentally changed the solution it would have manifested itself in a much larger difference between the perturbation mean and the primary experiment solution. Although this was not the case, it would be interesting in the future to directly compare the results of this perturbation analysis with different implementations of horizontal diffusivity in the model.

## 5. Summary

Based on these experiments, Hanna Shoal supplies diapause competent *C. glacialis* that originated in the southern Chukchi Sea and the Northern Bering Sea to both the Beaufort Slope and the Chukchi Cap. The experiments show that Hanna Shoal mainly receives juveniles from the broad slope between Hanna Shoal and Herald Canyon and receives second year adults from as far south as the Anadyr Gulf and as near as the broad slope between Hanna Shoal and Herald Canyon. The 2013 sink region was shifted west relative to the 2012 region and the 2013 adult source region was shifted north relative to the 2012 region, consistent with differences in the circulation between the two years. The locations of these regions were not sensitive to precise times and locations of release, so these interannual differences are significant. The positioning of these regions was quite sensitive to depth of release. Better information regarding the depth distribution of *C. glacialis* over Hanna Shoal as well as better information as to their vertical behavior throughout the spring and fall would provide for better predictions of their sink and source regions.

## 6. Acknowledgements

The Captain, officers, and crew of *USCGC Healy* are greatly appreciated for their instrumental help with completing the fieldwork. R. Ji, P. Alatalo, J. Boucher, X. Lyu, Y. Li, T. Weingartner, and Y.-C. Fang and our colleagues in the Hanna Shoal project provided invaluable support, advice and assistance. C. Gelfman enumerated the plankton samples. This study was funded by

the U.S. Department of the Interior, Bureau of Ocean Energy Management (BOEM), Alaska Outer Continental Shelf Region, Anchorage, Alaska under BOEM Cooperative Agreement No. M11AC00007 as part of the Chukchi Sea Offshore Monitoring in Drilling Area (COMIDA) through subcontracts from the University of Texas to the Woods Hole Oceanographic Institution and the University of Rhode Island. S. Elliott's participation was made possible and funded by the Woods Hole Oceanographic Institution – Massachusetts Institution of Technology Joint Program in Oceanography and the United States Coast Guard.

## 7. References

- Ashjian, C.J., Campbell, R.G., Welch, H.E., Butler, M., Van Keuren, D., 2003. Annual cycle in abundance, distribution, and size in relation to hydrography of important copepod species in the western Arctic Ocean. *Deep-Sea Res. I.* 50(10-11), 1235–1261. doi:10.1016/S0967-0637(03)00129-8.
- Bérline, L., Spitz, Y.H., Ashjian, C.J., Campbell, R.G., Maslowski, W., Moore, S.E., 2008. Euphausiid transport in the Western Arctic Ocean. *Mar. Ecol. Prog. Ser.* 360, 163–178. <http://doi.org/10.3354/meps07387>.
- Bureau of Ocean Energy Management (BOEM) Environmental Studies Program. 2015. <http://www.boem.gov/Studies> (accessed 15.02.16).
- Brugler, E.T., Pickart, R.S., Moore, G.W.K., Roberts, S., Weingartner, T.J., Statscewich, H., 2014. Seasonal to interannual variability of the Pacific water boundary current in the Beaufort Sea. *Prog. Oceanogr.* 127(C), 1–20. <http://doi.org/10.1016/j.pocean.2014.05.002>.
- Campbell, R.G., Sherr, E.B., Ashjian, C.J., Plourde, S., Sherr, B.F., Hill, V., Stockwell, D.A., 2009. Mesozooplankton prey preference and grazing impact in the western Arctic Ocean. *Deep-Sea Res. II.* 56(17), 1274–1289. doi:10.1016/j.dsr2.2008.10.027.
- Campbell, R., Wagner, M., Teegarden, G., Boudreau, C., Durbin, E., 2001. Growth and development rates of the copepod *Calanus finmarchicus* reared in the laboratory. *Mar. Ecol. Prog. Ser.* 221, 161-183.
- Carmack, E. Wassmann, P. 2006. Food webs and physical-biological coupling on pan-Arctic shelves: Unifying concepts and comprehensive perspectives. *Prog. Oceanogr.* 71, 446-477.
- Chen, C., Gao, G., Qi, J., Proshutinsky, A., Beardsley, R.C., Kowalik, Z., et al., 2009. A new high-resolution unstructured grid finite volume Arctic Ocean model (AO-FVCOM): An application for tidal studies. *J. Geophys. Res.* 114(C8), 08017. doi:10.1029/2008JC004941.
- Corkett, C.J., McLaren, I.A. and Sevigny, J.M., 1986. The rearing of the marine calanoid copepods *Calanus finmarchicus* (Gunnerus), *C. glacialis* Jaschnov and *C. hyperboreus* Kroyer with comment on the equiproportional rule. *Syllogeus*, 58: 539–546.
- Daase, M., Falk-Petersen, S., Varpe, Ø., Darnis, G., Søreide, J.E., Wold, A., et al., 2013. Timing of reproductive events in the marine copepod *Calanus glacialis*: a pan-Arctic perspective. *Can. J. Fish. Aquat. Sci.*, 70(6), 871–884. doi:10.1139/cjfas-2012-0401.
- Day, R.H., Weingartner, T.J., Hopcroft, R.R., Aerts, L.A.M., Blanchard, A.L., Gall, A.E., et al., 2013. The offshore northeastern Chukchi Sea, Alaska: A complex high-latitude ecosystem. *Cont. Shelf Res.* 67(C), 147–165. doi:10.1016/j.csr.2013.02.002.

- Durbin, E.G. Casas, M.C., 2014. Early reproduction by *Calanus glacialis* in the Northern Bering Sea: the role of ice algae as revealed by molecular analysis. *J. Plankton Res.* 36: 523-541.
- Falk-Petersen, S., Mayzaud, P., Kattner, G., Sargent, J.R., 2009. Lipids and life strategy of Arctic *Calanus*. *Mar. Biol. Res.* 5(1), 18–39. doi:10.1080/17451000802512267.
- Grebmeier, J.M., Bluhm, B.A., Cooper, L.W., Danielson, S.L., Arrigo, K.R., Blanchard, A.L., Clarke, J.T., Day, R.H., Frey, K.E., Gradinger, R.R., Kedra, M., Konar, B., Kuletz, K.J., Lee, S.H., Lovvorn, J.R., Norcross, B.L., Okkonen, S.R. 2015. Ecosystem characteristics and processes facilitating persistent macrobenthic biomass hotspots and associated benthivory in the Pacific Arctic. *Prog. Oceanogr.* 136, 92-114.  
<http://dx.doi.org/10.1016/j.pocean.2015.05.006>.
- Hopcroft, R.R., Kosobokova, K.N., Pinchuk, A.I., 2010. Zooplankton community patterns in the Chukchi Sea during summer 2004. *Deep-Sea Res. II.* 57(1-2), 27–39.  
doi:10.1016/j.dsr2.2009.08.003.
- Hunt, G.L., Jr., Blanchard, A.L., Boveng, P., Dalpadado, P., Drinkwater, K.F., Eisner, L., et al., 2013. The Barents and Chukchi Seas: Comparison of two Arctic shelf ecosystems. *J. Mar. Syst.* 109-110, 43–68. doi:10.1016/j.jmarsys.2012.08.003.
- Ji, R., Ashjian, C.J., Campbell, R.G., a, C., Gao, G., Davis, C.S., et al., 2012. Life history and biogeography of *Calanus* copepods in the Arctic Ocean: An individual-based modeling study. *Prog. Oceanogr.* 96(1), 40–56. doi:10.1016/j.pocean.2011.10.001.
- Lane, P.V., Llinás, L., Smith, S.L., Pilz, D. 2008. Zooplankton distribution in the western Arctic during summer 2002: hydrographic habitats and implications for food chain dynamics. *J. Mar. Sys.* 70, 97-133.
- Llinás, L., Pickart, R.S., Mathis, J.T., Smith, S.L., 2009. Zooplankton inside an Arctic Ocean cold-core eddy: Probable origin and fate. *Deep-Sea Res. II.* 56(17), 1290–1304.  
doi:10.1016/j.dsr2.2008.10.020.
- Nelson, R.J., Carmack, E.C., McLaughlin, F.A., Cooper, G.A., 2009. Penetration of Pacific zooplankton into the western Arctic Ocean tracked with molecular population genetics. *Mar. Ecol. Prog. Ser.* 381, 129–138. <http://doi.org/10.3354/meps07940>.
- Pickart, R.S., Weingartner, T.J., Pratt, L.J., Zimmermann, S., Torres, D.J., 2005. Flow of winter-transformed Pacific water into the Western Arctic. *Deep-Sea Res. Pt II.* 52 (24-26), 3175–3198. doi: 10.1016/j.dsr2.2005.10.009.
- Plourde, S., Campbell, R.G., Ashjian, C J., Stockwell, D.A., 2005. Seasonal and regional patterns in egg production of *Calanus glacialis/marshallae* in the Chukchi and Beaufort Seas during spring and summer, 2002. *Deep-Sea Res. II.* 52(24-26), 3411–3426.  
doi:10.1016/j.dsr2.2005.10.013.
- Quakenbush, L.T., Citta, J.J., George, J.C., Small, R.J., 2010. Fall and winter movements of bowhead whales (*Balaena mysticetus*) in the Chukchi Sea and within a potential petroleum development area. *Arctic.* <http://doi.org/10.1098/rsbl.2011.0731>.
- Questel, J.M., Clarke, C., Hopcroft, R.R., 2013. Seasonal and interannual variation in the planktonic communities of the northeastern Chukchi Sea during the summer and early fall. *Cont. Shelf Res.* 67(C), 23–41. doi:10.1016/j.csr.2012.11.003.

- Rose, K.A., Roth, B.M., Smith, E.P., 2009. Skill assessment of spatial maps for oceanographic modeling. *J. Mar. Syst.* 76(1-2), 34–48. doi: 10.1016/j.jmarsys.2008.05.013.
- Weingartner, T., Aagaard, K., Woodgate, R., Danielson, S., Sasaki, Y., Cavalieri, D. 2005. Circulation on the north central Chukchi Sea shelf. *Deep-Sea Res. II* 52, 3150–3174.
- Weingartner, T., Dobbins, E., Danielson, S., Winsor, P., Potter, R., Statscewich, H., 2013. Hydrographic variability over the northeastern Chukchi Sea shelf in summer-fall 2008–2010. *Cont. Shelf Res.* 67(C), 5–22. doi:10.1016/j.csr.2013.03.012.
- Woodgate, R.A., Aagaard, K., Weingartner, T.J., 2005. A year in the physical oceanography of the Chukchi Sea: Moored measurements from autumn 1990–1991. *Deep-Sea Res. II.* 52(24-26), 3116–3149. doi: 10.1016/j.dsr2.2005.10.016.
- Woodgate, R.A., Weingartner, T.J., Lindsay, R. 2012. Observed increases in Bering Strait oceanic fluxes from the Pacific to the Arctic from 2001 to 2011 and their impacts on the Arctic Ocean water column. *Geophys. Res. Ltrs.*, 39(24).
- Zhang, J., Spitz, Y.H., Steele, M., Ashjian, C., Campbell, R., Bérline, L., Matrai, P., 2010. Modeling the impact of declining sea ice on the Arctic marine planktonic ecosystem. *J. Geophys. Res.*, 115(C10), C10015. doi:10.1029/2009JC005387.

# Interannual Variability of Epibenthic Communities in the Chukchi Sea Alaska

Kimberly Powell<sup>a\*</sup>, Brenda Konar<sup>b</sup>, Jaqueline M. Grebmeier<sup>c</sup>

<sup>a\*</sup> Corresponding author: School of Fisheries and Ocean Sciences, University of Alaska Fairbanks, 905 N. Koyukuk Drive, 245 O'Neill Building, PO Box 757220 Fairbanks, Alaska, USA 99775-7220, Present address: Po Box 464 Homer, AK 99603,

<sup>b</sup> School of Fisheries and Ocean Sciences, University of Alaska Fairbanks, 905 N. Koyukuk Drive, 245 O'Neill Building, PO Box 757220 Fairbanks, Alaska, USA 99775-7220,

<sup>c</sup> University of Maryland Center for Environmental Science, Chesapeake Biological Laboratory, 146 Williams Street, PO Box 38 Solomons, Maryland, USA 20688,

[kkpowell2@alaska.edu](mailto:kkpowell2@alaska.edu), [bhkonar@alaska.edu](mailto:bhkonar@alaska.edu), [jgrebmei@umces.edu](mailto:jgrebmei@umces.edu)

## Abstract

Epibenthic communities contain many types of organisms and serve an important role in marine ecosystems. They are involved in carbon remineralization, benthic production, and are important prey items for higher trophic levels. While Arctic epibenthic communities may be experiencing changes due to long term shifts in the environment, differentiating these long term trends from short term interannual variation can be problematic. This study examined interannual differences of epibenthic community structure and potential environmental drivers of their variability in the Chukchi Sea. For this, a plumb-staff beam trawl was used to quantify epibenthic invertebrate composition based on their relative abundance and biomass at 71 stations in the NE Chukchi Sea during the ice free seasons of 2009, 2010, 2012, and 2013. At these same stations, we also examined bottom water temperature, salinity, dissolved oxygen, mean sediment chlorophyll *a*, sediment grain size, and sediment organic matter (TOC, TON, and the ratio of C:N). Over the entire study area and within a smaller area around Hanna Shoal with the most spatial and temporal coverage, variability between community structure was greatest from 2009 to 2013, and greater between 2009 and 2010 than between 2012 and 2013. For proportional biomass and abundance, crustaceans and echinoderms were the most important taxa, with only the crustaceans *Chionoecetes opilio*, *Pagurus spp.*, and Caridea varying significantly over time. The environmental drivers that were important in describing the epibenthic community in some, but not all years included bottom water temperature, salinity, dissolved oxygen, mean sediment chlorophyll *a*, and sediment organic matter. In contrast, sediment grain size was important in all years and, therefore, was the least likely to contribute to the biological variability among years. Of all the variables examined, only three varied significantly over time based on an ANOVA test (temperature, salinity, and dissolved oxygen). While these data provide a benchmark on interannual variability of epibenthic community structure in the Chukchi Sea, more monitoring is essential to determine long term trends.

## 1. Introduction

Similar to other Arctic seas, the Chukchi Sea is a dynamic ecosystem with considerable long and short term variability in both its biological and physical environment. Long term variability in this study is defined as a change to the ecosystem over a timescale of many (10+) years, whereas short term refers to shifts an ecosystem experiences from one year to the next. Short term variability in the abundance and biomass of epibenthic organisms is a natural phenomenon and may be caused by a variety of environmental drivers, which we define as variation in local current regimes, the amount of production that reaches the benthos, and water mass properties (such as temperature and salinity) (Winsor and Chapman, 2002; Grebmeier et al., 2006; Blanchard et al., 2013a; Questel et al., 2013).

The current regimes are complex and vary on both short and long time scales in the Chukchi Sea. There are three main currents with unique water mass properties that flow northward into the system: Alaska Coastal Water, Anadyr Water, and Bering Shelf Water (Grebmeier, 1987; Grebmeier et al., 1989). Anadyr Water and Bering Shelf water converge to form Bering Shelf-Anadyr Water (Grebmeier et al., 1989). The Alaska Coastal Water flows on the eastern side of the Chukchi Sea and is characterized by higher temperature ( $> + 2^{\circ}\text{C}$ ) and lower salinity ( $< 31.8$ ) than Bering Shelf-Anadyr Water in the west, which is characterized by low temperature ( $-1$  to  $+2^{\circ}\text{C}$ ) and relatively high salinity ( $> 31.8$ ) (Grebmeier et al., 1989). The coastal current can alter direction, flowing in a southward direction instead of northward (Weingartner et al., 2005). The Chukchi Sea undergoes large variation in temperature, salinity, and overall flow characteristics of these current regimes on monthly, annual, and even decadal scales (Weingartner et al., 2005). If variation occurs, it can cause a shift in important drivers that shape the structure of benthic communities. In this study, we define these drivers as sediment grain size, salinity, temperature, and the quality (carbon and nitrogen content within the sediment) and quantity of production reaching the seafloor (Winsor and Chapman, 2002; Grebmeier et al. 2006; Blanchard et al., 2013a; 2013b; Questel et al., 2013). Understanding short term variability is essential if we are to properly interpret long term changes in biological communities.

Previous studies of the Chukchi Sea have found that this region has the highest abundance and biomass of benthic organisms in the Arctic, in spite of the low temperatures and high temporal variation in particulate fluxes to the seafloor (White, 1977; Grebmeier, 1987). Benthic fauna, therefore, play a much greater role in benthic turnover and production in the Arctic than in lower latitudes (Feder et al., 2005; Blanchard et al., 2013a). High benthic abundance and biomass despite the harsh environment have been linked to a high deposition of organic material, particularly in cold waters (Haflinger, 1981; Stoker, 1981). In addition, benthic community composition is different, and abundance and biomass is higher, in offshore regions compared with the coast in arctic regions (Stoker, 1981). The pattern of abundance, biomass, and overall community composition conforms to current patterns and water mass distributions for the Chukchi Sea as there is a higher macrofaunal abundance and biomass under the offshore Bering Shelf Anadyr Water (1684-6940 ind/m<sup>2</sup> and 22.2-24.2 g C/m<sup>2</sup>, respectively) than under the inshore Alaska Coastal Current (641-4193 ind/m<sup>2</sup> and 2.0-15.4 g C/m<sup>2</sup>, respectively) (Grebmeier et al., 1989).

Echinoderms and crustaceans make up the majority of the epibenthic community in the Chukchi Sea and are, therefore, important in this environment (Piepenburg, 2000; Feder et al., 2005;

Bluhm et al., 2009; Ravelo et al., 2014). For example, brittle stars can number as high as several hundred individuals  $m^2$  (Piepenburg, 2000). Both echinoderms and crustaceans play important roles in the remineralization of organic matter, bioturbation of the surrounding sediment, and linking the benthic food chain to higher trophic levels (Piepenburg et al., 1995; Bluhm et al., 1998; Summers and Nybakken, 2000; Ambrose et al., 2001). It has been estimated that a significant portion of energy in Arctic shelf systems may pass through the epibenthos (Piepenburg et al., 1995; Piepenburg and Schmid, 1996). The abundance and biomass of echinoderms and crustaceans are sensitive to the amount of available primary production (McMahon et al., 2006), as well as to the temperature and salinity regimes of various water masses (Grebmeier et al., 1988; Feder et al., 1994). Therefore, the relative proportion of echinoderms and crustaceans can shift along with the seasonal and annual variation in the main currents flowing into the Chukchi, since current variation could change the sinking of production to the benthic environment. In a previous study, these two taxa varied spatially in both abundance and biomass across the Chukchi Sea, and generally had an inverse relationship in their dominance distribution (Blanchard et al., 2013a).

Epibenthic (and macrofaunal) organisms display a variety of sediment regime preferences and are strongly influenced by sediment grain size and quality (carbon and nitrogen content within the sediment) (Taghon, 1982; Etter and Grassle, 1992). For instance, polychaetes and brittle stars dominate in muddy substrates, whereas amphipods and crabs dominate in coarser grained regimes (Highsmith and Coyle, 1992; Feder et al., 1994). Finer grained sediments contain more organic matter, and have higher microbial activity than coarse substrata (Boos and Franke, 2004). Substrate, therefore, strongly influences community composition and likewise provides essential components needed to maintain metabolic processes (Tenore, 1988). If shifts in sediment grain size or sediment quality occur, then changes in benthic communities are expected (Grebmeier et al., 1989). Sediment organic content (hereon referred to as sediment quality) is important in maintaining cellular structure and influences amino acid synthesis (Tenore, 1988). Carbon and nitrogen are therefore needed in a large supply to support the extensive benthic communities. Since sediment grain size and quality are determined by hydrodynamic events such as current speed and duration, sediment quality can be used to infer hydrodynamic processes and physical ocean events, which affect food supply and habitat structure for epibenthic communities. Sediment characteristics are a vital factor in predicting how these communities are structured, both spatially and temporally (Blanchard and Feder, 2014).

In shallow seas, like the Chukchi Sea, particles quickly sink to the benthos, thus allowing for a fresh supply of productivity to the epibenthic environment. It is ultimately the flux of energy from nutrient rich surface waters to the benthos that links pelagic production to benthic production (Grebmeier and Barry, 1991; Wassmann, 1991; Dunton et al., 2005). Since benthic-pelagic coupling is a product of depth and the amount of pelagic production, which is driven by the advection of nutrient rich waters from the Bering Sea through the Bering Strait into the shallow Chukchi Sea (Coachman et al., 1975; Springer and McRoy, 1993; Grebmeier et al., 2006), tight benthic-pelagic coupling is very important in supporting the large epibenthic communities found in the Chukchi Sea. Organic matter flux to the benthos is highly variable interannually for high latitudes (Wassmann et al., 2006). Overall, abundance and biomass of epibenthic organisms has been decreasing on a decadal time scale in some high latitude regions, and has been thought to be due to a reduction in the amount of carbon flux to the benthos (Baldwin and Smith Jr., 2003). A decrease in benthic-pelagic coupling could put stress on the



large epibenthic communities of the Chukchi Sea (Ruhl, 2007), resulting in an overall reduction in organism size (Baldwin and Smith Jr., 2003). Since the Chukchi Sea is such a dynamic environment, benthic community structure may be driven by many environmental drivers. It is, therefore, important to understand which drivers are important in this system, and in particular, which are influencing the short term variability in the biology.

This study presents information on the short term variation and the species composition of the epibenthic community at stations on the northeastern Chukchi Sea shelf occupied in 2009 – 2013 (Figure 1). Comparisons were made between 2009 and 2010 and between 2012 and 2013 as well as between the earlier and later year groups. The objectives of this current study were to (1) describe the interannual variability of the epibenthic community structure in the Chukchi Sea, (2) determine which taxa specifically contributed to the interannual differences in community structure, and (3) determine which environmental drivers, if any, influence the community variability. Along with these objectives, the following hypotheses were tested: (1) the epibenthic community structure in the Chukchi Sea will vary interannually, (2) the variability in epibenthic community structure is driven by crustaceans and echinoderms, and (3) current regime proxies, such as sediment grain size and sediment carbon and nitrogen content, will be the main drivers of epibenthic community structure variability.

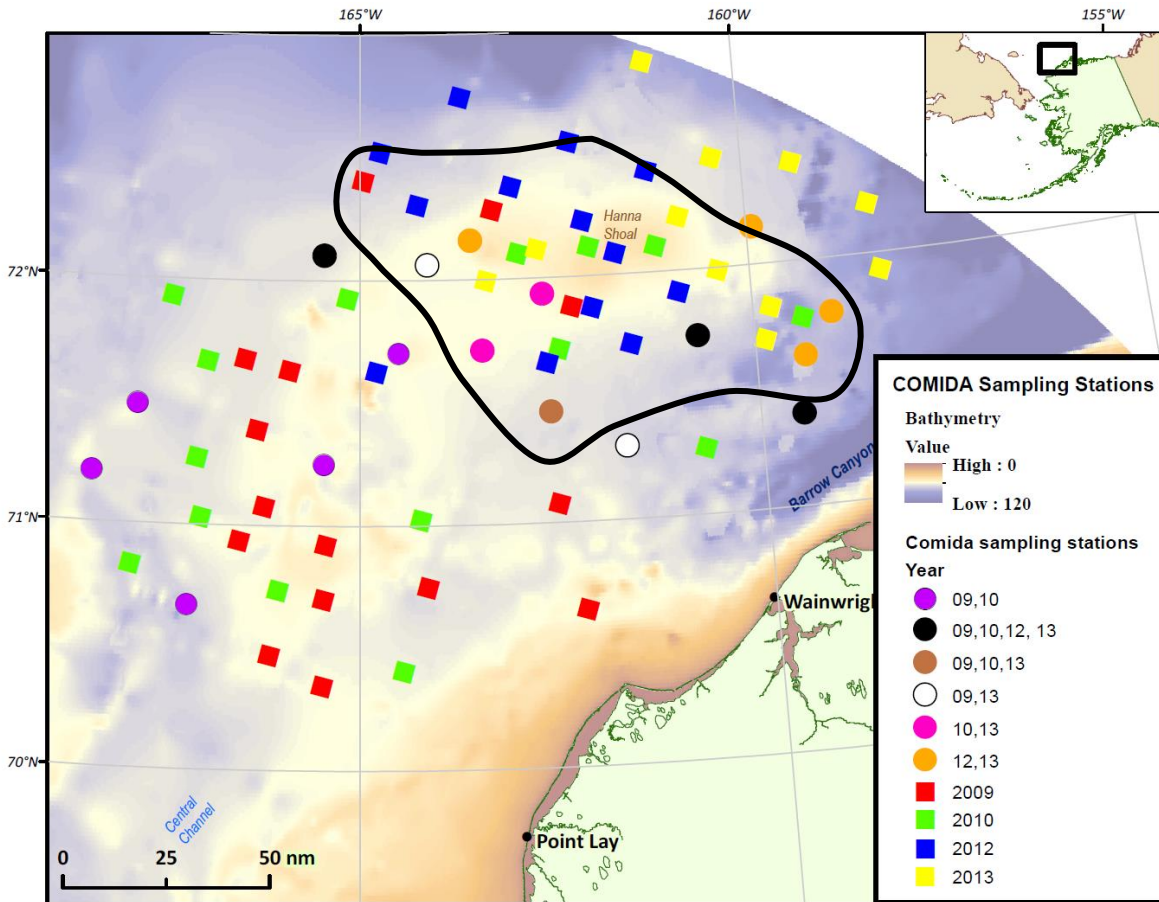
## **2. Materials and Methods**

### **2.1 Sampling Site Description**

The present study was carried out in the northeastern Chukchi Sea, Alaska extending from 70<sup>0</sup> to 73<sup>0</sup>N and 168<sup>0</sup> to 157<sup>0</sup>W. Sampling took place at stations in the ice-free seasons in 2009 (n=26), 2010 (n=26), 2012 (n=20), and 2013 (n=23). Of the 71 total stations, 24 were sampled in multiple years, with three being sampled all four years (Figure 1). In 2009 and 2010, the study area was more widespread, while the 2012 and 2013 study area focused on the northeast region around Hanna Shoal. Stations ranged in depth from 24 to 65 m. In 2009 and 2012, stations were initially selected using a tessellation method in GIS that ensured random selection and even station distribution (White et al., 1992). The following years (2010 and 2013), stations were again randomly designated; however, some previously sampled stations were opportunistically resampled.

### **2.2 Sampling Strategy**

The epibenthic communities were sampled at each station with a 3.05 m plumb-staff beam trawl (Gunderson and Ellis, 1986). The trawl had a 7 mm mesh and a 4 mm codend liner, and was modified with a lead line and 15 cm chain pieces tied to the footrope every 15 cm to increase connectivity with the seafloor. Bottom time for the trawl ranged from 1 min and 15 sec to 5 min, depending on substrate composition and epifaunal density for each specific area, which was determined visually using a benthic camera deployed prior to each trawl. The resulting trawl sample was then sieved on deck and sorted into the lowest taxonomic level possible, after which taxa were counted and weighed. To describe community structure for this study, we examined proportional data of each taxa in terms of abundance and biomass. If a station was resampled, the same trawl parameters were used (wire length, boat speed and bottom time). When a trawl sample was too large to feasibly process, it was subsampled by dividing the sample into equal



**Figure 1.** Epibenthic stations sampled in 2009, 2010, 2012, and 2013 in the Chukchi Sea, Alaska. The color of the circles represent the number of years that a station was sampled. Square symbols denote stations only sampled in one year, and circles are stations sampled in multiple years. Circled stations are a subset of stations with the maximum spatial overlap for all years based on ArcGIS spatial analysis.

portions and choosing one portion at random. Any unknown organisms were preserved in a 10% formalin solution for later identification at the University of Alaska Fairbanks.

Environmental drivers were sampled in the same years and at the same stations as the biological data. Sediments were collected with 0.1 m<sup>2</sup> van Veen grabs, and were used for sediment grain size analysis and for determining sediment quality, defined as total organic carbon, total organic nitrogen, sediment chlorophyll *a*, and C:N (details in Grebmeier and Cooper, 1995; Cooper et al., 2002). In addition, water column characteristics (bottom water temperature, salinity, and dissolved oxygen) were determined via a YSI 6600 V2-4 data sonde (YSI Inc., Yellow Springs, Ohio, USA) in 2009 and 2010, and by a Seabird CTD rosette in 2012 and 2013.

### 2.3 Data Analysis

Data analyses were performed through ArcGIS, PRIMER v. 6 (Clarke and Gorley, 2006), and R (www.r-project.org, V2.15.0). As an initial examination into the study area, a CLUSTER

analysis was run on the proportion, or relative abundance and biomass of major taxa in PRIMER to determine how stations grouped together based on taxon similarity both spatially and temporally. This was done via a similarity matrix utilizing the Bray-Curtis coefficient on 4<sup>th</sup> root transformed data. The SIMPROF routine was then used to determine significantly different cluster groupings based on taxa similarity. Since stations varied in spatial coverage from year to year, GIS was used to determine the area of maximum spatial overlap of stations across years (2009 to 2010 and 2012 to 2013). The Generate Near Table tool was used to determine which stations were closest to one another among the year pairs, and the Join Field tool was used to determine the proximity by year. The CLUSTER analysis was rerun on the stations with maximum overlap to ensure the pattern seen was not due to the spatial mis-match among study years. Finally, to examine the amount of separation between years, an ANOSIM test in PRIMER was run on proportional biomass and abundance of the spatially overlapping stations. The R values, or the measure of scaled separation between groups, were compared.

To determine which specific taxa were responsible for differences in community composition between years, a SIMPER test in PRIMER was run on a Bray-Curtis similarity matrix on 4<sup>th</sup> root transformed data to determine which taxa contributed to the differences among clusters and years for the spatially overlapping stations. An ANOVA test in R was performed on arcsine transformed relative biomass and abundance to see if proportions of major taxa varied significantly from 2009 to 2013 using the subset of spatially overlapping stations. Since proportional data have a binomial distribution, an arcsine transformation was used to standardize the data. A Tukey test was then performed to determine which years were statistically different from one another.

The temporally variable environmental drivers (bottom water temperature, salinity, dissolved oxygen, sediment grain size, C:N, and sediment chlorophyll *a* content) that were concurrently sampled at each station were normalized in PRIMER so drivers at a range of scales could be compared, and would contribute equally to the analysis. To normalize data, PRIMER subtracts the mean and divides by the standard deviation over all samples, which makes the variance along all axes similar. Collinearity between drivers was visually inspected using a Draftman's plot in PRIMER. If two drivers were found to be correlated at 90% or greater, determined by the underlying correlation matrix of the Draftman's plot, one was removed from further analysis. Sand, mud and gravel (coarse, fine, very fine) all correlated with one another, and, therefore, percent mud (sediment grain size >5 phi) was used as the sediment grain size variable. A Euclidean distance similarity matrix was then created on normalized environmental drivers. The BIO-ENV analysis in PRIMER was run to determine if any environmental drivers might be responsible for differences in epibenthic community structure for each year. This was done by comparing the Bray-Curtis and Euclidean distance resemblance matrices of the biological and environmental data, respectively, to determine if any environmental drivers correlated with the biological communities across the study region. This test was once again repeated on the subset of spatially overlapping stations to ensure that the observed pattern was not driven by a mis-match in spatial coverage between years. The mean values of each of the important environmental variables in the overlapping stations for each year were calculated. In addition,

ANOVA and Tukey tests were run to determine if there were any significant differences over time, and between which years these significant differences occurred.

### 3. Results

#### 3.1 Abundance

Higher separation in the community composition based on abundance was observed between the earlier years (2009 and 2010) than between the later years (2012 to 2013); however, these R values are low and there is therefore little difference between these two year groups (ANOSIM; R= 0.082 and 0.029 for 09-10 and 12-13, respectively; Table 1). The most separation was found between 2009 and 2013, and the least from 2010 and 2013 (R= 0.277 and 0.009 for 2009 to 2013 and 2010 to 2013, respectively; Table 1).

**Table 1.** R-values, or the scaled degree of separation between years, based on the analysis of similarity (ANOSIM) test for epibenthic abundance and biomass.

	Years	R-value
<b>Abundance</b>	09-10	0.082
	09-12	0.111
	09-13	0.277
	10-12	0.033
	10-13	0.009
	12-13	0.029
<b>Biomass</b>	09-10	-0.058
	09-12	0.144
	09-13	0.275
	10-12	0.121
	10-13	0.184
	12-13	-0.075

For all years, the four taxa that best described overall epibenthic community structure based on abundance were the brittle star class Ophiuroidea, the snow crab *Chionoecetes opilio*, the hermit crabs *Pagurus* spp., and the infraorder of shrimp Caridea (SIMPER analysis, Spearman coefficient = 0.753, 0.818, 0.709, and 0.639 for 2009, 2010, 2012, and 2013, respectively). For subsequent analyses, all other taxa were included in the “others” category, and consisted of various gastropods, sea stars, bryozoans, the crab *Hyas coarctatus*, and the sea cucumber *Ocnus glacialis*. While the aforementioned groups were always the dominant taxa, the relative contribution of each group to total abundance varied significantly between years (Tables 2 and 3). In 2009 and 2010, the majority of the community was composed of Ophiuroidea. However, between 2009 and 2010, *Chionoecetes opilio* contributed most to the separation in total relative abundance between years (Tables 1 and 2). *Chionoecetes opilio* was a major contributor to proportional abundance in 2009 and 2010 (southern region), but not in 2012 and 2013 (northern region), when the major contributors were Caridea and *Pagurus* spp. In 2012, the majority of the community was composed of Ophiuroidea and Caridea. In 2013, Caridea and Ophiuroidea contributed most to community abundance, and Caridea contributed most to the separation

between the years 2012 and 2013. Out of the major taxa describing the community, *C. opilio* decreased significantly in relative abundance across most year pairs, while *Pagurus* spp. increased significantly from 2009 to 2013 ( $p = <0.001$  and  $0.004$ , respectively; Tables 2 and 3). Specifically, *C. opilio* relative abundances were significantly different between the years 2009 and 2012, 2009 and 2013, and 2010 and 2012 (Table 2). For *Pagurus* spp., however, the only significant differences in relative abundance were between 2009 and 2012 and between 2009 and 2013 (Table 2).

**Table 2.** Top: One-way analysis of variance (ANOVA) of major taxa based on relative abundance and biomass within spatially overlapping stations by year. Asterisks represent statistically significant changes in taxon abundances over time. Bottom: Tukey test p-values for spatially overlapping stations of taxa with statistically significant differences in years: *C. opilio*, *Pagurus* spp., and Caridea

	Major Taxa	Sum of squares	Mean square	F-value	p-value
<b>Abundance</b>	Ophiuroidea	<0.001	<0.001	<0.001	0.994
	<i>Chionoecetes opilio</i>	0.277	0.277	13.45	<0.001*
	<i>Pagurus</i> spp.	0.070	0.070	8.788	0.004*
	Caridea	0.160	0.160	2.040	0.157
	Others	0.068	0.068	1.989	0.162
<b>Biomass</b>	Ophiuroidea	0.425	0.425	3.163	0.079
	<i>Chionoecetes opilio</i>	1.864	1.864	32.54	<0.001*
	<i>Pagurus</i> spp.	0.006	0.006	0.519	0.473
	Caridea	0.052	0.052	8.686	0.004*
	<i>Neptunea</i> spp.	<0.001	<0.001	0.394	0.532
	Others	0.170	0.170	3.055	0.084

Taxa	Year					
	10 – 09	12 – 09	13 – 09	12 – 10	13 – 10	13 – 12
<b>Abundance</b>						
<i>C. opilio</i>	0.433	<0.001*	0.050*	0.008*	0.660	0.153
<i>Pagurus</i> spp.	0.640	0.058	0.054*	0.544	0.519	0.999
<b>Biomass</b>						
<i>C. opilio</i>	0.965	<0.001*	<0.001*	<0.001*	<0.001*	0.999
Caridea	0.436	0.032*	0.029*	0.513	0.522	0.999

**Table 3.** Mean values for relative abundance and biomass for taxa that varied significantly between 2009, 2010, 2012, and 2013.

Organism	Year			
	2009	2010	2012	2013
<b>Abundance</b>				
<i>Chionoecetes opilio</i>	0.286±0.192	0.126±0.091	0.002±0.001	0.087±0.025
<i>Pagurus</i> spp.	0.122±0.095	0.092±0.072	0.056±0.028	0.055±0.037
<b>Biomass</b>				
<i>Chionoecetes opilio</i>	0.331±0.116	0.317±0.105	0.053±0.021	0.036±0.011
Caridea	0.011±0.001	0.044±0.005	0.098±0.020	0.168±0.053

The environmental drivers that best explained the patterns in community structure of spatially overlapping stations by abundance varied over time. In 2009, sediment grain size best matched the biological community patterns (BIO-ENV analysis,  $\rho = 0.576$ ). In 2010, sediment grain size, salinity, the C:N ratio within the sediment, and dissolved oxygen ( $\rho = 0.439$ ) were the most important drivers. In 2012, four drivers were also important but in this year, they were sediment grain size, salinity, the C:N ratio within the sediment, and bottom temperature ( $\rho = 0.481$ ). Finally, 2013 also indicated four important drivers: sediment grain size, the C:N ratio, temperature, and mean sediment chlorophyll *a* ( $\rho = 0.520$ ). Overall, sediment grain size was important in all years. Dissolved oxygen was only important in 2009, whereas mean sediment chlorophyll was only important in 2013. Temperature became important in the later years of the study (2012 and 2013) when the mean values switched from above zero to below zero degrees Celsius (Table 4). The C:N ratio within the sediment was important in all years except 2009, and salinity was only important in 2010 and 2012. This C:N ratio was low, suggesting that labile carbon was more important than terrigenous carbon. These patterns held true when community patterns were analyzed over all stations within the study area, as well as when only the stations with the maximum spatial overlap were considered. This suggests that the spatial mis-match in station location across years did not contribute to the selection of important environmental drivers. The ANOVA test showed that there were significant differences in temperature ( $p = <0.001$ ), salinity ( $p = <0.001$ ), and dissolved oxygen ( $p = <0.001$ ) over time, indicating that the differences seen in the biology was mostly due to these variables (Table 5). Bottom temperature was significantly different between 2009 and 2012 and 2013 as well as between 2010 and 2012. Salinity was significantly different between 2009 and 2012, 2010 and 2012, and 2012 and 2013. The final variable, dissolved oxygen, was significantly different between all years except 2009 and 2010 (Table 5).

**Table 4.** Mean values for the important environmental variables for 2009, 2010, 2012, and 2013.

Variable	Year			
	2009	2010	2012	2013
Salinity	32.83	32.83	33.32	32.80
C:N ratio	6.702	6.712	6.712	6.733
Dissolved Oxygen	11.25	11.16	11.23	11.24
Chlorophyll a	11.69	10.05	9.563	9.415
Bottom Temperature	0.238	0.146	-1.550	-1.515

**Table 5.** One-way analysis of variance (ANOVA) of important environmental variables for abundance and biomass within spatially overlapping stations by year. Asterisks represent statistically significant differences environmental variables over time. Bottom: Tukey test p-values for spatially overlapping stations of Environmental variables with statistically significant differences.

Environmental Variable	Sum of squares	Mean square	F-value	p-value
Bottom Temperature	1.099	0.366	10.63	<0.001*
Salinity	0.002	0.001	21.105	<0.001*
Dissolved Oxygen	2.555	0.852	334.44	<0.001*
Ratio of C:N	0.013	0.004	1.590	0.209
Mean Sediment Chlorophyll a	0.357	0.119	0.484	0.695

Environmental Variable	Year					
	10 – 09	12 – 09	13 – 09	12 – 10	13 – 10	13 – 12
Bottom Temperature	0.057	<0.001*	<0.001*	0.028*	0.062	0.871
Salinity	0.999	<0.001*	0.979	<0.001*	0.962	<0.001*
Dissolved Oxygen	0.932	<0.001*	<0.001*	<0.001*	<0.001*	0.012 *
Ratio of C:N	0.979	0.241	0.707	0.378	0.890	0.771
Mean Sediment Chlorophyll a	0.836	0.970	0.710	0.950	0.997	0.849

### 3.2 Biomass

In the latter years of this study (2012 and 2013), community composition based on biomass was more evenly distributed across stations. There was no difference in community structure between 2009 and 2010 and between 2012 and 2013, since negative R-values are considered zero. More separation in communities based on biomass was seen between 2009 and 2010 than between 2012 and 2013 ( $R = -0.058$  and  $-0.075$  for 09-10, and 12-13 respectively; Table 1). Based on the stations with maximum spatial overlap, the most separation was found between 2009 and 2013, and the least between 2009 and 2010 as well as between 2012 and 2013 ( $R = 0.275$ ,  $-0.058$ , and  $-0.075$  for 09-13, 09-10, and 12-13, respectively; Table 1).

The five taxa that best described overall epibenthic community structure based on biomass for all years were Ophiuroidea, *Chionoecetes opilio*, *Pagurus* spp., Caridea, and the large predatory gastropod *Neptunea* spp. (SIMPER analysis, Spearman coefficient = 0.745, 0.783, 0.751, and 0.649 for 2009, 2010, 2012, and 2013, respectively). All other taxa were included in “others”, which was defined as various gastropods, sea stars, bryozoans, the soft coral *Gersemia* spp., the crab *Hyas coarctatus*, the anemone *Stomphia* spp., and the sea cucumber *Ocnus glacialis*. The “dominant” groups mentioned above did not differ among years; however, the relative contribution of each group to total biomass (the difference seen in the percent biomass) varied significantly between years (Tables 2-3). In 2009, the majority of the community was composed of Ophiuroidea and *C. opilio*. Between 2009 and 2010, *C. opilio* contributed most to the separation between years (Tables 2-3). Stations sampled in 2010 were composed mainly of *C. opilio*, but both *C. opilio* and Ophiuroidea contributed most to the separation between years. *Chionoecetes opilio* was a major contributor to biomass in 2009 and 2010, and Caridea and *Pagurus* spp. were the major biomass contributors in 2012 and 2013. In 2012 and 2013, the majority of the community was composed of Ophiuroidea. Between 2012 and 2013, *C. opilio* and Caridea contributed most to the separation between years (Table 2-3). Of the major taxa that described the community, only *C. opilio* and Caridea varied significantly over the four years of the study ( $p = 1.37e-07$  and  $4.05e-03$ , respectively; Tables 2-3). The proportion of *C. opilio* significantly decreased across most year pairs, whereas Caridea significantly increased from 2009-2012 and 2009-2013 (Tables 2-3). Specifically, relative *C. opilio* biomass was significantly different between the years 2009 and 2012, 2009 and 2013, 2010 and 2012, and between 2010 and 2013 (Table 2). For Caridea, however, the only significant differences were between 2009 and 2012, and 2009 and 2013 (Table 2).

The environmental drivers that best matched the biological community patterns for spatially overlapping stations based on biomass changed over the study years. In 2009, it was sediment grain size (BIO-ENV analysis,  $\rho = 0.618$ ), while in 2010, they were sediment grain size, salinity, the C:N ratio within the sediment, and dissolved oxygen ( $\rho = 0.488$ ). For 2012, sediment grain size, salinity, the C:N ratio within the sediment, and temperature were most important ( $\rho = 0.532$ ), while in 2013, sediment grain size, the C:N ratio, temperature, and mean sediment chlorophyll *a* had the highest correlation to epibenthic community patterns ( $\rho = 0.451$ ). Overall, sediment grain size was important in all years. In contrast, dissolved oxygen and mean sediment chlorophyll *a* were only important in 2010 and 2013, respectively. Temperature became important in the last two years of the study. The C:N ratio within the sediment was important in 2010, 2012 and 2013. The environmental drivers best matching community biomass variability were the same when analyzed over all stations, or when only the stations with the maximum



spatial overlap were considered. This suggests that the spatial mis-match in station location among years did not contribute to the selection of important environmental drivers. The ANOVA test revealed that there were significant differences in temperature ( $p = <0.001$ ), salinity ( $p = <0.001$ ), and dissolved oxygen ( $p = <0.001$ ) over time, indicating that the differences seen in the biology was mostly due to these variables (Table 5). Bottom temperature was significantly different between 2009 and 2012 and 2013 as well as between 2010 and 2012. Salinity was significantly different between 2009 and 2012, 2010 and 2012, and 2012 and 2013. The final variable, dissolved oxygen, was significantly different between all years except 2009 and 2010 (Table 5).

## **4. Discussion**

### **4.1 Community Composition Patterns**

Epibenthic community structure demonstrated short term variability across the Chukchi Sea study area. This supports our first hypothesis that the epibenthic community structure in the Chukchi Sea will vary interannually. Specifically, there was more separation in epibenthic community composition between 2009 and 2013 for both relative proportions of taxa by abundance and by biomass in the spatially overlapping stations around Hanna Shoal. The least separation was found between 2010 and 2013 for proportion of taxa by abundance, and between 2009 and 2010 as well as 2012 and 2013 for proportion of taxa by biomass. Previous studies in the Chukchi Sea have shown a very productive and dynamic system with high abundance, biomass, and temporal as well as spatial variation of both epi- and infaunal communities (Grebmeier et al., 2006; Piepenburg, 2006; Ravelo et al., 2014). A so-called “hotspot” of benthic abundance and biomass exists southeast of Hanna Shoal (Grebmeier et al., 2006, 2015), where a convergence of currents increases deposition of organic matter to the epibenthic environment (Weingartner et al., 2013). The variation in the epibenthic hotspot could be due to changes in current regimes, which may lead to a decrease in the amount of primary production reaching the seafloor. Another possibility is the persistence of regionally colder temperatures that have been observed in recent years, which could be due to slower flushing times of the cold dense winter water that forms on Hanna Shoal that normally gets replaced by Bering Sea-Anadyr Water in early summer (Day et al., 2013). Colder temperatures are not favorable for several of the major epibenthic players in the Chukchi Sea, as colder temperatures have been found to inhibit larval recruitment and development (Ernst et al., 2005; Day et al., 2013; Balazy et al., 2015). Most studies focusing on variability in Arctic benthic communities have examined long term changes in abiotic drivers, such as sea ice cover and circulation patterns (Walsh, 1978; Semtner Jr., 1987; Johannessen et al., 2004; Stroeve et al., 2007). The Chukchi Sea varies greatly in ice cover, circulation, temperature, salinity, and the amount of production sinking to the benthos from year to year (Grebmeier and Barry, 1991; Winsor and Chapman, 2002; Arrigo and van Dijken, 2004; Grebmeier et al., 2006). This current study agrees with past studies in that the Chukchi Sea is dynamic, and that the importance of environmental drivers of epibenthic communities varies by year. The important drivers of community structure in this study were temperature, and the C:N ratio. This environmental variability probably influences interannual variability in the biological community.

While both crustaceans and echinoderms were the major contributors to total abundance and biomass across the study region in every year, only crustaceans varied significantly across years.

These results only partially support our second hypothesis, that the variability in epibenthic community structure is driven by crustaceans and echinoderms. One species, *Chionoecetes opilio* was particularly variable in relative abundance and biomass over time (Table 1-2). In addition, the sizes of *C. opilio* have also varied over spatial and temporal scales in this study area (Konar et al., 2014; Groß 2015; Groß and Konar, this issue). Previous studies in the Bering Sea reported *C. opilio* migration patterns that would be reflected in abundance, biomass and size frequency patterns (Somerton, 1981a; Ernst et al., 2005). Bering Sea *C. opilio* can undergo ontogenetic migrations of 73.5 nautical miles from shallow to deeper water (Ernst et al., 2005); although traditionally, migrations have been regarded as negligible since only shorter migrations have been found (Somerton, 1981b; Incze et al., 1987). In the Bering Sea, eggs are hatched in shallow waters because these regions are suitable for the survival, retention, and settlement of pelagic larvae (Ernst et al., 2012). Juvenile crabs also tend to stay in shallow water because they prefer the increased dissolved oxygen associated with these depths (Dionne et al., 2003). Once they settle, crabs grow to maturity, mate, and migrate to deep water (Ernst et al., 2005; Parada et al., 2010). This shallow to deep migration cycle has been monitored for three decades in the Bering Sea, and appears to have a mean period of seven years per cohort (Ernst et al., 2012). The same migratory pattern/periodicity in cohort development could be happening in the Chukchi Sea, as evidenced by the variability in relative abundance and biomass over time, and the overall decrease in mean proportional values of *C. opilio* in this current study. Migrations of *C. opilio* may be following environmental gradients. Bering Sea mature female *C. opilio* follow bottom temperature gradients and population movements are prevented by excessive cooling or heating of water, since crabs have preferred temperature ranges of 0-4.5<sup>0</sup>C (Dionne et al., 2003; Ernst et al., 2005). This observed temperature preference matches the present study, as temperatures were measured above 0<sup>0</sup>C in 2009 and 2010 and below 0<sup>0</sup>C in 2012 and 2013 (Table 4). If these temperature constraints are the same for Chukchi Sea crabs, mature crabs might migrate off the shelf onto the slope to find warmer water flowing in from the Atlantic, reaching 1<sup>0</sup>C at depth (Coachman and Barnes, 1963). Temperatures below 0<sup>0</sup>C are not suitable for adult crabs, and may help explain the decrease in abundance and biomass that was observed in the latter two study years if the temperature point measurements are representative of a more permanent decrease of temperature in the region.

Colder water may also have implications for Caridea and *Pagurus* spp.. The proportion of shrimp biomass became higher from 2009 to 2013 and less variable over time. The Gulf of Alaska experienced a regime shift in 1977 from a cold to warm temperature regime, which negatively affected the pandalid shrimp population (Anderson, 2000; Hare and Mantua, 2000; Overland et al., 2008). Shrimp are ecologically important, since they can occupy all depths and are common in high latitude food webs (Anderson, 2000). In the northeastern Chukchi Sea, decreasing temperatures may support higher shrimp recruitment and may help explain the increase in shrimp biomass over the study years, if caridean shrimp in the Arctic exhibit a similar temperature preference as pandalid shrimp in the Gulf of Alaska.

There have been very few studies on *Pagurus* spp. in the Arctic, but through the use of gastropod shells they not only provide transportation, but important habitat for epibionts (Williams and McDermott, 2004; Balazy et al., 2015), and are therefore considered important ecosystem engineers (Balazy et al., 2015). In a laboratory study, *Pagurus* spp. collected from northern Norway were found to decrease in number with a decrease in temperature because lower

temperatures inhibited larval development (Balazy et al., 2015). This temperature dependence could explain the observed decrease of relative *Pagurus* spp. abundance over time in the present study. Both Caridea and *Pagurus* spp. are important players in Arctic ecosystems, and therefore, variation in the relative abundance and biomass of these species will impact other trophic levels.

This current study found a decrease in epibenthic community complexity, and a change in community structure, especially in the later years of the study when comparing the stations within the area of maximum spatial overlap around Hanna Shoal. The variability in the epibenthic community observed in the current study has implications for higher trophic levels, such as benthic feeding marine mammals who utilize the NE Chukchi Sea epibenthos as a prey source. For example, Hanna Shoal is a preferred feeding ground for walrus (Jay et al., 2012). Walrus rarely dive deeper than 100 m, so the shallow environment of the Chukchi Sea and specifically Hanna Shoal in the NE regions is ideal for walrus foraging (Fay, 1982; Moore and Huntington, 2008). In addition, there is a hotspot of benthic fauna around Hanna Shoal (Schonberg et al., 2014), where ice remains until late into the summer (Martin and Drucker, 2012). This is especially important for walrus, which utilize ice for resting between feeding bouts to conserve energy and maintain their blubber layer (Moore and Huntington, 2008).

## 4.2 Environmental Analysis

The Chukchi Sea is a physically dynamic ecosystem, with much variability in its environmental drivers along with its biological communities. The correlations of environmental drivers with biological communities were reasonably strong and demonstrated that most of the primary drivers (bottom water temperature, salinity, dissolved oxygen, mean sediment chlorophyll *a*, and sediment organic matter) differed over time. One exception was sediment grain size, which was an important driver for describing community composition in all years for both relative proportions of taxa by abundance and biomass. These environmental drivers are associated with hydrodynamic regimes (currents and water mass characteristics), which are known to vary across years in the Chukchi Sea (Weingartner et al., 1998; Winsor and Chapman, 2002; Weingartner et al., 2005). Sediment grain size and sediment quality characteristics are thought to be proxies for current features. Faster currents produce coarser sediment whereas slower currents create fine grained sediment habitats (Grebmeier et al., 1989; 2015). In addition, currents determine how much organic matter reaches the benthos. The Chukchi Sea current systems are highly variable and have been known to change direction with strong wind regimes, which can also vary interannually (Weingartner et al., 1998; 2005; 2013). For example, reversal of the Alaska Coastal Current would ultimately change the sediment grain size and the amount of production reaching the benthos, which might impact the resident organisms (Blanchard et al., 2013a). The results of this study only partially support our third hypothesis that current regime proxies, such as sediment grain size and sediment carbon and nitrogen content, will be the main drivers of epibenthic community structure variability. It was found that only three of the six important variables changed significantly over time. Out of the drivers that we examined, temperature, salinity, and dissolved oxygen were the most important in driving the difference between the early years (2009 and 2010) and the later years (2012 and 2013) of the study.

Interannual variation in water mass characteristics is also high in the Chukchi Sea, with large differences in temperature and salinity between successive winters (Winsor and Chapman,

2002). Of the environmental drivers that were found to be important in describing the epibenthic community, only three were found to be varying significantly: temperature, salinity, and dissolved oxygen content. These variables define water masses, which subsequently can cause variation in the amount of productivity in the water column. A shift in temperature would cause zooplankton grazing rates to change, since as temperature increases or decreases so too does metabolism. A larger fraction of primary production retained in the pelagic system would subsequently affect the amount of primary production available to epibenthic organisms (Arrigo and van Dijken, 2004). Density in high latitude systems is mostly driven by salinity, which influences deep water formation and therefore ventilation of benthic systems (Winsor and Chapman, 2002). Benthic biomass is two to ten times greater under the nutrient-rich Bering Shelf-Anadyr Water than it is under Alaska Coastal Water (Springer and McRoy, 1993; Grebmeier et al. 2006; Blanchard and Feder, 2014). Bering Sea-Anadyr Water flows northward offshore, and splits around Hanna Shoal in the northeast. The upper arm of this split continues around the top of the shoal, and then wraps back on itself to meet up with the lower arm of the split, ultimately forming a convergence south of Hanna Shoal (Weingartner et al., 2005; 2013). This convergence allows for slower water motion, and thus retains a cold pool of salty winter water with a slow flushing of this water in the summer, when it is commonly replaced by Bering Shelf-Anadyr Water (Weingartner et al., 1998; 2005; 2013). Based on previous studies, the region south of Hanna Shoal is thought to be much more oceanographically stable than the surrounding waters (Weingartner et al., 1998; 2005; 2013). The later years of this present study had colder bottom water overall than in the earlier years, suggesting cold winter water was not fully flushed out of the system in the summer. Cold bottom waters have been recorded previously in summer months on Hanna Shoal; however, these conditions are not constant, varying nearly 4°C from year to year (Weingartner et al., 2013). Temperature changes have implications for the benthic community, since many biological processes are temperature dependent. Recent evidence has suggested that there has been a 50% increase of flow through the Bering Strait over the past decade (Woodgate et al., 2012). Increased flow has led to an increase in heat and freshwater fluxes into the Chukchi Sea (Woodgate et al., 2012), and a coarser sediment grain size (Grebmeier and Cooper, 1995). Changes in the drivers that structure the epibenthic communities were seen in this study, but their relative importance varied for all years. The ultimate cause of the variation in the epibenthic community structure seen in this study was most likely a result of a variety of environmental variables working in conjunction. The data from this study were a “snapshot”, and not from long term observations. Since Arctic benthic organisms are long lived and slow growing (Gage, 1990; Piepenburg et al., 1995), they integrate processes over time (Bluhm et al., 2005). Therefore, the inclusion of longer term and winter environmental data in future studies would increase the confidence in the results. For instance, total organic carbon and nitrogen, and pigment concentration (chlorophyll *a*) in the sediment change along with spring bloom timing and duration (Baldwin and Smith Jr., 2003). The reason these variables may have been important in some years and not others, and the reason for a lack of a significant difference over the four study years could be that the timing and duration of the bloom changed in the spring, and was missed in the summer signal because the production was already degraded.

One environmental driver that was not examined in the current study, but that may impact the Chukchi Sea, is sea ice (Gutt, 2001). Sea ice in the northern hemisphere ranges from year-round thick ice (rarely exceeds depths > 40 m) to thin seasonal ice (on average 0.5-2 m) that only

occurs in the winter months (Gutt, 2001). Thick ice prevents sunlight from reaching the sea surface, which in turn prevents photosynthesis and development of an underlying ice algal layer (Fisher et al., 1988; Fortier et al., 2002). When thick ice is present, there is little flux of particulates to the benthos. When the ice thins, ice algae are exposed to adequate sunlight for photosynthesis, seeding the phytoplankton bloom in the spring. The seasonal flux in ice melt timing as well as direction will cause considerable variation in magnitude and location of epibenthic communities (Fisher et al., 1988; Fortier et al., 2002). Ice scour is another physical driver of epibenthic communities in the Chukchi Sea since it is a shallow shelf system. Ice drift is mainly current driven and can run aground at depths of 600 m, leaving deep gouges (Sanderson, 1988; Gutt, 2001). In the Canadian Arctic, a benthic community that was once dominated by suspension feeders shifted to a community of scavengers and deposit feeders after scour occurred (Conlan et al., 1998; Gutt, 2001; Conlan and Kvitek, 2005). Scour has the potential to increase diversity within the system when different recolonization stages coexist, and scour can open up space for organisms (Gutt, 2001). Ice presence could therefore explain some variability seen in the biological community from 2009 to 2013.

## 5. Conclusions

The present study observed significant differences in the epibenthic community structure in the Chukchi Sea from 2009 to 2013. Ophiuroidea and Crustacea were the two taxa that contributed most to abundance and biomass; however, contributions of *Chionoecetes opilio*, Caridea, and *Pagurus* spp. to the communities were more variable over time. The environmental drivers that best described community structure were bottom water temperature, salinity, dissolved oxygen, mean sediment chlorophyll *a*, and sediment grain size and organic matter. Of these, sediment grain size was a consistent driver in all years of the study, and likely had a minimal impact on the differences in epibenthic communities among years. In addition, we found that out of the environmental variables that we examined, bottom temperature, salinity, and dissolved oxygen differed the most between years. This shift in temperature, salinity, and dissolved oxygen could be due to a shift in current regime and water mass characteristics, which could have led to a slower flushing of winter water from the area. It is this cold water that determines the recruitment success of various organisms, including Caridea and crab larvae. However, the Chukchi Sea ecosystem is highly dynamic, and, therefore, the variability seen in this study could be due to natural system variability as well, but more testing is needed to confirm this.

## 6. Acknowledgements

This study was funded by the U.S. Department of the Interior, Bureau of Ocean Energy Management (BOEM), Alaska Outer Continental Shelf Region, Anchorage, Alaska under BOEM Cooperative Agreement No. M11AC00007 as part of the Chukchi Sea Offshore Monitoring in Drilling Area (COMIDA). Additional funding was provided by the Robert Byrd Scholarship Program, the Matthew Iya Memorial Foundation, and the Francis “Bud” Fay Memorial Foundation. Environmental data for this project, along with information from the camera survey, was generously provided by Lee Cooper, University of Maryland Center for Environmental Science. Unknown organism identification was provided by Nora Foster, Ben Daly, and Ken Coyle. Statistical advice and guidance was given by Bob Clarke, Paul Somerfield, and Katrin Iken. From BOEM, we thank Heather Crowley for her continued support of this

project and enthusiastic assistance during our cruises. This work could not have been completed without the additional field assistance of Alexandra Ravelo, Tanja Schollmeier, and Martin Schuster. We thank Katrin Iken, Ken Coyle and Peter Winsor for comments on a previous version of this report. We thank the captains and crew of the R/V Alpha Helix, R/V Moana Wave and USCGC Healy for their dedication and effort at sea. Lastly, we thank all our field assistants and the rest of the COMIDA team for making this such a great group with which to work.

## 7. References

- Ambrose, W., Clough, L., Tilney, P., Beer, L., 2001. Role of echinoderms in benthic remineralization in Chukchi Sea. *Mar. Biol.* 139, 937-949.
- Anderson, P.J., 2000. Pandalid shrimp as indicators of ecosystem regime shift. *J. Northw. Atl. Fish Sci.* 27, 1-10.
- Arrigo, K.R., van Dijken, G.L., 2004. Annual cycles of sea ice and phytoplankton in Cape Bathurst polynya, southeastern Beaufort Sea, Canadian Arctic. *Geophys. Res. Lett.* DOI:10.1029/2003GL018978.
- Balazy, P., Kuklinski, P., Włodarska-Kowalczyk, M., Barnes, D., Kędra, M., Legeżyńska, J., Węślawski, J.M., 2015. Hermit crabs (*Pagurus* spp.) at their northernmost range: distribution, abundance and shell use in the European Arctic. *Polar Res.* Doi: <http://dx.doi.org/10.3402/polar.v34.21412>.
- Baldwin, R.J., Smith Jr., K.L., 2003. Temporal dynamics of particulate matter fluxes and sediment community response in Port Foster, Deception Island, Antarctica. *Deep-Sea Res. II.* 50, 1707-1725.
- Blanchard, A.L., Feder, H.M., 2014. Interactions of habitat complexity and environmental characteristics with macrobenthic community structure at multiple spatial scales in the northeastern Chukchi Sea. *Deep-Sea Res. II.* Doi: 10.1016/j.dsr2.2013.09.022.
- Blanchard, A.L., Parris, C.L., Knowlton, A.L., Wade, N.R., 2013a. Benthic ecology of the northeastern Chukchi Sea. Part II. Spatial variation of megafaunal community structure, 2009-2010. *Cont. Shelf Res.* 67, 67-76.
- Blanchard, A.L., Parris, C.L., Knowlton, A.L., Wade, N.R., 2013b. Benthic ecology of the northeastern Chukchi Sea. Part I. Environmental characteristics and macrofaunal community structure, 2008-2010. *Cont. Shelf Res.* 67, 52-66.
- Bluhm, B.A., MacDonald, I.R., Debenham, C., Iken, K., 2005. Macro- and megabenthic communities in the high Arctic Canada Basin: initial findings. *Polar Biol.* 28, 218-231.
- Bluhm, B.A., Iken, K., Hardy, S.M., Holladay, B.A., 2009. Community structure of epibenthic megafauna in the Chukchi Sea. *Aquat. Biol.* 7, 269-293.
- Bluhm, B.A., Piepenburg, D., von Juterzenka, K., 1998. Distribution, standing stock, growth, mortality, and production of *Strongylocentrotus pallidus* (Echinodermata: Echinoidea) in the northern Barents Sea. *Polar Biol.* 20, 325-334.
- Boos, K., Franke, H.D., 2004. Abundance and distribution of ophiuroids off Helgoland, German Bight (North Sea), in: Heinzeller, T., Nebelsick, J.H., (Eds.) *Echinoderms: Munchen.* Taylor

- & Francis Group plc, London, UK, pp 157-158.
- Clarke, K.R., Gorley, R.N., 2006. PRIMER v6: User manual/tutorial, in: PRIMER-E, Plymouth.
- Coachman, L.K., Aagaard, K., Tripp, R.B., 1975. Bering Strait: The regional physical oceanography. Seattle, Washington, USA. pp 111-131.
- Coachman, L.K., Barnes, C.A., 1963. The movement of Atlantic water in the Arctic Ocean. ANIA. Doi: <http://dx.doi.org/10.14430/arctic3517>.
- Conlan, K.E., Lenihan, H.S., Kvitek, R.G., Oliver, J.S., 1998. Ice scour disturbance to benthic communities in the Canadian high Arctic. *Mar. Ecol. Prog. Ser.* 166, 1-16.
- Conlan, K.E., Kvitek, R.G., 2005. Recolonization of soft-sediment ice scours on an exposed Arctic coast. *Mar. Ecol. Prog. Ser.* 286, 21-42.
- Cooper, L.W., Grebmeier, J.M., Larson, I.L., Egorov, V.G., Theodorakis, C., Kelly, H.P., Lovvorn, J.R., 2002. Seasonal variation in sedimentation of organic materials in the St. Lawrence Island polynya region, Bering Sea. *Mar. Ecol. Prog. Ser.* 226, 13-26.
- Day, R.H., Weingartner, T.J., Hopcroft, R.R., Aerts, A.M., Blanchard, A.L., Gall, A.E., Gallaway, B.J., Hannay, D.E., Holladay, B.A., Mathis, J.T., Norcross, B.L., Questel, J.M., Wisdom, S.S., 2013. The offshore northeastern Chukchi Sea, Alaska: A complex high-latitude ecosystem. *Cont. Shelf Res.* 67, 147-165.
- Dionne, M., Sainte-Marie, B., Bourget, E., Gilbert, D., 2003. Distribution and habitat selection of early benthic stages of snow crab *Chionoecetes opilio*. *Mar. Ecol. Prog. Ser.* 259, 117-128.
- Dunton, K.H., Goodall, J.L., Schonberg, S.V., Grebmeier, J.M., Maidment, D.R., 2005. Multi-decadal synthesis on benthic-pelagic coupling in the western Arctic: Role of cross-shelf advective processes. *Deep-Sea Res. II.* 52, 3462-3477.
- Ernst, B., Orensanz, J.M., Armstrong, D.A., 2005. Spatial dynamics of female snow crab (*Chionoecetes opilio*) in the eastern Bering Sea. *Can. J. Fish. Aquat. Sci.* 62, 250-268.
- Ernst, B., Armstrong, D.A., Burgos, J., Orensanz, J.M., 2012. Life history schedule and periodic recruitment of female snow crab (*Chionoecetes opilio*) in the eastern Bering Sea. *Can. J. Fish. Aquat. Sci.* 69, 532-550.
- Etter, R.J., Grassle, J.F., 1992. Patterns of species diversity in the deep sea as a function of sediment particle size diversity. *Nature.* 360, 576-578.
- Fay, F.H., 1982. Ecology and biology of the Pacific walrus, *Odobenus rosmarus divergens* Illiger. *N. Am. Fauna.* 74, 1-279.
- Feder, H.M., Naidu, A.S., Jewett, S.C., Hameedi, J.M., Johnson, W.R., Witledge, T.E., 1994. The northeastern Chukchi Sea: Benthos-environmental interactions. *Mar. Ecol. Prog. Ser.* 111, 171-190.
- Feder, H.M., Jewett, S.C., Blanchard, A., 2005. Southeastern Chukchi Sea (Alaska) epibenthos. *Polar Biol.* 28, 402-421.
- Fisher, G., Fütterer, D., Gersonde, R., Honjo, S., Ostermann, D., Wefer, G., 1988. Seasonal variability of particle flux in the Weddell Sea and its relation to ice cover. *Nature.* 335, 426-428.

- Fortier, M., Fortier, L., Michel, C., Legendre, L., 2002. Climatic and biological forcing of the vertical flux of biogenic particles under seasonal Arctic sea ice. *Mar. Ecol. Prog. Ser.* 225, 1-16.
- Gage, J., 1990. Skeletal growth bands in brittle stars: microstructure and significance as age markers. *J. Mar. Biol. Assoc. U.K.* 70, 209–224.
- Grebmeier, J.M., 1987. The ecology of benthic carbon cycling in the northern Bering and Chukchi Seas. PhD Thesis University of Alaska, Fairbanks.
- Grebmeier, J.M., Barry, J.P., 1991. The influence of oceanographic processes on pelagic-benthic coupling in polar regions: A benthic perspective. *J. Marine Syst.* 2, 495-518.
- Grebmeier, J.M., Cooper, L.W., 1995. Influence of the St. Lawrence Island Polynya upon the Bering Sea benthos. *J. Geophys. Res.-Oceans.* 100, 4439-4460.
- Grebmeier, J.M., Cooper, L.W., Feder, H.M., Sirenko, B.I., 2006. Ecosystem dynamics of the Pacific-influenced northern Bering and Chukchi Seas in the Amerasian Arctic. *Prog. Oceanogr.* 71, 331-361.
- Grebmeier, J.M., Feder, H.M., McRoy, C.P., 1989. Pelagic-benthic coupling on the shelf of the northern Bering and Chukchi Seas. II. Benthic community structure. *Mar. Ecol. Prog. Ser.* 51, 253-268.
- Grebmeier, J.M., McRoy, C.P., Feder, H.M., 1988. Pelagic-benthic coupling on the shelf of the northern Bering and Chukchi seas. 1. Food supply source and benthic biomass. *Mar. Ecol. Prog. Ser.* 48, 57-67.
- Groß, J., 2015. Variability in the size-frequency distribution and growth of snow crab (*Chionoecetes opilio*) and lyre crab (*Hyas coarctatus*) in the Chukchi Sea from 2009-2013. MS Thesis, University of Bremen.
- Groß, J., Konar, B., Grebmeier, J., Brey, T. this issue. Size-frequency distribution, growth, and mortality of snow crab (*Chionoecetes opilio*) and Lyre crab (*Hyas coarctatus*) in the Chukchi Sea from 2009-2013. *Deep-Sea Res. Pt II.*
- Gunderson, D.R., Ellis, I.E., 1986. Development of a plumb staff beam trawl for sampling demersal fauna. *Fish. Res.* 4, 35-41.
- Gutt, J., 2001. On the direct impact of ice on marine benthic communities, a review. *Polar Biol.* 24, 553-564.
- Haflinger, K., 1981. A survey of benthic infaunal communities of the southeastern Bering Sea, in: Hood, D.W., Calder, J.A., (Eds.) *The eastern Bering Sea shelf: Oceanography and resources*, Vol 2. Univ. Washington Press, Seattle, Washington, pp 1091-1104.
- Hare, S.R., Mantua, N.J., 2000. Empirical evidence for North Pacific regime shifts in 1977 and 1989. *Prog. Oceanogr.* 47, 103-145.
- Highsmith, R.C., Coyle, K.O., 1992. Productivity of Arctic amphipods relative to gray whale energy requirements. *Mar. Ecol. Prog. Ser.* 83, 141-150.
- Incze, L.S., Armstrong, D.A., Smith, S.L., 1987. Abundance of larval Tanner crabs (*Chionoecetes* spp.) in relation to adult females and regional oceanography of the southeastern Bering Sea. *Can. J. Fish. Aquat. Sci.* 44, 1143-1156.



- Jay, C.V., Fischbach, A.S., Kochnev, A.A., 2012. Walrus areas of use in the Chukchi Sea during sparse sea ice cover. *Mar. Ecol. Prog. Ser.* Doi: 10.3354/meps10057.
- Johannessen, O.M., Bengtsson, L., Miles, M.W., Kuzmina, A.I., Semenov, V.A., Alekseev, G.V., Nagurnya, A.P., Zakharov, V.F., Bobylev, L.P., Pettersson, L.H., Hasselmann, K., Cattle, H.P., 2004. Arctic climate change: Observed and modelled temperature and sea-ice variability. *Tellus A.* 56, 328-341.
- Konar, B., Ravelo, A., Grebmeier, J., Trefry, J.H., 2014. Size frequency distributions of key epibenthic organisms in the eastern Chukchi Sea and their correlations with environmental parameters. *Deep-Sea Res. Pt II.* 102, 107-118.
- Martin, S., Drucker, R., 2012. The effects of possible Taylor columns on the summer ice retreat in the Chukchi Sea. *J. Geophys. Res.* 102, 10473-10482.
- McMahon, K.W., Ambrose, W.G., Johnson, B.J., Sun, M., Lopez, G.R., Clough, L.M., Carroll, M.L., 2006. Benthic community response to ice algae and phytoplankton in Ny Alesund, Svalbard. *Mar. Ecol. Prog. Ser.* 310, 1-14.
- Moore, S.E., Huntington, H.P., 2008. Arctic marine mammals and climate change: Impacts and resilience. *Ecol. Appl.* 18, 157-165.
- Overland, J., Rodionov, S., Minobe, S., Bond, N., 2008. North Pacific regime shifts: Definitions, issues and recent transitions. *Prog. Oceanogr.* 77, 92-102.
- Parada, C., Armstrong, D.A., Ernst, B., Hinckley, S., Orensanz, J.M., 2010. Spatial dynamics of snow crab (*Chionoecetes opilio*) in the eastern Bering Sea – Putting together the pieces of the puzzle. *Bull. Mar. Sci.* 86, 413-437.
- Piepenburg, D., 2000. Arctic brittle stars (Echinodermata: Ophiuroidea), in: Gibson, R.N., Barnes, M., (Eds.), *Oceanography and marine biology: An annual review volume 38*. Taylor & Francis Inc., New York, NY, pp 189-256.
- Piepenburg, D., Blackburn, T.H., von Dorrien, C.F., Gutt, J., Hall, P.O.J., Hulth, S., Kendall, M.A., Opalinski, K.W., Rachor, E., Schmid, M.K., 1995. Partitioning of benthic community respiration in the Arctic (northwestern Barents Sea). *Mar. Ecol. Prog. Ser.* 118, 199-213.
- Piepenburg, D., 2006. The seafloor fauna in a changing Arctic – a review on its past, present, and future. *Polarforschung.* 75, 63-76.
- Piepenburg, D., Schmid, M.K., 1996. Brittle star fauna (Echinodermata: Ophiuroidea) of the Arctic northwestern Barents Sea: Composition, abundance, biomass, and spatial distribution. *Polar Biol.* 16: 383-392.
- Questel, J.M., Clarke, C., Hopcroft, R.R., 2013. Seasonal and interannual variation in the planktonic communities of the northeastern Chukchi Sea during the summer and early fall. *Cont. Shelf Res.* 67, 23-41.
- Ravelo, A.M., Konar, B., Trefry, J.H., Grebmeier, J.M., 2014. Epibenthic community variability in the northeastern Chukchi Sea. *Deep-Sea Res. Pt II.* Doi: 10.1016/j.dsr2.2013.07.017.
- Ruhl, H.A., 2007. Abundance and size distribution dynamics of abyssal epibenthic megafauna in the northeast Pacific. *Ecology.* 88, 1250-1262.
- Sanderson, T.J., 1988. Ice mechanics and risks to offshore structures. Graham and Trotman,

London.

- Schonberg S.V., Clarke, J.T., Dunton, K.H., 2014. Distribution, abundance, biomass, and diversity of benthic infauna in the northeast Chukchi Sea, Alaska: relation to environmental variables and marine mammals. *Deep Sea Res Pt II.* 102, 144-163.
- Semtner Jr., A.J., 1987. A numerical study of sea ice and ocean circulation in the Arctic. *J. Phys. Oceanogr.* 17, 1077-1099.
- Somerton, D.A., 1981a. Life history and population dynamics of two species of Tanner crab, *Chionoecetes bairdi* and *C. opilio*, in the eastern Bering Sea with implications for the management of the commercial harvest. PhD thesis, University of Washington, Seattle, Washington.
- Somerton, D.A., 1981b. Regional variation in the size at maturity of two species of Tanner Crab (*Chionoecetes bairdi* and *C. opilio*) in the eastern Bering Sea, and its use in defining management subareas. *Can. J. Fish. Aquat. Sci.* 38, 163-174.
- Springer, A.M., McRoy, C.P., 1993. The paradox of pelagic food webs in the northern Bering Sea-III. Patterns of primary production. *Cont. Shelf Res.* 13, 575-599.
- Stoker, S.W., 1981. Benthic invertebrate macrofauna of the eastern Bering/Chukchi continental shelf: oceanography and resources, Vol. 2. Univ. Washington Press, Seattle, Washington, pp 1069-1090.
- Stroeve, J., Holland, M.M., Meier, W., Scambos, T., Serreze, M., 2007. Arctic sea ice declines: Faster than forecast. *Geophys. Res. Lett.* Doi:10.1029/2007GL029703.
- Summers, A.C., Nybakken, J., 2000. Brittle star distribution patterns and population densities on the continental slope off central California (Echinodermata: Ophiuroidea). *Deep-Sea Res. Pt II.* 47, 1107-1137.
- Taghon, G.L., 1982. Optimal foraging by deposit-feeding invertebrates: Roles of particle size and organic coating. *Oecologia.* 52, 295-304.
- Tenore, K.R., 1988. Nitrogen in benthic food chains, in: Blackburn, T.H., Sørensen, J., (Eds.), Nitrogen cycling in coastal marine environment. John Wiley & Sons Ltd, pp 191-206.
- Walsh, J.E., 1978. Temporal and spatial scales of the Arctic circulation. *Mon. Weather Rev.* 106, 1532-1544.
- Wassmann, P., 1991. Dynamics of primary production and sedimentation in shallow fjords and pols of western Norway. *Oceanogr. Mar. Biol.* 29, 87-154.
- Wassmann, P., Slagstad, D., Riser, C.W., Reigstad, M., 2006. Modelling the ecosystem dynamics of the Barents Sea including the marginal ice zone: II. Carbon flux and interannual variability. *J. Mar. Sys.* 59, 1-24.
- Weingartner, T., Aagaard, K., Woodgate, R., Danielson, S., Sasaki, Y., Cavalieri, D., 2005. Circulation on the north central Chukchi Sea shelf. *Deep-Sea Res. II.* 52, 3150-3174.
- Weingartner, T.J., Cavalieri, D.J., Aagaard, K., Sasaki, Y., 1998. Circulation, dense water formation, and outflow on the northeast Chukchi shelf. *J. Geophys. Res. – Oceans.* 103, 7647-7661.
- Weingartner, T., Dobbins, E., Danielson, S., Winsor, P., Potter, R., Statscewich, H., 2013.

Hydrographic variability over the northeastern Chukchi Sea shelf in summer-fall 2008-2010. *Cont. Shelf Res.* 67, 5-22.

White, M.G., 1977. Ecological adaptations by Antarctic poikilotherms to the polar marine environment, in: Liano, G.A., (Ed.) *Adaptations within Antarctic ecosystems*. Gulf Publishing Co, Houston, pp 197-208.

White, D., Kimerling, J.A., Overton, S.W., 1992. Cartographic and geometric components of a global sampling design for environmental monitoring. *Cart. Geogr. Inform.* 19, 5-22.

Williams, J.D., McDermott, J.J., 2004. Hermit crab biocoenoses: A worldwide review of the diversity and natural history of hermit crab associates. *J. Exp. Mar. Biol. Ecol.* 305, 1-128.

Winsor, P., Chapman, D.C., 2002. Distribution and interannual variability of dense water production from coastal polynyas on the Chukchi Shelf. *J. Geophys. Res.-Oceans*. Doi: 10.1029/2001JC000984.

Woodgate, R.A., Weingartner, T.J., Lindsay, R., 2012. Observed increases in Bering Strait oceanic fluxes from the Pacific to the Arctic from 2001 to 2011 and their impacts on the Arctic Ocean water column. *Geophys. Res. Lett.* Doi: 10.1029/2012GL054092.

# Size-frequency Distribution, Growth, and Mortality of snow crab (*Chionoecetes opilio*) and Arctic Lyre Crab (*Hyas coarctatus*) in the Chukchi Sea from 2009 to 2013

Jasmin Groß<sup>a</sup>, Brenda Konar<sup>a</sup>, Thomas Brey<sup>b</sup>, Jacqueline M. Grebmeier<sup>c</sup>

<sup>a</sup>School of Fisheries and Ocean Sciences, University of Alaska Fairbanks, Fairbanks, AK 99775, USA

<sup>b</sup>Alfred-Wegner-Institute, Helmholtz-Centre for Polar and Marine Research, Bremerhaven, D-27570

<sup>c</sup>Chesapeake Biological Laboratory, University of Maryland Center for Environmental Science, Solomons, MD 20688, USA

[jasmin4689@me.com](mailto:jasmin4689@me.com)

## Abstract

The snow crab *Chionoecetes opilio* and Arctic lyre crab *Hyas coarctatus* are prominent members of the Chukchi Sea epifaunal community. A better understanding of their life history will aid in determining their role in this ecosystem in light of the changing climate and resource development. In this study, the size frequency distribution, growth, and mortality of these two crab species was examined in 2009, 2010, 2012, and 2013 to determine temporal and spatial patterns within the eastern Chukchi Sea, and to identify potential environmental drivers of the observed patterns. Temporally, the mean size of both sexes of *C. opilio* and *H. coarctatus* decreased significantly from 2009 to 2013, with the number of rare maximum sized organisms decreasing significantly to near absence in the latter two study years. Spatially, the mean size of male and female crabs of both species showed a latitudinal trend, decreasing from south to north in the investigation area. Growth of both sexes of *C. opilio* and *H. coarctatus* was linear over the sampled size range, and mortality was highest in the latter two study years. Life history features of both species related to different environmental parameters in different years, ranging from temperature, the sediment carbon to nitrogen ratio of the organic content, and sediment grain size distribution. Plausible explanations for the observed temporal and spatial variability are ontogenetic migrations of mature crabs to warmer areas possibly due to cooler water temperatures in the latter two study years, or interannual fluctuations, which have been reported for *C. opilio* populations in other areas where successful waves of recruitment were estimated to occur in eight year intervals. Further research is suggested to determine if the spatial and temporal patterns found in this study are part of the natural variability in this system or if they are an indication of long-term trends.

**Keywords:** Crustacea, Decapoda, temporal variability, spatial variability, latitudinal cline, benthos, environmental variables

## 1. Introduction

Epibenthic organisms dominate the lower trophic-level benthic standing stock in the Chukchi Sea with crustaceans being one of the most abundant taxa (Bluhm et al., 2009; Feder et al., 2005). As highly mobile organisms, crustaceans contribute to the redistribution and remineralisation of organic carbon that falls to the sea floor (Lovrich et al., 1995; Piepenburg et al., 1997). They are one of the main predators in the benthic community, and they also contribute to total benthic energy turnover by providing an important prey base for higher trophic levels such as demersal fish and benthic feeding marine mammals (Frost and Lowry, 1983; Jewett and Feder, 1981).

In the Chukchi Sea, the snow crab *Chionoecetes opilio* (O. Fabricius, 1788) can be one of the most abundant benthic taxa, with the Arctic lyre crab *Hyas coarctatus* (Leach, 1816) also being fairly abundant (Bluhm et al., 2009; Ravelo et al., 2014). Both species have a boreal-arctic range distribution around North America (Alvsvåg et al., 2009; Bluhm et al., 2009; Bryant, 1991; Comeau et al., 1998; Rand and Logerwell, 2011). They are found over a wide depth range, with *C. opilio* occurring between 30-1400 m water depth at year round bottom water temperatures of -1.5 to 4°C (Dawe and Colbourne, 2002), and *H. coarctatus* occurring between 2 and 457 m water depth and a similar temperature range as *C. opilio* (Bryant, 1991). Both species are found on muddy or sandy grounds, and are carnivorous, cannibalistic and opportunistic feeders, preying on gastropods, ophiuroids, crustaceans, bivalves and polychaetes (Bryant, 1991; Dawe and Colbourne, 2002; Ernst et al., 2005; Kolts et al., 2013; Wiczorek and Hooper, 1995).

While *H. coarctatus* is not economically important, *C. opilio* is one of the most important commercially fished crab species in the North Atlantic and Pacific (Bailey and Elner, 1989; Lanteigne et al., 1996). Heavy exploitation of male *C. opilio* occurs in Atlantic Canada, Alaska, and the Sea of Japan. The U.S. fishery is constrained to the eastern Bering Sea (EBS) but it is the most valuable crab fishery in the country with over \$155 million ex-vessel value (Bailey and Elner, 1989; NPFMC, 2010). The EBS fishery is managed as one continuous population with a legal fisheries size of 78 mm carapace width (CW) (NPFMC, 2010). All *C. opilio* fisheries are male-only fisheries to protect the reproductive potential of the stock, with the minimum legal catch limit set to a size that females do not reach (Comeau et al., 1998; Sainte-Marie and Gilbert, 1998; Sainte-Marie et al., 2008). Snow crab fisheries in all regions have exhibited great fluctuations over time due to highly variable recruitment with alternating strong and weak cohorts (Ernst et al., 2012). The observed fluctuations in the *C. opilio* fisheries have caused debates whether this temporal variability is regulated by bottom-up or top-down controls (Émond et al., 2015). It is suggested that bottom-up processes related to climate variability may strongly influence the survival of early benthic life stages, as *C. opilio* is a cold-stenothermic species (Dionne et al., 2003; Émond et al., 2015). As a top-down control, predation pressure by cod, the main vertebrate predator of *C. opilio*, can also be a major source of juvenile mortality (Orensanz et al., 2004). Even though multiple explanations for temporal recruitment variability have been suggested, its causes remain unknown (Émond et al., 2015). Along with temporal variability, spatial variability has been observed along a latitudinal cline in the Bering Sea and the Gulf of St. Lawrence, with *C. opilio* size decreasing with increasing latitude (Ernst et al., 2005; Sainte-Marie and Gilbert, 1998). This finding seems to be directly related to lower bottom water temperatures or an environmental covariate (Burmeister and Sainte-Marie, 2010; Somerton, 1981).

Both, *C. opilio* and *H. coarctatus* have a lifecycle that is marked by a pelagic larval phase after hatching, and various juvenile benthic stages. The larvae of *C. opilio* and *H. coarctatus* are pelagic for several months before settling to the seafloor, facilitating potentially long larval dispersal distances, which would allow genetic mixing between distant populations (Bryant, 1991; Puebla et al., 2008). Once the larvae settle to the seafloor, there are three described allometric (defined by CW) and gonad maturity stages (aka, morphology description): (1) immature ( $\leq 34$  mm CW), (2) adolescent ( $> 34$  mm CW with non-differentiated claw), and (3) mature ( $> 40$  mm CW, males with differentiated claw) (Conan et al., 1992). In all crustaceans, somatic growth is discrete and occurs as a series of moults separated by intermoult periods called instars. Moulting increments decrease in frequency after the puberty moult and moulting occurs at most once a year from instar VI onwards, which is similar for both sexes (Bryant, 1991; Comeau et al., 1998; Sainte-Marie et al., 1995). However, it was noticed that the size increment and growth pattern of *C. opilio* males and females differ after instar VII (Comeau et al., 1998). The moult to maturity, or terminal moult is present in both species but combining male-female spawning indices can be problematic because females mature at a substantially smaller mean size than males, causing variation in male and female spawning biomasses. The size at terminal moult varies for *C. opilio* within and among populations (Bailey and Elner, 1989; Bryant, 1991; Sainte-Marie et al., 1995, 2008).

Estimating the age and growth of crustaceans is extremely difficult because crustaceans periodically cast off their rigid, calcareous exoskeleton, leaving no recognizable aging structures such as growth rings (Hartnoll, 1982; Watson, 1969). Growth is not continuous but discrete and biphasic as it is limited to brief moulting events (Hartnoll, 1982). This finding means that the most frequently used measure of growth, CW, is a discontinuous function over time (Fisher, 1999; Welch and Epifanio, 1995). There are various means to study crustacean growth but size frequency distributions (SFD) are often used to make inferences about growth, and also age, physiology, survival/mortality, competitive ability, reproductive status, market value of commercial crabs, and population productivity (Bluhm et al., 2009; Brey, 2001; Calder, 1984). However, uncertainty in the estimation of crustacean growth parameters is introduced by the absence of permanent hard exoskeletons, the use of laboratory grown individuals, the margin of error in detecting modes from SFD, and also intrinsic factors such as moult cycles, synchronisation between moulting and reproduction, and size-related growth rates (Company and Sarda, 2000). Nevertheless, somatic growth is one of the most easily measured responses of organisms to environmental conditions because it is influenced by temperature, food availability and quality, water chemistry, biotic factors such as competition or diseases, and environmental stressors such as pollutants (Teissier, 1960). Specifically, temperature and food availability impact growth, and hence body size of invertebrates (MacDonald and Thompson, 1985). In the Chukchi Sea, many studies have shown that environmental drivers are important in structuring the epibenthic community abundance and biomass (Bluhm et al., 2009; Feder et al., 2005; Hardy et al., 2011), but only a few have shown how the same drivers may affect the SFD of these organisms (Konar et al., 2014).

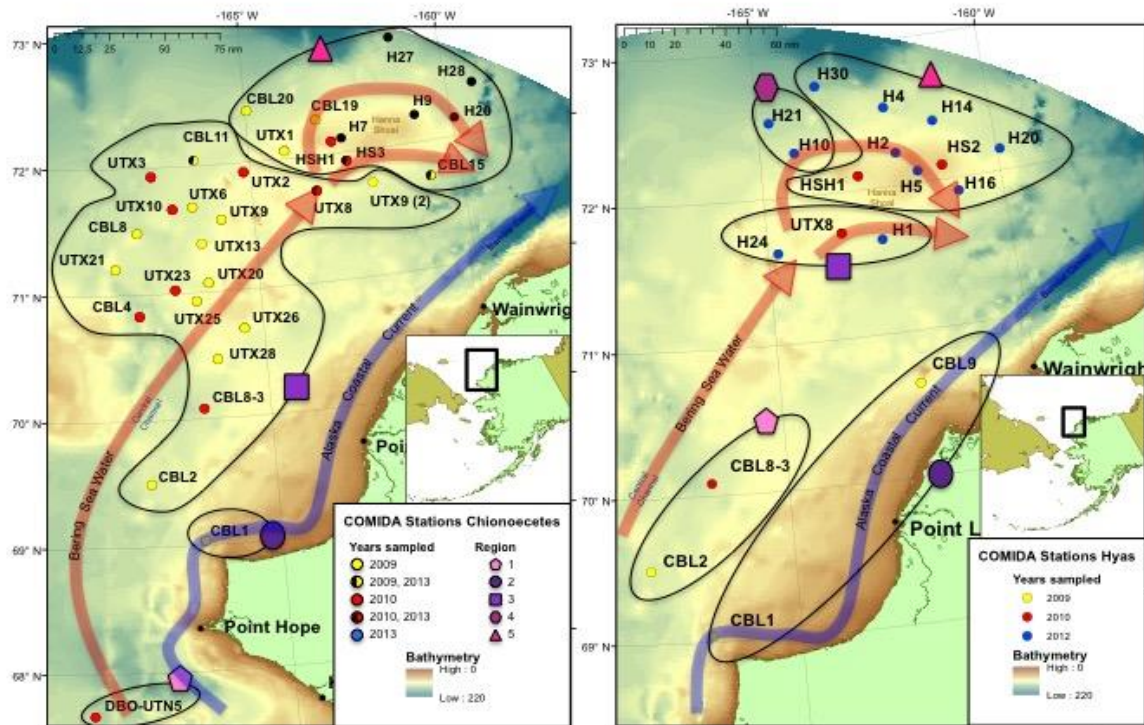
To manage crustaceans in the Chukchi Sea, it is important to understand their size distribution and growth, especially as increasing human activity in the Chukchi Sea and global climate change have raised concerns that the stability of the epibenthic community might be negatively impacted (Bluhm et al., 2009; Grebmeier, 2012; Piepenburg, 2005). The objectives of this study were to determine the SFD, growth and mortality of both sexes of *C. opilio* and *H. coarctatus* per

year and region to determine temporal and spatial trends within the eastern Chukchi Sea, and to identify environmental drivers that explain the observed patterns of these SFD. Three specific hypotheses were formulated based on pre-existing knowledge. As growth and size-at-maturity differ between male and female crabs during later life stages in some areas, it was hypothesized that the size frequency distribution of male and female *C. opilio* and *H. coarctatus* would differ significantly from each other in the Chukchi Sea. On the basis of known temporal variation in *C. opilio* fisheries in the Bering Sea and the Gulf of St. Lawrence, it was also hypothesized that there would be significant interannual variability in the SFD of *C. opilio* and *H. coarctatus* on the Chukchi Sea shelf, and that this variability would be explained by changing environmental parameters, specifically bottom water temperature, sediment total organic carbon content, sediment carbon to nitrogen ratio, and sediment chlorophyll *a* content.

## 2. Materials and Methods

### 2.1. Study Site

Crabs and environmental data were collected from 71 stations sampled in the northeast Chukchi Sea (67°N to 72°N, 168°W to 157°W) during four summer cruises (July/August in 2009, 2010, 2012 and 2013) as part of the Chukchi Sea Offshore Monitoring in Drilling Area (COMIDA) Chemical and Benthos (CAB) and COMIDA Hanna Shoal projects. For this study, size frequency distributions (SFD) were determined for *C. opilio* and *H. coarctatus* from 32 and 18 stations, respectively, over the 4 cruises (Figure 1). These 50 stations were chosen because their sample sizes were large enough ( $n=42$  for *C. opilio*,  $n=20$  for *H. coarctatus*) to create sensible SFD. In 2012, *C. opilio* and in 2013, *H. coarctatus*, were not abundant enough at any stations so these years were left out of the analysis of the respective species. Sites used in these analyses ranged in water depth from 28 m to 65 m. The 2009 and 2010 cruises covered a broad spatial area, while the 2012 and 2013 cruises focused on the northeast Chukchi Sea around Hanna Shoal (Figure 1). Two methods were used for the selection of sampling sites to ensure that sites were randomly distributed. The first sites were chosen with a general randomised tessellation stratified design (GRTS) in GIS, while the other sites were spatially oriented, nearshore to offshore, on a south to north grid that overlaid the GRTS design. For the spatial analysis, stations were grouped into regions based on the prevailing currents in the sampling area (Figure 1). Two major currents influence the northeast Chukchi Sea: the Alaska Coastal Current (ACC) and the Bering Sea Water (BSW) (Weingartner et al., 2005, 2013). The ACC flows northward along the coast of Alaska and is characterised by warm, low salinity water with a low nutrient content (Weingartner et al., 2005; Figure 1). The BSW flows through the Central Channel and is characterised by cold, high salinity water with a high nutrient content (Weingartner et al., 2005; Figure 1). It continues to Hanna Shoal in a slow flow, displaces the cold, saline winter waters that form during the ice-covered season and merges with the ACC close to Barrow Canyon (Weingartner et al., 2005, 2013). Region 1 is the most southern region, influenced by BSW that comes through the Bering Strait. Region 2 includes the coastal stations, influenced by the ACC (Figure 1). Regions 3 and 4 include the furthest offshore stations influenced by the BSW that flows through the Central Channel and along the western side of Hanna Shoal. Region 3 also includes stations influenced by the slow flowing BSW south of Hanna Shoal. Region 5 is the most northern region, influenced by BSW flowing around northern Hanna Shoal (Figure 1).



**Figure 1.** Map displaying the stations that were used for the analyses of the size frequency distribution of *Chionoectes opilio* (left) and *Hyas coarctatus* (right) in the years 2009, 2010, 2012 and 2013. Stations allocated to a specific region are encircled with a black line, and the attached symbol indicates the region number.

## 2.2. Sampling technique

### 2.2.1. Epibenthic sampling

The epibenthos was sampled with a 3.05 m plumb-staff beam trawl with a 7 mm mesh and a 4 mm codend liner, which was modified with lead-filled line and 15 cm sections of chain seized to the footrope every 15 cm. The net was deployed at an average vessel speed of 1.5 knots, with an average bottom time of 2.5 minutes depending on the relative epibenthic density, which was determined by a drop video camera (LW Cooper, personal communication). The mouth of the net was held open with a rigid 3 m pipe allowing an effective swath of 2.26 m. The vertical net opening was 1.2 m wide and catch weight ranged between 40 and 100 kg. It has to be noted that early settlement cohorts are probably not adequately represented using this mesh size because small individuals (<7 mm) are excluded from sampling with the occasional exception of smaller individuals found in the mud that accumulated in the net.

Each trawl catch was sieved over 4 mm mesh to remove sediments. Crabs were sorted by species and sex and then counted, weighed, and carapace size was measured to the nearest millimetre using calipers. In 2009 and 2010, the carapace length was measured and converted to carapace width. In 2012, carapace length and width were measured to establish a conversion factor



between carapace length and width. In 2013, only carapace width was measured to ensure standardization with literature data where carapace width is commonly reported. For each data point, carapace width was divided by the corresponding carapace length. The average of all data points was used as the conversion factor as there was no significant difference in conversion factor between the different size classes, which was determined through a regression analysis (Groß, 2015).

### 2.2.2. Environmental analysis

Parameters that have been reported as influential to the epibenthic community structure in the Chukchi Sea (Ravelo et al., 2014) were measured at each station and in each year. Water temperature (°C), pH, salinity, and dissolved oxygen ( $\text{mg L}^{-1}$ ) were measured as a continuous vertical profile using a YSI Sonde 6600V2-4 (Yellow Springs, Ohio, USA) but only bottom water parameters were used in the analysis. A  $0.1 \text{ m}^2$  van Veen grab was used to collect surface sediment to determine total organic carbon (TOC, %), total organic nitrogen (TON, %), the carbon to nitrogen (C/N) ratio, sediment chlorophyll *a* (sed chl *a*,  $\text{mg m}^{-2}$ ), and sediment grain size (% phi size).

## 2.3. Data Analysis

The size frequency distributions (SFD) were generated in Excel by station and region, and transposed onto ArcGIS maps. The regional SFD were standardized to relative proportions because of unequal station numbers among regions. The size frequency data for both species were square root transformed to normalise the spread of the data around its mean for multivariate analysis. To determine differences among years, region, and between sex, a three-factor mixed model permutational analysis of variance (PERMANOVA) was run in PRIMER v.6 package based on a Bray Curtis resemblance matrix. Year, region and sex were treated as fixed factors. A pairwise comparison of means was calculated at a 0.05 significance level for all years and regions. Differences of maximum sizes among years of males and females of both species were determined by comparing the average maximum size of the highest percentile (10% largest individuals) with a one-way analysis of variance (ANOVA) in R. A Tukey's HSD post hoc test was performed in R for significant results of the one-way ANOVA at a 0.05 significance level.

The environmental data collected in all four years were normalized and a Euclidean distance resemblance matrix was created. Based on this matrix, the Distance Based Linear Model (DistLM) routine in PRIMER was used to establish which environmental variables best correlated with the SFD of both species. Latitude (°W), longitude (°N) and depth (m) were used as indirect determinants, while sed chl *a*, TOC, TON, and the C/N ratio were used as indicators of food supply and quality. Also included in the analysis were salinity, temperature, dissolved oxygen, pH, and sediment grain size. Correlating environmental variables (conductivity, oxygen saturation) were excluded from the analysis based on a Draftsman's plot, and when necessary, variables were log or square root transformed.

Size-at-age data (SAD), adapted from Comeau et al. (1998) for *C. opilio*, were used to determine a growth function as it was not possible to determine age from the data sampled in this study. SAD for *H. coarctatus* were also adapted from Comeau et al. (1998), as there is no published SAD for *H. coarctatus* covering the same size range that was recorded in this study. Growth of males and females of both species was linear for the size range recorded in this study, which is not necessarily true for sizes beyond the sampled range. The data were fitted with adequate

precision to a linear growth model using the equation:  $S_t = a + b \times t$ , where  $S_t$  is the size at time  $t$ ,  $a$  is the intercept of the linear growth function,  $b$  is the slope of the linear growth function, and  $t$  is time. An analysis of covariance (ANCOVA) was performed in R to determine if growth differed significantly between males and females of both species. Sex was treated as the categorical variable, age as the covariate, and size as the dependent variable. The type III sum of squares was calculated, as the design was unbalanced. The analysis was run with and without the interaction term, and an ANOVA was used to compare which statistical design was more appropriate. Mortality was determined using a numbers versus age curve, where the basic model consists of a plot of the natural logarithm of the number of crabs caught in various age groups against their corresponding age groups. The natural logarithm of the frequency of all data points of the descending right arm of the numbers versus age curve was calculated. The natural logarithm of the frequency of all data points was plotted against age, and a linear trendline was fitted to the scatter for 2009, 2010 and 2013 for *C. opilio*, and 2009, 2010 and 2012 for *H. coarctatus*. The following equation was used to determine mortality from the resulting linear equation of the trendline:  $Z = -b$ , where  $Z$  is the instantaneous total mortality coefficient, which in this case is equal to natural mortality as *C. opilio* and *H. coarctatus* are not commercially fished in the Chukchi Sea, and  $b$  is the slope of the linear trendline. An ANCOVA was also performed for this model, with year as the categorical variable, age as the covariate and the natural logarithm of frequency as the dependent variable. The type III sum of squares was calculated here as well, because the design was unbalanced. The analysis was also run with and without the interaction term, and an ANOVA was used to determine which design was more appropriate.

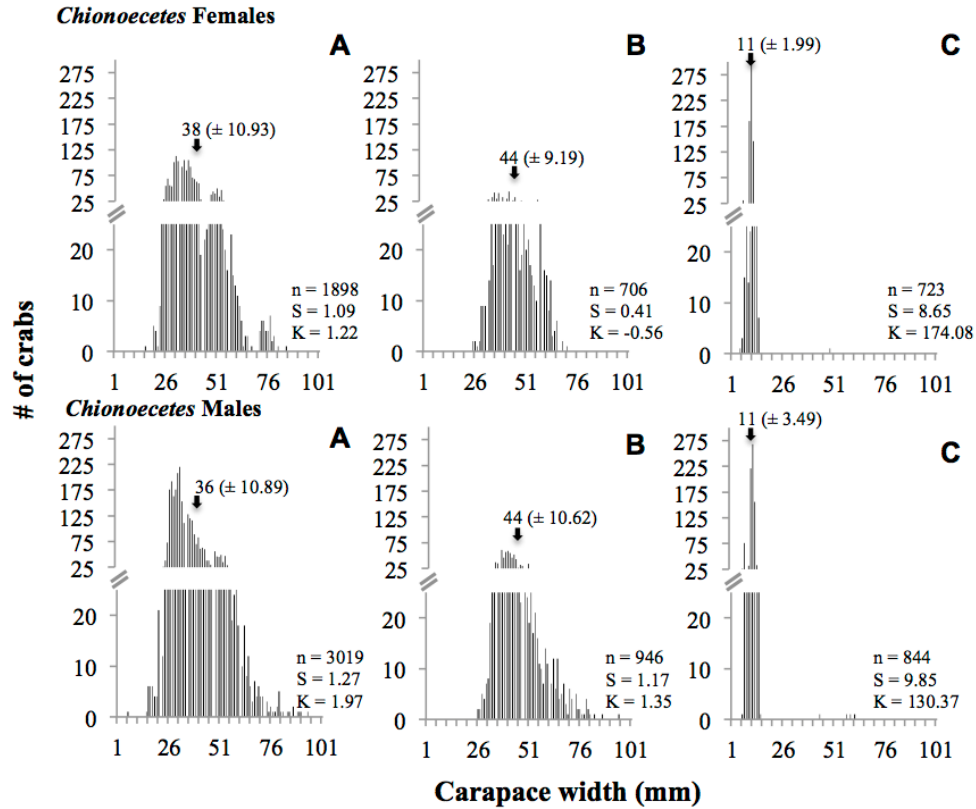
### 3. Results

The snow crab *C. opilio* was found at more sampling stations and was more abundant in all sampling years than the Arctic lyre crab *H. coarctatus* (Figures 1, 2 and 3). Female crabs of both species were consistently less abundant than male crabs, with the male crabs also reaching larger maximum sizes than the females (Figures 2 and 3). However, female crabs had equal or larger mean sizes in all years with the exception that for *H. coarctatus*, females had a smaller mean size ( $44 \pm 11.05$  mm) than males in 2009 ( $51 \pm 23.28$  mm; Figures 2 and 3). The largest *C. opilio* male was 94 mm while the largest female was 84 mm. The largest *H. coarctatus* male was 115 mm while the largest female was 76 mm (Figures 2 and 3). These maximum sized specimens were all caught in the first sampling year (2009), except the male *C. opilio*, which was caught in 2010 (Figures 2 A, B and 3 A). The decrease in maximum size was not gradual for both sexes of *C. opilio*, as the average size of the highest percentile increased from 60 mm in 2009 to 67 mm and 61 mm in 2010 for males and females, respectively. It then dropped to 14 mm and 13 mm in 2013 for males and females, respectively (Table 1). The average maximum size of the highest percentile of both sexes of *H. coarctatus* decreased from 101 mm and 64 mm in 2009 to 33 mm and 32 mm for males and females, respectively (Table 1). The average maximum size of the highest percentile of male and female crabs of both species differed significantly among years (ANOVA, *C. opilio* male:  $F_2 = 1276.3$ ,  $p < 2.2e-16$ ; *C. opilio* female:  $F_2 = 1618.9$ ,  $p < 2.2e-16$ ; *H. coarctatus* male:  $F_2 = 456.49$ ,  $p < 2.2e-16$ ; *H. coarctatus* female:  $F_2 = 137.77$ ,  $p < 2.2e-16$ ). A pairwise comparison showed that the maximum size of both species of male crabs differed significantly among all years, but that for females, *C. opilio* were only significantly different between 2009 and 2013, and 2010 and 2013, and *H. coarctatus* between 2009 and 2012, and

2010 and 2012 (Tukey's HSD,  $p < 0.05$ ; Table 2). The SFD of male and female *H. coarctatus* differed significantly (PERMANOVA, Pseudo- $F_1 = 4.35$ ,  $p = 0.0001$ ), in contrast to male and female *C. opilio*, which did not differ significantly in their SFD (PERMANOVA, Pseudo  $F_1 = 1.29$ ,  $p = 0.2202$ ; Table 3). However, the interaction term between year and sex was significant for both species (PERMANOVA, *C. opilio*: Pseudo- $F_2 = 1.64$ ,  $p = 0.0485$ ; *H. coarctatus*: Pseudo- $F_2 = 1.76$ ,  $p = 0.0549$ ; Table 3). A pairwise comparison showed that the interaction between year and sex was significant for *C. opilio* in 2010 while it was significant for *H. coarctatus* in 2012, meaning that the hypothesis that the size frequency distribution of male and female snow and Arctic lyre crab would differ significantly from each other in the Chukchi Sea was not fully supported as they did not differ significantly from one another in each year sampled (Pairwise comparison,  $p < 0.05$ ; Table 4).

**Table 1.** Table displaying the average maximum size (Max) of the highest percentile (10% largest individuals), sample number (n) and standard deviation (SD) for males and females of both sexes.

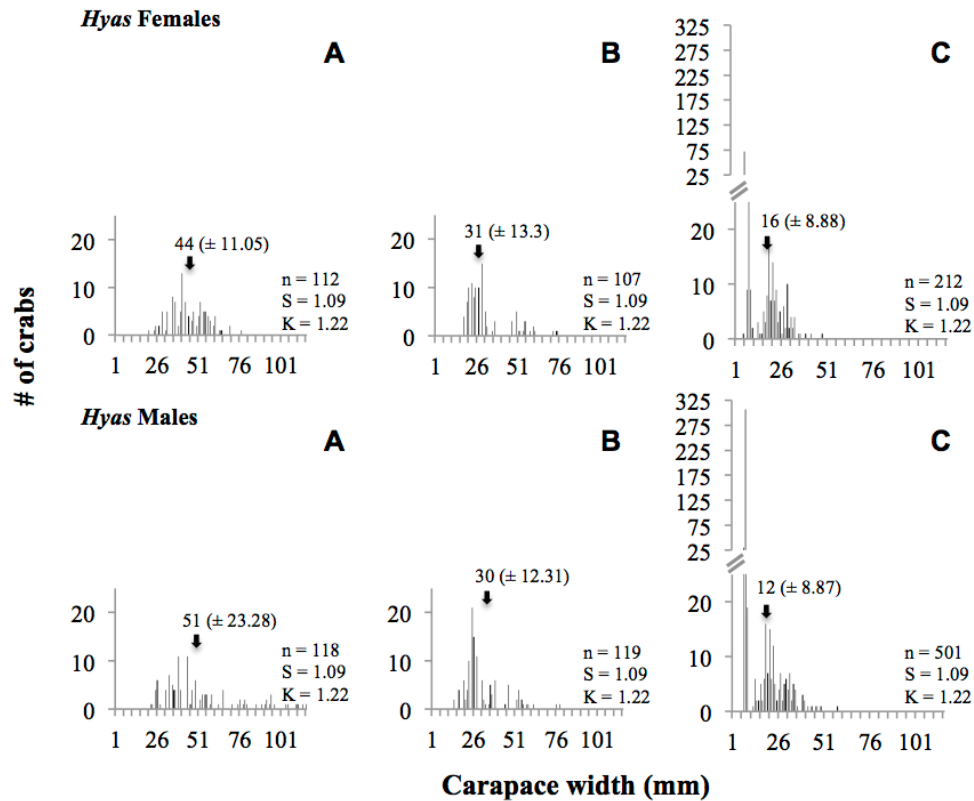
Year	<u><i>Chionoecetes opilio</i></u>						<u><i>Hyas coarctatus</i></u>					
	Female			Male			Female			Male		
	n	Max	SD	n	Max	SD	n	Max	SD	n	Max	SD
<b>2009</b>	190	60	7.82	302	60	7.84	11	64	5.54	12	101	8.7
<b>2010</b>	71	61	2.51	95	67	6.7	11	61	8.05	12	58	8.76
<b>2012</b>	-	-	-	-	-	-	21	32	4.77	50	33	6.29
<b>2013</b>	72	13	4.24	84	14	9.09	-	-	-	-	-	-



**Figure 2.** The combined size frequency distribution of *Chionoecetes opilio* females (top) and males (bottom) from 2009 (A), 2010 (B) and 2013 (C). Arrows indicate the mean with the standard deviation in brackets. n = sample size, S = Skewness, K = Kurtosis.

**Table 2.** Tukey's HSD results comparing the average maximum size of the highest percentile for both species, *Chionoecetes opilio* and *Hyas coarctatus*, among all possible pairs of the factor year, showing the p-values with a significance level of  $\alpha=0.05$  (\* denotes significant results). The dash (-) indicates that values were not calculated.

Year	<i>Chionoecetes opilio</i>		<i>Hyas coarctatus</i>	
	Female	Male	Female	Male
2009, 2010	0.5379	< 0.0001*	0.5115	< 0.0001*
2009, 2012	-	-	< 0.0001*	< 0.0001*
2009, 2013	< 0.0001*	< 0.0001*	-	-
2010, 2012	-	-	< 0.0001*	< 0.0001*
2010, 2013	< 0.0001*	< 0.0001*	-	-



**Figure 3.** The combined size frequency distribution of *Hyas coarctatus* females (top) and males (bottom) from 2009 (A), 2010 (B) and 2012 (C). Arrows indicate the mean with the standard deviation in brackets.  $n$  = sample size,  $S$  = Skewness,  $K$  = Kurtosis.

**Table 3.** PERMANOVA results for both species, *Chionoecetes opilio* and *Hyas coarctatus*, showing the Pseudo-F statistic with corresponding degrees of freedom (df) and p-values with a significance level of  $\alpha = 0.05$  (\* denotes significant results).

Factor	<i>Chionoecetes opilio</i>			<i>Hyas coarctatus</i>		
	Pseudo-F	df	p-value	Pseudo-F	df	p-value
Year	38.689	2	0.0001*	4.0384	2	0.0007*
Region	2.6466	3	0.0029*	1.7409	4	0.0262*
Sex	1.2909	1	0.2202	4.3516	1	0.0001*
Year x Region	1.4196	2	0.12	1.532	1	0.16
Year x Sex	1.6352	2	0.0485*	1.763	2	0.0549*
Region x Sex	1.1931	3	0.2378	0.7318	4	0.8346
Year x Region x Sex	1.2583	2	0.1946	0.29412	1	0.9617

### 3.1. Temporal comparison

A decrease in size was observed for both species throughout the sampling time. Mean size of female *C. opilio* decreased from 38 ( $\pm 10.93$ ) mm in 2009 to 11 ( $\pm 1.99$ ) mm in 2013, and males decreased from 36 ( $\pm 10.89$ ) mm in 2009 to 11 ( $\pm 3.49$ ) mm in 2013 (Figure 3) with a total absence of sizes above 48 mm for females and 60 mm for males (Figure 2). The standard deviation in 2013 was much smaller than in 2009 and 2010, indicating that the spread around the mean was much greater in 2009 and 2010 (Figure 2). The mean size of *H. coarctatus* females decreased from 44 ( $\pm 11.05$ ) mm in 2009 to 16 ( $\pm 8.88$ ) mm in 2012, while males decreased from 51 ( $\pm 23.28$ ) mm in 2009 to 12 ( $\pm 8.87$ ) mm in 2012 (Figure 3). The SFD of both males and females were widely spread around the mean in 2009 and 2010, while the standard deviation was lower in 2012 (Figure 3). The hypothesis that there would be significant interannual variability in the SFD of snow and Arctic lyre crabs was only partially supported by the data. The difference in size was significant among years for both species (PERMANOVA, *C. opilio*: Pseudo- $F_2 = 38.69$ ,  $p = 0.0001$ ; *H. coarctatus*: Pseudo- $F_2 = 4.04$ ,  $p = 0.0007$ ; Table 3) but a pairwise comparison showed that *C. opilio* differed significantly in size among all years while *H. coarctatus* only differed significantly in size between 2010 and 2012 (Pairwise comparison,  $p < 0.05$ ; Table 4). The SFD of both species were asymmetrically distributed and right skewed. The SFD of the males of both species were more highly skewed than females (Figures 2 and 3). Skewedness was most pronounced for male and female *C. opilio* in 2013 (females: 8.65, males: 9.85), while skewedness for *H. coarctatus* males was most pronounced in 2012 (1.84) and for females in 2010 (1.57). Kurtosis was mostly positive with exceptions for the SFD of female *C. opilio* in 2010 (-0.56) and female *H. coarctatus* in 2009 (-0.24) and 2012 (-0.32). Kurtosis for the SFD of males of both species was more positive than the SFD of the females (Figures 2 and 3).

### 3.2. Spatial comparison

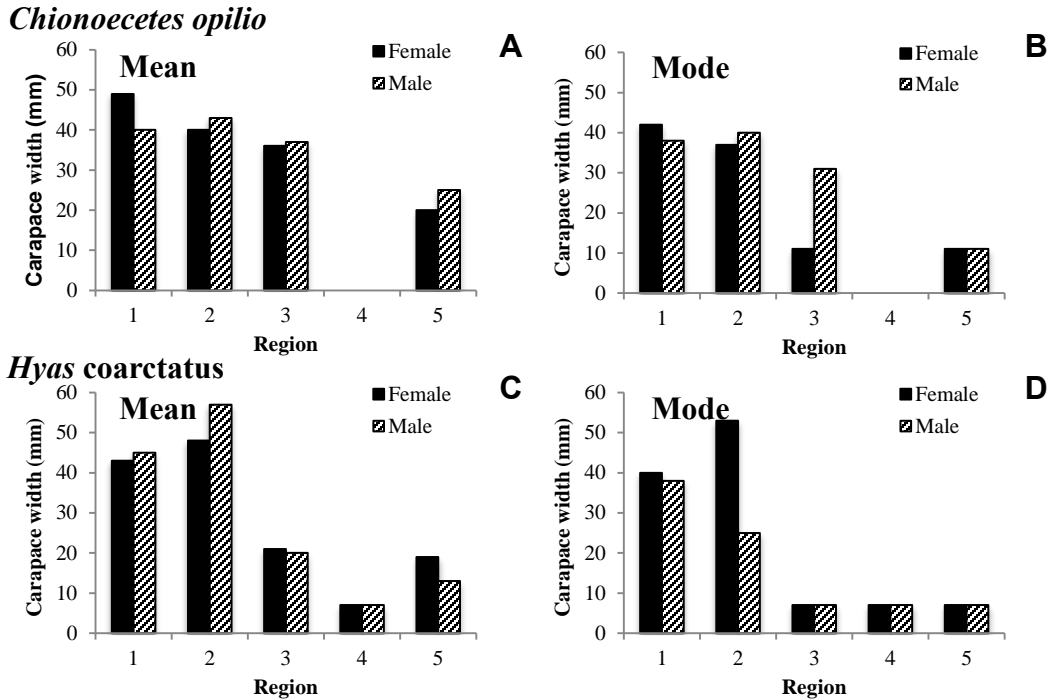
To observe spatial trends, the SFD data of all stations across years were combined by region. The mean size of *C. opilio* females showed a clear trend of decreasing mean size from south (region 1) to north (region 5). The same decreasing trend was observed for the mode of each region, with regions 3 and 5 having equal modes (Figure 4). This decreasing trend was not as pronounced for *C. opilio* males, as a peak in mean size was present in region 2, which was closest to the coast. The mode of each region of *C. opilio* males showed the same pattern as the mean (Figure 4). The SFD differed significantly among regions (PERMANOVA, Pseudo- $F_3 = 2.65$ ,  $p = 0.0029$ ; Table 3). A pairwise comparison showed that region 2, in the southern part of the sampling area, differed significantly from regions 3 and 5, which are both located further north. Region 5, which is furthest north, also differed significantly from regions 3 and 1, indicating that there was a difference between northern and southern stations that might not have been represented by means alone (Table 4).

The mean size of *H. coarctatus* was smaller in northern regions compared to the south; however, this trend was not as pronounced as for *C. opilio* females. Both mean and mode showed a peak in region 2, which was also observed for *C. opilio* males (Figure 4). The mean and mode were smallest in region 4, which was furthest offshore. This could indicate that male and female *H. coarctatus* decrease in size with increasing distance from coast. Patterns for the mean and mode were similar for both males and females; however, the mode of both sexes was equal in regions 3, 4 and 5, while the mean varied among those northern regions (Figure 4). The SFD differed significantly among regions (PERMANOVA, Pseudo- $F_4 = 1.74$ ,  $p = 0.0262$ ; Table 3), but a

pairwise comparison did not reveal which regions differed significantly among each other as sample sizes were too small to establish a test statistic (Table 4).

**Table 4.** Pairwise comparison of the factors that showed a significant result in the PERMANOVA for both species *Chionoecetes opilio* and *Hyas coarctatus*. Displayed are the t-statistic with the corresponding degrees of freedom (df) and the p-values with a significance level of  $\alpha=0.05$  (\* denotes significant results). The dash (-) indicates that values were not calculated.

Comparison	Group	<u><i>Chionoecetes opilio</i></u>			<u><i>Hyas coarctatus</i></u>		
		t-value	df	p-value	t-value	df	p-value
<b>Year</b>	2009, 2010	2.8549	42	0.0001*	0.85991	4	0.6173
	2009, 2012	-	-	-			
	2009, 2013	7.9224	42	0.0001*	-	-	-
	2010, 2012	-	-	-	2.7664	18	0.0003*
	2010, 2013	7.4696	28	0.0001*	-	-	-
<b>Region</b>	1, 2	-	-	-	0.77396	2	0.7043
	1, 3	0.86559	36	0.5772	1.1976	2	0.3005
	1, 4	-	-	-			
	1, 5	1.4836	20	0.0363*	1.3033	14	0.1295
	2, 3	1.6872	36	0.033*			
	2, 4	-	-	-			
	2, 5	2.5044	20	0.0008*			
	3, 4	-	-	-	1.6822	4	0.087
	3, 5	1.8022	56	0.0023*	1.2598	16	0.1441
	4, 5	-	-	-	1.3803	16	1.3803
<b>Year x Sex Female, Male</b>	2009	1.4382	28	0.0816	1.3727	2	0.2185
	2010	1.4777	14	0.0321*	1.8262	2	0.0883
	2012	-	-	-	1.7416	16	0.0098*
	2013	1.257	14	0.1986	-	-	-



**Figure 4.** The mean (A, C) and mode (B, D) of the combined SFD data of all stations across years of *Chionoecetes opilio* (A, B) and *Hyas coarctatus* (C, D) males and females separated in regions.

### 3.3. Environmental analysis

The environmental variables that best explained the variation in the SFD data matrixes varied between species, sexes, and among years. While none of the tested environmental variables significantly explained the variation in the SFD of *C. opilio* females in 2009, three explained the variation for *C. opilio* males in 2009. Overall, the sediment C/N ratio, bottom water temperature, and salinity explained 43.67 % of variability in the data matrix, with the sediment C/N ratio accounting for 15.7 % of the variability (Table 5). In 2010, two environmental parameters significantly explained the variation in the SFD of *C. opilio* females, while none explained the variation for *C. opilio* males. Longitude and sediment grain size <math><0 \phi</math> explained 60.24 % of the variability in the data matrix of *C. opilio* females, with longitude accounting for 40.55 % of the explained variability (Table 5). In 2013, three environmental variables significantly explained the variation in the SFD of *C. opilio* females, while only one explained the variation in *C. opilio* males. Sediment modal size, sediment grain size 2  $\phi$ , and salinity explained 53.95 % of the variability in the SFD data matrix of *C. opilio* females while sediment C/N ratio explained 33.35 % of the variability for the males (Table 5).



**Table 5.** DistLM results for *Chionoecetes opilio* showing the variable, the relative contribution to the explained variation (Contrib.), the cumulative contribution of the explained variation (Cum.) and p-values with a significance level of  $\alpha=0.05$  (\* denotes significant results).

Sex	Number of Variables	<i>Chionoecetes opilio female</i>			<i>Chionoecetes opilio male</i>				
		Variable	Contrib. (%)	Cum. (%)	p-value	Variable	Contrib. (%)	Cum. (%)	p-value
2009	1.	Longitude (°W)	13.71	13.71	0.0656	C/N (%)	15.7	15.7	0.0146*
	2.	Temperature (°C)	10.42	24.13	0.1347	Temperature (°C)	12.11	27.81	0.0329*
	3.	Sediment Grain Size 2 $\phi$	8.92	33.05	0.1906	Salinity	15.86	43.67	0.0011*
	4.	Latitude (°N)	8.8	41.85	0.1444	Latitude (°N)	6.19	49.86	0.1457
2010	1.	Longitude (°W)	40.55	40.55	0.0007*	TOC (%)	14.36	14.36	0.1972
	2.	Sediment Grain Size <0 $\phi$	19.69	60.24	0.0021*	TON (%)	17.15	31.51	0.1157
	3.	TOC (%)	9.89	70.13	0.0751	Mean Sediment Grain Size 1-4 $\phi$	16.1	47.61	0.1093
2013	1.	Temperature (°C)	30.5	30.5	0.1119	C/N (%)	33.35	33.35	0.0375*
	2.	Sediment Modal Size	31.61	62.11	0.0146*	Sediment Grain Size 3 $\phi$	16.6	49.95	0.0776
	3.	Sediment Grain Size 2 $\phi$	12.45	74.56	0.0484*	Depth (m)	15.53	65.47	0.0969
	4.	Salinity	9.89	84.45	0.0372*	Temperature (°C)	13.35	78.82	0.107
	5.	Sediment Grain Size 4 $\phi$	5.78	90.24	0.2537	Mean Sediment Chlorophyll <i>a</i>	7.63	86.44	0.1941

Fewer environmental parameters explained the variation in the SFD of *H. coarctatus*, which may be because the number of stations per year was smaller than for *C. opilio*. In 2009, depth explained 61.61 % and 71.84 % of the variability in the SFD matrix of *H. coarctatus* males and females, respectively, but neither was significant (Table 6). In 2010, no variable significantly explained the variation in the SFD for males but temperature explained 48.12 % of the variability for females (Table 6). In 2012, one environmental variable significantly explained the variation for females while two did for males. The dissolved oxygen concentration explained 34.83 % of

the variability for females while sediment grain size  $>5 \phi$  and sediment grain size  $<0 \phi$  explained 45.6 % of the variability for males (Table 6).

**Table 6.** DistLM results for *Hyas coarctatus* showing the variable, the relative contribution to the explained variation (Contrib.), the cumulative contribution of the explained variation (Cum.) and p-values with a significance level of  $\alpha = 0.05$  (\* denotes significant results).

Sex	Number of variables	<i>Hyas coarctatus female</i>			<i>Hyas coarctatus male</i>				
		Variable	Contrib. (%)	Cum. (%)	p- value	Variable	Contrib. (%)	Cum. (%)	p- value
2009	1.	Depth (m)	71.84	71.84	0.1708	Depth (m)	61.61	61.61	0.1679
	1.	Temperature (°C)	48.12	48.12	0.046*	Temperature (°C)	49.57	49.57	0.1283
2010	2.	Salinity	29.77	77.88	0.3716	Dissolved Oxygen Concentration	31.2	80.77	0.3019
	1.	Dissolved Oxygen Concentration	34.83	34.83	0.0025*	Sediment Grain Size $>5 \phi$	31.52	31.52	0.0021*
2012	2.	Sediment Grain Size $<0 \phi$	13.22	48.05	0.0695	Sediment Grain Size $<0 \phi$	14.09	45.6	0.0527*
	3.	Specific Conductivity (mS/cm)	12.23	60.27	0.0813	Sediment Modal Size	10.75	56.35	0.1317

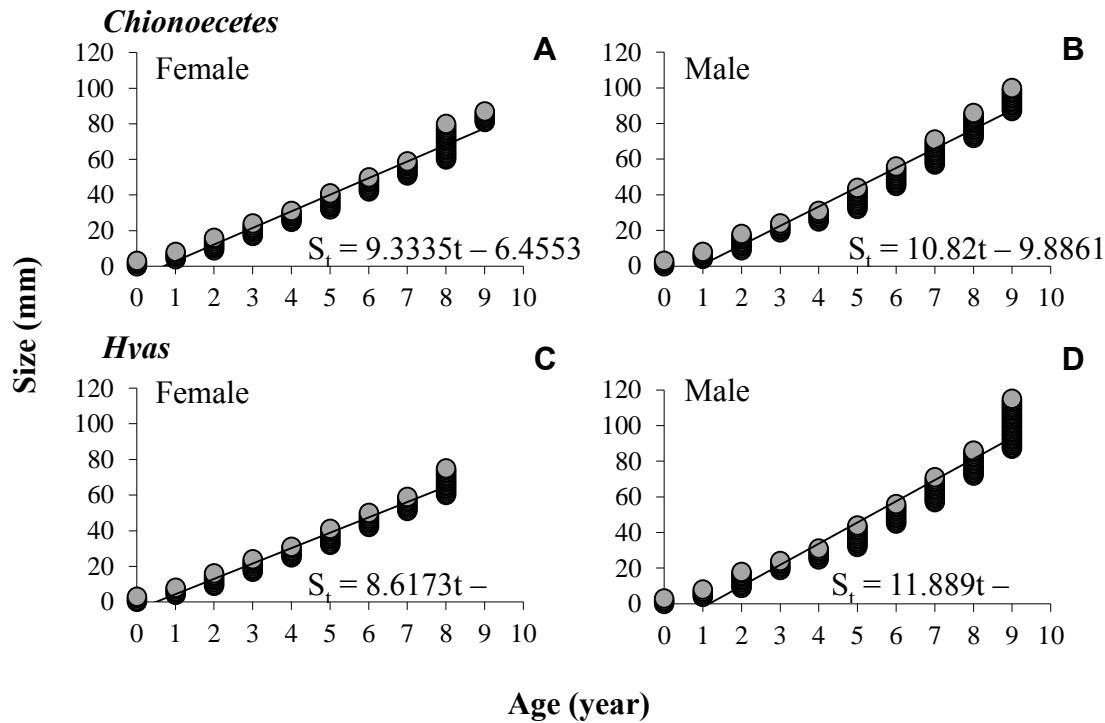
These results indicate that the variation in SFD of Chukchi Sea crabs was only partially explained by changing environmental parameters, in particular bottom water temperature, sediment TOC, sediment C/N ratio, and chlorophyll *a* content in the sediment. Of these, the latter three can be used as proxies for food availability and quality. In some years, the variation in the SFD of both species was not significantly explained by any of the tested environmental parameters. Sediment TOC and chlorophyll *a* did not explain any of the variation in the SFD for either species in any year (Tables 5 and 6). The variation in the SFD of female *C. opilio* and male *H. coarctatus* was not explained by temperature or sediment C/N ratio but the variation in the SFD of male *C. opilio* was significantly explained by temperature and sediment C/N ratio in 2009, and only by the sediment C/N ratio in 2013, and the variation in the SFD of female *H. coarctatus* was significantly explained by bottom water temperature in 2012 (Tables 5 and 6).

### 3.4. Growth and mortality models

Individual growth of both species could be approximated by linear models in the size range sampled in this study. Female crabs of both species grew slower than males, as the slope and the intercept of the linear growth model of the females were significantly smaller than the slope and the intercept of the males (ANCOVA, *C. opilio*:  $F_1 = 18.68$ ,  $p = 2.582e-05$ ; *H. coarctatus*:  $F_1 = 63.852$ ,  $p = 1.289e-13$ ; Figure 5, Table 7). The negative intercept of the trendline showed that the growth of both sexes of both species was not linear in the first year, as they did not fall on the linear trendline fitted to the data (Figure 5). Mortality of both sexes of *C. opilio* and *H. coarctatus* females was lowest in 2010, while it was lowest for *H. coarctatus* males in 2009 (Figure 6). The highest mortality of both sexes for both crabs was observed in the latter two sampling years (Figure 6). The rise in mortality in the latter two study years was, however, only

significant for *C. opilio* females and *H. coarctatus* males (ANCOVA, *C. opilio*:  $F_1 = 60.4835$ ,  $p = 0.0001091$ ; *H. coarctatus*:  $F_1 = 9.4802$ ,  $p = 0.008795$ ; Table 8). For *C. opilio* males and *H. coarctatus* females, the ANOVA showed that the ANCOVA design without the interaction was more parsimonious (Table 8). Mortality of *H. coarctatus* males increased gradually from 2009 to 2012. Overall, *C. opilio* had greater mortality coefficients than *H. coarctatus* (Figure 6).

Mortality of both sexes of both crabs increased with rising age. It was fairly constant over the entire size spectrum sampled in this study for both sexes of *C. opilio*, except in 2009, where a sudden rise in mortality of the females was observed between age eight and age nine (Figure 6). Mortality of both sexes of *H. coarctatus* was less constant across all sizes in this study than that of *C. opilio*, as outliers were present in all sampling years. This discontinuity in mortality was more pronounced for *H. coarctatus* females than males, and outliers varied among age groups (Figure 6).



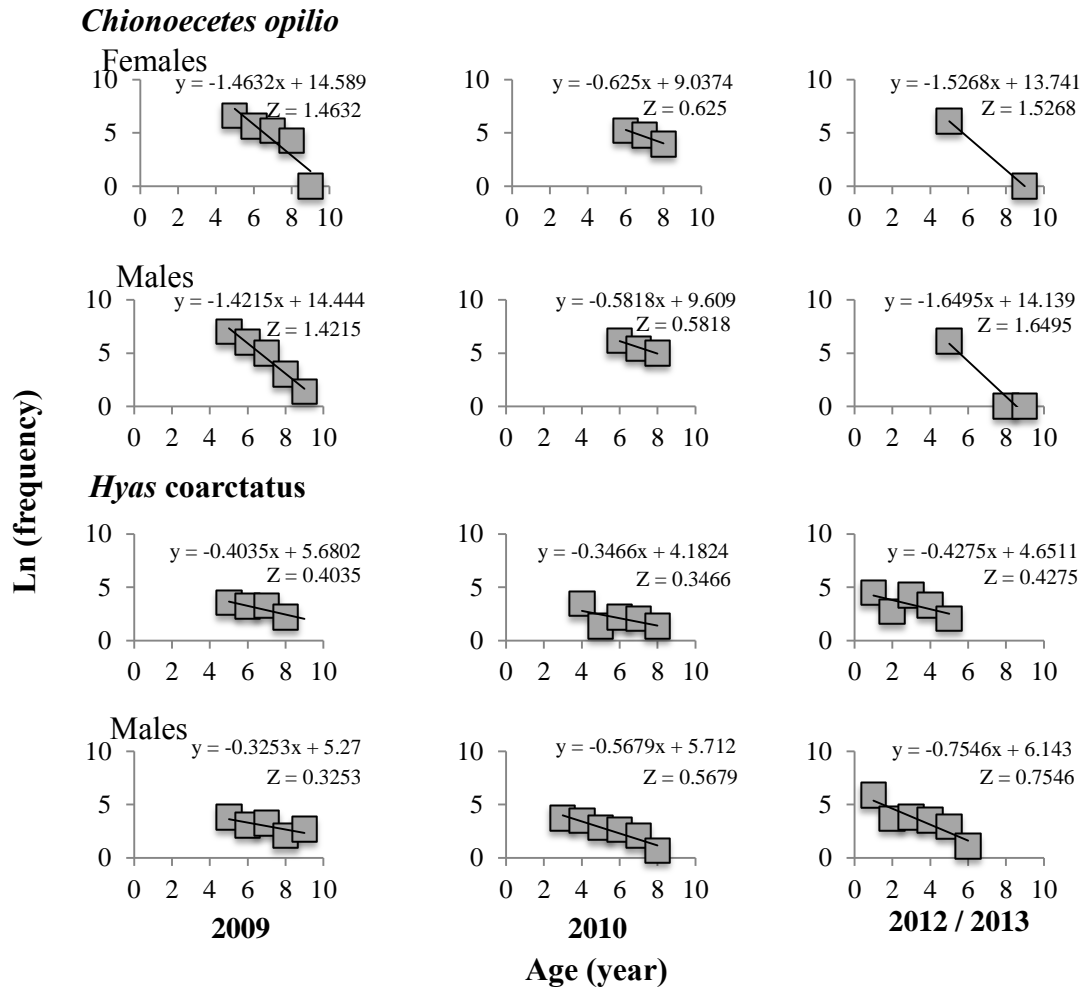
**Figure 5.** Linear growth model shown as a size-at-age graph for males (right) and females (left) of *Chionoecetes opilio* (A, B) and *Hvas coarctatus* (C, D), including the corresponding equation to the fitted linear trendline.

**Table 7.** ANCOVA results for the growth model of *Chionoecetes opilio* and *Hyas coarctatus*, with sex as the categorical factor, age as the covariate and size as the dependent variable. Displayed are the test statistic (F-value), the degrees of freedom (df) and the significance value (p-value) at a 0.05 significance level (\* denotes significant results).

Variable	<u><i>Chionoecetes opilio</i></u>			<u><i>Hyas coarctatus</i></u>		
	F-value	df	p-value	F-value	df	p-value
Age	4316.482	1	2.2e-16*	3391.585	1	2.2e-16*
Sex	27.547	1	4.376e-07*	52.348	1	1.130e-11*
Age: Sex	18.68	1	2.582e-05*	63.852	1	1.289e-13*

**Table 8.** ANCOVA results for the mortality model of both sexes of *Chionoecetes opilio* and *Hyas coarctatus*, with year as the categorical factor, age as the covariate and natural logarithm (ln) of the frequency as the dependent variable. Displayed are the test statistic (F-value), the degrees of freedom (df) and the significance value (p-value) at a 0.05 significance level (\* denotes significant results). The dash (-) indicates that models without the interaction term were more appropriate than the ones with the interaction term.

Variable	<u><i>Chionoecetes opilio</i></u>						<u><i>Hyas coarctatus</i></u>					
	Female			Male			Female			Male		
	F-value	df	p-value	F-value	df	p-value	F-value	df	p-value	F-value	df	p-value
Age	21.1503	1	0.0024873*	9.1327	1	0.0116134*	9.2252	1	0.0113*	46.4701	1	1.23e-05*
Year	0.8611	1	0.3843079	28.4171	1	0.0002408*	2.063	1	0.1787	9.2285	1	0.009520*
Age: Year	60.4835	1	0.0001091*	-	-	-	-	-	-	9.4802	1	0.008795*



**Figure 6.** The natural logarithm of the frequency of crabs caught in an age group plotted against age for males and females of *Chionoecetes opilio* (top) for the years 2009 (left), 2010 (middle) and 2013 (right) and *Hyas coarctatus* (bottom) for the years 2009 (left), 2010 (middle) and 2012 (right), including the corresponding equation to the fitted linear trendline and the mortality factor (Z).

#### 4. Discussion

This paper presents the first temporal record of size frequency distributions (SFD) of *Chionoecetes opilio* and *Hyas coarctatus* in the Chukchi Sea from 2009 to 2013. The first hypothesis that the size frequency distribution of male and female *C. opilio* and *H. coarctatus* would differ significantly from each other was not fully supported as *C. opilio* females only differed significantly from males in 2010, and the two sexes of *H. coarctatus* only differed significantly from each other in 2012. As in previous studies, male crabs obtained larger maximum sizes than females for both species (Alvsvåg et al., 2009; Bryant, 1991). The largest *C. opilio* female was larger (84 mm) than the largest published size for *C. opilio* females (63 mm) in the Chukchi Sea (Jewett and Feder, 1981). The largest male in this study (94 mm) was larger

than the largest male found in the literature (75 mm) in the Chukchi Sea (Frost and Lowry, 1983). The majority of *C. opilio* from this study were sub-legal size for the eastern Bering Sea snow crab fishery, which has a legal catch size of males larger than 78 mm (NPFMC, 2010). *Chionoecetes opilio* below the legal catch size in the northeastern Chukchi Sea are well documented in the literature as most large crabs from this area are between 35 to 70 mm in size (Burmeister and Sainte-Marie, 2010; Frost and Lowry, 1983; Somerton, 1981). A recent study found *C. opilio* individuals up to 119 mm in the Beaufort Sea (Rand and Logerwell 2011). Larger maximum sizes in other areas demonstrate that *C. opilio* may be experiencing reduced growth in the Chukchi Sea. Historic size data for *H. coarctatus* do not exist for the Chukchi Sea but the mean sizes reported around the Isle of Man, Scotland (20-29 mm and 17-28 mm for males and females, respectively) (Bryant, 1991) are smaller than those found in this study (12-51 mm and 16-44 mm for males and females, respectively).

#### 4.1. Temporal comparisons

Two clear temporal trends were observed in the SFD of *C. opilio* and *H. coarctatus*. The mean size and the rare maximum sized individuals of both sexes decreased from 2009 to 2013. The decline in mean size of *C. opilio* was not gradual. The mean size of males changed from 36 to 44 to 11 mm, in 2009, 2010, and 2013, respectively. Females changed from 38 to 44 to 11 mm, respectively. The mean size of both sexes of *H. coarctatus* declined from 51 mm and 44 mm in 2009 to 12 mm and 16 mm in 2012 for males and females, respectively. These data only partially support the second hypothesis, that there is significant interannual variability in the SFD of *C. opilio* and *H. coarctatus*. The SFD of *C. opilio* differed significantly between all years while the SFD of *H. coarctatus* only differed significantly between 2010 and 2012. This suggests that the SFD of *C. opilio* started changing earlier than the SFD of *H. coarctatus*. However, speculations about temporal trends made in this study are questionable due to the limited number of repeat stations and the limited (four years) temporal spread of the data.

There are many possibilities as to why mean carapace width decreased during the study period and why mature crabs (>40 mm) of both species were nearly absent in 2012 and 2013 while immature crabs (<34 mm) were fairly abundant. One possibility could be ontogenetic migrations of larger crabs to areas with warmer bottom water temperatures as colder temperatures were observed around Hanna Shoal in the latter two study years compared to previous years (Groß, 2015). The occurrence of colder bottom water temperatures around Hanna Shoal could be caused by a shift in the local current regime. Bering Sea water usually replaces the cold, dense winter water that forms on Hanna Shoal in the early summer but slower flushing times could result in the colder bottom water temperatures observed in 2012 and 2013 (Day et al., 2013; Weingartner et al., 2005). The reduced productivity of brachyuran crabs in sub-zero temperatures may be causing ontogenetic migrations to deeper waters (Ernst et al., 2005; Orensanz et al., 2007; Sainte-Marie and Gilbert, 1998). Sub-zero temperatures limit or even inhibit crab growth and lead to smaller size-at-maturity (Ernst et al., 2005; Kolts et al., 2015). Adult *C. opilio* females not only follow ontogenetic migrations because growth is limited at cold temperatures but also because a reduced size-at-maturity decreases their reproductive potential. Clutch size is reduced in smaller females and egg developmental rate is slowed down in colder temperatures, resulting in a two year incubation at temperatures below 2°C (Burmeister, 2002; Comeau et al., 1999; Kolts et al., 2015). The relation between body and clutch size has also been noted in *H. coarctatus* females (Bryant, 1991). Female body size is important in determining population growth, through fecundity and reproductive output, which may be why mature females actively

seek out habitats with warmer temperatures (Bryant, 1991; Conan et al., 1996). The scarcity of mature crabs is an indication that ontogenetic migration may even begin before maturity is reached, leading to spatial segregation of mature and immature crabs (Comeau et al., 1998).

One other possibility for the near absence of mature crabs in the latter study years may be that juveniles are less mobile than mature crabs and most likely limited to the area of settlement. However, it is unknown if initial recruitment to an area depends on larval settlement or post-settlement dispersal of instars I to III (0~8 mm) (Kolts et al., 2013), as only immature crabs of instar IV (>9 mm) were consistently found in this and one other study (Kolts et al., 2015). One indication that larval settlement determines higher juvenile crab abundance is the slowing of water around Hanna Shoal, which favors larval settlement (Kolts et al., 2015; Weingartner et al., 2005). Larval settlement conditions were also more favorable around Hanna Shoal due to shallow waters with coarse grain sediment and cold bottom water temperatures. Predation and cannibalism are assumed to be reduced in those habitats making them favorable for more frequently moulting immature crabs (Bryant, 1991; Comeau et al., 1998; Kolts et al., 2015; Lovrich et al., 1995). Cannibalism on immature crabs was reduced in 2012 and 2013, as large crabs were nearly absent during that time. Predation may also have been reduced around Hanna Shoal as only 16-91 fish 1000 m<sup>-2</sup> were found in the pool of cold winter water south of Hanna Shoal, whereas 207 fish 1000 m<sup>-2</sup> were found in warmer regions in the northeastern Chukchi Sea in 2009 and 2010 (Day et al. 2013). This finding could explain why cold temperatures reduce predation on small crabs, and why small crabs were present in high numbers in 2012 and 2013. The scarcity of mature crabs and the high numbers of immature crabs on Hanna Shoal in 2012 and 2013 also suggests that the population is being sustained from elsewhere, and that larvae advected from one area are deposited in another. This is not uncommon for brachyuran crabs as female breeding habitats are often disjunct from nursery grounds (Parada et al., 2010). It seems that immature and mature crabs not only have different habitat preferences, in terms of depth and sediment grain size, but that the distribution of crabs is also influenced by habitat adequacy, current flow and their migration behavior.

Findings where larger crabs excluded smaller crabs from the same habitat due to cannibalism were made in Bonne Bay and the Gulf of St. Lawrence, Canada (Comeau et al., 1998; Wieczorek and Hooper, 1995). This interaction led to habitat segregation where immature *C. opilio* inhabited shallower waters with coarser, gravelly sediment and mature crabs inhabited deeper waters with finer, muddy sediment. The coarser, gravelly sediment provides refuge from predators and higher food abundance (Comeau et al., 1998; Lovrich et al., 1995; Robichaud et al., 1989). Observed differences in the feeding behavior and diet of small and large crabs could also lead to habitat segregation, and explain the near absence of mature crabs in 2012 and 2013, as immature and mature crabs have been found in different benthic communities in other areas (Lefebvre and Brêthes, 1991). Overall prey abundance, regardless of prey taxa, can determine the distribution of crabs as feeding is largely opportunistic (Kolts et al., 2013). It could be that the overall decline in the prey base, reported as a drop in abundance and biomass of the majority of the benthic fauna in 2012 and 2013, caused a decline in the abundance of mature *C. opilio* and *H. coarctatus* in the same years (Kolts et al., 2013; Powell et al., this issue). Mature crabs of both species preferably feed on other, larger epibenthic organisms while immature crabs feed on amphipods and small bivalves with soft shells (Kolts et al., 2013). It is unknown if the preferred prey of immature crabs was present in high abundances north of Hanna Shoal in 2012 and 2013 allowing higher abundances of immature crabs. Inferences about habitat segregation in the

Chukchi Sea on the basis of food availability and feeding behavior are therefore hard to make as the abundance of all components of the food web is not well known.

## 4.2. Spatial comparisons

The one clear spatial trend that was observed in the size frequency distribution (SFD) of both crab species was that mean size decreased from south to north. This trend was more pronounced for *C. opilio* than *H. coarctatus*, and it was most prominent for *C. opilio* females. This result confirms previous findings of a spatial north-south trend in the SFD of both species in the Chukchi Sea (Burmeister and Sainte-Marie, 2010; Jewett and Feder, 1981; Orensanz et al., 2007). This latitudinal cline in size is most likely a reflection of the impact of conditions that vary with latitude such as bottom water temperature, primary productivity distribution or current regime (Stoker, 1981). Bottom water temperatures have been assumed to play a substantial role in the latitudinal cline, as temperature affects growth and hence body size of organisms (MacDonald and Thompson, 1985; McCormick and Molony, 1995). Cold temperatures may be the greatest limitation on population productivity, as it decreases growth, size-at-maturity, clutch size and slows egg development (Bryant, 1991; Burmeister and Sainte-Marie, 2010; Kolts et al., 2015; Orensanz et al., 2007). Observations of *C. opilio* from west Greenland have shown that the mean CW at instar is similar or larger in colder areas than warmer areas, showing that the relative moult increment is generally invariable (Burmeister and Sainte-Marie, 2010). Differences in size-at-maturity may be due to differences in the intermoult period. Immature crabs can moult more frequently in warmer than colder environments, before the onset of pre-puberty, when the moulting cycle becomes annual (Burmeister and Sainte-Marie, 2010). A north-south variation in the intermoult period was found in the Gulf of St. Lawrence and the Sea of Japan (Comeau et al., 1998; Kon, 1980).

Movement patterns of *C. opilio* in the Chukchi and Beaufort Seas are unknown but the finding of large mature crabs in the Beaufort Sea suggests that conditions varying with latitude might not be the only factors influencing the distribution of this species (Logerwell et al., 2011; Rand and Logerwell, 2011). The study from the Beaufort Sea is the first breaking the pattern of a well-documented latitudinal cline of size-at-maturity, with mature *C. opilio* only reaching a size of 40-94 mm in the Chukchi Sea (Burmeister and Sainte-Marie, 2010; Rand and Logerwell, 2011; Somerton, 1981). Migrations of adolescent and mature crabs could play a role in explaining this unconventional finding of large *C. opilio* in the Beaufort Sea, and the observed latitudinal cline in this study. Ontogenetic migrations tend to follow an “upstream” pattern regarding local currents (Ernst et al., 2005). This seems contrary to the observed pattern as larger crabs were found in the southern regions of the study area; however, large *C. opilio* have also been found in the Beaufort Sea, and southwestward migrations of females were also observed in the Bering Sea (Ernst et al., 2005; Rand and Logerwell, 2011). Since females track environmental gradients along their migrations, especially temperature, movement to warmer areas likely increases their reproductive input to the population (Burmeister and Sainte-Marie, 2010; Ernst et al., 2005). The area in the Beaufort Sea where large individuals of *C. opilio* were found has warmer bottom water temperatures due to upwelling, warm deep water of Atlantic origin, which likely contributes to the enhanced crab growth (Burmeister and Sainte-Marie, 2010; Orensanz et al., 2007; Pickart et al., 2005). It can be suggested that adolescent and mature *C. opilio* might migrate to warmer areas in the Chukchi Sea, which could explain why smaller individuals were found further north of Hanna Shoal. The constant cold pool of winter water around Hanna Shoal leads to lower average temperatures compared to the southern part of the study region or the



deeper areas in the Beaufort Sea (Pickart et al., 2005; Weingartner et al., 2005). Both, a migration of adolescent and mature crabs to the southern regions of the study area as well as an “upstream” migration with the northeastward flowing currents to the Beaufort Sea are possible explanations for the latitudinal cline in body size.

A second spatial trend was observed in this study with a peak in mean size in region 2 for all but *C. opilio* females, and a minimum in region 4 for both sexes of *H. coarctatus*. Region 2 included the coastal stations, while region 4 included the furthest offshore stations, indicating an inshore-offshore trend in the distribution of both sexes of *H. coarctatus*. Water masses may also provide insights in the longitudinal pattern observed, as it is thought that crabs might track water masses in the Chukchi Sea (Ravelo et al., 2014). The largest mean size of *C. opilio* males and both sexes of *H. coarctatus* were found close to the shore under the warmer Alaska Coastal Current (ACC) water while the smallest mean size of both sexes of *H. coarctatus* were found offshore under colder Bering Sea Water in the Central Channel. It could be that the larger mean size was found close to the coast because crabs show seasonal migrations to shallower waters in the spring for reproduction. The warmer waters of the ACC could attract mature crabs undergoing ontogenetic migrations, and foster enhanced growth (Lovrich et al., 1995; Orensanz et al., 2007). However, this trend of larger mean sizes close to the coast was not observed for female *C. opilio*, which stay longer in shallower areas than the males (Conan et al., 1996). In addition, findings from the Gulf of St. Lawrence demonstrated that female adult size followed a longitudinal cline that correlated with increasing temperature (Sainte-Marie and Gilbert, 1998). These seasonal migrations into coastal waters have not yet been observed in the eastern Bering Sea (Ernst et al., 2005). Another explanation could be the greater influence of water dynamics through storms and disturbances from ice gouging, which co-vary with the shallower water depth and are better tolerated by mature, larger crabs, especially the males, as they are highly mobile and can travel several miles within a few days to avoid big disturbance events (Blanchard and Knowlton, 2013; Kon, 1980; Lovrich et al., 1995).

### 4.3 Environmental analysis

The environmental analysis only partially supported the final hypothesis, that the variation in the size frequency distribution would be significantly explained by changing environmental parameters (i.e., bottom water temperature, and sediment TOC, C/N ratio, and chlorophyll *a* content). Total organic carbon and chlorophyll *a* content in the sediment did not explain any of the SFD in this study. Bottom water temperature explained the variation in the SFD of male *C. opilio* in 2009 and female *H. coarctatus* in 2012, suggesting that temperature itself is not important in structuring the SFD of crabs in the Chukchi Sea. The C/N in the sediment only explained the SFD for *C. opilio* males in 2009 and 2013. This suggests that food availability and nutrient abundance does not structure the SFD of these crabs, even though higher abundances of epifaunal and infaunal organisms have been correlated with low C/N ratios (high quality primary production) around Hanna Shoal and Barrow Canyon (Grebmeier and McRoy, 1989; Ravelo et al., 2014; Schonberg et al., 2014). These results are similar to findings from west Greenland where food supply did not structure the observed cline in *C. opilio* adult size (Burmeister and Sainte-Marie, 2010), even though reduced growth would be expected with less food quality or quantity (Atkinson and Sibly, 1997). Food limitation could lead to a lengthening in the intermoult period, resulting in a smaller size at instar (Burmeister and Sainte-Marie, 2010; Hartnoll, 2001). This does not seem to be the case in the Chukchi Sea, showing that food quality and quantity are not solely structuring the SFD of these crabs. It could be that water masses are

the driving factor of crab size distribution patterns in the Chukchi Sea, as temperature, sediment granulometry, C/N ratios and salinity differ between water masses (Schaff et al., 1992; Thomsen et al., 1995).

#### 4.4. Growth and Mortality

Applying the modeled age from the study by Comeau et al. (1998) to this data set showed that growth appeared to be constant for all the sampled crabs. This is very similar to the results by Comeau et al. (1998) for *C. opilio* females, which showed a constant increase in the percent growth increment with no effect of the terminal molt. However, growth of male *C. opilio* was not constant in other studies, which showed a larger increase of percent carapace width per moult during the immature phase and a further decline in growth after the moult to maturity (Comeau et al., 1998; Watson, 1969). Both these studies showed that growth in each phase (immature, adolescent and mature phase) was constant but that it changed between the phases. For *H. coarctatus* females, constant growth was found in this and one other study (Bryant, 1991). In contrast to results of constant growth in this study, growth of *H. coarctatus* males has been found to be similar to that of *C. opilio* males discussed above (Bryant 1991). There, growth could be broken down into three phases, immature, adolescent, and mature, with a relative decrease of the moult increments between each phase (Bryant, 1991). The decrease in moult increment from the immature phase to the adolescent phase at the puberty moult is assumed to be caused by an early investment into reproductive organs (Bryant, 1991). While both *C. opilio* and *H. coarctatus* females exhibit gonad development before the puberty moult, the testes of *H. coarctatus* males only mature after the puberty moult (Bryant, 1991; Watson, 1970). This does not fully support the findings of this or other studies (Bryant, 1991; Comeau et al., 1998). The constant growth of females of both species would indicate that no energy is diverted from somatic growth to gonad production at the puberty moult. A changing energy investment would only hold true for *C. opilio* males in the studies that show growth decreasing after the puberty moult (Comeau et al., 1998; Watson, 1969). Constant growth in females of both species could be interpreted as a tactic for maximizing body size to the terminal moult, as larger females are more fertile because they are able to produce more eggs (Bryant, 1991).

Mortality of male and female crabs of both species was highest in the latter two study years, and increased with age. This result supports the previously discussed drop in abundance and average maximum size of the highest percentile of all mature crabs in 2012 and 2013. Comparisons of *H. coarctatus* mortality to other studies were not made, as they are scarce. However, mortality of male and female *C. opilio* in 2013 was higher (1.65 and 1.53 per year, respectively) compared to other studies. A trawl and commercial catch study showed that mortality was lowest for immature male crabs with 0.136 per year, and highest for mature males of 80-90 mm CW with 0.701 per year (Zheng, 2003). Zheng (2003) also showed that a scenario of constant mortality was the most parsimonious model tested. Constant mortality seems more plausible as direct fishing mortality rates for small *C. opilio* males were very small or close to zero in the eastern Bering Sea snow crab fishery. The natural mortality rate of sublegal mature *C. opilio* males in the northwestern Gulf of St. Lawrence, Canada, derived from a model, was 0.53-1.02 per year while it was 0.66 per year for *C. opilio* females (Drouineau et al., 2013; Wade et al., 2003). Those mortality estimates are in the same range as the estimates from this study in 2010, the year with the lowest mortality. However, mortality was much higher in this study in 2012 and 2013, indicating that the near absence of adolescent and mature crabs may be caused by increased mortality. Besides the prominent causes for natural mortality, such as predation and diseases,

mortality of mature females could be higher than that of immature females due to density-dependent sexual conflicts arising during the female's mating period (Sainte-Marie et al., 2008). If the adult *C. opilio* sex ratio is biased towards males, as in this study, dominant males may forcefully take over females from other males, inflicting immediate death or severe injuries that may shorten female life expectancy (Sainte-Marie et al., 2008).

## 5. Conclusions

To determine if the absence of adolescent and mature crabs of both species in the northeastern Chukchi Sea is a directional size decrease or short-term variability will only be determined through future monitoring. However, variability is likely as interannual fluctuations have been reported for *C. opilio* populations in other areas, and successful waves of recruitment were estimated to occur in seven or eight year intervals (Ernst et al., 2012; NPFMC, 2010; Sainte-Marie et al., 1995; Zheng et al., 2001). It is still uncertain if these fluctuations are cyclic or chronically instable but they are thought to be an advantage over predators, which may not specialize on a species that is not readily available every year (Bailey and Elner, 1989; Conan et al., 1992, 1996). The observed changes in the distribution pattern of *C. opilio* and *H. coarctatus* can be used as potential ecological indicators of climate warming as the distribution and growth of both species partly depends on bottom water temperatures and available food sources in the benthic community (Alvsvåg et al., 2009; Comeau et al., 1999; Kon, 1980; Orensanz et al., 2007; Parada et al., 2010; Powell, this issue). As these factors are likely to change in the Arctic, it is important to study the SFD of *C. opilio* and *H. coarctatus* further to be able to discern if the near absence of adolescent and mature crabs is caused by ontogenetic migrations, interannual fluctuations or if it is an early indication of a further northward extension, a shift in the southern distribution limit, or a regime shift in the Chukchi Sea (Dionne et al., 2003; Orensanz et al., 2004). Findings from this study are not only of ecological importance but they also have implications for future Arctic *C. opilio* fisheries. The small number of mature male crabs sampled that reached the legal fishing size (>78 mm) of the current eastern Bering Sea *C. opilio* fishery shows that a *C. opilio* fishery is currently not viable in the Chukchi Sea.

## 6. Acknowledgments

This study was funded by the U.S. Department of the Interior, Bureau of Ocean Energy Management (BOEM), Alaska Outer Continental Shelf Region, Anchorage, Alaska under BOEM Cooperative Agreement No. M11AC00007 as part of the Chukchi Sea Offshore Monitoring in Drilling Area (COMIDA). From BOEM, we thank Heather Crowley for her continued support of this project and enthusiastic assistance during our cruises. We thank the Fulbright Commission who supported Jasmin Groß during this study. Environmental data were collected by Lee Cooper, Jackie Grebmeier, and John Trefry. We thank Tom Weingartner for sharing his expertise of Chukchi Sea oceanography, David Verbyla for his help with ArcGIS, Bob Clark for all his statistical help with PRIMER, and Katrin Iken, Lauren Bell, Alyssa Lind, Kimberley Powell, Alexandra Ravelo, Tanja Schollmeier and Carlos Serratos for their valuable comments on this manuscript. We thank the captains and crew of the R/V Alpha Helix, R/V Moana Wave and USCGC Healy for their dedication and effort at sea. Lastly, we thank all our

field assistants and the rest of the COMIDA team for making this such a great group with which to work.

## 7. References

- Alvsvåg, J., Agnalt, A.-L., Jørstad, K.E., 2009. Evidence for a permanent establishment of the snow crab (*Chionoecetes opilio*) in the Barents Sea. *Biol. Invasions* 11, 587–595.  
doi:10.1007/s10530-008-9273-7
- Atkinson, D., Sibly, R.M., 1997. Why are organisms usually bigger in colder environments? Making sense of a life history puzzle. *Trends Ecol. Evol.* 12, 235–239.
- Bailey, R.F.J., Elnor, R.W., 1989. Northwest Atlantic snow crab fisheries: lessons in research and management, in: Caddy, J.F., Wiley, J. & S. (Eds.), *Marine Invertebrate Fisheries: Their Assessment and Management of Shellfish Resources*. New York, NY, pp. 261–280.
- Blanchard, A.L., Knowlton, A.L., 2013. Chukchi Sea Environmental Studies Program: Benthic Ecology of the Northeastern Chukchi Sea, 2008–2013. Fairbanks, AK.
- Bluhm, B.A., Iken, K., Mincks Hardy, S., Sirenko, B.I., Holladay, B.A., 2009. Community structure of epibenthic megafauna in the Chukchi Sea. *Aquat. Biol.* 7, 269–293.  
doi:10.3354/ab00198
- Brey, T., 2001. Population dynamisc in benthic invertebrates. A virtual handbook. Version 01.2. <http://www.thomas-brey.de/science/virtualhandbook> (accessed 18.04.15).
- Bryant, A.D., 1991. The life history patterns of brachyuran crabs. University of Liverpool.
- Burmeister, A., 2002. Preliminary notes on the reproduction conditions of mature female snow crab (*Chionoecetes opilio*) from Disko Bay and Sisimiut, West Greenland, in: Paul, A.J., Dawe, E.G., Elnor, R., Jamieson, G.S., Kruse, G.H., Otto, R.S., Sainte-Marie, B., Shirley, T.C., Woodby, D. (Eds.), *Crab 2001: Crabs in Cold Water Regions: Biology, Management and Economics*. University of Alaska Sea Grant.
- Burmeister, A., Sainte-Marie, B., 2010. Pattern and causes of a temperature-dependent gradient of size at terminal moult in snow crab (*Chionoecetes opilio*) along West Greenland. *Polar Biol.* 33, 775–788. doi:10.1007/s00300-009-0755-6
- Calder, W.A., 1984. *Size, function, and life history*. Harvard University Press, Cambridge, Mass.
- Comeau, M., Conan, G.Y., Maynou, F., Robichaud, G., Therriault, J.-C., Starr, M., 1998. Growth, spatial distribution, and abundance of benthic stages of the snow crab (*Chionoecetes opilio*) in Bonne Bay, Newfoundland, Canada. *Can. J. Fish. Aquat. Sci.* 55, 262–279.  
doi:10.1139/cjfas-55-1-262
- Comeau, M., Starr, M., Conan, G.Y., Robichaud, G., Therriault, J.-C., 1999. Fecundity and duration of egg incubation for multiparous female snow crabs (*Chionoecetes opilio*) in the fjord of Bonne Bay, Newfoundland. *Can. J. Fish. Aquat. Sci.* 56, 1088–1095.
- Company, J.B., Sarda, F., 2000. Growth parameters of deep-water decapod crustaceans in the Northwestern Mediterranean Sea: a comparative approach. *Mar. Biol.* 136, 79–90.  
doi:10.1007/s002270050011

- Conan, G.Y., Comeau, M., Robichaud, G., 1992. Life history and fishery management of majid crabs: the case study of the Bonne Bay (Newfoundland) *Chionoecetes opilio* population. Int. Counc. Explor. Sea C.M. 1992/K 21, 24 pp.
- Conan, G.Y., Starr, M., Comeau, M., Therriault, J.-C., Hernandez, F.X.M., Robichaud, G., 1996. Life History Strategies, Recruitment Fluctuations, and Management of the Bonne Bay Fjord Atlantic Snow Crab (*Chionoecetes opilio*), in: High Latitude Crabs: Biology, Management, and Economics. Alaska Sea Grant College, Anchorage, AK, pp. 59–97.
- Dawe, E.G., Colbourne, E.B., 2002. Distribution and Demography of Snow crab (*Chionoecetes opilio*) males on the Newfoundland and Labrador shelf, in: Paul, A.J., Dawe, E.G., Elner, R., Jamieson, G.S., Kruse, G.H., Otto, R.S., Sainte-Marie, B., Shirley, T.C., Woodby, D. (Eds.), Crabs in Cold Water Regions: Biology, Ma.
- Day, R.H., Weingartner, T.J., Hopcroft, R.R., Aerts, L.A.M., Blanchard, A.L., Gall, A.E., Gallaway, B.J., Hannay, D.E., Holladay, B.A., Mathis, J.T., Norcross, B.L., Questel, J.M., Wisdom, S.S., 2013. The offshore northeastern Chukchi Sea, Alaska: A complex high-latitude ecosystem. Cont. Shelf Res. 67, 147–165. doi:10.1016/j.csr.2013.02.002.
- Dionne, M., Sainte-Marie, B., Bourget, E., Gilbert, D., 2003. Distribution and habitat selection of early benthic stages of snow crab *Chionoecetes opilio*. Mar. Ecol. Prog. Ser. 259, 117–128. doi:10.3354/meps259117.
- Drouineau, H., Sainte-Marie, B., Duplisea, D., 2013. Estimating natural mortality and egg production of snow crab *Chionoecetes opilio* adult females. Aquat. Biol. 18, 261–270. doi:10.3354/ab00513.
- Émond, K., Sainte-Marie, B., Galbraith, P.S., Bêty, J., 2015. Top-down vs. bottom-up drivers of recruitment in a key marine invertebrate: investigating early life stages of snow crab. ICES J. Mar. Sci. 1–13.
- Ernst, B., Armstrong, D.A., Burgos, J., Orensanz, J.M. (Lobo), 2012. Life history schedule and periodic recruitment of female snow crab (*Chionoecetes opilio*) in the eastern Bering Sea. Can. J. Fish. Aquat. Sci. 69, 532–550. doi:10.1139/f2011-173.
- Ernst, B., Orensanz, J.M. (Lobo), Armstrong, D.A., 2005. Spatial dynamics of female snow crab (*Chionoecetes opilio*) in the eastern Bering Sea. Can. J. Fish. Aquat. Sci. 62, 250–268. doi:10.1139/F04-201.
- Feder, H.M., Jewett, S.C., Blanchard, A.L., 2005. Southeastern Chukchi Sea (Alaska) epibenthos. Polar Biol. 28, 402–421. doi:10.1007/s00300-004-0683-4.
- Fisher, M.R., 1999. Effect of temperature and salinity on size at maturity of female blue crabs. Trans. Am. Fish. Soc. 128, 499–506.
- Frost, K.J., Lowry, L.F., 1983. Demersal fishes and invertebrates trawled in the northeastern Chukchi and western Beaufort Seas, 1976-77.
- Grebmeier, J.M., 2012. Shifting Patterns of Life in the Pacific Arctic and Sub-Arctic Seas. Ann. Rev. Mar. Sci. 4, 63–78. doi:10.1146/annurev-marine-120710-100926.
- Grebmeier, J.M., McRoy, C.P., 1989. Pelagic-benthic coupling on the shelf of the northern Bering and Chukchi Seas. III. Benthic food supply and carbon cycling. Mar. Ecol. Prog. Ser. 53, 79–91.

- Groß, J., 2015. Variability in the Size Frequency Distribution and Growth of Snow Crab (*Chionoecetes opilio*) and Lyre Crab (*Hyas coarctatus*) in the Chukchi Sea from 2009 to 2013. University of Bremen, Bremen, Germany.
- Hardy, S.M., Lindgren, M., Konakanchi, H., Huettmann, F., 2011. Predicting the Distribution and Ecological Niche of Unexploited Snow Crab (*Chionoecetes opilio*) Populations in Alaskan Waters: A First Open-Access Ensemble Model. *Integr. Comp. Biol.* 51, 608–622. doi:10.1093/icb/icr102.
- Hartnoll, R.G., 1982. Growth, in: Abele, L.G. (Ed.), *The Biology of the Crustacea*. Academic Press, New York, NY, pp. 111–196.
- Hartnoll, R.G., 2001. Growth in Crustacea—20 years on. *Hydrobiologia* 449, 111–122.
- Jewett, S.C., Feder, H.M., 1981. Epifaunal invertebrates of the continental shelf of the eastern Bering and Chukchi Seas, in: Hood, D.W., Calder, J.A. (Eds.), *The Eastern Bering Sea Shelf: Oceanography and Resources*, Vol 2. U S Department of Commerce, NOAA, Rockville, Maryland.
- Kolts, J., Lovvorn, J.R., North, C.A., Janout, M.A., 2015. Oceanographic and demographic mechanisms affecting population structure of snow crabs in the northern Bering Sea. *Mar. Ecol. Prog. Ser.* 518, 193–208. doi:10.3354/meps11042.
- Kolts, J.M., Lovvorn, J.R., North, C.A., Grebmeier, J.M., Cooper, L.W., 2013. Effects of body size, gender, and prey availability on diets of snow crabs in the northern Bering Sea. *Mar. Ecol. Prog. Ser.* 483, 209–220. doi:10.3354/meps10292.
- Kon, T., 1980. Studies on the life history of the Zuwai crab, *Chionoecetes opilio* (O. Fabricius). Spec. Publ. from Sado Mar. Biol. Station. Niigata Univ. 2.
- Konar, B., Ravelo, A.M., Grebmeier, J.M., Trefry, J.H., 2014. Size frequency distributions of key epibenthic organisms in the eastern Chukchi Sea and their correlations with environmental parameters. *Deep Sea Res. Part II Top. Stud. Oceanogr.* 102, 107–118.
- Lanteigne, C., Beninger, P.G., Gionet, C., 1996. Ontogeny of Female Primary Sexual Characters in the Majid Crabs *Chionoecetes opilio* and *Hyas coarctatus*. *J. Crustac. Biol.* 16, 501–514.
- Lefebvre, L., Brêthes, J.-C.F., 1991. Influence de la croissance et de facteurs du milieu sur l'alimentation du crabe des neiges, *Chionoecetes opilio* (O. Fabricius), dans le sud-ouest du golfe du Saint-Laurent. *Can. J. Zool.* 69, 489–494.
- Logerwell, E.A., Rand, K., Weingartner, T.J., 2011. Oceanographic characteristics of the habitat of benthic fish and invertebrates in the Beaufort Sea. *Polar Biol.* 34, 1783–1796.
- Lovrich, G.A., Sainte-Marie, B., Smith, B.D., 1995. Depth distribution and seasonal movements of *Chionoecetes opilio* (Brachyura: Majidae) in Baie Sainte-Marguerite, Gulf of Saint Lawrence. *Can. J. Zool.* 73, 1712–1726.
- MacDonald, B., Thompson, R.J., 1985. Influence of temperature and food availability on the ecological energetics of the giant scallop *Placopecten magellanicus*. I. Growth rates of shell and somatic tissue. *Mar. Ecol. Prog. Ser.* 25, 279–294.

- McCormick, M.I., Molony, B.W., 1995. Influence of Water Temperature During the Larval Stage on Size, Age and Body Condition of a Tropical Reef Fish at Settlement. *Mar. Ecol. Ser.* 118, 59–68.
- NPFMC, 2010. Stock assessment and fishery evaluation report for the King and Tanner Crab fisheries of the Bering Sea and Aleutian Islands Regions. Anchorage, AK.
- Orensanz, J.M. (Lobo), Ernst, B., Armstrong, D.A., 2007. Variation of female size and stage at maturity in snow crab (*Chionoecetes opilio*) (Brachyura: Majidae) from the Eastern Bering Sea. *J. Crustac. Biol.* 27, 576–591. doi:10.1651/S-2790.1.
- Orensanz, J.M. (Lobo), Ernst, B., Armstrong, D.A., Stabeno, P., Livingston, P., 2004. Contraction of the geographic range of distribution of snow crab (*Chionoecetes opilio*) in the eastern Bering Sea: An environmental ratchet? *Calif. Coop. Ocean. Fish. Investig. Reports* 45, 65–79. doi:10.1016/j.fishres.2003.09.029.
- Parada, C., Armstrong, D.A., Ernst, B., Hinckley, S., Orensanz, J.M. (Lobo), 2010. Spatial Dynamics of Snow Crab (*Chionoecetes opilio*) in the Eastern Bering Sea—Putting Together the Pieces of the Puzzle. *Bull. Mar. Sci.* 86, 413–437.
- Pickart, R.S., Weingartner, T.J., Pratt, L.J., Zimmermann, S., Torres, D.J., 2005. Flow of winter-transformed Pacific water into the Western Arctic. *Deep. Res. Part II Top. Stud. Oceanogr.* 52, 3175–3198.
- Piepenburg, D., 2005. Recent research on Arctic benthos: Common notions need to be revised. *Polar Biol.* 28, 733–755.
- Piepenburg, D., Ambrose, W.G.J., Brandt, A., Renaud, P.E., Ahrens, M.J., Jensen, P., 1997. Benthic community patterns reflect water column processes in the Northeast Water polynya (Greenland). *J. Mar. Syst.* 10, 467–482.
- Powell, K., Konar, B., Grebmeier, J.M., 2016. Interannual Variation of Epibenthic Communities in the Chukchi Sea, Alaska. University of Alaska Fairbanks, Fairbanks, AK., this report.
- Puebla, O., Sévigny, J.-M., Sainte-Marie, B., Brêthes, J.-C.F., Burmeister, A., Dawe, E.G., Moriyasu, M., 2008. Population genetic structure of the snow crab (*Chionoecetes opilio*) at the Northwest Atlantic scale. *Can. J. Fish. Aquat. Sci.* 65, 425–436. doi:10.1139/f07-163.
- Rand, K.M., Logerwell, E.A., 2011. The first demersal trawl survey of benthic fish and invertebrates in the Beaufort Sea since the late 1970s. *Polar Biol.* 34, 475–488. doi:10.1007/s00300-010-0900-2.
- Ravelo, A.M., Konar, B., Trefry, J.H., Grebmeier, J.M., 2014. Epibenthic community variability in the northeastern Chukchi Sea. *Deep Sea Res. Part II Top. Stud. Oceanogr.* 102, 119–131. doi:10.1016/j.dsr2.2013.07.017.
- Robichaud, D.A., Bailey, R.F.J., Elnor, R.W., 1989. Growth and distribution of snow crab, *Chionoecetes opilio*, in the southern Gulf of St. Lawrence. *J. Shellfish Res.* 8, 13–23.
- Sainte-Marie, B., Gilbert, D., 1998. Possible effects of change in CIL temperature and thickness on population dynamics of snow crab, *Chionoecetes opilio*, in the Gulf of Saint Lawrence. *Can. Stock Assess. Secr. Res. Doc.* 98, 19.

- Sainte-Marie, B., Gosselin, T., Sévigny, J.-M., Urbani, N., 2008. The snow crab mating system: Opportunity for natural and unnatural selection in a changing environment, in: *Bulletin of Marine Science*. pp. 131–161.
- Sainte-Marie, B., Raymond, S., Brêthes, J.-C.F., 1995. Growth and maturation of the benthic stages of male snow crab, *Chionoecetes opilio* (Brachyura: Majidae). *Can J Fish Aquat Sci* 52, 903–924.
- Schaff, T., Levin, L., Blair, N., DeMaster, D., Pope, R., Boehme, S., 1992. Spatial heterogeneity of benthos on the Carolina continental slope: large (100 km)-scale variation. *Mar. Ecol. Prog. Ser.* 88, 143–160.
- Schonberg, S. V., Clarke, J.T., Dunton, K.H., 2014. Distribution, abundance, biomass and diversity of benthic infauna in the Northeast Chukchi Sea, Alaska: Relation to environmental variables and marine mammals. *Deep. Res. Part II Top. Stud. Oceanogr.* 102, 144–163. doi:10.1016/j.dsr2.2013.11.004.
- Somerton, D.A., 1981. Life history and population dynamics of two species of Tanner crab, *Chionoecetes bairdi* and *C. opilio*, in the eastern Bering Sea with implications for the management of the commercial harvest. University of Washington, Seattle.
- Stoker, S., 1981. Benthic invertebrate macrofauna of the Eastern Bering/Chukchi Continental Shelf, in: Hood, D.W., Calder, J.A. (Eds.), *The Eastern Bering Sea Shelf: Oceanography and Resources*, Vol. 2. U S Department of Commerce, NOAA, Rockville, Maryland, pp. 1069–1090.
- Teissier, G., 1960. Relative growth, in: Waterman, T.H. (Ed.), *The Physiology of Crustacea*, Vol I. Metabolism and Growth. Academic Press, New York, NY, pp. 537–560.
- Thomsen, L., Graf, G., Von Juterzenka, K., Witte, U., 1995. An in situ experiment to investigate the depletion of seston above an interface feeder field on the continental slope of the western Barents Sea. *Mar. Ecol. Prog. Ser.* 123, 295–300.
- Wade, E., Surette, T., Apaloo, J., Moriyasu, M., 2003. Estimation of mean annual natural mortality for adult male snow crab *Chionoecetes opilio* in the southern Gulf of St. Lawrence.
- Watson, J., 1969. Biological investigations on the spider crab, *Chionoecetes opilio*. Fredericton, CA.
- Watson, J., 1970. Maturity, mating, and egg laying in the spider crab, *Chionoecetes opilio*. *J. Fish. Res. Board Canada* 27, 1607–1616.
- Weingartner, T.J., Aagaard, K., Woodgate, R.A., Danielson, S., Sasaki, Y., Cavalieri, D., 2005. Circulation on the north central Chukchi Sea shelf. *Deep Sea Res. Part II Top. Stud. Oceanogr.* 52, 3150–3174. doi:10.1016/j.dsr2.2005.10.015.
- Weingartner, T.J., Dobbins, E., Danielson, S., Winsor, P., Potter, R., Statscewich, H., 2013. Hydrographic variability over the northeastern Chukchi Sea shelf in summer-fall 2008–2010. *Cont. Shelf Res.* 67, 5–22. doi:10.1016/j.csr.2013.03.012.
- Welch, J.M., Epifanio, C.E., 1995. Effect of variations in prey abundance on growth and development of crab larvae reared in the laboratory and in large field-deployed enclosures. *Mar. Ecol. Prog. Ser.* 116, 55–64.



- „Wieczorek, S.K., Hooper, R.G., 1995. Relationship between Diet and Food Availability in the Snow Crab *Chionoecetes opilio* (O. Fabricius) in Bonne Bay, Newfoundland. *J. Crustac. Biol.* 15, 236–247.
- Zheng, J., 2003. Uncertainties of natural mortality estimates for eastern Bering Sea snow crab, *Chionoecetes opilio*. *Calif. Coop. Ocean. Fish. Investig. Reports* 65, 411–425.  
doi:10.1016/j.fishres.2003.09.029.
- Zheng, J., Kruse, G.H., Ackley, D.R., 2001. Spatial distribution and recruitment patterns of snow crabs in the eastern Bering Sea. In *Spatial processes and management of marine populations*. Fairbanks, AK.

# Sediment Deposition Patterns on the Chukchi Shelf Using Radionuclide Inventories

Lee W. Cooper and Jacqueline M. Grebmeier

Chesapeake Biological Laboratory, University of Maryland Center for Environmental Science, Solomons, MD

[cooper@umces.edu](mailto:cooper@umces.edu), [jgrebmei@umces.edu](mailto:jgrebmei@umces.edu)

## Abstract

Forty sediment cores collected on the Chukchi shelf and adjacent portions of the East Siberian Sea have been assayed for the sedimentation tracers  $^{137}\text{Cs}$  and  $^{210}\text{Pb}$ . Radiocesium deposition patterns indicate that cores can be separated into two broad categories, first, cores where sedimentation influence exceeds bioturbation, and second, those where bioturbation is the dominant redistribution process. The first category generally includes cores collected in high current areas such as Herald Canyon, and comparatively low sedimentation areas such as Hanna Shoal, as well as some portions of the northeast Chukchi shelf. In other portions of the northeast Chukchi shelf and in productive benthic “hotspots,” the influence of bioturbation exceeds sedimentation, and radiocesium is more evenly distributed within the sediments. Sedimentation rates were also calculated for 14 of the 40 cores where there was a consistent decline in excess sedimentary  $^{210}\text{Pb}$  with depth in the core, but sedimentation rate estimates were only consistent with estimated  $^{137}\text{Cs}$  sedimentation rates in 5 of the 14 cores. These data show the complexities of considering sedimentation rate estimates for productive continental shelves in comparison with cores collected at deeper depths, such as one collected from 400 m in the Bering Sea. Despite these limitations on continental shelves, distribution patterns of these radionuclides, particularly the depth where  $^{137}\text{Cs}$  reaches maximum activity and the activity of  $^{137}\text{Cs}$  at that depth provide new insights on the interplay between sedimentation and bioturbation in influencing the broader distribution of contaminants within continental shelf sediments.

## 1. Introduction

Sediment rates and associated processes that control the accumulation of materials on the sea floor are critical to understanding the linkages between pelagic and benthic systems (Hargrave, 1973; Grebmeier et al., 1988). Radionuclides such as  $^{137}\text{Cs}$  and  $^{210}\text{Pb}$  can be used in many circumstances to help inform our understanding of the linkages to water column sedimentation, e.g. (Koide et al., 1972; Robbins and Edgington, 1975; Smith and Walton, 1980). On Arctic shelves in the North American Arctic, the recognition of the strong pelagic-benthic coupling between seasonally productive water column and underlying shallow, broad shelves has led to several prior studies documenting sedimentation rates and accumulation patterns of specific radionuclides, e.g. (Baskaran and Naidu, 1995; Cooper et al., 1998a; Cooper et al., 2005; Pirtle-Levy et al., 2009).

We follow on these earlier studies here by presenting radionuclide data from cores collected at a wide variety of locations on the Chukchi and East Siberian shelves during programs supported by the US National Oceanographic and Atmospheric Administration (the Russian-American

Long-term Census of the Arctic---RUSLACA), and the US Bureau of Ocean Energy Management (Chukchi Sea Offshore Monitoring in Drilling Area ---COMIDA Chemistry and Benthos and COMIDA Hanna Shoal). Data from a relatively deep core (400 m water depth) on the Bering Sea slope is also presented here to provide a comparison to processes north of Bering Strait on the shallow shelf (<50 m). Each of these programs had different motivations for undertaking these studies. For example in the case of the COMIDA program, concern about the ultimate potential fate of contaminants associated with industrial activities that include oil and gas drilling on the Chukchi shelf required a better understanding of the dynamics and depth of bioturbation in shelf sediments, and how long contaminants might be expected to persist. The RUSALCA program is motivated by the need for better understanding of arctic biodiversity, so the relationship of overlying water production on the structuring of marine benthic communities and associated sediment characteristics was the primary motivation.

The two radioisotopes that we chose to meet these objectives were  $^{137}\text{Cs}$  and  $^{210}\text{Pb}$ .  $^{137}\text{Cs}$  is a bomb fallout product (30.2 year half life) with a maximum deposition on the Earth's surface coinciding with the signing of the Limited Nuclear Test Ban Treaty in 1963, which ended most atmospheric nuclear weapons testing. Other secondary sources include the Chernobyl and Fukushima-Daiichi nuclear plant accidents, point pollution sources such as the La Hague (France) and Sellafield (UK) nuclear fuel cycle reprocessing plants, nuclear weapons manufacturing and waste generation facilities such as Hanford (Columbia River, USA) and Zheleznogorsk (Yenisei River, Russia). As an alkali metal, cesium is highly soluble in water and most radiocesium in the world ocean remains dissolved. It reaches the sediments by complexation with clay particles, particularly in soils that are eroded into the ocean, as well as ion exchange at the sediment-water interface, authigenesis and biological uptake (Noshkin and Bowen, 1973; Livingston and Bowen, 1979; Ritchie and McHenry, 1990; Avery, 1996). Because no  $^{137}\text{Cs}$  was present on Earth prior to the development of nuclear weapons and stratospheric bomb fallout reached a maximum in 1963-1964, the depth of penetration of the radionuclide and the distribution of the radioisotope in sediments reflects sedimentation rates and bioturbation.

$^{210}\text{Pb}$  is another independent tracer of sedimentation (Koide et al., 1972). It is a natural radioisotope (22.3 year half-life) that is a daughter product of the  $^{238}\text{U}$  decay series. Some  $^{210}\text{Pb}$  is present that falls to the Earth's surface because one of the immediate precursors to  $^{210}\text{Pb}$  in the uranium decay series is the radioactive gas  $^{222}\text{Rn}$ . Sedimentation studies of this radionuclide require determining the "supported" or background activities of  $^{210}\text{Pb}$  in the sediments, i.e. the inventory of the radionuclide present naturally without considering the contributions of "excess"  $^{210}\text{Pb}$  that is derived from atmospheric deposition (as radon decays). Once the supported  $^{210}\text{Pb}$  inventory has been determined, a sedimentation rate can be estimated by plotting the logarithm of the  $^{210}\text{Pb}$  activity against the mid-depth point of each core increment. The decay constant for  $^{210}\text{Pb}$  ( $-0.01352 \text{ year}^{-1}$ ), reflecting its 22.3 year half-life, is then divided by the calculated slope of this line, below any surface mixed layer, and above the point at which  $^{210}\text{Pb}$  activities decline to a background level supported by in-situ radioactive decay.

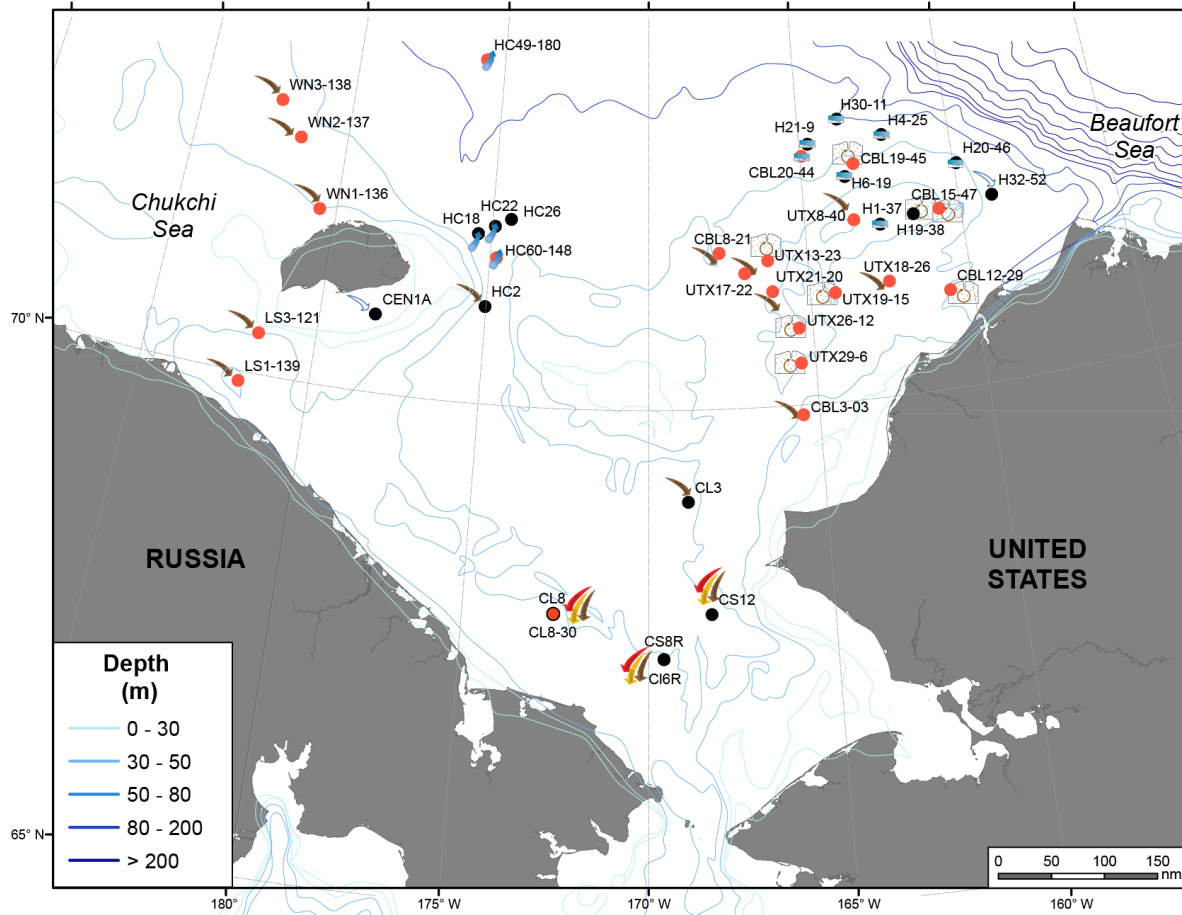
## 2. Methods

Sediment cores were collected using a HAPS benthic corer (Kannevorff and Nicolaisen, 1973) or a Benthos gravity corer (Teledyne Benthos, North Falmouth, Massachusetts) during research cruises conducted during the RUSALCA program in September 2009 and September 2012 (Crane and Ostrovskiy, 2015) and during the COMIDA CAB and Hanna Shoal Ecosystem

projects in August 2009 and August 2012 (Dunton et al., 2014; Dunton, 2015). A HAPS core collected in the north Bering Sea slope on 17 June 2007 from the USCGC Healy was also included in our sampling and the analysis is presented here. Typically, HAPS cores were sectioned in one-centimeter segments to a depth of 4 cm, then every 2 cm below that depth. Gravity cores were sectioned every 2 cm beginning at the surface. Sediments were canned within 90 cm<sup>3</sup> aluminum cans at sea and returned to the laboratory for direct gamma spectroscopy using a Canberra GR4020/S reverse electrode closed-end coaxial detector with low background shielding (Nuclear Lead Co., Oak Ridge, Tennessee) at the Chesapeake Biological Laboratory. Corrections for efficiency and calibrations for all samples were made prior to counting with a mixed gamma standard traceable to the National Institute for Standards and Technology. Background corrections and control samples were analyzed prior to counting to verify a calibrated geometry and detector performance. Data for <sup>137</sup>Cs inventories are reported on an area (per cm<sup>2</sup>) basis, using the 661.5 KeV peak on the gamma spectrum. Sediments were dried after counting (160,000-200,000 seconds) and <sup>210</sup>Pb activity data are reported on a gram dry weight basis, using the 46.5 KeV gamma decay peak. A self-absorption correction for <sup>210</sup>Pb (Cutshall et al., 1983) was determined by counting each sediment sample for 10 minutes in the presence of a sealed <sup>210</sup>Pb source (20kBq) relative to activity associated with the source placed upon an empty aluminum can. All activities are reported relative to the date of collection. Given the comparatively small range of sampling dates (2009 and 2012) on the Chukchi shelf relative to half-life, we assume that differences in collection dates over the 3-year study interval do not introduce any significant differences to interpretations that would be reached if all sampling was corrected to a common date.

### 3. Results

Radiocesium data for 40 cores from the Chukchi continental shelf are reported here (Figure 1). Broad geographical patterns in deposition are evident from the depth in the sediments where maximum <sup>137</sup>Cs activity is observed (Figure 2), reflecting the sedimentation rates of clay particles the isotope is bound too. The activity of radiocesium at the sediment maximum (Figure 3) in addition reflects a combination of sedimentation as well as bioturbation that diminishes the intensity of the <sup>137</sup>Cs activity maximum. We divided cores based upon deposition patterns into two specific categories, depending upon the influence of sedimentation relative to bioturbation, and then further divided those two categories into several general patterns (Figure 1). First, cores collected at the most southern locations to the north of Bering Strait are in areas with high particle deposition and high benthic biological activities, leading to even deposition of <sup>137</sup>Cs over depth due to bioturbation and relatively high activities due to deposition (Figure 4). A similar pattern was observed in many cores collected in the northeast Chukchi shelf, particularly on the southeast portion of Hanna Shoal (Figure 5), which has been identified in other studies as an important benthic biological hotspot with high biological activity (Grebmeier et al., 2015). However, on other parts of the northeast Chukchi shelf, sedimentation dominates over bioturbation processes, leading to cores with mid-depth maxima of <sup>137</sup>Cs (Figure 6). In almost all cases, surface sediment <sup>137</sup>Cs activities were lower than activities deeper within the cores, implying initial burial of radiocesium on clay particles during the bomb fallout era of the 1960's, followed by continued deposition of clay particles with lower radiocesium burdens, and less sediment mixing than observed in more productive areas of the shelf with higher bioturbation. Another common pattern on the northeast Chukchi shelf were



**Figure 1.** Location of the cores studied in the Chukchi and adjacent East Siberian Sea. Red circles were stations sampled in 2009 and black circles were sampled in 2013. Station names are adjacent to the symbols. A few stations (with two station names next to circles) were sampled in both 2009 and 2012. Sediment profile categories based upon  $^{137}\text{Cs}$  distributions:



Cores collected in productive areas with high benthic bioturbation and high sedimentation;




Cores with sedimentation exceeding bioturbation ( $^{137}\text{Cs}$  maximum present);



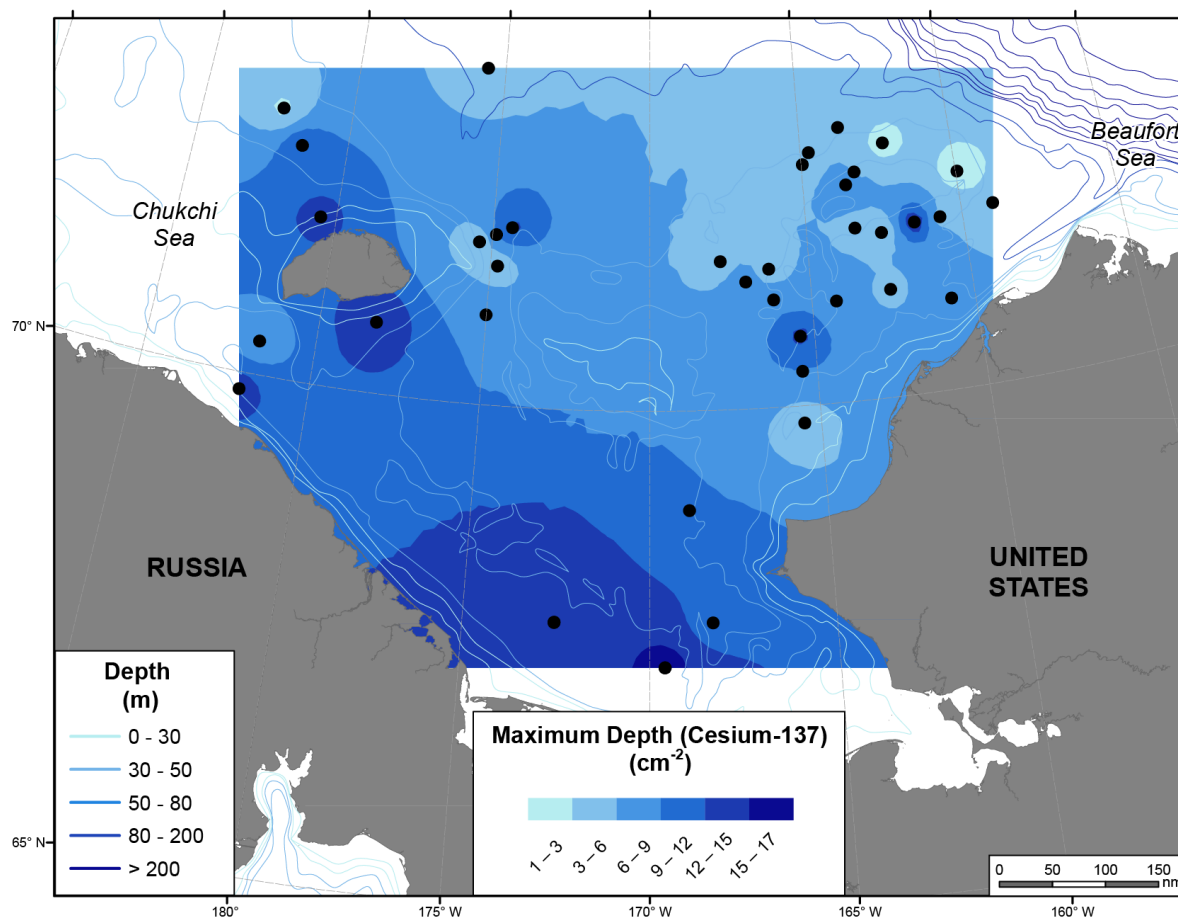
Cores where bioturbation influence exceeded sedimentation (no clear  $^{137}\text{Cs}$  maximum present);

cores collected in Hanna Shoal area showed generally low sediment deposition and shallow if

any  $^{137}\text{Cs}$  maxima;  high current area cores with shallow if any  $^{137}\text{Cs}$  maxima and lower

overall  $^{137}\text{Cs}$  inventories.

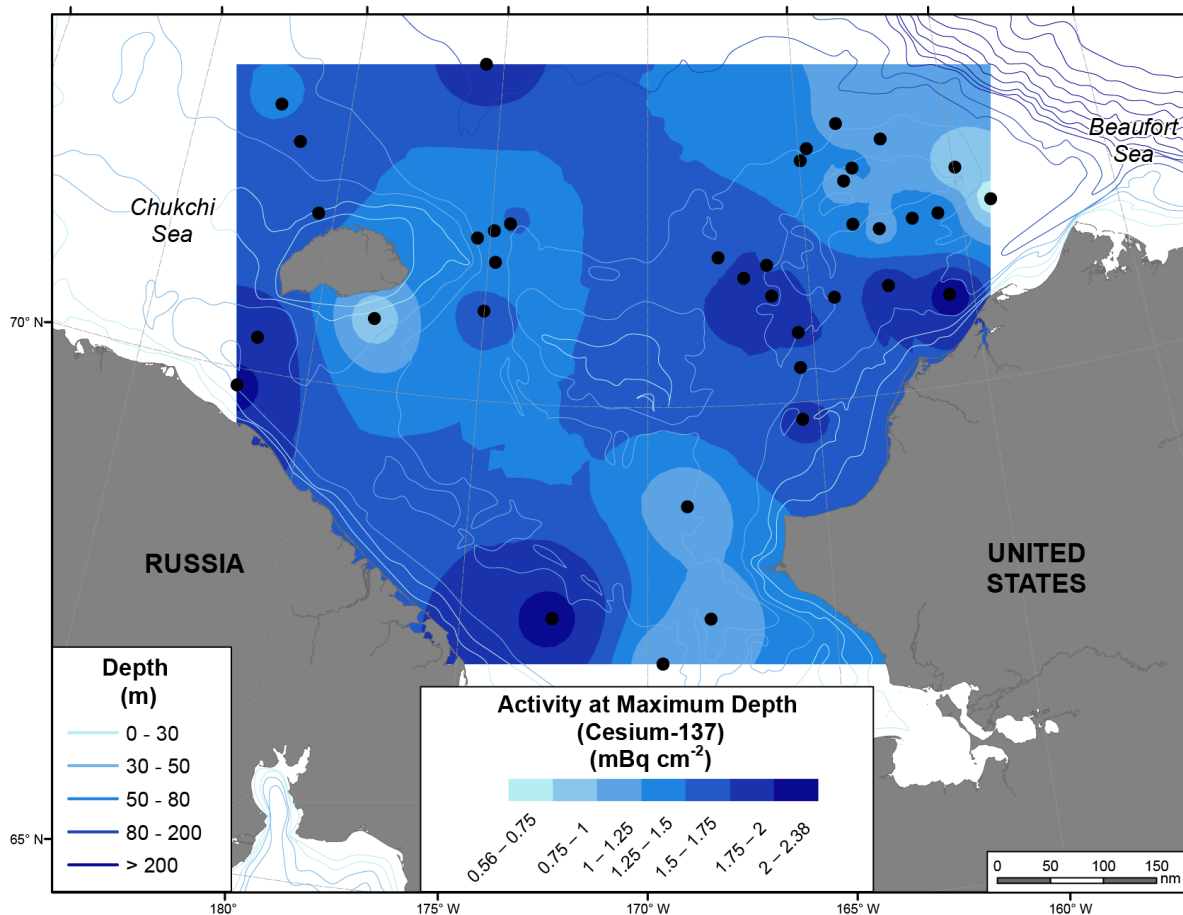
cores without clear maxima in radiocesium content (Figure 7), indicating, as at the southeast of Hanna Shoal and southern Chukchi Sea benthic biological “hotspots,” that bioturbation was a dominant process relative to sedimentation. A variation from these patterns was observed for cores collected from Hanna Shoal (Figure 8), where total radiocesium deposition over the whole sediment core was generally lower, and radiocesium maxima were at shallower depths,



**Figure 2.** Maximum depth (in cm) of radiocesium maximum observed in cores collected in 2009 and 2012.

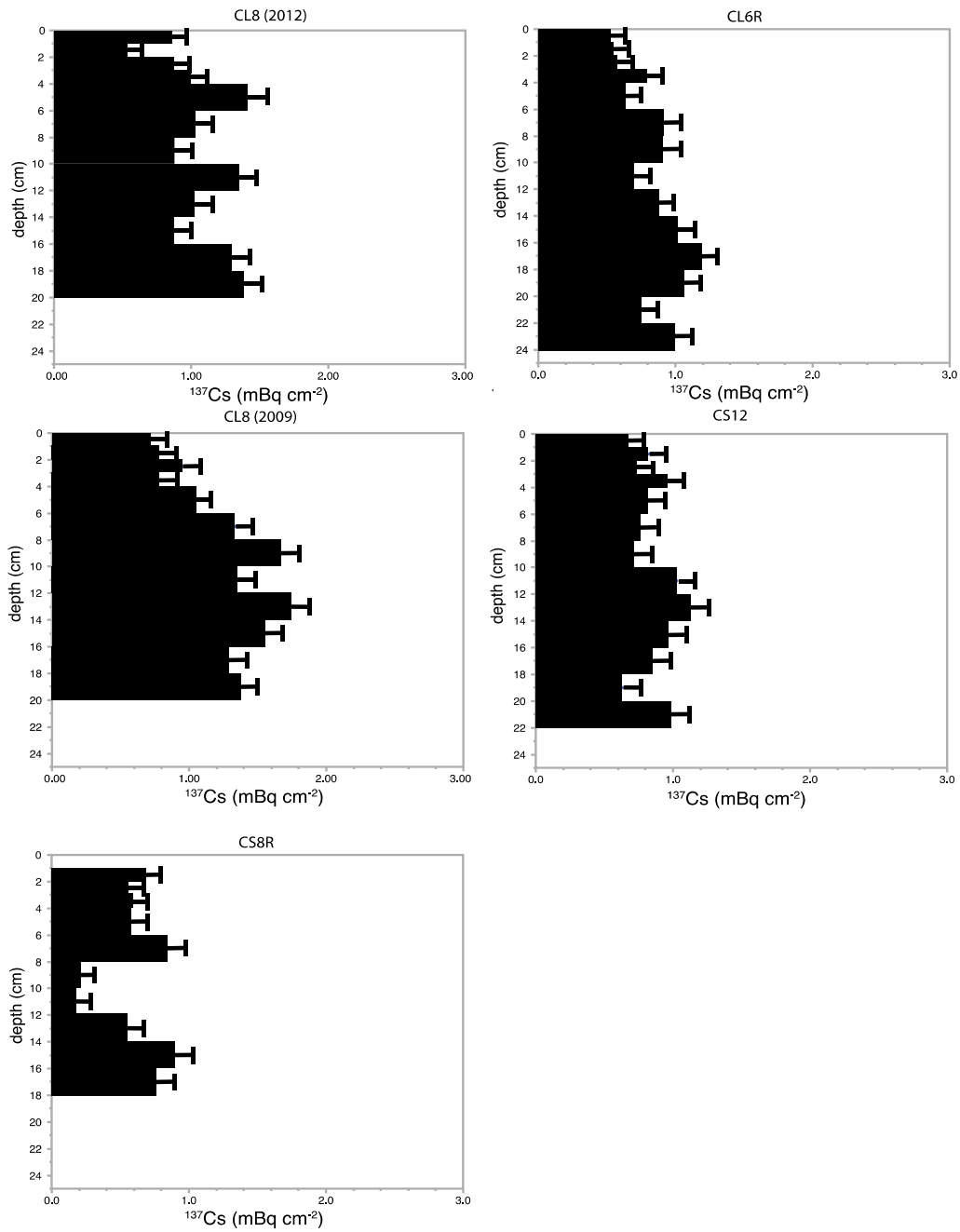
suggesting higher currents, lower deposition, and moderate bioturbation. In areas with higher current flow, such as the Herald Canyon undersea feature on the northern shelf, <sup>137</sup>Cs sediment activities tended to be higher nearer to the sediment surface than elsewhere, implying lower clay particle deposition, and lower sedimentation rates (Figure 9). In five cores collected north of Wrangel Island, East Siberian Sea, and in Long Strait between Wrangel Island and the Russian mainland in 2009, lower current flow, and dominance of bioturbation over sedimentation was implied by deeper sediment <sup>137</sup>Cs activities (Figure 10).

A final category of core deposition patterns were two cores with very low <sup>137</sup>Cs inventories, (Figure 11), south of Wrangel Island, and in the far northeastern Chukchi shelf. We also present here for comparison with all Chukchi and East Siberian sea cores, the <sup>137</sup>Cs activity in a core collected on 17 June 2007 at 400 m depth on the Bering Sea slope (Figure 12). Probably due to the greater water depth of collection and lower sedimentation rates, <sup>137</sup>Cs activity is lower throughout the core (<1 mBq cm<sup>-2</sup>), and is concentrated nearer the surface. Bioturbation of radiocesium also extended no deeper than 16 cm depth, so the patterns of deposition of radiocesium on the Bering Sea slope are significantly different than observed on the Chukchi shelf.



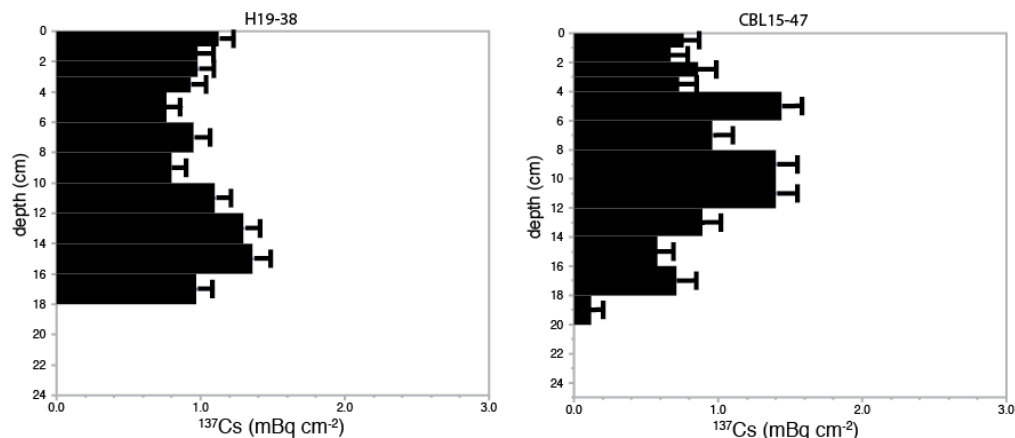
**Figure 3.** Radiocesium activity at the depth where maximum activity was observed. Data are corrected to core collection data in 2009 or 2013.

In most of these 40 cores,  $^{137}\text{Cs}$  activity was still detected at the bottom of cores recovered, so total inventories are larger than the integrated sums of activity data that are available, although for many cores much of the total inventory was recovered, based upon low or near detection activities at the base of each core. The distributions of  $^{210}\text{Pb}$  within these 40 cores from the Chukchi shelf reflect many of the same bioturbation and sedimentation patterns. However, the use of  $^{210}\text{Pb}$  as a sedimentation indicator compared to radiocesium requires more than simply identifying a maximum  $^{137}\text{Cs}$  peak in a sediment core and dividing that depth by the number of years since the bomb fallout peak in 1963-1964. Bioturbation limited the number of cores with steady, logarithmic declines in  $^{210}\text{Pb}$  to only 14 of the 40 cores collected, plus the single core collected on the Bering slope in 2007 (Figure 13). In addition, sedimentation rate estimates obtained for the 14 Chukchi shelf cores were consistent with sedimentation rate estimates obtained from maximum  $^{137}\text{Cs}$  peaks in only 5 of the 14 cores (Figure 13). The  $^{210}\text{Pb}$  profile with the most robust regression coefficient was the 400-m water depth core collected in the



**Figure 4.** Radiocesium distributions in sediment cores categorized as having more influence from bioturbation than sedimentation and located in areas of high biological activity north of Bering Strait. In general these are cores with no identifiable <sup>137</sup>Cs maxima and even distribution of radiocesium throughout the sediment core.



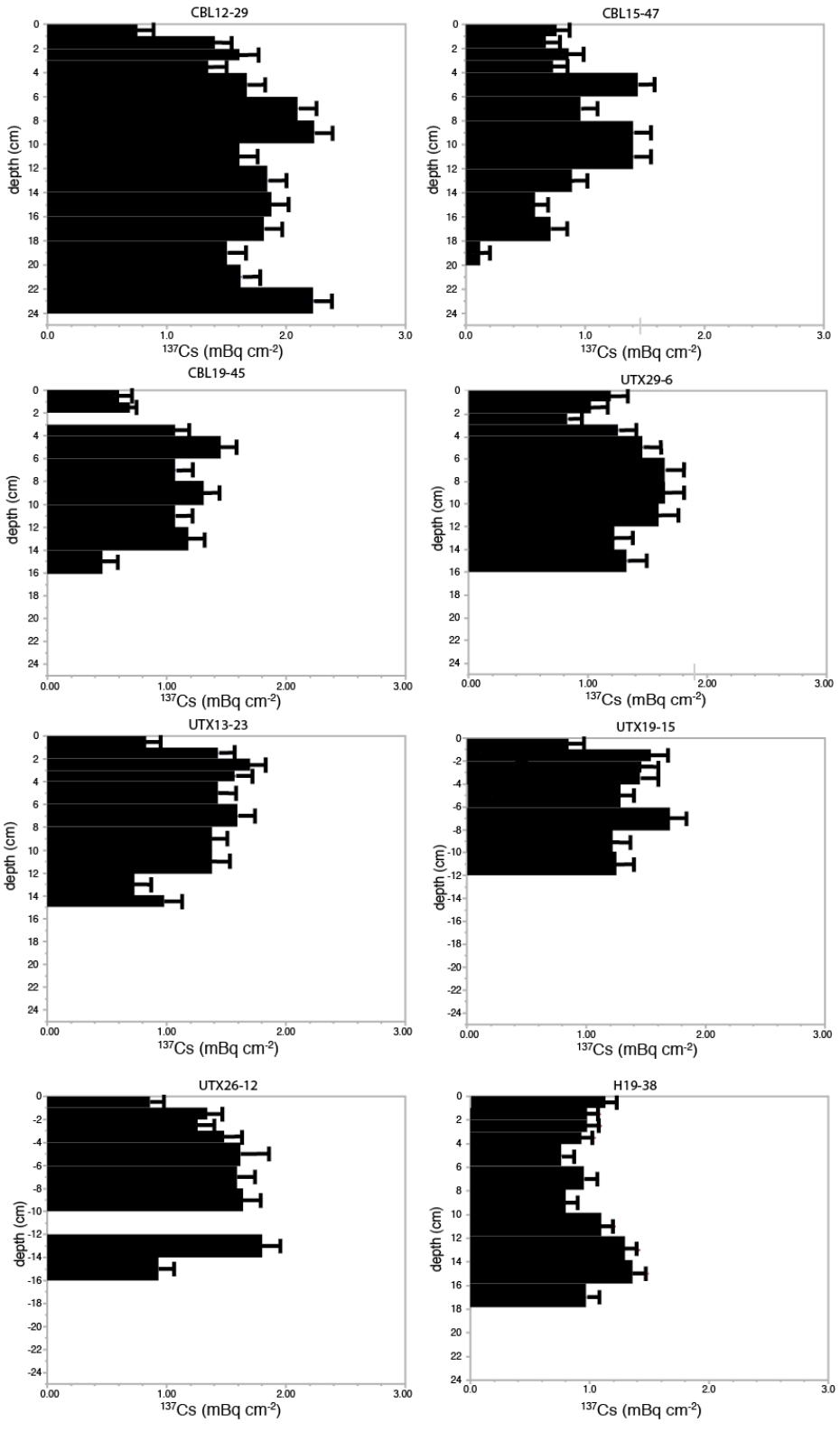


**Figure 5.** Radiocesium distributions in two cores collected from a biologically active location on the southeast side of Hanna Shoal. As with cores shown in Figure 4, these are cores with no identifiable  $^{137}\text{Cs}$  maxima and even distribution of radiocesium throughout the sediment core.

Bering Sea in 2007 (Figure 13, lower right hand sub-plot). Surface (0-1 cm) activities for  $^{210}\text{Pb}$  in this core were anomalously low and  $^{137}\text{Cs}$  activities were anomalously high (Figure 12). If this 0-1 cm depth is excluded, sedimentation rates were similar for this core ( $0.11 \text{ cm year}^{-1}$ ) for both ( $^{210}\text{Pb}$  and  $^{137}\text{Cs}$ ) sedimentation estimate methods.

#### 4. Discussion

The sedimentation of  $^{137}\text{Cs}$  and  $^{210}\text{Pb}$  observed in 40 cores collected in 2009 and 2012 on the Chukchi shelf and adjoining areas of the East Siberian Sea demonstrate the complexity associated with evaluating sedimentation processes on biologically productive continental shelves. Prior work has demonstrated that sedimentation at deeper depths such as on the Chukchi outer continental shelf can be reasonably estimated, e.g. (Cooper et al. 1998a; Pirtle-Levy et al. 2009), and our own measurements of both  $^{137}\text{Cs}$  and  $^{210}\text{Pb}$  from a 400 m water depth core on the Bering slope are also consistent with those findings. However, on the shallow shelf (<50m), bioturbation dominates or at least significantly alters sedimentation patterns recorded by radionuclide tracers such as  $^{137}\text{Cs}$  and  $^{210}\text{Pb}$ . We divided  $^{137}\text{Cs}$  deposition patterns into several different categories depending upon whether bioturbation or sedimentation dominates (Figure 1). In areas that are highly productive with high sedimentation, such as immediately north of Bering Strait and at the localized “hotspot” on the southeast side of Hanna Shoal, no distinct peak in  $^{137}\text{C}$  is observed and total radionuclide inventories tend to be high (Figure 4). By comparison, at a wide variety of locations on the Chukchi shelf, particularly the northeastern Chukchi shelf (Figure 1), sedimentation is a larger influence than bioturbation, and  $^{137}\text{Cs}$  maxima can be observed in sediment cores (Figure 7). A continuum exists in other parts of the northeastern Chukchi shelf, where bioturbation is a greater influence on sediment radiocesium inventories than sedimentation, and no distinct peak in  $^{137}\text{Cs}$  is observed (Figure 6), although total



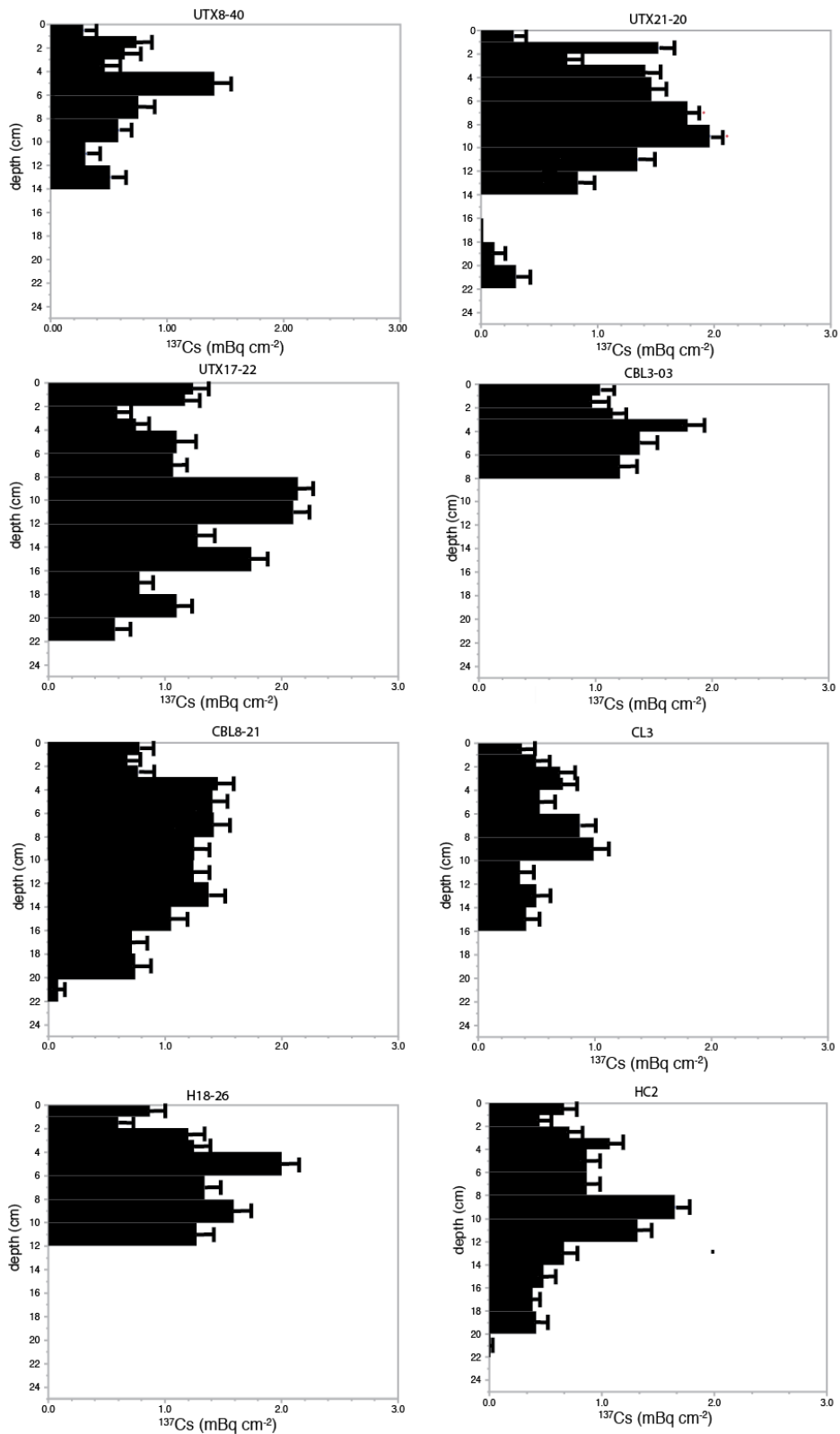
**Figure 6.** Radiocesium distributions in sediment cores categorized as having more influence from bioturbation than sedimentation. In general these are cores with no identifiable  $^{137}\text{Cs}$  maxima and even distribution of radiocesium throughout the sediment core.

radiocesium inventories can be lower than in biological hotspots (Figure 4, 5). On Hanna Shoal itself, low sedimentation leads to lower total inventories, with  $^{137}\text{Cs}$  maxima often nearer to the surface of cores (Figure 8). A similar pattern of shallow radiocesium burial was observed in areas with high current flow such as Herald Canyon (Figure 9), while other sampling in Long Strait and north of Wrangel Island in the East Siberian Sea identified more quiescent regions with deeper deposition of clay particles carrying  $^{137}\text{Cs}$  than in Herald Canyon. Finally, localized areas of anomalously low radiocesium deposition were also identified in the far northeastern Chukchi Sea and south of Wrangel Island (Figure 11), probably reflecting high current flow and low clay particle deposition.

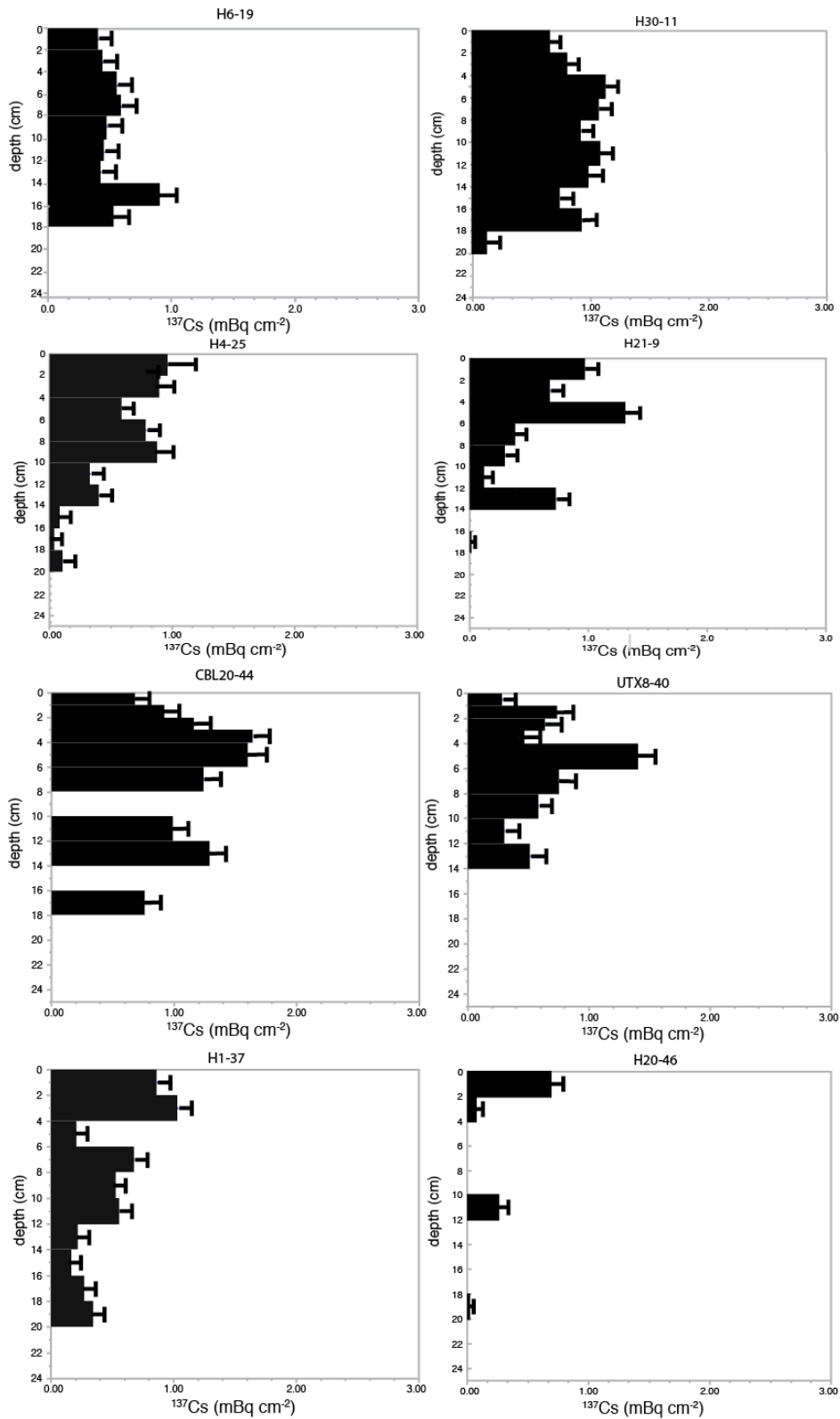
These patterns demonstrate some of the complexities of considering sedimentation processes on a shelf system where accumulation of contaminants, e.g. from industrial oil and gas development, may be a concern. The depth of sediment penetration of bomb fallout  $^{137}\text{Cs}$  can reach 20 cm or more and bioturbation can be the dominant process where contaminants are spread evenly throughout this bioturbated layer.  $^{210}\text{Pb}$  is an independent indicator of sedimentation, but application is more problematic because it requires a steady decrease in  $^{210}\text{Pb}$  downwards through the sediment core as the activities decline for the proportion of the  $^{210}\text{Pb}$  that are in excess of the supported (background) activities in the sediments. Thus a valid  $^{210}\text{Pb}$  deposition estimate depends upon steady declines in  $^{210}\text{Pb}$  throughout the sediment core, and not activities at any single depth. This is a more rigorous requirement than the simple assumption that a maximum in  $^{137}\text{Cs}$  represents the deposition that was concentrated at the time of the 1963-1964 bomb fallout peak that has been since re-distributed to some extent by bioturbation. In our study of 40 sediments cores, only 14 cores, and the core collected on the Bering Slope in 2007 met the requirement for steady decreases in excess  $^{210}\text{Pb}$  over the length of the sediment core (Figure 13).

Seven cores collected in Herald Canyon, near Wrangel Island, and in Long Strait (HC, WN and LS stations on Figure 13, respectively), where there are more distinct  $^{137}\text{Cs}$  sediment maxima, were the most consistent locations where  $^{210}\text{Pb}$  sedimentation estimates were feasible. Two cores collected from Hanna Shoal (H30-11 and H6-19), and two cores from the northeastern Chukchi Sea that were judged to be dominated by sedimentation relative to bioturbation in  $^{137}\text{Cs}$  analyses (UTX8-40 and CBL8-21) also met these  $^{210}\text{Pb}$  sedimentation rate criteria of steady declines in excess  $^{210}\text{Pb}$  through the sediment core. However, in only 5 of the 14 cores were the excess  $^{210}\text{Pb}$  sedimentation rate estimates consistent with the estimates based upon the depth of  $^{137}\text{Cs}$  sediment maxima (Figure 13). The decline in excess  $^{210}\text{Pb}$  activity was best correlated with sediment depth in the core collected from slope (400 m depth) sediments in the Bering Sea (Figure 12), which is consistent with collections made on the Chukchi slope at similar depths to our Bering Sea sample (Cooper et al., 1998a; Pirtle-Levy et al., 2009). It is possible of course that the  $^{210}\text{Pb}$  sedimentation estimates obtained here (Figure 13) are more accurate than those obtained from  $^{137}\text{Cs}$  analyses, which are based upon the single point where a maxima was reached. However a broader point is simply the problematic challenge that is poised by needs to estimate sedimentation rates on biologically active shelves.

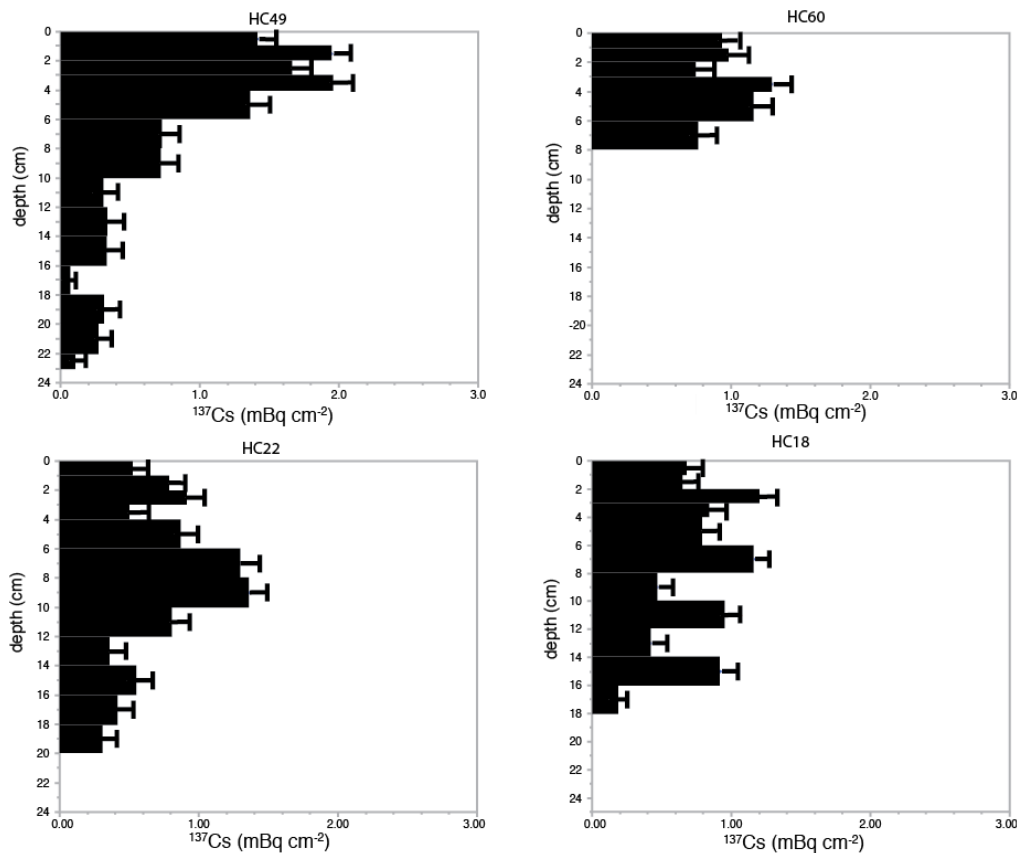
Nevertheless, broad geographical patterns are apparent in the distribution of radiocesium in sediments, both the depth of maximum activity, and the activity at that depth, depending upon current flow, biological activity, and sedimentation and the combined interplay of those factors (Figure 2, 3). The intensity of the peak radiocesium activity is influenced by bioturbation (e.g. less intense in the most productive benthic communities), and the depth of the radiocesium



**Figure 7.** Radiocesium distributions in sediment cores categorized as having more influence from sedimentation than bioturbation. In general these are cores with identifiable <sup>137</sup>Cs maxima.



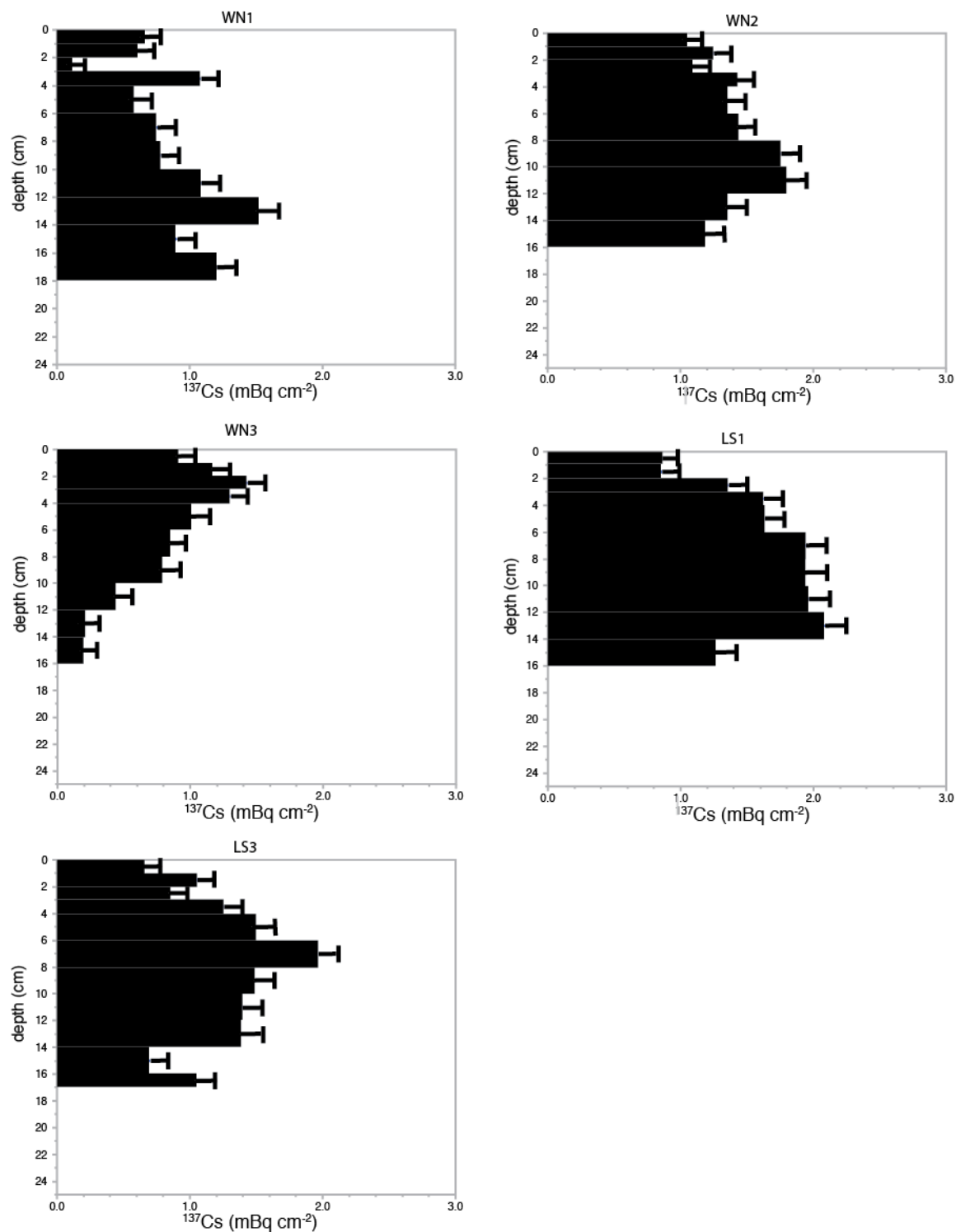
**Figure 8.** Radiocesium distributions in sediment cores collected from Hanna Shoal that show relatively low deposition and shallow maxima.



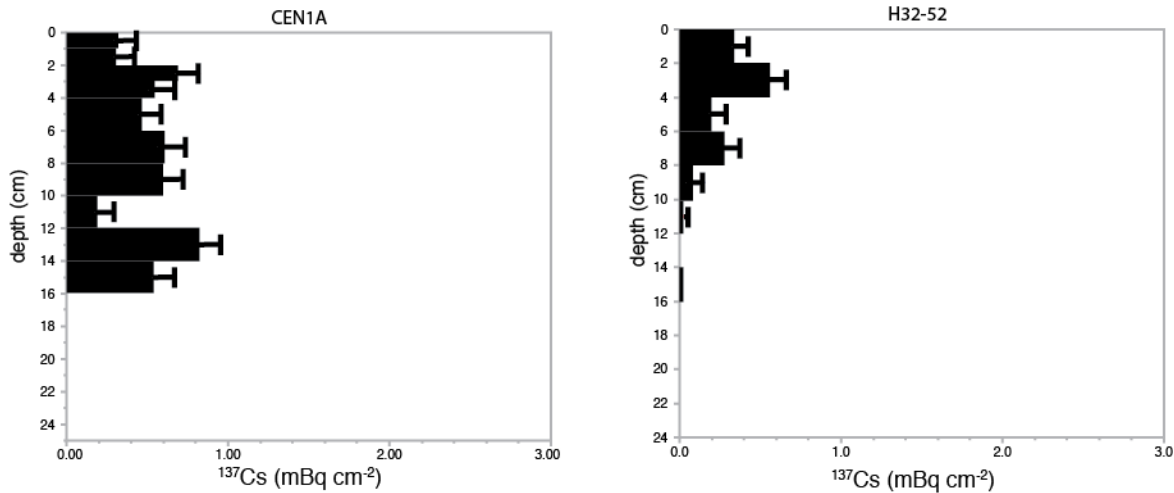
**Figure 9.** Radiocesium distributions in sediment cores collected from high current regions within Herald Canyon, showing relatively low deposition and shallow maxima.

activity maximum is influenced by sedimentation. For example, deep and well-mixed  $^{137}\text{Cs}$  inventories are observed in known areas of high benthic biological activities north of Bering Strait that also have high sedimentation and southeast of Hanna Shoal. Current flow can reduce the depth of radiocesium distribution within the sediments (e.g. Hanna Shoal and Herald Canyon), as well as overall deposition. As better understanding is developed of biogeochemical processes on arctic shelves, e.g. (Grebmeier, 2012), the measurements of these two radioactive tracers, and probably other stable and radioisotopes show promise for helping to improve understanding of re-distribution mechanisms for biological and mineralogical materials in marine sediments.

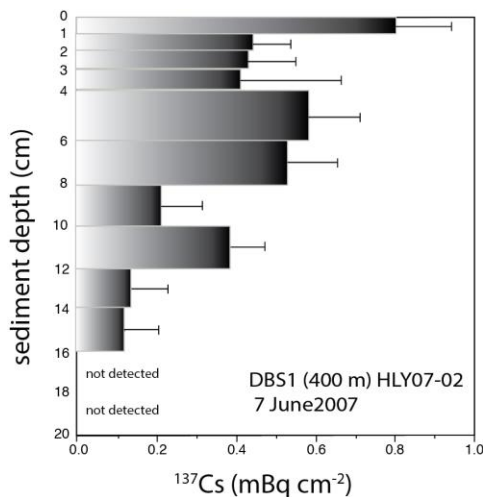
Finally, a related uncertainty is suggested by the activities of  $^{137}\text{Cs}$  observed in surface sediments in this study. Measurements of  $^{137}\text{Cs}$  in surface sediments of the Beaufort, Chukchi and East Siberian seas in 1991-1995 showed activities averaging  $3.5 \pm 2.3 \text{ Bq kg}^{-1}$  dry weight ( $n=145$ ); (Cooper et al., 1998b). Converted to a dry weight basis from the per square meter inventory data provided in this study, almost no surface samples in this study have even 50% of the average burden by weight present during the 1990's. Given the 30.2 year half life of  $^{137}\text{Cs}$ , and the <20 year period that has elapsed since collection of those samples and the cores in this study, it is apparent that  $^{137}\text{Cs}$  is disappearing faster from Chukchi sea sediments than would be expected



**Figure 10.** Radiocesium distributions in sediment cores collected north of Wrangel Island and in Long Strait, generally showing relatively low current flow and lower bioturbation than from Herald Canyon (Figure 8).



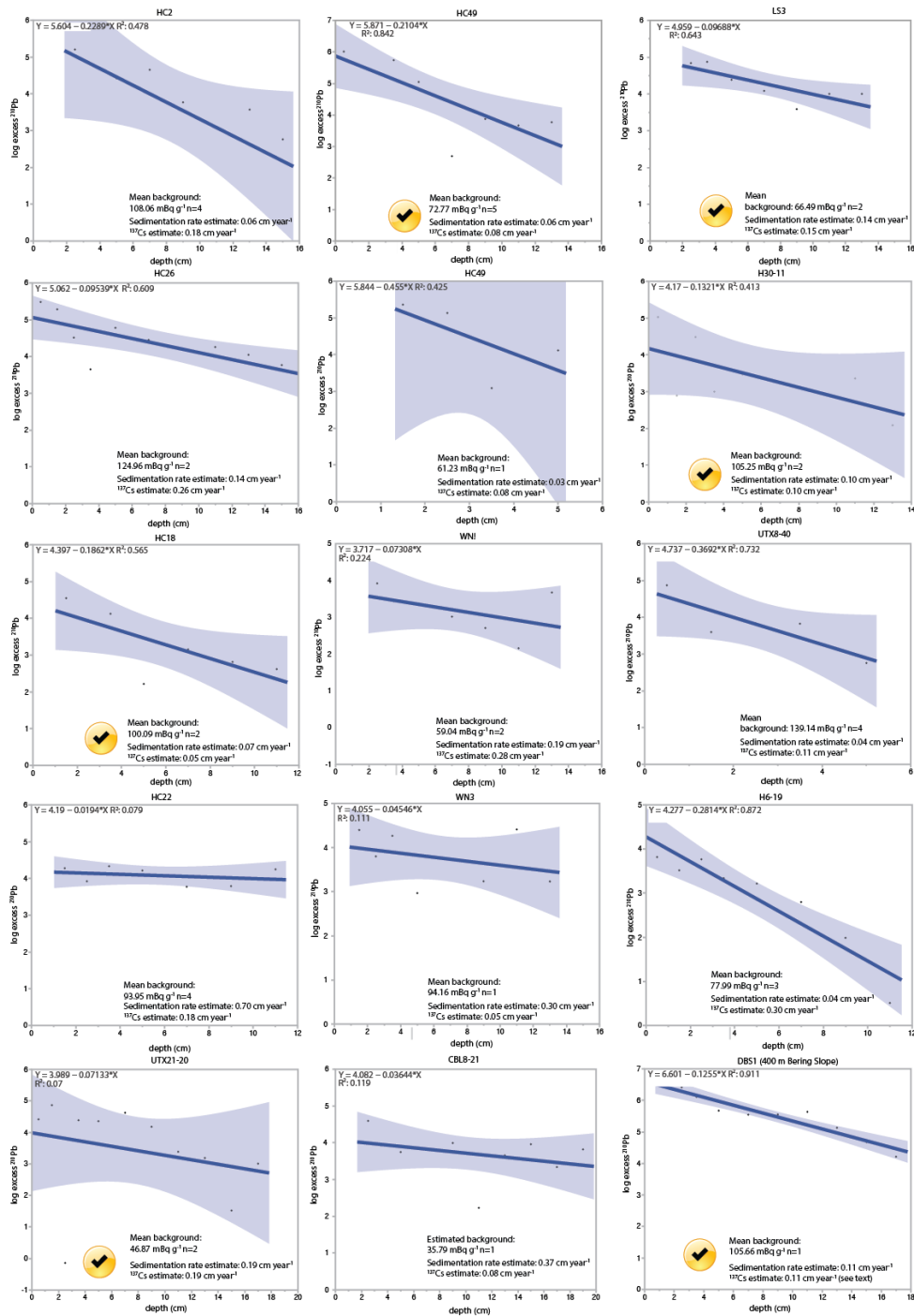
**Figure 11.** Radiocesium distributions in two sediment cores with low overall deposition south of Wrangel Island and in the northeast Chukchi Sea.



**Figure 12.** Radiocesium distribution in a sediment core collected on the Bering continental slope (400 m water depth) in June 2007 from the USCGC Healy. Station location is 60.0469°N, 179.6632°W.

solely based upon radioactive decay. The sink for the radioisotope may be mixing deeper into the sediments, loss from the sediments by dissolution from clay particles, entrainment with fine particles onto sea ice that is forming or downstream transport into the deeper Arctic Ocean. The probable arrival of radiocesium into the Arctic through Bering Strait from the Fukushima-Daiichi nuclear power plant accident will make these determinations more difficult to make, but also suggests that any loss of cesium from the mostly dissolved radiocesium plume in the water column onto fine particles could be potentially detected by comparing with the radiocesium content of sediments measured on the Chukchi shelf both in the 1990's and during this study.





**Figure 13.** Log of  $^{210}\text{Pb}$  excess regressions relative to sediment depth for 14 cores (of 40) where there was a steady decline in excess  $^{210}\text{Pb}$  (above background or supported), moving down the sediment core. Background or supported  $^{210}\text{Pb}$  provided for each core is based upon activities at the base of the core (number of activities averaged is given as n=). Sedimentation estimates from  $^{210}\text{Pb}$  were calculated from the activity co-efficient for  $^{210}\text{Pb}$  ( $-0.1352 \text{ year}^{-1}$ ) divided by slope of the line relating log excess  $^{210}\text{Pb}$  to sediment depth (cm). The yellow checked circles indicate cores where there was good agreement between sedimentation rate estimates provided by both  $^{210}\text{Pb}$  and  $^{137}\text{Cs}$ .

## 5. Acknowledgements

This study was funded by the U.S. Department of the Interior, Bureau of Ocean Energy Management (BOEM), Alaska Outer Continental Shelf Region, Anchorage, Alaska under BOEM Cooperative Agreement No. M11AC00007 as part of the Chukchi Sea Offshore Monitoring in Drilling Area (COMIDA). Funding for the RUSALCA program was provided by NOAA. We thank the US Coast Guard, COMIDA HS colleagues and shipboard team, including Christian Johnson, Mengjie Zhang, Laura Gemery, Dubrava Kirievskaya, Holly Kelly, Christina Goethel, and Piper Lewis. In addition, we thank Christian Johnson (assistance with gamma spectroscopy), and Alynne Bayard (GIS mapping).

## 6. References

- Avery, S.V. 1996. Fate of caesium in the environment: Distribution between the abiotic and biotic components of aquatic and terrestrial ecosystems. *Journal of environmental radioactivity* 30:139-171.
- Baskaran, M., Naidu, A.S., 1995.  $^{210}\text{Pb}$ -derived chronology, and the fluxes of  $^{210}\text{Pb}$  and  $^{137}\text{Cs}$  isotopes into continental shelf sediments, East Chukchi Sea, Alaskan Arctic. *Geochimica et Cosmochimica Acta* 59:4435-4448.
- Cooper, L.W., Grebmeier, J.M., Larsen, I.L., Dolvin, S.S., Reed, A.J., 1998a. Inventories and distribution of radiocesium in arctic marine sediments: Influence of biological and physical processes. *Chemistry and Ecology* 15:27-46.
- Cooper, L.W., Larsen, I.L., Beasley, T.M., Dolvin, S.S., Grebmeier, J.M., Kelley, J.M., Scott, M., Johnson-Pyrtle, A., 1998b. The distribution of radiocesium and plutonium in sea ice-entrained Arctic sediments in relation to potential sources and sinks. *Journal of environmental radioactivity* 39:279-303.
- Cooper, L.W., Larsen, I.L., Grebmeier, J.M., Moran, S.B., 2005. Detection of rapid deposition of sea ice-rafted material to the Arctic Ocean benthos using the cosmogenic tracer  $^7\text{Be}$ . *Deep Sea Research Part II: Topical Studies in Oceanography* 52:3452-3461.
- Crane, K., Ostrovskiy A., 2015. Introduction to the Special Issue: Russian-American Long-term Census of the Arctic: RUSALCA. *Oceanography* 28:18-23.
- Cutshall, N.H., Larsen, I.L., Olsen, C.R., 1983. Direct analysis of  $^{210}\text{Pb}$  in sediment: self-absorption corrections. *Nuclear Instrument Methods* 206:309-312.
- Dunton, K. 2015. Hanna Shoal: An integrative study of a high arctic marine ecosystem. *Environment, Coastal and Offshore (Eco) Magazine*:24-33.
- Dunton, K.H., Grebmeier, J.M., Trefry, J.H., 2014. The benthic ecosystem of the northeastern Chukchi Sea: An overview of its unique biogeochemistry and biological characteristics. *Deep Sea Research Part II: Topical Studies in Oceanography*.
- Grebmeier, J.M. 2012. Shifting Patterns of Life in the Pacific Arctic and Sub-Arctic Seas. *Annual Review of Marine Science* 4:63-78.
- Grebmeier, J.M., Bluhm, B.A., Cooper, L.W., Danielson, S., Arrigo, K.R., Blanchard, A.L., Clark, J.T., Day, R.H., Frey, K.E., Gradinger, R.R., Kedra, M., Konar, B., Kuletz, K.J., Lee,

- S.H., Lovvorn, J.R., Norcross, B.L., Okkonen, S.R., 2015. Ecosystem characteristics and processes facilitating persistent macrobenthic biomass hotspots and associated benthivory in the Pacific Arctic Progress In Oceanography 136:92-114.
- Grebmeier, J.M., McRoy, C.P., Feder, H.M., 1988. Pelagic-benthic coupling on the shelf of the northern Bering and Chukchi Seas. I. Food supply source and benthic biomass. Marine Ecology - Progress Series 48:57-67.
- Hargrave, B.T. 1973. Coupling carbon flow through some pelagic and benthic communities. Limnology and Oceanography 14:801-805.
- Kanneworff, E., Nicolaisen W., 1973. The "HAPS:" A frame supported bottom corer. Ophelia Supplement 10:119-129.
- Koide, M., Soutar, A., Goldberg, E.D., 1972. Marine geochronology with <sup>210</sup>Pb. Earth and Planetary Science Letters 44:442-446.
- Livingston, H.D., Bowen, V.T., 1979. Pu and 137Cs in coastal sediments. Earth and Planetary Science Letters 43:29-45.
- Noshkin, V., Bowen, V.T., 1973. Concentrations and distributions of long-lived fallout radionuclides in open ocean sediments. Pages 671-686 Radioactive contamination of the marine environment. IAEA Vienna.
- Pirtle-Levy, R., Grebmeier, J.M., Cooper, L.W., Larsen, I.L., 2009. Chlorophyll *a* in Arctic sediments implies long persistence of algal pigments. Deep Sea Research Part II: Topical Studies in Oceanography 56.
- Ritchie, J.C., McHenry, J.R., 1990. Application of radioactive fallout Cesium-137 for measuring soil erosion and sediment accumulation rates and patterns: A review. Journal of Environmental Quality 19:215-233.
- Robbins, J.A., Edgington, D.N., 1975. Determination of recent sedimentation rates in Lake Michigan using Pb-210 and Cs-137. Geochimica et Cosmochimica Acta 39:285-304.
- Smith, J.N., Walton, A., 1980. Sediment accumulation rates and geochronologies measured in the Saguenay Fjord using the Pb-210 dating method. Geochimica et Cosmochimica Acta 44:225-240.

# **Water Column Chemistry, Benthic Macroinfaunal Populations, and Sediment Tracer Measurements**

**Jacqueline Grebmeier, Lee Cooper**

**Chesapeake Biological Laboratory, University of Maryland Center for Environmental Science, Solomons, MD**

[jgrebmei@umces.edu](mailto:jgrebmei@umces.edu), [cooper@umces.edu](mailto:cooper@umces.edu)

## **Abstract**

The shallow, but complex bathymetry of Hanna Shoal influences the productivity of the water column and organic sedimentation processes. The Chesapeake Biological Laboratory research group undertook both water column and sediment sample collections as part of the BOEM-funded COMIDA Hanna Shoal project during the HLY1201 (August 9-25, 2012) and HLY1301 (July 29-August 15, 2013) cruises, including a sub-set of stations on the Distributed Biological Observatory transect line across Barrow Canyon. Based upon field efforts in 2012 and 2013, as well as prior work, we identified that inshore waters are less nutrient rich and lower in chlorophyll content than offshore waters, especially to the north and west. However, although areas of high benthic biomass, sediment oxygen demand and chlorophyll deposited to the surface sediments are higher in the offshore regions, these parameters do not always mimic the water column processes. These organic sedimentation indicators tend to be higher to the south, including in waters to the south and east of Hanna Shoal where large populations of walrus have also been observed to forage on the benthos in the summer from remnant sea ice. The emerging picture suggests that the complex current system rotates richer organic materials around the periphery of Hanna Shoal in a clockwise direction, with shoreward enhancement of organic material deposition. These pelagic – benthic coupling characteristics are considered in the context of the larger Chukchi marine ecosystem.

## **1. Introduction**

The shallow, but complex bathymetry of Hanna Shoal influences the productivity of the water column and organic sedimentation processes. Based upon field efforts in 2012 and 2013, as well as prior work, inshore waters are less nutrient rich and water column chlorophyll also increases offshore to the north and west. However, benthic biomass, sediment oxygen demand and chlorophyll deposited to the surface sediments do not always mimic these water column processes. These organic sedimentation indicators tend to be higher to the south, including in waters to the south and east of Hanna Shoal where large populations of walrus have also been observed to forage on the benthos in the summer from seasonal sea ice that remains. The emerging picture suggests that the complex current system rotates richer organic materials around the periphery of Hanna Shoal in a clockwise direction, with shoreward enhancement of organic material deposition. These pelagic - benthic coupling characteristics are being evaluated

in the context of the larger Chukchi marine ecosystem. The following report has a brief introduction to our project, then methods, findings and conclusions.

### **1.1 A physical and ecological overview of the Chukchi Sea ecosystem**

The Chukchi Sea is an inflow shelf of the Arctic Ocean, with advection of Pacific water through Bering Strait a driving factor for ecosystem structure (Carmack and Wassmann, 2006, Grebmeier et al., 2006). With the declining trend of sea ice extent and increasing duration of ice-free season, along with increasing Pacific water temperatures, the NE Chukchi Sea has been the focus of collaborative and interdisciplinary scientific studies as part of the BOEM COMIDA project (Dunton et al., 2014), funded by the Bureau of Ocean Energy Management, and the environmental program sponsored by the oil and gas industry (Day et al., 2013).

The Chukchi shelf is complex topographically, with variable environmental factors, including retreating sea ice, increasing organic matter and nutrient input, and increasing light availability. The Chukchi Sea is known for regions of strong pelagic-benthic coupling and high benthic macrofaunal biomass estimated to reach  $> 4000$  g wet weight  $m^{-2}$  (or  $\sim 150$  g C  $m^{-2}$ ; Grebmeier et al., 2015). The physical features play an important role in biological community structure and ecosystem variation in the northeastern Chukchi Sea (Blanchard and Feder, 2014, Schonberg et al., 2014). The northward water transport of Pacific water from the Bering Strait during summer and fall includes three major water masses: cold, salty and nutrient-rich Anadyr Water (AW) in the western Bering Strait, warm, fresh and nutrient-poor Alaskan Coastal Current (ACW) formed by an eastern branch of Bering Strait inflow and the intermediate Bering Shelf water. AW and BSW merge through Bering Strait to form Bering Sea Water (BSW) in the Chukchi Sea, while ACW maintains its freshwater features moving northward (Grebmeier et al., 2015). The BSW flows over the central shelf and bifurcates into two branches west of Hanna Shoal. One of them moves north, east and southeast around Hanna Shoal and northward on the western side of Barrow Canyon, while the other flows eastward along the southern flank of Hanna Shoal and converges with the ACW at Barrow Canyon (Weingartner et al., 2013). The BSW provides high quality organic carbon and nutrient supply to the shelf and fosters high primary production in the water column and large biomass of benthos in the summer (Grebmeier et al., 2006). The advection of organic matter from the south and production associated with different water masses are important drivers on dynamic benthic food-web structure in the northeast Chukchi Sea.

Sediment grain size is related to the strength of the flow field, with finer silt and clay sediments being deposited as currents slow down as well as commonly co-varying with sediment total organic carbon (TOC) content (Grebmeier et al., 2006, 2015). More positive stable carbon isotopes and lower C/N values in the organic carbon content of surface sediments are also an indicator of the quality of organic carbon (Grebmeier et al., 2006, 2015). Surface sediment chlorophyll *a* and sediment community oxygen consumption (SCOC) can also be indicative of the supply of organic carbon to the sediments (Grebmeier et al., 2006, 2015). Carbon and nitrogen stable isotope ratios can be used to determine trophic levels and ultimate carbon sources when end members of different carbon isotope compositions exist. Iken et al. (2010) showed that  $\delta^{13}C$  values of particulate organic material were more depleted in the relatively unproductive Alaska Coastal Water compared to the enriched values of the highly productive Anadyr Water.

## 1.2 Objectives

The Chesapeake Biological Laboratory (CBL) research group undertook both water column and sediment sample collections during the HLY1201 (August 9-25, 2012) and HLY1301 (July 29-August 15, 2013) COMIDA Hanna Shoal cruises, including a sub-set of stations on the Distributed Biological Observatory transect line across Barrow Canyon during both cruises (Figure 1.) The shallow, but complex bathymetry of Hanna Shoal appears to influence the productivity of the water column and organic sedimentation processes. The Hanna Shoal area has been identified as an area of biological interest because it is one of the last areas used by walrus while sea ice is still present in late summer over the Chukchi Shelf. Even in those years when sea ice is no longer present on the Shoal as a resting platform, some walrus return from shore beaches such as at Point Lay to forage in this area (Jay et al., 2012).

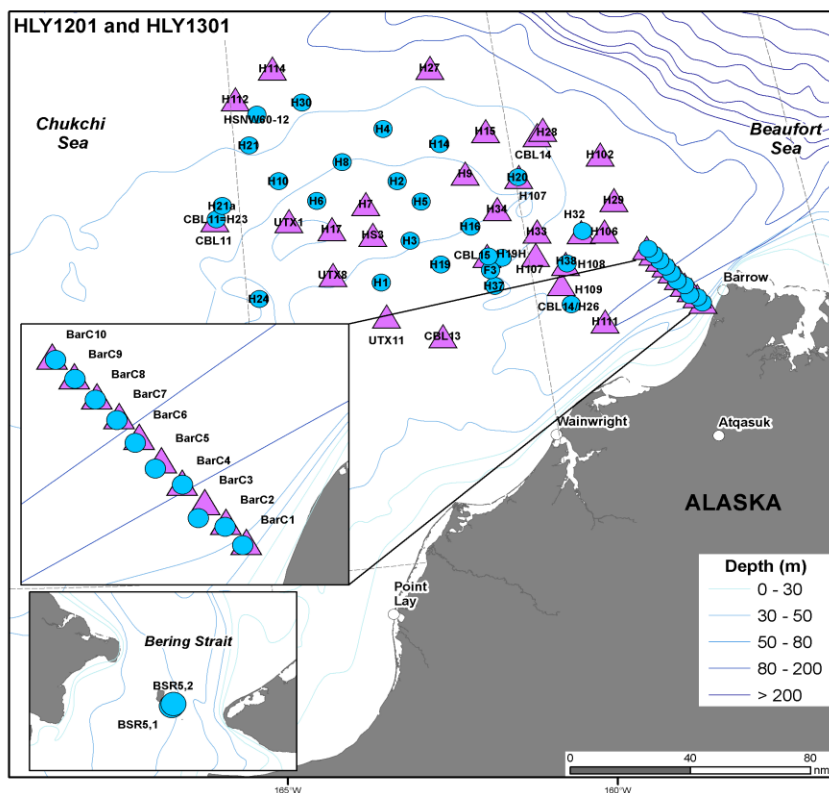
## 2. Methods

Water column collections included sampling for inorganic nutrients, chlorophyll *a* and stable oxygen isotopes from the CTD/rosette system. The water column and sediment chlorophyll concentrations were analyzed shipboard using a Turner Designs AU-20 fluorometer (non-acidification or Welschmeyer method) following a 24-hour (water) or 12-hour (sediment) in the dark extraction period in 90% acetone at 4°C. Inorganic nutrients were also collected from the CTD rosette, filtered shipboard, frozen, and subsequently analyzed at the Nutrient Analytical Service Laboratory (NASL) at CBL (NASL, 2016). Procedures and techniques used by NASL are available at <http://nasl.cbl.umces.edu/>. Water samples for <sup>18</sup>O/<sup>16</sup>O ratios were also collected in small glass vials, stored at room temperature, and analyzed at CBL using a Thermo DeltaPlus Stable Isotope mass spectrometer. For a graduate student supported project evaluating the stable isotope composition of amino acid isotopes within the foodweb, phytoplankton samples were collected with 20 m mesh nets and filtered onto 25mm Whatman GF/F filters that were pre-combusted at 450° (for 24 h to remove trace organic material). Ice collected at selected stations was thawed in the dark environment under room temperature. The melted ice water was then filtered onto pre-combusted 25mm Whatman GF/F filters to get ice algae samples. Bottom water samples (~5m above bottom) were collected during the CTD water column collection casts, and then filtered onto Whatman GF/F filters for suspended particulate organic matter.

Surface sediment and benthic macrofaunal samples were collected using a 0.1 m<sup>2</sup> Van Veen grab, weighted with 32 kg. Surface sediments were collected throughout the cruise from the top of the single van Veen grab before it was opened to minimize disturbance of surface sediments. These collections included determination of inventories of chlorophyll *a* (chl *a*) in surface sediments shipboard (as described above) as well as subsamples to determine total organic carbon (TOC) and nitrogen (TON) content, C/N ratios, δ<sup>13</sup>C and δ<sup>15</sup>N (bulk organic analyses), and grain size determination. Additional subsamples of sediments were collected to assay surface sediments for ostracod abundance (Laura Gemery; both 2012 and 2013 cruises) and rare earth elements (Dubrava Kirievskaya, Russian State Hydrometeorological University, St. Petersburg; 2013 cruise).

The rest of the sediment from the first grab was sieved through 1mm screen mesh and the retained macrofauna were subsequently sorted shipboard to family or lowest taxon possible, frozen, and returned to CBL in Solomons, Maryland, where they were stored in a -20°C freezer

prior to processing for compound specific isotope analyses. Four additional quantitative grabs were collected, with the sediments sieved to retain the animals on a 1 mm screen, and subsequently preserved in 10% buffered seawater formalin, for post cruise analyses of taxonomic identification, abundance and biomass determinations in our CBL laboratory. Replicate sediment cores were also collected by the single or multiple HAPS coring systems and used for shipboard incubations in the dark and at in-situ bottom water temperatures using one of the temperature controlled chamber rooms on the USCGC Healy. Oxygen utilization, inorganic nutrient and



**Figure 1.** Stations sampled during Healy 1201 (August 2012) and Healy1301 (July-August 2013).

inorganic carbon exchange were measured during these incubations, specifically for 17 stations during HLY1201 and 18 stations during HLY1301. Additionally, HAPS core and gravity core collections of sediments were used to support measurements of sedimentation rates. Cores were sectioned and canned in calibrated geometric containers and analyzed on gamma counters at CBL. Radiogenic isotopes, such as  $^{137}\text{Cs}$  and  $^{210}\text{Pb}$ , were counted at CBL using two low background gamma spectrometers in order to determine sedimentation rates. We have completed 22 down core radioisotopic analyses (several hundred samples) as part of this project that is part of the Cooper et al. draft manuscript prepared for the special issue of Deep-sea Research II.

Finally, at each station where it was practical, and dependent upon sea state and ice conditions, a submersible video camera system was lowered to the seafloor to document the epibenthic communities at each station. These video clips were used by the University of Alaska Fairbanks research trawling team, and have been analyzed on a semi-quantitative basis to estimate organisms per square meter and/or to qualitatively characterize the epibenthic communities at

each location sampled in a collaborative study between our CBL technician, Christian Johnson at CBL and Ph.D. candidate, Alexandra Ravelo at UAF.

### 3. Results

The results presented in this final report were data collected during both the 2012 and 2013 COMIDA Hanna Shoal cruises (HLY1201 and HLY1301, respectively). Our efforts included sampling the benthos to identify specific communities of importance to walrus and other benthic feeding predators. Taxonomic identification of invertebrates with relatively high biomass particularly occurred on the southeast side of the Shoal. We are working with other members of the COMIDA team to understand the biogeochemical and physical basis for the apparent biological importance of Hanna Shoal.

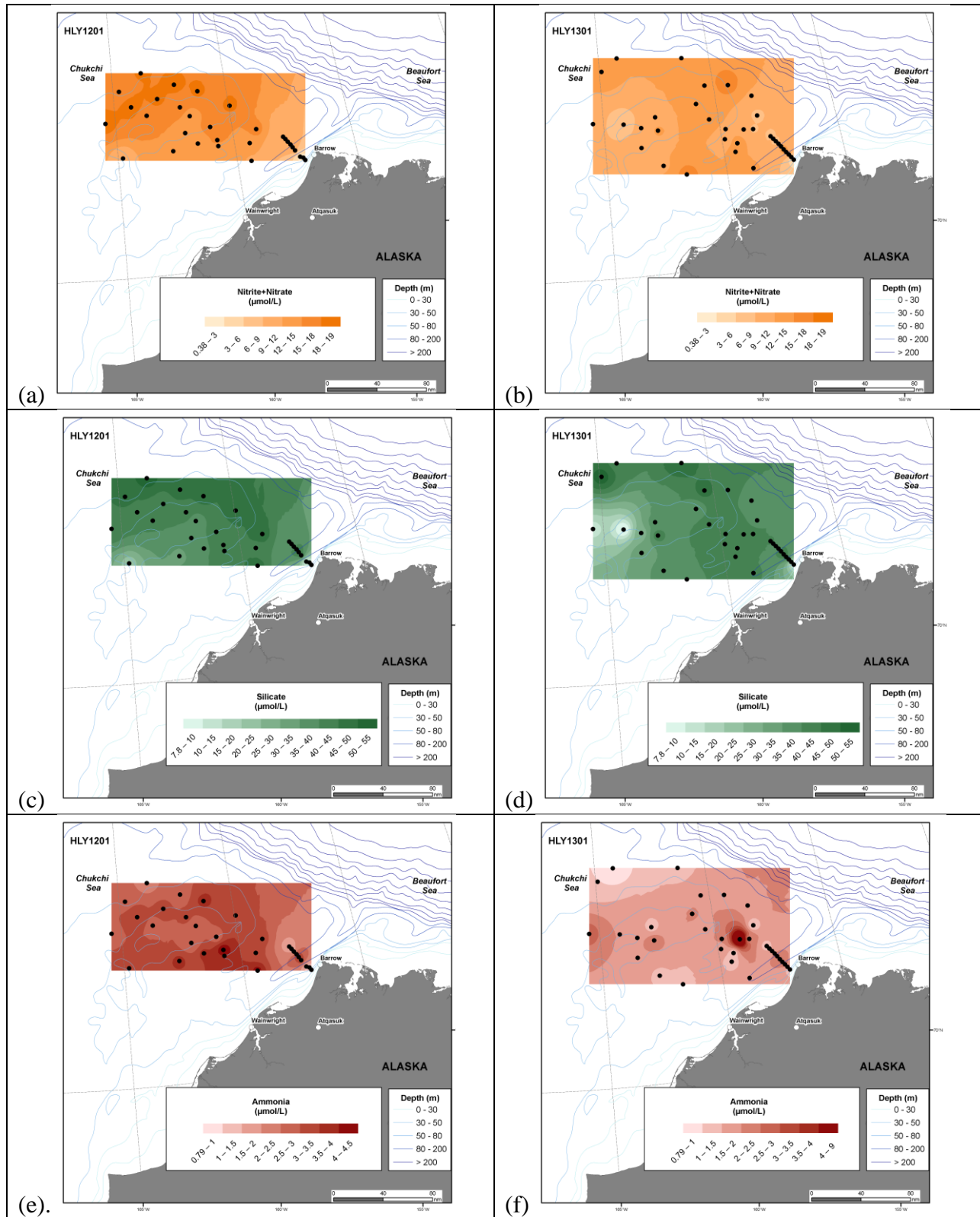
#### 3.1 Water column nutrients and chlorophyll *a*

Water column nutrients in surface and bottom waters (Figure 2) indicate interannual variability due to the different water masses of Pacific origin transported to the region, along with their associated nutrient content. Figure 2 shows the nitrite/nitrate (Figure 2a,b), silicate (Figure 2c, d) and ammonium (Figure 2e,f) for HLY1201 and HLY1301, all that indicate the clockwise circulation of northward transiting Bering Sea water around Hanna Shoal, with the 2013 bottom water ammonium data (Figure 2f) having the highest values in the SE section of Hanna Shoal.

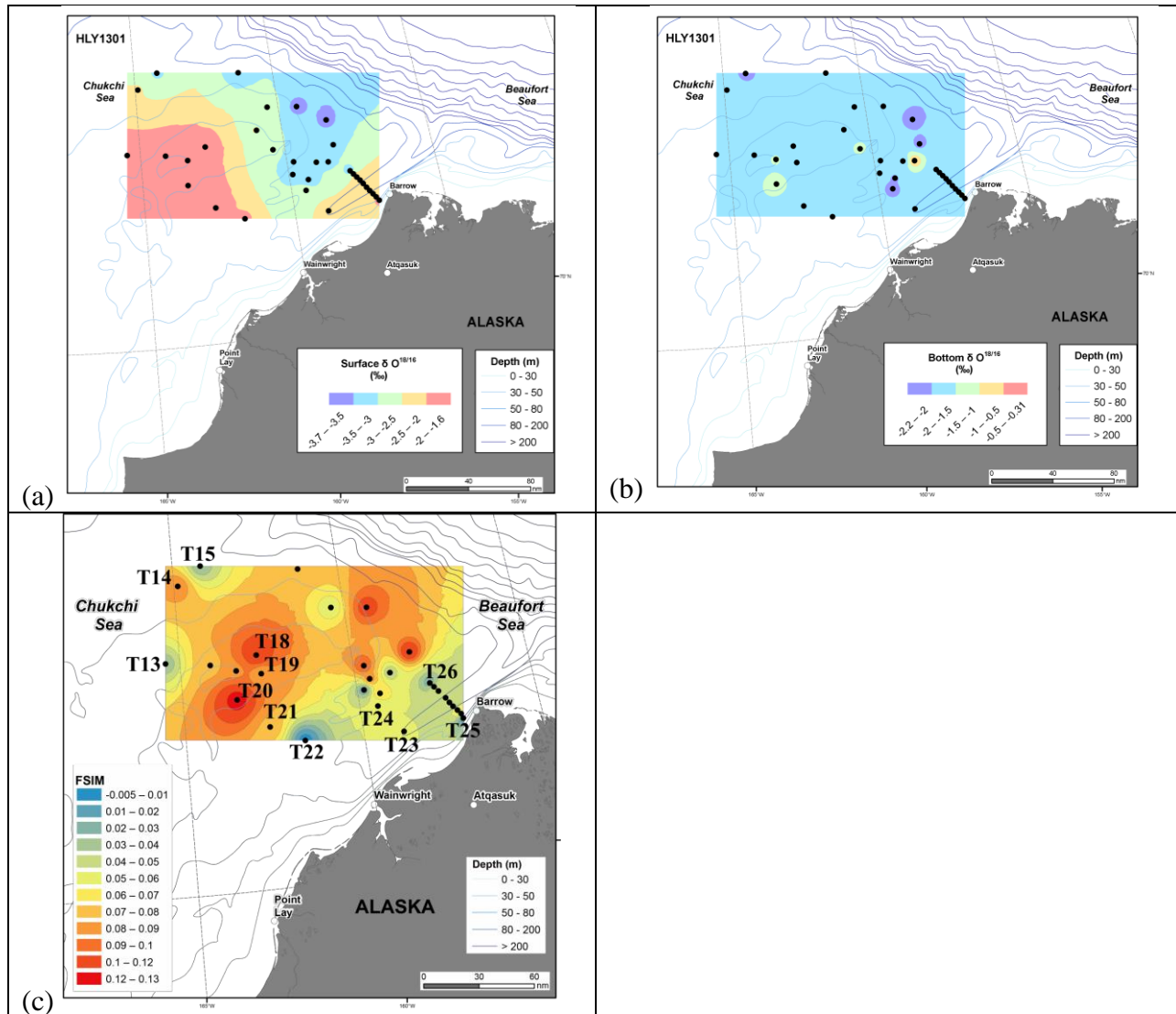
Figure 3a shows the stable oxygen isotope values in: 3a. surface seawater and 3b. bottom waters during HLY1301. Figure 3a indicates more sea ice melt at the surface in the area over a wide portion of Hanna Shoal and in Barrow Canyon (red colors, -1.6 to -2 ‰), with the northeastern area of Hanna Shoal with more Atlantic-type water at the surface (blue colors, -3 ‰). By comparison, most of the bottom water over the study area has expected values associated with Bering Sea winter water (~ -2‰). Figure 3c. shows a three end-member mixing model can be used to estimate the fraction of melted sea ice relative to Atlantic water and runoff, using stable isotopes of oxygen and salinity as variables. Negative fractions of sea ice melt result from contributions of brine injected during sea ice formation. Data shown are for the 2012 Healy cruise and have been incorporated into a manuscript, “Optical Properties and Molecular Diversity of Dissolved Organic Matter in the Bering Strait and Chukchi Sea,” by Gonsior et al. that has been submitted to the COMIDA Hanna Shoal Deep-Sea Research II special issue.

Figure 4a indicates higher water column integrated chlorophyll (chl) *a* biomass to the north and west of the study area in 2012 whereas water column chl *a* biomass was highest in the eastern section in 2013 (Figure 4b). These data are consistent with a growing understanding of the flow of more nutrient-rich water clockwise around the northern periphery of the Shoal, but the variability between years is influenced by time of sampling and hydrographic variability. The slightly earlier sampling in 2013 may have influenced the variable integrated chl *a* values in 2013 vs. 2012. The sediment chlorophyll *a* data (Figure 4 c,d) reflect recent sedimentation (~weeks, based upon distribution of the short-term <sup>7</sup>Be tracer) of live chlorophyll to the sediments. The distribution of sediment chlorophyll relative to water column chlorophyll suggests some lateral advection to the south and east. Other data to be used to help confirm these indications include bottom water nutrients (Figure 2), sediment respiration measurements and longer-term sedimentation indicators.

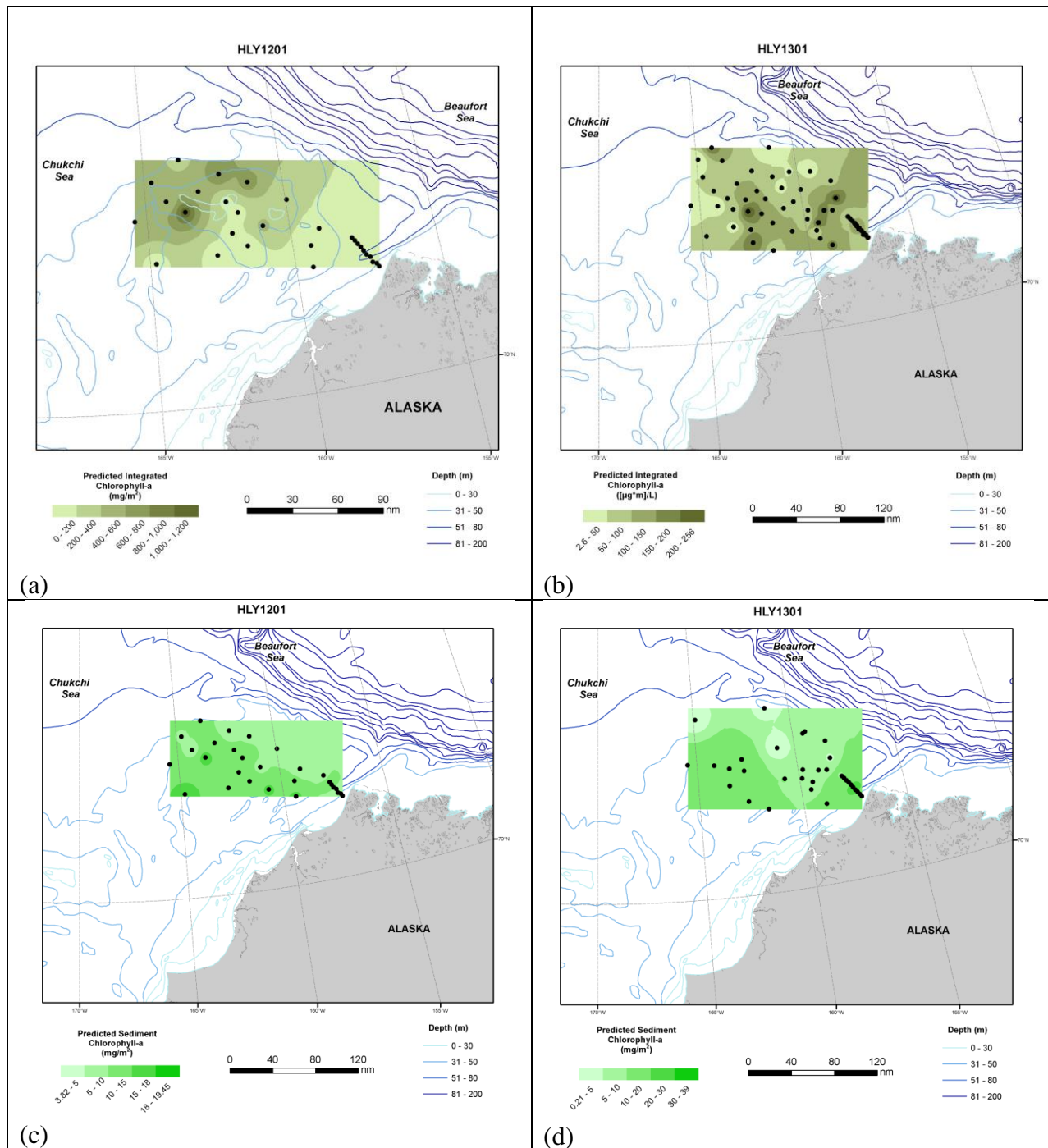




**Figure 2.** Bottom water nutrients: nitrate/nitrite (a,b), silicate (c,d) and ammonium (e,f) for HLY1201 (left) and HLY1301 (right).



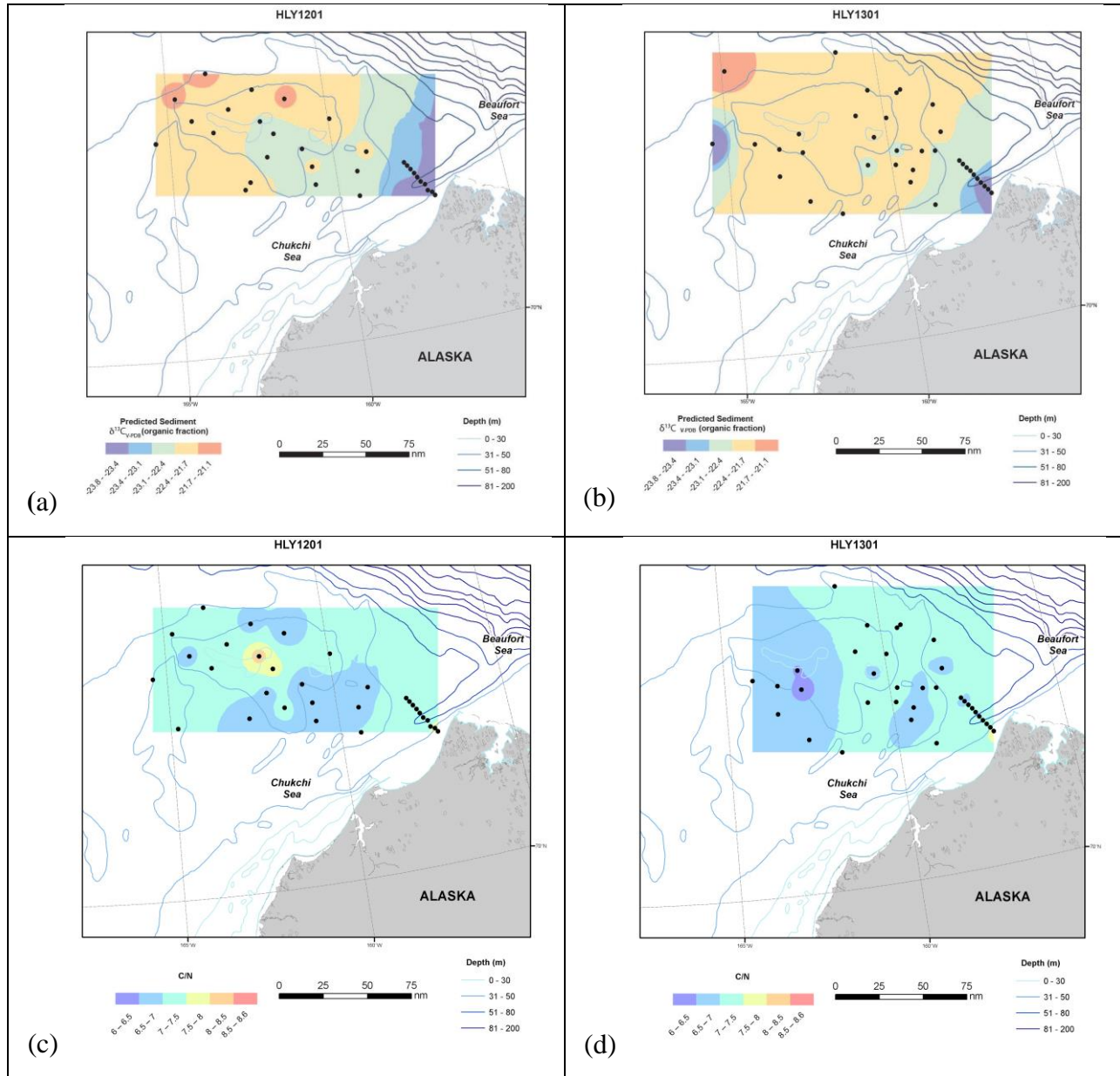
**Figure 3.**  $\delta^{18}\text{O}$  for surface seawater (a) and bottom seawater (b) during HLY1301 in 2013, along with fractional sea ice melt (FSIM) (c) present in surface waters during HLY1201 in 2012. See text for brief description of three end member mixing model that was used.



**Figure 4.** Water column chlorophyll *a*, integrated from sea surface to bottom during (a) HLY1201 in 2012 and (b) HLY1301 in 2013. Sediment chlorophyll *a* on surface sediments (0-1 cm) during (a) HLY1201 in 2012 and (d) HLY1301 in 2013.

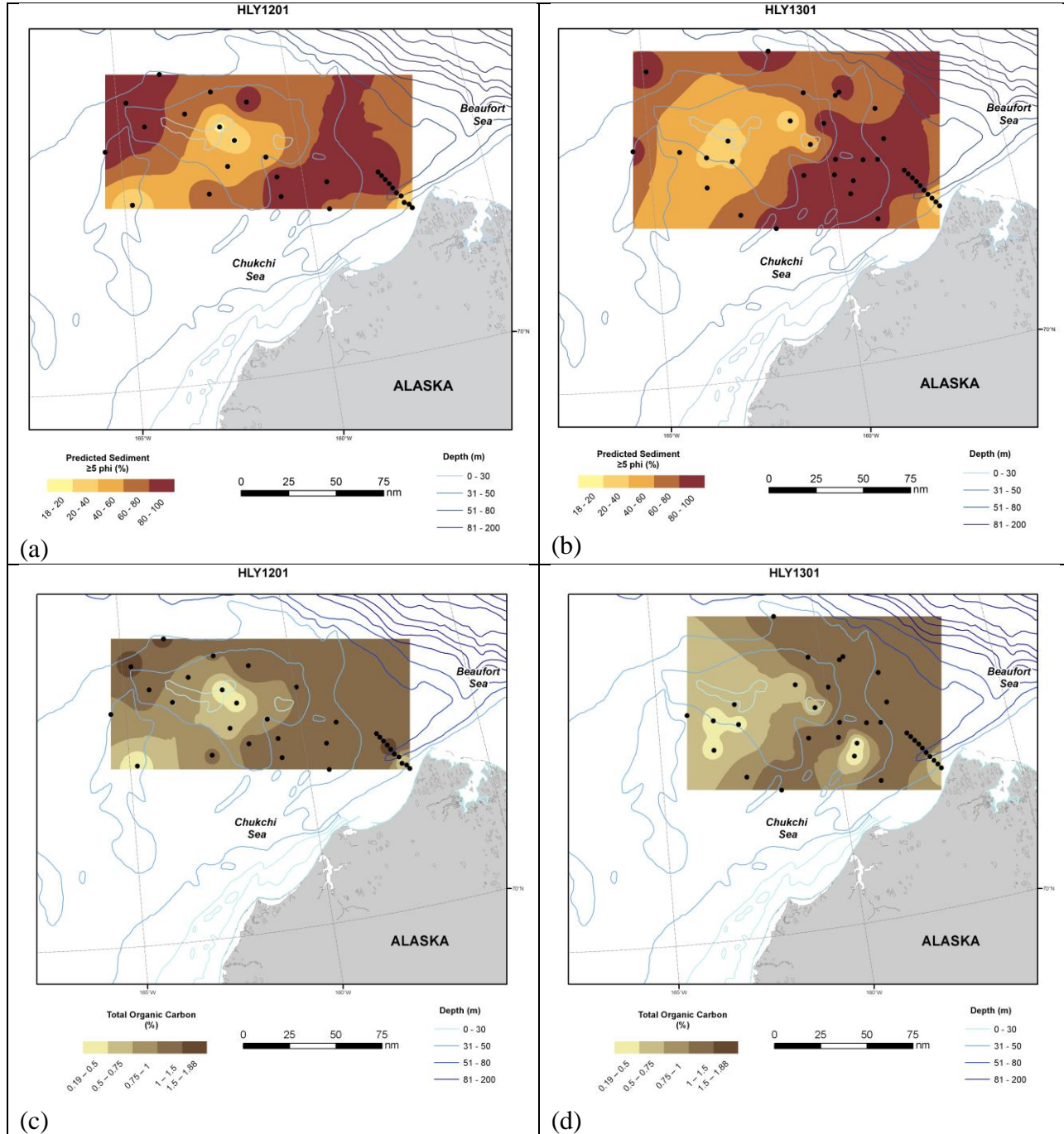
### 3.2 Sediments

Stable isotopes of carbon in the organic fraction of surface sediments ( $\delta^{13}\text{C}_{\text{org}}$ ) and surface sediment C/N ratios (Figure 5c,d) provides insights on the biogeochemistry of organic carbon and nitrogen as more nutrient rich water flow clockwise around the northern periphery of the Shoal. In general, less negative  $\delta^{13}\text{C}$  and lower C/N values reflect organic matter synthesized under higher rates of biological productivity and lower terrestrial inputs, and possibly higher sea ice. Higher  $\delta^{15}\text{N}$  and C/N values indicate additional cycling of organic nitrogen in the sediments and water column as organic materials. Grain size distributions (Figure 6 a,b) clearly show the coarser

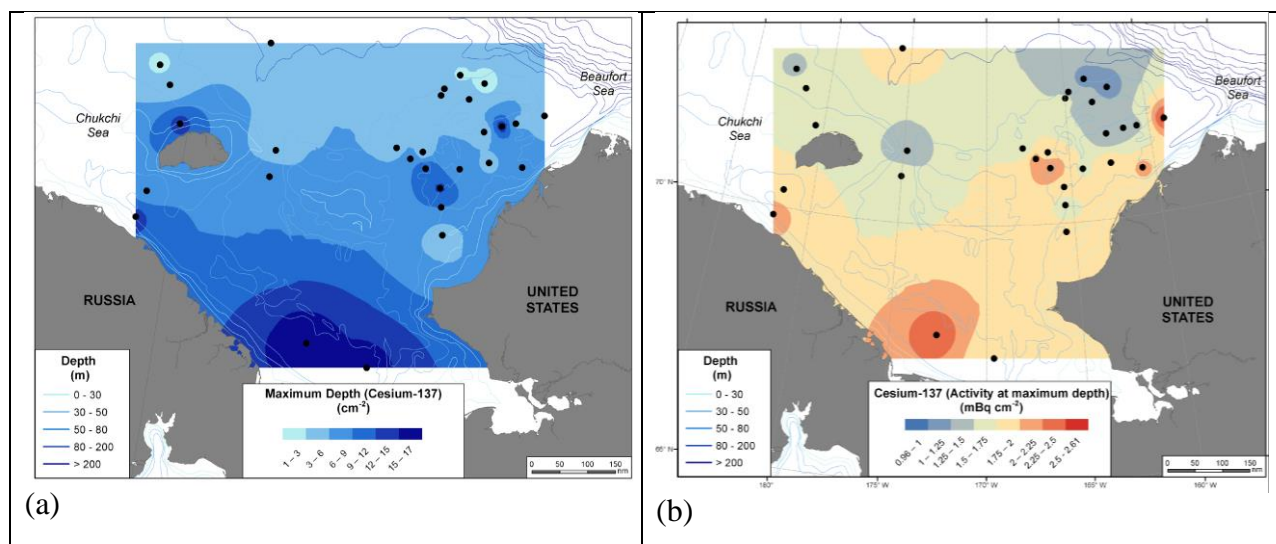


**Figure 5.** Stable carbon isotope ratios observed in the organic fraction of surface sediments during (a) HLY1201 and (b) HLY1301 and surface sediment C/N ratios for (c) HLY1201 and (d) HLY1301.

sediments on Hanna Shoal and mud in deeper waters offshore and in western Barrow Canyon. Sediment total organic carbon content (Figure 6c,d) indicates similar patterns with lowest %TOC over Hanna Shoal and higher TOC content coinciding with finer grained sediments to the west and east of Hanna Shoal and the western side of Barrow Canyon. The depth of surface Cs-137 (Figure 7) indicates areas of bioturbation (Figure 7a) and the level of the associated radioactivity (Figure 7b). The results indicated highest inventories of Cs-137 are in the southern Chukchi Sea and to the SE of Hanna Shoal.



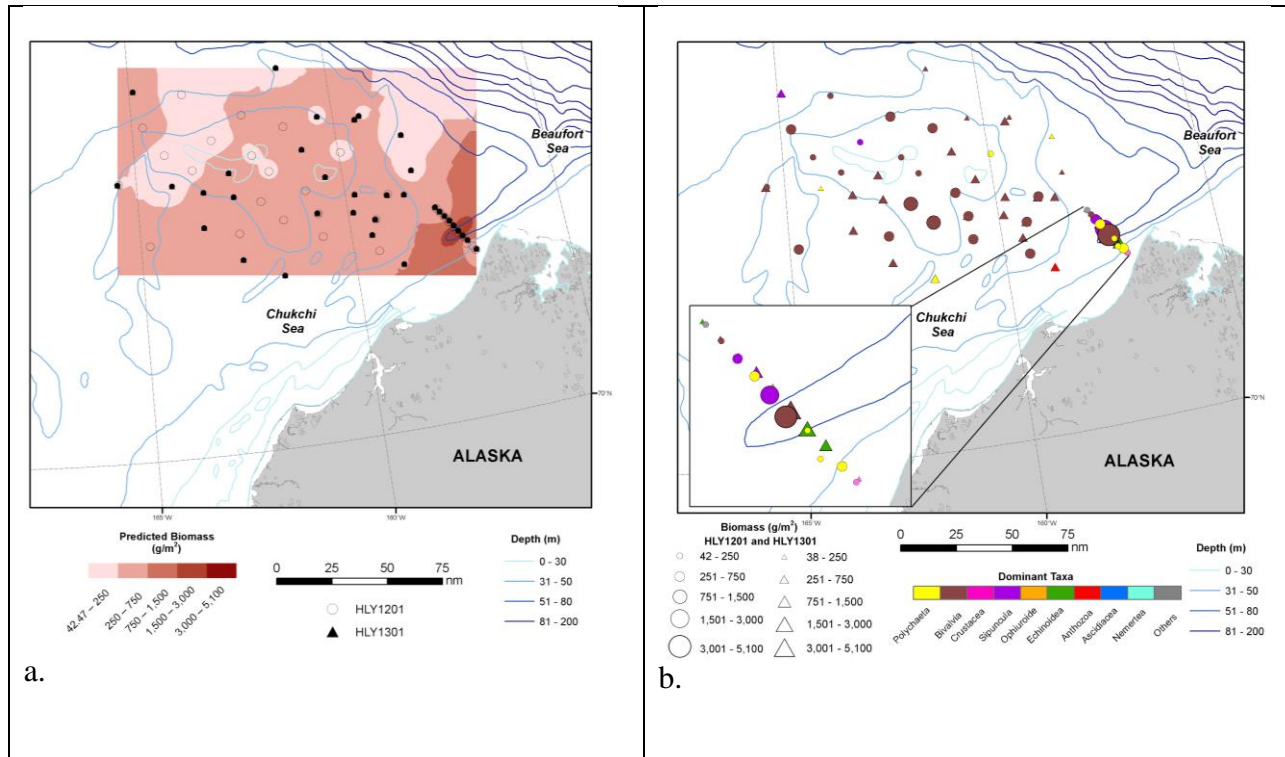
**Figure 6.** Grain size distributions ( $\geq 5 \phi$ ) in surface sediments for (a) HLY1201 and (b) HLY1301 and total organic carbon content (%) for (c) HLY1201 and (d) HLY1301.



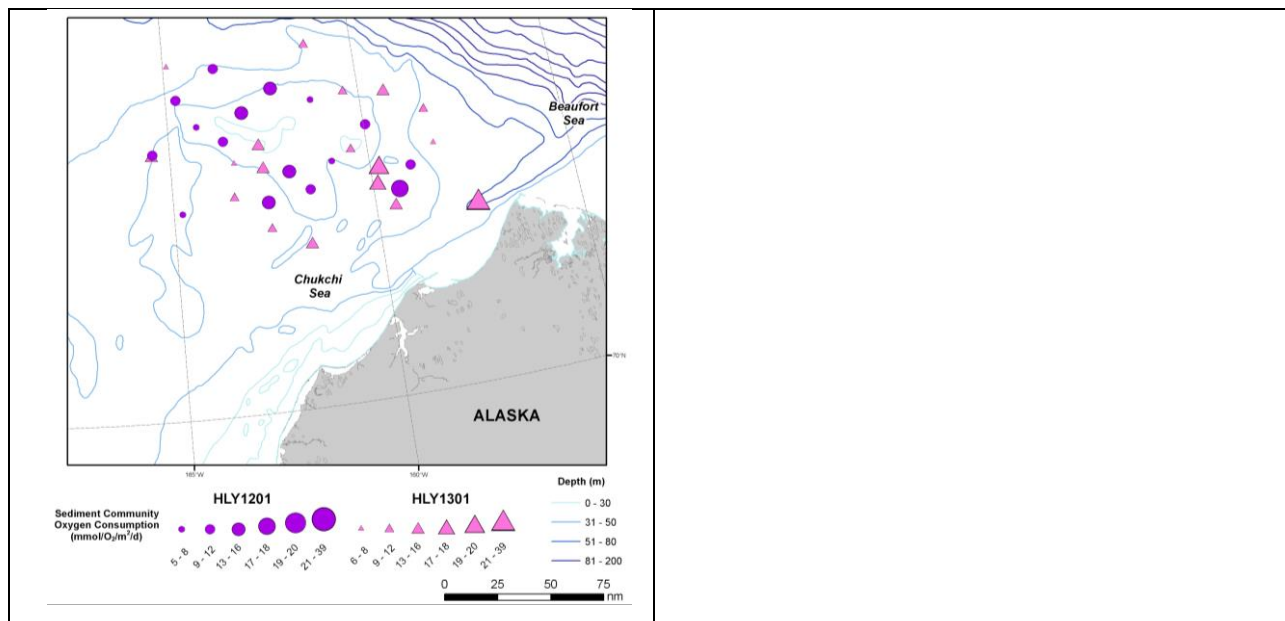
**Figure 7.** Sediment radioisotope isopleth of (a) depth of  $^{137}\text{Cs}$  maximum and (b) radioactivity at that depth for the combined HLY1201 and HLY1301 cruises.

Benthic macroinfauna ( $\text{gww/m}^2$ ) biomass data collected during HLY1201 and HLY1301 shows the lowest total station wet weight biomass in the offshore regions of the western and northeastern regions of Hanna Shoal, with highest areas south and east of Hanna shoal, including in western Barrow Canyon (Figure 8a). Bivalves dominant the macrofaunal groups overall, with polychaetes and sipunculids the second most dominant fauna (Figure 8b). The highest bivalve biomass are clearly shown in the southern and SE regions of Hanna Shoal and in the center of Barrow Canyon (Figure 8b).

For HLY1201 only (Table 1) total station abundance across the study area ranged from 868-47,550 individuals/ $\text{m}^2$  and biomass was 42.47-4532.91 g wet weight/ $\text{m}^2$ . The lowest and highest values occurred in Barrow Canyon along the DBO5 line. Excluding Barrow Canyon, the total station abundance and biomass ranged from 868-5478 individuals/ $\text{m}^2$  and wet weight biomass from 95.41-816.66 g wet weight / $\text{m}^2$ . In composite, the highest macroinfaunal biomass occurred in the center and western side of Barrow Canyon (stations BarC 5-7), being dominated by mytilid bivalves, golfingiid sipunculids and maldanid polychaetes, and just south of Hanna Shoal (stations H1, H3, H19) being dominated by tellinid bivalves (Figure 8b, Table 1 (HLY1201 only). The next highest biomass stations occurred southeast of Hanna Shoal (stations H16, CBL15, H37, CBL14) and were dominated by tellinid, nuculid and astartid bivalves (Figure 8b, Table 1). Figure 9 shows the distribution of sediment community oxygen consumption (SCOC), with highest values to the SE of Hanna Shoal, indicative of a region of high pelagic-benthic coupling of organic matter to the benthos. This region corresponds to high benthic macrofaunal biomass south and southeast of Hanna Shoal (Figure 8b), indicative of a deposition region. Fine silt and clay deposition areas associated with higher TOC are also observed in these same regions (Figure 6).



**Figure 8.** (a) Distribution of macroinfaunal station biomass (grams wet weight per  $m^2$  ( $gww/m^2$ )) in the main study area in the northern Chukchi Sea for HLY1201 and (b) the dominant macrofauna by biomass in relation to total station biomass for HLY1201.



**Figure 9.** Distribution of sediment community oxygen uptake (SCOC;  $mmol O_2/m^2/d$ ) during HLY1201 and HLY1301.

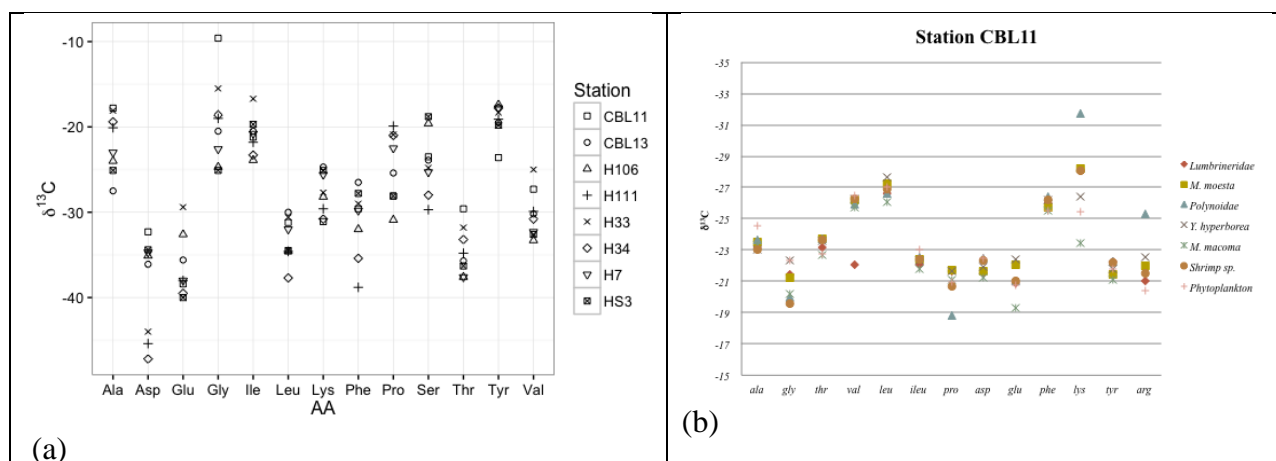
**Table 1.** Summary of HLY1201 stations (stn) by number (#), name, macroinfaunal abundance (#/m<sup>2</sup>) and wet weight biomass (grams wet weight, gww/ m<sup>2</sup>), number of taxa, and percent of top 3 dominant family types in each station (abundance and biomass).

Stn #	Station Name	Station Abundance (#/m <sup>2</sup> )	Station Wet Weight Biomass (gww/m <sup>2</sup> )	# of Taxa by Family	Taxon Family by Abundance-Top 3	% Abundance	Taxon Family by Wet Weight Biomass -Top 3	% Wet weight biomass
6	H24	3428	379.63	57	NUCULIDAE	11.4	ASTARTIDAE	34.8
					YOLDIIDAE	10.2	MALDANIDAE	19.4
					PHOXOCEPHALIDAE	8.8	GOLFINGIIDAE	18.3
7	CBL1 1	1250	185.98	37	NUCULIDAE	34.2	GOLFINGIIDAE	40.4
					TELLINIDAE	17.0	YOLDIIDAE	29.7
					NUCULANIDAE	9.4	TELLINIDAE	8.9
9	H21	1443	324.04	33	NUCULANIDAE	43.3	YOLDIIDAE	55.5
					YOLDIIDAE	19.9	NUCULANIDAE	22.1
					NUCULIDAE	13.2	NEPHTYIDAE	12.8
10	H10	1193	220.16	43	NUCULIDAE	17.8	YOLDIIDAE	37.1
					ISAEIDAE	15.7	TELLINIDAE	18.6
11	H30	1995	175.37	39	NEBALIIDAE	27.6	TELLINIDAE	24.8
					NUCULIDAE	24.4	NUCULIDAE	20.1
					YOLDIIDAE	7.4	NEPHTYIDAE	16.0
19	H6	1888	164.23	45	NUCULIDAE	30.5	TELLINIDAE	35.8
					TELLINIDAE	23.0	NUCULIDAE	15.8
					YOLDIIDAE	12.1	YOLDIIDAE	8.4
20	H8	878	138.25	38	NUCULIDAE	28.2	GOLFINGIIDAE	45.4
					TELLINIDAE	18.2	YOLDIIDAE	17.7
					YOLDIIDAE	9.1	NUCULANIDAE	8.7
25	H4	1945	272.38	43	TELLINIDAE	35.5	TELLINIDAE	48.8
					NUCULIDAE	19.2	YOLDIIDAE	19.1
					YOLDIIDAE	10.5	NEPHTYIDAE	6.9
26	H14	1740	328.80	41	TELLINIDAE	24.1	TELLINIDAE	49.1
					NUCULIDAE	13.9	NUCULIDAE	16.8
					CAPITELLIDAE	10.6	YOLDIIDAE	13.4
30	H2	4625	189.92	53	TELLINIDAE	19.5	TELLINIDAE	54.2
					SABELLIDAE	19.5	CARDIIDAE	9.1
					ISAEIDAE	7.0	ASTARTIDAE	6.1
31	H5	868	121.85	37	MOLGULIDAE	17.6	TELLINIDAE	38.2
					LYSIANASSIDAE	11.8	ASTARTIDAE	22.8
					SPIONIDAE	11.5	CARDIIDAE	8.8
32	H3	5168	816.66	60	NUCULIDAE	24.1	TELLINIDAE	39.3
					TELLINIDAE	15.1	NUCULIDAE	32.1
					CIRRATULIDAE	13.6	NUCULANIDAE	9.2
37	H1	5478	702.68	57	CIRRATULIDAE	25.7	TELLINIDAE	58.6
					TELLINIDAE	18.5	ASTARTIDAE	16
					YOLDIIDAE	7.0	GOLFINGIIDAE	6.6
38	H19	2998	801.74	45	TELLINIDAE	21.3	TELLINIDAE	67.9
					NUCULIDAE	13.7	NUCULIDAE	7.9
					CIRRATULIDAE	13.1	ASTARTIDAE	4.7



The  $\delta^{13}\text{C}_{\text{AA}}$  patterns of phytoplankton samples across 8 stations were quite similar. The mean range in  $\delta^{13}\text{C}_{\text{AA}}$  values for the 13 amino acids was  $9.9 \pm 0.8$  ‰, with the maximum of 15.5 ‰ for glycine and the minimum of 6.2 ‰ for tyrosine. The amino acids with the least variability of normalized  $\delta^{13}\text{C}_{\text{AA}}$  values were leucine, isoleucine phenylalanine and valine, which are all essential amino acids for animals. However, certain essential amino acids such as threonine had greater  $\delta^{13}\text{C}$  variation than nonessential amino acids such as alanine. We also explored the spatial variability of  $\delta^{13}\text{C}_{\text{AA}}$  values across 8 stations (Figure 10a). Over half of the amino acids including alanine, glycine, threonine, valine, leucine, isoleucine, aspartic acid and phenylalanine showed similar trend of more depleted  $\delta^{13}\text{C}_{\text{AA}}$  values at near-shore stations, while proline and glutamic acid showed the opposite pattern.

We also evaluated the compound-specific amino acid isotope composition of different trophic level components of the NE Chukchi Sea food web. Figure 10b provides an example of different benthic infaunal values at one (CBL11) of nearly 20 stations where samples were collected samples during the HLY1201 and HLY1301 cruises.



**Figure 10.** (a) Distribution of  $\delta^{13}\text{C}$  in various amino acids for different trophic level components of the NE Chukchi at different stations, and (b)  $\delta^{13}\text{C}$  in various amino acids for different trophic level components (phytoplankton, crustacean, bivalves and polychaetes) in the food web at station CBL11.

#### 4. Summary

The Chukchi Sea Offshore Monitoring in Drilling Area (COMIDA) project expanded field efforts in 2012 and 2013 focused on the shallow Hanna Shoal region of the northern Chukchi Sea, as well as the Distributed Biological Observatory transect across Barrow Canyon. The shallow, but complex bathymetry of Hanna Shoal influences the productivity of the water column and organic sedimentation processes. Based upon field efforts in 2012 and 2013, as well as prior work, inshore waters are less nutrient rich and water column chlorophyll (up to 1000 mg chlorophyll *a* per square meter over the whole water column) also increases offshore to the north and west. However, benthic biomass, sediment oxygen demand and chlorophyll deposited to the surface sediments (up to 20 mg per square meter) do not always mimic these water column processes. These organic sedimentation indicators tend to be higher to the south, including in

waters to the south and east of Hanna Shoal where large populations of walrus have also been observed to forage on the benthos in the summer from remnant sea ice. The emerging picture suggests that the complex current system rotates richer organic materials around the periphery of Hanna Shoal in a clockwise direction, with shoreward enhancement of organic material deposition. These pelagic – benthic coupling characteristics will be considered in the context of the larger Chukchi marine ecosystem.

## 5. Acknowledgements

This study was funded by the U.S. Department of the Interior, Bureau of Ocean Energy Management (BOEM), Alaska Outer Continental Shelf Region, Anchorage, Alaska under BOEM Cooperative Agreement No. M11AC00007 as part of the Chukchi Sea Offshore Monitoring in Drilling Area (COMIDA). We thank the US Coast Guard, COMIDA HS colleagues and shipboard team, including Christian Johnson, Mengjie Zhang, Laura Gemery, Dubrava Kirievskaya, Holly Kelly, Christina Goethel, and Piper Lewis. In addition, we thank Dana Biasatti (isotope data), Christian Johnson (grain size data, sorting), Alynne Bayard (GIS mapping), and Linton Beaven, Stephanie Soques and Monika Kedra (sorting laboratory).

## 6. References

- Blanchard A.L., Feder H.M., 2014. Interactions of habitat complexity and environmental characteristics with macrobenthic community structure at multiple spatial scales in the northeastern Chukchi Sea. *Deep-Sea Res. Pt II* 102:132–143.
- Carmack E., Wassmann, P., 2006. Food webs and physical-biological coupling on pan-arctic shelves: comprehensive perspectives, unifying concepts and future research. *Prog. Oceanogr.* 71, 446–477.
- Day R.H., Weingartner T.J., Hopcroft R.R., Aerts L.A.M., Blanchard A.L., Gall A.E., Gallaway B.J., Hannay D.E., Holladay B.A., Mathis J.T., Norcross B.L., Questel J.M., Wisdom S.S., 2013. The offshore northeastern Chukchi Sea: a complex high-latitude system. *Cont. Shelf Res.* 67, 147–165.
- Dunton K.H., Grebmeier J.M., Trefry J.H., 2014. The benthic ecosystem of the northeastern Chukchi Sea: An overview of its unique biogeochemistry and biological characteristics. *Deep-Sea Res. II*, 102, 1-8.
- Grebmeier J.M., Cooper, L.W., Feder H.M., Sirenko S.I., 2006. Ecosystem dynamics of the Pacific-influenced Northern Bering and Chukchi Seas in the Amerasian Arctic. *Prog. Oceanogr.* 71, 331-361.
- Grebmeier J.M., Bluhm B.A., Cooper L.W., Danielson S., Arrigo K.R., Blanchard A.L., Clark J.G., Day R.H., Frey K.E., Gradinger R.R., Kedra M., Konar, B., Kuletz, K.J., Lee, S.H., Lovvorn, J.R., Norcross, B.L., Okkonen S.R., 2015.. Ecosystem characteristics and processes facilitating persistent macrobenthic biomass hotspots and associated benthivory in the Pacific Arctic. *Prog. Oceanogr.* 136, 92-114.
- Iken K., Bluhm B.A., Dunton K.H., 2010. Benthic food web structure serves as indicator of water mass properties in the southern Chukchi Sea. *Deep-Sea Res. Pt II* 57:71–85.

- Jay, C.V., Fischbach, A.S., Kochnev, A.A., 2012. Walrus areas of use in the Chukchi Sea during sparse sea ice cover. *Mar. Ecol. Prog. Ser.* 468: 1–13.
- NASL. 2016. Procedures and techniques are available at <http://nasl.cbl.umces.edu/>.
- Schonberg, S.V., Clarke, J.T., Dunton, K.H., 2014. Distribution, abundance, biomass and diversity of benthic infauna in the northeast Chukchi Sea, Alaska: relation to environmental variables and marine mammals. *Deep-Sea Res. Part II*, 102, 144–163.
- Weingartner T., Dobbins E., Danielson S., Winsor P., Potter R., Statscewich H., 2013. Hydrographic variability over the northeastern Chukchi Sea shelf in summer-fall 2008–2010. *Cont. Shelf Res.* 67, 5–22.

# Arctic Shelves as Platforms for Active Biogeochemical Activity: Nitrogen and Carbon Transformations in the Chukchi Sea, AK.

Amber K. Hardison<sup>a</sup>, Nathan D. McTigue<sup>b</sup>, Wayne S. Gardner<sup>a</sup>, Kenneth H. Dunton<sup>a</sup>

<sup>a</sup>University of Texas at Austin Marine Science Institute, Port Aransas, TX, 78373

<sup>b</sup>NOAA Lab, Beaufort, NC 28516

[amber.hardison@utexas.edu](mailto:amber.hardison@utexas.edu), [nathan.mctigue@noaa.gov](mailto:nathan.mctigue@noaa.gov), [wayne.gardner@utexas.edu](mailto:wayne.gardner@utexas.edu),  
[ken.dunton@utexas.edu](mailto:ken.dunton@utexas.edu)

## Abstract

Continental shelves comprise <5% of global ocean area yet are the site for a disproportionate 30% of primary production, 80% of organic matter (OM) burial, and >50% of marine denitrification. The Hanna Shoal region in the northeast Chukchi Sea, Alaska, is recognized for its high biodiversity and productivity. We investigated the role of sediments in OM decomposition and nutrient cycling at 5 stations on the shallow Hanna Shoal. In particular, we asked (1) how much OM is remineralized by benthic microbes in the Chukchi Sea and (2) whether sediments functioned as a net source for nitrogen (N), thus fueling primary production in the overlying water, or as a net sink for N, thereby removing it from the system. We conducted dark sediment core incubations to measure sediment O<sub>2</sub> consumption, net N<sub>2</sub> and nutrient (NH<sub>4</sub><sup>+</sup>, NO<sub>3</sub><sup>-</sup>, NO<sub>2</sub><sup>-</sup>, PO<sub>4</sub><sup>3-</sup>) fluxes, and rates of sediment NH<sub>4</sub><sup>+</sup> cycling, including uptake and regeneration. Sediment O<sub>2</sub> consumption rates and NH<sub>4</sub><sup>+</sup> and PO<sub>4</sub><sup>3-</sup> efflux suggests that high OM remineralization rates occurred in these cold (-2°C) sediments. We estimated that microbial aerobic remineralization accounted for 19 – 28% of summer export production measured on the Chukchi Shelf. Net N<sub>2</sub> release was the dominant N flux, indicating that sediments acted as a net sink for bioavailable N via denitrification. From our rates, we estimated that 22% of total denitrification occurring on Arctic shelves occurs in the Chukchi Sea. Organic carbon remineralization via denitrification accounted for 6 – 12% of summer export production. Oxic mineralization and denitrification together oxidized 31 – 37% of export production, with denitrification making up 16 – 39% of the total. These shallow, productive Arctic shelves may be local hotspots for OM remineralization.

## 1. Introduction

The majority of global marine primary production takes place on continental shelves, as their shallow nature and high nutrient content make them hot spots for organic matter production and export (Bauer et al., 2013; Smith and Hollibaugh, 1993). The Arctic contains ~20% of the world's continental shelves even though it represents only 4 % of the ocean area, and this region is recognized for high rates of primary production during the ice-free growing season (see review by Grebmeier and colleagues (2006). The Chukchi Sea is a dynamic region within the Arctic through which upwelled, nutrient-rich Pacific Ocean water flows from the Bering Strait towards the Arctic Ocean. The high nutrient levels support high levels of primary production over the broad northern Chukchi Sea shelf, averaging 80-90 g C m<sup>-2</sup> y<sup>-1</sup>, and a remarkable 430 g C m<sup>-2</sup> y<sup>-1</sup> in Barrow Canyon (Grebmeier et al., 2006). Low levels of grazing and remineralization in the shallow water column lead to high rates of export production to the benthos, which fuels a productive benthic faunal community and sediment decomposition (Chang and Devol, 2009; Grebmeier et al., 2006; Moran et al., 2005).

Sediments are critical zones of organic matter cycling, including recycling and removal of carbon and nutrients. Recycling involves aerobic and anaerobic breakdown of organic matter into dissolved inorganic forms (CO<sub>2</sub>, NH<sub>4</sub><sup>+</sup>, NO<sub>3</sub><sup>-</sup>, PO<sub>4</sub><sup>3-</sup>), which can be released to the overlying water and may fuel further pelagic productivity. In some systems, sediment nutrient release satisfies a large proportion of the inorganic nitrogen and phosphorus needs of the pelagic communities (Joye and Anderson, 2008; Nixon, 1981). This “internal” loading of nutrients, particularly nitrogen, may be important in the Chukchi Sea, as previous work suggests that nitrogen is the limiting macronutrient over the Chukchi shelf (Brown et al., 2015; Deutsch and Weber, 2012; Gruber and Sarmiento, 1997). Sediments also play an important role in nitrogen loss. The processes of denitrification and anammox, which occur in anoxic sediments, completely remove fixed nitrogen from a system via N<sub>2</sub> gas, which is largely unavailable to organisms. Denitrification is the major removal pathway of bioavailable nitrogen in the ocean, although transfer up the food chain is also important in many systems (Devol, 2015; Nixon, 1981). Burial is an additional removal pathways of both carbon and nutrients (Burdige, 2006). Understanding the role of sediments in the fate of organic matter is a critical aspect of ecosystem functioning in continental shelf systems. Specifically, the dominant nitrogen cycling pathway occurring in sediments will determine whether sediments act as a net source or a sink for bioavailable nitrogen.

Globally, continental shelves are major sites of organic matter remineralization, via processes such as aerobic respiration and denitrification (Bauer et al., 2013; Devol, 2015). Few studies of these rates have been conducted in the Arctic due largely to the logistical difficulties of studying the region, which is ice-covered for the majority of the year. Oxidation of organic carbon via O<sub>2</sub> respiration has been studied in the Chukchi Sea relatively recently (see Grebmeier et al. 2006 review). Sediment nitrogen cycling, including ammonification and denitrification have been studied less (Chang and Devol, 2009; Christensen, 2008; Devol et al., 1997; McTigue et al., in review; Souza et al., 2014b), and only twice have O<sub>2</sub> respiration and sediment nitrogen cycling been studied together (Christensen 1987; Souza et al., 2014). These and other studies suggest that Arctic sediments are dynamic zones of organic matter remineralization that vary over space and time.

This study builds on these findings to focus on a highly productive region of the Chukchi shelf called the Hanna Shoal. The Hanna Shoal is unique in that it has extremely high production and particle flux due to hydrodynamic forcings that focus export production to the seafloor (Schonberg et al., 2014; Grebmeier et al., 2015; Weingartner et al., 2013). It has notably high benthic fauna, marine mammals, and birds, largely due to its shallow nature and the presence of ice during the summer, which make it easy to access for feeding (Schonberg et al., 2014). We know little about the role of the sediments in the fate of this organic matter, including, carbon and nutrient recycling and removal. To that end, we measured simultaneous fluxes of O<sub>2</sub>, N<sub>2</sub>, and dissolved inorganic nutrients at the sediment-water interface at the Hanna Shoal in summer 2013. This research is guided by the following questions: (1) How much organic carbon is remineralized in the sediments, specifically by microbial processes? (2) Are the sediments a net sink or source of fixed nitrogen? We aim to understand the role of sediments in organic matter cycling in this biologically rich region.

## **2. Materials and methods**

### **2.1 Study site and sampling**

The study was conducted on board the USCGC *Healy* in the northeastern Chukchi Sea, Alaska from July to August 2013 as part of the Hanna Shoal Ecosystem Study (<http://arcticstudies.org/hannashoal/>). Five stations were sampled across the Hanna Shoal region for biogeochemical rate determination (Figure 1). At each station bottom water samples (40 L) for incubations were collected by CTD cast, and four sediment cores with intact sediment-water interfaces were collected using a modified HYPOX corer (Gardner et al., 2009). Sediments and water were stored in an environmental chamber at 4 °C.

### **2.2 Oxygen microprofiles**

At each station, three to five O<sub>2</sub> microprofiles were measured in two of the intact cores using Clark-type O<sub>2</sub> microelectrodes (OX-50, Unisense). O<sub>2</sub> measurements were made in vertical steps of 500 μm in the dark at 4 °C. Oxygen penetration depth (OPD) and diffusive O<sub>2</sub> fluxes (diffusive O<sub>2</sub> utilization, DOU) were determined by applying Fick's First Law calculation to microelectrode profiles (Boudreau, 1997; Soetaert and Meysman, 2009) using R ([www.r-project.org](http://www.r-project.org); R Development Core Team 2013). Sediment porosity values for the calculations were obtained for each station from J. Trefry (unpublished).

### **2.3 Measuring solute fluxes at the sediment-water interface**

All four cores per station were incubated in the environmental chamber at 4 °C. Cores were connected to a flow-through incubation system as described by McTigue et al. (in review). Briefly, an air-tight cap was placed in each core, leaving ~230 mL of water overlying the sediments. Aerated, unfiltered site water was then pumped continuously through inflow tubing, over the sediment-water interface, then through outflow tubing at ~1.2 mL min<sup>-1</sup>. The inflow bottom water was divided into two treatments: (1) unamended, control water, and (2) spiked with <sup>15</sup>N-NH<sub>4</sub><sup>+</sup> (99.9 % <sup>15</sup>N-NH<sub>4</sub>Cl) to final concentrations between 15-18 μm NH<sub>4</sub><sup>+</sup>, depending on

ambient  $\text{NH}_4^+$  concentrations (Table 1). Each feed water reservoir fed duplicate cores, and cores were wrapped in aluminum foil to ensure dark conditions.

**Table 1.** Characterization of bottom water and surface sediment. Sediment TOC, TN, and benthic chlorophyll *a* were measured in top 2 cm. CTD and sediment organic content from McTigue et al. (in revision); Benthic chl *a* from Dunton (unpublished).

Station	Depth	Bottom temperature	Bottom salinity	Bottom D.O.	Bottom $\text{NH}_4^+$	Bottom $\text{NO}_3^-$	Sediment TOC	Sediment TN	Benthic Chl <i>a</i>	$\text{O}_2$ penetration depth
	<i>m</i>	$^\circ\text{C}$		%	$\mu\text{M}$	$\mu\text{M}$	%	%	$\text{mg m}^{-2}$	<i>mm</i>
<b>CBL11</b>	47	-1.6	32.7	84	2.6	5.2	0.9	0.14	TBD	6.1 (0.8)
<b>CBL13</b>	50	-1.7	32.7	74	1.6	4.7	1.8	0.23	35.2	5.5 (0.5)
<b>H17</b>	41	-1.6	32.7	83	1.7	5.1	0.7	0.09	10.2	5.8 (1.9)
<b>H29</b>	66	-1.6	32.8	79	1.4	5.5	1.5	0.21	8.3	7.6 (0.2)
<b>H33</b>	50	-1.7	32.7	76	2.4	6.8	1.2	0.15	15.4	6.8 (0.7)
<b>Station mean (SD)</b>		-1.6 (0.1)	32.7 (0)	79 (4)	1.9 (0.5)	5.5 (0.8)	1.2 (0.5)	0.2 (0.1)	TBD	6.4 (0.4)

After an initial 12 h pre-incubation to allow the flow-through system to reach equilibrium, inflow and outflow water were sampled for dissolved gas and nutrient concentrations once daily for four days. Samples for dissolved gases ( $\text{O}_2$ ,  $\text{N}_2$ ) were collected from the control cores in 13 mL Exetainers (Labco, UK) by allowing the vials to overflow three times, ensuring no air bubbles were captured. Each sample was killed with 200  $\mu\text{L}$  of 100%  $\text{ZnCl}_2$ , capped, and stored underwater at 4  $^\circ\text{C}$ . Samples were collected from the control cores for dissolved nutrient concentrations. 30 mL of water was passed through a 0.2  $\mu\text{m}$  filter into a Whirlpak bag and frozen until analysis. All water samples were collected in duplicate for analytical replication. All samples were transported to the University of Texas Marine Science Institute (UTMSI) for analyses.

Dissolved gases ( $\text{O}_2$ ,  $\text{N}_2$ ) were measured using membrane inlet mass spectrometry (MIMS) (Kana et al., 1994). Samples for  $\text{NO}_3^-$ ,  $\text{NO}_2^-$ ,  $\text{NH}_4^+$ , and  $\text{PO}_4^{3-}$  concentrations were prepared using standard colorimetric techniques adapted to a microplate spectrophotometer (Mooney and McClelland, 2012), as described previously in McTigue et al. (in review).

Benthic fluxes of dissolved constituents ( $\mu\text{mol m}^{-2} \text{h}^{-1}$ ) were calculated as the difference between outflow and inflow concentrations at the same time point:

$$flux = (C_o - C_i) \times \frac{F}{A} \quad (1)$$

where  $C_o$  and  $C_i$  are the outflow and inflow concentrations, respectively ( $\mu\text{M}$ ),  $F$  is the flow rate ( $\text{L h}^{-1}$ ), and  $A$  is the sediment cross-sectional area ( $\text{m}^2$ ) (Lavrentyev et al., 2000). A positive flux

indicates release from the sediments to the overlying water, or efflux, while a negative flux designates uptake by the sediments, which we also refer to as influx, consumption, or demand. Specifically, a negative O<sub>2</sub> flux corresponds to sediment O<sub>2</sub> demand, or total O<sub>2</sub> utilization (TOU). A positive N<sub>2</sub> flux corresponds to net denitrification, while a negative N<sub>2</sub> flux indicates net nitrogen fixation.

## 2.4 Measuring NH<sub>4</sub><sup>+</sup> cycling rates at the sediment-water interface

Sediment NH<sub>4</sub><sup>+</sup> uptake and regeneration rates were determined in the <sup>15</sup>NH<sub>4</sub><sup>+</sup> core incubations according to Lin and colleagues (2011). Inflow and outflow water samples were collected as described above for nutrient analyses. NH<sub>4</sub><sup>+</sup> isotopic composition was measured at UTMSI using ammonium isotope retention time shift (AIRTS) high-performance liquid chromatography (HPLC) (Gardner, 1995). Each sample was run in triplicate, and an internal NH<sub>4</sub><sup>+</sup> standard was included between samples.

NH<sub>4</sub><sup>+</sup> regeneration and uptake rates were calculated according to the isotope dilution equations developed by Blackburn (1979) and modified by Lin et al. (2011) for the flow-through incubation technique. The calculations require the relative abundance of <sup>15</sup>NH<sub>4</sub><sup>+</sup> in the total NH<sub>4</sub><sup>+</sup> pool, as follows:

$$r = {}^{15}\text{NH}_4^+ / ({}^{15}\text{NH}_4^+ + {}^{14}\text{NH}_4^+). \quad (2)$$

The actual NH<sub>4</sub><sup>+</sup> regeneration (*REG*) and potential uptake (*U<sub>pot</sub>*) rates are calculated as:

$$REG = \frac{\ln\left(\frac{r_i}{r_o}\right)}{\ln\left(\frac{C_o}{C_i}\right)} \times (C_o - C_i) \times \frac{F}{A} \quad (3)$$

$$U_{pot} = \left(1 - \frac{\ln\left(\frac{r_i}{r_o}\right)}{\ln\left(\frac{C_o}{C_i}\right)}\right) \times (C_o - C_i) \times \frac{F}{A} \quad (4)$$

where rates are in μmol m<sup>-2</sup> h<sup>-1</sup>; *r<sub>i</sub>* and *r<sub>o</sub>* are the inflow and outflow isotope ratios of <sup>15</sup>NH<sub>4</sub><sup>+</sup> in the <sup>15</sup>NH<sub>4</sub><sup>+</sup> treatments, respectively; and *C<sub>i</sub>* and *C<sub>o</sub>* are the inflow and outflow NH<sub>4</sub><sup>+</sup> concentrations in the <sup>15</sup>NH<sub>4</sub><sup>+</sup> treatments, respectively (μM). Regeneration is expressed as a positive flux. The potential uptake rate (expressed as a negative flux) includes consumption via nitrification, assimilation, and other NH<sub>4</sub><sup>+</sup> removal processes (Lin et al., 2011).

The net flux of NH<sub>4</sub><sup>+</sup> across the sediment-water interface at each site is estimated using the net NH<sub>4</sub><sup>+</sup> flux from the control cores. We assume that the <sup>15</sup>NH<sub>4</sub><sup>+</sup> addition and control cores have the same NH<sub>4</sub><sup>+</sup> regeneration fluxes because the added <sup>15</sup>NH<sub>4</sub><sup>+</sup> is the end product rather than the substrate of regeneration. Based on this assumption, the actual uptake flux (*U<sub>act</sub>*) is defined as the net NH<sub>4</sub><sup>+</sup> flux from the control cores (*NET*) minus the actual NH<sub>4</sub><sup>+</sup> regeneration rate in the <sup>15</sup>NH<sub>4</sub><sup>+</sup> cores (*REG*):

$$U_{act} = NET - REG \quad (5)$$



where  $U_{act}$  rates (expressed as a negative flux) are in  $\mu\text{mol m}^{-2} \text{h}^{-1}$ . The difference between potential and actual uptake can be described as “Sediment  $\text{NH}_4^+$  Demand” (SAD; expressed as a positive value), which reflects the degree of  $\text{NH}_4^+$  limitation on the microbial community:

$$\text{SAD} = U_{pot} - U_{act} \quad (6)$$

As the difference between potential and actual uptake decreases, addition of  $\text{NH}_4^+$  is less likely to stimulate microbial activity, and SAD decreases.

## 2.5 Statistical analyses

All statistics were computed using R. For all fluxes, the mean value for each core was obtained by averaging the daily measurements ( $T_0, T_1, T_2, T_3; n = 4$ ). Repeated measures ANOVA was performed to ensure that cores had reached steady-state conditions by the first sampling. The results underwent post-hoc testing using Tukey’s comparisons, and significantly lower rates at  $T_0$  or  $T_1$  were omitted. The mean value for each treatment (control vs.  $^{15}\text{NH}_4^+$ ) was obtained by averaging the duplicate core means ( $n = 2$ ).

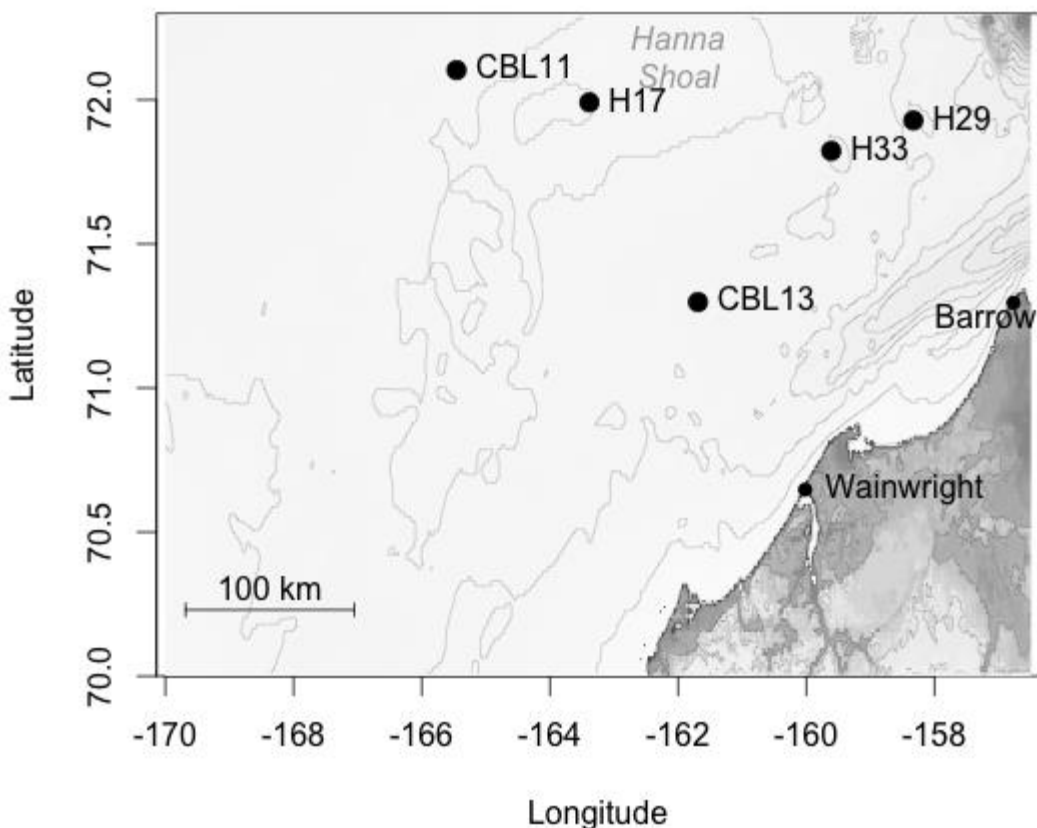
## 3. Results

### 3.1 Site characteristics

The five stations spanned a region that was approximately 250 km x 100 km (Figure 1). The stations were alike in many aspects: water depths ranged from 41 to 66 m, bottom water temperature (mean  $-1.6 \pm 0.1$  °C), salinity (mean 32.7), dissolved  $\text{O}_2$  (mean  $79.1 \pm 0.5\%$ ) and nutrient data were comparable, and surface sediment organic content (TOC mean  $1.2 \pm 0.5\%$ ; TN mean  $0.2 \pm 0.1\%$ ) was similar (see Table 1 for selected and McTigue et al., in review, for full site metadata). Moderate sediment organic content corresponded to moderately shallow OPDs, which ranged from  $5.5 \pm 0.5$  mm at CBL11 to  $7.6 \pm 0.2$  mm at H29 (Table 1).

### 3.2 Net dissolved gas and nutrient fluxes

DOU rates obtained from  $\text{O}_2$  microprofiles ranged from  $-139 \pm 43$  (CBL11) to  $-222 \pm 33$   $\mu\text{mol O}_2 \text{ m}^{-2} \text{h}^{-1}$  (CBL13) (Figure 2a; Table 2). Whole core dissolved gas fluxes from incubations are unavailable for station H17 due to instrument malfunction. Net  $\text{O}_2$  fluxes, or total  $\text{O}_2$  uptake (TOU) at the remaining 4 stations were all directed into the sediments, indicating net  $\text{O}_2$  consumption by sediment organisms.  $\text{O}_2$  fluxes ranged from  $-157 \pm 11$  to  $-452 \pm 166$   $\mu\text{mol O}_2 \text{ m}^{-2} \text{h}^{-1}$  at CBL13 and H33, respectively, with significantly higher  $\text{O}_2$  consumption at H33 (Figure 2a; Table 2). Net  $\text{N}_2$  fluxes were directed out of the sediments at all stations, indicating net  $\text{N}_2$



**Figure 1.** Sample stations along the Hanna Shoal in the Northeast Chukchi Sea, Alaska. Depth contour lines are 20 m increments.

**Table 2.** Gas and nutrient benthic fluxes in control cores. Values are mean (SE). “DNF eff.” = denitrification efficiency

Station	DOU	TOU	TOU:D OU	N <sub>2</sub>	NH <sub>4</sub> <sup>+</sup>	NO <sub>3</sub> <sup>-</sup>	NO <sub>2</sub> <sup>-</sup>	NO <sub>x</sub>	DIN	PO <sub>4</sub> <sup>3-</sup>	NO <sub>x</sub> /N <sub>2</sub>	DNF eff.
	$\mu\text{mol O}_2 \text{ m}^{-2} \text{ h}^{-1}$			$\mu\text{mol m}^{-2} \text{ h}^{-1}$							%	%
<b>CBL11</b>	-139 (43)	-277 (32)	2.0	55 (3)	6.3 (2.3)	-8.2 (4.4)	0.5 (0.3)	-7.7	1.5 (4.0)	2.2 (1.4)	16 (10)	86 (3)
<b>CBL13</b>	-222 (33)	-157 (11)	0.7	28 (4)	10.7 (3.6)	-9.0 (2.0)	-0.3 (0.2)	-9.3	1.3 (3.4)	0.8 (0.3)	37 (8)	69 (4)
<b>H17</b>	-177 (76)				-0.1 (4.3)	-6.1 (5.9)	-0.7 (0.09)	-6.8	-6.1 (4.4)	-0.5 (0.5)		
<b>H29</b>	-201 (4)	-176 (33)	0.9	24 (4)	2.3 (1.7)	-3.8 (0.9)	0.03 (0.09)	-	-0.5 (2.2)	3.3 (1.2)	30 (7)	86 (4)
<b>H33</b>	-158 (25)	-452 (166)	2.9	43 (8)	3.5 (3.1)	-23 (7.5)	-0.3 (0.3)	-	-14.8 (8.8)	1.6 (0.8)	65 (28)	82 (6)
<b>Station mean (SE)</b>	-179 (15)	-266 (68)	1.6 (0.5)	38 (7)	4.5 (1.9)	-10 (3.4)	-0.2 (0.2)		-3.7 (3.1)	1.5 (0.6)		

production via denitrification or anammox (Figure 2b; Table 2). Values ranged from  $24 \pm 4$  (H29) to  $55 \pm 3 \mu\text{mol N m}^{-2} \text{h}^{-1}$  (CBL11) and were significantly higher at CBL11.

Net  $\text{NH}_4^+$  and  $\text{PO}_4^{3-}$  fluxes were mostly directed out of the sediments, and  $\text{NH}_4^+$  fluxes always exceeded  $\text{PO}_4^{3-}$  fluxes (Figure 2c, 2d; Table 2). Net  $\text{NH}_4^+$  fluxes ranged from  $-0.1 \pm 4.3$  (H17) to  $10.7 \pm 3.6 \mu\text{mol NH}_4^+ \text{m}^{-2} \text{h}^{-1}$  (CBL13) and were not significantly different among stations. Net  $\text{PO}_4^{3-}$  fluxes ranged from  $-0.5 \pm 0.5$  (H17) to  $3.3 \pm 1.2 \mu\text{mol PO}_4^{3-} \text{m}^{-2} \text{h}^{-1}$  (H29).  $\text{PO}_4^{3-}$  fluxes at station H29 and H17 were significantly different from each other, but not from the other stations.  $\text{NH}_4^+$  and  $\text{PO}_4^{3-}$  fluxes at H17 were not significantly different from zero, indicating no net release or uptake by sediments. In contrast to  $\text{NH}_4^+$  and  $\text{PO}_4^{3-}$ , net  $\text{NO}_3^-$  fluxes at all stations were negative, indicating uptake into sediments, and all stations were statistically equivalent (Figure 2e; Table 2). Values ranged from  $-3.8 \pm 0.9$  (H29) to  $-23.5 \pm 7.5 \mu\text{mol NO}_3^- \text{m}^{-2} \text{h}^{-1}$  (H33). Net  $\text{NO}_2^-$  fluxes were not significantly different from zero at CBL13, H29, and H33, indicating no net  $\text{NO}_2^-$  flux into or out of these sediments (Figure 2f; Table 2). CBL 11 and H17 were significantly different from one another but not from the other stations. CBL11 showed a small net  $\text{NO}_2^-$  efflux while H17 showed a small net  $\text{NO}_2^-$  influx.

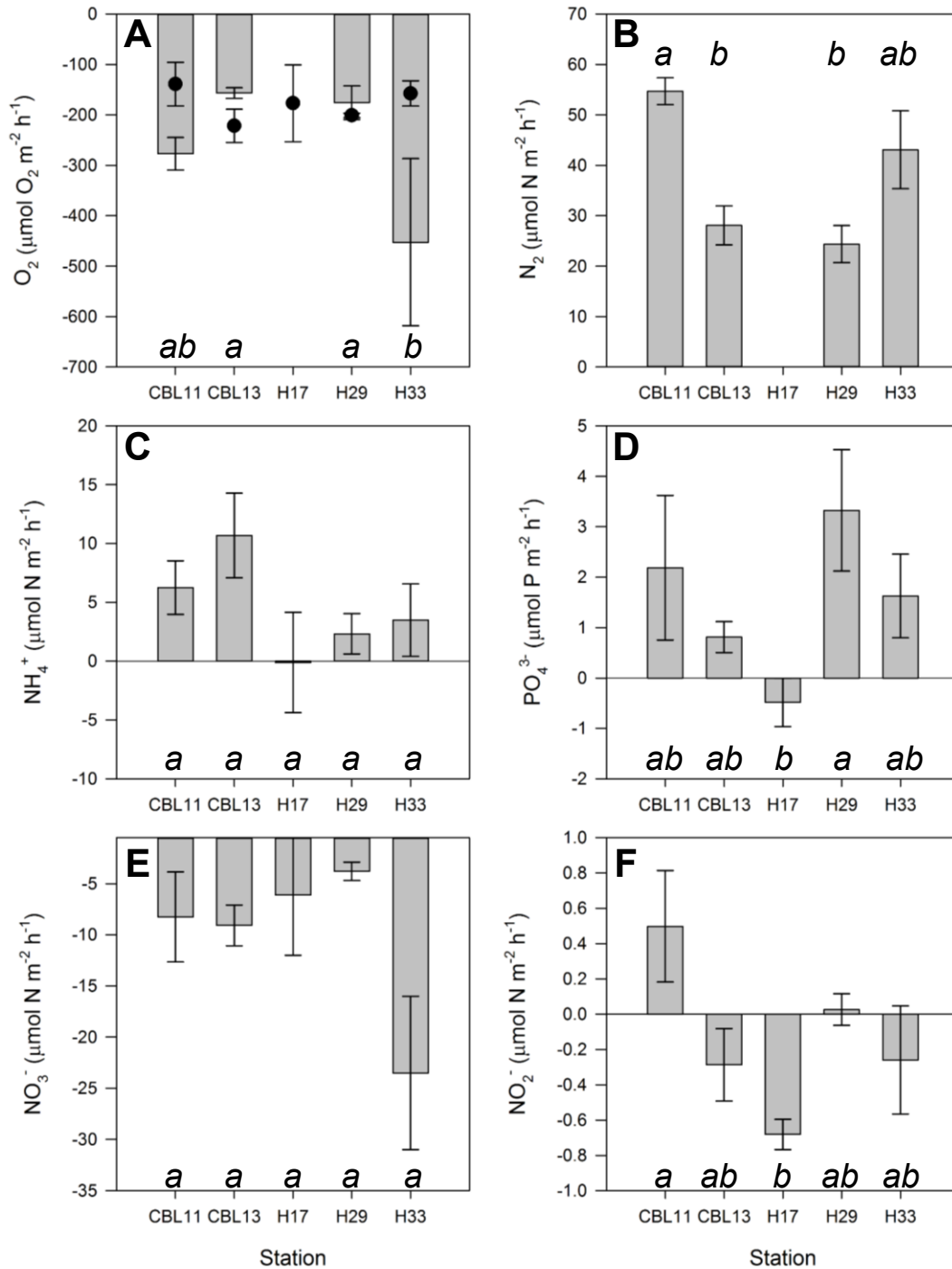
### 3.3 $\text{NH}_4^+$ cycling

Although net  $\text{NH}_4^+$  fluxes were zero at H17 and showed net release at the other stations (Figure 2c), the  $^{15}\text{NH}_4^+$  addition treatment allowed a more detailed analysis of  $\text{NH}_4^+$  cycling at the sediment-water interface. Actual  $\text{NH}_4^+$  regeneration rates ranged from  $5 \pm 2$  to  $15 \pm 2 \mu\text{mol N m}^{-2} \text{h}^{-1}$  with lowest rates at H29 and highest rates at CBL11 (Figure 3a; Table 3). Potential uptake rates, measured after  $^{15}\text{NH}_4^+$  addition, were highest at CBL11 and lowest at H33, ranging from  $-16 \pm 13$  to  $-48 \pm 20 \mu\text{mol N m}^{-2} \text{h}^{-1}$  (Figure 3b; Table 3). Actual uptake rates at CBL13 were positive, indicating no uptake, while rates ranged from  $-1.6 \pm 1.6$  to  $-17 \pm 9 \mu\text{mol N m}^{-2} \text{h}^{-1}$  at the other four stations, with highest actual uptake rates measured at H17 (Figure 3c; Table 3). The differences between actual and potential uptake rates across stations resulted in similar sediment  $\text{NH}_4^+$  demand (SAD) at stations CBL11, CBL13, and H29 (range  $36 \pm 22$  to  $46 \pm 20 \mu\text{mol N m}^{-2} \text{h}^{-1}$ ) while stations H17 and H33 were not significantly different from zero (Figure 3d; Table 3). All  $\text{NH}_4^+$  cycling rates were not significantly different among stations.

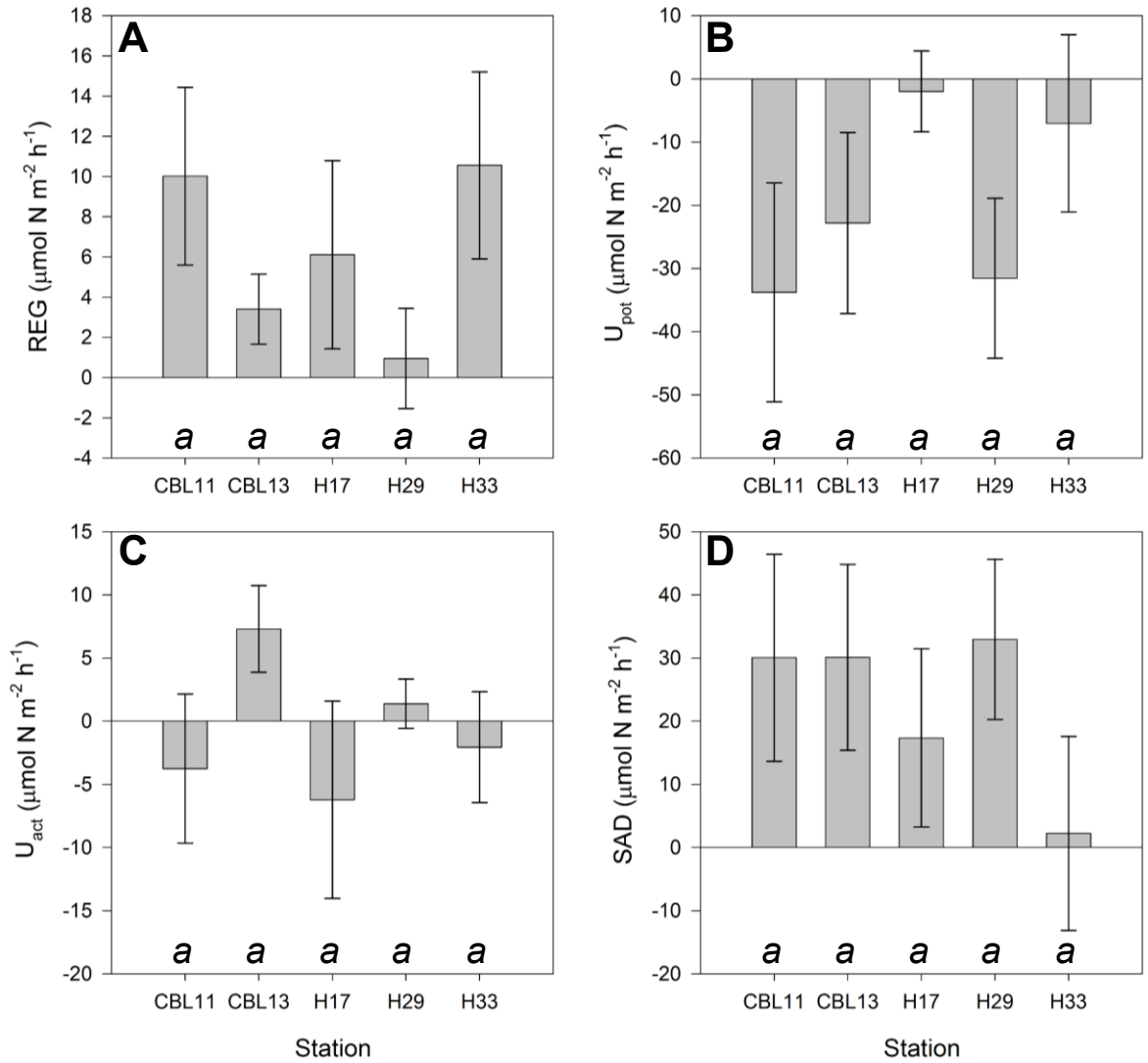
## 4. Discussion

### 4.1 Active organic matter remineralization at cold sites

Sediment  $\text{O}_2$  consumption has been widely used to assess benthic organic matter mineralization (Glud et al., 1994; Lansard et al., 2008). Total oxygen uptake (TOU) can be split into (1) diffusive  $\text{O}_2$  uptake (DOU), due to sediment bacteria conducting aerobic respiration, and (2) advective  $\text{O}_2$  uptake, generally governed by benthic faunal activities. TOU can be measured using benthic chambers settled on the seafloor (e.g., Reimers et al., 2001) or, as in the current study, ex situ using sediment core incubations (Archer and Devol, 1992; Lansard et al., 2008). DOU is quantified by the use of microelectrodes performed in situ or ex situ with sediment cores (Glud et al., 1994; Lansard et al., 2008). All  $\text{O}_2$  microprofiles in this study showed rapid



**Figure 2.** Gas (O<sub>2</sub>, N<sub>2</sub>) and nutrient (NH<sub>4</sub><sup>+</sup>, PO<sub>4</sub><sup>3-</sup>, NO<sub>3</sub><sup>-</sup>, NO<sub>2</sub><sup>-</sup>) fluxes at the sediment-water interface measured in control cores. Values are mean (SE) for duplicate cores. In panel A, grey bars correspond to total O<sub>2</sub> utilization (TOU) from core incubations while circles correspond to diffusive O<sub>2</sub> utilization (DOU) from microelectrode profiles. Error bars for DOU represent SE for duplicate cores. Letters in italics designate groups from a post-hoc Tukey's test. Means with the same letter are not significantly different. In panel A, letters correspond to TOU values.



**Figure 3.**  $\text{NH}_4^+$  cycling rates at the sediment-water interface measured in  $^{15}\text{NH}_4^+$  treated cores. Values are mean (SE) for replicate sampling days. Letters in italics designate groups from a post-hoc Tukey's test. Means with the same letter are not significantly different. REG = regeneration;  $U_{\text{pot}}$  = potential uptake;  $U_{\text{act}}$  = actual uptake; SAD = sediment  $\text{NH}_4^+$  demand.

**Table 3.**  $\text{NH}_4^+$  recycling rates from  $^{15}\text{NH}_4^+$  cores. All units are  $\mu\text{mol N m}^{-2} \text{h}^{-1}$ . Values are mean (SE).

Station	NET	REG	$U_{\text{pot}}$	$U_{\text{act}}$	SAD
CBL11	6.3 (2.3)	14.9 (4.0)	-47.6 (20.2)	-11.3 (4.1)	36.3 (21.6)
CBL13	10.7 (3.6)	6.6 (1.3)	-39.7 (19.0)	6.2 (4.5)	45.9 (20.5)
H17	-0.1 (4.3)	13.5 (4.9)	-36.8 (24.1)	-17.1 (8.6)	19.7 (22.6)
H29	2.3 (1.7)	5.3 (1.8)	-38.7 (18.1)	-1.6 (1.6)	37.0 (18.0)
H33	3.5 (3.1)	12.3 (5.1)	-15.5 (13.2)	-4.9 (4.1)	9.1 (16.8)
<b>Station mean (SE)</b>	4.5 (1.9)	10.5 (1.9)	-35.7 (5.4)	-5.7 (4.0)	29.6 (6.6)

consumption of  $\text{O}_2$  within a few mm of the sediment-water interface, indicating the high reactivity of these surficial sediments. The OPD into sediments reflects the balance between downward diffusive transport of  $\text{O}_2$  from the overlying water and  $\text{O}_2$  consumption processes in the sediments. OPD ranged from 5.5 to 7.5 mm, displaying little variability among stations. The DOU rates, which are calculated based on the  $\text{O}_2$  profiles, varied only by ~8% across stations. TOU rates, measured in the core incubations, were more variable ( $\text{CV} = 25\%$ ) and were highest at H33 and lowest at CBL13 and H29. The ratio of TOU to DOU reflects the degree of macrofaunal irrigation and respiration activities, with higher values corresponding to more macrofaunal activity (Wenzhofer and Glud, 2002). The higher between-station variability in TOU values relative to DOU was reflected in the more variable TOU:DOU ratios, which ranged from 2.9 to 0.7 (Table 2). Macrofaunal bioirrigation at H33 and CBL11 appeared to contribute more to enhancement of the total  $\text{O}_2$  flux than at H29 and CBL13. Both stations were dominated by bivalves while CBL13 and H29 were dominated by polychaetes (McTigue et al., in review). Organic matter mineralization due to sediment bacteria, represented by DOU, varied little across stations, which may be explained by the relatively similar environmental conditions (e.g., bottom water temperature and dissolved  $\text{O}_2$ , sediment organic matter) across stations.

Our  $\text{O}_2$  fluxes were within the range of other studies at similar depths in the Chukchi. For example, Grebmeier and colleagues (2006) reviewed patterns of organic carbon production, export, and utilization in the northern Bering and Chukchi Seas (Table 4). They reported sediment community oxygen consumption (SCOC, equivalent to TOU) in the northern Chukchi shelf at depths of 50 – 200 m of 125 – 1,667  $\mu\text{mol O}_2 \text{m}^{-2} \text{h}^{-1}$ , with highest rates in the Barrow Canyon region, where benthic infaunal biomass also peaked. SCOC rates were positively correlated to integrated water column chlorophyll *a* concentration and benthic biomass and negatively correlated with depth, showing evidence for tight benthic-pelagic coupling in the Chukchi. Souza and colleagues (2014) sampled stations in the southern and northern Chukchi shelf at depths of 34 – 46 m and reported sediment  $\text{O}_2$  demand (TOU) of -150 to -569  $\mu\text{mol O}_2 \text{m}^{-2} \text{h}^{-1}$ , which are nearly identical to those measured in the current study.

In addition to consuming  $\text{O}_2$ , benthic organic matter remineralization often results in release of  $\text{NH}_4^+$  and  $\text{PO}_4^{3-}$  from the benthos to the overlying water, which may fuel water column production. We observed  $\text{NH}_4^+$  and  $\text{PO}_4^{3-}$  release at all stations except H17, where fluxes were not significantly different from zero. This may be explained by the slightly lower sediment

**Table 4.** Literature comparison of N<sub>2</sub>, O<sub>2</sub>, and nutrient fluxes in the Chukchi Sea.

Location	Depth range (m)	Season year	N <sub>2</sub>	TOU	NO <sub>3</sub> <sup>-</sup>	NH <sub>4</sub> <sup>+</sup>	PO <sub>4</sub> <sup>3-</sup>	Citation
Hanna Shoal	41 - 66	summer 2013	24 - 55	-157 - -452	-3.8 - -23	-0.1 - 10.7	-0.5 - 3.3	this study
Chukchi shelf	50 - 1450	spring 2004	nd. - 65.8	-	-	-	-	Chang and Devol 2009
Chukchi shelf	34 - 46	summer 2010	-27 - 286	-150 - -569	-0.8 - 4.1	-	-1.1 - 13.2	Souza et al. 2014
Chukchi shelf	11 - 48	summer 1992; winter 1993	0.03 - 0.2	-688 - -825	-6.3 - 27	-1.7 - 31.3	-	Devol et al. 1997
Chukchi & Beaufort shelf-slope	50 - 3894	summer 2004	12.2 - 105	-9 - -355	-	-	-	Christensen 2008
Northern Chukchi shelf	50 - 200	spring, summer		125 - 1667				Grebmeier et al. 2006

not reflected in the O<sub>2</sub> fluxes. At the other 4 stations, NH<sub>4</sub><sup>+</sup> and PO<sub>4</sub><sup>3-</sup> fluxes were variable within and between stations, but showed no significant spatial patterns. NH<sub>4</sub><sup>+</sup> may be released through processes other than ammonification, including dissimilatory NO<sub>3</sub><sup>-</sup> reduction to NH<sub>4</sub><sup>+</sup> (DNRA) and faunal excretion. Our companion study at these stations using <sup>15</sup>N tracers detected DNRA but the rates were very low (McTigue et al. in review), thus it is most likely that NH<sub>4</sub><sup>+</sup> release from these sediments resulted from ammonification or faunal excretion. The elevated NH<sub>4</sub><sup>+</sup> release at CBL13 may have resulted from the high abundance of infauna there (6,713 ± 678 inv. m<sup>-2</sup>) relative to the other stations, as described by McTigue et al. (in review). Infauna abundance at CBL13 was dominated by *Maldane sarsi*, a tube-building polychaete, which are known to influence NH<sub>4</sub><sup>+</sup> fluxes. In contrast to NH<sub>4</sub><sup>+</sup> and PO<sub>4</sub><sup>3-</sup>, all NO<sub>3</sub><sup>-</sup> and most NO<sub>2</sub><sup>-</sup> fluxes were directed into the sediments, with NO<sub>3</sub><sup>-</sup> values exceeding NO<sub>2</sub><sup>-</sup>. At stations CBL11 and CBL13, NH<sub>4</sub><sup>+</sup> efflux was greater than NO<sub>x</sub> uptake, while at stations H17, H29, and H33, NO<sub>x</sub> uptake rates were greatest, yielding net DIN (NO<sub>x</sub> + NH<sub>4</sub><sup>+</sup>) fluxes ranging from -14.8 ± 8.8 to 1.5 ± 4.0 μmol

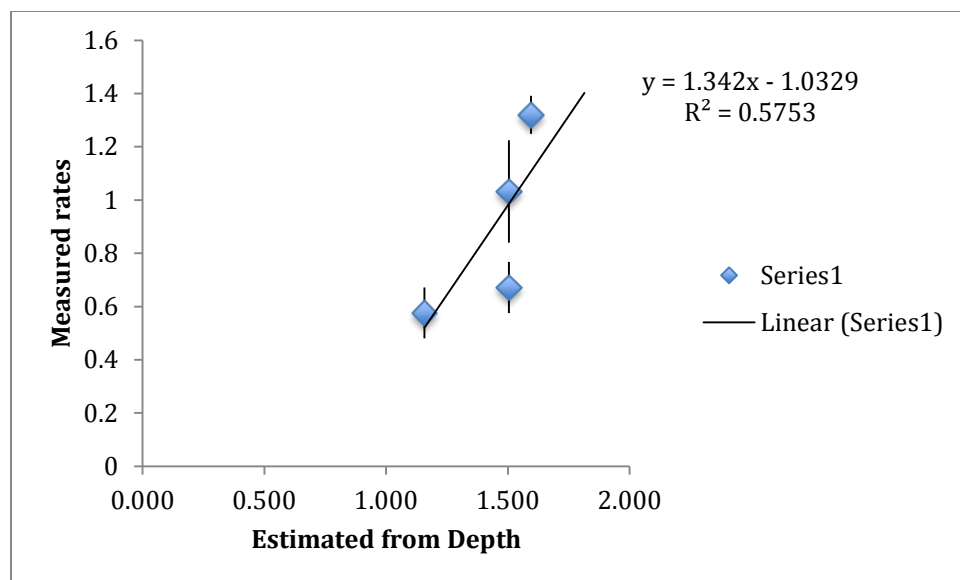
$\text{N m}^{-2} \text{ h}^{-1}$  (Table 2). Averaging across stations, sediments at the Hanna Shoal were a small net sink for DIN, taking up  $3.7 \pm 3.1 \mu\text{mol N m}^{-2} \text{ h}^{-1}$ .

Net  $\text{N}_2$  fluxes were always directed out of the sediments, indicating the occurrence of net denitrification, or possibly anammox. Denitrification is the largest global fixed N sink (Devol, 2015). The majority of sedimentary denitrification occurs on continental margins (Christensen et al., 1987; Seitzinger et al., 2006). Anammox is another pathway of  $\text{NO}_2^-$  reduction that releases  $\text{N}_2$  gas and has been detected in continental margins (Thamdrup and Dalsgaard, 2002; Trimmer et al., 2013). Our companion study at the Hanna Shoal using  $^{15}\text{N}$  tracers measured anammox at these stations, but denitrification rates exceeded anammox rates by one to two orders of magnitude (McTigue et al., in review). Our results are in good agreement with the limited studies of  $\text{N}_2$  flux in the Chukchi Sea. For example, Chang and Devol (2009) reported  $\text{N}_2$  fluxes of n.d. –  $65.8 \mu\text{mol N m}^{-2} \text{ d}^{-1}$  at stations ranging from 50 – 1,450 m. Their highest rates occurred at the shallowest station, and the authors developed a predictive relationship between  $\text{N}_2$  flux and depth. This relationship likely reflected the relationship between POC delivery to the seafloor and denitrification, a heterotrophic process, since shallower depths are more tightly coupled to water column production. The current study covers a more narrow depth range (41 – 66 m) than Chang and Devol’s (2009) study area that focused on shelf-basin interactions, but  $\text{N}_2$  flux and depth were significantly negatively correlated (Table 5), with highest average rates occurring at the shallowest station with gas flux data (CBL11). Moreover, when the Chang and Devol (2009) relationship between  $\text{N}_2$  flux and depth are used to predict  $\text{N}_2$  fluxes at the stations in the current study by depth alone, we get good agreement (Figure 4). The depth-estimated rates are always higher than the measured rates but are within the range of natural variability that we observed between replicate cores from the same station. Denitrification at our stations likely reflected variations in time-integrated POC flux to the sediments, which often correlates with depth, as concluded by Chang and Devol (2009). Interestingly,  $\text{N}_2$  fluxes were negatively correlated and  $\text{O}_2$  fluxes positively correlated with sediment TOC and TN (Table 5), thus stations with more organic matter standing stock favored  $\text{O}_2$  over  $\text{NO}_3^-$  respiration. This may indicate production of  $\text{H}_2\text{S}$  via  $\text{SO}_4^{2-}$  reduction, which would be favored under high organic carbon loading, and  $\text{H}_2\text{S}$  is a known inhibitor of nitrification. Alternatively, these correlations may reflect a relatively fresh deposition of organic carbon at the stations with highest sediment organic content, which would be respired in order of decreasing free energy yield, first by aerobic heterotrophic bacteria, consuming the most labile fraction of the organic carbon.

**Table 5.** Pearson Correlation coefficients (R) between benthic fluxes and environmental parameters. Values in bold are significant at the  $p < 0.05$  level.

	depth	temp	D.O.	TOC	TN
$\text{N}_2$	<b>-0.47</b>	0.05	0.34	<b>-0.6</b>	<b>-0.61</b>
$\text{O}_2$	0.25	0.09	-0.09	<b>0.38</b>	<b>0.49</b>
$\text{NO}_2$	0.19	0.15	0.16	0.05	0.14
$\text{NO}_3$	0.1	<b>0.36</b>	0.26	-0.03	0.05
$\text{NH}_4$	0	-0.24	-0.21	0.27	0.28
SRP	<b>0.43</b>	0.08	-0.04	0.21	0.27





**Figure 4.** Relationship between measured  $N_2$  fluxes and estimated  $N_2$  fluxes based on station depth and equation developed in Chang and Devol (2009). Rates are  $\text{mmol N m}^{-2} \text{d}^{-1}$ .

Over time, the denitrifiers would then be left with less labile organic carbon, which would be consumed more slowly. Thus, stations with more recent deposition of sediment organic carbon favored  $O_2$  over  $NO_3^-$  respiration, which has been observed in other studies (e.g., Chang and Devol, 2009; Sayles et al., 1994). Souza and colleagues (2014) reported  $N_2$  fluxes in the southern and northern Chukchi shelf that ranged from net nitrogen fixation to net denitrification,  $-27$  to  $286 \mu\text{mol N m}^{-2} \text{h}^{-1}$ . Interestingly, their net nitrogen fixation data was measured at their station closest to the Hanna Shoal. Our data do not support net nitrogen fixation, nor do the other studies that have measured net  $N_2$  flux in this region (Chang and Devol, 2009; Devol et al., 1997; Christensen 2008), but this is a topic that warrants further investigation.

Denitrifiers can use  $NO_3^-$  directly from the overlying water diffusing into porewater ( $D_w$ ), or by coupling to nitrification of  $NH_4^+$  to  $NO_3^-$  in sediments ( $D_n$ ). The observed  $NO_x$  fluxes into the sediments suggests that 16 – 65 % of denitrification may have occurred via  $D_w$  (Table 2). This corresponds well to our estimates of  $D_w$  from a  $^{15}N$  tracer study, which ranged from 8 – 42 % (McTigue et al., in review). Generally, coupled  $D_n$  is thought to account for ~80 % of total denitrification in continental shelves assuming bottom water  $NO_3^-$  concentrations  $< 10 \mu\text{M}$ , as at our stations (Table 1; Seitzinger et al., 2006). Porewater  $NH_4^+$  concentrations, ranging from 39 – 86  $\mu\text{M}$ , were high enough to support nitrification (McTigue et al., in review). For example, at H33, where we observed the highest  $NO_x$  uptake rates, porewater  $NH_4^+$  concentration in the top 5 cm was  $76.5 \pm 10.9 \mu\text{M}$ . However,  $NH_4^+$  concentrations near the zone of  $NO_3^-$  reduction (OPD = 6.8 mm) may have been more limiting, as concentrations are usually depleted near the surface, and overlying  $NO_3^-$  concentrations were adequate to support  $D_w$ . DIN uptake by microalgae may take place in situ at the Hanna Shoal, as light levels are  $4\text{--}20 \mu\text{mol photons m}^{-2} \text{s}^{-1}$  at the sediment surface (40 – 50 m depth) (McTigue and Dunton, 2014), which is suggested to be adequate to support benthic microalgal photosynthesis in this region. Benthic microalgae are capable of dark DIN uptake, so they may have contributed to our observed DIN influxes. DIN

uptake may also represent incorporation into microbial biomass and/or subsequent incorporation into higher trophic levels (Berelson et al., 1998; Hammond et al., 1999).

## 4.2 $\text{NH}_4^+$ cycling at the sediment-water interface

There was no net  $\text{NH}_4^+$  flux at H17, and the other stations showed net  $\text{NH}_4^+$  release, but the  $^{15}\text{NH}_4^+$  treatment allowed a more detailed analysis of  $\text{NH}_4^+$  cycling at the sediment-water interface. Measurement of net flux alone may underestimate actual  $\text{NH}_4^+$  regeneration because  $\text{NH}_4^+$  uptake (removal) processes may occur at similar rates as  $\text{NH}_4^+$  production, so that the measured net flux is low even though actual regeneration is high (Gardner and McCarthy, 2009). This is demonstrated at station H17, where net flux was zero but both active  $\text{NH}_4^+$  regeneration and uptake were simultaneously taking place (Figure 3). In fact, station H17 had the highest rates of actual uptake and nearly the highest rates for regeneration. All stations showed active  $\text{NH}_4^+$  regeneration, and most showed net release to the overlying water. In many systems, this is a vital internal source of recycled nitrogen that can fuel overlying production and/or bacteria such as nitrifiers (Tobias et al., 2003). At the Hanna Shoal, net  $\text{NH}_4^+$  flux contributed to the DIN pool in the overlying water, although this was not the primary fate of nitrogen processed in the sediments, as discussed below. Despite the net release of  $\text{NH}_4^+$ , all stations except CBL13 showed actual  $\text{NH}_4^+$  uptake, indicating use of  $\text{NH}_4^+$  by microbes such as nitrifiers.  $\text{NH}_4^+$  is also used by some heterotrophic bacteria as an energetically less expensive source of nitrogen than  $\text{NO}_3^-$  (Hoellein et al., 2009; Middelburg and Nieuwenhuize, 2000). After the addition of  $^{15}\text{NH}_4^+$ , all stations showed additional  $\text{NH}_4^+$  uptake, revealing some degree of  $\text{NH}_4^+$  limitations at the sediment-water interface, which is quantified as sediment  $\text{NH}_4^+$  demand (SAD; Figure 3d). Although porewater  $\text{NH}_4^+$  concentrations in the top 5 cm were high, concentrations may have been more limiting closer to the sediment surface where high rates of uptake by nitrifiers, anammox bacteria, and heterotrophic bacteria may have removed  $\text{NH}_4^+$  more quickly than it could be resupplied via organic matter remineralization.

Numerous water column studies and a limited number of sediment studies have investigated  $\text{NH}_4^+$  cycling. These data and other studies highlight the importance of measuring  $\text{NH}_4^+$  uptake and regeneration as opposed to only measuring net fluxes, as in other studies (Bruesewitz et al., 2015; 2011; Lin et al., 2011; McCarthy et al., 2007; Paerl et al., 2011; Souza et al., 2014a). The sediment water interface is dynamic and complex zone for  $\text{NH}_4^+$  cycling in the Hanna Shoal.

## 4.3 System-wide nitrogen cycling

Sediments are major sites for nitrogen uptake, transformation, and removal through microbial processes such as ammonification and denitrification. The relative proportion of different types of nitrogen fluxing into or out of the sediments has important implications for the nitrogen budget for the ecosystem. For example, nitrogen released as  $\text{N}_2$  gas is lost from the system, whereas nitrogen released as  $\text{NH}_4^+$  or  $\text{NO}_x$  may further stimulate primary production in the overlying water.  $\text{N}_2$  was the largest of the dark nitrogen fluxes, indicating that these sediments are efficient at removing nitrogen through denitrification. Even though most stations released  $\text{NH}_4^+$  to the overlying water, they functioned as a net sink for DIN, largely driven by greater  $\text{NO}_x$  uptake. As discussed above, this  $\text{NO}_3^-$  influx likely fueled denitrification. The denitrification efficiency is a useful term used to quantify how much of the nitrogen released from the sediments comes from denitrification. It is the percentage of total inorganic nitrogen released as

$\text{N}_2$  during organic matter decomposition (Eyre and Ferguson, 2002), or  $\text{N}_2\text{-N}/(\text{NH}_4^+ + \text{N}_2\text{-N})$ . The efficiencies ranged from 69 - 86%, indicating a dominance by denitrification (Table 2). The lowest efficiency occurred at CBL13, which had the highest  $\text{NH}_4^+$  efflux of the stations. As discussed previously, this may reflect the notably high levels of polychaetes found at this station (McTigue et al., in review), which would have contributed to total  $\text{NH}_4^+$  release via excretion. Overall, the net release of nitrogen as  $\text{N}_2$  gas is the major nitrogen pathway in the sediments, resulting in net removal of nitrogen during the summer. A previous study of denitrification in this system suggests that denitrification rates vary little from ice-covered spring to ice-free summer (Chang and Devol, 2009), thus we would expect our results to extend to spring, and possibly fall and winter, as well. Denitrification in these perennially cold, shelf sediments may not vary seasonally because the timescale on which POC is denitrified is long relative to the seasonal pulses of organic matter.

There is a paucity of denitrification data from the Arctic, so these Hanna Shoal rates can inform our limited knowledge of denitrification in this region. If we assume that the Hanna Shoal summer rates are maintained throughout the year, and we take a simplistic view and scale up the rates to the entire Chukchi Sea ( $620,000 \text{ km}^2$ ), denitrification in the Chukchi Sea removes  $2.89 \text{ Tg N yr}^{-1}$  (range  $1.82 - 4.18 \text{ Tg N yr}^{-1}$ ). This represents on average 22 % of total denitrification occurring on Arctic shelves ( $13 \text{ Tg N yr}^{-1}$ ), as estimated by Chang and Devol (2009), and 1.2% of total shelf sediment denitrification globally ( $250 \text{ Tg N yr}^{-1}$ ; Seitzinger et al. 2006). Our estimate agrees remarkably well with the areal denitrification rate for the Chukchi Sea of  $3.059 \text{ Tg N yr}^{-1}$  estimated by Chang and Devol (2009) using the derived relationship between depth and denitrification. Despite the cold temperatures, Arctic continental shelves are important nitrogen loss regions to consider in constructing global nitrogen budgets.

#### **4.4 System-wide organic carbon remineralization**

Sediment  $\text{O}_2$  uptake has been widely used to assess benthic organic carbon mineralization during early diagenesis (Epping and Helder, 1997; Glud et al., 1994; Lansard et al., 2008; Wenzhofer and Glud, 2002). Although both aerobic and anaerobic remineralization are occurring, most of the reduced species produced by anaerobic degradation (e.g.,  $\text{H}_2\text{S}$ ,  $\text{NH}_4^+$ ,  $\text{Fe}^{2+}$ ) are ultimately reoxidized by an equivalent amount of  $\text{O}_2$ . Thus,  $\text{O}_2$  uptake rate can be used as a proxy for the total benthic carbon remineralization rate, which includes both oxic and anoxic mineralization. If we consider only DOU, which excludes the role of benthic fauna in bioturbation and bioirrigation on  $\text{O}_2$  fluxes, we can estimate the amount of organic carbon mineralized in these sediments. Assuming Redfield stoichiometry (138O:106C), our  $\text{O}_2$  consumption rates yield benthic carbon remineralization rates of  $107 \pm 33$  to  $170 \pm 25 \mu\text{mol C m}^{-2} \text{ h}^{-1}$  (Table 6). These values account for approximately 19 - 28% of summer export production ( $13.2 \pm 13.0 \text{ mmol C m}^{-2} \text{ d}^{-1}$ ) measured on the northern Chukchi shelf (Table 6; Moran et al., 2005). POC export accounted for ~37% of summer primary production on the shelf (Moran et al., 2005). Previous estimates of POC export and benthic carbon remineralization on the shelf showed a strong correspondence at shallow (<300 m) stations, indicating strong benthic-pelagic coupling, relative to deeper slope stations (Moran et al., 2005). They estimated benthic carbon respiration to account for ~55% of export production in the summer, which is greater than our estimate; however their estimate also includes respiration by benthic macrofauna, which we do not include, as our focus is microbial remineralization. The previous study noted that benthic-pelagic coupling was stronger during the spring than in the summer, and that much of the carbon not

being remineralized in the sediments was likely exported at the shelf-break region (Moran et al., 2005). Our relatively low fraction of export production mineralized at the shallow Hanna Shoal stations in the summer supports the conclusions of Moran et al. 2005.

**Table 6.** Organic carbon remineralization estimates. Carbon mineralization estimate from DOU uses 106C:138O Redfield ratio. Carbon oxidation via denitrification uses 1N:1.25C ratio (Hardison et al., 2015). Percent of export production is based on summer export production =  $13.2 \pm 13 \text{ mmol C m}^{-2} \text{ d}^{-1}$ , Moran et al., 2005.

Station	C mineralized (DOU)	% export production	C mineralized (denitrification)	% export production
	$\mu\text{mol C m}^{-2} \text{ h}^{-1}$	%	$\mu\text{mol C m}^{-2} \text{ h}^{-1}$	%
<b>CBL11</b>	107 (33)	19 (6)	68 (3)	12 (0.6)
<b>CBL13</b>	170 (25)	31 (5)	35 (5)	6 (0.9)
<b>H17</b>	136 (59)	25 (11)		
<b>H29</b>	154 (3)	28 (0.6)	30 (5)	6 (0.8)
<b>H33</b>	120 (19)	22 (4)	54 (10)	10 (1.8)
<b>Station mean (SE)</b>	137 (11)	25 (2)	47 (9)	9 (2)

The amount of organic carbon oxidized via denitrification can be estimated using the reaction stoichiometry of the complete denitrification pathway, from  $\text{NO}_3^-$  reduction to  $\text{N}_2$  gas production (see Hardison et al., 2015). Assuming stoichiometry of 1N:1.5C yields carbon mineralization rates of  $30 \pm 5$  to  $68 \pm 3 \mu\text{mol C m}^{-2} \text{ h}^{-1}$  (Table 6). These values account for approximately 6 - 12% of summer export production ( $13.2 \pm 13.0 \text{ mmol C m}^{-2} \text{ d}^{-1}$ ) measured on the northern Chukchi shelf (Moran et al., 2005). Oxidic mineralization and denitrification together oxidized 31 - 37% of export production, with denitrification making up 16 - 39% of the total carbon oxidation. These percentages reflect global trends, as  $\text{O}_2$  is responsible for more than 80% of total organic carbon oxidation in continental shelf sediments (Lefevre et al., 1997; Martin and Sayles, 2003). Denitrification at the Hanna Shoal and elsewhere in the productive Chukchi Sea may be enhanced relative to global averages due to the high abundance of benthic infauna, which enhance denitrification via bioirrigation and bioturbation activities that expand the zone of  $\text{NO}_3^-$  reduction (Braeckman et al., 2014; Kristensen et al., 1991). Thus, these shallow, productive Arctic shelves may be local hotspots for organic carbon remineralization.

## 5. Acknowledgments

We are enormously grateful to the captain and crew of the USCGC *Healy* for the productive and safe research voyage, HLY1301. We thank M. McCarthy for much helpful discussion of  $^{15}\text{NH}_4^+$  data, K. Liu for analyzing AIRTS samples, and N. Reyna and A. Wohlrab for dedicated assistance with nutrient analyses. This study was funded by the U.S. Department of the Interior, Bureau of Ocean Energy Management (BOEM), Alaska Outer Continental Shelf Region, Anchorage, Alaska under BOEM Cooperative Agreement No. M11AC00007 as part of the Chukchi Sea Offshore Monitoring in Drilling Area (COMIDA) and through support by the National Science Foundation under Grant No. EAR-1417433 to AKH.

## 6. References

- Archer, D., Devol, A., 1992. Benthic Oxygen Fluxes on the Washington Shelf and Slope - a Comparison of Insitu Microelectrode and Chamber Flux Measurements. *Limnology and Oceanography* 37, 614-629.
- Bauer, J.E., Cai, W.J., Raymond, P.A., Bianchi, T.S., Hopkinson, C.S., Regnier, P.A.G., 2013. The changing carbon cycle of the coastal ocean. *Nature* 504, 61-70.
- Berelson, W.M., Heggie, D., Longmore, A., Kilgore, T., Nicholson, G., Skyring, G., 1998. Benthic nutrient recycling in Port Phillip Bay, Australia. *Estuarine Coastal and Shelf Science* 46, 917-934.
- Blackburn, T.H., 1979. Method for Measuring Rates of  $\text{NH}_4^+$  Turnover in Anoxic Marine-Sediments, Using a N-15-  $\text{NH}_4^+$  Dilution Technique. *Applied and Environmental Microbiology* 37, 760-765.
- Boudreau, B.P., 1997. Diagenetic Models and Their Implementation: Modelling Transport and Reactions in Aquatic Sediments. Springer.
- Braeckman, U., Foshtomi, M.Y., Van Gansbeke, D., Meysman, F., Soetaert, K., Vincx, M., Vanaverbeke, J., 2014. Variable Importance of Macrofaunal Functional Biodiversity for Biogeochemical Cycling in Temperate Coastal Sediments. *Ecosystems* 17, 720-737.
- Brown, Z.W., Casciotti, K.L., Pickart, R.S., Swift, J.H., Arrigo, K.R., 2015. Aspects of the marine nitrogen cycle of the Chukchi Sea shelf and Canada Basin. *Deep-Sea Research II-Topical Studies in Oceanography* 118, 73-87.
- Bruesewitz, D.A., Gardner, W.S., Mooney, R.F., Buskey, E.J., 2015. Seasonal Water Column  $\text{NH}_4^+$  Cycling Along a Semi-arid Sub-tropical River-Estuary Continuum: Responses to Episodic Events and Drought Conditions. *Ecosystems* 18, 792-812.
- Chang, B.X., Devol, A.H., 2009. Seasonal and spatial patterns of sedimentary denitrification rates in the Chukchi sea. *Deep-Sea Research II-Topical Studies in Oceanography* 56, 1339-1350.
- Christensen, J.P., 2008. Sedimentary Carbon Oxidation and Denitrification on the Shelf Break of the Alaska Beaufort and Chukchi Seas. *The Open Oceanography Journal* 2, 6-17.
- Christensen, J.P., Murray, J.W., Devol, A.H., Codispoti, L.A., 1987. Denitrification in continental shelf sediments has major impact on the ocean nitrogen budget. *Global Biogeochemical Cycles* 1, 97-116.
- Deutsch, C., Weber, T., 2012. Nutrient Ratios as a Tracer and Driver of Ocean Biogeochemistry. *Annual Review of Marine Science*, Vol 4 4, 113.
- Devol, A.H., 2015. Denitrification, Anammox, and  $\text{N}_2$  Production in Marine Sediments. *Annual Review of Marine Science*, Vol 7 7, 403.
- Devol, A.H., Codispoti, L.A., Christensen, J.P., 1997. Summer and winter denitrification rates in western Arctic shelf sediments. *Continental Shelf Research* 17, 1029.
- Epping, E.H.G., Helder, W., 1997. Oxygen budgets calculated from in situ oxygen microprofiles for Northern Adriatic sediments. *Continental Shelf Research* 17, 1737-1764.

- Eyre, B.D., Ferguson, A.J.P., 2002. Comparison of carbon production and decomposition, benthic nutrient fluxes and denitrification in seagrass, phytoplankton, benthic microalgae- and macroalgae-dominated warm-temperate Australian lagoons. *Marine Ecology Progress Series* 229, 43-59.
- Gardner, C.W., 1995. High-Performance Liquid-Chromatography - an Introduction to the Chemistry of HPLC. *Abstracts of Papers of the American Chemical Society* 209, 23-TECH.
- Gardner, W.S., McCarthy, M.J., 2009. Nitrogen dynamics at the sediment-water interface in shallow, sub-tropical Florida Bay: why denitrification efficiency may decrease with increased eutrophication. *Biogeochemistry* 95, 185-198.
- Gardner, W.S., McCarthy, M.J., Carini, S.A., Souza, A.C., Lijun, H., McNeal, K.S., Puckett, M.K., Pennington, J., 2009. Collection of intact sediment cores with overlying water to study nitrogen- and oxygen-dynamics in regions with seasonal hypoxia. *Continental Shelf Research* 29, 2207-2213.
- Glud, R.N., Gundersen, J.K., Jorgensen, B.B., Revsbech, N.P., Schulz, H.D., 1994. Diffusive and Total Oxygen-Uptake of Deep-Sea Sediments in the Eastern South-Atlantic Ocean - in-Situ and Laboratory Measurements. *Deep-Sea Research Part I-Oceanographic Research Papers* 41, 1767-1788.
- Grebmeier, J.M., Bluhm, B., Cooper, L.W., Danielson, S.L., Arrigo, K.R., Blanchard, A.L., Clarke, J.T., Day, R.H., Frey, K.E., Gradinger, R.R., Kedra, M., Konar, B., Kuletz, K.J., Lee, S.H., Lovvorn, J.R., Norcross, B.L., Okkonen, S.R., 2015. Ecosystem characteristics and processes facilitating persistent macrobenthic biomass hotspots and associated benthivory in the Pacific Arctic. *Progress in Oceanography* 136, 92-114.
- Grebmeier, J.M., Cooper, L.W., Feder, H.M., Sirenko, B.I., 2006. Ecosystem dynamics of the Pacific-influenced Northern Bering and Chukchi Seas in the Amerasian Arctic. *Progress in Oceanography* 71, 331-361.
- Gruber, N., Sarmiento, J.L., 1997. Global patterns of marine nitrogen fixation and denitrification. *Global Biogeochemical Cycles* 11, 235-266.
- Hammond, D.E., Giordani, P., Berelson, W.M., Poletti, R., 1999. Diagenesis of carbon and nutrients and benthic exchange in sediments of the Northern Adriatic Sea. *Marine Chemistry* 66, 53-79.
- Hardison, A.K., Algar, C.K., Giblin, A.E., Rich, J.J., 2015. Influence of organic carbon and nitrate loading on partitioning between dissimilatory nitrate reduction to ammonium (DNRA) and N<sub>2</sub> production. *Geochimica et Cosmochimica Acta* 164, 146-160.
- Hoellein, T.J., Tank, J.L., Rosi-Marshall, E.J., Entekin, S.A., 2009. Temporal variation in substratum-specific rates of N uptake and metabolism and their contribution at the stream-reach scale. *Journal of the North American Benthological Society* 28, 305-318.
- James, R.T., Gardner, W.S., McCarthy, M.J., Carini, S.A., 2011. Nitrogen dynamics in Lake Okeechobee: forms, functions, and changes. *Hydrobiologia* 669, 199-212.
- Joye, S.B., Anderson, I.C., 2008. Nitrogen cycling in coastal sediments, in: Capone, D.G., Bronk, D.A., Mulholland, M.R., Carpenter, E.J. (Eds.), *Nitrogen in the Marine Environment*, 2 ed. Academic Press, pp. 867-915.

- Kana, T.M., Darkangelo, C., Hunt, M.D., Oldham, J.B., Bennett, G.E., Cornwell, J.C., 1994. Membrane Inlet Mass-Spectrometer for Rapid High-Precision Determination of N<sub>2</sub>, O<sub>2</sub>, and Ar in Environmental Water Samples. *Analytical Chemistry* 66, 4166-4170.
- Kristensen, E., Jensen, M.H., Aller, R.C., 1991. Direct Measurement of Dissolved Inorganic Nitrogen Exchange and Denitrification in Individual Polychaete (*Nereis-Virens*) Burrows. *J. Mar. Res.* 49, 355-377.
- Lansard, B., Rabouille, C., Denis, L., Grenz, C., 2008. In situ oxygen uptake rates by coastal sediments under the influence of the Rhone River (NW Mediterranean Sea). *Cont. Shelf Res.* 28, 1501-1510.
- Lavrentyev, P.J., Gardner, W.S., Yang, L.Y., 2000. Effects of the zebra mussel on nitrogen dynamics and the microbial community at the sediment-water interface. *Aquat. Microbial Ecol.* 21, 187-194.
- Lefevre, D., Minas, H.J., Minas, M., Robinson, C., Williams, P.J.L., Woodward, E.M.S., 1997. Review of gross community production, primary production, net community production and dark community respiration in the Gulf of Lions. *Deep-Sea Research Part II-Topical Studies in Oceanography* 44, 801-&.
- Lin, X.A., McCarthy, M.J., Carini, S.A., Gardner, W.S., 2011. Net, actual, and potential sediment-water interface NH<sub>4</sub><sup>+</sup> fluxes in the northern Gulf of Mexico (NGOMEX): Evidence for NH<sub>4</sub><sup>+</sup> limitation of microbial dynamics. *Cont. Shelf Res.* 31, 120-128.
- Martin, W.R., Sayles, F.L., 2003. The Recycling of Biogenic Material at the Seafloor, in: Mackenzie, F.T., Holland, H.D., Turekian, K.K. (Eds.), *Treatise on Geochemistry*. Elsevier, pp. 37-65.
- McCarthy, M.J., Gardner, W.S., Lavrentyev, P.J., Moats, K.M., Joehem, F.J., Klarer, D.M., 2007. Effects of hydrological flow regime on sediment-water interface and water column nitrogen dynamics in a great lakes coastal wetland (Old Woman Creek, Lake Erie). *J. Great Lakes Res.* 33, 219-231.
- McTigue, N.D., Dunton, K.H., 2014. Trophodynamics and organic matter assimilation pathways in the northeast Chukchi Sea, Alaska. *Deep-Sea Res. II-Topical Studies in Oceanography* 102, 84-96.
- McTigue, N.D., Gardner, W.S., Dunton, D.H., Hardison, A.K., in review. Biotic and abiotic controls on co-occurring denitrification, anammox, and DNRA in shallow Arctic shelf sediments. *Nat Commun.*
- Middelburg, J.J., Nieuwenhuize, J., 2000. Nitrogen uptake by heterotrophic bacteria and phytoplankton in the nitrate-rich Thames estuary. *Mar. Ecol. Progr. Ser.* 203, 13-21.
- Mooney, R.F., McClelland, J.W., 2012. Watershed Export Events and Ecosystem Responses in the Mission-Aransas National Estuarine Research Reserve, South Texas. *Estuaries and Coasts* 35, 1468-1485.
- Moran, S.B., Kelly, R.P., Hagstrom, K., Smith, J.N., Grebmeier, J.M., Cooper, L.W., Cota, G.F., Walsh, J.J., Bates, N.R., Hansell, D.A., Maslowski, W., Nelson, R.P., Mulrow, S., 2005. Seasonal changes in POC export flux in the Chukchi Sea and implications for water column-

- benthic coupling in Arctic shelves. *Deep-Sea Res. I -Topical Studies in Oceanography* 52, 3427-3451.
- Nixon, S., 1981. Remineralization and nutrient cycling in coastal marine ecosystems, in: Neilson, B., Cronin, L. (Eds.), *Estuaries and Nutrients*. Humana Press, Clifton, NJ, pp. 111-138.
- Paerl, H.W., Xu, H., McCarthy, M.J., Zhu, G.W., Qin, B.Q., Li, Y.P., Gardner, W.S., 2011. Controlling harmful cyanobacterial blooms in a hyper-eutrophic lake (Lake Taihu, China): The need for a dual nutrient (N & P) management strategy. *Water Res.* 45, 1973-1983.
- Reimers, C., Jahnke, R.A., Thomson, L., 2001. In situ sampling in the benthic boundary layer, in: Boudreau, B.P., Jorgensen, B.B. (Eds.), *The Benthic Boundary Layer--Transport Processes and Biogeochemistry*. Oxford University Press, Oxford, pp. 245-268.
- Sayles, F.L., Martin, W.R., Deuser, W.G., 1994. Response of Benthic Oxygen-Demand to Particulate Organic-Carbon Supply in the Deep-Sea near Bermuda. *Nature* 371, 686-689.
- Schonberg, S.V., Clarke, J.T., Dunton, K.H., 2014. Distribution, abundance, biomass and diversity of benthic infauna in the Northeast Chukchi Sea, Alaska: Relation to environmental variables and marine mammals. *Deep-Sea Res. I-Topical Studies in Oceanography* 102, 144-163.
- Seitzinger, S., Harrison, J.A., Bohlke, J.K., Bouwman, A.F., Lowrance, R., Peterson, B., Tobias, C., Van Drecht, G., 2006. Denitrification across landscapes and waterscapes: A synthesis. *Ecolog. Applications* 16, 2064-2090.
- Smith, S.V., Hollibaugh, J.T., 1993. Coastal Metabolism and the Oceanic Organic-Carbon Balance. *Rev. Geophys.* 31, 75-89.
- Soetaert, K., Meysman, F., 2009. *ReacTran: Reactive transport modeling in 1D, 2D, and 3D*, R package version 2.1. <http://cran.r-project.org/web/packages/ReacTran/index.html>.
- Souza, A.C., Gardner, W.S., Dunton, K.H., 2014a. Rates of nitrification and ammonium dynamics in northeastern Chukchi Sea shelf waters. *Deep-Sea Res. I-Topical Studies Oceanogr.* 102, 68-76.
- Souza, A.C., Kim, I.N., Gardner, W.S., Dunton, K.H., 2014b. Dinitrogen, oxygen, and nutrient fluxes at the sediment-water interface and bottom water physical mixing on the eastern Chukchi Sea shelf. *Deep-Sea Res. II -Topical Studies in Oceanography* 102, 77-83.
- Thamdrup, B., Dalsgaard, T., 2002. Production of N<sub>2</sub> through anaerobic ammonium oxidation coupled to nitrate reduction in marine sediments. *Appl. Environ. Microbiol.* 68, 1312-1318.
- Tobias, C., Giblin, A., McClelland, J., Tucker, J., Peterson, B., 2003. Sediment DIN fluxes and preferential recycling of benthic microalgal nitrogen in a shallow macrotidal estuary. *Mar.Ecol. Progr. Ser.* 257, 25-36.
- Trimmer, M., Engstrom, P., Thamdrup, B., 2013. Stark Contrast in Denitrification and Anammox across the Deep Norwegian Trench in the Skagerrak. *Appl. Environ. Microbiol.* 79, 7381-7389.
- Weingartner, T., Dobbins, E., Danielson, S., Winsor, P., Potter, R., Statscewich, H., 2013. Hydrographic variability over the northeastern Chukchi Sea shelf in summer-fall 2008-2010. *Cont. Shelf Res.* 67, 5-22.



Wenzhofer, F., Glud, R.N., 2002. Benthic carbon mineralization in the Atlantic: a synthesis based on in situ data from the last decade. *Deep-Sea Res. I -Oceanographic Research Papers* 49, 1255-1279.

# Trophodynamics of the Hanna Shoal Ecosystem (Chukchi Sea, Alaska): Connecting Multiple End-members to a Rich Benthic Food Web

Nathan D. McTigue<sup>a</sup>, Kenneth H. Dunton<sup>b</sup>

<sup>a</sup>NOAA Center for Coastal Fisheries and Habitat Research, Beaufort, NC 28516

<sup>b</sup>University of Texas at Austin Marine Science Institute, Port Aransas, TX, 78373

[nathan.mctigue@noaa.gov](mailto:nathan.mctigue@noaa.gov), [ken.dunton@utexas.edu](mailto:ken.dunton@utexas.edu)

## Abstract

We used stable carbon and nitrogen isotopes to determine the dietary contribution of multiple end-members to the consumers in the Hanna Shoal ecosystem using the mixing model *simmr*. Trophic redundancy and plasticity was assessed by measuring the standard ellipses of each consumer in bivariate  $\delta^{13}\text{C}$  and  $\delta^{15}\text{N}$  isospace. Phytoplankton, sediment organic matter (SOM), and ice algae, which were collected from the study area, were used as food web end-members. We also included a  $^{13}\text{C}$ -enriched microphytobenthos (MPB) end-member, an isotopically distinct organic matter source that is hypothesized to exist in the shallow benthos of the Chukchi Sea, in our mixing model. Consumers were grouped into five different trophic guilds: suspension feeder, surface deposit feeder, subsurface deposit feeder, predator, and scavenger. Phytoplankton and SOM were isotopically similar and considered the same ultimate organic matter source by the mixing model. Most suspension feeders and predator/scavengers obtained a large proportion of their nutrition from phytoplankton/SOM, while deposit feeders assimilated combinations of all end-members. MPB was assimilated by deposit-feeding bivalves and passed to higher trophic levels by predatory gastropod feeding. Trophic redundancy and consumer reliance on specific organic matter sources in the benthic food web can be used to predict changes in the food web as ice-mediated primary production regimes shift in the future.

## 1. Introduction

The impetus of many recent Arctic food web studies has been to elucidate how climate change-mediated alterations in sea ice extent and duration will impact the timing and delivery of ice algae and phytoplankton food resources to the shallow shelf communities, i.e. investigating alterations to cryo-pelagic-benthic coupling (Bluhm and Gradinger, 2008). There is clear evidence that primary production in the Arctic is mediated by sea ice cover (Sakshaug, 2004; Wassmann and Reigstad, 2011), which has steadily decreased in extent and volume over the past three decades. With the onset of open water occurring earlier, it is possible that primary production might be reduced given lower light levels earlier in the growing season (Kahru et al., 2011; Saitoh et al., 2002). But long-term observations have shown that the lengthening of the open water season by about 30 days from 1998 to 2012 in the Arctic Ocean coincides with increases in annual net primary production (Arrigo and van Dijken, 2015). However, more pelagic primary production does not necessarily yield increased export to the seafloor. The earlier onset of open water could reduce the strength of the rapidly-sinking ice algae bloom,

prevent water column stratification due to wind mixing, and cause a later-occurring bloom that is dominated by phytoplankton (Bluhm and Gradinger, 2008). Later in the growing season, pelagic grazers that are not present in the early spring could efficiently reduce the quantity and quality of carbon that reaches the benthic food web on the seafloor (Carroll and Carroll, 2003). While testing these hypotheses is beyond the scope of this study, we aim to address the long-term impacts of the current and imminent alterations in primary production by tracking the assimilation of different carbon sources into the benthic food web and assessing consumers' reliance on different organic matter sources. By assessing if consumers rely heavily on one organic matter source or have flexibility in their diet, we can better understand how the ripples of primary production regime shifts will be felt across the food web.

Overwhelmingly, stable isotopes are the choice tool to track the assimilation of different carbon sources into a food web. The stable isotope composition of consumer tissue reflects that of the food source; therefore, if multiple food web end-members possess differing stable isotope signatures, then the dietary contributions to a consumer's diet can be discerned by using mixing models. Previous insights in applying stable isotopes to trophic ecology have developed the 'isotopic niche', quantified by the plotted bivariate  $\delta^{13}\text{C}$  and  $\delta^{15}\text{N}$  space, or  $\delta$ -space, of a species or population (Bearhop et al., 2004; Newsome et al., 2007). The isotopic niche is a robust measure of dietary niche width in that it allows the direct comparison of individuals or populations, combines information on richness and evenness of food resources, and allows the temporal integration of dietary information over different timescales (Bearhop et al., 2004). Several metrics (e.g.,  $\delta^{13}\text{C}$  range,  $\delta^{15}\text{N}$  range, area) can be used to quantify the character and size of each isotopic niche (Layman et al., 2007). However, limitations still exist in using stable isotopes to solve mixing models and quantify niche space, particularly the natural variation of stable isotope values exhibited by both consumers and end-members and the uncertainty surrounding the use of appropriate trophic enrichment factors (TEFs), which are typically assumed from broad ecosystem surveys (Post, 2002; Vander Zanden and Rasmussen, 2001) or a lab study using several different organisms but only one marine invertebrate (*Artemia salina*) (DeNiro and Epstein, 1978, 1981). These authors clearly showed that there is normally-distributed natural variation in TEFs, up to 4‰ for  $\delta^{13}\text{C}$  and  $\delta^{15}\text{N}$  TEFs ranged from -0.5 to 9.2‰, while the mean, median, and mode TEFs are ~1‰ and ~3.3‰ for  $\delta^{13}\text{C}$  and  $\delta^{15}\text{N}$ , respectively. Recent revelations suggest utilizing Bayesian inference to evade these limitations (Parnell et al., 2010, 2015; Jackson et al., 2011). This approach incorporates uncertainty surrounding assumptions of TEFs and variation of stable isotope values into the model, thereby generating potential solutions (e.g., of isotopic niche width or mixing model proportions) as true probability distributions, thus improving upon linear mixing equations that produce only one solution (Parnell et al., 2010).

The northeast Chukchi Sea is a unique location to conduct food web studies. It has been identified as a benthic 'hotspot' due to its persistent, seasonally intense primary production, which is efficiently exported to the benthos to support high macrofaunal biomass (Grebmeier et al. 2015). The northeast Chukchi Sea, particularly near Hanna Shoal, hosts multiple end-members that can supply nutrition to the benthic food web. The nutrient rich waters in the Chukchi Sea support some of the highest pelagic primary production and organic carbon flux to the seafloor in the Arctic (Sakshaug et al., 2004; Moran et al., 2005). Due to its unique hydrology, Hanna Shoal eddies currents of northward-advected, nutrient-rich Pacific Ocean water (Weingartner et al., 2013). Thus, sea ice is retained in the region late into summer providing an ice algae subsidy to the benthos. Sea ice algae can have a wide range of  $\delta^{13}\text{C}$

values, greatly depending on algae health, from -24 to -14‰ (Sørense et al., 2006), Gradinger, 2009, Tremblay et al. 2006). Conversely, phytoplankton and particulate organic matter (POM) are typically entrained between  $\delta^{13}\text{C}$  values of -25 and -22‰, so ice- and water column-derived organic matter can potentially be isotopically disparate. Sediment organic matter (SOM), the feeding substrate for deposit feeders, is usually isotopically similar to overlying POM, which demonstrates the tight pelagic-benthic coupling on the Arctic shelf (Iken et al., 2010; McTigue and Dunton, 2014; Tu et al., 2015).

Another organic matter source has been hypothesized by the scientific community to exist in the Chukchi Sea benthos that supplies a  $^{13}\text{C}$ -enriched signal to the benthic food web: benthic microalgae (Glud et al., 2009; Wulff et al., 2009; McTigue and Dunton, 2014; Tu et al., 2015) and/or microbially degraded detrital material (McCaughnahan and McRoy, 1979; Lovvorn et al., 2009; North et al., 2014; McTigue et al., 2015). Benthic microalgae have eluded stable isotope analysis in the Chukchi Sea, but they have been identified in other systems as  $^{13}\text{C}$ -enriched primary producers relative to phytoplankton (France, 1995; Dubois et al., 2009). Benthic microalgae exhibit values that fit within the expected range of an OM source that would explain some  $^{13}\text{C}$ -enriched benthic consumers in the Bering and Chukchi Seas (Lovvorn et al., 2005; North et al., 2014; McTigue et al., 2014; Tu et al., 2015). Oxtoby et al. (2015) have modeled stable isotope values for benthic microalgae using  $\delta^{13}\text{C}$  values of dissolved inorganic carbon (DIC) from Beaufort Sea bottom water, benthic microalgae growth rates, and fractionation factors from photosynthesis. They estimated that values would range between -30 and -23‰ since slow growth conditions at the seafloor would allow cells to discriminate against  $^{13}\text{C}$  despite having a limited DIC pool from benthic boundary conditions (Hecky and Hesslein, 1995). While this range does not fit our expected values of benthic microalgae from stable isotope values reported from other systems (-20 to -16‰), it is possible that either Chukchi Sea DIC is more  $^{13}\text{C}$ -enriched or that growth rates are higher for benthic microalgae in the shallow Hanna Shoal system that receives higher photosynthetically active radiation (PAR).

An alternative to benthic microalgae that could provide a  $^{13}\text{C}$ -enriched OM source for benthic consumers is microbially degraded OM, first hypothesized by McConnaughey and McRoy (1979) for the Bering Sea. Since microalgae have been observed to pass through a consumer's gut undigested (Hansen and Josefson, 2004), it is plausible that microalgae are not bioavailable to the food web until they have entered the phytodetritus pool via microbial re-working (North et al., 2014), which occurs readily to recently deposited microalgae in Arctic sediments (Sun et al., 2009). Microbial re-working of a carbon pool should preferentially release  $^{13}\text{C}$ -depleted  $\text{CO}_2$ , causing  $^{13}\text{C}$ -enrichment of the remaining substrate (Coffin et al., 1991; Macko and Estep, 1984). Bolstering this hypothesis, there is a striking correlation with sedimentary biomarkers of degraded microalgae and  $\delta^{13}\text{C}$  values of benthic consumers (McTigue et al., 2015). However, predicting how microbial degradation affects  $^{15}\text{N}$  fractionation is complicated as it can deplete or enrich the substrate, and the N dynamics in the Chukchi Sea seafloor is complicated still requiring some resolution (Brown et al., 2015; Hardison et al., this issue).

Regardless of the true identity of the 'missing' source (Dunton et al. 2014), the  $\delta^{13}\text{C}$  values of benthic fauna in the Arctic strongly suggest that an organic matter source is assimilated into the food web that exhibits  $^{13}\text{C}$ -enriched values that cannot be explained by POM, SOM, or sea ice algae (McTigue and Dunton, 2014; Lovvorn et al. 2005, North et al. 2014; Lalande et al., 2007). Since we are applying stable isotope mixing models to elucidate diet proportions of consumers and it is required to include all potential end-members in analysis (Philips et al., 2014), we

included a  $^{13}\text{C}$ -enriched and  $^{15}\text{N}$ -depleted OM source we termed benthic microalgae using a range of literature values of benthic microalgae that incorporate its isotopic variation. Hereafter, this source is referred to as microphytobenthos (MPB), which is considered benthic microalgae and/or microbially-derived products.

This study investigates the plasticity of the benthic food web in order to elucidate its ability to adapt to current and imminent shifts in primary production. This is accomplished in two steps: first, we quantified the plasticity of isotopic trophic niches for multiple species in the benthic food web including suspension feeders, deposit feeders, and predator/scavengers; second, we identified the importance of various food web end-members in consumer diets using a stable isotope mixing model. We address the questions (1) are there consumers or trophic groups that heavily rely on only one organic matter source, and (2) what is the relative importance of the multiple end-members, including the hypothesized  $^{13}\text{C}$ -enriched MPB, for the Hanna Shoal ecosystem?

## **2. Methods**

### **2.1 Study area**

This project was one component of the Hanna Shoal Ecosystem Study ([www.arcticstudies.org/hannashoal](http://www.arcticstudies.org/hannashoal)), an interdisciplinary, multi-year project that focused on defining the chemical, biological, and physical properties that contribute to the high primary and secondary production in the Hanna Shoal ecosystem. Aboard the USCGC *Healy*, 25 stations were occupied from 9 – 25 August 2012, and 33 stations were occupied from 29 July – 15 August 2013. Nine stations were occupied both years. The sampling stations were oriented around the bathymetric feature Hanna Shoal in the northeast Chukchi Sea (72 °N, 162 °W).

### **2.2 End-members**

Phytoplankton were collected with vertical plankton tows using a 20  $\mu\text{m}$  mesh net (Sea-Gear, Melbourne, FL). Since non-phytoplankton particles and organisms can be obtained during sampling, concentrated samples were passed over a 180  $\mu\text{m}$  screen to remove small zooplankton and other large extraneous particles. Sieved phytoplankton were filtered onto a pre-combusted 25 mm GF/F (0.7  $\mu\text{m}$  pore size) under low vacuum. Samples were stored in opaque vials and frozen for shipment.

Ice algae were obtained by collecting sea ice visibly discolored by algal pigments from a Zodiac boat excursion. Sea ice was slowly melted into basins, and meltwater was then filtered through pre-combusted 25 mm GF/F. Filters were frozen immediately in opaque vials.

Sediment organic matter (SOM) was collected from the upper 2 cm of an undisturbed 0.1  $\text{m}^2$  van Veen grab with the barrel of a 20  $\text{cm}^3$  syringe (1.8 cm diameter). Surface sediment was extruded into a pre-labeled vial and frozen for shipment.

MPB are another potential food web end-member (Matheke and Horner, 1974; McTigue et al., 2015). Since stable isotope mixing models can produce erroneous results if all end-members are not included (Phillips et al., 2014), this potential end-member, despite not being sampled directly, was included in analysis. The microalgae that specifically make up the microphytobenthos are typically disparate in stable isotope signatures from the bulk conglomeration that makes up SOM and are treated separately. In order to include MPB as a

potential end-member, literature values were used for stable carbon and nitrogen isotope values from temperate locations (Cloern et al., 2002; France, 1995; Kang et al., 2003; Dubois et al., 2007). MPB have a wide range of  $\delta^{13}\text{C}$  values in the literature, but are typically more  $^{13}\text{C}$ -enriched than phytoplankton and sometimes ice algae. Due to the variation in the literature and lack of actual measured values for the study area, the standard deviation around the literature mean of both stable isotopes was relatively large at 1.5‰. This variation assumedly encompasses the possible values of Chukchi Sea MPB.

### 2.3 Consumers

Benthic fauna were collected from the seafloor with either a 0.1 m<sup>2</sup> van Veen grab or a 3 m beam trawl with a 7 mm mesh and 4 mm cod-end liner. Organisms collected with van Veen grab were washed with surface seawater over a 1 mm screen to remove extraneous sediment. Propeller wash while retrieving the net off the stern A-frame removed most of the sediment from the trawl, but organisms were still washed with flowing surface water on deck. Larger epifauna obtained from the beam trawl were sorted and kept in a basin with flowing seawater. Zooplankton (specifically *Calanus* spp. copepods and *Sagitta* spp. chaetognaths) were obtained from either vertical tows of a 335  $\mu\text{m}$  net or bongo nets by Carin Ashjian and her group. Organisms were sorted and keyed to lowest taxonomic classification possible (oftentimes species level) while shipboard. In some cases, voucher specimens were kept in 90% ethanol until later identification. For larger fauna, muscle tissue was excised, while smaller organisms (e.g., amphipods, polychaetes) were kept whole. Organisms were labeled in aluminum tins and dried at 60 °C shipboard. All consumer and end-member samples were shipped to The University of Texas Marine Science Institute for sample preparation and analyses.

### 2.4 Sample analyses

End-members and consumers were analyzed for stable carbon and nitrogen isotopes. To remove inorganic carbon from samples prior to analysis of stable carbon isotopes, sub-samples were removed and underwent an acidification regimen so that the sub-sample analyzed for stable nitrogen isotopes was not subjected to acid. SOM and tissue from calcareous organisms (e.g., echinoderms) sub-samples were soaked in 1 N HCl until bubbling stopped, then rinsed with deionized water and dried at 60 °C.

Samples were not lipid extracted prior to stable isotope analyses so that data could be comparable to other studies from the region (e.g., McTigue and Dunton 2014, Iken et al. 2010, Tu et al., 2014). Previous work determined a low likelihood that lipids in Arctic consumers influenced  $\delta^{13}\text{C}$  values (Graeve et al., 1997; Iken et al., 2010, Dunton et al., 2012).

Dried tissue and SOM samples were manually homogenized with a mortar and pestle, and weighed to the nearest 10<sup>-6</sup> g into tin capsules. Samples on filters were also wrapped in tin capsules. All samples were analyzed for dual stable carbon and nitrogen isotopes on a Finnegan MAT Delta Plus mass spectrometer attached to a CE Instruments (NC 2500) elemental analyzer at The University of Texas Marine Science Institute. Samples were combusted at 1020 °C and injected into the mass spectrometer on a helium carrier. Isotopic ratios are reported in standard  $\delta$  notation using the equation

$$\delta X = [(R_{\text{sample}}/R_{\text{standard}})-1] \times 1000$$

where X corresponds to either  $^{13}\text{C}$  or  $^{15}\text{N}$ , R is the ratio of heavy to light isotopes, and the standard is either PDB for  $^{13}\text{C}$  or atmospheric  $\text{N}_2$  for  $^{15}\text{N}$ . Analytical sample error was  $\pm 0.2\%$  based on internal standards from the U.S. National Institute of Science and Technology and the International Atomic Energy Agency.

## 2.5 Data analyses

All analyses were computed in R 3.2.0 (R Development Core Team, 2007). The first goal of this research was to identify and compare the isotopic niche space occupied by each species and feeding guild. Isotopic niches are related to ecological niches in that the location of organisms in bivariate  $\delta^{13}\text{C} : \delta^{15}\text{N}$  space is a metric that can quantify an organism's trophic role in an ecosystem (Bearhop et al., 2004; Newsome et al., 2007). Therefore, isotopic niches are tightly correlated with trophic niches. For example, overlapping isotopic niches would suggest trophic redundancy between the two consumers. Likewise, a wide isotopic niche with a large area would indicate trophic plasticity (i.e., obtaining OM from isotopically disparate sources), whereas a small isotopic niche would indicate trophic rigidity. One strategy to quantify isotopic niche space is by quantifying the total area (TA) of the convex hull for a group of data points (Layman et al. 2007). Shortcoming of this method is that TA is highly influenced by outliers, TA increases as  $n$  increases, and that comparisons between groups with differing  $n$  are difficult to standardize (Jackson et al., 2011). An alternative approach uses standard ellipses (Batschelet, 1981), which are comparable to bivariate standard deviations and contain  $\sim 40\%$  of the data, which is typical of 1 standard deviation in univariate space. A standard ellipse, then, is less influenced by extreme values (Jackson et al., 2011). On a bivariate  $\delta^{13}\text{C} : \delta^{15}\text{N}$  plot, the area encompassed by a standard ellipse is reported in squared axes units, technically 'parts per thousand-squared', which is given the notation  $\text{‰}^2$ .

Incorporation of Bayesian inference to determine standard ellipse areas (SEAs) is an elegant solution to deal with the variation and uncertainty associated with sampling to generate a robust metric of isotopic niche area for groups with different sampling size (Jackson et al. 2011). The package Stable Isotope Bayesian Ellipses in R (*SIBER*; Jackson et al. 2011) was used to compute and compare SEAs among species and feeding guilds, using scripts modified from Passoti et al., (2015). The model fitting algorithm iteratively guesses at possible solutions, then discards those not probabilistically consistent with the data (Parnell et al., 2010; Phillips et al., 2014). The number of iterations to sample was  $2 \times 10^4$ , the number of iterations to discard as a burn-in from the start of the sampling was  $10^4$ , the number of samples to thin by was 10, and the number of chains to fit was 2. Per the recommendation of Jackson et al. (2011) of using at least  $n > 9$ , not all species collected and analyzed could be individually assessed. Therefore, in order to include all organisms collected from the benthic community, species were grouped into feeding guilds. These included suspension feeders, surface deposit feeders, subsurface deposit feeders, scavenger/omnivores, and predators. The end-members (phytoplankton, SOM, and ice algae) were also included as the baseline trophic guild. Guild membership was determined from literature (MacDonald et al., 2010) or from the World Register of Marine Species (<http://www.marinespecies.org>). SEAs were determined for each trophic guild, and then for each species with  $n > 9$ .

The second goal of this research was to determine the contribution of end-members to consumers' diets using a stable isotope mixing model. We used the package Stable Isotope Mixing Models in R (*simmr*) to compute possible contributions of end-members to consumer diets (Parnell et al., 2013). *simmr* is the designated upgrade to *siar* (Parnell et al., 2010) in that it

has a slightly richer mixing model and uses JAGS (Plummer, 2003) to implement the mixing model. Similar to computing SEAs, Bayesian inference was applied to the variation and uncertainty of sampling. Unlike previous mixing models, *simmr* incorporates uncertainty in trophic enrichment factors (TEFs) into the likelihoods of source contributions. Assigning TEFs to consumers is one of the largest sources of uncertainty in using stable isotopes to investigate trophodynamics (Phillips et al., 2014), so incorporating that uncertainty in the model makes this procedure a powerful quantitative tool. Since few controlled feeding studies exist for organisms found in the Arctic (McMahon et al., 2006) and there is considerable range of measured TEFs (Vander Zanden and Rasmussen, 2001; Post, 2002; Eggers and Jones, 2000), we chose to incorporate moderate variation into the TEFs for this model. Mean  $\pm$  standard deviation  $\Delta\delta^{13}\text{C}$  and  $\Delta\delta^{15}\text{N}$  for suspension feeders, surface deposit feeders, and subsurface deposit feeders were  $1.1\pm 1.0\text{‰}$  and  $3.4\pm 1.0\text{‰}$ , respectively. TEFs were doubled for predators and scavenger/omnivores, assuming that they occupy a higher trophic level and undergo more fractionation from their ultimate organic matter sources. A species must qualify at  $n>4$  to undergo analysis in *simmr* (Parnell et al., 2010; Parnell et al., 2013).

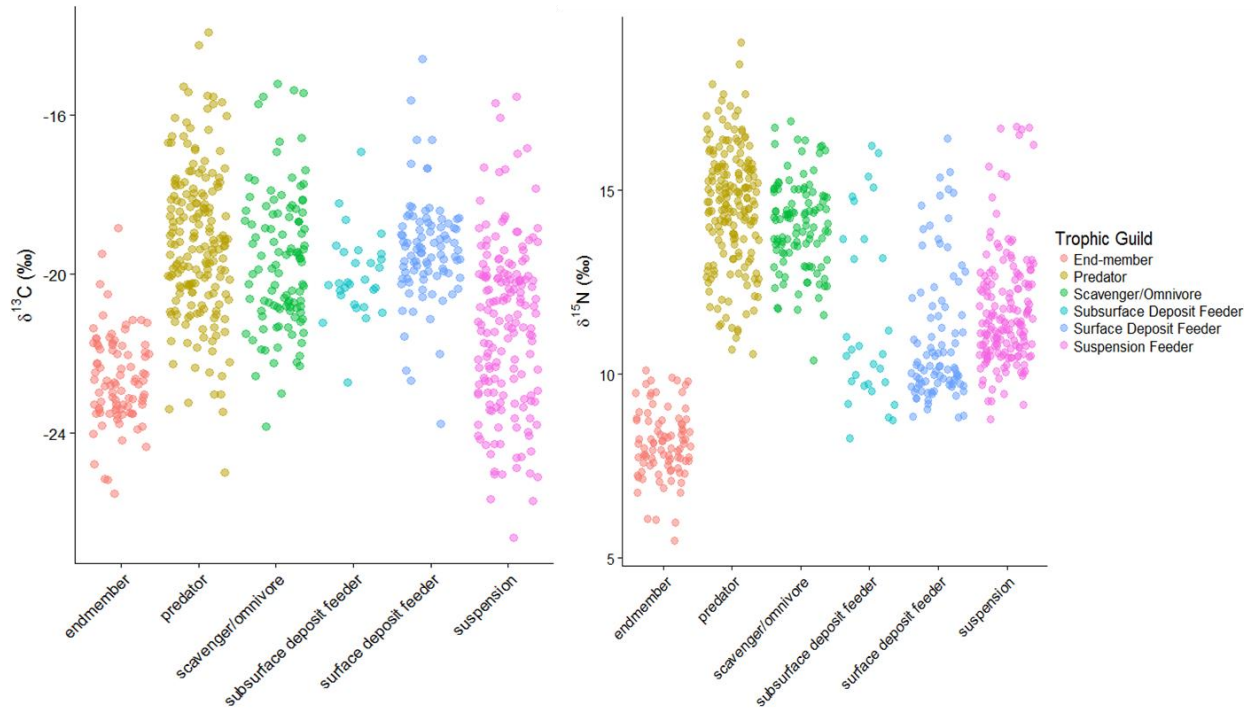
### 3. Results

#### 3.1 Standard ellipse areas (SEAs) for trophic guilds

SEAs could only be computed for samples measured during analysis, omitting the literature values for MPB we used in the mixing model. The  $\delta^{13}\text{C}$  values for the end-members guild (phytoplankton, SOM, and ice algae) were most constrained in isotopic niche space compared to any other guild (Figure 1). The most  $^{15}\text{N}$ -enriched end-members overlapped with some of the most  $^{15}\text{N}$ -depleted consumers at  $\sim 10\text{‰}$ . The suspension feeders and deposit feeders possessed approximately the same  $\delta^{15}\text{N}$  value range, which overlapped with some predators and scavengers. However, most of the primary consumers were less than  $13\text{‰}$  for  $\delta^{15}\text{N}$ . The suspension feeders possessed the largest range in  $\delta^{13}\text{C}$  values, whereas the surface and subsurface deposit feeders had the same  $\delta^{13}\text{C}$  values as the predators and scavengers. The predatory trophic guild possessed the highest  $\delta^{13}\text{C}$  and  $\delta^{15}\text{N}$  values, and the scavenger/omnivores possessed similar values.

When the entire stable isotope inventory was used for SEA determination, the only group that occupied a distinct isospace was the end-members guild (Figure 2). The end-members guild also occupied the smallest area of isospace (Table 1). The five remaining consumer guilds' SEAs overlapped each other to some extent. The predator guild, which should contain the highest trophic level organisms, did not overlap with surface deposit feeders and only overlapped  $0.03\text{‰}^2$  with suspension feeders, both of which likely contain primary consumers (Table 2). The predator SEA overlapped 87% of the scavenger/omnivore guild occupying the same  $5.8\text{‰}^2$ . Likewise, the surface and subsurface deposit feeders overlapped 60 and 66% of their SEAs, respectively, in  $4.9\text{‰}^2$  of isospace. The suspension feeding guild, despite employing different morphological adaptations to obtain food sources, overlapped with both the surface and subsurface guilds occupying 22 and 42% of the same isospace, respectively. Since there was significant SEA overlap between surface and subsurface deposit feeders, they were combined into one deposit feeder guild for species-level analysis. Likewise, a single predator/scavenger guild was used for subsequent species-level analysis since the scavenger/omnivore guild's SEA was almost completely enveloped by the predator SEA.

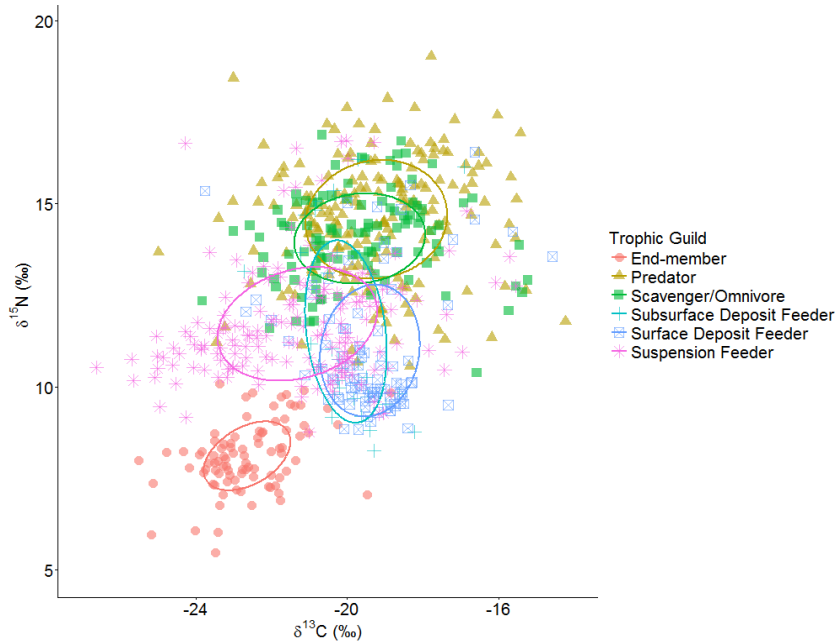




**Figure 1.** Jitterplot projecting the distribution of  $\delta^{13}\text{C}$  and  $\delta^{15}\text{N}$  values for six trophic guilds.

**Table 1.** Statistics describing the SEAs for the Hanna Shoal food web. Units are ‰<sup>2</sup>.

Trophic Descriptor	mean	sd	mode	l095	hi95
endmember	3.078511	0.3279278	3.004983	2.460901	3.734272
predator	9.528063	0.7031594	9.432000	8.190444	10.920639
scavenger/omnivore	6.687527	0.6468731	6.618219	5.466322	7.971526
subsurface deposit	8.244242	1.5949100	7.565260	5.417682	11.416476
surface deposit	7.431061	0.7803321	7.319028	5.960033	8.990599
suspension	10.032027	0.7862824	9.902134	8.539700	11.593609



**Figure 2.**  $\delta^{13}\text{C}:\delta^{15}\text{N}$  biplot for all organisms analyzed for stable isotopes. Color and shape denotes trophic guild membership. Solid lines correspond to the standard ellipse for each trophic guild and are color-coded respectively.

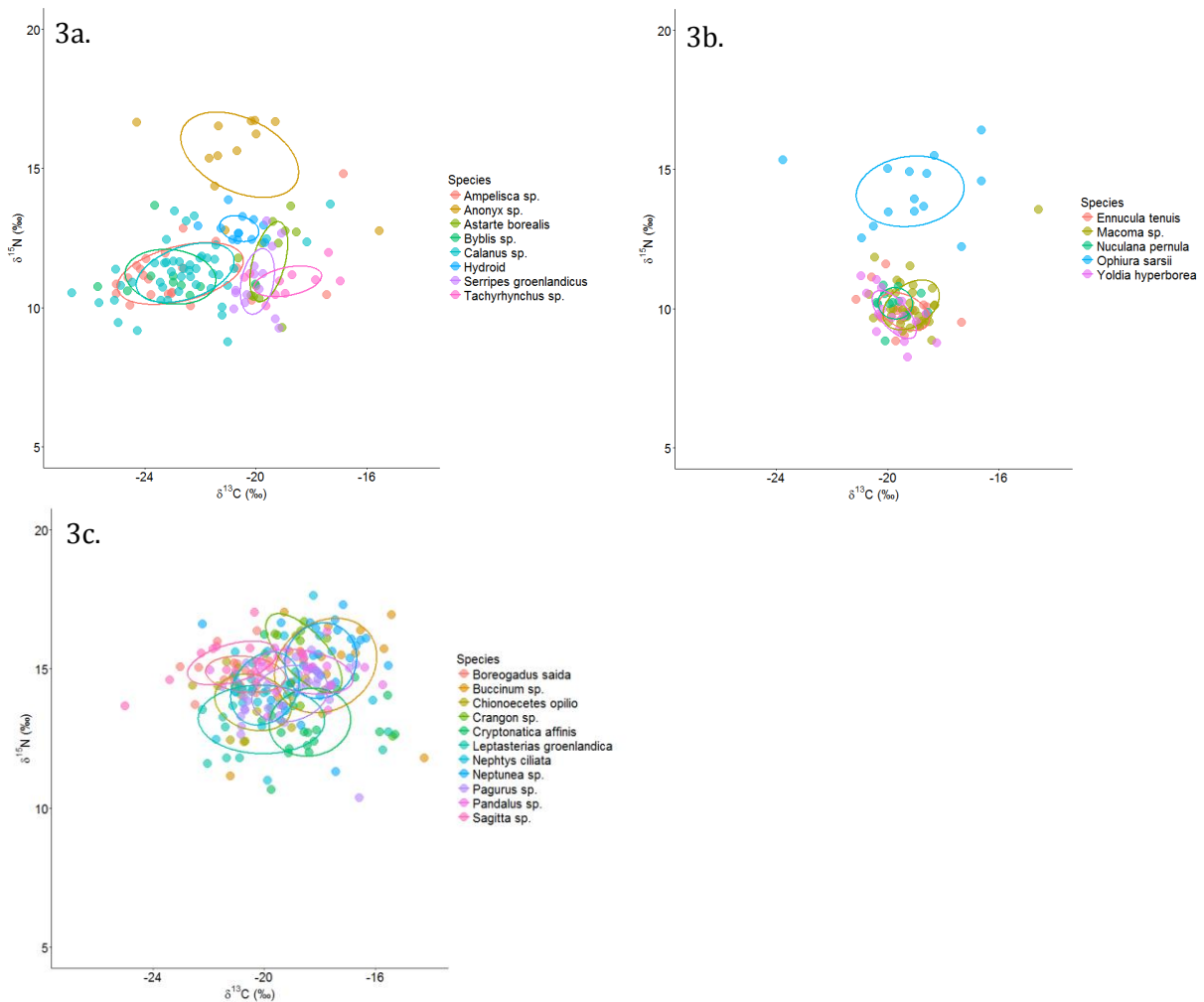
**Table 2.** Overlapped area of trophic guild SEAs. Overlap refers to area ( $\%^2$ ) that g1 overlaps with g2. Area 1 and Area 2 respectively correspond with g1 and g2.

g1	g2	overlap	area1	area2
endmember	predator	0.00000	3.0694	9.52774
endmember	scavenger/omnivore	0.00000	3.0694	6.69186
endmember	subsurface deposit	0.00000	3.0694	8.24852
endmember	surface deposit	0.00000	3.0694	7.42932
endmember	suspension	0.00000	3.0694	10.02960
predator	scavenger/omnivore	5.78723	9.5277	6.69186
predator	subsurface deposit	0.90194	9.5277	8.24852
predator	surface deposit	0.00000	9.5277	7.42932
predator	suspension	0.03248	9.5277	10.02960
scavenger/omnivore	subsurface deposit	1.34934	6.6918	8.24852
scavenger/omnivore	surface deposit	0.00000	6.6918	7.42932
scavenger/omnivore	suspension	0.36916	6.6918	10.02960
subsurface deposit	surface deposit	4.92006	8.2485	7.42932
subsurface deposit	suspension	4.17112	8.2485	10.02960
surface deposit	suspension	2.17196	7.4293	10.02960

### 3.2 Standard ellipse areas (SEAs) for species

Species that were analyzed in sufficient replication of  $n > 9$  were analyzed individually for their SEAs and grouped by feeding guild (Figure 3a-c). Among the suspension feeders that met this qualification, the amphipod *Anonyx* sp. and hydroids occupied distinct SEAs from other suspension feeders (Figure 3a). *Anonyx* sp. had a relatively wide  $\delta^{13}\text{C}$  and  $\delta^{15}\text{N}$  range, but its SEA was separate from other suspension feeders because of its enriched  $\delta^{15}\text{N}$  values. Hydroids'

SEA did not overlap with other suspension feeders and coincidentally had the smallest SEA<sub>c</sub> (SEA corrected for sample size) of all individuals analyzed of 1.0‰<sup>2</sup> (Table 3). Two suspension feeding amphipods *Ampelisca* sp. and *Byblis* sp. had overlapping SEAs with the copepod *Calanus* sp. The bivalves *Astarte borealis* and *Serripes groenlandicus* and the gastropod *Tachyrhynchus* sp. had SEAs in distinct isospace from the other suspension feeders. These three occupied isospace slightly more enriched in  $\delta^{13}\text{C}$  values but within the same  $\delta^{15}\text{N}$  range as Hydroids, *Ampelisca* sp., *Byblis* sp., and *Calanus* sp.



**Figure 3.**  $\delta^{13}\text{C}:\delta^{15}\text{N}$  biplot for species in the suspension feeder guild (a), deposit feeder guild (b), and predator/scavenger guild (c). Solid lines correspond to the standard ellipse for each trophic guild and are color-coded, respectively, per plot. Axes represent the same range in each plot.

Of the five deposit feeders whose SEAs were calculated, the brittle star *Ophiura sarsii* did not overlap with the others (Figure 3b). *O. sarsii* occupied a wide range of  $\delta^{13}\text{C}$  and  $\delta^{15}\text{N}$  values spanning from -23.8 to -16.6‰ and 12.2 to 16.4‰, respectively. While its SEA possessed similar values to the other deposit feeders, it was more  $^{15}\text{N}$ -enriched. The four other deposit feeders were all bivalves (*Ennucula tenuis*, *Macoma* sp., *Nuculana pernula* and *Yoldia*

*hyperborea*) and occupied essentially the same isospace as each other. They ranked second, third, fourth, and seventh smallest in SEAc area of the 24 consumers analyzed (Table 3).

The predator/scavenger guild contained mostly overlapping SEAs, although individuals ranged in  $\delta^{13}\text{C}$  from -25.0 to -15.4‰ and in  $\delta^{15}\text{N}$  from 10.1 to 17.6‰ (Figure 3c). The SEAs for this trophic guild were larger than most of the suspension and deposit feeder SEAs (Table 3). The predatory gastropod *Buccinum* sp. had the largest SEAc at 9.7‰<sup>2</sup>. Other notably large predator SEAs were the sea star *Leptasterias groenlandica* (8.8‰<sup>2</sup>) and the gastropod *Cryptonatica affinis* (5.6‰<sup>2</sup>). The copepod-consuming chaetognath *Sagitta* sp. was the predator with the smallest SEAc at 3.6‰<sup>2</sup> (Table 3). Individuals *Sagitta* sp. analyzed were constrained in  $\delta^{13}\text{C}$  and  $\delta^{15}\text{N}$  values ranging from -25.0 to -18.6‰<sup>2</sup> and from 13.7 to 17.0‰<sup>2</sup>.

**Table 3.** SEAs for species analyzed by SIBER. SEAc is corrected for sample size. Units are ‰.

Species	mean	sd	mode	lo95	hi95	SEAc
<i>Ampelisca</i> sp.	7.320649	1.617603	6.777902	4.542697	10.46043	7.217958
<i>Anonyx</i> sp.	9.504246	3.012994	8.535882	4.45416	15.34294	9.368848
<i>Astarte borealis</i>	2.75174	0.90085	2.508172	1.298087	4.54408	2.707
<i>Boreogadus saida</i>	2.881943	0.684187	2.763548	1.667543	4.178012	2.904549
<i>Buccinum</i> sp.	9.584588	2.483141	8.427608	5.221714	14.33493	9.653073
<i>Byblis</i> sp.	4.905143	1.717316	4.189902	2.067429	8.082691	5.022789
<i>Calanus</i> sp.	5.427675	0.802576	5.118885	3.902647	7.003954	5.402531
<i>Chionoecetes opilio</i>	4.322761	1.267278	3.982395	2.186887	6.885726	4.339405
<i>Crangon</i> sp.	4.763678	1.697932	3.87531	2.092138	8.043492	4.513819
<i>Cryptonatica affinis</i>	5.572135	1.232471	5.133056	3.464501	8.049679	5.602551
<i>Ennucula tenuis</i>	1.799199	0.464233	1.628153	1.017675	2.695108	1.79618
Hydroid	1.004794	0.333369	0.922791	0.468288	1.664449	1.008632
<i>Leptasterias groenlandica</i>	8.706901	2.485504	7.813033	4.344013	13.44713	8.774583
<i>Macoma</i> sp.	2.643555	0.456205	2.428207	1.826198	3.515961	2.624356
<i>Nephtys ciliata</i>	4.984184	1.077982	4.71482	3.077329	7.132161	4.975064
<i>Neptunea</i> sp.	5.519179	1.095904	5.094179	3.536854	7.693729	5.507561
<i>Nuculana pernula</i>	1.086028	0.348462	0.957081	0.5226	1.780355	1.095777
<i>Ophiura sarsii</i>	7.675792	2.18154	6.898831	3.962713	12.0697	7.656551
<i>Pagurus</i> sp.	4.332493	0.762486	4.055314	2.948588	5.8499	4.325613
<i>Pandalus</i> sp.	4.233053	0.924885	3.90636	2.618647	6.032791	4.208638
Phyto 20um	2.907799	0.428677	2.8259	2.117711	3.75107	2.91602
<i>Sagitta</i> sp.	3.613231	1.027943	3.133331	1.923635	5.563335	3.560694
sediment	1.302868	0.211882	1.206324	0.915643	1.719972	1.302685
<i>Serripes groenlandicus</i>	2.151575	0.633545	1.848461	1.08707	3.415292	2.173206
<i>Tachyrhynchus</i> sp.	1.963986	0.682471	1.648578	0.87314	3.359777	1.967426
<i>Yoldia hyperborea</i>	1.717866	0.459424	1.497427	0.939354	2.605041	1.65521

### 3.3 Mixing model end-member differentiation

The *simmr* model reports its capability for discriminating between end-members [when fitting possible contributions to consumer diets] by correlating end-member probabilities of diet incorporation of consumers. A large negative correlation between end-members indicates that the model is replacing one end-member with the other when fitting possible dietary proportions of the two to a consumer. This would suggest that the model could not differentiate between the sources and reliably assign dietary proportions to consumers. Phytoplankton and SOM had high negative correlations ( $> -0.9$ ) for almost all consumers. Therefore, subsequent analyses combined phytoplankton and SOM into one source that occupies a distinct isospace (hereafter, PSOM). The three end-members analyzed in subsequent runs of the model (PSOM, ice algae, and MPB) were generally well discriminated (Table 4). In several instances, however, ice algae and PSOM were poorly differentiated due to their close proximity in isospace. Determining dietary assimilation of PSOM and ice algae is ecologically important, and for most species the distinction was clear; therefore, these end-members were not pooled. Gelman-Rubin convergence statistics were also computed to determine if the model had properly run with a suitable number of iterations. Diagnostics for each end-member were between 1.00 and 1.01, which indicate satisfactory runs since values  $> 1.1$  diagnose unsatisfactory runs (Gelman et al., 2004).

### 3.4 End-member proportions in consumers diets

The mixing model *simmr* has slightly less restrictive specification for sampling size ( $n > 4$ ) than *SIBER*, so some species that could not be analyzed for SEAs were included in the mixing model. The posterior distributions (i.e., the model outputs) of dietary proportions created by *simmr* show that suspension feeders have a high probability of incorporating more PSOM into their diets than other sources. The interquartile range (IQR), which encompasses 50% of the model's observations around the median, provides a metric for assessing the likelihoods of dietary contributions for each end-member and is used here to discuss the proportion of assimilation.

A low proportion of MPB and ice algal material was likely assimilated by *Ampelisca* sp., *Byblis* sp., or *Calanus* sp., all of which had overlapping SEAs in distinct isospace (Figure 4a-c, Figure 3a). For these species, no more than 13% of their diets consist of ice algae or MPB, while between 74% and 96% of their diets incorporate PSOM. Conversely, the molluscan suspension feeders (*Astarte borealis*, *Liocyma fluctuosa*, *Serripes groenlandicus*, and *Tachyrhynchus* sp.) likely incorporate all three end-members to some degree. In the molluscan suspension feeders, the IQR for ice algae ranged from 8 to 42%, while it was between 21 and 51% for MPB, and from 31 to 63% for PSOM.

The proportions of endmembers incorporated in the diet of the holothuroidean *Ocnus glacialis* were poorly constrained. The mixing model shows that all end-members are likely incorporated in its diet, but the range of proportions was expansive. For example possible proportions between the 2.5% and 97.5% quantiles ranged from 4% to 67% for ice algae, and 8 to 86% for PSOM. Seven *O. glacialis* individuals from Hanna Shoal were analyzed. Five of the seven individuals had stable isotope values similar to each other with  $\delta^{13}\text{C}$  values between  $-24$  and  $-21\text{‰}$  and  $\delta^{15}\text{N}$  near  $11\text{‰}$ . However, two of the individuals analyzed had  $\delta^{13}\text{C}$  values  $\sim -16\text{‰}$  and  $\delta^{15}\text{N}$  values  $\sim 13\text{‰}$ . Here, the model assigns almost every possible combination of end-members to its diet because the range of stable isotope values for this organism spanned the range of  $\delta^{13}\text{C}$  values of

potential end-members. Some individuals reflect the isotope signature of PSOM, while others had assimilated a more  $^{13}\text{C}$ - and  $^{15}\text{N}$ -enriched source like ice algae.

**Table 4.** End-member discrimination correlations reported by the mixing model as its effectiveness to discern differences in end-member contribution for consumers. High negative correlations indicate poor discrimination (highlighted). For the column labeled Trophic, susp = suspension feeder, depo = deposit feeder, and pred = predator/scavenger. Group indicates position on x-axis in Figure 4.

Trophic	Group	Ice Algae~MPB	Ice.Algae~Phyto	MPB~Phyto
susp	1	0.09	-0.75	-0.75
susp	2	-0.71	-0.85	0.24
susp	3	0.18	-0.74	-0.8
susp	4	0.06	-0.84	-0.61
susp	5	-0.46	-0.67	-0.36
susp	6	-0.12	-0.73	-0.59
susp	7	-0.58	-0.76	-0.09
susp	8	-0.33	-0.68	-0.46
depo	1	-0.52	-0.92	0.13
depo	2	0	-0.97	-0.22
depo	3	-0.54	-0.63	-0.31
depo	4	-0.73	-0.64	0.01
depo	5	-0.54	-0.65	-0.28
depo	6	-0.67	-0.68	-0.07
depo	7	-0.56	-0.67	-0.25
depo	8	-0.82	-0.83	0.35
depo	9	0.01	-0.87	-0.45
depo	10	-0.61	-0.74	0.02
pred	1	0.001	-0.85	-0.54
pred	2	0.001	-0.69	-0.69
pred	3	-0.43	-0.57	-0.49
pred	4	-0.46	-0.55	-0.49
pred	5	0.07	-0.72	-0.74
pred	6	0.001	-0.68	-0.74
pred	7	-0.09	-0.80	-0.52
pred	8	0	-0.64	-0.76
pred	9	-0.30	-0.65	-0.53
pred	10	-0.28	-0.45	-0.73
pred	11	-0.44	-0.73	-0.29
pred	12	0	-0.79	-0.64
pred	13	0.16	-0.92	-0.54

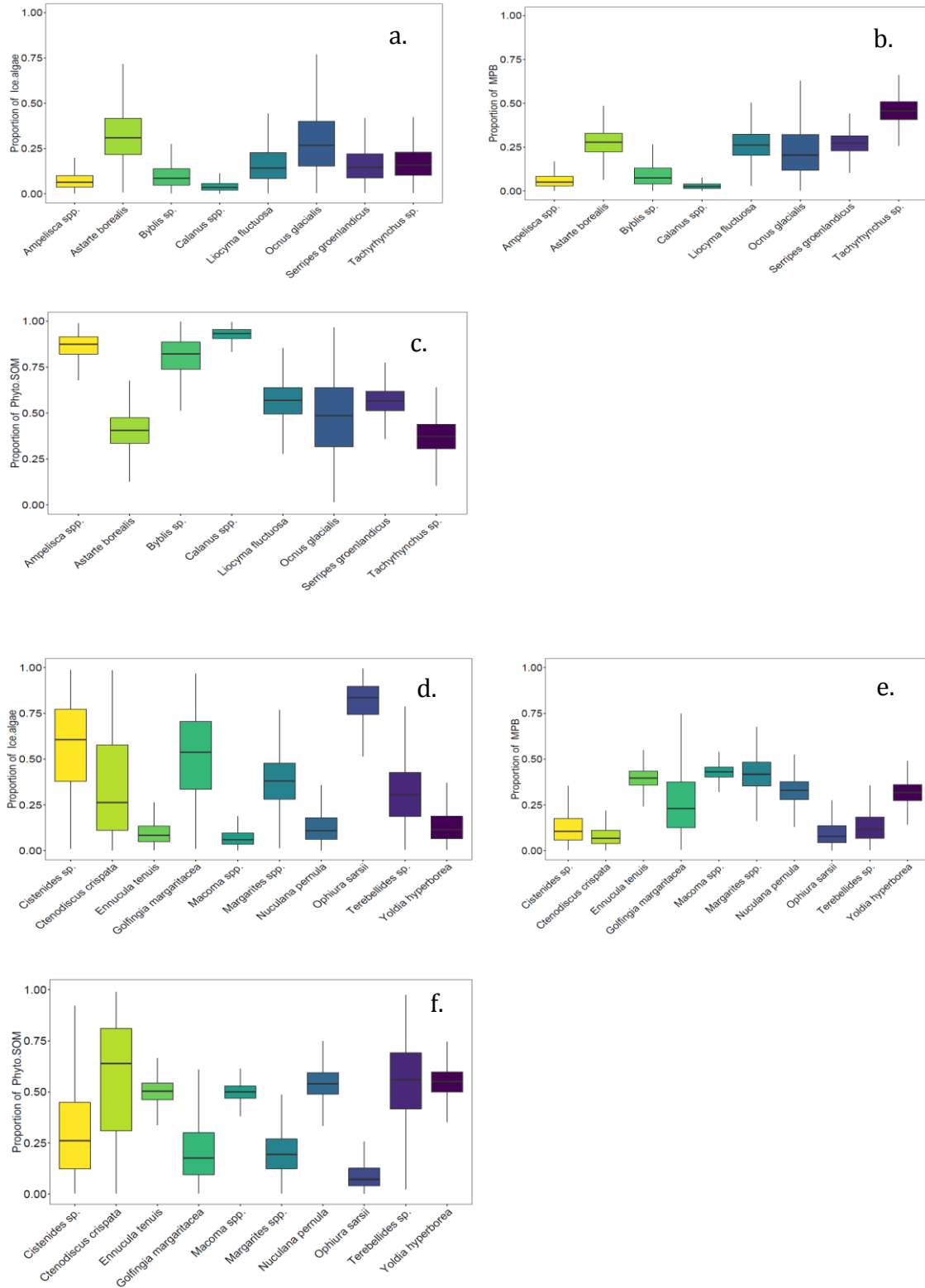
The deposit feeding bivalves *Ennucula tenuis*, *Macoma* spp., *Nuculana pernula*, and *Yoldia hyperborea* had similar dietary proportions just as their SEAs were overlapping (Figure 4d-f). The bivalves had low proportions of ice algae in their diets (<19%), but relatively equal proportions of MPB and PSOM (up to 45 and 60%, respectively). *O. sarsii* was shown to have 74 to 90% of its diet consisting of ice algae. Like *O. glacialis*, the range of stable isotope values was wide for the sipunculid *Golfingia margaritacea* (-20.9 to -15.6‰ for  $\delta^{13}\text{C}$  and 11.1 to 14.2‰ for  $\delta^{15}\text{N}$ ) providing many combinations of dietary proportions in the model output. For the polychaetes *Cistenides* sp. and *Terebellides* sp. and the seastar *Ctenodiscus crispatus*, MPB was a low proportion of their diets (<19%). These organisms had notably large negative correlations in their end-member correlations for PSOM and ice algae dietary incorporation; thus, proportions of those two sources could not be effectively differentiated by the mixing model. For this reason, their wide dietary proportions of PSOM and ice algae for these three species were likely an artefact of the model.

While the predator/scavenger guild does not directly consume end-members, their stable isotope ratios can be used to assess their ultimate organic matter sources using different TEFs than the suspension and deposit feeder guilds. The majority of species analyzed in the predator/scavenger guild were highly connected to PSOM as their ultimate organic matter sources (Figure 4g-i). Two species that stand out from this trend are the predatory gastropods *Cryptonatica affinis* and *Euspira* sp. The IQR for their dietary contribution from MPB was 35 to 44% and 31 to 49%, respectively. Ice algae was a low proportion for all analyzed predator/scavenger diets.

## 4. Discussion

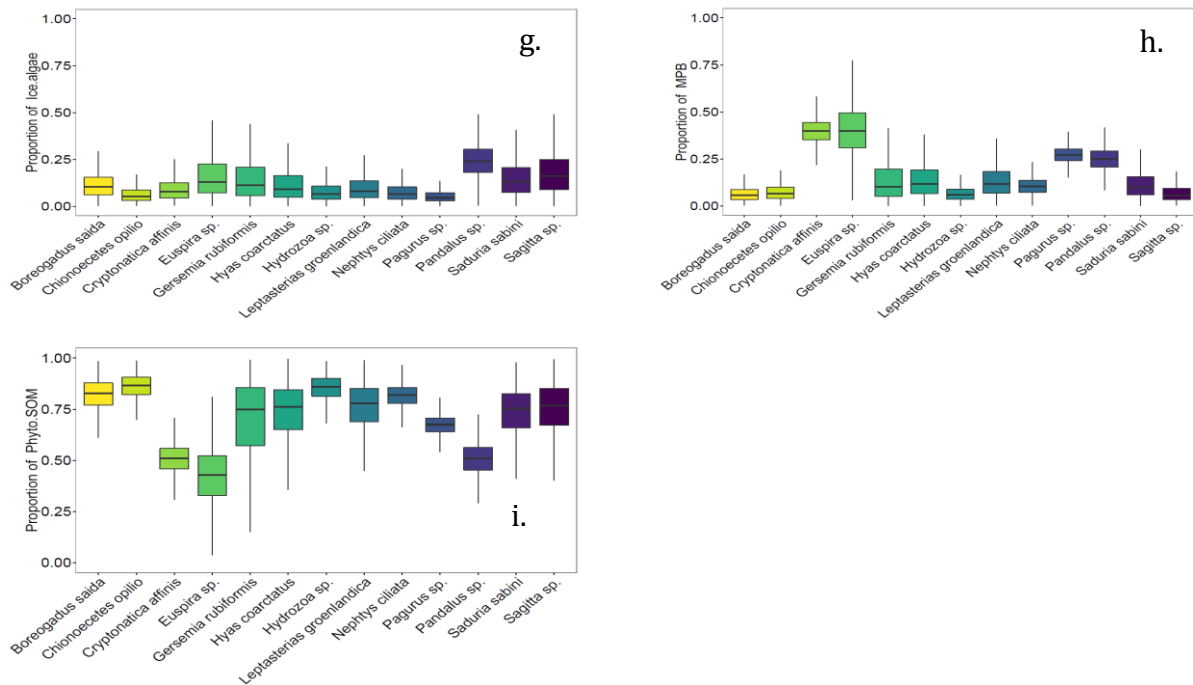
### 4.1 Connecting multiple end-members to the food web

Many reports exist of consumers from the Arctic seas exhibiting  $\delta^{13}\text{C}$  values >4‰ more enriched than the available end-members (Lovvorn et al., 2005, McTigue and Dunton, 2014; Tu et al., 2015; Divine et al., 2015; Iken et al., 2010; McConaughy and McRoy, 1979), and this study is no exception. The most common explanation of this recurring trend is that consumers are not directly assimilating the end-members isolated and measured during sampling, but instead are assimilating organic matter that is microbially degraded and, therefore,  $^{13}\text{C}$ -enriched. Lovvorn et al. (2005) provide compelling discussion of this topic, while North et al. (2014) show significant portions of bacterial fatty acids in deposit feeder tissues. McTigue et al. (2015) show significant trends between  $^{13}\text{C}$ -enriched consumers and organic matter degradation biomarkers (pheopigments). This hypothesis remains viable by these cases of ancillary evidence, although it has proven difficult to demonstrably isolate  $^{13}\text{C}$ -enriched bacteria or bacterial by-products from sediment. In this study, we don't dismiss or refute this notion, but rather supplement it by testing whether an end-member in the isospace we have defined as MPB is assimilated into the food web.



**Figure 4.1.** Boxplots of the distribution of possible dietary contributions for consumers in the suspension feeder guild (a-c), and deposit feeder guild (d-f.). Figure continues on next page (Figure 4.2).





**Figure 4.2** Boxplots of the distribution of possible dietary contributions for consumers in the predator/scavenger guild (g-i). Outliers were omitted for clarity. Contributions are represented as proportions (0-1). The whiskers extend to the 95% credible interval. The three end-members used in the mixing model were ice algae (a, d, g), MPB (b, e, h), and phytoplankton/SOM (c, f, i).

In addition to microbially-degraded OM, benthic microalgae, which typically have enriched  $\delta^{13}\text{C}$  values (France et al., 1995; Doi et al., 2010; Dubois et al., 2007; Cloern et al., 2002) might represent another food web end-member assimilated by the Hanna Shoal food web, especially given high chlorophyll *a*:pheopigment ratios and high chlorophyll *a* concentrations in surface sediments in the Chukchi Sea (McTigue et al., 2015, Pirtle-Levy et al., 2009). Although we did not isolate MPB for stable isotope analysis, nor is there any non-modeled value in the literature of Arctic benthic microalgae stable isotopes to our knowledge (e.g., Oxtoby et al., 2015), we can only posit this as another hypothesis to explain the  $^{13}\text{C}$ -enriched values of consumers. It is possible that if viable benthic microalgae do exist in the Arctic sediments but have a slow growth rate since only limited PAR reaches the sediments, then they may discriminate against  $^{13}\text{C}$  and have a more  $^{13}\text{C}$ -depleted value than the literature values of temperate MPB we use as our end-member (Rau et al., 1996, Oxtoby et al. 2015). Regardless, it is important to emphasize that many benthic fauna are  $^{13}\text{C}$ -enriched, which can be explained by one of two possibilities: either some Arctic fauna exhibit trophic enrichment factors (TEFs) for  $\delta^{13}\text{C}$  that are much larger than the median and mode values reported in the literature, or a  $^{13}\text{C}$ -enriched end-member exists in the Arctic sediments and is preferentially consumed and assimilated by benthic fauna (as discussed in Lovvorn et al., 2005, North et al., 2014, and McTigue and Dunton, 2014). In the present study, we show compelling evidence that suspension feeders and deposit feeders incorporate a  $^{13}\text{C}$ -enriched end-member (what we termed MPB) as at least 50% of their diet, and that  $^{13}\text{C}$ -enriched carbon is transferred into higher trophic levels (Figure 4).

Ice algae is cited as a  $^{13}\text{C}$ -enriched microalgae source available to Arctic benthic food webs (Hobson et al. 2002), but it can have a wide  $\delta^{13}\text{C}$  range from -25 to -14 ‰ (Tremblay et al. 2006; Gradinger, 2009). The stable carbon isotope values of ice algae can change throughout a season, especially due to health of the cells (Søreide et al., 2006). In the present study, ice algae from sea ice that was retained in the Hanna Shoal late into the season was collected and analyzed. Interestingly, the ice algae was more  $^{13}\text{C}$ -enriched than phytoplankton and SOM, but it was also  $^{15}\text{N}$ -enriched comparatively ( $\delta^{13}\text{C} = -20.4$  to  $-18.9\text{‰}$ ;  $\text{d}15\text{N} = 9.4$  to  $9.9$ ). The high values of ice algae  $\delta^{15}\text{N}$  effectively precluded ice algae as a possible contributor to the diets of the  $^{15}\text{N}$ -depleted lower trophic consumers, particularly the bivalves that were  $^{13}\text{C}$ -enriched whose  $\delta^{15}\text{N}$  values are  $\sim 10\text{‰}$ . Therefore, these consumers must have assimilated a  $^{13}\text{C}$ -enriched end-member that was not ice algae.

Ice algae and PSOM were still important end-members to the food web. *Ophiura sarsii* was the organism we analyzed that likely relied most on ice algae. This mobile consumer might take advantage of finding freshly deposited ice algae, whereas the sessile consumers can only assimilate the ice algae deposited to them (North et al., 2014). Ice algal carbon was also important to *Cistenides*, *Ctenodiscus*, *Golfingia*, *Margarites*, and *Terebellides*. The suspension feeders, particularly *Ampelisca*, *Byblis*, and *Calanus*, had a high proportion of their diet sourced to PSOM. Most of the higher trophic level organisms were traced back to PSOM as their ultimate organic matter sources, which suggests that they were preying on consumers of PSOM like *Ampelisca*, *Byblis*, *Calanus*, *Liocyma*, and *Serripes* (Figure 4).

## 4.2 Trophic Redundancy in the Hanna Shoal food web

Using standard ellipse isospace as a long-term integrator of a consumer's trophic habit provided a quantifiable means to assess trophic redundancy and plasticity in the Hanna Shoal ecosystem. The food web showed marked trophic redundancy where certain feeding guilds' standard ellipses overlapped in isospace. Predators and scavenging omnivores occupied similar isospace, which indicated trophic redundancy between the groups. There was a 0.998 probability that the predators' SEA was larger than the omnivore/scavengers' SEA, but their  $\delta^{13}\text{C}$  and  $\delta^{15}\text{N}$  ranges were quite similar (Table 5, Figure 1). Therefore, both groups obtained nutrition from the same wide range of sources, but the scavengers were more densely aggregated in isospace subsequently reducing the size of their standard ellipse, whereas predators were more distributed in isospace.

Likewise, the surface and subsurface deposit feeders were largely overlapping in isospace. Despite feeding on separate sediment horizons, surface and subsurface deposit feeders are often indecipherable in stable isotope values (North et al., 2014; McTigue and Dunton, 2014). This implies that bioturbation mixes the organic matter from surface layers down to depths of subsurface feeders. North et al. (2014) compared the stable isotope values and fatty acid profiles of the subsurface deposit feeder *Cistenides* (formerly *Pectinaria*) to the surface deposit feeders *Ophiura*, *Macoma*, *Ennucula*, and *Nuculana* in the Bering Sea throughout the major seasonal microalgal bloom. They found that *Cistenides* was isotopically similar and had similar gut contents to surface deposit feeders from the same site. Additionally, deposit feeders did not change markedly in stable isotope values from pre-bloom to post-bloom despite the end-members (ice algae and suspended particulate organic matter) changing in both  $\delta^{13}\text{C}$  and  $\delta^{15}\text{N}$  through the bloom cycle. They reason that the sediments are repositories for organic matter (Mincks et al., 2005; McTigue et al., 2015) and that these deposit feeders select and assimilate a consistent labile fraction of OM from the sediments that is  $^{13}\text{C}$ -enriched to the fresher end-

members. In our study, *Cistenides* ranged in individual  $\delta^{13}\text{C}$  values from -22.7 to -16.9‰. For *Cistenides*, the mixing model could not parse out the potential diet contribution between the  $^{13}\text{C}$ -enriched signal of ice algae from the  $^{13}\text{C}$ -depleted value of PSOM due to the wide range of consumer stable isotope values. Since individuals spanned the same isotopic range as the potential end-members, every combination of ice algae and PSOM assimilation was possible. Therefore, despite a wide range of possible solutions, the modelling effort was successful in fitting the data. *Cistenides* was a consumer that exhibited profound trophic plasticity in that its  $\delta^{13}\text{C}$  range was ~6‰. Other consumers that exhibit relatively high trophic plasticity based on their range of  $\delta^{13}\text{C}$  values were *Ocnus glacialis* (-24.1 to -15.7‰), *Ophiura sarsii* (-23.7 to -16.6‰), *Buccinum* sp. (-21.2 to -15.4‰), *Chionoecetes opilio* (-22.6 to -17.9‰), and *Golfingia margaritacea* (-20.9 to -15.6‰). These are compared to consumers with trophic rigidity like *Serripes groenlandicus* (-20.8 to -19.1‰), *Macoma* spp. (-20.7 to -18.3‰), *Liocyma fluctuosa* (-20.5 to -18.9‰), and the hydroids (-22.1 to -19.7‰). Trophic plasticity and rigidity directly correlate to SEA area (Table 3). Some organisms with high trophic plasticity might be indiscriminant feeders utilizing the same feeding mode (e.g., the deposit feeder *Golfingia*), whereas others might utilize different feeding modes in order to opportunistically obtain food sources (Slattery et al., 1997).

The stable isotope mixing model could be validated by post hoc investigations of known trophic connections. For example, the chaetognath *Sagitta* sp. are voracious predators on the copepods *Calanus* spp. In turn, *Calanus* spp. are suspension feeders of phytoplankton. *Sagitta* was the predator with the smallest SEA suggesting the individuals analyzed here assimilated consistently similar prey, thus exhibiting the least plasticity of the predators (Table 3). *Calanus* ranked among the highest probabilities of assimilating only PSOM (Figure 4c). That isotopic signal was reflected in the diet proportions of *Sagitta* that mostly reflecting PSOM, but not ice algae or MPB (Figure 4i). Similarly, the predators *Cryptonatica* and *Euspira* were the only two predators analyzed that had remarkable dietary contributions from MPB (Figure 4h). The  $^{13}\text{C}$ -enriched signal incorporated by the bivalves was transferred up the food web to upper trophic level consumers.

**Table 5.** Probabilities that Group 1 has a larger SEA than Group 2 from the Bayesian fitting of multiple SEAs (see Methods).

Group 1	Group 2	prop
endmember	predator	0.000000
endmember	scavenger/omnivore	0.000000
endmember	subsurface deposit feeder	0.000000
endmember	surface deposit feeder	0.000000
endmember	suspension	0.000000
predator	scavenger/omnivore	0.9982105
predator	subsurface deposit feeder	0.7886579
predator	surface deposit feeder	0.9743684
predator	suspension	0.3182105
scavenger/omnivore	subsurface deposit feeder	0.1790000
scavenger/omnivore	surface deposit feeder	0.2308158
scavenger/omnivore	suspension	0.0006053
subsurface deposit feeder	surface deposit feeder	0.6604737
subsurface deposit feeder	suspension	0.1505000
surface deposit feeder	suspension	0.0111053

## References

- Arrigo, K. R., and G. L. van Dijken. 2015. Continued increases in Arctic Ocean primary production. *Progress in Oceanography* 136:60-70.
- Batschelet, E. 1981. *Circular Statistics in Biology*. Academic Press, London.
- Bearhop, S., C. E. Adams, S. Waldron, R. A. Fuller, and H. MacLeod. 2004. Determining trophic niche width: a novel approach using stable isotope analysis. *Journal of Animal Ecology* 73:1007-1012.
- Bluhm, B. A., and R. Gradinger. 2008. Regional variability in food availability for Arctic marine mammals. *Ecological Applications* 18:S77-S96.
- Board, W. E. 2016 World Register of Marine Species A. f. h. w. m. o. a. VLIZ. doi:10.14284/170
- Brown, Z. W., K. L. Casciotti, R. S. Pickart, J. H. Swift, and K. R. Arrigo. 2015. Aspects of the marine nitrogen cycle of the Chukchi Sea shelf and Canada Basin. *Deep Sea Research Part II: Topical Studies in Oceanography* 118:73-87.
- Carroll, M. L., and J. Carroll. 2003. The Arctic Seas. Pages 127-156 in K. D. Black and G. B. Shimmield, editors. *Biogeochemistry of Marine Systems*, Oxford.
- Cloern, J. E., E. A. Canuel, and D. Harris. 2002. Stable carbon and nitrogen isotope composition of aquatic and terrestrial plants of the San Francisco Bay estuarine system. *Limnology and Oceanography* 47:713-729.
- Coffin, R. B., D. J. Velinsky, R. Devereux, W. A. Price, and L. A. Cifuentes. 1990. Stable carbon isotope analysis of nucleic-acids to trace sources of dissolved substrates used by estuarine bacteria. *Applied Environmental Microbiology* 56:2012-2020.
- DeNiro, M. J., and S. Epstein. 1978. Influence of diet on the distribution of carbon isotopes in animals. *Geochimica et Cosmochimica Acta* 42:495-506.
- DeNiro, M. J., and S. Epstein. 1981. Influence of diet on the distribution of nitrogen isotopes in animals. *Geochimica et Cosmochimica Acta* 45:341-351.
- Divine, L. M., K. Iken, and B. A. Bluhm. 2015. Regional benthic food web structure on the Alaska Beaufort Sea shelf. *Marine Ecology Progress Series* 531:15-32.
- Doi, H., E. Kikuchi, S. Shikano, and S. Takagi. 2010. Differences in nitrogen and carbon stable isotopes between planktonic and benthic microalgae. *Limnology* 11:185-192.
- Dubois, S., B. Jean-Louis, B. Bertrand, and S. Lefebvre. 2007. Isotope trophic-step fractionation of suspension-feeding species: Implications for food partitioning in coastal ecosystems. *Journal of Experimental Marine Biology and Ecology* 351:121-128.
- Dunton, K. H., J. M. Grebmeier, and J. H. Trefry. 2014. The benthic ecosystem of the northeastern Chukchi Sea: An overview of its unique biogeochemical and biological characteristics. *Deep Sea Research Part II: Topical Studies in Oceanography* 102:1-8.

- Dunton, K. H., S. V. Schonberg, and L. W. Cooper. 2012. Food Web Structure of the Alaskan Nearshore Shelf and Estuarine Lagoons of the Beaufort Sea. *Estuaries and Coasts* 35:416-435.
- Eggers, T., and T. H. Jones. 2000. You are what you eat ... or are you? *Trends in ecology & evolution* 15:265-266.
- France, R. L. 1995. Carbon-13 Enrichment in Benthic Compared to Planktonic Algae: Foodweb Implications. *Marine Ecology Progress Series* 124:307-312.
- Glud, R. N., J. Woelfel, U. Karsten, M. Kuhl, and S. Rysgaard. 2009. Benthic microalgal production in the Arctic: applied methods and status of the current database. *Botanica Marina* 52:559-571.
- Gradinger, R. 2009. Sea-ice algae: Major contributors to primary production and algal biomass in the Chukchi and Beaufort Seas during May/June 2002. *Deep Sea Research Part II: Topical Studies in Oceanography* 56:1201-1212.
- Graeve, M., G. Kattner, and D. Piepenburg. 1997. Lipids in Arctic benthos: Does the fatty acid and alcohol composition reflect feeding and trophic interactions? *Polar Biol* 18:53-61.
- Grebmeier, J., B. A. Bluhm, L. W. Cooper, S. L. Danielson, K. R. Arrigo, A. L. Blanchard, J. T. Clarke, R. H. Day, K. E. Frey, R. Gradinger, M. Kedra, B. Konar, K. J. Kuletz, S. H. Lee, J. R. Lovvorn, B. L. Norcross, and S. R. Okkonen. 2015. Ecosystem characteristics and processes facilitating persistent macrobenthic biomass hotspots and associated benthivory in the Pacific Arctic. *Progress in Oceanography* 136:92-144.
- Hansen, J. L. S., and A. B. Josefson. 2004. Ingestion by deposit-feeding macro-zoobenthos in the aphotic zone does not affect the pool of live pelagic diatoms in the sediment. *Journal of Experimental Marine Biology and Ecology* 308:59-84.
- Hardison, A. K., N. D. McTigue, W. S. Gardner, and K. H. Dunton. this issue. Arctic shelves as platforms for active biogeochemical activity: nitrogen and carbon transformations in the Chukchi Sea, AK. Bureau of Ocean Energy Management, Chukchi Sea Offshore Monitoring in Drilling Area (COMIDA): Hanna Shoal Ecosystem Study Final Report, Anchorage, AK, Bureau of Ocean Energy Management.
- Hecky, R. E., and R. H. Hesslein. 1995. Contributions of benthic algae to lake food webs as revealed by stable isotope analysis. *J N Am Benthol Soc* 14:631-653.
- Iken, K., B. Bluhm, and K. Dunton. 2010. Benthic food-web structure under differing water mass properties in the southern Chukchi Sea. *Deep Sea Research Part II: Topical Studies in Oceanography* 57:71-85.
- Jackson, A. L., R. Inger, A. C. Parnell, and S. Bearhop. 2011. Comparing isotopic niche widths among and within communities: SIBER - Stable Isotope Bayesian Ellipses in R. *The Journal of animal ecology* 80:595-602.
- Kahru, M., V. Brotas, M. Manzano-Sarabia, and B. G. Mitchell. 2011. Are phytoplankton blooms occurring earlier in the Arctic? *Global Change Biology* 17:1733-1739.
- Kang, C. K., J. B. Kim, K. S. Lee, J. B. Kim, P. Y. Lee, and J. S. Hong. 2003. Trophic importance of benthic microalgae to macrozoobenthos in coastal bay systems in Korea: dual stable C and N isotope analyses. *Marine Ecology Progress Series* 259:79-92.

- Lalande, C., J. M. Grebmeier, P. Wassmann, L. W. Cooper, M. V. Flint, and V. M. Sergeeva. 2007. Export fluxes of biogenic matter in the presence and absence of seasonal sea ice cover in the Chukchi Sea. *Continental Shelf Research* 27:2051-2065.
- Layman, C. A., D. A. Arrington, C. G. Montana, and D. M. Post. 2007. Can Stable Isotope Ratios Provide for Community-Wide Measures of Trophic Structure? *Ecology* 88:42-48.
- Lovvorn, J. R., L. W. Cooper, M. L. Brooks, C. C. De Ruyck, J. K. Bump, and J. M. Grebmeier. 2005. Organic matter pathways to zooplankton and benthos under pack ice in late winter and open water in late summer in the north-central Bering Sea. *Marine Ecology Progress Series* 291:135-150.
- Macdonald, T. A., B. J. Burd, V. I. Macdonald, and A. van Roodselaar. 2010. Taxonomic and feeding guild classification for the marine benthic macroinvertebrates of the Strait of Georgia, British Columbia. Canadian Technical Report of Fisheries and Aquatic Sciences.
- Macko, S. A., and M. Estep. 1984. Microbial alteration of stable nitrogen and carbon isotopic compositions of organic matter. *Organic Geochemistry* 6:787-790.
- Matheke, G. E. M., and R. Horner. 1974. Primary production of the benthic microalgae in the Chukchi Sea near Barrow, Alaska. *Journal of Fisheries Research Board of Canada* 31:1779-1786.
- McConnaughey, T., and C. P. McRoy. 1979. Food-web structure and the fractionation of carbon isotopes in the Bering Sea. *Marine Biology* 53:257-262.
- McMahon, K. W., W. G. Ambrose, B. J. Johnson, M. Y. Sun, G. R. Lopez, L. M. Clough, and M. L. Carroll. 2006. Benthic community response to ice algae and phytoplankton in Ny Alesund, Svalbard. *Marine Ecology Progress Series* 310:1-14.
- McTigue, N. D., P. Bucolo, Z. Liu, and K. H. Dunton. 2015. Pelagic-benthic coupling, food webs, and organic matter degradation in the Chukchi Sea: Insights from sedimentary pigments and stable carbon isotopes. *Limnology and Oceanography* 60:429-445.
- McTigue, N. D., and K. H. Dunton. 2014. Trophodynamics and organic matter assimilation pathways in the northeast Chukchi Sea, Alaska. *Deep Sea Research Part II: Topical Studies in Oceanography* 102:84-96.
- Mincks, S. L., C. R. Smith, and D. J. DeMaster. 2005. Persistence of labile organic matter and microbial biomass in Antarctic shelf sediments: evidence of a sediment 'food bank'. *Marine Ecology Progress Series* 300:3-19.
- Moran, S. B., R. P. Kelly, K. Hagstrom, J. N. Smith, J. Grebmeier, L. W. Cooper, G. F. Cota, J. J. Walsh, N. Bates, D. A. Hansell, W. Maslowski, R. P. Nelson, and S. Mulsow. 2005. Seasonal changes in POC export flux in the Chukchi Sea and implications for water column-benthic coupling in Arctic shelves. *Deep Sea Research Part II: Topical Studies in Oceanography* 52:3427-3451.
- Newsome, S. D., C. M. del Rio, S. Bearhop, and D. L. Phillips. 2007. A niche for isotopic ecology. *Frontiers in Ecology and the Environment* 5:429-436.
- North, C. A., J. R. Lovvorn, J. M. Kolts, M. L. Brooks, L. W. Cooper, and J. Grebmeier. 2014. Deposit-feeder diets in the Bering Sea: potential effects of climatic loss of sea ice-related microalgal blooms. *Ecological Applications* 24:1525-1542.

- Oxtoby, L. E., J. T. Mathis, L. W. Juranek, and M. J. Wooller. 2016. Estimating stable carbon isotope values of microphytobenthos in the Arctic for application to food web studies. *Polar Biol* 39:473-483.
- Parnell, A. C., R. Inger, S. Bearhop, and A. L. Jackson. 2010. Source partitioning using stable isotopes: coping with too much variation. *PloS one* 5:e9672.
- Parnell, A. C., D. L. Phillips, S. Bearhop, B. X. Semmens, E. J. Ward, J. W. Moore, A. L. Jackson, J. Grey, D. J. Kelly, and R. Inger. 2013. Bayesian stable isotope mixing models. *Environmetrics*:n/a-n/a.
- Pasotti, F., L. A. Saravia, M. De Troch, M. S. Tarantelli, R. Sahade, and A. Vanreusel. 2015. Benthic Trophic Interactions in an Antarctic Shallow Water Ecosystem Affected by Recent Glacier Retreat. *PLoS One* 10:e0141742.
- Phillips, D. L., R. Inger, S. Bearhop, A. L. Jackson, J. W. Moore, A. C. Parnell, B. X. Semmens, and E. J. Ward. 2014. Best practices for use of stable isotope mixing models in food-web studies. *Canadian Journal of Zoology* 92:823-835.
- Pirtle-Levy, R., J. M. Grebmeier, L. W. Cooper, and I. L. Larsen. 2009. Chlorophyll a in Arctic sediments implies long persistence of algal pigments. *Deep-Sea Res Pt II* 56:1326-1338.
- Post, D. M. 2002. Using stable isotopes to estimate trophic position: models, methods, and assumptions. *Ecology* 83:703-718.
- Rau, G. H., U. Riebesell, and D. WolfGladrow. 1996. A model of photosynthetic C-13 fractionation by marine phytoplankton based on diffusive molecular CO<sub>2</sub> uptake. *Marine Ecology Progress Series* 133:275-285.
- Saitoh, S., T. Iida, and K. Sasaoka. 2002. A description of temporal and spatial variability in the Berine Sea spring phytoplankton blooms (1997-1999) using satellite multi-sensor remote sensing. *Progress in Oceanography* 55:131-146.
- Sakshaug, E. 2004. Primary and secondary production in the Arctic seas. Pages 57-81 in R. Stein and R. W. Macdonald, editors. *Organic Carbon Cycle in the Arctic Ocean*. Springer-Verlag, Berlin, Germany.
- Slattery, M., J. B. McClintock, and S. S. Bowser. 1997. Deposit feeding: A novel mode of nutrition in the Antarctic colonial soft coral *Gersemia antarctica*. *Marine Ecology Progress Series* 149:299-304.
- Sørenseide, J. E., H. Hop, M. L. Carroll, S. Falk-Petersen, and E. N. Hegseth. 2006. Seasonal food web structures and sympagic-pelagic coupling in the European Arctic revealed by stable isotopes and a two-source food web model. *Progress in Oceanography* 71:59-87.
- Sun, M. Y., L. Clough, M. L. Carroll, J. Dai, W. G. Ambrose, Jr., and G. R. Lopez. 2009. Different responses of two common Arctic macrobenthic species (*Macoma balthica* and *Monoporeia affinis*) to phytoplankton and ice algae: Will climate change impacts be species specific? *Journal of Experimental Marine Biology and Ecology* 376:110-121.
- Tremblay, J.-É., S. Bélanger, D. G. Barber, M. Asplin, J. Martin, G. Darnis, L. Fortier, Y. Gratton, H. Link, P. Archambault, A. Sallon, C. Michel, W. J. Williams, B. Philippe, and M. Gosselin. 2011. Climate forcing multiplies biological productivity in the coastal Arctic Ocean. *Geophysical Research Letters* 38.

- Tu, K. L., A. L. Blanchard, K. Iken, and L. Horstmann-Dehn. 2015. Small-scale spatial variability in benthic food webs in the northeastern Chukchi Sea. *Marine Ecology Progress Series* 528:19-37.
- Vander Zanden, J., and J. B. Rasmussen. 2001. Variation in  $\delta^{15}\text{N}$  and  $\delta^{13}\text{C}$  trophic fractionation: Implications for aquatic food web studies. *Limnology and Oceanography* 46:2061-2066.
- Wassmann, P., and M. Reigstad. 2011. Future Arctic Ocean seasonal ice zones and implications for pelagic-benthic coupling. *Oceanography* 24:220-231.
- Weingartner, T., E. Dobbins, S. Danielson, P. Winsor, R. Potter, and H. Statscewich. 2013. Hydrographic variability over the northeastern Chukchi Sea shelf in summer-fall 2008–2010. *Continental Shelf Research* 67:5-22.
- Wulff, A., K. Iken, M. L. Quartino, A. Al-Handal, C. Wiencke, and M. N. Clayton. 2009. Biodiversity, biogeography and zonation of marine benthic micro- and macroalgae in the Arctic and Antarctic. *Bot Mar* 52:491-507.



# Distribution, Abundance, Biomass and Diversity of Benthic Infauna in the Northeastern Chukchi Sea, Alaska

Susan Schonberg , Ken Dunton

The University of Texas Marine Science Institute  
750 Channel View Dr.  
Port Aransas, TX 78373

[susan.schonberg@utexas.edu](mailto:susan.schonberg@utexas.edu), [ken.dunton@utexas.edu](mailto:ken.dunton@utexas.edu)

## Abstract

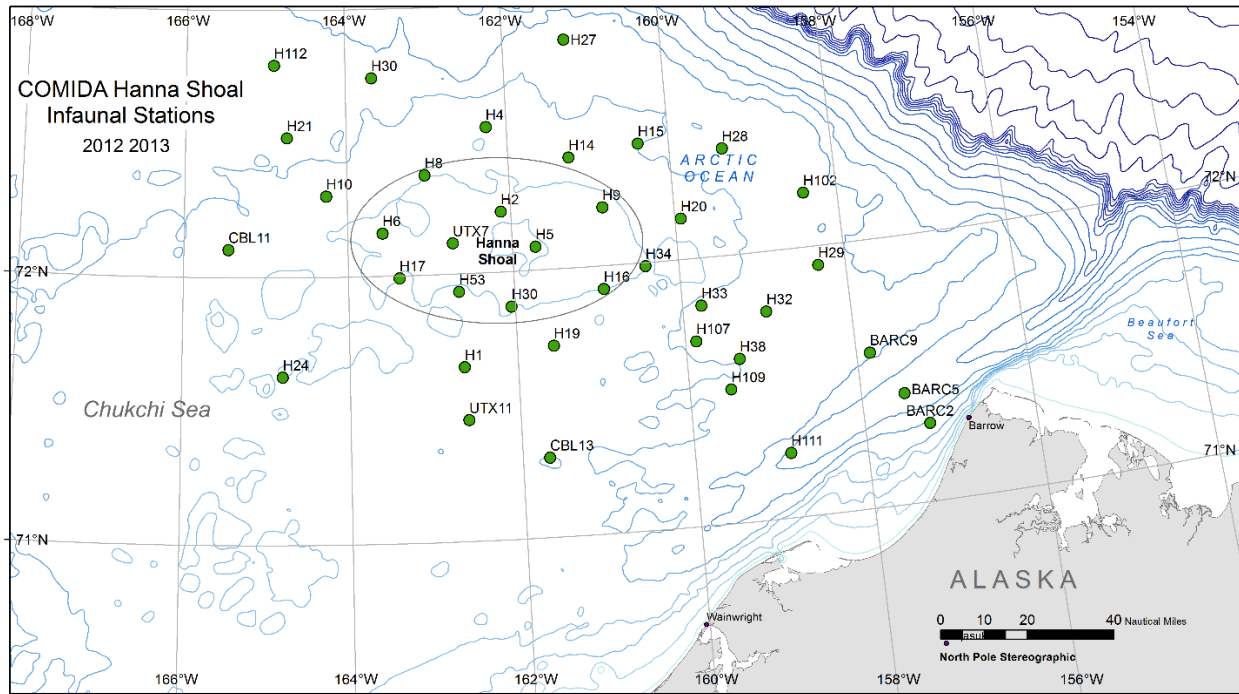
In summer 2012 and 2013, as part of the Hanna Shoal Ecosystem program, we performed a quantitative assessment of the biomass, abundance, and community structure of benthic infaunal populations of the northeastern Chukchi Sea. This analysis documented a benthic species inventory of 380 taxa collected from 85 individual van Veen grab samples ( $0.1 \text{ m}^2$ ) at 39 stations. Infaunal abundance was dominated by Polychaeta, Mollusca, and Crustacea. Percentage contribution of three infaunal groups (amphipod, polychaetes, bivalves) to total abundance and biomass revealed areas of group dominance and sparseness in distribution over the study area. The high diversity of the infauna was characterized by abundance Shannon diversity values that ranged from 3.1 to 4.6 (mean =  $3.7 \pm \text{SD } 0.36$ ). Twenty seven of the 39 stations had diversity values between 3.1 and 3.9 and 12 stations ranged between 4.0 and 4.6 (out of a maximum of 5). Pielou's evenness index values ranged from 0.89 to 0.98 (mean =  $0.94 \pm \text{SD } 0.02$ ; maximum 1) demonstrating balanced contributions from all species collected at each station. To examine the relationships between infaunal distributions of all collected taxa with the physical environment, we used a Biota and Environment matching routine. A combination of water depth, sediment chlorophyll *a* concentration and sediment C:N molar ratio, correlated closest with infaunal abundance distribution ( $\rho = 0.25$ ). Infaunal biomass distribution had a stronger prediction with water depth, percentage of sand, and C:N molar ratio producing the best fit ( $\rho = 0.45$ ). Overall, our results reveal that the northeast Chukchi Sea in the vicinity of Hanna Shoal and Barrow Canyon support a relatively high diversity of benthic infauna that is reflective of the overall high productivity of this region.

*Keywords:*

Arctic, Chukchi Sea, infauna, diversity, amphipods, bivalves, polychaetes, Hanna Shoal

## 1. Introduction

This report presents the results of the Chukchi Sea Monitoring in the Drilling Area (COMIDA) Hanna Shoal program, an extension of the multi-disciplinary COMIDA Chemical and Benthos (CAB) program funded by the Bureau of Ocean Energy Management (BOEM). Our results complement the benthic sampling performed under COMIDA CAB (Schonberg et al., 2014) with additional benthic sampling that provides a comprehensive overview of the spatial patterns and inventories of infaunal organisms. Since earlier results (sampling in summers 2009 and 2010 under COMIDA CAB) revealed that the Hanna Shoal and Barrow Canyon regions were extremely productive, a renewed focus was placed on the collection of additional samples in these areas during summers 2012 and 2013 (Figure 1). In addition to creating an inventory of



**Figure 1.** Hanna Shoal 2012 and 2013 University of Texas infaunal sampling station locations.

species occurrence, we assessed the spatial patterns of abundance, biomass and diversity of the benthic infaunal communities in the Hanna Shoal region.

## 2. Methods

### 2.1 Benthic infauna collection

Infaunal sampling was conducted during August 2012 and 2013 aboard the Coast Guard ice breaker *Healy*. Stations were selected using a probability-based computation in ArcGIS 10 to create random locations within thirty 1260 km<sup>2</sup> hexagonal tessellated grid cells (White et al., 1992) that spanned the northeast Chukchi Sea. All benthic sampling occurred within a 0.5 nautical mile (nm) radius of the predetermined site location.

Benthic infaunal invertebrates were collected from double van Veen grabs (3 grabs per station) at 19 stations in 2012 and twenty stations in 2013 (Figure 1). Use of a double van Veen grab (0.1 m<sup>2</sup>) insured that the physical and chemical properties associated with the sediments could be matched to the biological samples obtained from the companion grabs. Samples were sieved through a 1 mm mesh using a low-flow sieve table to ensure gentle handling of soft-tissue invertebrates (i.e. polychaetes) to aid in taxonomy. Soft-tissue organisms were preliminarily identified to lowest possible taxonomic level onboard the ice breaker *Healy*. All samples were preserved in 80% ethanol.

Upon arrival to The University of Texas Marine Science Institute, infaunal samples were reexamined. Taxonomic specialists were used to verify identifications of dominant groups

including crustaceans (Ken Coyle, University of Alaska, Fairbanks), molluscs (Nora Foster, Fairbanks, AK) and polychaetes (Leslie Harris, Natural History Museum of Los Angeles County). After identifications were complete, species within each grab sample were blotted and measured for wet biomass (including mollusc shells).

## 2.2 Community Structure - Species Diversity

An ecological analysis of infaunal species abundance was performed using routines available in the PRIMER v6 software package (Clarke and Gorley 2006; Primer-e 2016). The Shannon Diversity Index ( $H'$ ) and Pielou's Evenness Index ( $J'$ ) were calculated for species abundance data ( $m^{-2}$ ) using the DIVERSE routine in PRIMER (Clarke and Warwick 2001). The Shannon Diversity routine assumes that individuals are randomly sampled from a large population:

$$H' = - \sum_{i=1}^R p_i \ln p_i$$

where  $p_i$  is the proportion of individuals that belong to species  $i$  and  $R$  is richness (the number of species in the dataset). Mathematically, the Shannon diversity value has the potential to range from 0–5 but in practice it usually lies between 1.5 and 3.5 and only rarely is  $>4$  (Magurran, 2004). The higher values indicate greater species diversity.

Pielou's Evenness Index ( $J'$ ) is a measurement of the proportion of dominant species in a community. It uses the following formulas where  $H'$  is the number derived from the Shannon diversity index where  $H'_{\max}$  is the maximum value of  $H'$ , and  $S$  is the number of species.

$$J' = \frac{H'}{H'_{\max}} = - \sum_{i=1}^S \frac{1}{S} \ln \frac{1}{S} = \ln S$$

$J'$  values range from 0, indicating that species distribution is maximally uneven, to 1, if the species distribution is completely even with balanced contributions from all species collected at the station.

## 2.3 Community Structure - Environmental Variables

Environmental variables were plotted using the PRIMER v6 Principal Component Analysis (PCA) routine to determine how a set of environmental factors collected at 24 stations related to each other. Environmental variables included total water depth, bottom water temperature and salinity, sediment chlorophyll  $a$ , grain size (gravel, sand, mud), sediment total organic carbon (TOC), total organic nitrogen (TON), and carbon to nitrogen molar ratio (C:N). Sediment grain size data were provided by Jackie Grebmeier, and bottom water temperature and salinity data were collected from ship's CTD. All other analyses were performed in the laboratory at The University of Texas.

Principal component analysis (PCA) is a mathematical procedure that uses an orthogonal transformation to convert a set of possibly correlated variable values into a set of values of linearly uncorrelated variables called principal components. The first principal component (PC1, x axis) accounts for as much of the variability in the data as possible, with each succeeding component having the highest variance possible under the constraint that it be uncorrelated with the preceding components. The data were normalized prior to running the PCA function to fulfill the requirement that the data be normally distributed.

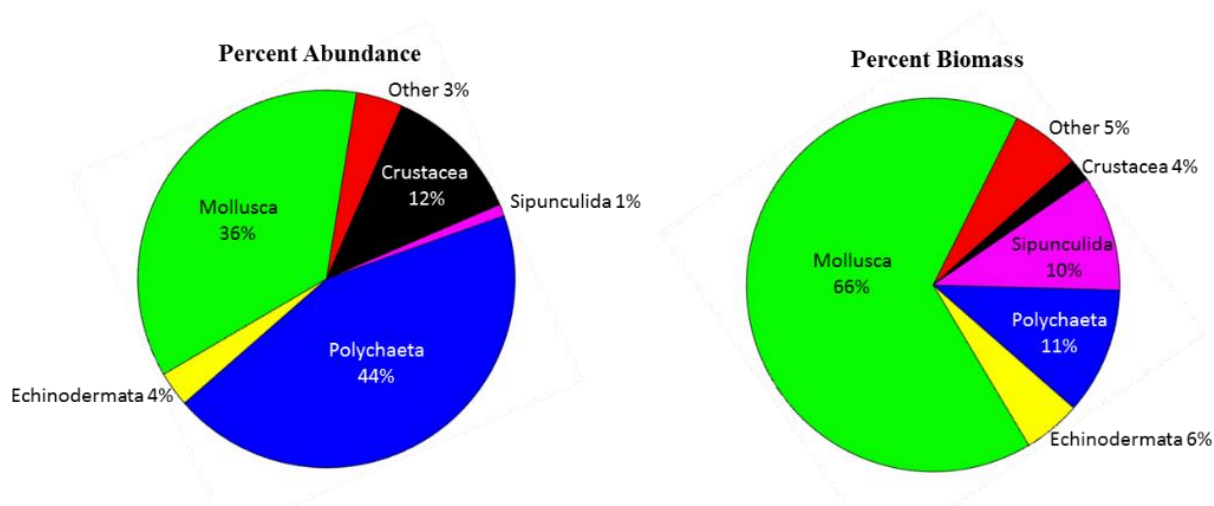
The Biota-Environmental (BIO-ENV) routine in PRIMER v6 was used to explore relationships between COMIDA Hanna Shoal species abundance and biomass and selected environmental variables (same variables as listed above for the PCA analysis). Only 12 stations from 2012 and another 12 from 2013 were included in the analyses due to lack of one or more environmental parameter for the other stations. The BIO-ENV routine calculates Spearman rank correlations between the similarity matrix derived from infaunal species abundance or biomass data and matrices derived from environmental variables that could explain the biotic structure (Clarke and Warwick, 2001). The statistical significance of the results was tested by the global BIO-ENV match permutation test whereby each set of samples was randomly permuted relative to the other. The null hypothesis was that there is no relationship between the species abundance matrix and any of the possible resemblance matrices subsets of the environmental variables. The real rank correlation coefficient was compared with the permuted null hypothesis values, and if the actual coefficient was larger than any of the permuted coefficients, then the null hypothesis was rejected with a  $p < 1\%$ . Biota abundance values were square root transformed prior to analysis to meet assumptions of normality, and environmental parameters were log-transformed and normalized prior to analysis in order to derive meaningful Euclidean distances between environmental data variables with different scales.

### 3. Results and Discussion

#### 3.1 Infauna inventory

A total of 380 taxa were identified from 85 van Veen grab samples ( $0.1 \text{ m}^{-2}$ ) collected from 39 stations in 2012 and 2013. Species occurrence by abundance included Polychaeta (44%) followed by Mollusca (36%), Crustacea (12%), Echinodermata (4%), Sipunculida (1%) and other phyla (3%). Species distribution by biomass was dominated by Mollusca (66%) followed by Polychaeta (11%), Crustacea (4%), Echinodermata (6%), Sipunculida (10%) and other phyla (5%; Figure 2). All annelid species except one oligochaete belonged to Polychaeta (160 species). The dominant mollusc groups were Gastropoda (30 species) and Bivalvia (42 species). Within the Arthropoda, Malacostraca represented the most diverse class, including 186 species of Amphipoda, nine Cumacea, and three Decapoda. The remaining taxa ('Other' in Figure 2) included Porifera, Bryozoa, Hydrozoa, Nemertea, Asterozoa, Holothurozoa, Ophiurozoa, Isopoda, Pycnogonida, Priapulida, Echinozoa, Alcyonaria, Actinaria, and Ascidiacea. COMIDA Hanna Shoal 2012 and 2013 infaunal abundance and biomass station data was combined with COMIDA CAB 2009 and 2010 and mapped using GIS ArcMap 10.3 (Figure 3). The general community structure trend for the northeast Chukchi Sea shows a concentration of organisms in the Hanna Shoal-Barrow Canyon vicinity that was initially revealed during COMIDA CAB 2009 and 2010 sampling (Schonberg et al. 2014). Feder et al. (1989) also measured elevated levels of infauna in this same general area. (Figure 3, bottom panel, large orange circles near Icy Cape). Other stations with larger biomass values reflect the presence of bivalves.

The distribution of infaunal organisms reveal the existence of dense polychaete mats associated with muddy sediments (Figure 3, top panel, three green bubbles on the northwest flanks of Barrow Canyon). Large concentrations of sand dollars (Echinoderms) inhabit sandy sediments near Icy Cape in the biomass map (bottom panel; two large orange circles).

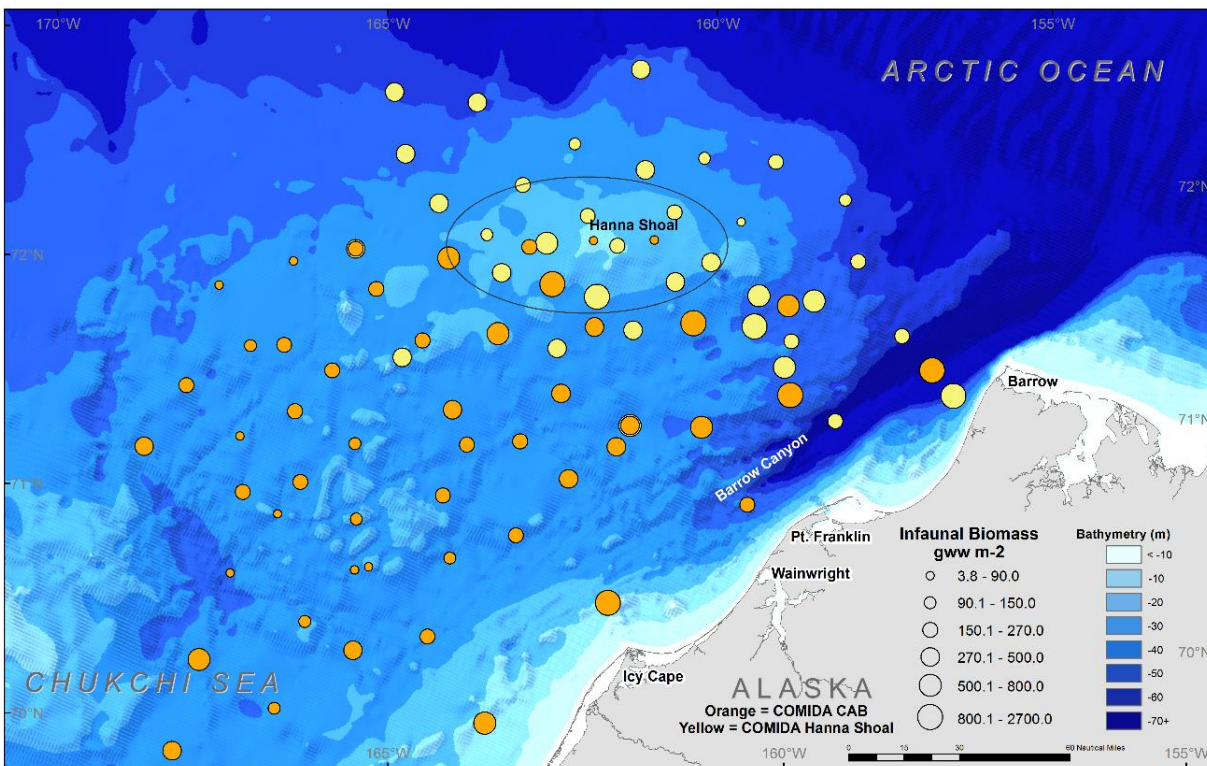
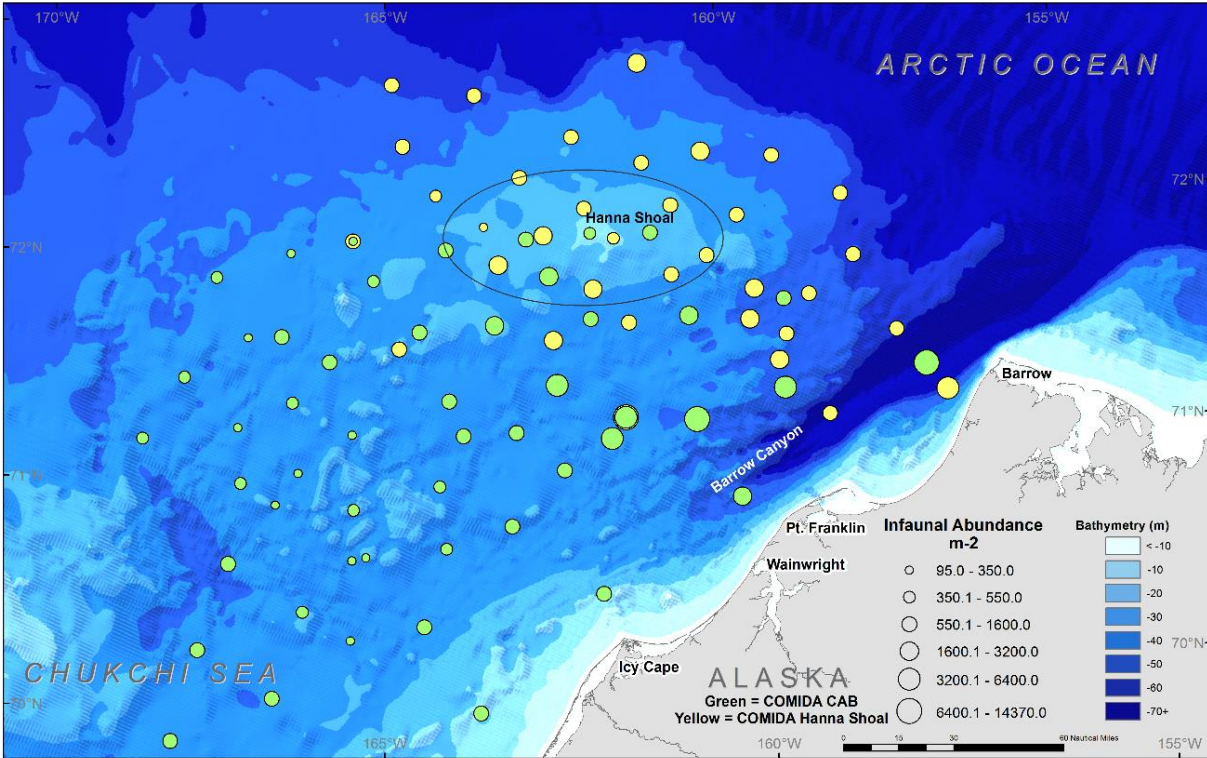


**Figure 2.** Percent abundance (top graph) and percent biomass of major phyla of infauna samples collected in the COMIDA Hanna Shoal project (2012 and 2013 combined).

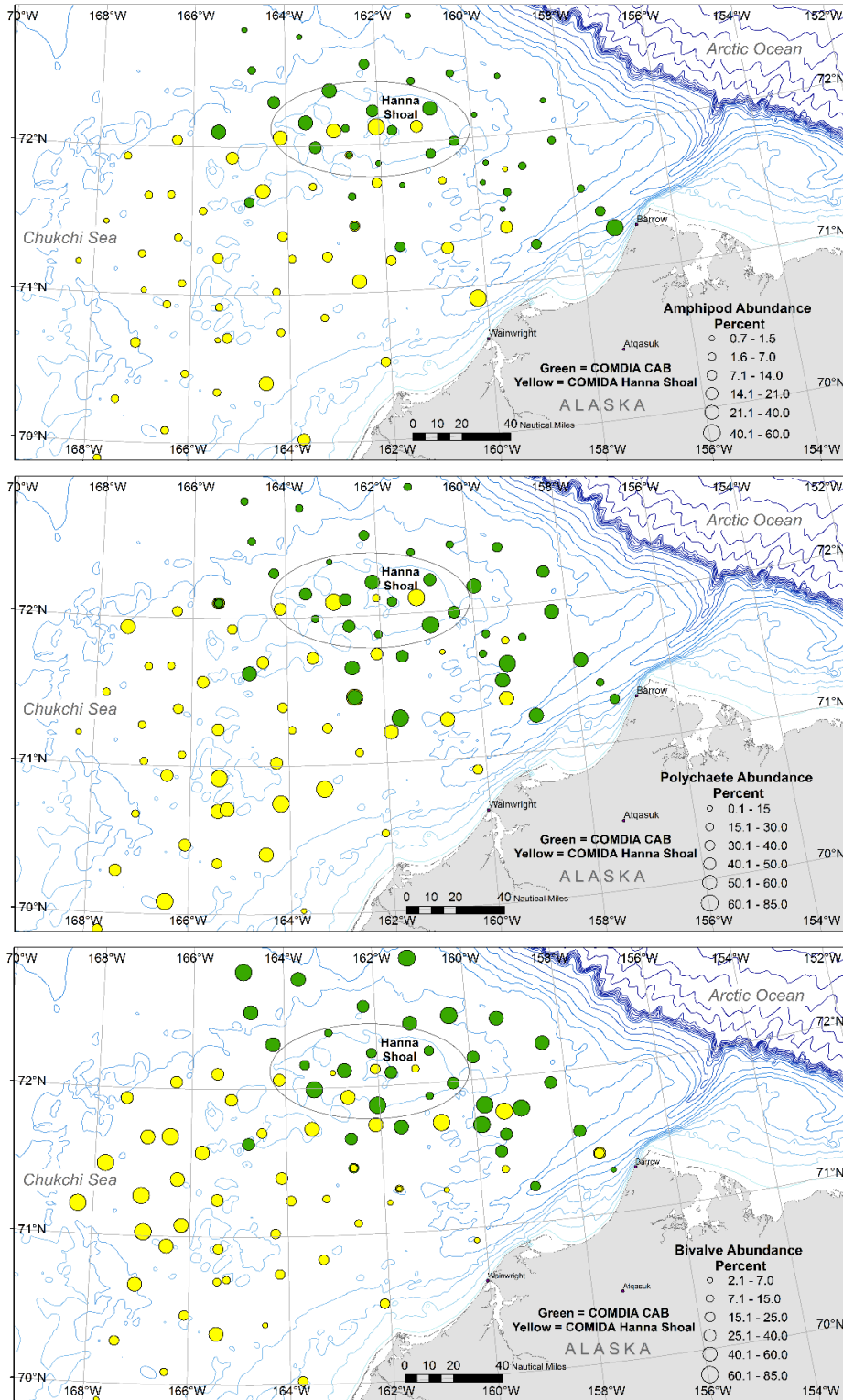
Three major infaunal groups (amphipods, polychaetes and bivalves), are most important to the Northeast Chukchi Sea area because they are widespread, can be numerous, and are an important prey source for marine mammals and birds (Grebmeier et al. 2006). To illustrate their relative importance at each station, the percentage of the total station abundance and biomass represented by each of these three groups revealed some interesting differences (Figures 4, 5). Amphipods have a higher percentage of presence on Hanna Shoal and along Barrow Canyon than in other parts of the study area. This pattern was also observed with the COMIDA CAB data (Schonberg et al., 2014). Polychaetes percentages have higher values on the southeast flank of Hanna Shoal over to a line that runs west of the Alaskan Coastal Current. Bivalve percentages are small in the region west of Wainwright to Icy Cape, but large elsewhere.

### 3.2 Infauna diversity

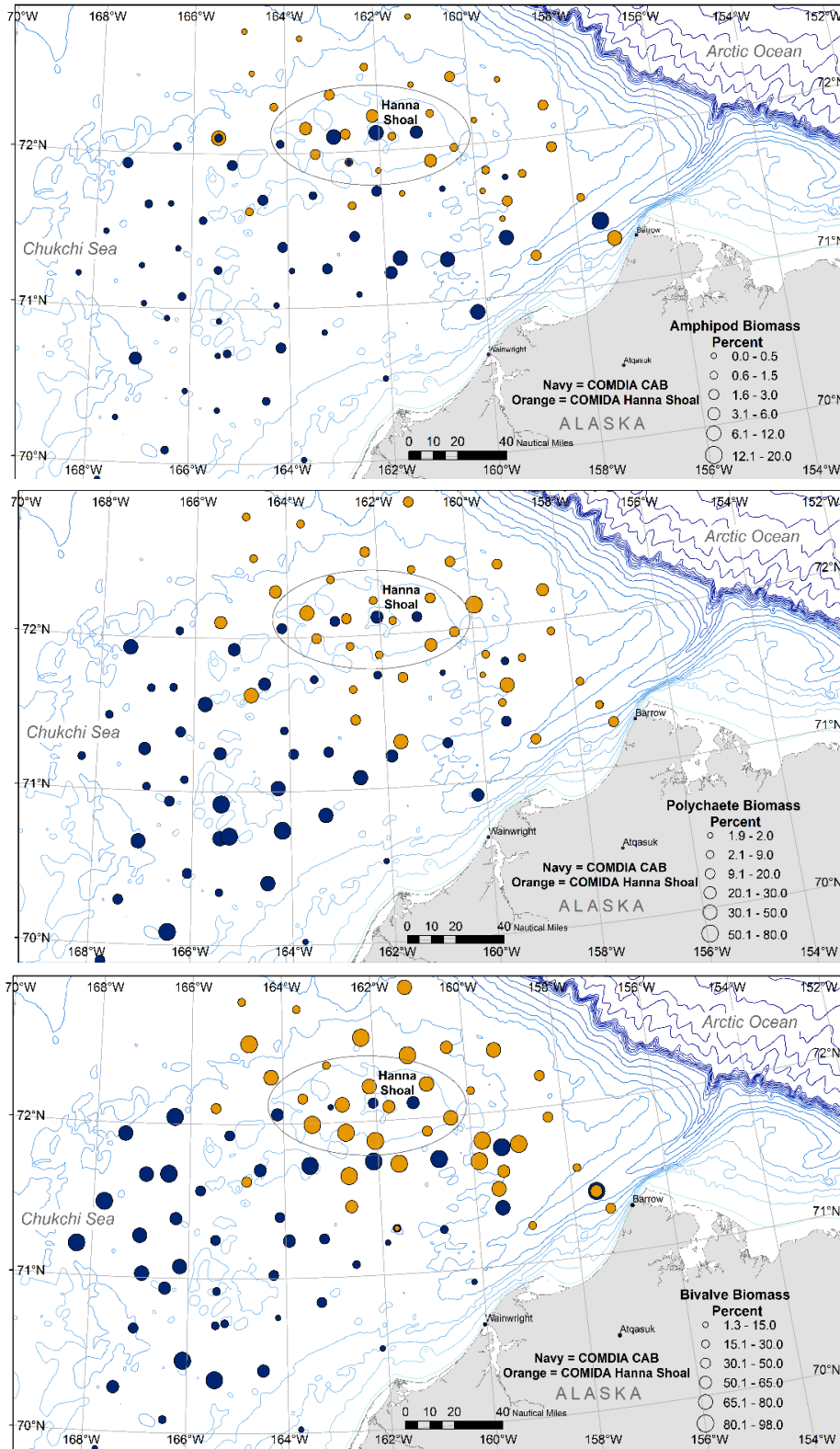
Shannon Diversity and Pielou Evenness were calculated to explore trends in infaunal community structure in the study area. Shannon index values were calculated for species abundance and biomass measurements. The abundance Shannon diversity values ranged from 3.1 to 4.6 with a mean =  $3.7 \pm \text{SD } 0.36$  (Figure 6). Twenty seven of the 39 stations had diversity values between 3.1 and 3.9 and 12 stations ranged between 4.0 and 4.6 (out of a maximum of 5) indicating that the seafloor in this study area supports an extremely diverse ecosystem. Pielou index values ranged from 0.89 to 0.98 with a mean =  $0.94 \pm \text{SD } 0.02$  signifying that the infauna is not dominated by a few or a single species. The relationships between infaunal abundance, Shannon diversity and Pielou's evenness indicated that low abundance did not necessarily correspond with low species diversity or evenness (Figure 6). For instance, some stations located within the Hanna Shoal oval graphic had low or medium abundance (top panel) but the diversity and evenness values were the opposite (middle and bottom panels). The biomass Shannon diversity values followed a similar trend to the abundance numbers. They ranged from 2.4 to 4.1 with a mean =  $3.3 \pm \text{SD } 0.38$  (Figure 7). Seven of the 39 stations had diversity values between 2.4 and 3.0, 31 stations ranged from 3.0 to 3.9 and 1 station was greater than 4.0 (4.1). Pielou index values were between 0.72 and 0.88 with a mean =  $0.83 \pm \text{SD } 0.03$ .



**Figure 3.** COMIDA CAB (2009, 2010) and COMIDA Hanna Shoal (2012, 2013) infaunal station abundance (top) and biomass (bottom) means (m<sup>-2</sup>).

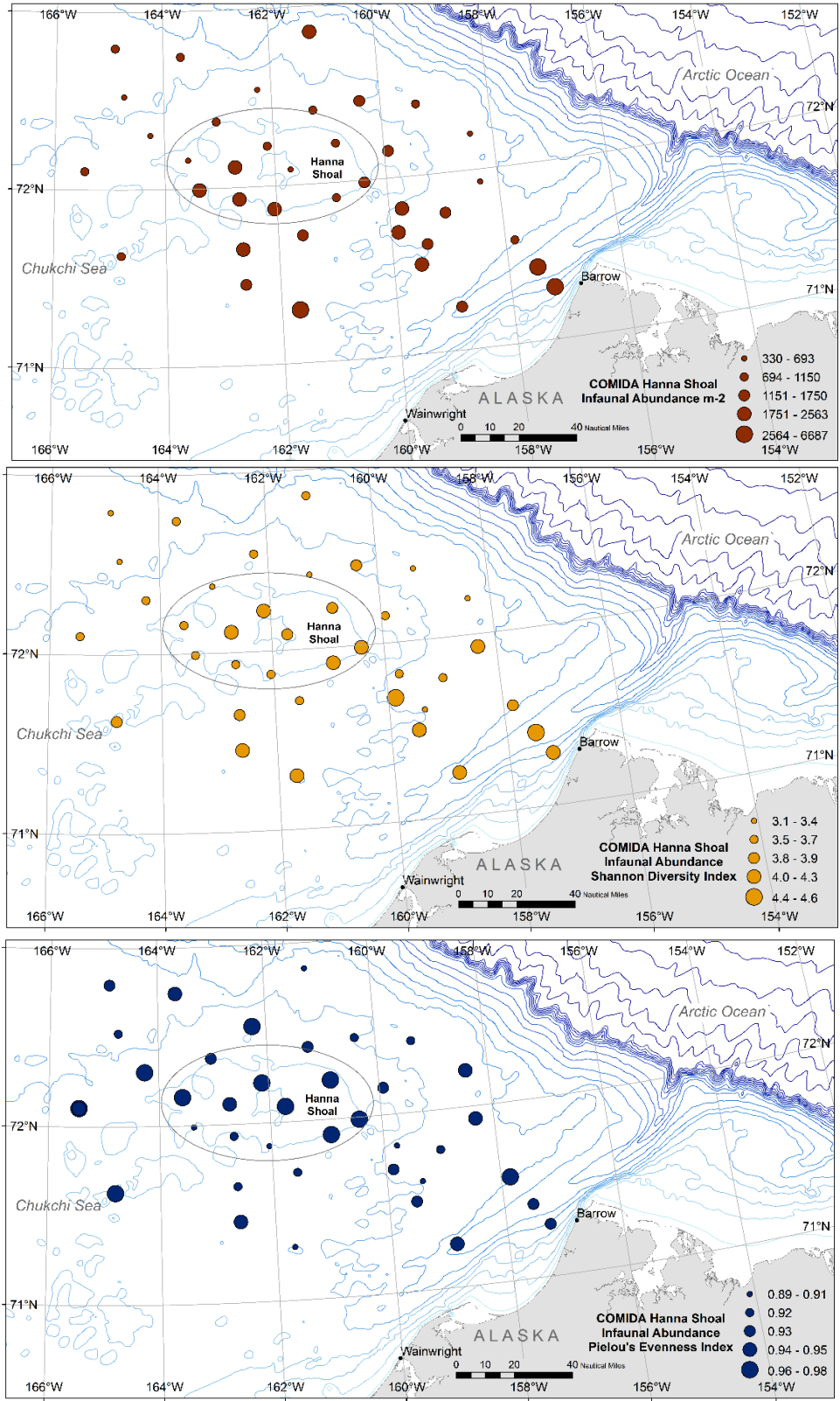


**Figure 4.** Percentage of station infaunal abundance that is composed of amphipods (top), polychaetes (middle), and bivalves (bottom).

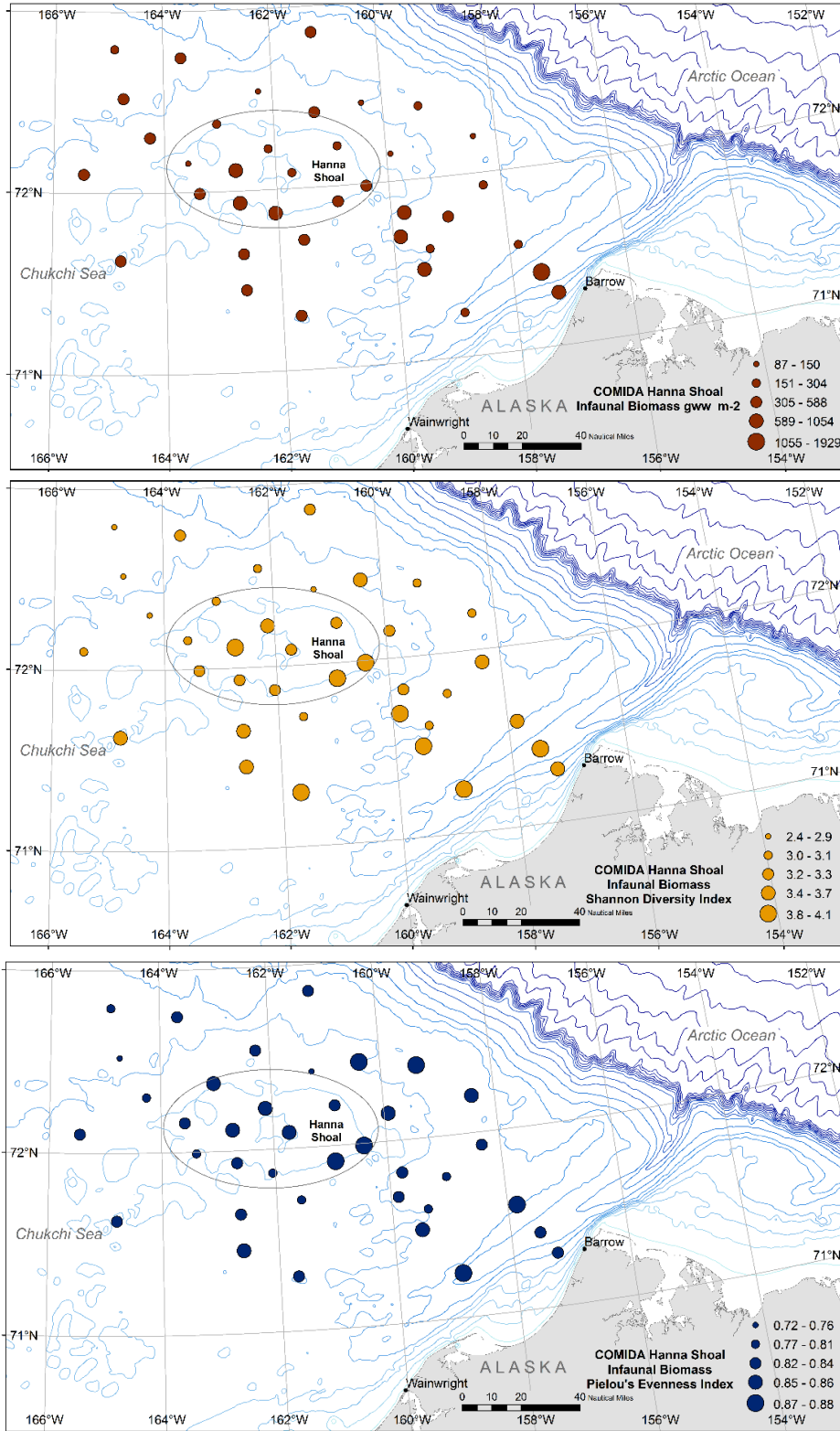


**Figure 5.** Percentage of station infaunal biomass that is composed of amphipods (top), polychaetes (middle), and bivalves (bottom).





**Figure 6.** COMIDA Hanna Shoal 2012 and 2013 infaunal abundance data. Station means (top), Simpson Diversity Index values (middle) and Pielou's Evenness Index (bottom).

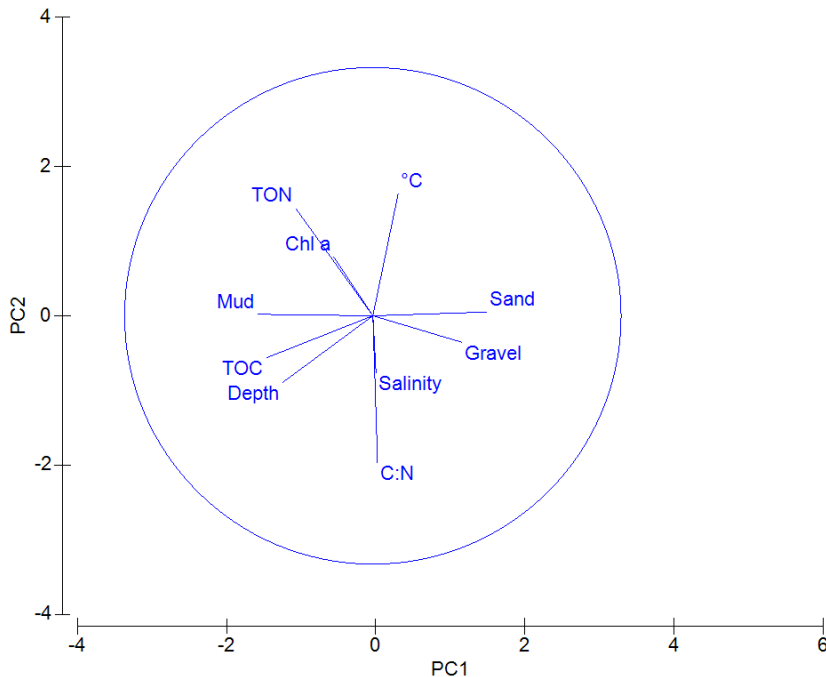


**Figure 7.** COMIDA Hanna Shoal 2012 and 2013 infaunal biomass data. Station means (top), Simpson Diversity Index values (middle), and Pielou's Evenness Index (bottom).

### 3.3 Environmental factors

#### 3.3.1 Principal Component Analysis

Environmental variables were plotted using PRIMER's Principal Components Analysis (PCA) to determine how a set environmental factors collected at 24 stations related to each other (Figure 8; Table 1). The length of the vector lines correspond with the variable influence or strength of each variable. The results on the PC1 axis show that stations with higher measurements of mud substrates (left side) have associated levels of TOC, TON, chlorophyll *a* and are in deeper water than sand and gravel areas (right side). On the PC2 axis, the opposition of temperature versus C:N and to a lesser degree salinity is shown.



**Figure 8.** A Principal Components Analysis (PCA) plot of environmental data collected at 24 stations located in the Hanna Shoal study area.

#### 3.3.2 Biota and Environment Analysis

A set of environmental variables including total water depth, bottom water temperature and salinity, sediment chlorophyll *a*, grain size (gravel, sand, mud), sediment total organic carbon (TOC), total organic nitrogen (TON), and carbon to nitrogen molar ratio (C:N) were incorporated into the Biota and Environment (BIO-ENV) matching routine in PRIMER v6 to determine which environmental factors had the strongest correlations with species abundance and biomass distribution. According to the highest Spearman correlation ( $\rho$ ) ranking, water depth, chlorophyll *a* concentrations and C:N had the most robust association (but not strong predictor value) with species abundance distributions for all collected infaunal invertebrate groups ( $\rho = 0.25$ ). Infaunal biomass distribution was most closely correlated with water depth, percentage of sand and C:N ( $\rho = 0.45$ ). Similarly, Schonberg et al. (2014) found that COMIDA CAB infauna abundance distribution was best predicted with water depth and sediment C:N ratios.

**Table 1.** Environmental data collected during the 2012 and 2013 COMIDA Hanna Shoal project and used for the Principal Component and Biota and Environment Analyses. Bottom water temperature are from the ship's CTD and all other data were processed from samples at The University of Texas. Grain size data are available from J. Grebmeier.

Date	Sta	Site	Depth m	Bottom water Temp °C	Bottom water Salinity	Chl <i>a</i> mg m- 2	TOC %	TON %	C:N mol/mol
20120813	6	H24	20	-1.489	33.086	33.57	7.02	1.10	6.60
20120814	9	H21	47	-1.700	33.440	112.09	30.10	4.72	6.47
20120814	10	H10	39	-1.651	33.458	73.75	21.40	3.39	6.70
20120815	11	H30	58	-1.540	32.442	82.09	42.33	4.50	8.87
20120816	20	H8	36	-1.549	32.707	71.06	15.49	2.92	5.00
20120817	25	H4	40	-1.709	33.352	82.88	38.30	4.93	7.95
20120817	26	H14	39	-1.618	32.693	91.33	20.39	3.90	5.13
20120818	30	H2	30	-1.683	33.316	80.04	10.92	0.53	20.88
20120819	37	H1	40	-1.619	33.240	23.10	37.88	2.29	17.75
20120820	45	H16	70	-1.694	33.376	16.01	28.68	1.81	15.06
20120822	57	BARC5	116	-1.673	33.396	55.83	42.98	3.68	10.98
20120823	66	H38	49	-1.631	33.014	104.99	31.36	2.68	11.78
20130802	3	H112	63	-1.717	32.961	20.38	37.14	0.46	81.63
20130804	14	H7	38	-1.685	32.804	5.62	8.30	0.93	8.95
20130804	15	H17	38	-1.628	32.702	10.24	15.34	1.87	8.45
20130805	17	H53	42	-1.702	32.905	30.82	16.61	0.48	35.31
20130805	25	CBL13	50	-1.700	32.718	35.25	42.32	4.71	9.22
20130807	37	H109	53	-1.724	33.188	14.85	34.14	0.49	75.43
20130809	52	H29	60	-1.583	32.546	8.25	37.69	4.36	8.52
20130810	57	H107	54	-1.715	33.020	20.42	33.56	0.45	74.49
20130810	58	H33	50	-1.694	32.684	15.41	29.04	3.03	9.81
20130811	63	H28	52	-1.692	32.714	31.74	44.37	4.95	8.98
20130811	64	H15	50	-1.686	32.733	15.40	23.88	2.83	8.84
20130812	73	H34	35	-1.675	32.681	7.28	18.22	2.19	7.68

#### 4. Acknowledgements

This study was funded by the U.S. Department of the Interior, Bureau of Ocean Energy Management (BOEM), Alaska Outer Continental Shelf Region, Anchorage, Alaska under BOEM Cooperative Agreement No. M11AC00007 as part of the Chukchi Offshore Monitoring in Drilling Area (COMIDA). We are very thankful to Heather Crowley of BOEM for her participation on collection cruises and support for the logistics and for the research team.

## 5. References

- Clarke, K.R., Gorely, R.N., 2006. PRIMER v6: User manual/tutorial, PRIMER-E, Plymouth UK, 192 pp.
- Clarke, K.R., Warwick, R.M., 2001. Change in Marine Communities: An Approach to Statistical Analysis and Interpretation. 2nd ed. PRIMER-E, Plymouth, UK, 172 pp.
- Feder, H.M., Naidu, A.S., Hameedi, M.J., Jewett, S.C., Johnson, W.R., 1989. The Chukchi Sea continental shelf: benthos-environmental interactions. U.S. Dept. Comm., NOAA, OCSEAP Final Rep. 68, 25-311.
- Grebmeier, J.M., Cooper, L.W., Feder, H.M., Sirenko, B.I., 2006a. Ecosystem dynamics of the Pacific-influenced Northern Bering and Chukchi Seas in the Amerasian Arctic. Prog. Oceanogr. 71, 331-361.
- Magurran, A.E., 2004. Measuring Biological Diversity. Blackwell Publishing. pp. 107-108.
- Primer-e, 2016. <http://www.primer-e.com>
- Schonberg, S.V., Clarke, J.T., Dunton, K.H., 2014. Distribution, abundance, biomass and diversity of benthic infauna in the Northeast Chukchi Sea, Alaska: Relation to environmental variables and marine mammals. Deep-Sea Res. II 102, 144-163.
- White, D., Kimerling, J.A., Overton, S.W., 1992. Cartographic and geometric components of a global sampling design for environmental monitoring. Cartogr. Geogr. Inf. Sci. 19, 5-22.

# **Data Management for the Hanna Shoal Ecosystem Study**

## **Tim Whiteaker, David Maidment**

The University of Texas at Austin  
Center for Research in Water Resources  
University of Texas at Austin  
10100 Burnet Rd., Bldg. 119  
Austin, TX 78758

[whiteaker@utexas.edu](mailto:whiteaker@utexas.edu)

### **Abstract**

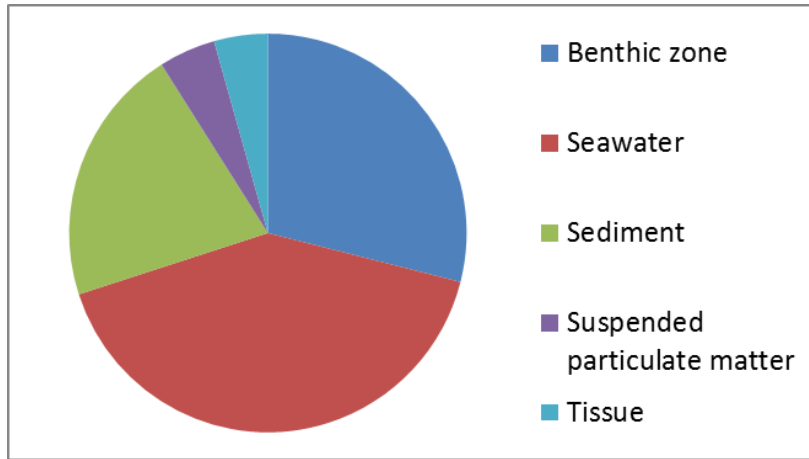
For this project, ten investigators submitted data files covering 125 sampling locations and containing more than 50,000 data values. Samples represent 200+ variables, 400+ taxonomic names, 30+ collection methods, and 30+ lab analysis methods. These data were harmonized according to a community driven set of controlled vocabularies for variable names, chemical speciations, units of measure, sample mediums, and sample types, and stored in an internal project database using a version of the CUAHSI Observations Data Model schema modified for inclusion of taxonomic information. To share with the public, data are exported from the project database into formats more typically used by scientists in this domain such as CSV, Excel, and ArcGIS geodatabase, for publication on the project website and in the NCEI archives. The data are accompanied by an entity relationship diagram, data dictionary, and ISO 19139 metadata explaining the data structure. As explained in a readme file within the dataset, data are available under the Creative Commons Attribution 3.0 United States (CC BY 3.0 US) license which states that the data are available for all to use provided that proper credit is given.

### **1. Introduction**

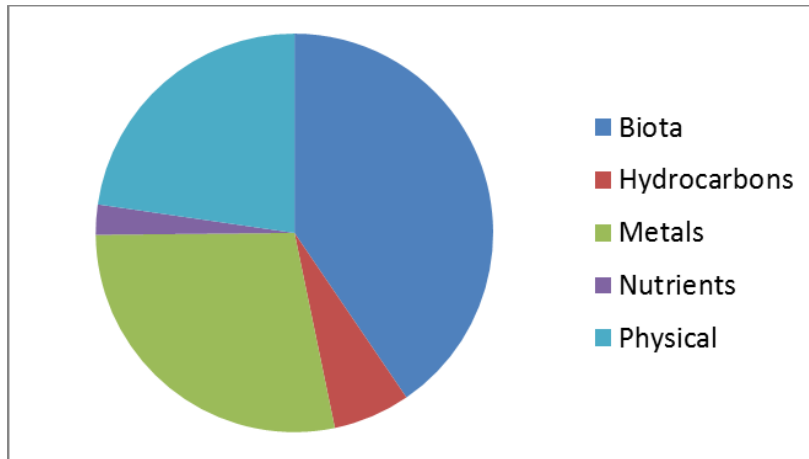
A key requirement of this project is to provide the public with a database of field sample results with sufficient metadata to enable others to understand and use the data. Data management for this project was carried out with this end goal in mind, with the data management workflow beginning prior to any field data collection, and ending with datasets published on the project website and in the National Oceanic Data Center's (NOODC) National Centers for Environmental Information (NCEI) archives. This section summarizes data collected for the project and describes the project's data management workflow.

### **2. Data Summary**

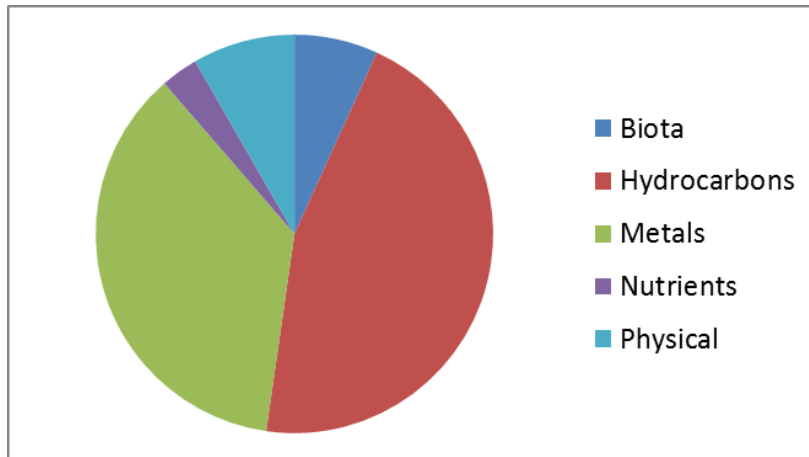
Ten investigators submitted data files covering 125 sampling locations and containing more than 50,000 data values. Samples represent 200+ variables, 400+ taxonomic names, 30+ collection methods, and 30+ lab analysis methods. Table 1 shows some of the variables collected in various sample media. Figure 1 shows the relative number of data values by sample medium, Figure 2 shows the relative number of data values by broad category, and Figure 3 shows the relative number of variables included in each category.



**Figure 1.** Distribution of data values by sample medium.



**Figure 2.** Distribution of data values by broad category.



**Figure 3.** Distribution of variables by broad category.

**Table 1.** Examples of the types of data collected in various sample media.

<b>Seawater</b>	<b>Benthic Zone</b>	<b>Sediment</b>
Salinity	Abundance	Hydrocarbons
Chlorophyll a	Biomass	Metals
Particulate organic carbon	Organic contaminants	Grain size distribution
Total suspended solids	Stable isotopes	Oxygen uptake
Dissolved oxygen	Metals	C-N mass ratio

The data are available on the project website (The University of Texas at Austin, 2016) and at the National Centers for Environmental Information archives (National Centers for Environmental Information, 2016).

### **3. Project Database**

Like the COMIDA CAB project, the Hanna Shoal Ecosystem Study uses the Consortium of Universities for the Advancement of Hydrologic Science, Inc. (CUAHSI) Observations Data Model (ODM) as the basis for its project database. This relational database is suitable for storing observations data at point sampling locations and includes sufficient metadata to enable discovery and interpretation (Horsburgh, et al., 2008). By storing data from all principal investigators (PIs) in a single ODM database, the data have been described in a consistent and well-documented manner.

At the core of an ODM database is a table of numerical data values, such as dissolved oxygen measurements, in a table called DataValues. Each data value includes the time at which the sample was taken, quality control level, and optional data qualifiers such as whether the phenomenon measured was below the detection limit of the sensor. Furthermore, each data value includes a relationship to other tables in the database describing where the measurement was taken, a description of the variable being measured (e.g., dissolved oxygen in units of micromoles per kilogram), sample identification, sample collection and lab analysis methods used, and who provided the data value. A diagram of the ODM database schema, a design specifications document describing the schema, a blank database, and a sample populated database are available on the CUAHSI Hydrologic Information Systems website (CUAHSI-HIS Project Team, 2010).

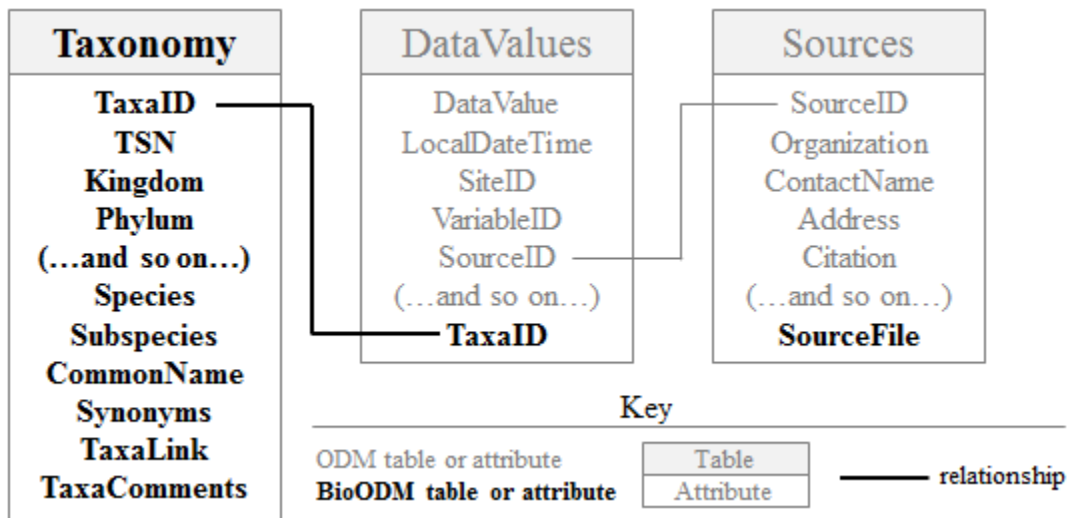
ODM requires data descriptors to be a valid entry in a set of community-driven controlled vocabularies maintained by CUAHSI. For example, dissolved oxygen is present in the Variable Name controlled vocabulary as “Oxygen, dissolved” (and not Dissolved oxygen or DO or D.O., for example). Using terms from controlled vocabularies improves data understanding and interoperability, and thus is a welcome feature for the project database. The master controlled vocabularies are available on the CUAHSI website (CUAHSI HIS, 2014).

As with COMIDA CAB, the ODM database is augmented to support taxonomic descriptors and source file provenance following the BioODM design of Hersh and Maidment, 2013. For taxonomy, a table in which each record represents a specific taxonomic entry is added to the database. Each record in this table includes taxonomic hierarchy for the entry (e.g., kingdom, phylum, class...genus, species, subspecies), common name, synonyms, taxonomic serial number



from the Integrated Taxonomic Information System (if available), a link to a description of the taxon online, and any PI comments about the entry. Each value in the DataValues table can optionally be related to a record in the Taxonomy table. For example, a data value of mercury concentration could be associated with Arctic cod.

To enhance provenance, a SourceFile attribute is added to the Sources table of ODM to store the name of the file that the PI submitted. Because each record in the DataValues table is related to a record in the Sources table, every data value in the database can be tracked back to the original file from which it came. Changes to the ODM design are highlighted in Figure 4.



**Figure 4.** BioODM enhancements to the CUAHSI Observations Data Model.

Based on experience with the COMIDA CAB project, the BioODM database includes sufficient detail to store data collected for the Hanna Shoal Ecosystem Study. With a database design chosen, a data management workflow was designed to facilitate loading data into the database.

#### 4. Data Management Workflow

The groundwork for the data management workflow was established during the COMIDA CAB project. This involves collecting quality controlled sample results from the project's multidisciplinary research staff, transforming the data to follow a common set of controlled vocabularies for variable names, units of measure, etc., loading data into a project database, exporting data to readily accessible formats for data sharing such as GIS files and comma delimited text files, and publishing data both on a project website and in NCEI archives. However, whereas COMIDA CAB relied upon technologies like iRODS and scripting to collect and transform data, for the Hanna Shoal Ecosystem Study a more flexible and yet simpler approach is taken.

The workflow begins prior to sample collection, when PIs are trained in the use of a data submission template created in Excel. While optional, using the data submission template enhances data submission because the template includes columns for each metadata element

required by the project database. Most PIs used the template. When PIs did not use the template, they often provided just the portions of the template with metadata not already included within the PI's own internal data file format.

In the field, samples are collected by PIs and analyzed either immediately or stored for later analysis onshore. Over the next few months, data are analyzed and assembled by PIs into the project data template or their own data format, typically an Excel spreadsheet.

Quality controlled data are submitted by each PI to Dr. Tim Whiteaker at The University of Texas at Austin. Dr. Whiteaker reviews the data for completeness. Metadata omissions, such as missing units of measure or ambiguities on sample collection method, are resolved via direct communication with the PI. During the data review, variables (the property measured within the sample), sample mediums, sample types, units of measure, and chemical speciations from submitted data files are checked against and mapped to the master set of controlled vocabularies used for the project. The rest of the data are associated with columns in the BioODM database, and the data files are typically transformed to a format recognized by the CUAHSI ODM Data Loader, a free tool for loading data into an ODM database. For this project, Dr. Whiteaker adapted the CUAHSI ODM Data Loader to handle the additional table and columns included with BioODM. The transformed files are then loaded into the project's BioODM database using the data loader, which is stored in a SQL Server database at The University of Texas at Austin.

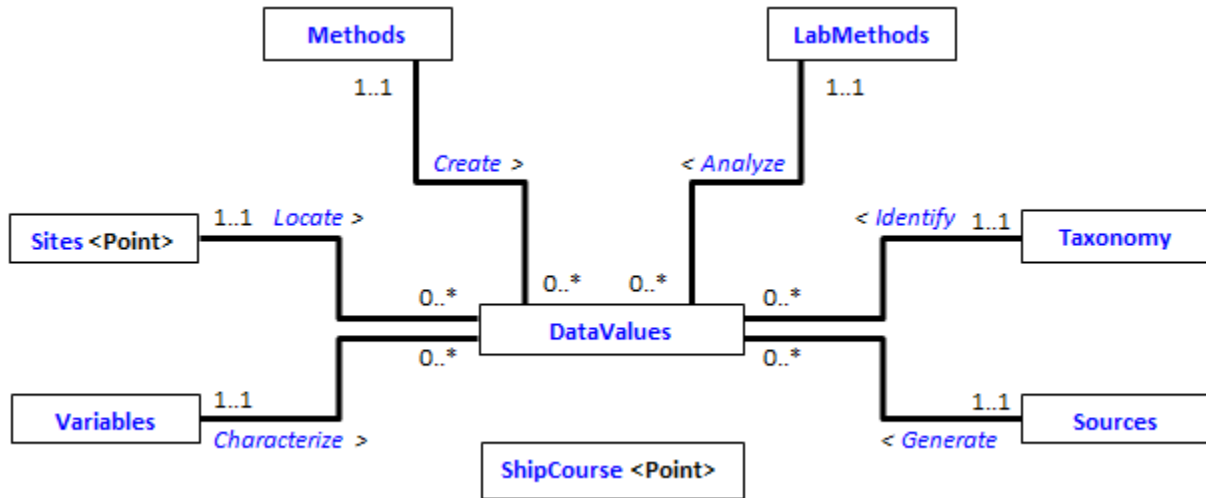
Periodically, data are extracted from the database into more widely used formats and shared with the public on the project website and in NCEI archives. This project has been assigned NODC Accession 0123220, so any updates to the archive submission result in a new version number under the same Accession number. Users can access any version desired from the archives, though the highest version number will represent the most current and most complete dataset.

## **5. Data Structure for Published Sample Results**

Internally, this project uses SQL Server to store project data. To better enable potential users of the data who may not have SQL Server expertise, and to comply with acceptable submission formats for both BOEM and NODC, the data are exported to formats more typically used by scientists in this domain for publication on the project website and in the NCEI archives. The formats include Esri file geodatabase, comma separated values (CSV) text file, and Excel format. Each format contains the same sample results as other formats. For example, the file geodatabase will include a table called Sources, the Excel spreadsheet will include a worksheet called Sources, a CSV file called Sources will be included, and all three formats will include the same data about data sources used in the project. Multiple formats are provided so that the user can choose the format most compatible with the user's software. Original files submitted by PIs are included as well so that each data value can be traced back and viewed in its file of origin.

Note that while NODC accepts file geodatabases, an NODC data officer will convert from file geodatabase to shapefile format as per their protocol. While shapefiles are more widely accessible to GIS users, they also suffer limitations such as coarse temporal resolution and 10-character field name lengths. However, the original file geodatabase will be available for users if needed, and shapefile users can still see full attribute details by viewing the version of the data in CSV or Excel format.

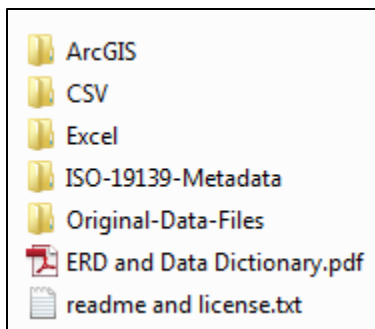
Per BOEM requirements and with guidance from Dan Holiday and Heather Crowley of BOEM, an entity relationship diagram of the tables included with this product, and a data dictionary describing each table, have been prepared for inclusion with the data submission. In addition, ISO 19139 metadata for the tables and fields was created in and exported from ArcGIS and is included with the data submission. A simplified version of the entity relationship diagram is shown in Figure 5. The diagram applies to all three file formats used for data publication.



**Figure 5.** Simplified Entity Relationship Diagram for Downloadable Data

As explained in a readme file within the dataset, data are available under the Creative Commons Attribution 3.0 United States (CC BY 3.0 US) license (Creative Commons, 2016). Basically, this license states that the data are available for all to use provided that proper credit is given. Because each data value in the project database includes a pointer back to the data source, users of the data should have no trouble assigning proper attribution. Furthermore, the Sources table includes a Citation field so that there is no ambiguity in how data should be cited.

The files described above are organized into folders based on file type, and the folder is zipped for posting online. An example of how the folder structure of this dataset might look in Microsoft’s Windows Explorer software is shown in Figure 6.



**Figure 6.** Example folder structure of project sampling results dataset

The following tables comprise the data dictionary for the downloadable project sampling results.  
**Table 2.** DataValues - numerical values representing sampling results.

<b>Field</b>	<b>Description</b>	<b>Type</b>
SiteID	References the site at which the observation was measured. This links data values to their locations in the Sites table.	Long Integer
VariableID	References the variable that was measured. This links data values to their variable in the Variables table.	Long Integer
TaxaID	References the taxonomic classification of the organism (if any) associated with the measurement. This links data values to their taxonomic record in the Taxonomy table.	Long Integer
DataValue	The numeric value of the observation.	Double
Qualifier	A data qualifying comment that may accompany the data value.	Text
CensorStatus	Indicates whether the data value is censored, e.g., below the detection limit of the sensor.	Text
OffsetValue	Distance from a datum or control point to the point at which a data value was observed. If not given, the OffsetValue is inferred to be 0, or not relevant/necessary.	Double
OffsetUnits	Units of measure used for the offset.	Text
OffsetDescription	Describes the offset type.	Text
SiteName	Full text name of sampling site from the Sites table, duplicated here for convenience.	Text
Latitude	Latitude in decimal degrees from the Sites table, duplicated here for convenience.	Double
Longitude	Longitude in decimal degrees from the Sites table, duplicated here for convenience.	Double
VariableCode	Unique variable code for the variable from the Variables table, duplicated here for convenience.	Text
VariableName	Name of the variable from the Variables table, duplicated here for convenience.	Text
Units	Units of measure used for the data value.	Text
SampleMedium	The medium of the sample from the Variables table, duplicated here for convenience.	Text
LocalDateTime	Local date and time at which the data value was observed.	Date
ValueAccuracy	Numeric value that describes the measurement accuracy of the data value. If not given, it is interpreted as unknown.	Double
MethodID	References the method used to generate the data value. This links data values to their methods in the Methods table.	Long Integer
LabSampleCode	Text code assigned to the sample (if any) associated with the data value.	Text
SampleType	Controlled vocabulary specifying the sample type.	Text
LabMethodID	References the lab method used to analyze the sample. This links data values to their lab method in the LabMethods table.	Long Integer
QualityControlLevel	Level of quality control that the value has been subjected to.	Text
SourceID	References the record in the Sources table giving the source of the data value.	Long Integer
ContactName	The contact name from the Sources table, duplicated here for convenience.	Text

**Table 3.** LabMethods - descriptions of the laboratory methods used to analyze physical samples for specific constituents.

Field	Description	Type
LabMethodID	Unique integer identifier for each laboratory method.	Long Integer
LabName	Name of the laboratory responsible for processing the sample.	Text
LabOrganization	Organization responsible for sample analysis.	Text
LabMethodName	Name of the method and protocols used for sample analysis.	Text
LabMethodDescription	Description of the method and protocols used for sample analysis.	Text
LabMethodLink	Link to additional reference material on the analysis method.	Text

**Table 4.**Methods - the methods used to collect samples and any additional information about the method.

Field	Description	Type
MethodID	Unique integer ID for each method.	Long Integer
MethodDescription	Text description of each method.	Text
MethodLink	Link to additional reference material on the method.	Text

**Table 5.** ShipCourse - the ship course for cruises undertaken during the Hanna Shoal Ecosystem Study. The table is intended to be visualized as a point feature class in a geographic information system, i.e., a set of point locations in a map.

Field	Description	Type
DateTime	The date and time when the ship arrived at a certain position.	Text
Latitude	Latitude in decimal degrees.	Double
Longitude	Longitude in decimal degrees. East positive, West negative.	Double
CruiseYear	The year when the cruise was carried out.	Short Integer

**Table 6.** Sites - the spatial location at which data values have been collected. The table is intended to be visualized as a point feature class in a geographic information system, i.e., a set of point locations in a map.

Field	Description	Type
SiteID	Unique identifier for each sampling location.	Long Integer
SiteName	Full name of the sampling site.	Text
Latitude	Latitude in decimal degrees.	Double
Longitude	Longitude in decimal degrees. East positive, West negative.	Double
PositionalAccuracy_meters	Value giving the accuracy with which the positional information is specified in meters.	Double
Comments	Comments related to the site.	Text
Datum	Spatial Reference System of the latitude and longitude coordinates.	Text

**Table 7.** Sources - the source organization and contact which originated the data values.

<b>Field</b>	<b>Description</b>	<b>Type</b>
SourceID	Unique integer identifier that identifies each data source.	Long Integer
Organization	Name of the organization that collected the data.	Text
SourceDescription	Full text description of the source of the data.	Text
SourceLink	Link for more information about the data source.	Text
ContactName	Name of the contact person for the data source.	Text
Phone	Phone number for the contact person.	Text
Email	Email address for the contact person.	Text
Address	Street address for the contact person.	Text
City	City in which the contact person is located.	Text
State	State in which the contact person is located.	Text
ZipCode	US Zip Code or country postal code.	Text
Citation	Text string that gives the citation to be used when the data from each source are referenced.	Text

**Table 8.** Taxonomy - the taxonomy information to describe organisms in the study.

<b>Field</b>	<b>Description</b>	<b>Type</b>
TaxaID	Unique ID for each taxonomic classification.	Long Integer
TSN	Taxonomic Serial Number, from itis.gov. Negative TSN values are used when an appropriate TSN could not be obtained from itis.gov.	Long Integer
Kingdom	Scientific Kingdom name.	Text
Subkingdom	Scientific Subkingdom name.	Text
Infrakingdom	Scientific Infrakingdom name.	Text
Superphylum	Scientific Superphylum name.	Text
Phylum	Scientific Phylum name.	Text
Subphylum	Scientific Subphylum name.	Text
Class	Scientific Class name.	Text
Subclass	Scientific Subclass name.	Text
Infraclass	Scientific Infraclass name.	Text
Superorder	Scientific Superorder name.	Text
Order_	Scientific Order name.	Text
Suborder	Scientific Suborder name.	Text
Infraorder	Scientific Infraorder name.	Text
Superfamily	Scientific Superfamily name.	Text
Family	Scientific Family name.	Text
Genus	Scientific Genus name.	Text
Species	Scientific Species name.	Text
Subspecies	Scientific Subspecies name.	Text
CommonName	Common name.	Text
Synonyms	Common synonyms.	Text
TaxaLink	Hyperlink to the taxa report on itis.gov or other authoritative website.	Text
TaxaComments	Comments on the taxonomic classification.	Text

**Table 9.** Variables - descriptive information about what variables have been measured.

<b>Field</b>	<b>Description</b>	<b>Type</b>
VariableID	Unique integer identifier for each variable.	Long Integer
VariableCode	Text code used by the organization that collects the data to identify the variable.	Text
VariableName	Full text name of the variable that was measured, observed, modeled, etc.	Text
Speciation	Text code used to identify how the data value is expressed (e.g., total phosphorus concentration expressed as P).	Text
UnitsName	Full text name of the units of the data values associated with the variable.	Text
SampleMedium	The medium in which the sample or observation was taken or made.	Text
ValueType	Text value indicating what type of data value is being recorded.	Text
DataType	Text value that identifies the data values as one of several data types.	Text
GeneralCategory	General category of the data values.	Text
NoDataValue	Numeric value used to encode no data values (i.e., null or missing values) for this variable.	Double

**Table 10.** Relationships - these relationships define ancillary information about data values.

<b>Name</b>	<b>Table</b>	<b>Field</b>	<b>Type</b>	<b>Field</b>	<b>Table</b>
<i>Locate</i>	DataValues	SiteID	* <-> 1	SiteID	Sites
<i>Characterize</i>	DataValues	VariableID	* <-> 1	VariableID	Variables
<i>Create</i>	DataValues	MethodID	* <-> 1	MethodID	Methods
<i>Analyze</i>	DataValues	LabMethodID	* <-> 1	LabMethodID	LabMethods
<i>Identify</i>	DataValues	TaxaID	* <-> 1	TaxaID	Taxonomy
<i>Generate</i>	DataValues	SourceID	* <-> 1	SourceID	Sources

## 6. Broader Impact

This project uses community-driven controlled vocabularies maintained by CUAHSI. These controlled vocabularies are dynamic in that users of the system can submit refinements or additions as needed. As a result of project needs for the Hanna Shoal Ecosystem Study, dozens of edits and additions were submitted to CUAHSI, and over the course of several months, Dr. Whiteaker worked with CUAHSI to refine the terms until reaching agreement on the final set, which is now officially part of the CUAHSI controlled vocabularies. Some of the new terms include Rosette sampler, Benthic zone, and 1,4,5-Trimethylnaphthalene. These enhancements will be available to all who use ODM or the CUAHSI controlled vocabularies. Working with CUAHSI personnel also provided independent review of the data descriptors used for this project, helping to ensure that our sample data will be interpretable by the broader community. A summary of controlled vocabulary edits is shown in Table 11.

**Table 11.** Number of updates to CUAHSI controlled vocabularies.

<b>Category</b>	<b>Additions</b>	<b>Edits</b>
<b>Variable Names</b>	23	3
<b>Chemical Speciations</b>	35	2
<b>Units of Measure</b>	4	0
<b>Sample Mediums</b>	2	0
<b>Sample Types</b>	2	0

## **7. Acknowledgements**

This study was funded by the U.S. Department of the Interior, Bureau of Ocean Energy Management (BOEM), Alaska Outer Continental Shelf Region, Anchorage, Alaska under BOEM Cooperative Agreement No. M11AC00007 as part of the Chukchi Sea Offshore Monitoring in Drilling Area (COMIDA) Project.

## **8. References**

- Creative Commons, 2016. Creative Commons - Attribution 3.0 United States - CC BY 3.0 US. <https://creativecommons.org/licenses/by/3.0/us/>.
- CUAHSI HIS, 2014. CUAHSI Hydrologic Information System - Master Controlled Vocabulary Registry. <http://his.cuahsi.org/mastercvreg/cv11.aspx>.
- CUAHSI-HIS Project Team, 2010. CUAHSI Hydrologic Information System - ODM Databases. <http://his.cuahsi.org/odmdatabases.html>.
- Hersh, E.S., Maidment, D.R., 2013. Extending Hydrologic Information Systems to accommodate Arctic marine observations data. *Deep-Sea Res. II* 102, 9-17, doi:10.1016/j.dsr2.2013.07.014.
- Horsburgh, J.S., Tarboton, D.G., Maidment, D.R., Zaslavsky, I., 2008. A relational model for environmental and water resources data. *Water Resour. Res.* 44, W05406, doi:10.1029/2007WR006392.
- National Centers for Environmental Information, 2016. Ecosystem monitoring information collected in Hanna Shoal in the Chukchi Sea for the COMIDA CAB project from August 2012 to August 2013 (NODC Accession 0123220). <http://data.nodc.noaa.gov/cgi-bin/iso?id=gov.noaa.nodc:0123220>.
- The University of Texas at Austin, 2016. Hanna Shoal. <http://arcticstudies.org/hannashoal/>.